AD NUMBER
ADC018373
CLASSIFICATION CHANGES
TO: unclassified
FROM: secret
LIMITATION CHANGES
TO: Approved for public release, distribution unlimited
FROM: Controlling DoD Organization: U.S. Naval Electronic Systems Command, Washington, DC 20360.
AUTHORITY
ONR ltr, 31 Jan 2006; ONR ltr, 31 Jan 2006

AD-C018374

SECRET (This page is UNCLASSIFIED.)

SECURITY CLASSIFICATION OF THIS PAGE (When Data Entered)

REPORT DOCUMENTATION PAGE	READ INSTRUCTIONS BEFORE COMPLETING FORM
1. REPORT NUMBER	2. GOVT ACCESSION NO. / 3. RECIPIENT'S CATALOG NUMBER (9)
4. TITLE (and Subtitle) (6) MOORED SURVEILLANCE SYSTEM FIELD VALIDATION TEST SENSOR PERFORMANCE ANALYSIS (U) STANDARD RESOLUTION DATA PRODUCTS (U) Volume II	5. TYPE OF REPORT & PERIOD COVERED final report 10 JAN 77 - 31 MAR 78
	6. PERFORMING ORG. REPORT NUMBER ARL-TR-78-2
7. AUTHOR(s) (10) Steven L. Watkins, Judith L. Winterkamp	8. CONTRACT OR GRANT NUMBER(s) (8) N00039-77-C-0003 (15)
9. PERFORMING ORGANIZATION NAME AND ADDRESS Applied Research Laboratories, The University of Texas at Austin, Austin, Texas 78712	10. PROGRAM ELEMENT, PROJECT, TASK AREA & WORK UNIT NUMBERS Items 0003 and 0004
11. CONTROLLING OFFICE NAME AND ADDRESS Naval Electronic Systems Command, Department of the Navy, Washington, DC 20360	12. REPORT DATE 31 December 1978
	13. NUMBER OF PAGES 427
14. MONITORING AGENCY NAME & ADDRESS (if different from Controlling Office) (11) ARL-TR-78-2	15. SECURITY CLASS. (of this report) SECRET
	15a. DECLASSIFICATION/DOWNGRADING SCHEDULE See reverse side.

16. DISTRIBUTION STATEMENT (of this Report)

None

(12) 432 p.

17. DISTRIBUTION STATEMENT (of the abstract entered in Block 20, if different from Report)

18. SUPPLEMENTARY NOTES

19. KEY WORDS (Continue on reverse side if necessary and identify by block number)

rapidly deployable surveillance system
moored surveillance system
DIFAR

20. ABSTRACT (Continue on reverse side if necessary and identify by block number)

(U) Volume II of this report contains the detailed standard frequency resolution data products used to analyze candidate sensor performance based on the Moored Surveillance System Field Validation Test. In addition, this volume contains a brief discussion of each type of display and the methods used to generate it.

DD FORM 1 JAN 73 1473 EDITION OF 1 NOV 65 IS OBSOLETE

(This page is unclassified)

SECRET 404 434

SECURITY CLASSIFICATION OF THIS PAGE (When Data Entered)

15a.

DD 254, 12/10/76,
Cont. N00039-77-C-0003
CLASSIFIED BY OPNAVINST S5510.72C, 4 Sep 73
EXEMPT FROM GDS OF E.O. 11652
EXEMPTION CATEGORY 3
DECLASSIFIED ON 31 Dec 2007

"NATIONAL SECURITY INFORMATION

"Unauthorized Disclosure Subject to Criminal Sanctions"

Accession For	
NTIS GRA&I	☐
DDC TAB	☒
Unannounced	☐
Justification	
By	
Distribution/	
Availability Codes	
Dist	Avail and/or special
9	

TABLE OF CONTENTS

(The reverse of this page is blank.)

LIST OF TABLES

(The reverse of this page is blank.)

LIST OF FIGURES

(The reverse of this page is blank.)

I. INTRODUCTION

(C) During November 1975, the Moored Surveillance System (MSS) Field Validation Test (FVT) was conducted under the sponsorship of the MSS Project Office (PME 124-30) of Naval Electronic Systems Command. Applied Research Laboratories, The University of Texas at Austin (ARL:UT), participated in the processing and analysis of the acquired ACODAC data. The results of this work, performed under Contract N00039-77-C-0003, are contained in a four-volume report describing the measurements and analyses of candidate sensor performance based on data from the MSS-FVT. Volume I describes the data collection system and the measurement system used to obtain the results. This volume, Volume II, contains data products obtained with standard frequency resolution processing. Volume III contains the data products obtained with vernier frequency resolution processing. Volume IV contains the background information, summary data products, and analysis.

(U) Since the MSS-FVT was completed, the name of the MSS program has been changed to Rapidly Deployable Surveillance System (RDSS). To avoid ambiguity, the term MSS will be used throughout this report. However, the issues addressed herein are those that were specified by the MSS Project Office and were of interest to RDSS at the time that this report was written.

(U) This volume, which contains the standard frequency resolution data products, is partitioned into four sections. The first section is this introduction. The second section describes the cw data products. The third section describes the ambient sound field (ASF) data products. The fourth section is a brief discussion of the utilization of these data products. Much of the text in this volume is similar to that in Volumes I and III, but is repeated here so that each volume can be used independently of the others.

(The reverse of this page is blank.)

II. cw DATA PRODUCTS

(U) The standard frequency resolution cw data products contained in this volume were extracted from the data intervals shown in Table II-1. The processing parameters are summarized in Table II-2. The cw projector characteristics used in the performance of these measurements are summarized in Table II-3. The cw projector source levels for the CFAV KAPUSKACING are higher than those reported previously (Ref. 1). These revisions were made in order to reconcile the propagation loss curves from the CFAV KAPUSKACING with those from the other sources. A detailed description of the measurement system can be found in Volume I.

(C) Several different types of cw data products are contained herein. Each type is described briefly, and a table of curves is given. The abbreviations used in these tables and the text are:

QT	CFAV QUEST
KP	CFAV KAPUSKACING
CH	R/V CHAIN
O	Omnidirectional Sensor
SC	Single Cardioids Sensor
MGL	Maximum Gain Limacons Sensor
VD	Vertical Dipole Sensor
DC	Differenced Cardioids Sensor.

These curves were included in this report to substantiate the observations in Volume IV, and to furnish a data base for future issues not addressed by this report. For completeness, each curve containing any data was included, even though the small number of samples may minimize its statistical significance.

(U) TABLE II-1

STANDARD RESOLUTION DATA BASE

Site A1 1200Z 17 Nov[321] - 2359Z 17 Nov[321]

Site A2 1200Z 17 Nov[321] - 1859Z 17 Nov[321]

Site A3 1200Z 17 Nov[321] - 2359Z 17 Nov[321]

[] Julian Day

Z Greenwich Mean Time

(S) TABLE II-2

STANDARD RESOLUTION PROCESSING PARAMETERS (U)

Parameter	Value
Sample Rate:	1250 Hz (obtained from zero crossings of tape servo signal)
Frequency Range	10 to 600 Hz (no acoustic data below 30 Hz)
FFT Length	6.55 sec (8192 samples)
Spectral Window	Hanning
Frequency Spacing	0.1526 Hz
3 dB Bandwidth	0.2197 Hz
Equivalent Noise Bandwidth	0.2289 Hz
FFT Overlap	50%
ALI Interval	5 min
ALI Type	Rectangular Integration
FFT/ALI	90
Time Bandwidth Product	66.4
Equivalent Degrees of Freedom	161.6
Probability of False Alarm	10^{-3}
Detection Threshold	-10.3 dB//Hz

(U) TABLE II-3

cw PROJECTOR CHARACTERISTICS FOR
STANDARD RESOLUTION DATA PRODUCTS

TOW PLATFORM	NOMINAL FREQUENCY (Hz)	NOMINAL LEVEL (dB//μPa)	17 NOV FIELD EVENT ON/OFF TIMES (Z)	17 NOV FIELD EVENT NOMINAL DEPTH (m)
CFAV	55	141	1230/2230	110
QUEST	155	134	1230/2230	110
	305	136	1230/2230	110
CFAV	64	162	1230/2318	110
KAPUSKACING	160	161	1230/2318*	110
	260	147	1230/2318	110
R/V	70	166	1225/2200	100
CHAIN	170	156	1225/2200	100
	335	154	1645/2200	100

*FREQUENCY VARYING 1 CYCLE

(C) Data products of the first type are termed summary detection plots (Appendix A, Figs. II-1 — II-15). These are plots of each detected line within a frequency band as a function of time. The solid symbols indicate that the line was detected in multiple cells and/or on multiple beams of the sensor. The X symbols indicate that the line was detected only in a single cell on a single beam of the sensor. The solid line emanating from each symbol indicates the maximum signal-to-noise ratio (S/N) of any cell of the line. If the sensor provides bearing information, the solid line also indicates the estimated bearing, north being the top of the plot. The dashed lines indicate which of the detections were linked by the tracking algorithm. These displays are intended to provide qualitative information about the environment in which the processor must function in terms of line loading and relative clutter density between sensors and frequency regimes. More quantitative information will be found in Section III of this volume.

(C) Data products of the next type (Appendix B, Figs. II-16 - II-142) are termed line history plots, and are cataloged in Table II-4. These are plots of the estimated cw signal parameters as a function of time. The top portion of the plot contains a solid line indicating ground truth source-to-receiver range in nautical miles and X's indicating the number of equivalent degrees of freedom for each ALI. The second portion contains a solid line denoting ground truth receiver-to-source bearing, X's indicating the estimated signal bearing, and ·'s indicating the estimated noise bearing. Gaps in the solid ground truth lines indicate intervals of missing data, such as calibration signal intervals. The third portion contains the estimated ambient sound field (ASF) levels in dB//μPa/Hz$^{1/2}$. The omnidirectional (O) and vertical dipole (VD) sensor curves contain a single trace of connected X's. The curves plotted for SC (single cardioids), MGL (maximum gain limacons), and DC (differenced cardioids) contain a trace for each beam, which is labeled by the first letter of its main axis bearing (north, east, south, and west). ASF level estimates

(U)

TABLE II-4

STANDARD RESOLUTION LINE HISTORY PLOTS

Source Platform	Source Frequency	17 NOV (321)														
		Site A1					Site A2					Site A3				
		0	SC	MGL	VD	DC	0	SC	MGL	VD	DC	0	SC	MGL	VD	DC
QT	55	16*	17*	18*	ND	ND	ND	58*	59	ND	ND	ND	100*	ND	101	102
KP	64	28	29	30	31	32	70	71	72	73	74	113	114	115	116	117
CH	70	43	44	45	46	47	85	86	87	88	89	128	129	130	131	132
QT	155	19	20	21	ND	22	60	61	62	63	64	103	104	105	106	107
KP	160	33	34	35	36	37	75	76	77	78	79	118	119	120	121	122
CH	170	48	49	50	51	52	90	91	92	93	94	133	134	135	136	137
KP	260	38	39	40	41	42	80	81	82	83	84	123	124	125	126	127
QT	305	23	24	25	26	27	65	66	67	68	69	108	109	110	111	112
CH	335	53	54	55	56	57	95	96	97	98	99	138	139	140	141	142

ND - Not Detected

Entries are plot numbers.

*Later Changed to Not Detected

(C) were displayed only when the signal was detected. The fourth portion of the plot contains the estimated sound pressure level (SPL) in dB//μPa of the received signal. The O and VD sensor curves each contain two traces; the X's denote the levels for the cell with the highest S/N (most detectable); the +'s denote the levels summed over all detected cells, as is normally done when computing propagation loss. The SC, MGL, and DC sensor curves each contain four traces, each giving the levels for the most detectable cell on a beam and annotated in the same manner as the ASF levels. The fifth portion of the plot contains the S/N in decibels relative to a 1 Hz noise band. The traces are defined in the same manner as the SPL curves. The dashed line denotes the detection threshold. The bottom portion of the plot contains two traces; the X's denote the estimated signal frequency, and the □'s denote the line's bandwidth. These displays contain all of the information known about the signal. All of the remaining cw data products are derived from these data.

(C) Data products of the next type (Appendix C, Figs. II-143 — II-150) are termed propagation loss plots, and are cataloged under the O sensor columns of Table II-5. These are plots of the estimated cw propagation loss in decibels as a function of range in nautical miles. Below these are other traces denoting the associated signal excess, (S+N)/N, at each range bin in decibels relative to the noise level in the analysis bandwidth. These traces indicate the confidence associated with the measurements. The bottom traces denote the estimated background ASF levels associated with each range bin. These measurements were derived for a 1 nmi range bin, and smoothed with a 3-bin sliding average. The received signal power was estimated from the cell with the highest S/N of any detected cell on any beam. Since these are single cell measurements, they will show more loss than the total received SPL technique, such as was used in Ref. 2. This difference is discussed in Volume IV.

(C) Data products of the next type (Appendix D, Figs. II-151 — II-182) are termed signal, noise, and array gain plots, and are listed in Table II-5

(U)

TABLE II-5

STANDARD RESOLUTION PROPAGATION LOSS OR
SIGNAL, NOISE, AND ARRAY GAIN VERSUS RANGE PLOTS

Source Platform	Source Frequency	17 NOV (321)														
		Site A1					Site A2					Site A3				
		0	SC	MGL	VD	DC	0	SC	MGL	VD	DC	0	SC	MGL	VD	DC
QT	55	ND	ND	ND	ND	ND	ND	ND	---	ND	ND	ND	ND	ND	---	---
KP	64	143	151	152	153	154	143	151	152	153	154	143	151	152	153	154
CH	70	144	155	156	157	158	144	155	156	157	158	144	155	156	157	158
QT	155	145	159	160	ND	162	145	159	160	161	162	145	159	160	161	162
KP	160	146	163	164	165	166	146	163	164	165	166	146	163	164	165	166
CH	170	147	167	168	169	170	147	167	168	169	170	147	167	168	169	170
KP	260	148	171	172	173	174	148	171	172	173	174	148	171	172	173	174
QT	305	149	175	176	177	178	149	175	176	177	178	149	175	176	177	178
CH	335	150	179	180	181	182	150	179	180	181	182	150	179	180	181	182

ND - Not Detected

Entries are plot numbers.

UNCLASSIFIED

(C) under sensors other than 0 (SC, MGL, etc.). These are plots of measured sensor signal, noise, and S/N levels relative to those of an omnidirectional sensor (0) as a function of range. The top portion of the plot indicates how many samples (0 sensor detections) occurred in each range bin. The next portion contains traces denoting the measured signal gain of the sensor, where signal gain is the ratio of the received SPL of this sensor over that of the 0 sensor. The next portion contains traces denoting the measured array gain of the sensor, where array gain is the ratio of the S/N of this sensor over that of the 0 sensor. The bottom portion contains traces denoting the measured noise gain of the sensor, where noise gain is the ratio of the ASF level of this sensor over that of the 0 sensor. Since signal gain is primarily a function of range, and noise gain is a function primarily of time, this display allows array gain to be interpreted in terms of both range and time. All of the traces were computed with 1 nmi range bins and smoothed with a 3 nmi sliding average.

(C) When computing average S/N as a function of range, if the signal is not detected during every ALI, the resultant average will be biased high. This bias occurs because only the highest S/N are detected. To reduce this bias, the detection threshold (Table II-2) has been substituted for the missing S/N whenever the target was not detected. This debiasing technique was used both for computing array gain and also for generating curves of S/N versus range.

(C) Data products of the next type (Appendix E, Figs. II-183 — II-225) are termed percentage detection plots, and are cataloged in Table II-6. These curves of single line detection percentages were calculated as the number of independent detection opportunities (ALI intervals) that the specified source was within a given integer 1 nmi range interval and was detected, divided by the number of such opportunities For multibeam sensors, detection on any beam was considered a detection for the sensor. If the number of equivalent degrees of freedom for an ALI was less than

(U)

TABLE II-6

STANDARD RESOLUTION PROBABILITY OF DETECTION VERSUS RANGE PLOTS

Source Platform	Source Frequency	17 NOV (321)														
		Site A1					Site A2					Site A3				
		0	SC	MGL	VD	DC	0	SC	MGL	VD	DC	0	SC	MGL	VD	DC
QT	55	ND	ND	ND	ND	ND	ND	ND	183	ND	ND	ND	ND	ND	184	185
KP	64	196	197	198	199	200	196	197	198	199	200	196	197	198	199	200
CH	70	211	212	213	214	215	211	212	213	214	215	211	212	213	214	215
QT	155	186	187	188	ND	190	186	187	188	189	190	186	187	188	189	190
KP	160	201	202	203	204	205	201	202	203	204	205	201	202	203	204	205
CH	170	216	217	218	219	220	216	217	218	219	220	216	217	218	219	220
KP	260	206	207	208	209	210	206	207	208	209	210	206	207	208	209	210
QT	305	191	192	193	194	195	191	192	193	194	195	191	192	193	194	195
CH	335	221	222	223	224	225	221	222	223	224	225	221	222	223	224	225

ND - Not Detected

Entries are plot numbers.

(C) that specified in Table II-2 (i.e., some portion of the ALI interval was missing), and the signal was not detected, then the ALI was not counted as a valid detection opportunity. This editing criterion was required because the detection threshold for each ALI was determined by its number of degrees of freedom. All of the traces were smoothed with a 3 nmi sliding average. If the sensor furnished a bearing estimate, its rms bearing error was also plotted as a function of range.

(C) Data products of the next type (Appendix F, Figs. II-226 — II-251) are termed bearing error plots, and are cataloged in Table II-7. These are curves of the number of bearing estimates (detections), the mean bearing error (estimated bearing/ground truth bearing), the rms bearing error, and the bearing error standard deviation, all plotted as a function of S/N (dB//1 Hz noise band). The ground truth bearing was computed from the navigation reconstruction as the great circle receiver-to-source bearing at the receiver and at the beginning of the ALI. The estimated bearings were corrected for magnetic variation and acoustically debiased (see Volume I). Each trace was smoothed with a 3 dB sliding average.

(C) Data products of the last type (Appendix G, Figs. II-252 — II-294) are curves of S/N (dB//1 Hz noise band) versus range (nmi), and are cataloged in Table II-8. These measurements were obtained from the detected cell with the highest S/N on any beam. As described earlier, these results are partially debiased by substitution of the detection threshold for ALI intervals without signal detections. The detection threshold is drawn on each plot. Each trace was smoothed with a 3 nmi sliding average.

(U)

TABLE II-7

STANDARD RESOLUTION BEARING ERROR VERSUS SIGNAL-TO-NOISE RATIO PLOTS

Source Platform	Source Frequency	17 NOV (321)														
		Site A1					Site A2					Site A3				
		0	SC	MGL	VD	DC	0	SC	MGL	VD	DC	0	SC	MGL	VD	DC
QT	55	---	ND	ND	---	ND	---	ND	226	---	ND	---	ND	ND	---	227
KP	64	---	234	235	---	236	---	234	235	---	236	---	234	235	----	236
CH	70	---	243	244	---	245	---	243	244	---	245	---	243	244	---	245
QT	155	---	228	229	---	230	---	228	229	---	230	---	228	229	---	230
KP	160	---	237	238	---	239	---	237	238	---	239	---	237	238	---	239
CH	170	---	246	247	---	248	---	246	247	---	248	---	246	247	---	248
KP	260	---	240	241	---	242	---	240	241	---	242	---	240	241	---	242
QT	305	---	231	232	---	233	---	231	232	---	233	---	231	232	---	233
CH	335	---	249	250	---	251	---	249	250	---	251	---	249	250	---	251

ND - Not Detected

Entries are plot numbers.

(U)

TABLE II-8

STANDARD RESOLUTION SIGNAL-TO-NOISE RATIO VERSUS RANGE PLOTS

Source Platform	Source Frequency	17 NOV (321)														
		Site A1					Site A2					Site A3				
		0	SC	MGL	VD	DC	0	SC	MGL	VD	DC	0	SC	MGL	VD	DC
QT	55	ND	ND	ND	ND	ND	ND	ND	252	ND	ND	ND	ND	ND	253	254
KP	64	265	266	267	268	269	265	266	267	268	269	265	266	267	268	269
CH	70	280	281	282	283	284	280	281	282	283	284	280	281	282	283	284
QT	155	255	256	257	ND	259	255	256	257	258	259	255	256	257	258	259
KP	160	270	271	272	273	274	270	271	272	273	274	270	271	272	273	274
CH	170	285	286	287	288	289	285	286	287	288	289	285	286	287	288	289
KP	260	275	276	277	278	279	275	276	277	278	279	275	276	277	278	279
QT	305	260	261	262	263	264	260	261	262	263	264	260	261	262	263	264
CH	335	290	291	292	293	294	290	291	292	293	294	290	291	292	293	294

ND - Not Detected

Entries are plot numbers.

(The reverse of this page is blank.)

III. AMBIENT SOUND FIELD DATA PRODUCTS

(U) Four types of ambient sound field (ASF) measurements were performed using the sound pressure levels at an omnidirectional sensor, noise gains of directional sensors, and clutter (processor loading) statistics of each sensor. The standard frequency resolution ASF data products cover a wide frequency range (40 to 600 Hz) at three sites, but are only of 12 hours duration. The vernier frequency resolution ASF data products in Volume III are of longer duration, but have only limited frequency coverage. Each data product set can be used to extrapolate the other to different frequencies or times.

(U) Data products of the first type (Appendix H, Figs. II-295 — II-297) are termed 3D plots. These are 3-dimensional representations of omnidirectional ASF levels (dB//μPa/Hz$^{1/2}$) as a function of time and frequency. Each trace denotes the average over a 10 min time interval, and has had no smoothing. These displays serve as a roadmap of the data since they reveal signatures, tones, artifacts, and broadband trends.

(U) Data products of the second type (Appendix I, Figs. II-298 — II-327), are termed timeseries plots, and reveal the time dependence of the ASF measured in selected 1/10-octave bands. The first three figures contain the omnidirectional ASF levels (dB//μPa/Hz$^{1/2}$) at each site. The remaining figures contain the noise gains (dB), where noise gain is the ratio of the ASF level of this sensor over that of the omnidirectional sensor.

(U) Data products of the third type (Appendix J, Figs. II-328 — II-357), are termed percentile distributions, and reveal the distribution of the ASF measurements in contiguous 1/10-octave bands. The first three figures contain the distributions of the omnidirectional ASF levels (dB//μPa/Hz$^{1/2}$)

(U) at each site. The remaining figures contain the noise gain (dB) distributions for each beam of the directional sensors. These displays denote the ASF distribution only for the shipping, environmental, and sea surface conditions encountered during the 17 November field event, and do not apply to other conditions, such as lower sea states.

(U) Both the timeseries plots and percentile distributions were derived from ASF measurements summed over 1/10-octave bands. These summations increase the number of equivalent degrees of freedom of the measurement, and thus decrease its observed variance. The high frequency bands are wider than the low frequency bands and therefore will appear to be more stable. This increased stability with frequency might not occur when the ASF is measured with bands of uniform width, and the ASF distributions will have a larger variance when measured with individual FFT cells.

(C) Data products of the last type (Appendix K, Figs. II-358 — II-372), are termed clutter timeseries plots. These are plots of the number of detected cells, the number of lines formed, and the number of lines linked, for each ALI interval as a function of time. The frequency range has been divided into four octaves, with separate curves for each.

Octave (Hz)	Number of Cells
40 to 80	260
80 to 160	520
160 to 320	1040
320 to 600	1830

Plots have been included for each site and each sensor. The detection, line formation, and line tracking algorithms are described in Volume I.

(C) The clutter timeseries plots are intended to portray the shore link and processor capacity required for operation in the absence of targets. To provide accurate clutter measurements it is necessary to first eliminate the loading incurred due to the presence of the exercise vessels

(C) and projectors. For example, a close inspection of the summary detection plots will reveal that, during phase II, the CFAV KAPUSKACING projector was generating at least eight lines in addition to the three scheduled lines. Such lines would have dominated the clutter counts had they not been removed. Table II-9 lists those lines which have been deleted from the clutter measurements along with their probable sources.

(C) TABLE II-9

LINES DELETED FROM CLUTTER MEASUREMENTS (U)

40 to 80 Hz OCTAVE

42 Hz	Recording System Artifact (Differenced Channels Only)
55 Hz	Scheduled QUEST Projector Line
64 Hz	Scheduled KAPUSKACING Projector Line
70 Hz	Scheduled CHAIN Projector Line

80 to 160 Hz OCTAVE

125 Hz	Recording System Artifact
128 Hz	KAPUSKACING Projector Harmonic (2×64)
132 Hz	KAPUSKACING Projector Artifact (260-2×64)
155 Hz	Scheduled QUEST Projector Line
160 Hz	Scheduled KAPUSKACING Projector Line

160 to 320 Hz OCTAVE

170 Hz	Scheduled CHAIN Projector Line
192 Hz	KAPUSKACING Projector Harmonic (3×64)
250 Hz	Recording System Artifact
260 Hz	Scheduled KAPUSKACING Projector Line
288 Hz	KAPUSKACING Projector Harmonic (160+2×64)
305 Hz	Scheduled QUEST Projector Line
320 Hz	KAPUSKACING Projector Harmonic (5×64 or 2×160)

320 to 600 Hz OCTAVE

324 Hz	KAPUSKACING Projector Artifact (64+260)
335 Hz	Scheduled CHAIN Projector Line
356 Hz	CHAIN Projector Artifact (Prior to Voltage Adjustment at 1645Z)
384 Hz	KAPUSKACING Projector Artifact (64+2×160)
388 Hz	KAPUSKACING Projector Artifact (2×64+260)
525 Hz	Recording System Artifact (Site A1 Only)
600 Hz	Recording System Artifact (Site A1 Only)

IV. DISCUSSION

(U) The analysis of the data presented in this volume is contained in Volume IV. However, some of the limitations of these data should be pointed out so that those without access to Volume IV will not draw unwarranted conclusions.

(C) The curves in this volume denote the estimated averages of complex stochastic processes. The estimates are displayed as a function of a single variable, such as range, even though they may be highly dependent on another variable, such as the time dependence of S/N or array gain. The signal, noise, and array gain displays allow the time and range dependencies to be somewhat separated, whereas the percentage detection and S/N versus range displays do not. Even though the propagation loss and signal, noise, and array gain displays separate the time dependence of the ASF from the range dependence of the signal field, they do not isolate the time dependence of the signal field. However, since these curves are in good agreement for all three data intervals at Site A3, the day-to-day time dependence of the signal field, as observed with a 5 min ALI, is probably small.

(U) Since the curves are estimated averages of complex stochastic processes (assumed to be, in a wide sense, stationary), the variance of these estimates is highly dependent on the number of sample measurements. For most of the cw curves, and particularly for the lower level signals, the number of samples is small (<10). The variance of each curve has been decreased by a smoothing window which effectively tripled the number of samples in each bin, but also decreased the resolution of the curve. However, the statistical fluctuations of these estimates do not entirely account for the apparently anomalous results from the low level signals. As is discussed in Volume IV, these results are sometimes severely biased. This is because a fixed threshold

(U) detection process was used to extract signal measurements, and thus only that portion of the signal SPL distribution lying above the threshold was used to estimate its average. For the higher level sources, more of the SPL distribution was detected and used to estimate its average. As was discussed earlier, a simple technique was used to partially debias the S/N results.

(C) The results which appear most anomalous, i.e., those at 55 Hz, were caused by the complete SPL distribution being undetectable. Detections at 55 Hz occurred only when the ASF level in the signal cell exceeded the estimated ASF mean level sufficiently that it forced the signal plus noise level above the detection threshold; this results in erroneous cw measurements (Ref. 3). This phenomenon is discussed more fully in Volume IV, pp. 62-65.

REFERENCES

1. Steven L. Watkins, "Moored Surveillance System Field Validation Test cw Projector Reconstruction," Applied Research Laboratories Technical Report No. 76-16 (ARL-TR-76-16), Applied Research Laboratories, The University of Texas at Austin, October 1976.

2. Steven L. Watkins, "Moored Surveillance System Field Validation Test Ambient Sound Field and cw Propagation Measurements for Near-Bottom Sensors at Site A3" (U), Applied Research Laboratories Technical Report No. 76-52 (ARL-TR-76-52), Applied Research Laboratories, The University of Texas at Austin, December 1976. CONFIDENTIAL

3. Jack A. Shooter and Steven L. Watkins, "Estimation of Background Ambient Noise Levels from the Spectral Analysis of Time Series with Application to cw Propagation Loss Measurements," J. Acoust. Soc. Am. 62, 84-90 (1977).

The reverse of this page is blank.)

APPENDIX A

SUMMARY DETECTION CURVES (U)

(FIGURES II-1 - II-15)

(The reverse of this page is blank.)

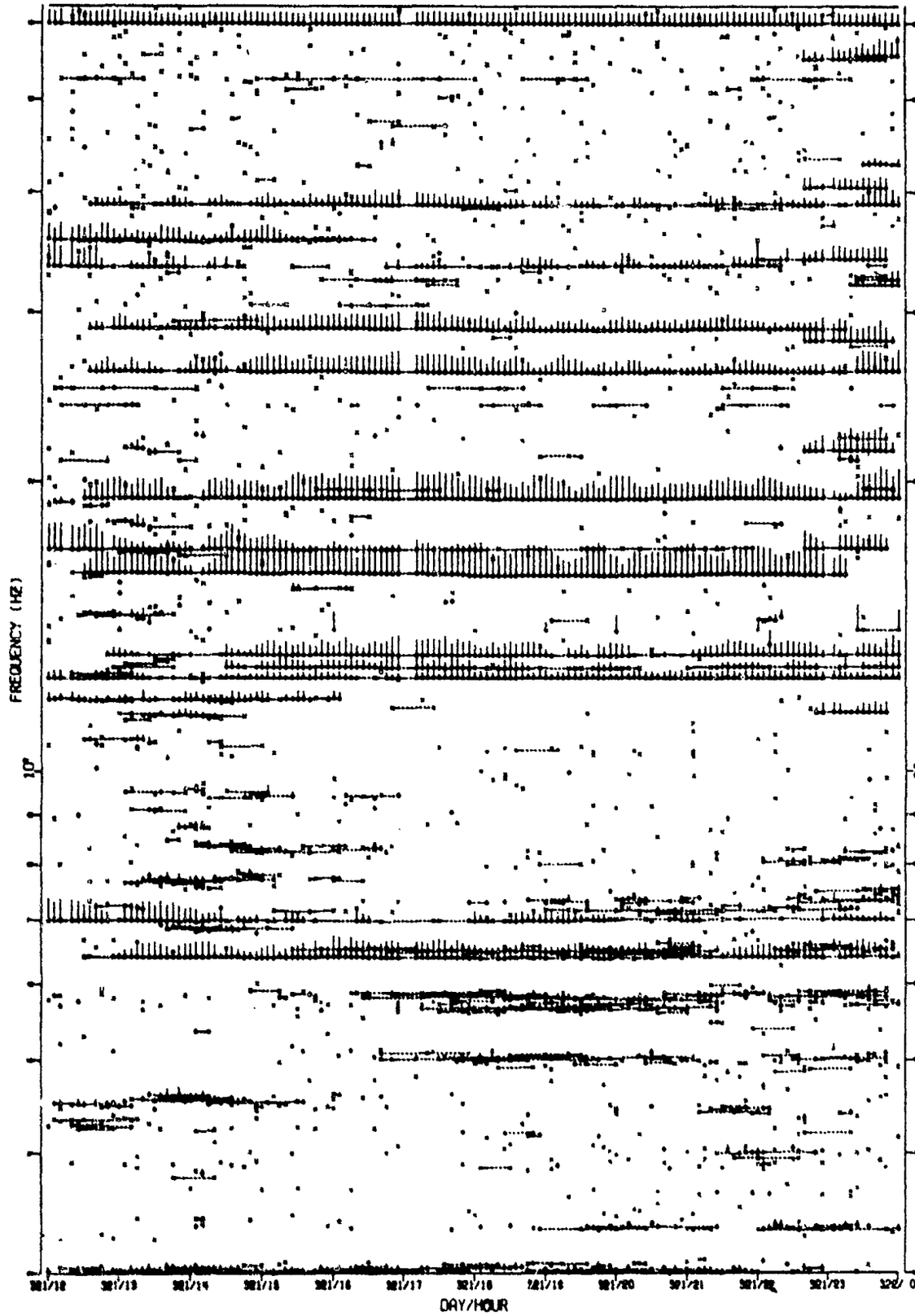

FIGURE II-1
KSS-FVT DETECTION OVERVIEW DURING THE 17 NOV FIELD EVENT AT SITE A1
OBTAINED VIA THE OMNIDIRECTIONAL SENSOR WITH STANDARD RESOLUTION (U)

AS-77-2928

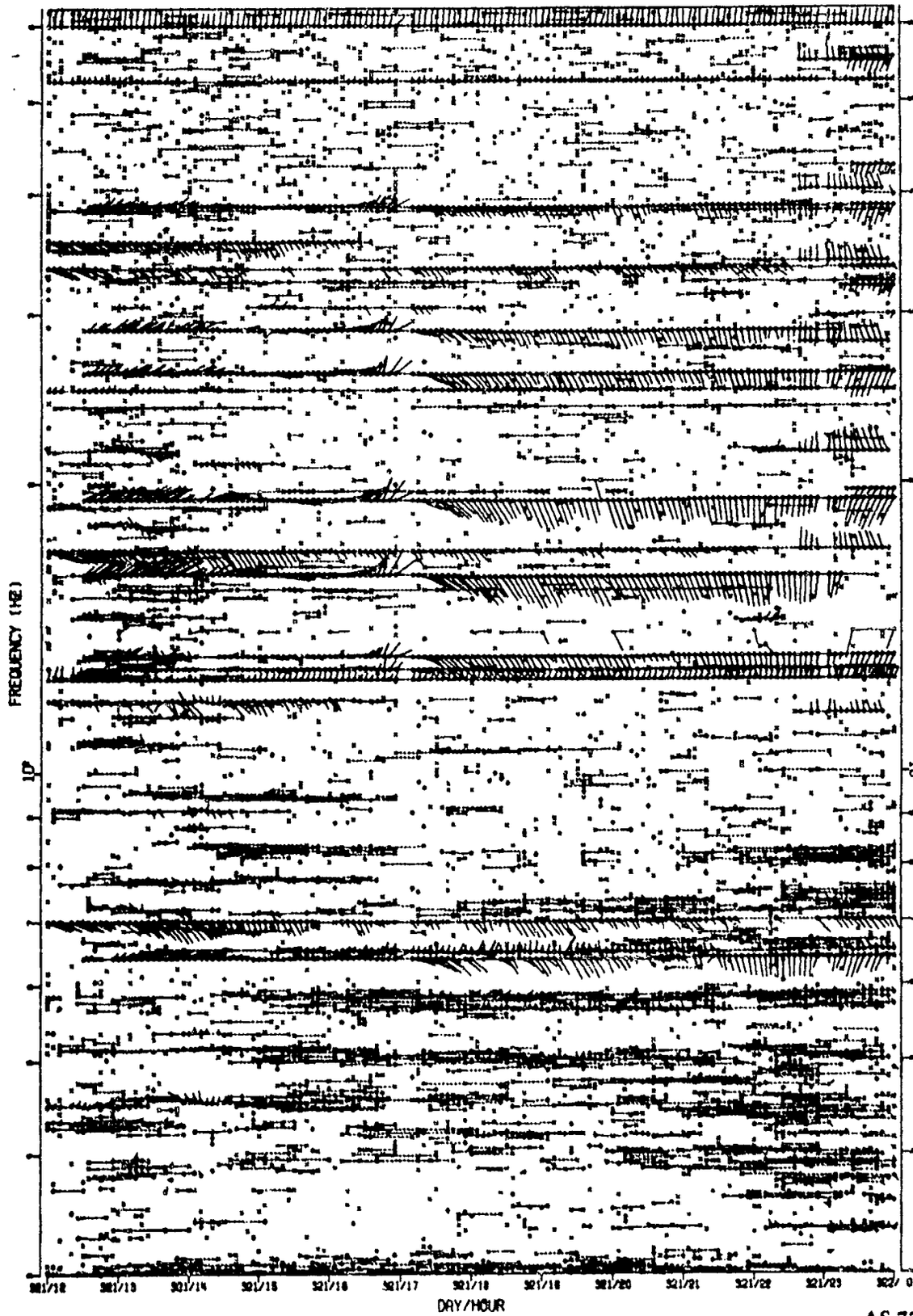

FIGURE II-2
NSS-FVT DETECTION OVERVIEW DURING THE 17 NOV FIELD EVENT AT SITE A1
OBTAINED VIA THE SINGLE CARDIOIDS SENSOR WITH STANDARD RESOLUTION (U)

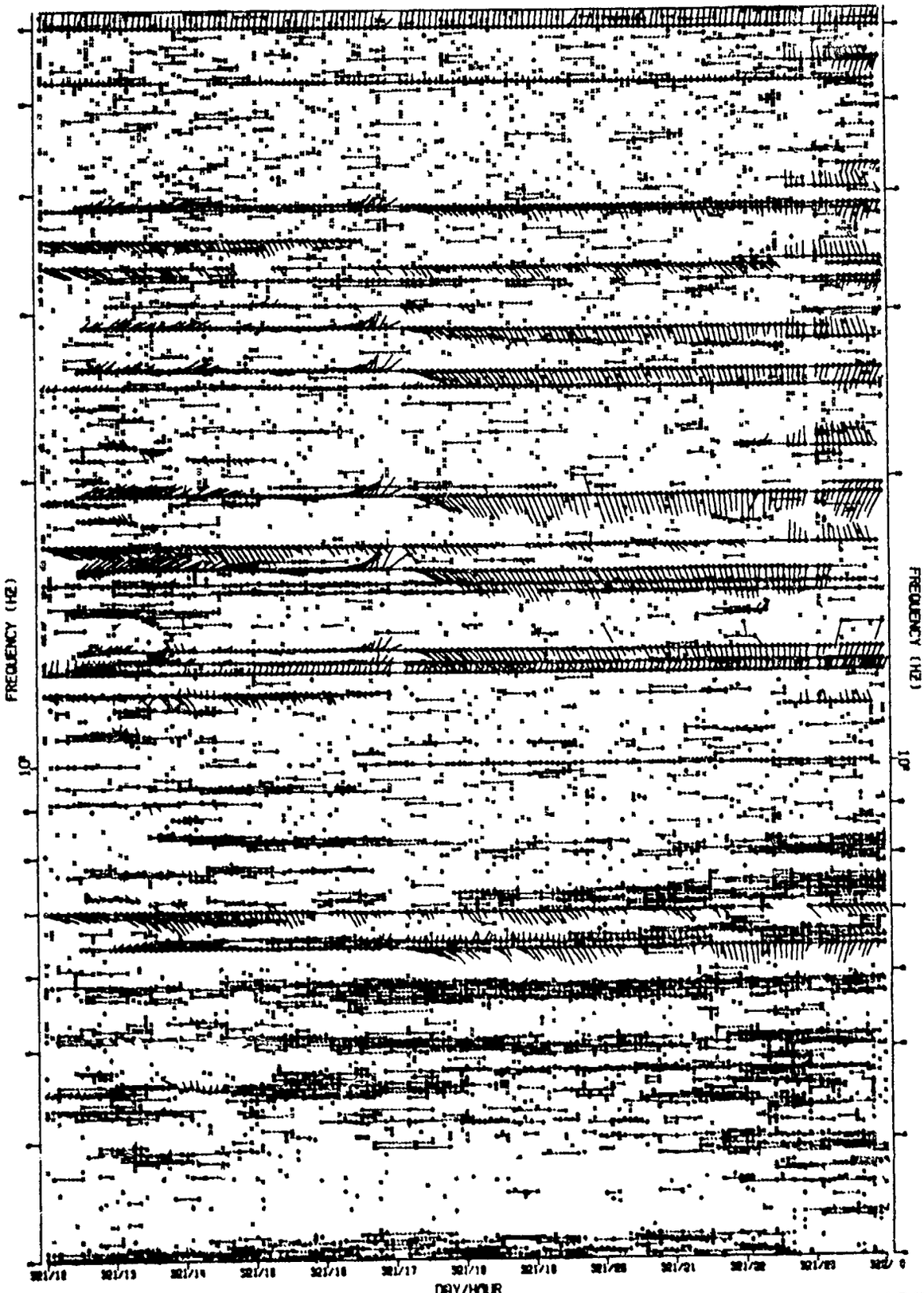

AS-77-2930

FIGURE II-9
MSS-FVT DETECTION OVERVIEW DURING THE 17 NOV FIELD EVENT AT SITE A1
OBTAINED VIA THE MAX GRIN LIMACONS SENSOR WITH STANDARD RESOLUTION (U)

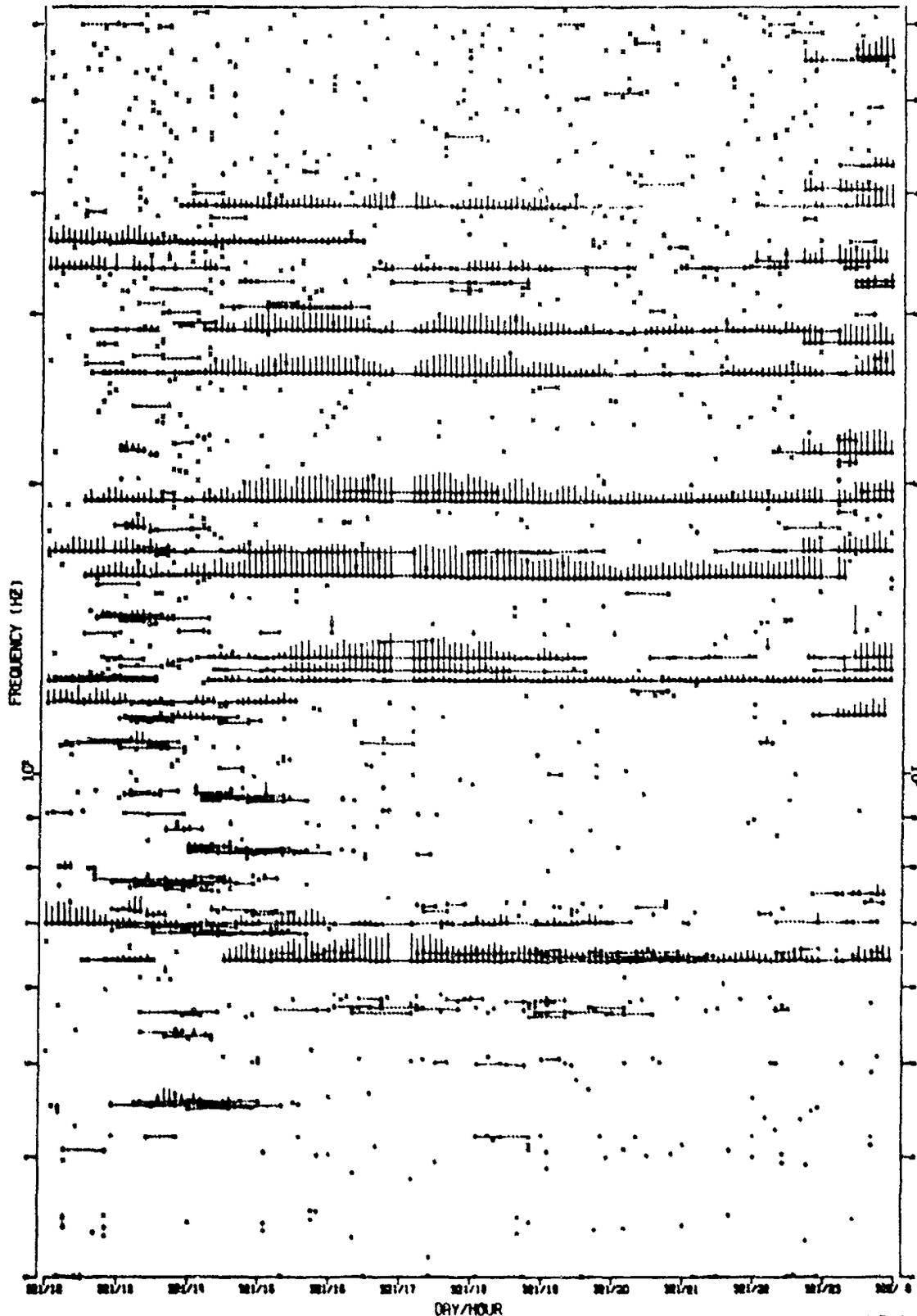

AS-77-2931

FIGURE II-4
MSS-FVT DETECTION OVERVIEW DURING THE 17 NOV FIELD EVENT AT SITE RI
OBTAINED VIA THE VERTICAL DIPOLE SENSOR WITH STANDARD RESOLUTION (U)

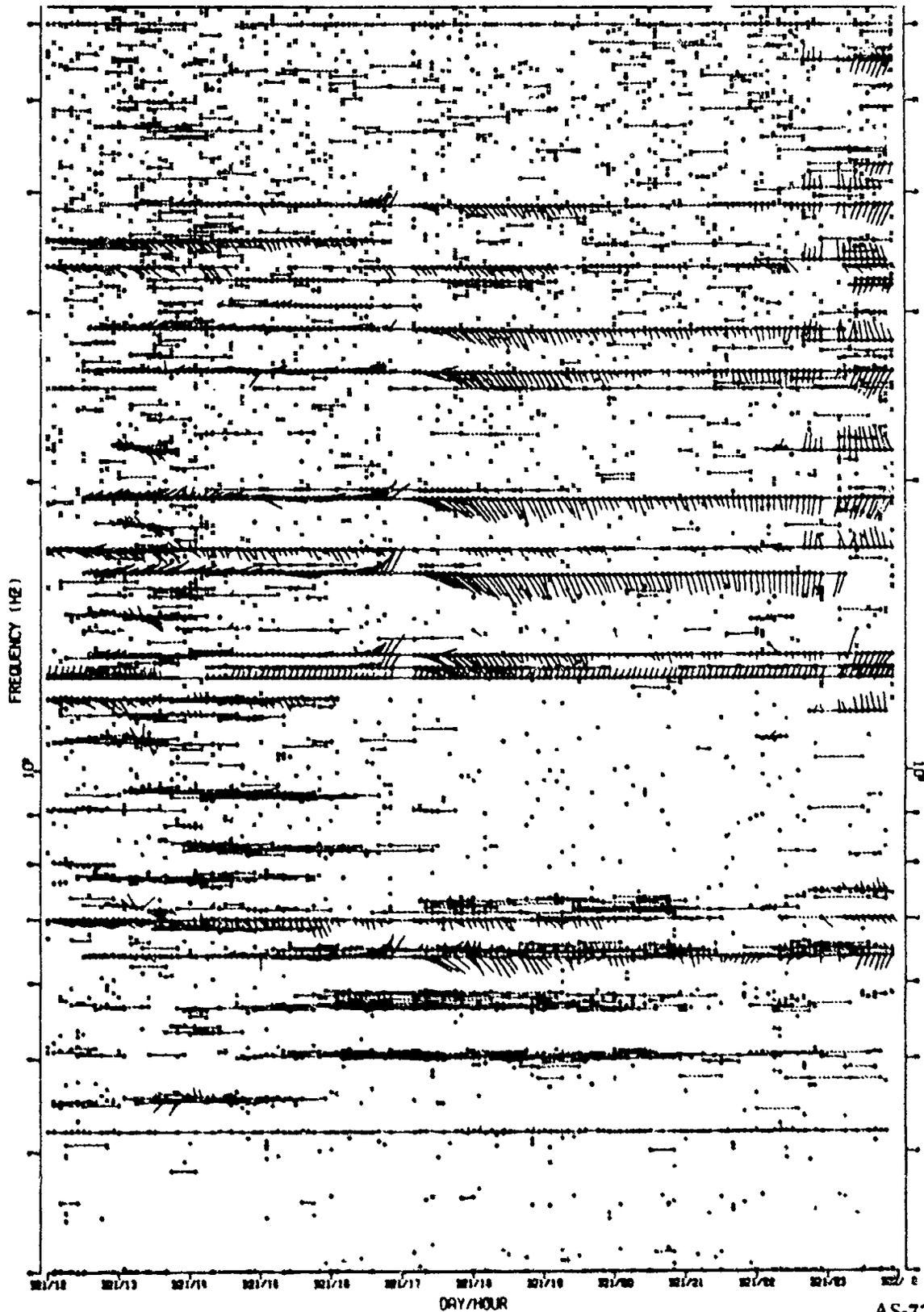

AS-77-2932

FIGURE II-5
KSS-FVT DETECTION OVERVIEW DURING THE 17 NOV FIELD EVENT AT SITE A1
OBTAINED VIA THE DIFFERENCED CARDIOIDS SENSOR WITH STANDARD RESOLUTION (U)

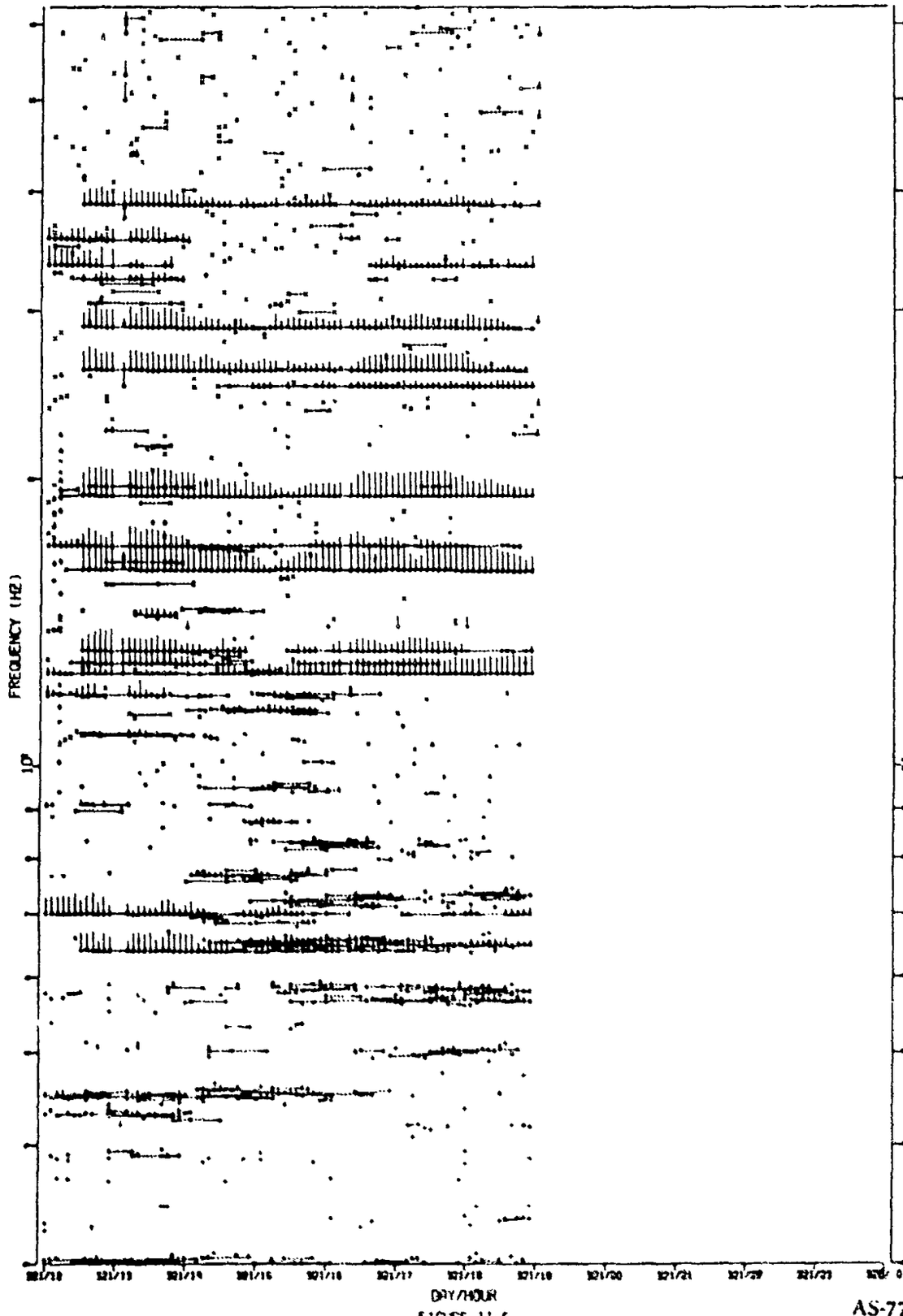

AS-77-2933

FIGURE II-6
HSS-FVT DETECTION OVERVIEW DURING THE 17 NOV FIELD EVENT AT SITE R2
OBTAINED VIA THE OMNIDIRECTIONAL SENSOR WITH STANDARD RESOLUTION (U)

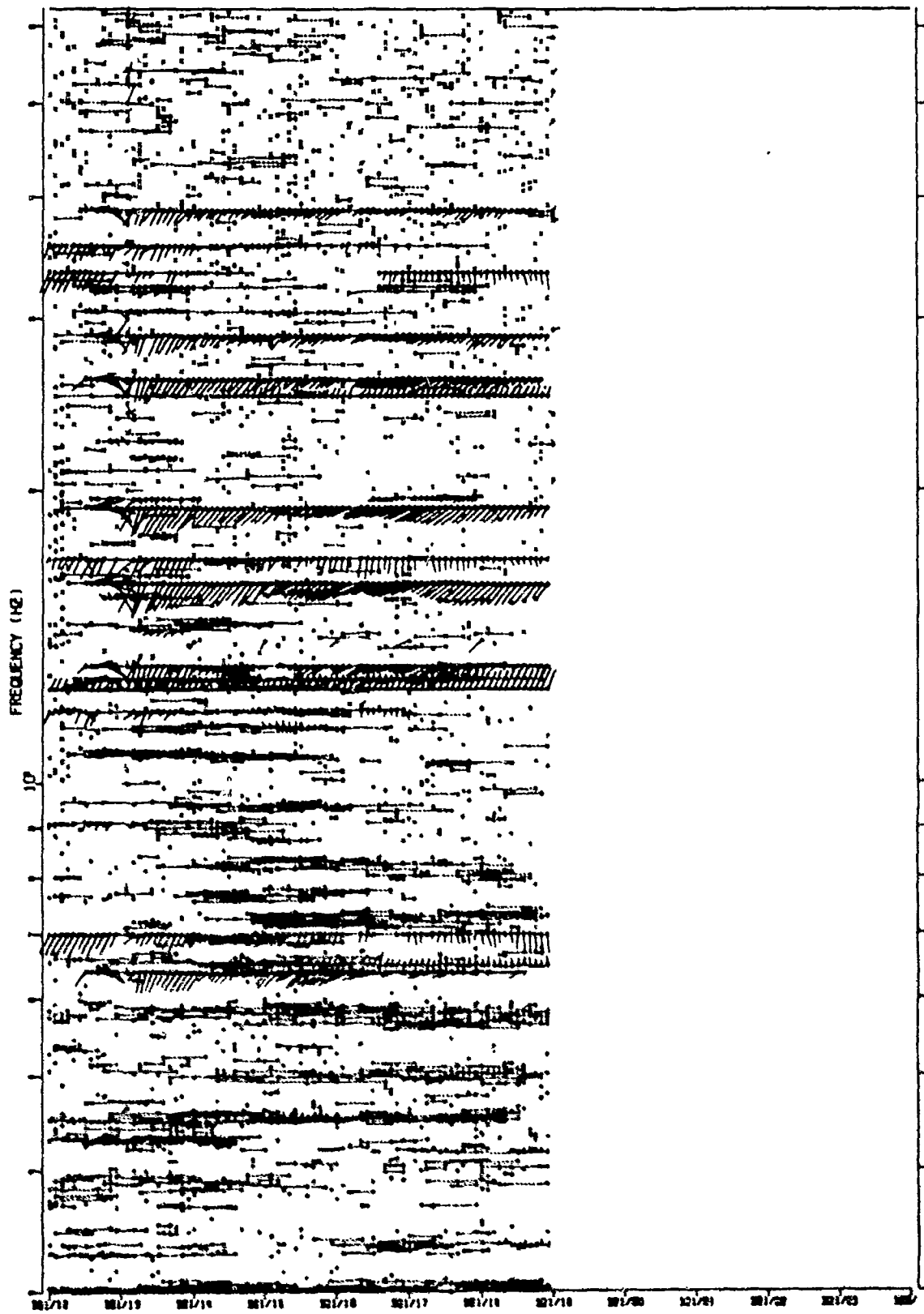

AS-77-2934

FIGURE II-7
KSS-FVT DETECTION OVERVIEW DURING THE 17 NOV FIELD EVENT AT SITE A2
OBTAINED VIA THE SINGLE COMPONENT SENSOR WITH STANDARD RESOLUTION (U)

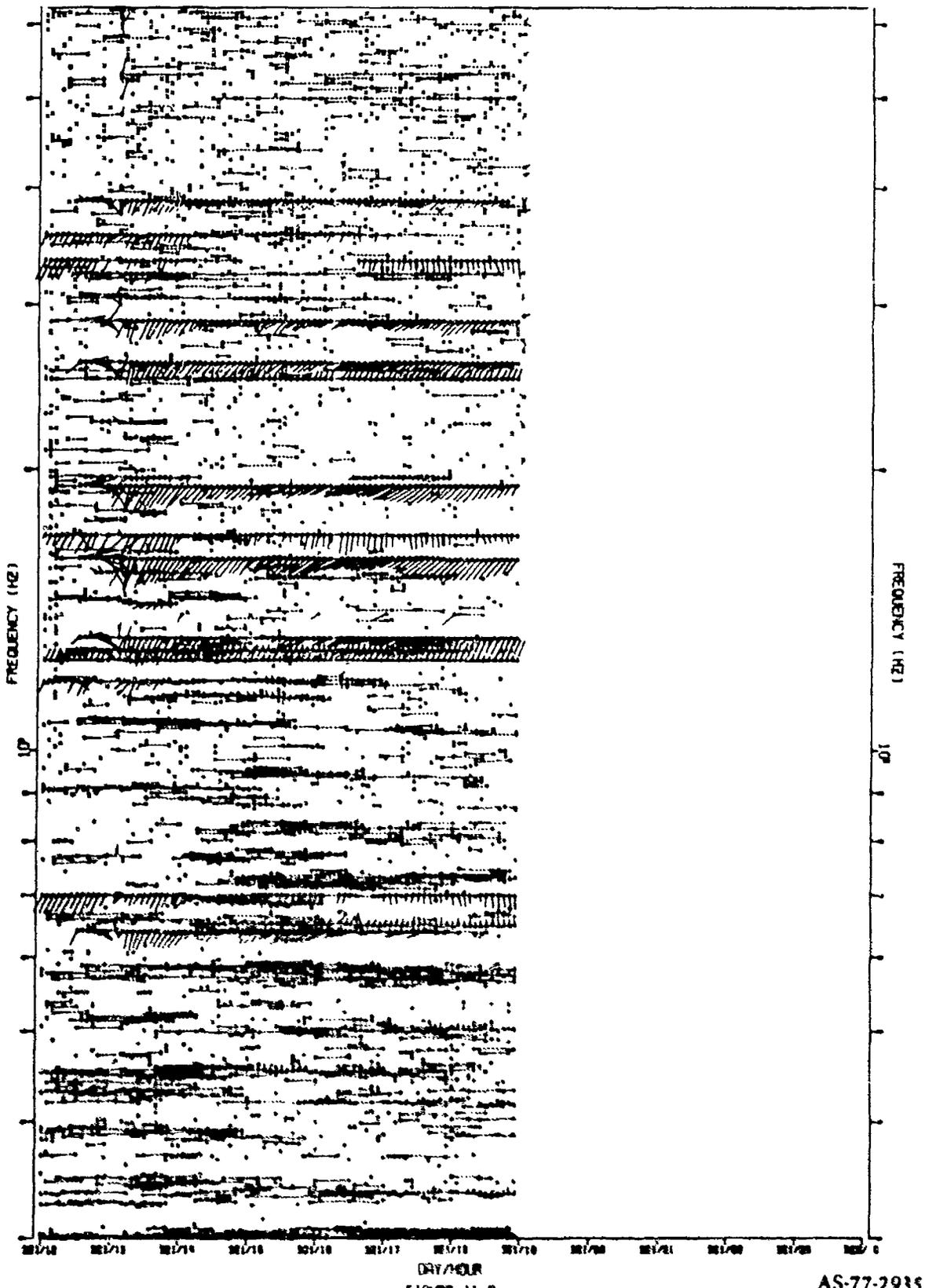

AS-77-2935

FIGURE II-8
MSS-FVT DETECTION OVERVIEW DURING THE 17 NOV FIELD EVENT AT SITE A2
OBTAINED VIA THE HAY PAIN LINEONS SENSOR WITH STANDARD [illegible]

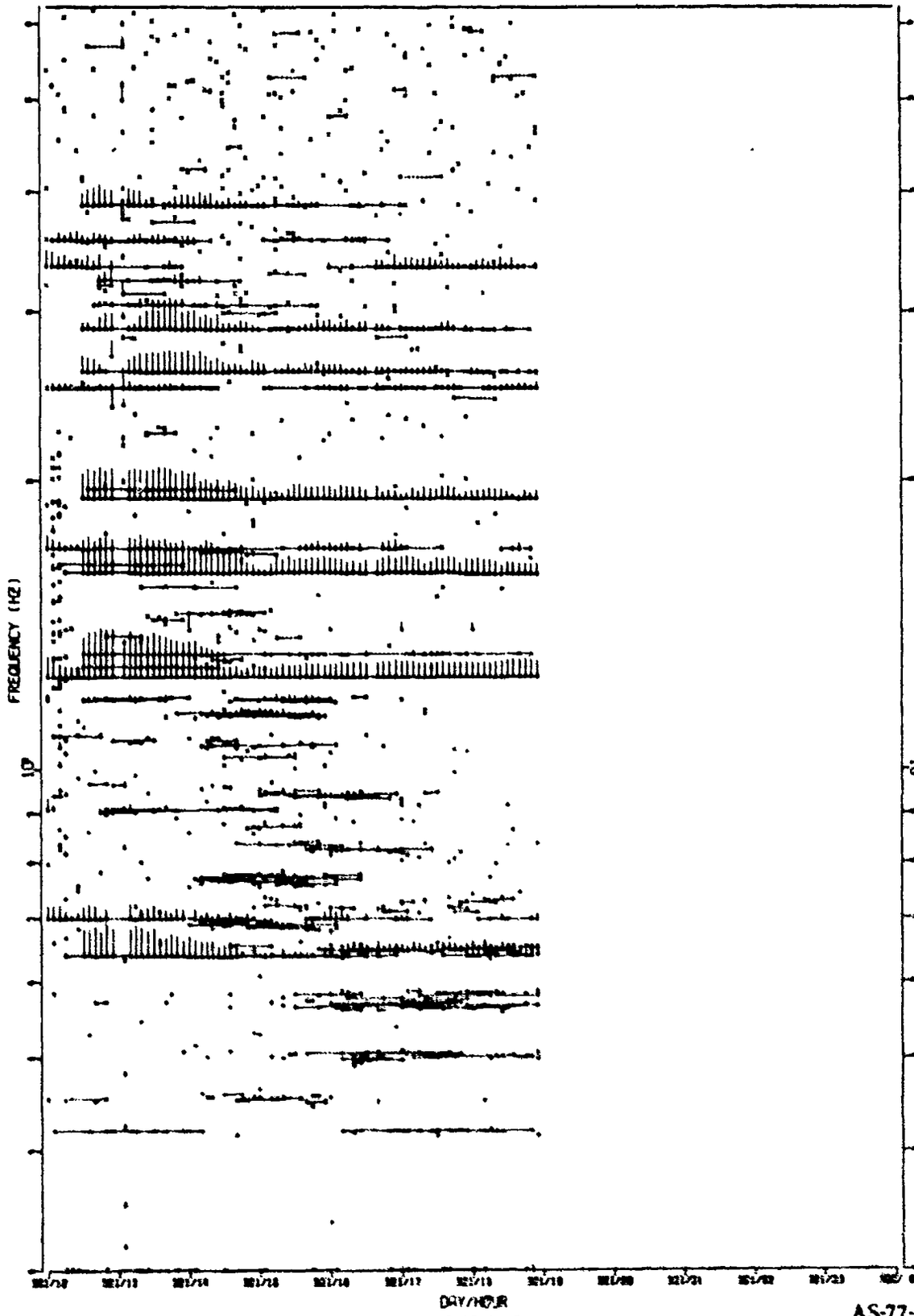

FIGURE II-9
MSS-FVT DETECTION OVERVIEW DURING THE 17 NOV FIELD EVENT AT SITE R2
OBTAINED VIA THE VERTICAL DIPOLE SENSOR WITH STANDARD RESOLUTION (U)

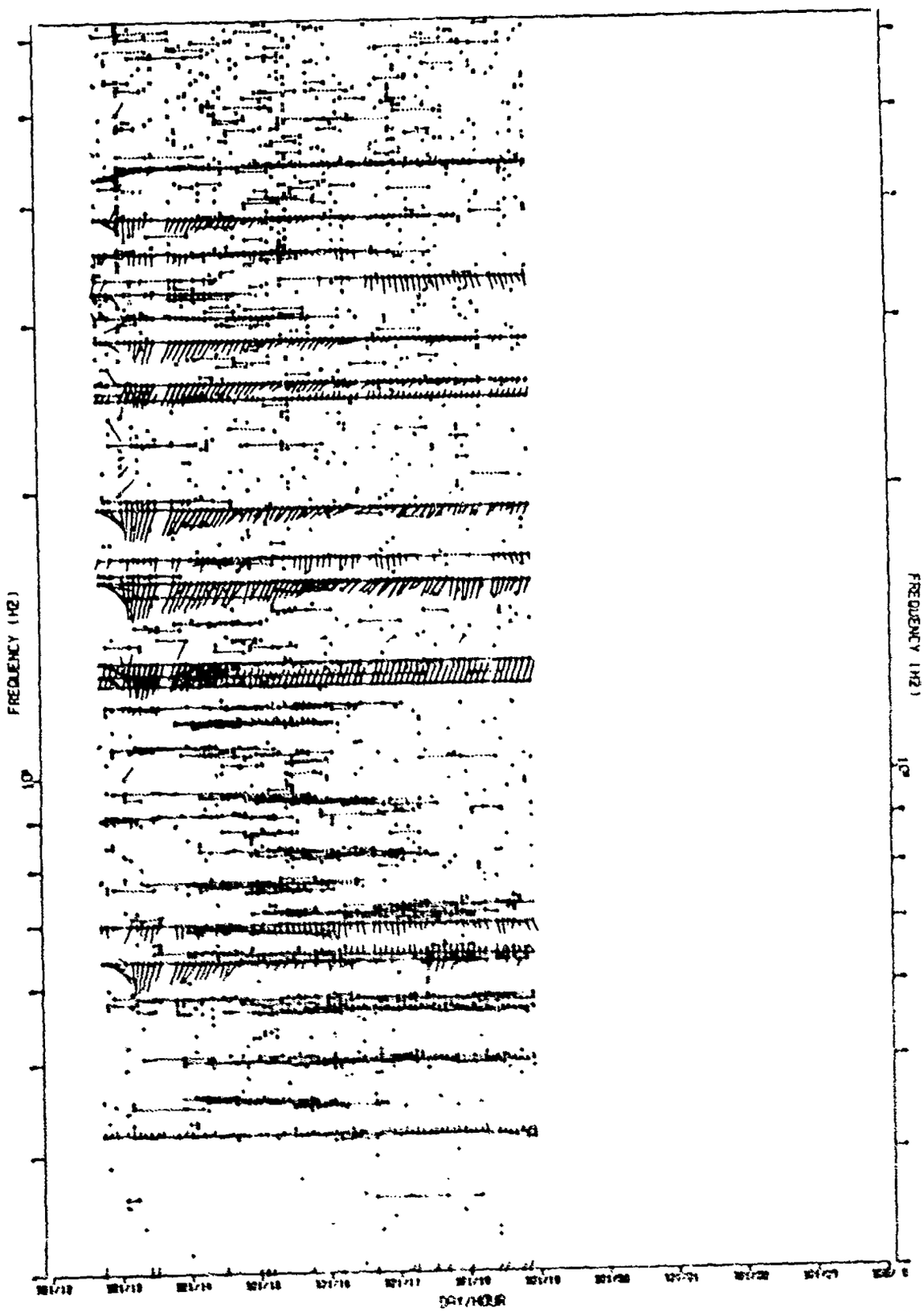

FIGURE 11-10
HSS-FVT DETECTION OVERVIEW DURING THE 17 NOV FIELD EVENT AT SITE 82
OBTAINED VIA THE DIFFERENCED CARDIOID SENSOR WITH STANDARD

AS-77-2937

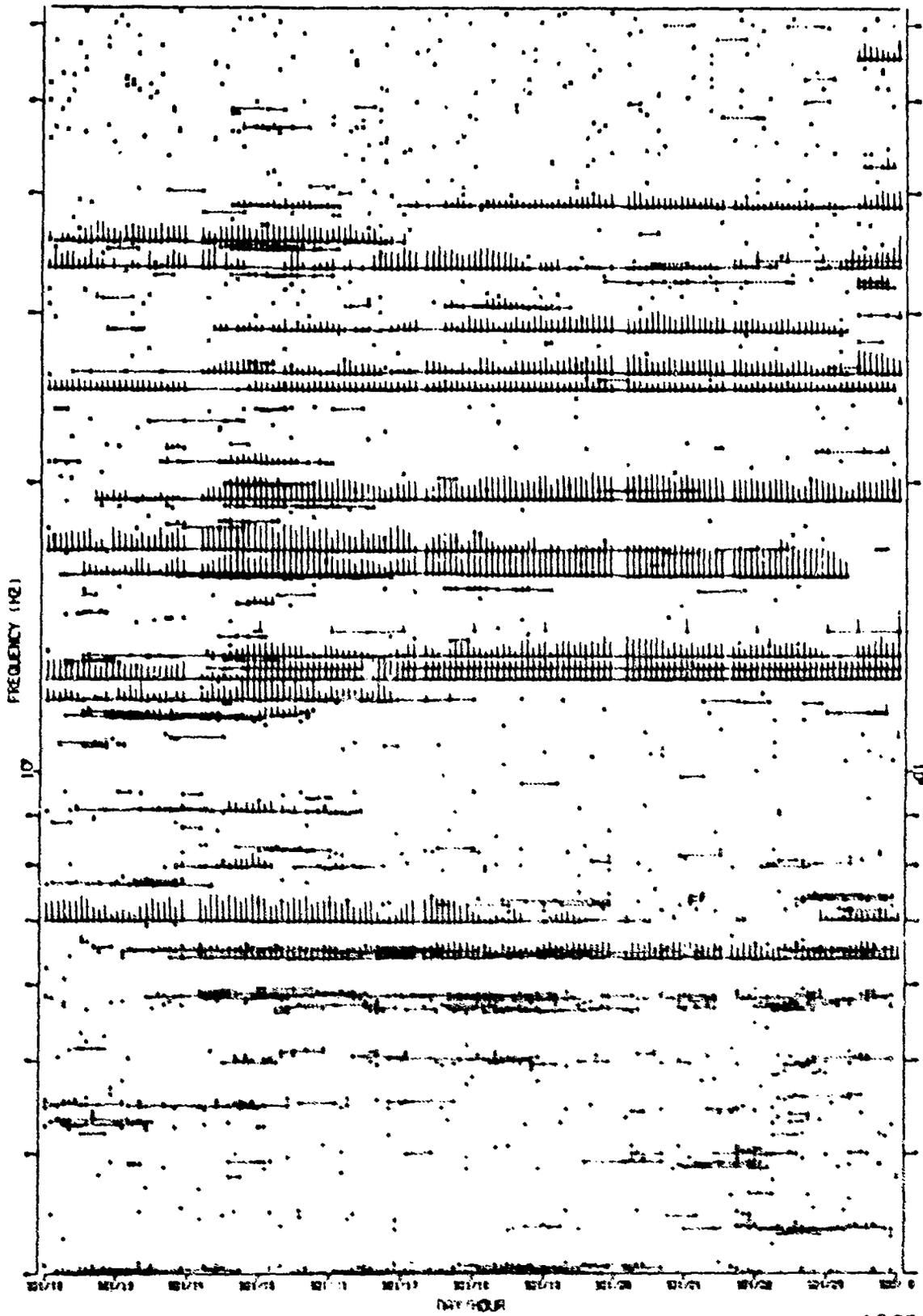

AS-77-2938

FIGURE II-11
HSS-FVI DETECTION OVERVIEW DURING THE 17 NOV FIELD EVENT AT SITE 03 OBTAINED VIA THE OMNIDIRECTIONAL SENSOR WITH STANDARD RESOLUTION (U)

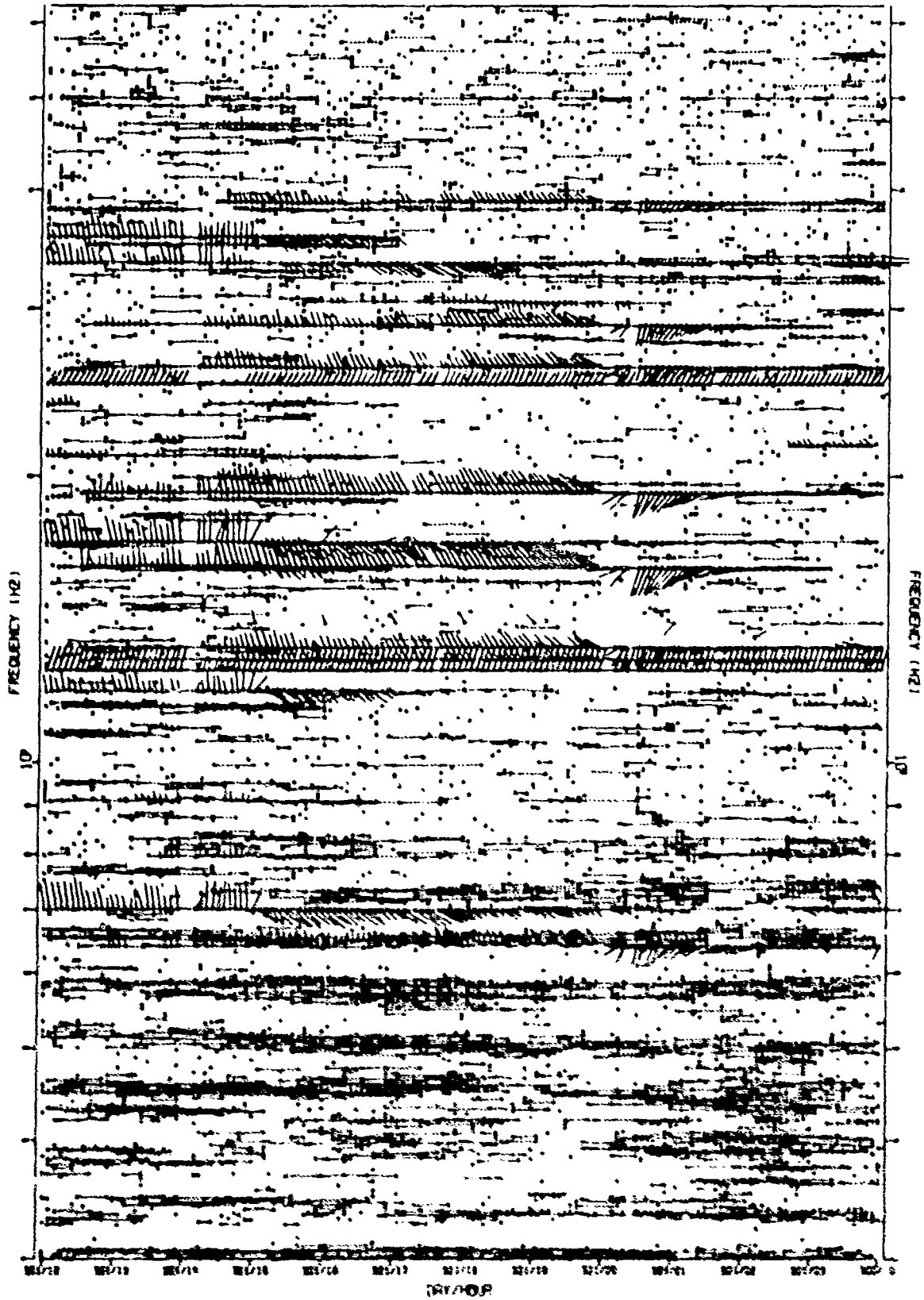

AS-77-2939

FIGURE 11-12
KSS-FVT DETECTION OVERVIEW DURING THE 17 NOV FIELD EVENT AT SITE R3
OBTAINED VIA THE SINGLE CORDICIDS SENSOR WITH STANDARD RESOLUTION (U)

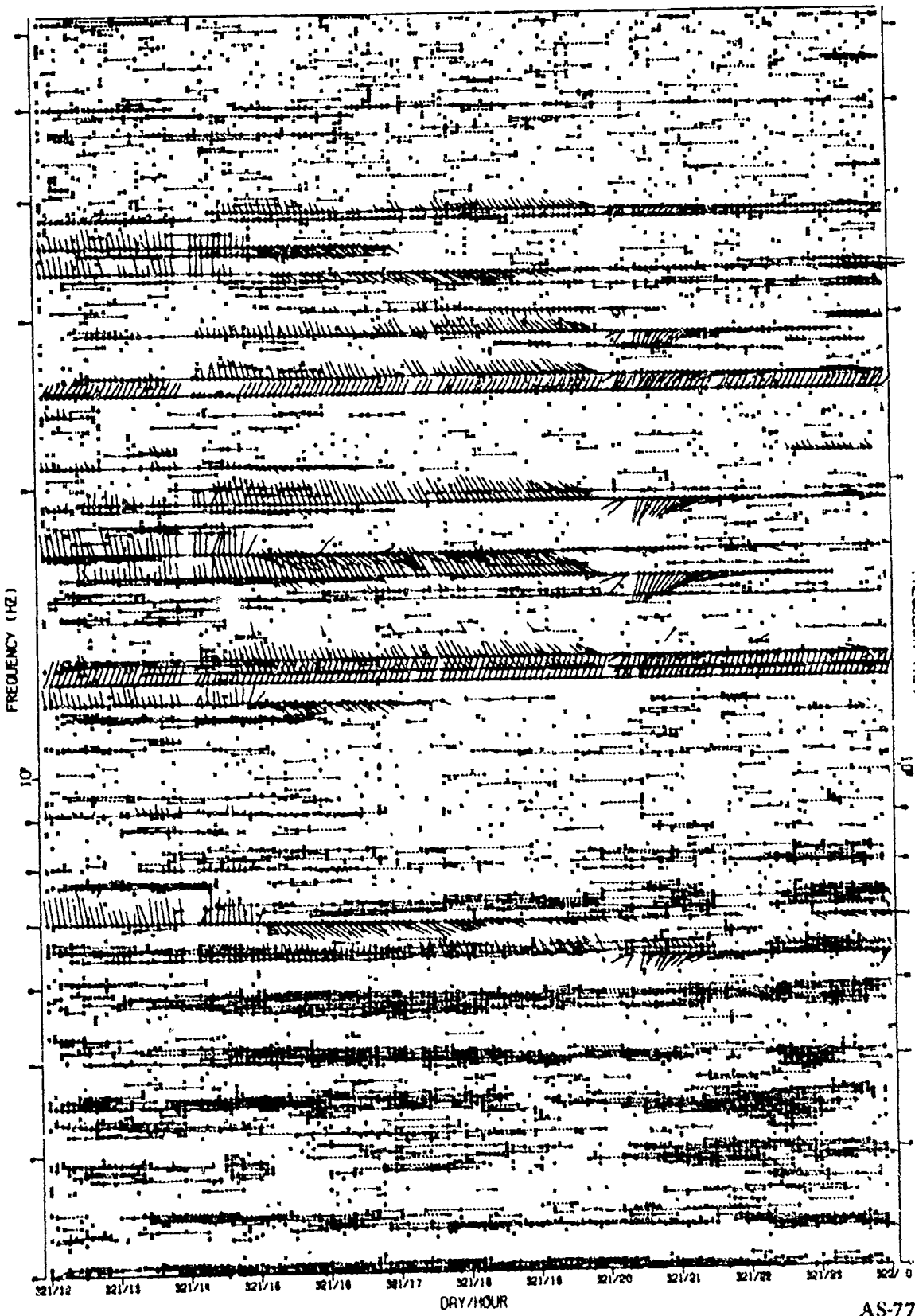

AS-77-2940

FIGURE II-13
NSS-FVT DETECTION OVERVIEW DURING THE 17 NOV FIELD EVENT AT SITE H3
OBTAINED VIA THE MAX GAIN LIMACONS SENSOR WITH STANDARD RESOLUTION (U)

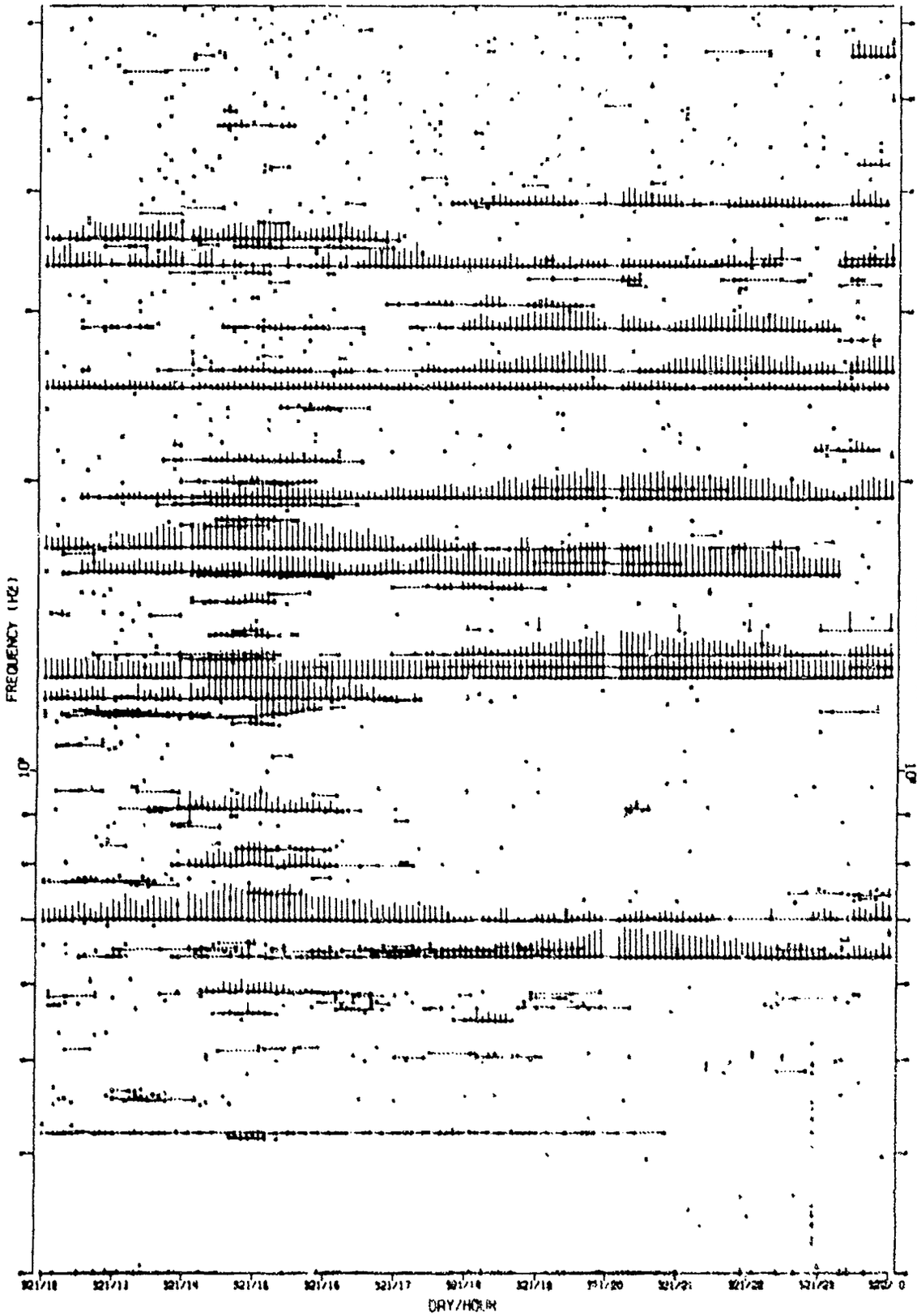

FIGURE II-14
MSS-FVT DETECTION OVERVIEW DURING THE 17 NOV FIELD EVENT AT SITE A3
OBTAINED VIA THE VERTICAL DIPOLE SENSOR WITH STANDARD RESOLUTION (U)

AS-77-2941

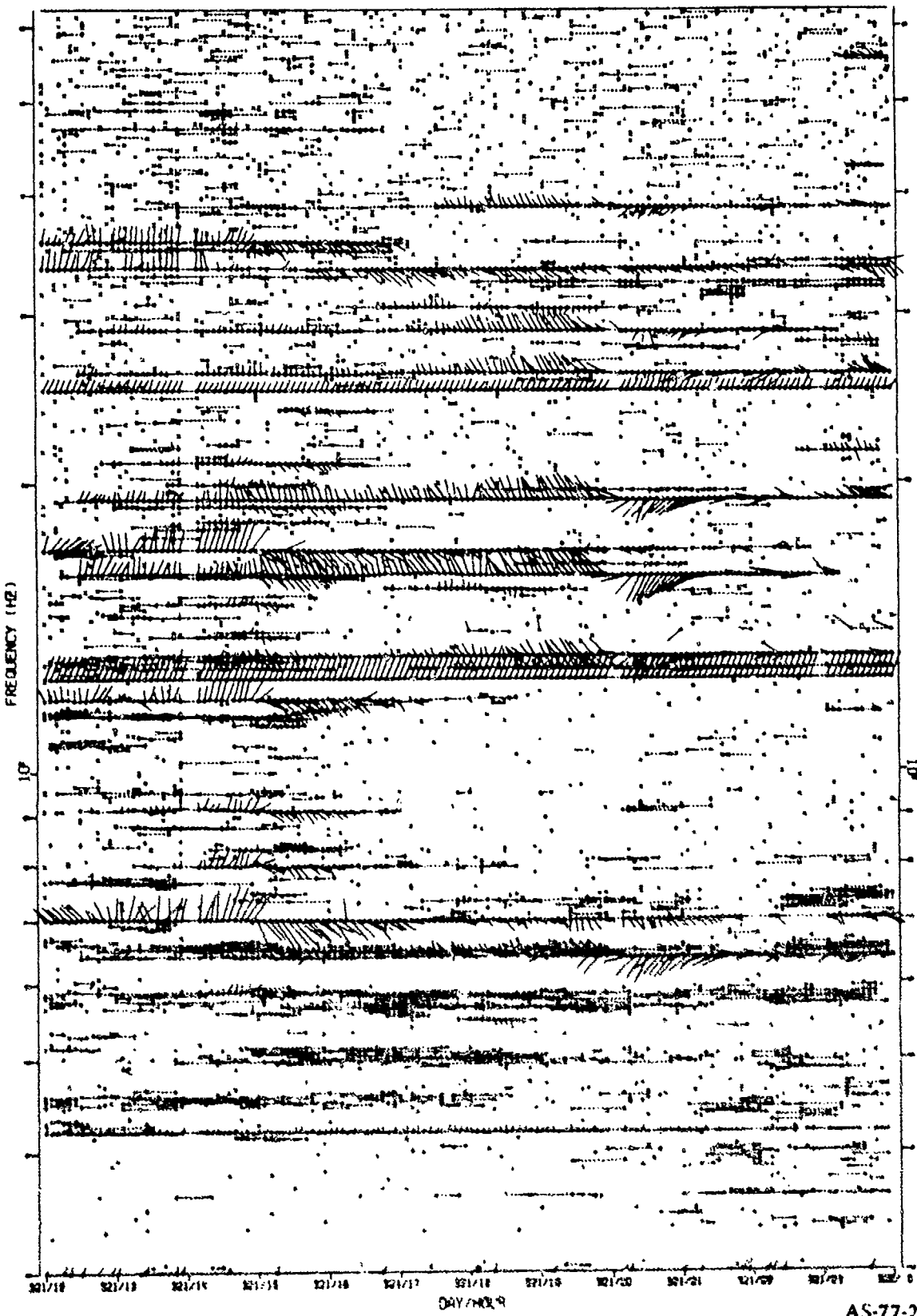

AS-77-2942

FIGURE 11-15
HSS-FVT DETECTION OVERVIEW DURING THE 17 NOV FIELD EVENT AT SITE 03
OBTAINED VIA THE DIFFERENCED CORIOLIS [illegible] RESOLUTION (U)

(The reverse of this page is blank.)

APPENDIX B

LINE HISTORY CURVES (U)

(FIGURES II-16 - II-142)

(The reverse of this page is blank.)

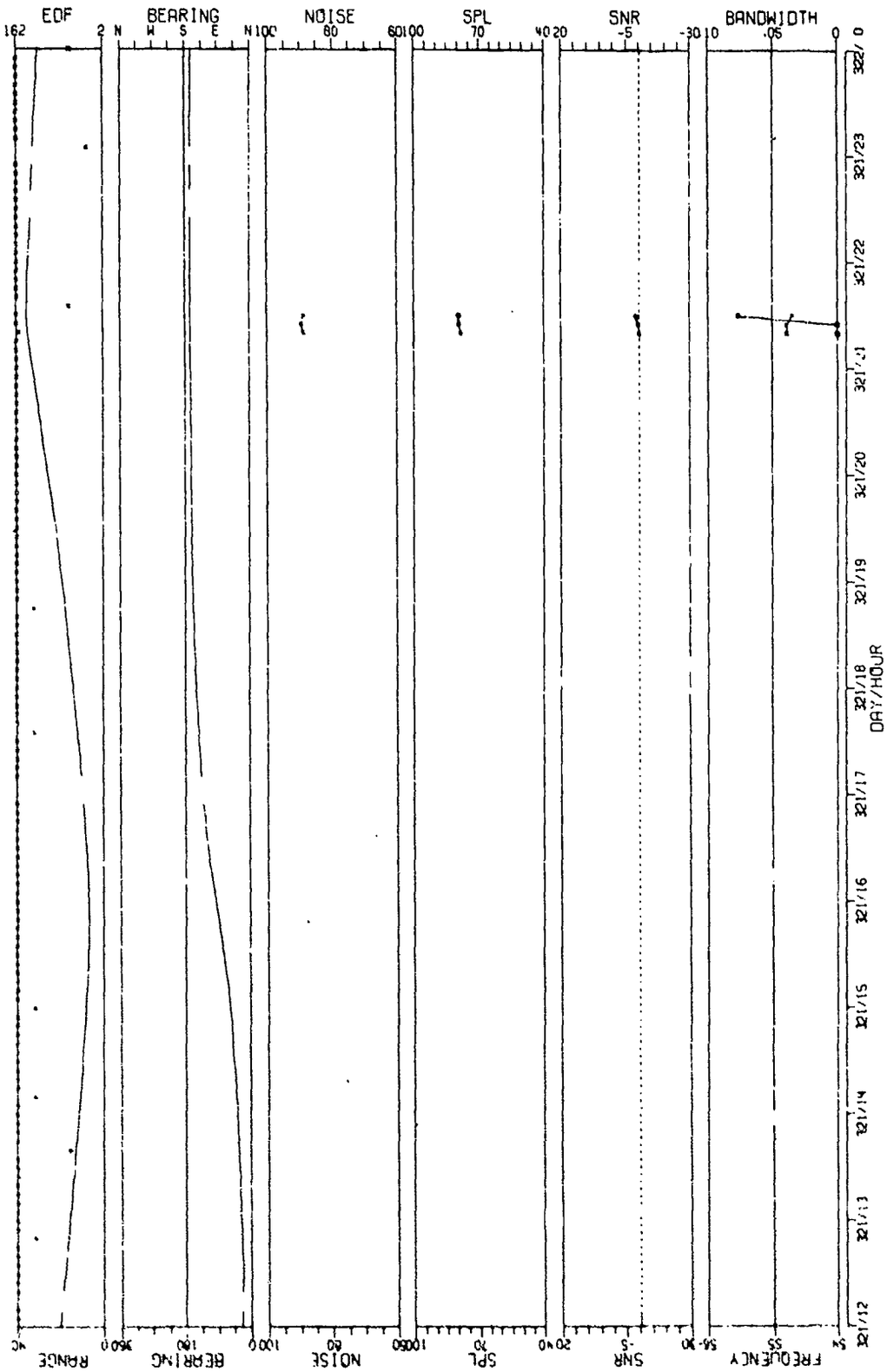

FIGURE II-16
MSS FVT 55HZ LINE HISTORY AS OBSERVED VIA THE OMNIDIRECTIONAL SENSOR
AT SITE A1 DURING THE 17 NOV FIELD EVENT WITH STANDARD RESOLUTION (U)

AS-77-2943

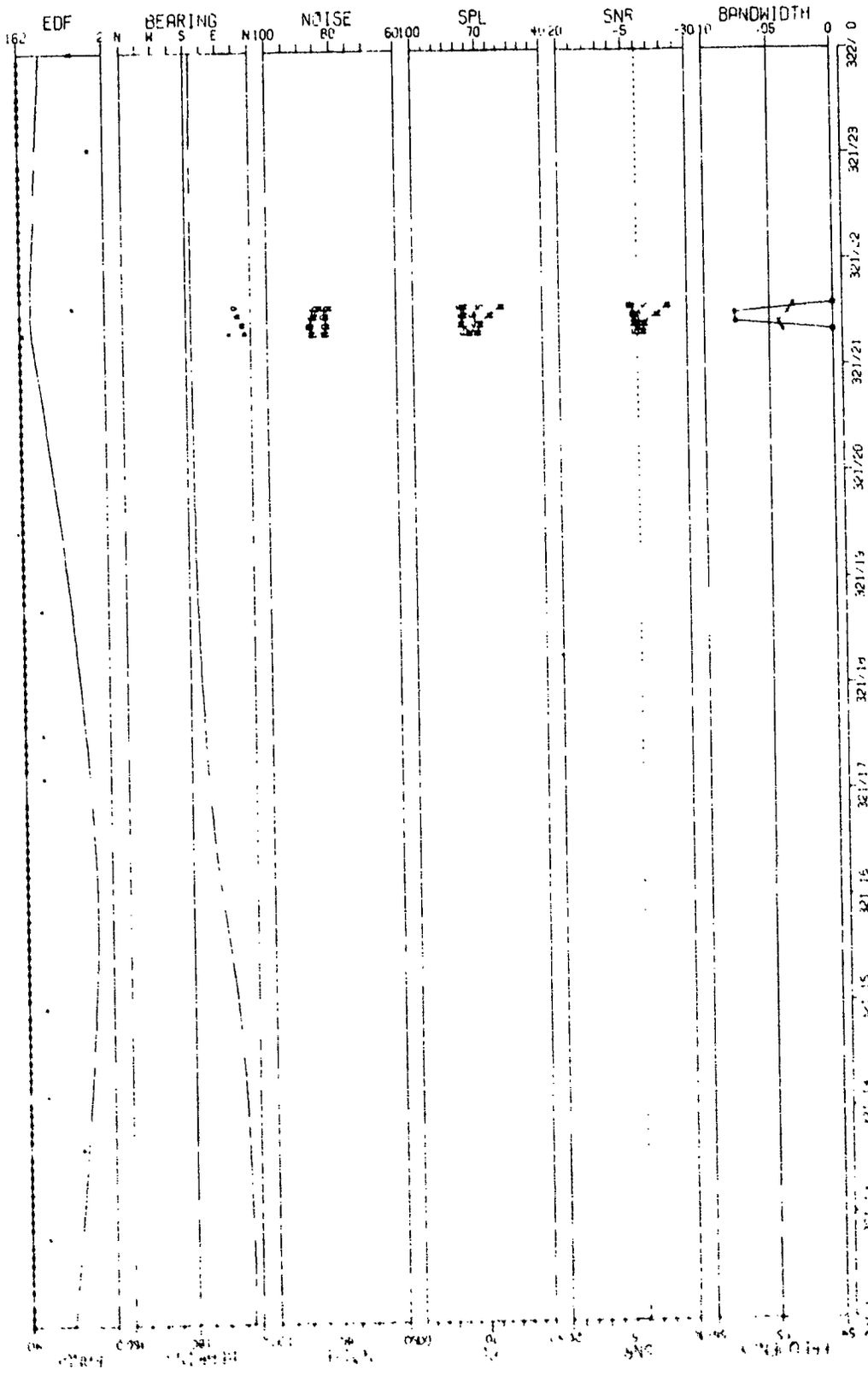

FIGURE LI-17
OBSERVED VIA THE SINGLE CARDIOIDS SENSOR
FIELD EVENT WITH STANDARD RESOLUTION LOI

AS-77-2944

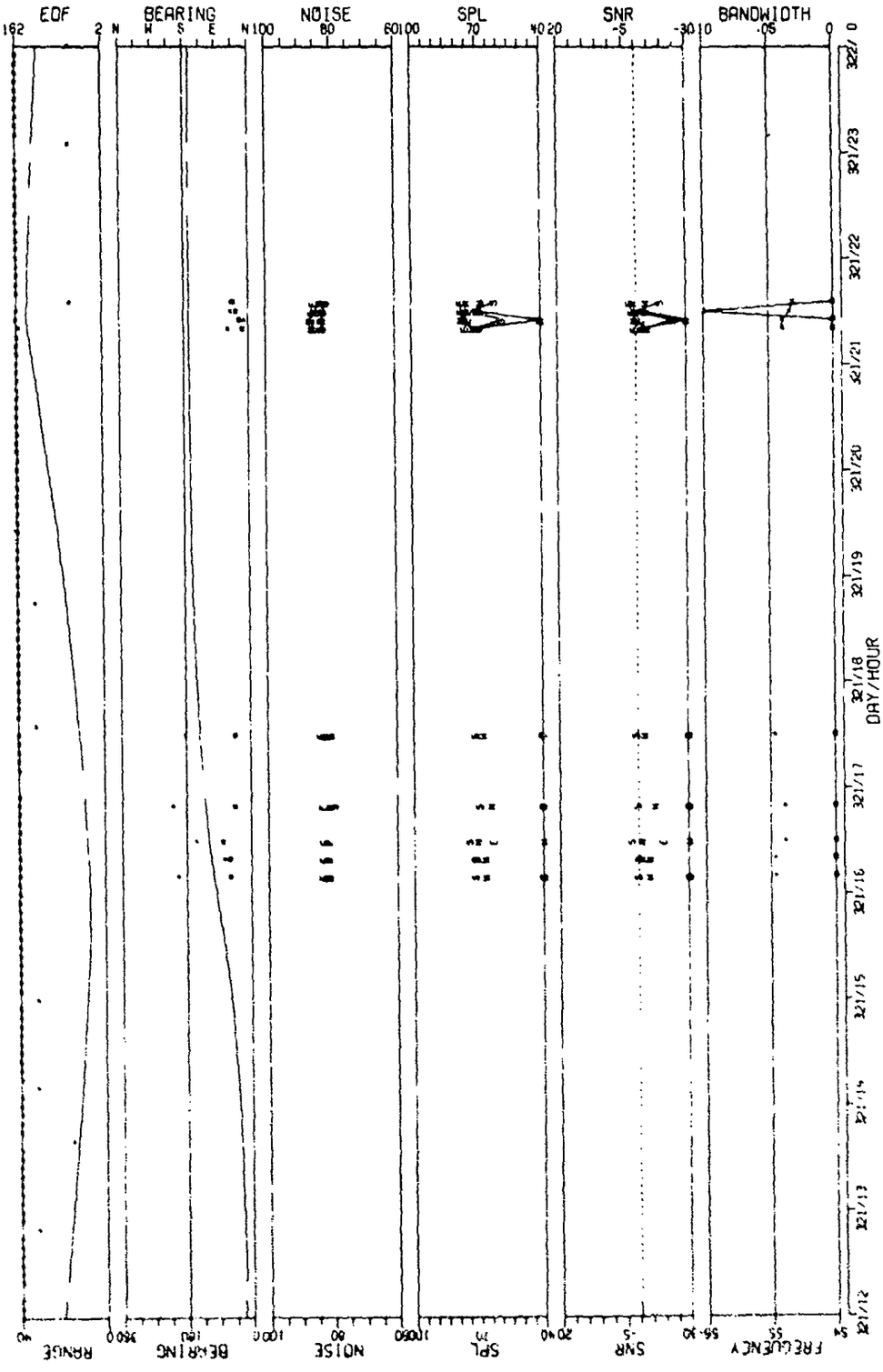

FIGURE 11-18
MSS-FV1 5512 LINE HISTORY AS OBSERVED VIA THE MAX GAIN LIMACONS SENSOR
AT SITE 61 DURING THE 17 NOV FIELD EVENT WITH STANDARD RESOLUTION IDI

AS-77-2945

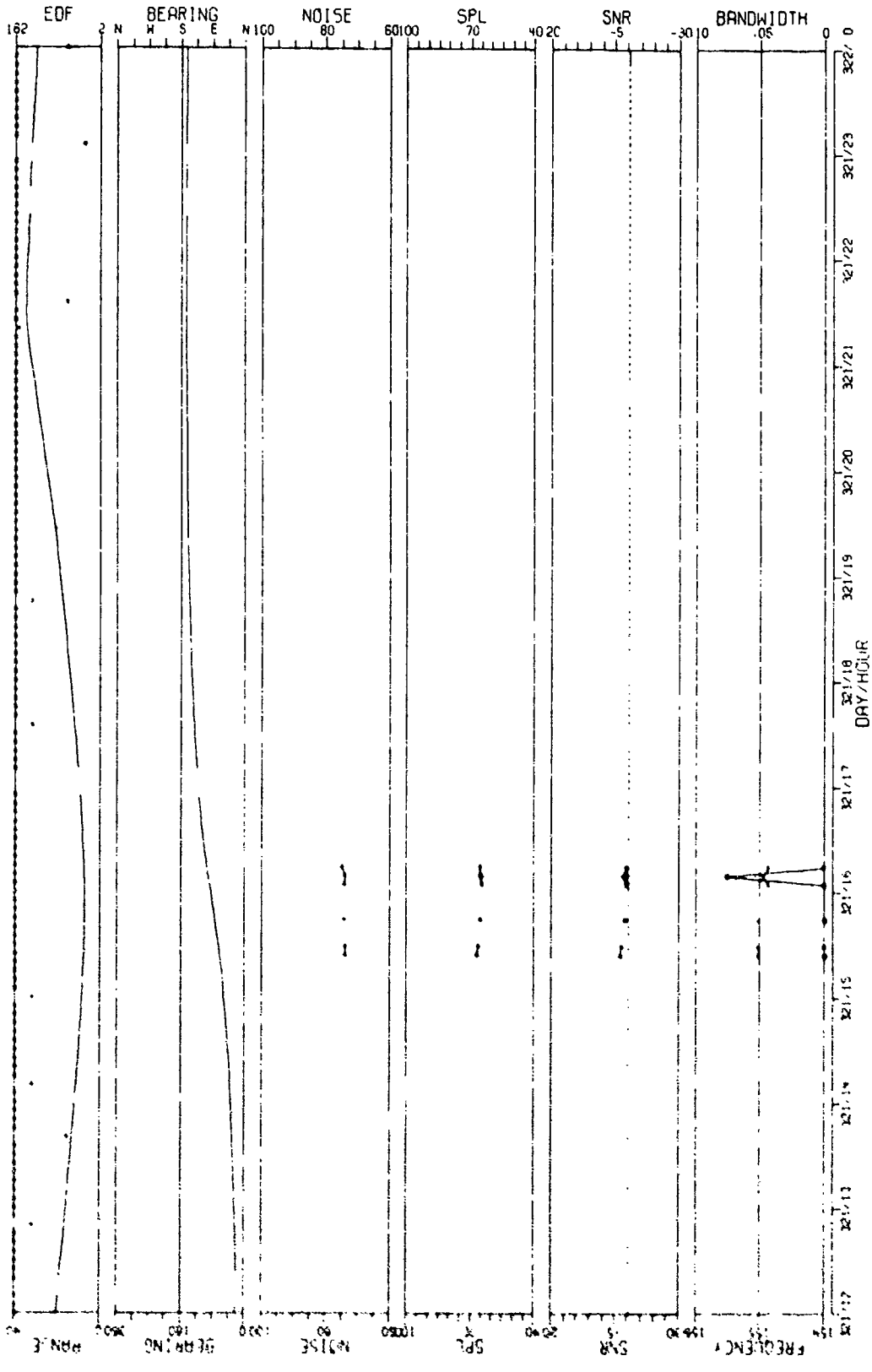

FIGURE II 19
MSS-F/T 155HZ LINE HISTORY AS OBSERVED VIA THE OMNIDIRECTIONAL SENSOR AT SITE A1 DURING THE 17 NOV FIELD EVENT WITH STANDARD RESOLUTION (U)

AS-77-2946

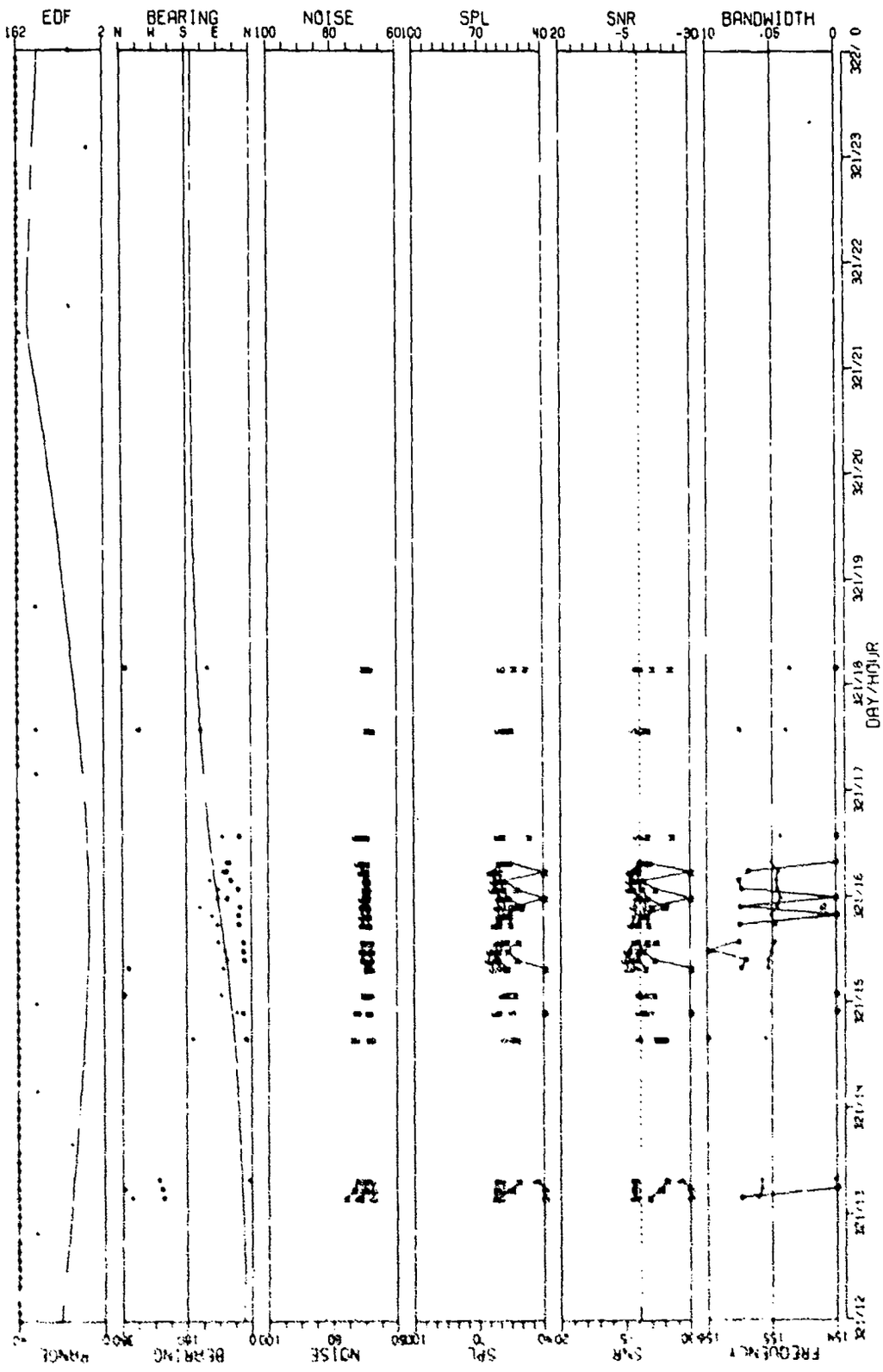

FIGURE II-29
MSS-FVV 155HZ LINE HISTORY AS OBSERVED VIA THE SINGLE CARDIOIDS SENSOR AT SITE A1 DURING THE 17 NOV FIELD EVENT WITH STANDARD RESOLUTION (U)

AS-77-2947

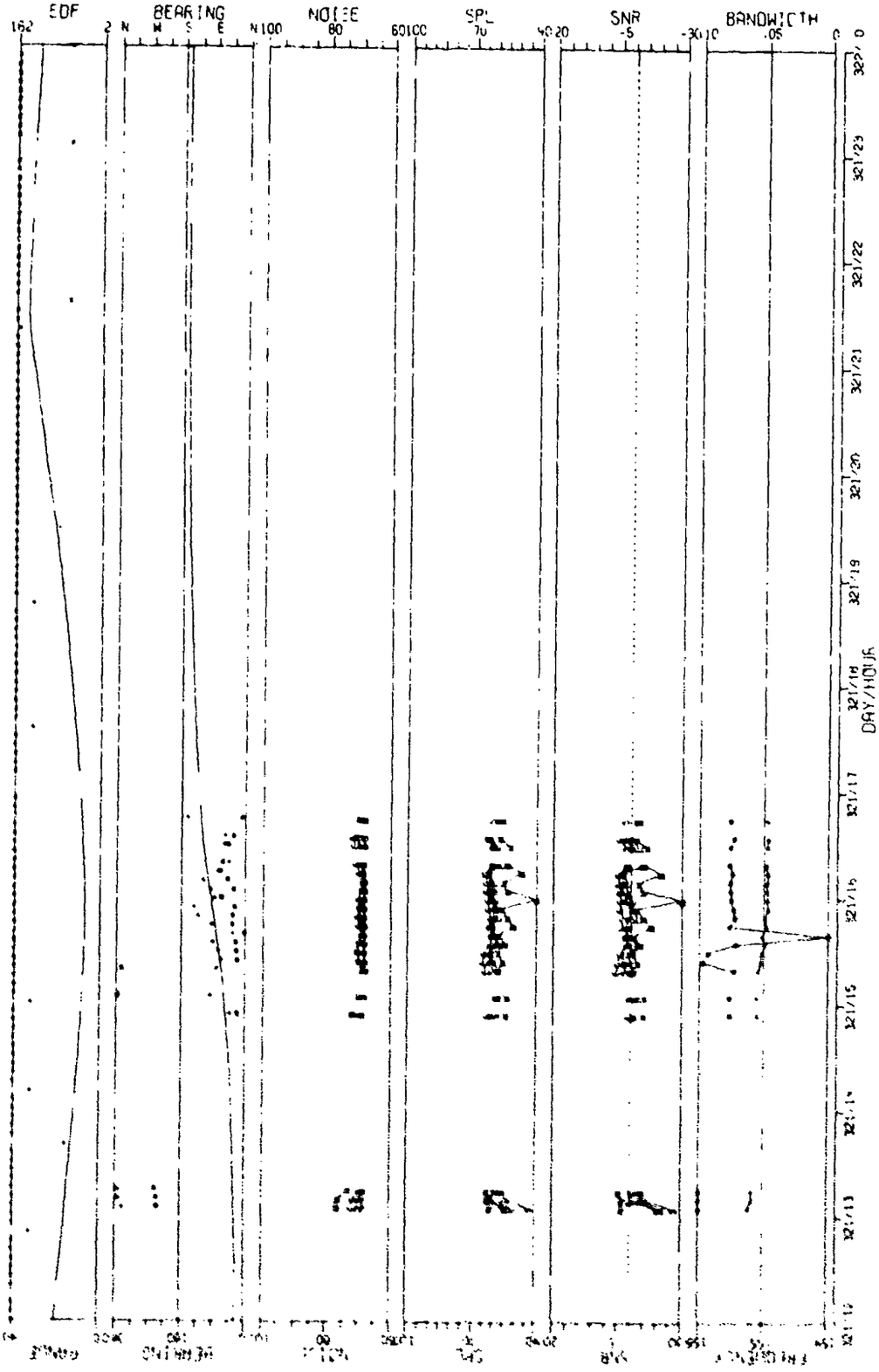

FIGURE 11-21
[illegible] LINE HISTORY AS OBSERVED /JA THE MAX GAIN LIMACONS SENSOR
[illegible] DURING THE 17 NOV FIELD EVENT WITH STANDARD RESOLUTION FUT

AS-77-2948

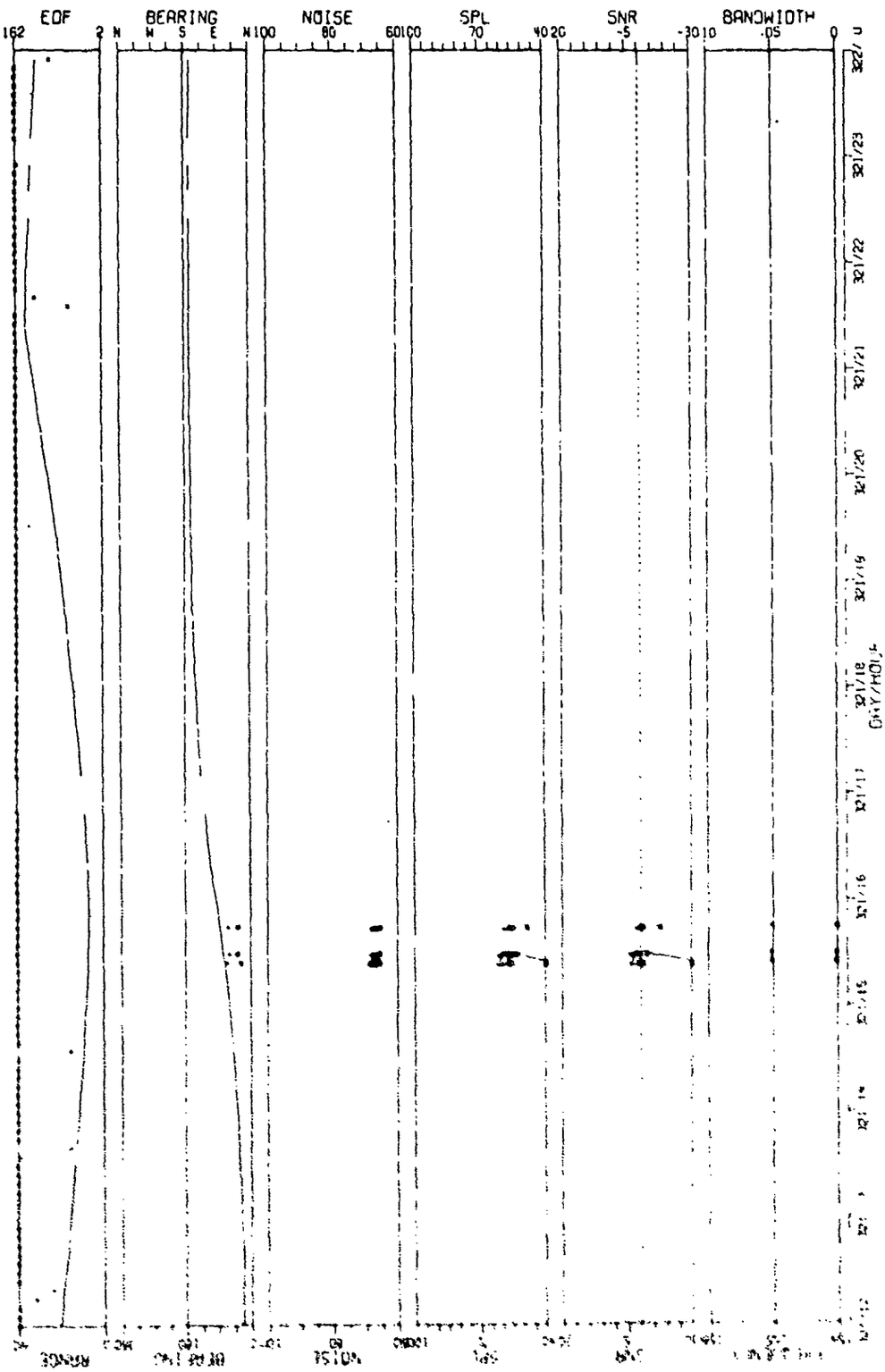

FIGURE 11-22

AS-77-2949

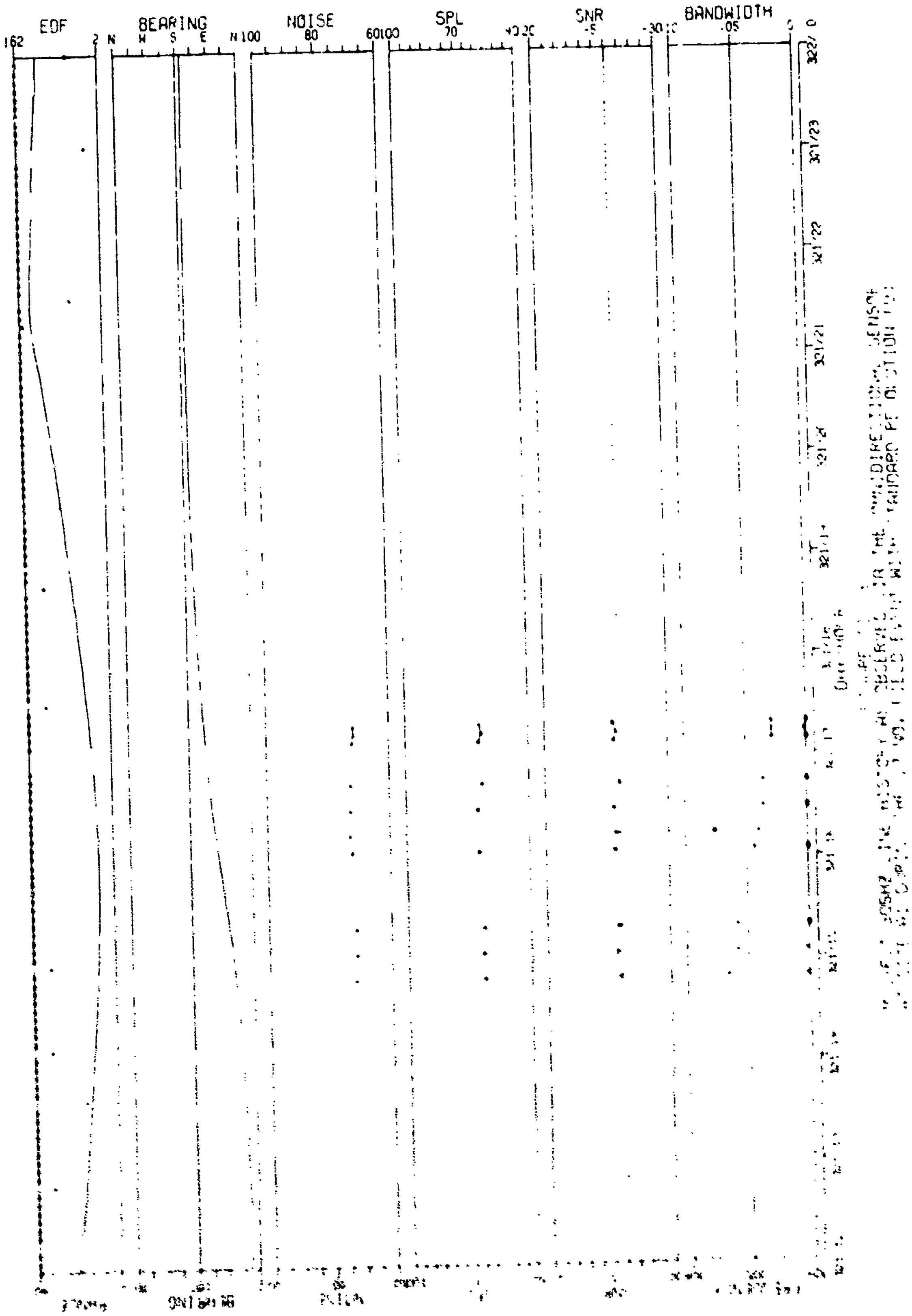

AS-77-2950

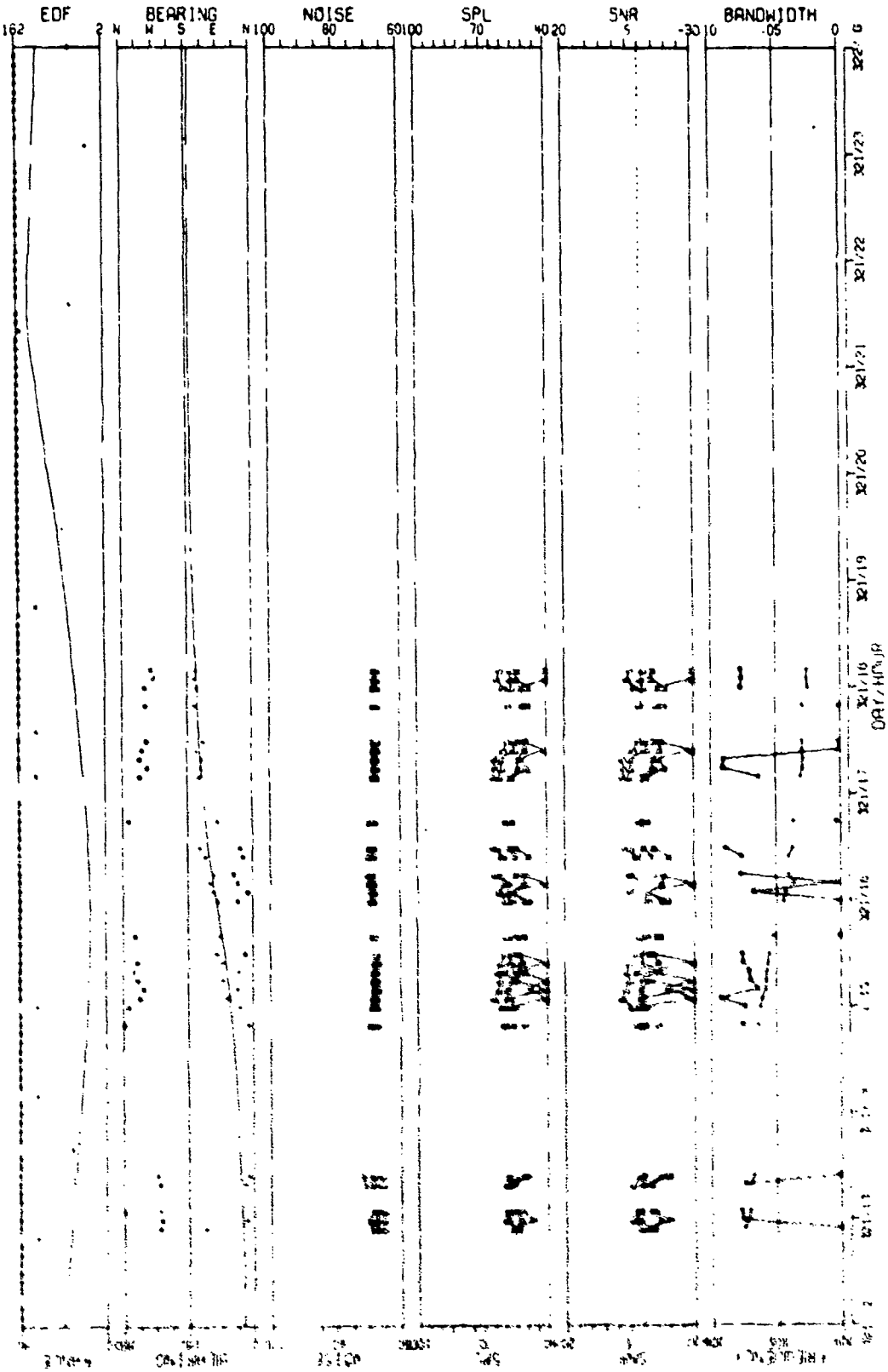

FIGURE II-24
OBSERVED VIA THE SINGLE CARDIOID SENSOR
THE 17 NOV FIELD EVENT WITH STANDARD RESOLUTION (U)

AS-77-2951

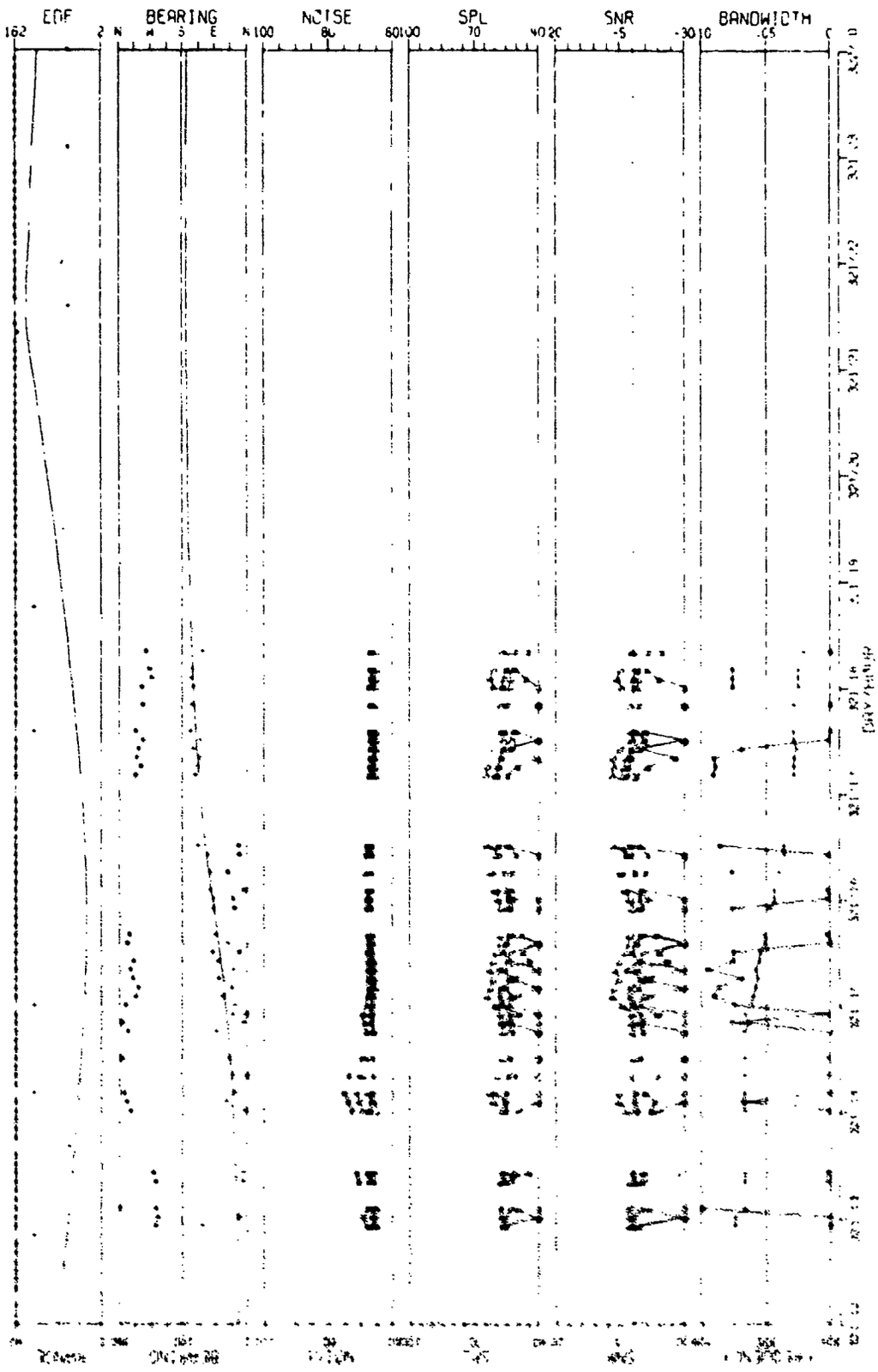

AS-77-2952

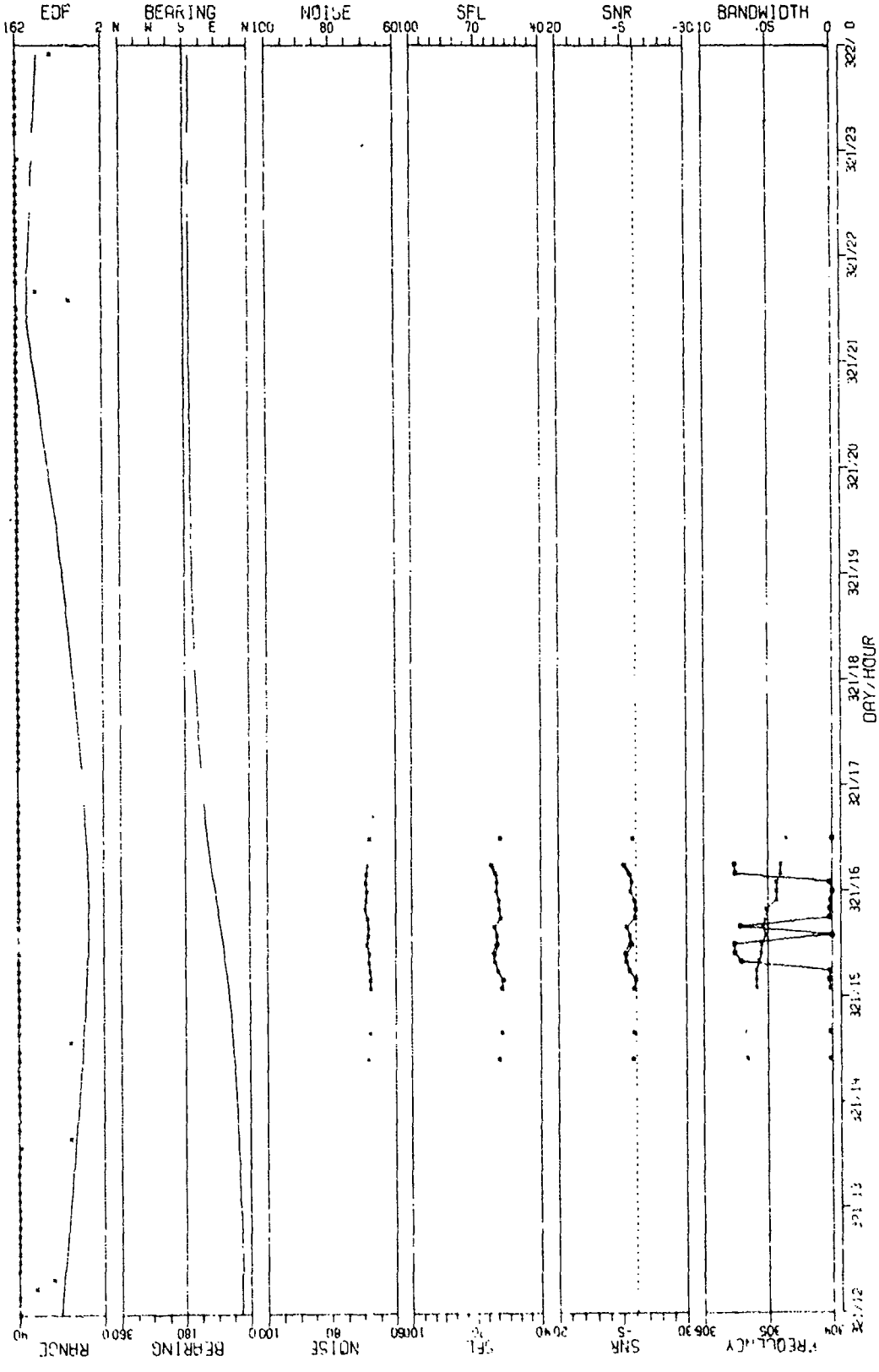

FIGURE II 25
MSS-FVT 305HZ LINE HISTORY AS OBSERVED VIA THE VERTICAL DIPOLE SENSOR AT SITE A1 DURING THE 17 NOV FIELD EVENT WITH STANDARD RESOLUTION (U)

AS-77-2953

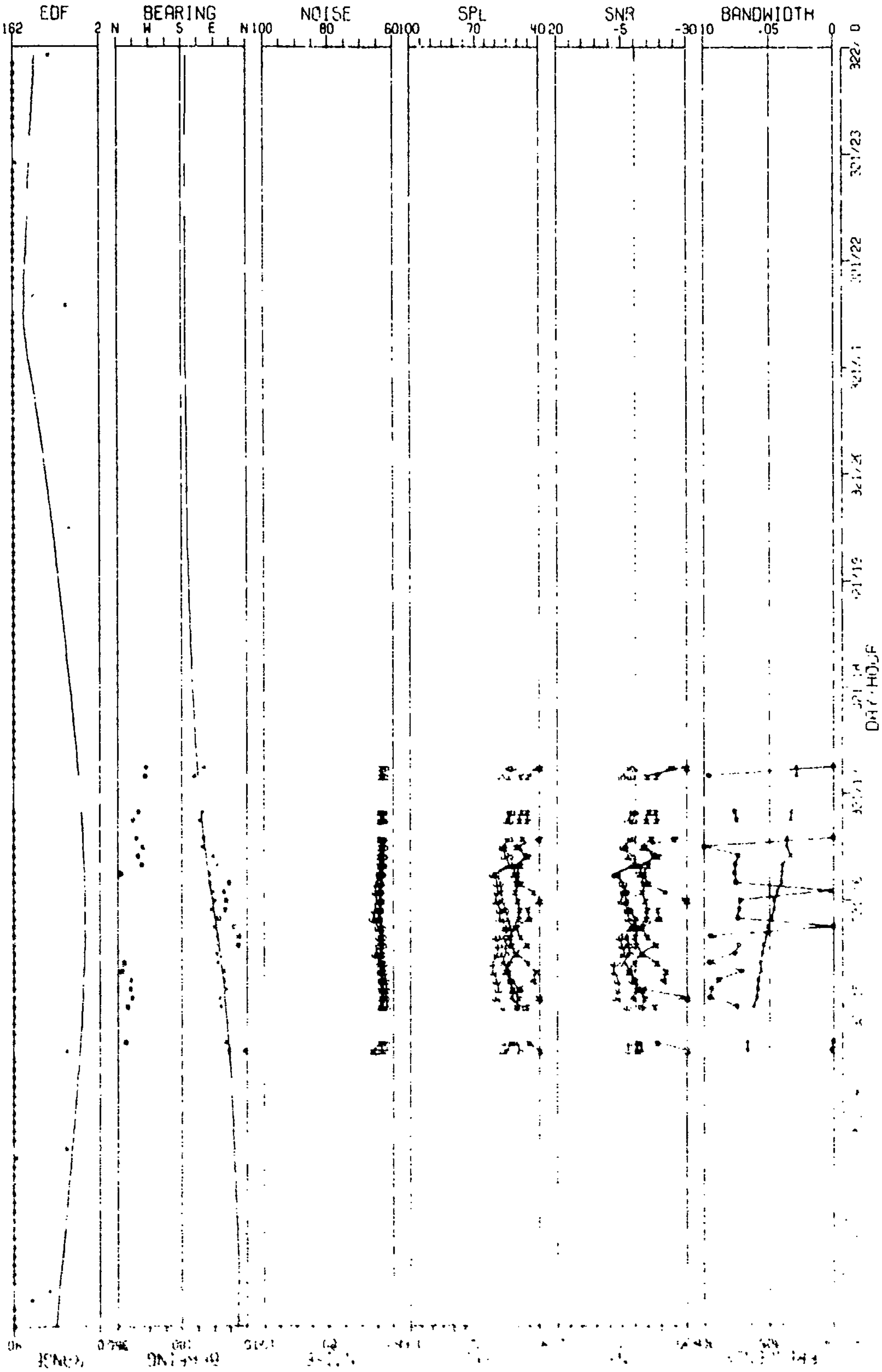

FIGURE II-27 [illegible] HISTORY [illegible] OBSERVED [illegible] THE DIFFERENCED CARDIOIDS SENSOR [illegible] DURING THE 17 NOV FIELD EVENT WITH STANDARD RESOLUTION [illegible]

AS-77-2954

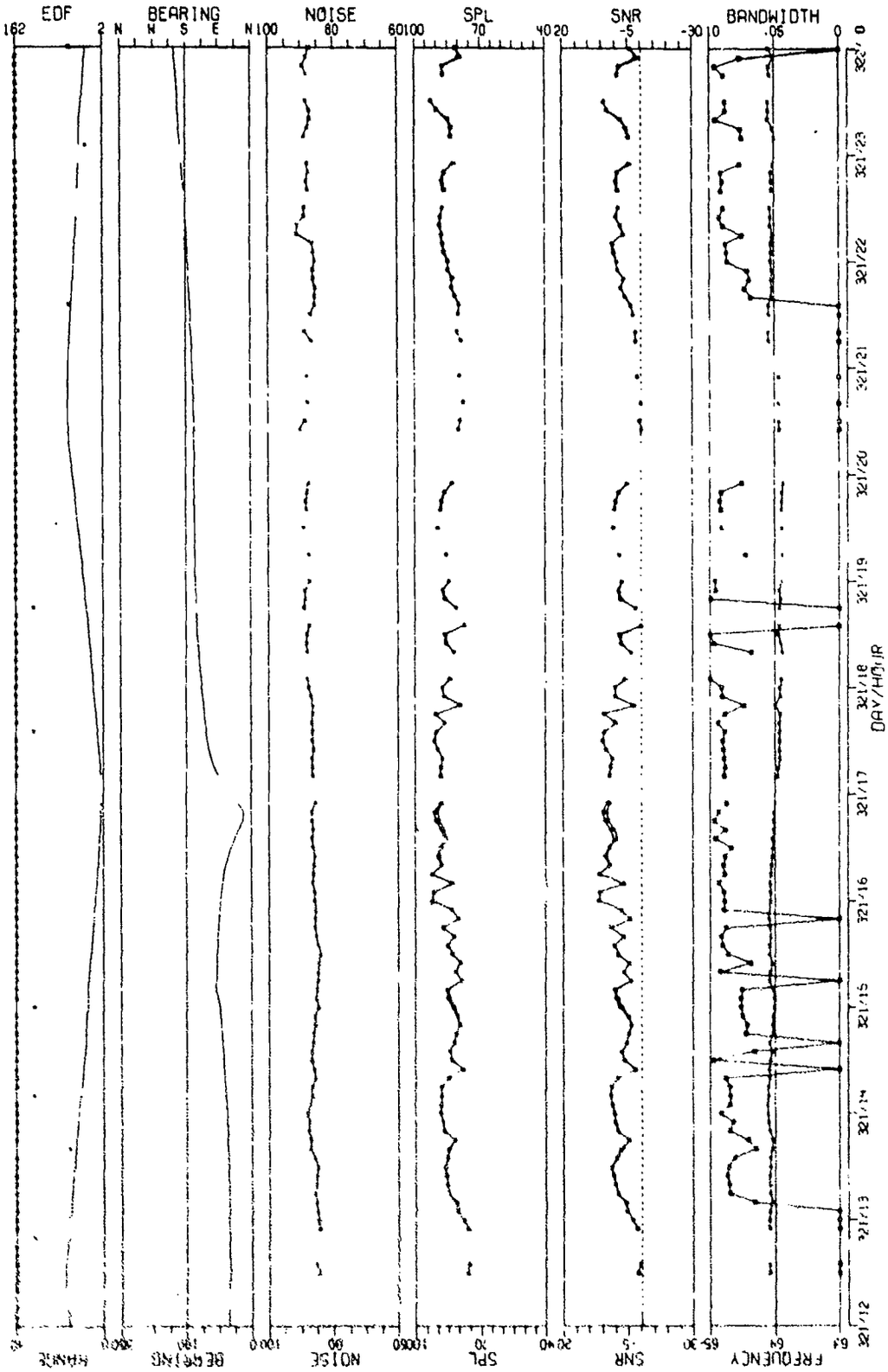

FIGURE II-28
MSS-FVT 6WHZ LINE HISTORY AS OBSERVED VIA THE OMNIDIRECTIONAL SENSOR AT SITE P1 DURING THE 17 NOV FIELD EVENT WITH STANDARD RESOLUTION (U)

AS-77-2955

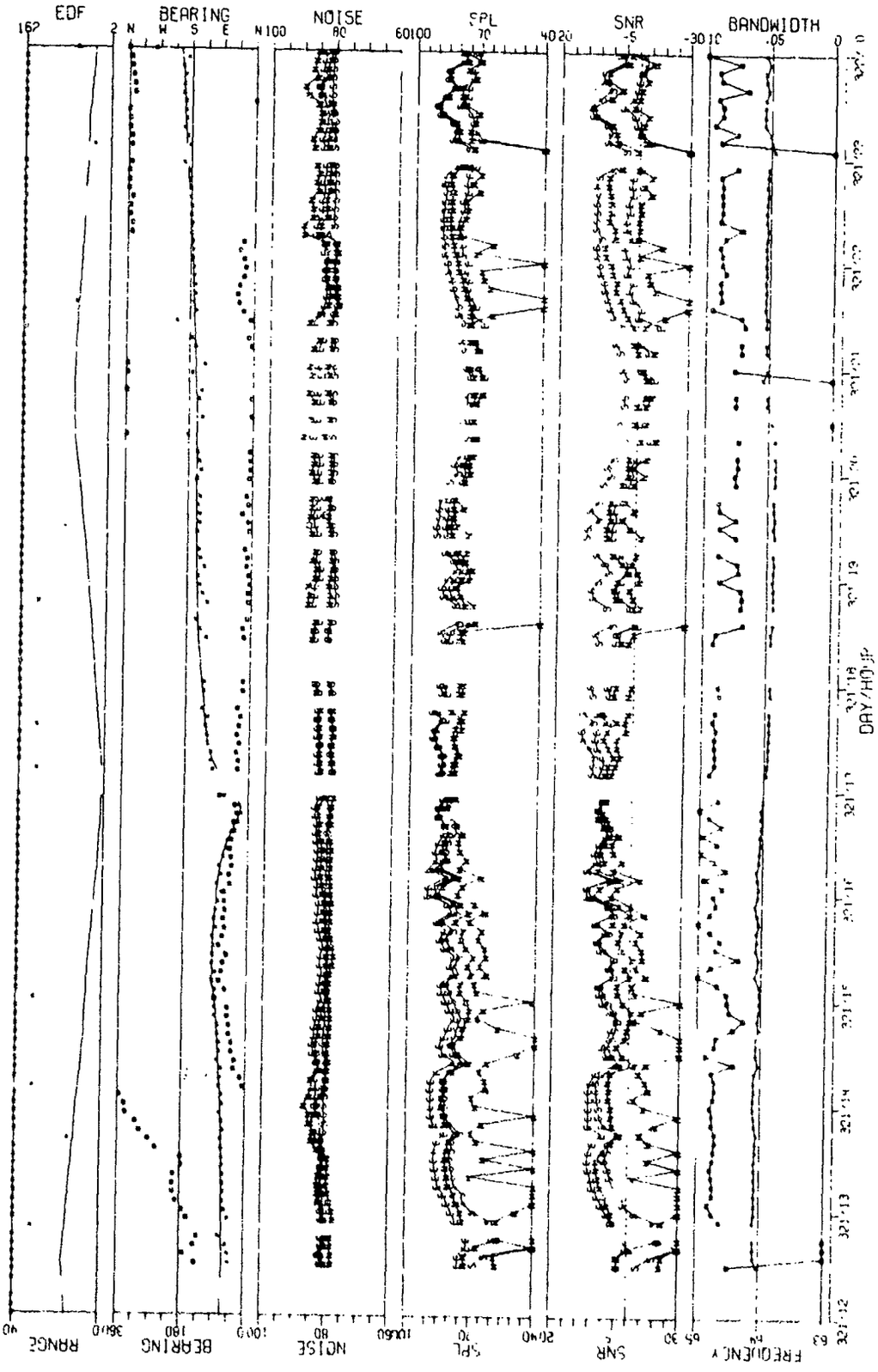

FIGURE 11-209
MSS-FYI 64HZ LINE HISTORY AS OBSERVED VIA THE SINGLE CARDIOID SENSOR AT SITE A1 DURING THE 17 NOV FIELD EVENT WITH STANDARD RESOLUTION FFT

AS-77-2956

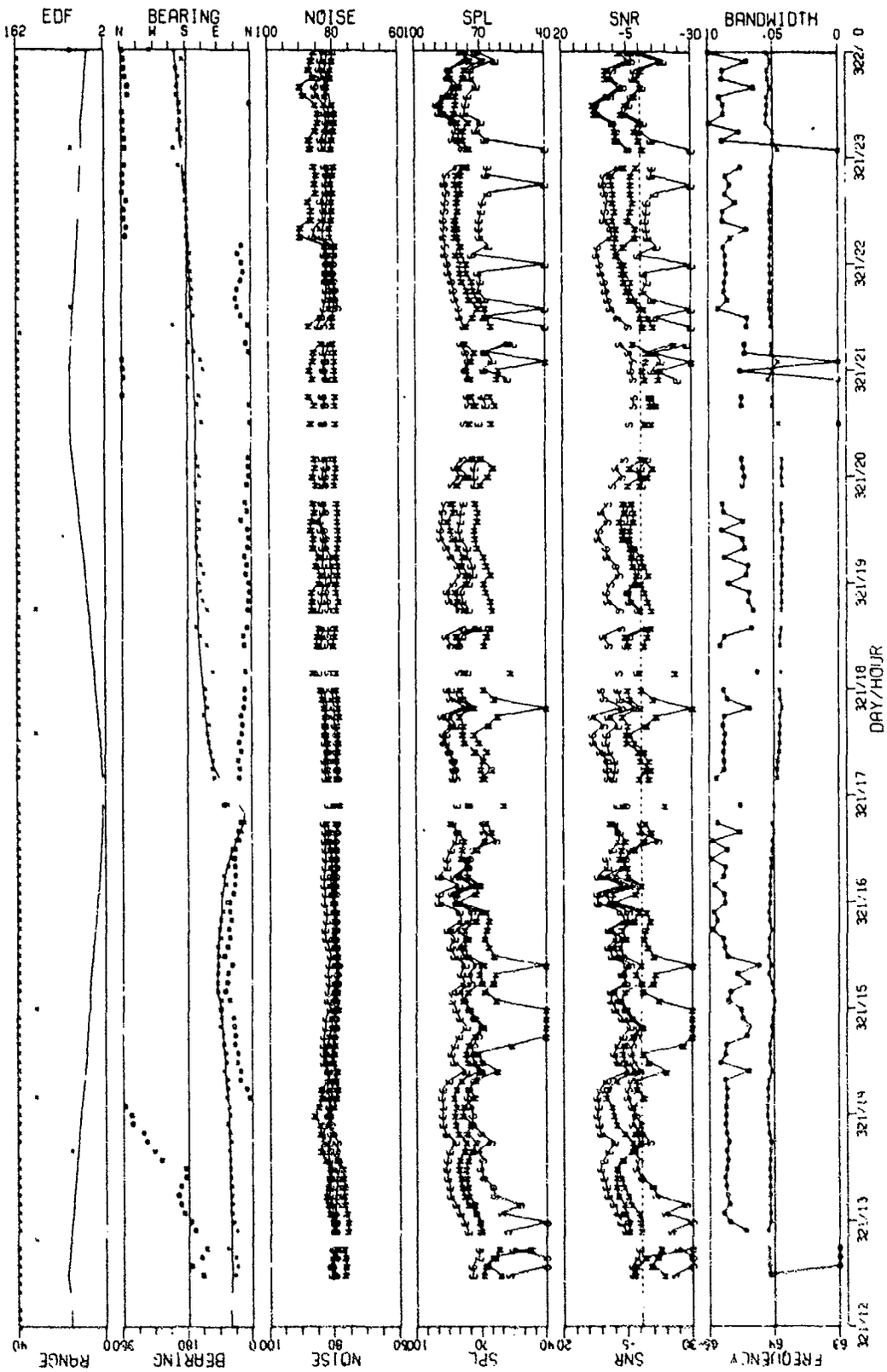

FIGURE II-30
M55-FVI 64HZ LINE HISTORY AS OBSERVED VIA THE MAX GAIN LIMACONS SENSOR
AT SITE A1 DURING THE 17 NOV FIELD EVENT WITH STANDARD RESOLUTION (U)

AS-77-2957

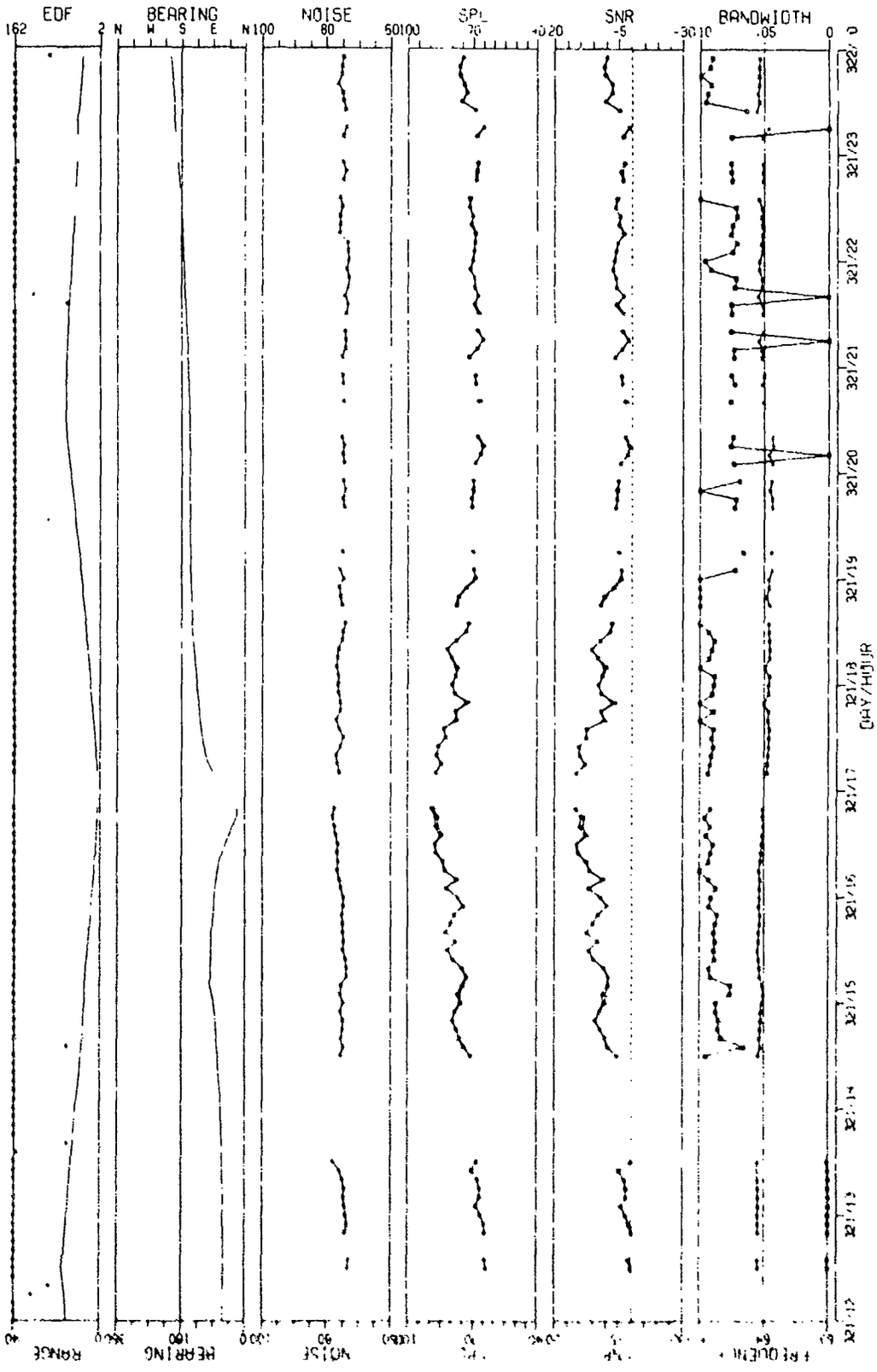

FIGURE 11-31
MSS-FM 6MHZ LINE HISTORY AS OBSERVED VIA THE VERTICAL DIPOLE SENSOR AT SITE 41 DURING THE 17 HOUR FIELD EVENT WITH STANDARD RESOLUTION (U)

AS-77-2958

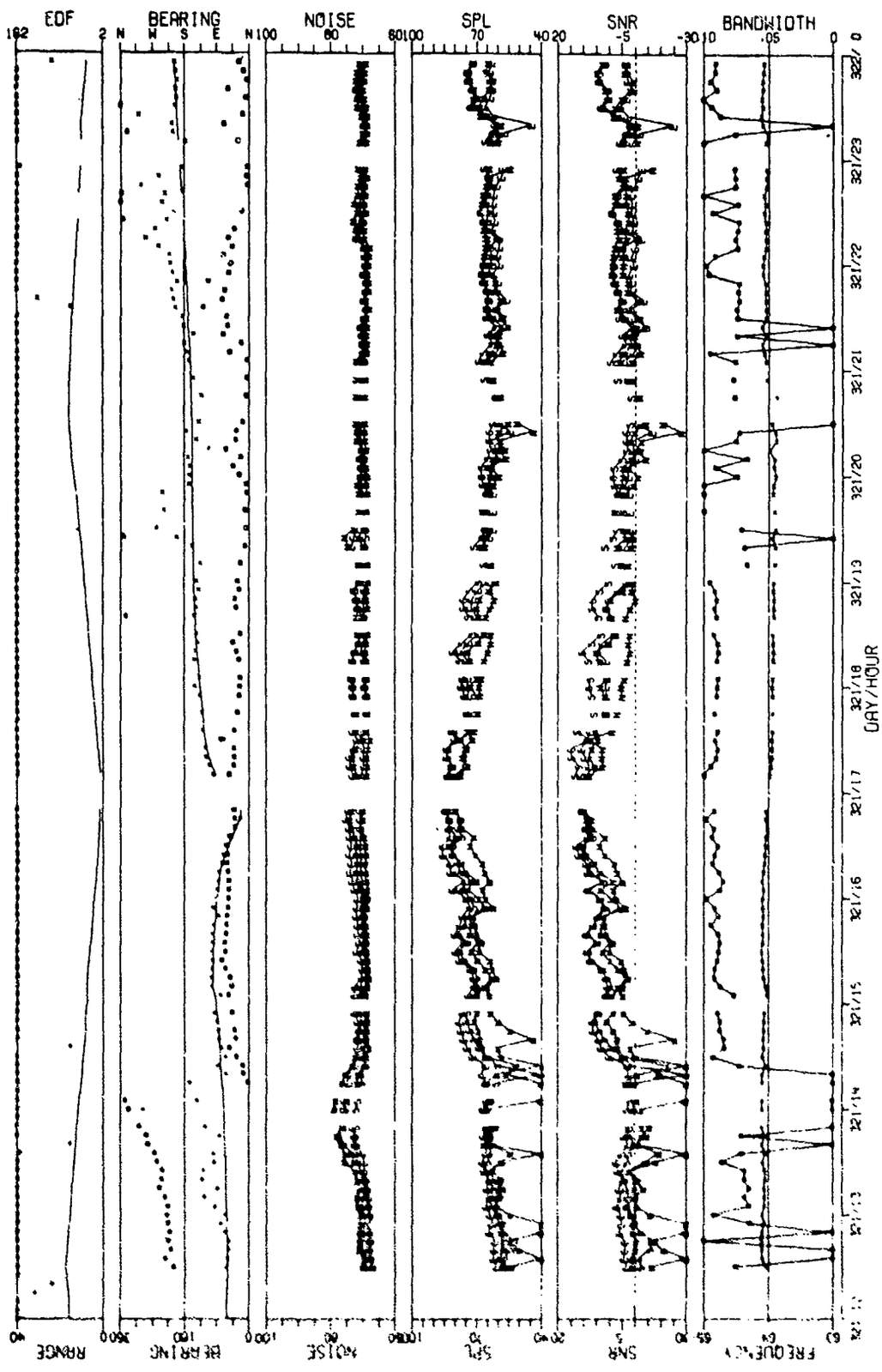

FIGURE II-32
MSS-FVI 64HZ LINE HISTORY AS OBSERVED VIA THE DIFFERENCED CARDIOIDS SENSOR AT SITE A1 DURING THE 17 NOV FIELD EVENT WITH STANDARD RESOLUTION (U)

AS-77-2959

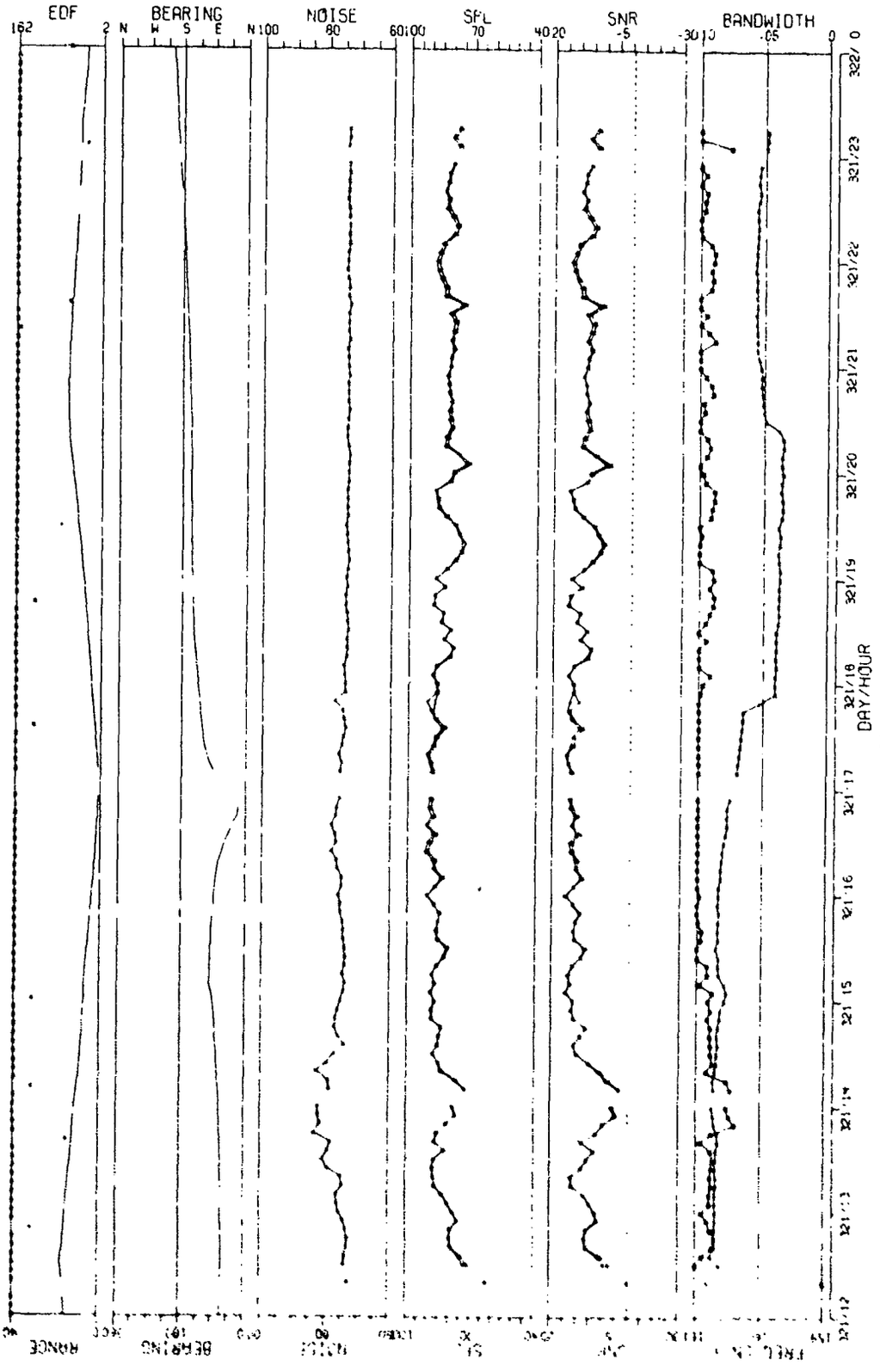

FIGURE II-33
MSS-FVT 150HZ LINE HISTORY AS OBSERVED VIA THE OMNIDIRECTIONAL SENSOR
AT SITE A1 DURING THE 17 NOV FIELD EVENT WITH STANDARD RESOLUTION (U)

AS-77-2960

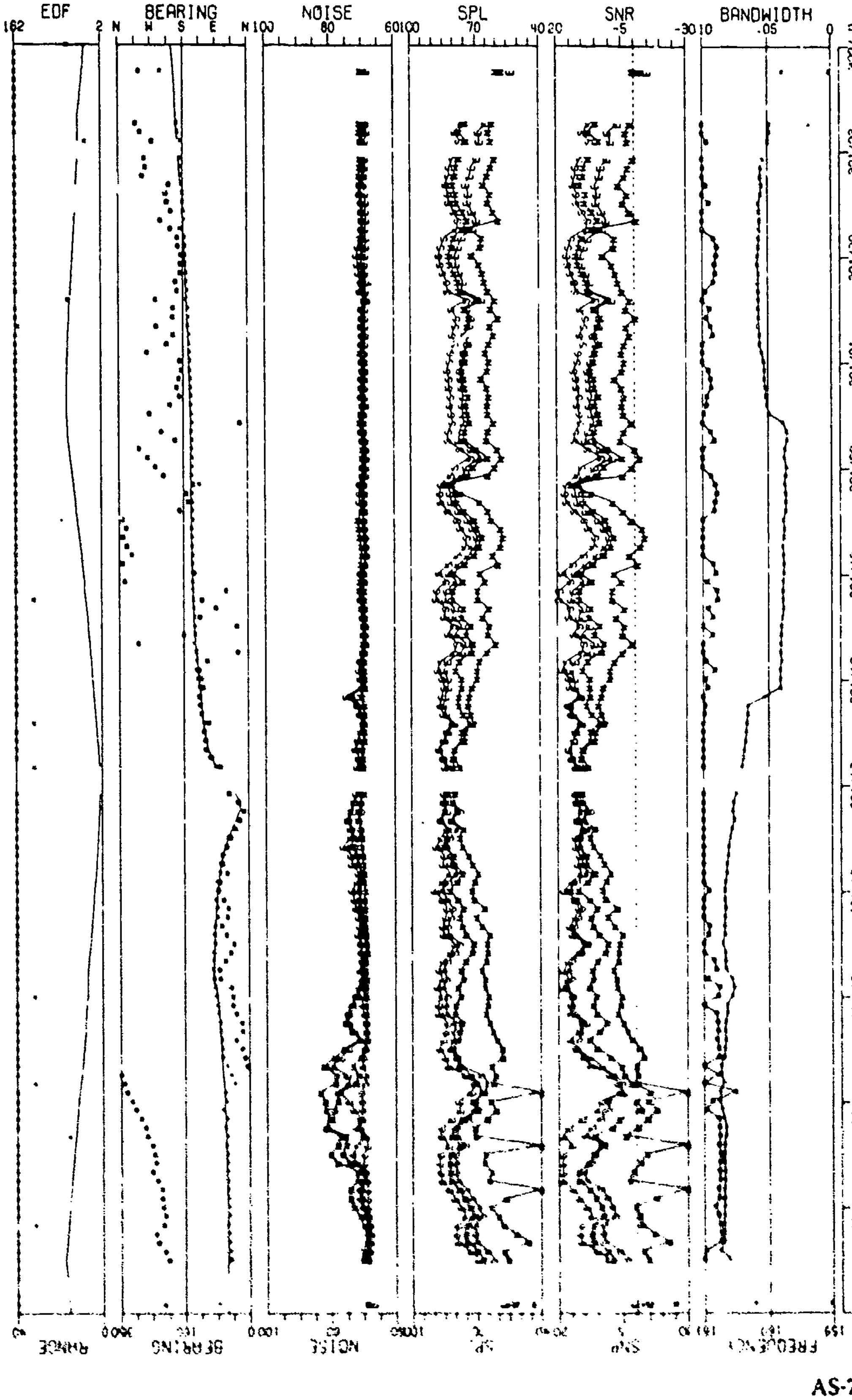

FIGURE II-34
MOS-AVT 160HZ LINE HISTORY AS OBSERVED VIA THE SINGLE CARDIOIDS SENSOR AT SITE A1 DURING THE 17 NOV FIELD EVENT WITH STANDARD RESOLUTION (U)

AS-77-2961

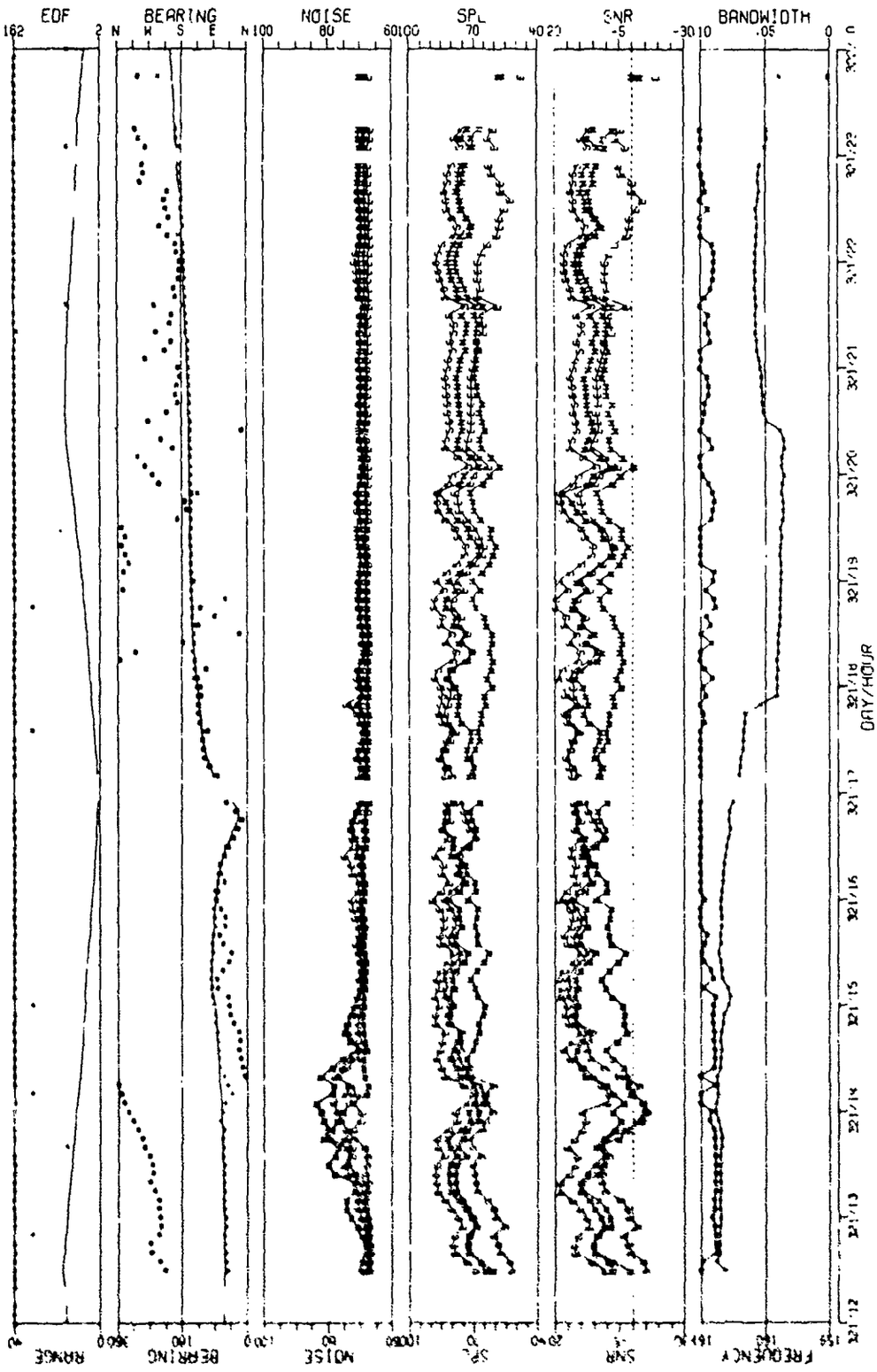

FIGURE II-35
MSS-FVT 160HZ LINE HISTORY AS OBSERVED VIA THE MAX GAIN LIMACONS SENSOR
AT SITE A1 DURING THE 17 NOV FIELD EVENT WITH STANDARD RESOLUTION (U)

AS-77-2962

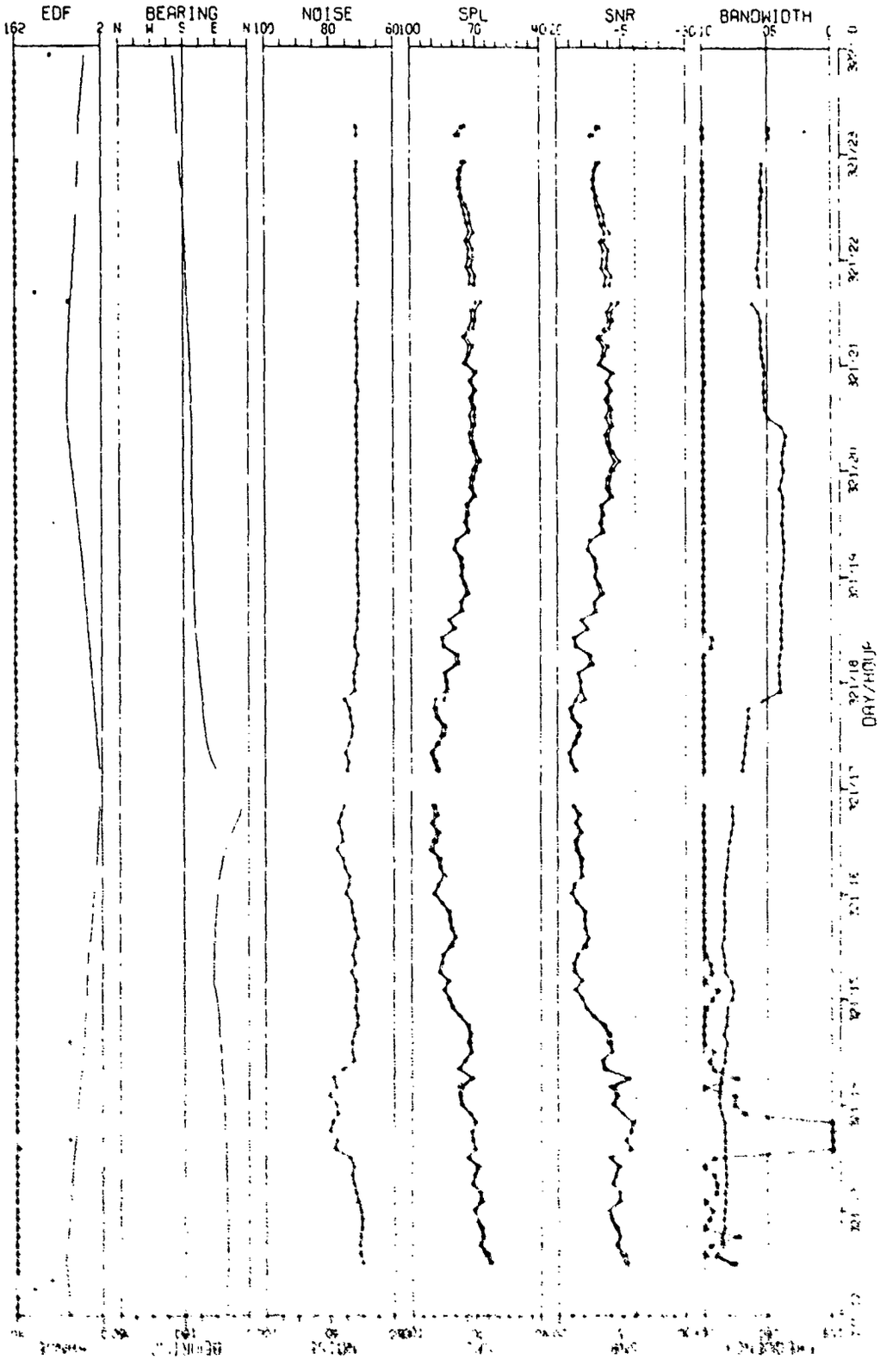

FIGURE 11 36
TIME LINE HISTORY AS OBSERVED VIA THE VERTICAL DIPOLE SENSOR
AT SITE A1 DURING THE 17 NOV FIELD EVENT WITH STANDARD RESOLUTION (U)

AS-77-2963

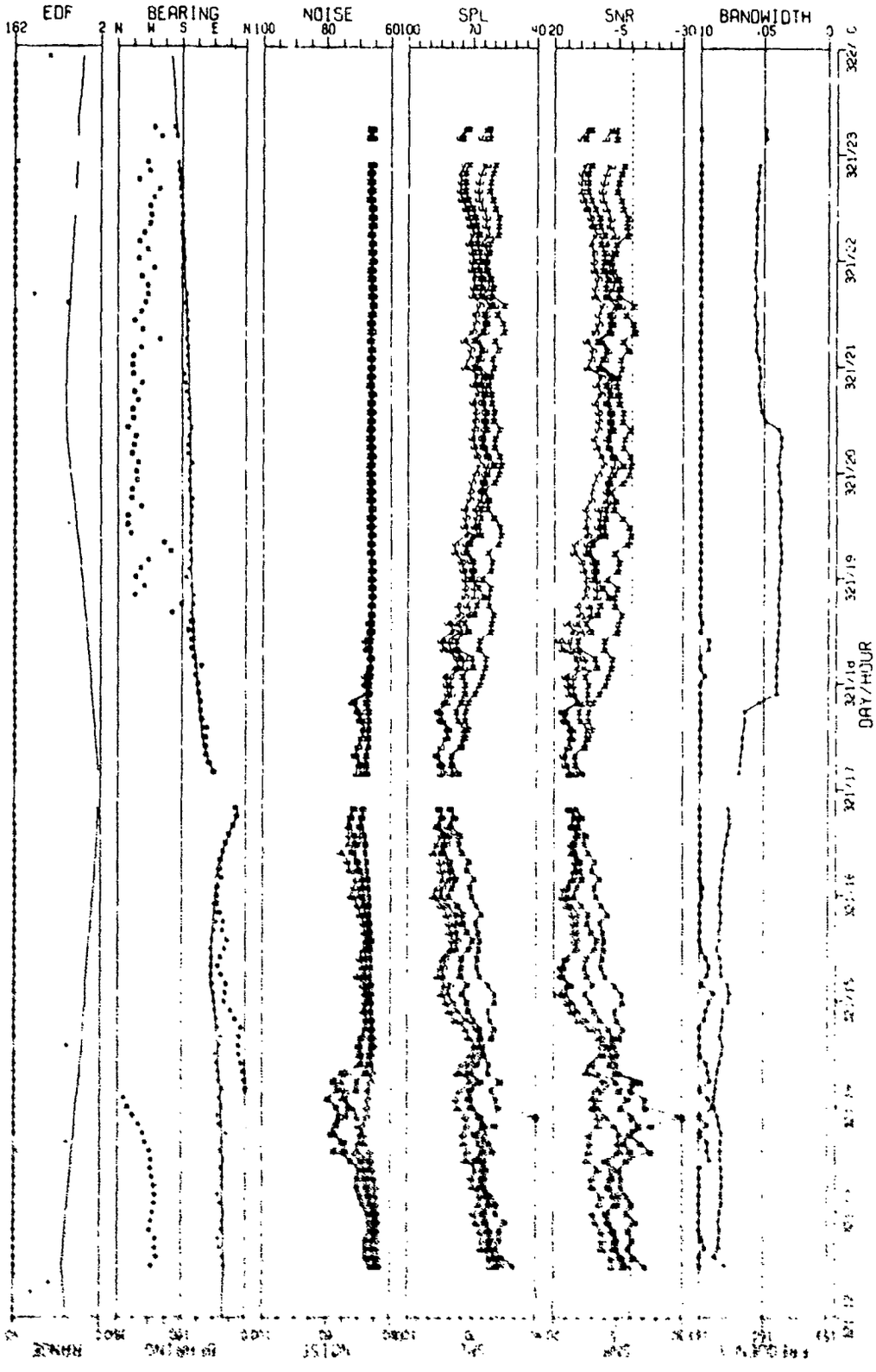

FIGURE 11-17
[illegible] AS OBSERVED VIA THE DIFFERENCED CARDIOID SENSOR
[illegible] DURING THE 17 NOV FIELD EVENT WITH STANDARD RESOLUTION (U)

AS-77-2964

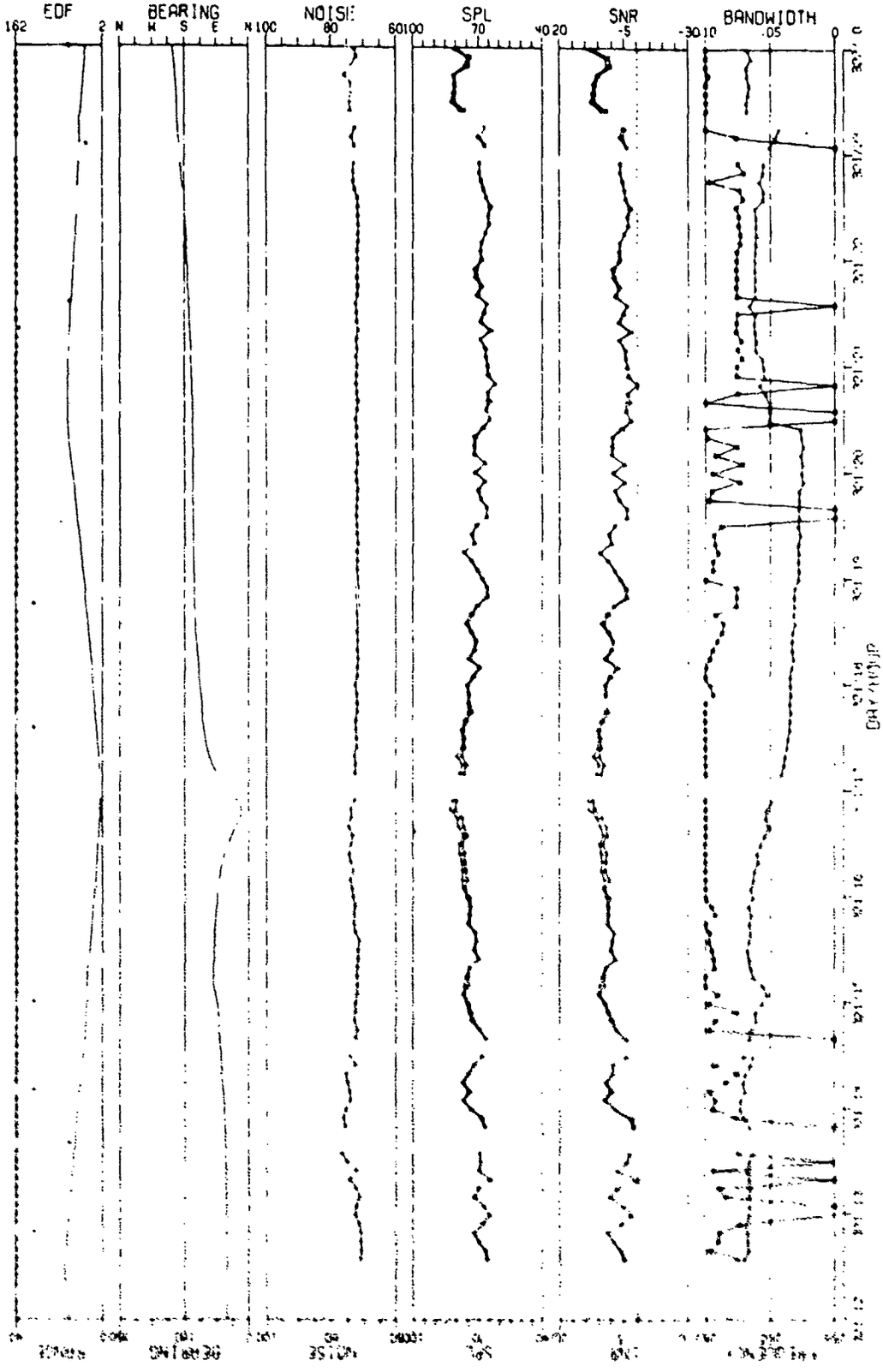

AS-77-2965

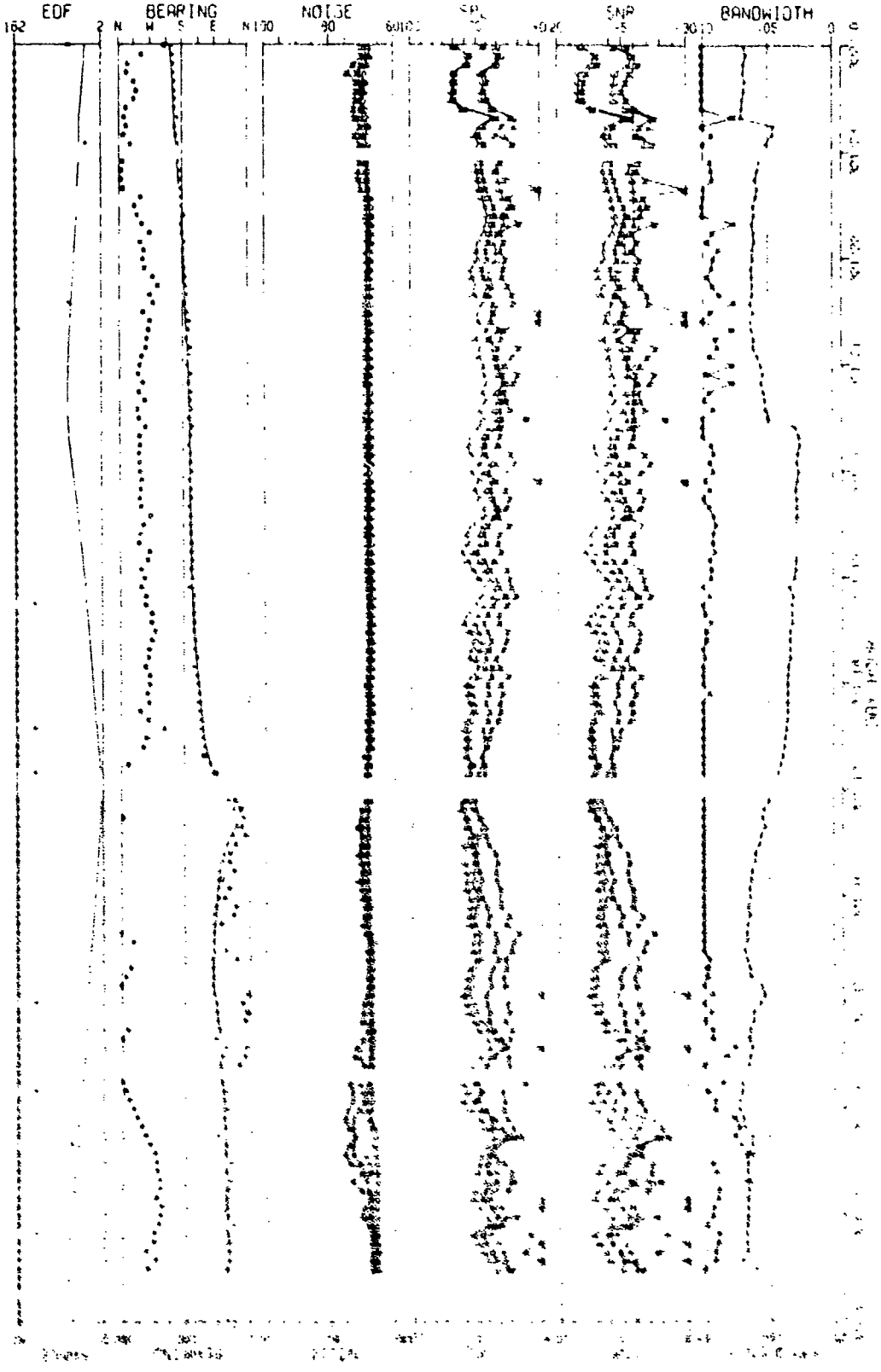

AS-77-2966

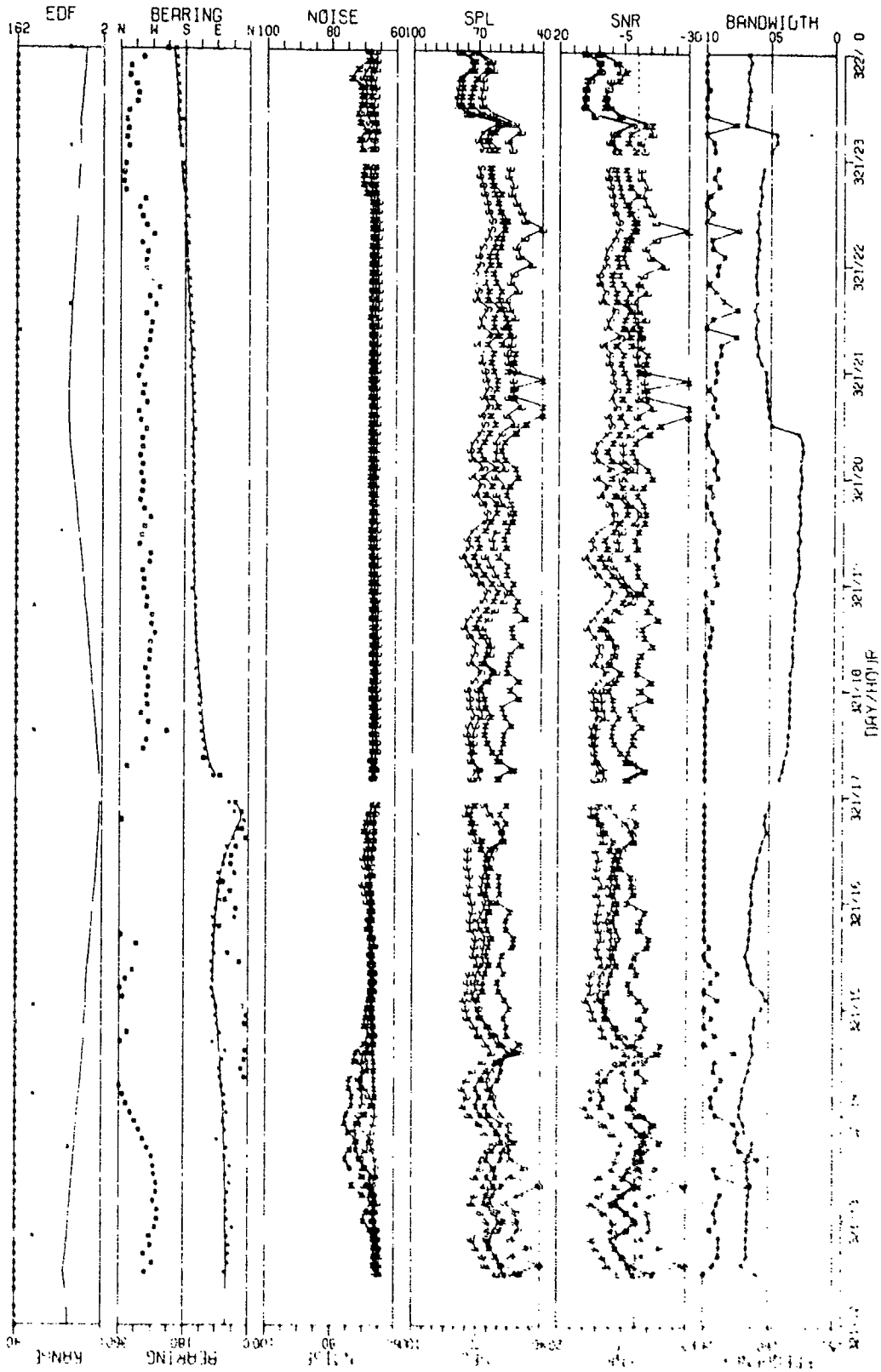

FIGURE II-43
[illegible] 26GHZ LINE HISTORY AS OBSERVED VIA THE MAX GAIN LIMACONS SENSOR
[illegible] DURING THE 17 MAY FIELD EVENT WITH STANDARD RESOLUTION FFT

AS-77-2957

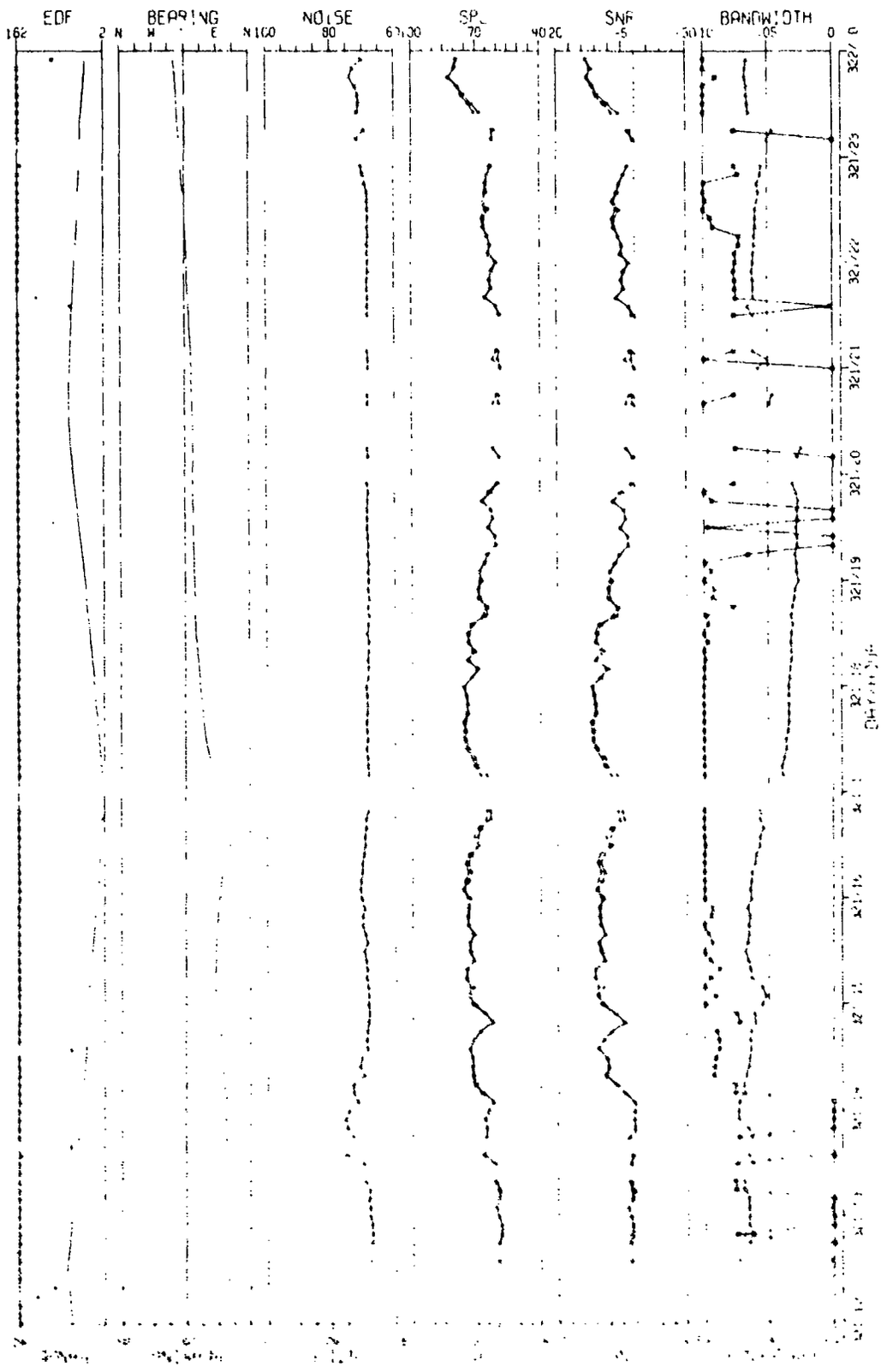

AS-77-2968

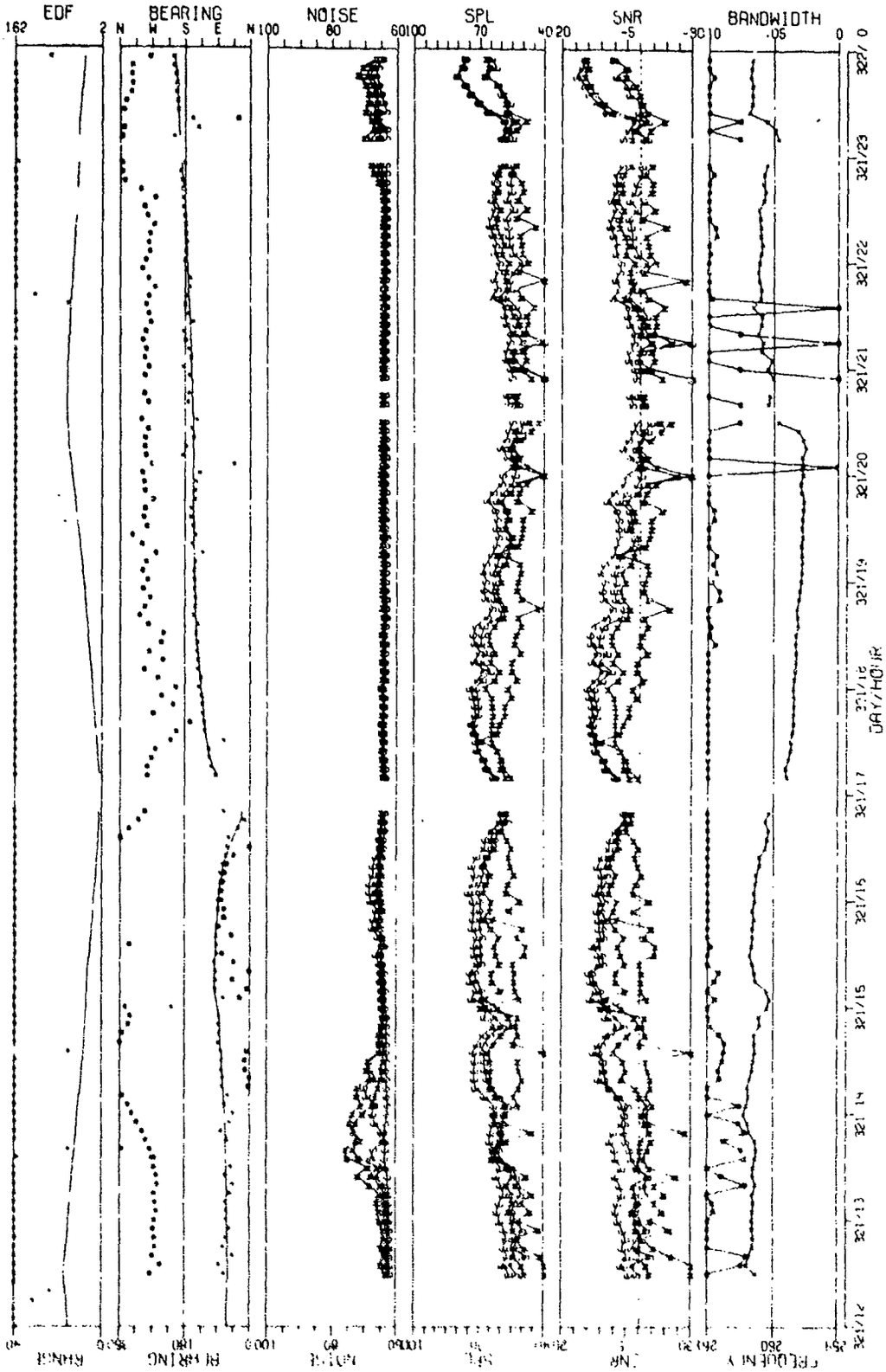

FIGURE 11-42
MSS-EVT 260HZ LINE HISTORY AS OBSERVED VIA THE DIFFERENCED CARDIOIDS SENSOR AT SITE A1 DURING THE 17 NOV FIELD EVENT WITH STANDARD RESOLUTION (U)

AS-77-2969

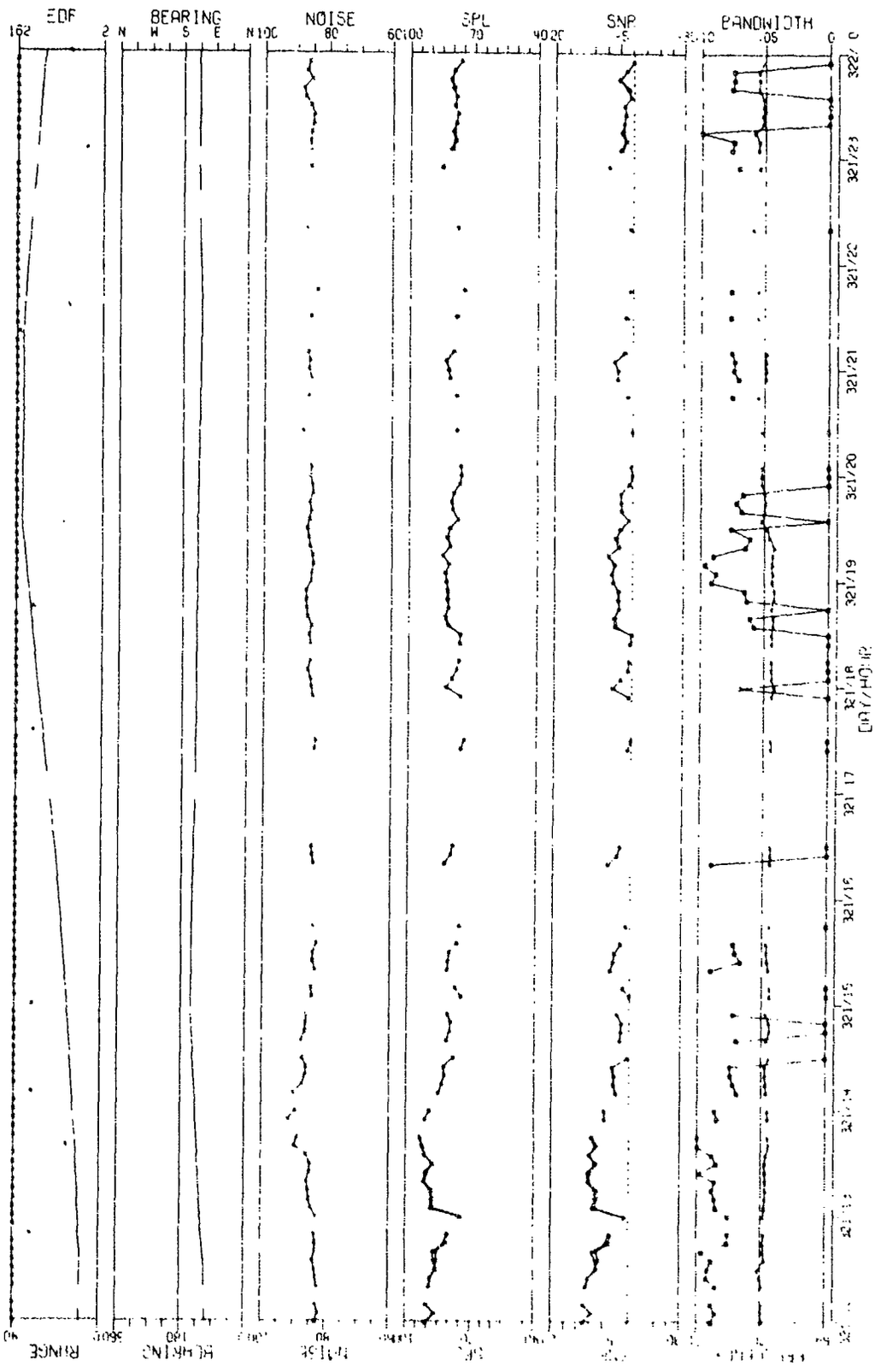

FIGURE 11-43
PROFILE LINE HISTORY AS OBSERVED VIA THE OMNIDIRECTIONAL SENSOR AT SITE 6 DURING THE 17 NOV FIELD EVENT WITH STANDARD RESOLUTION (U)

AS-77-2970

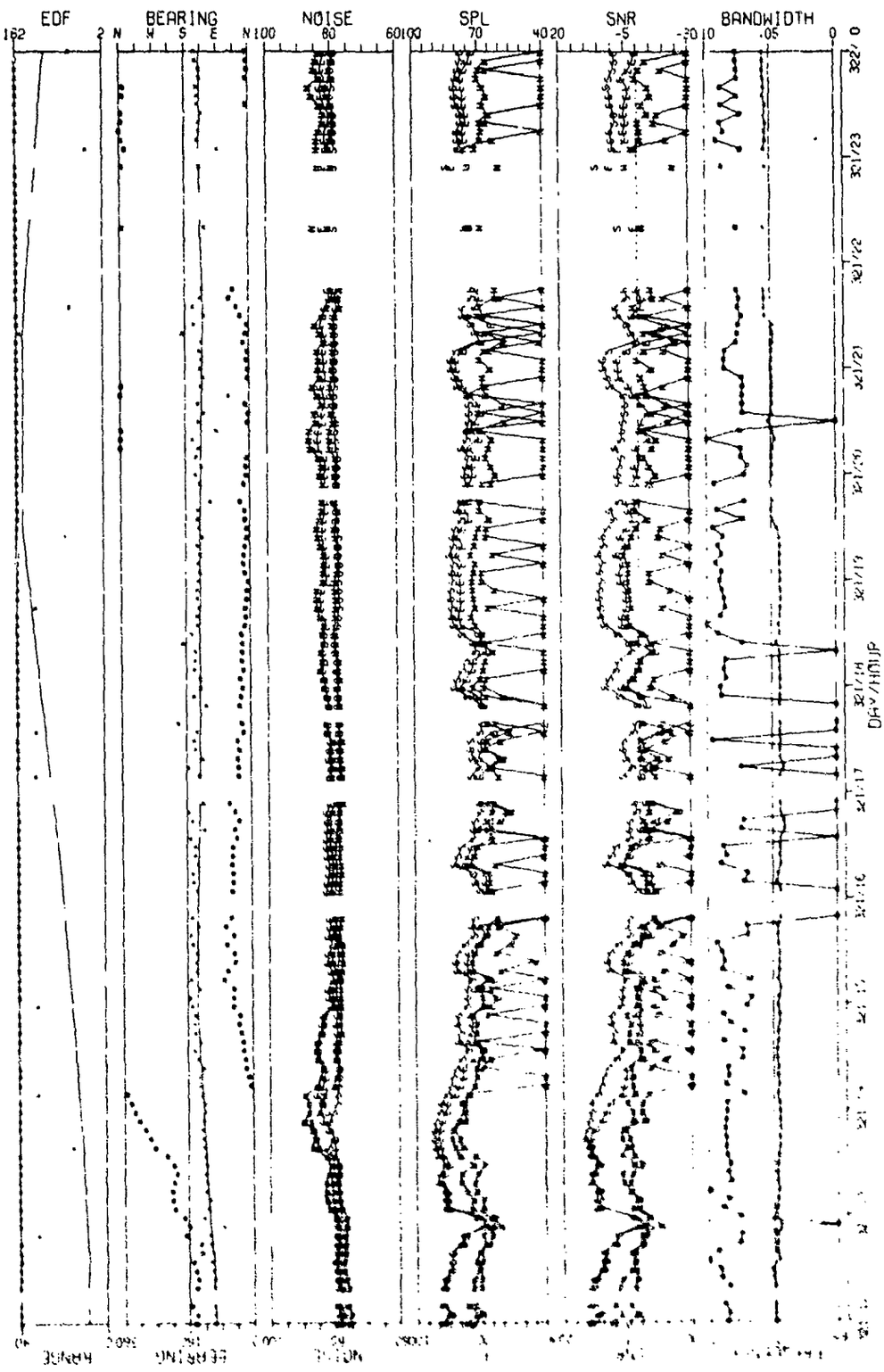

FIGURE 11-44. LINE HISTORY AS OBSERVED VIA THE SINGLE CARDIOIDS SENSOR [illegible] DURING THE 17 NOV FIELD EVENT WITH STANDARD RESOLUTION (U)

AS-77-2971

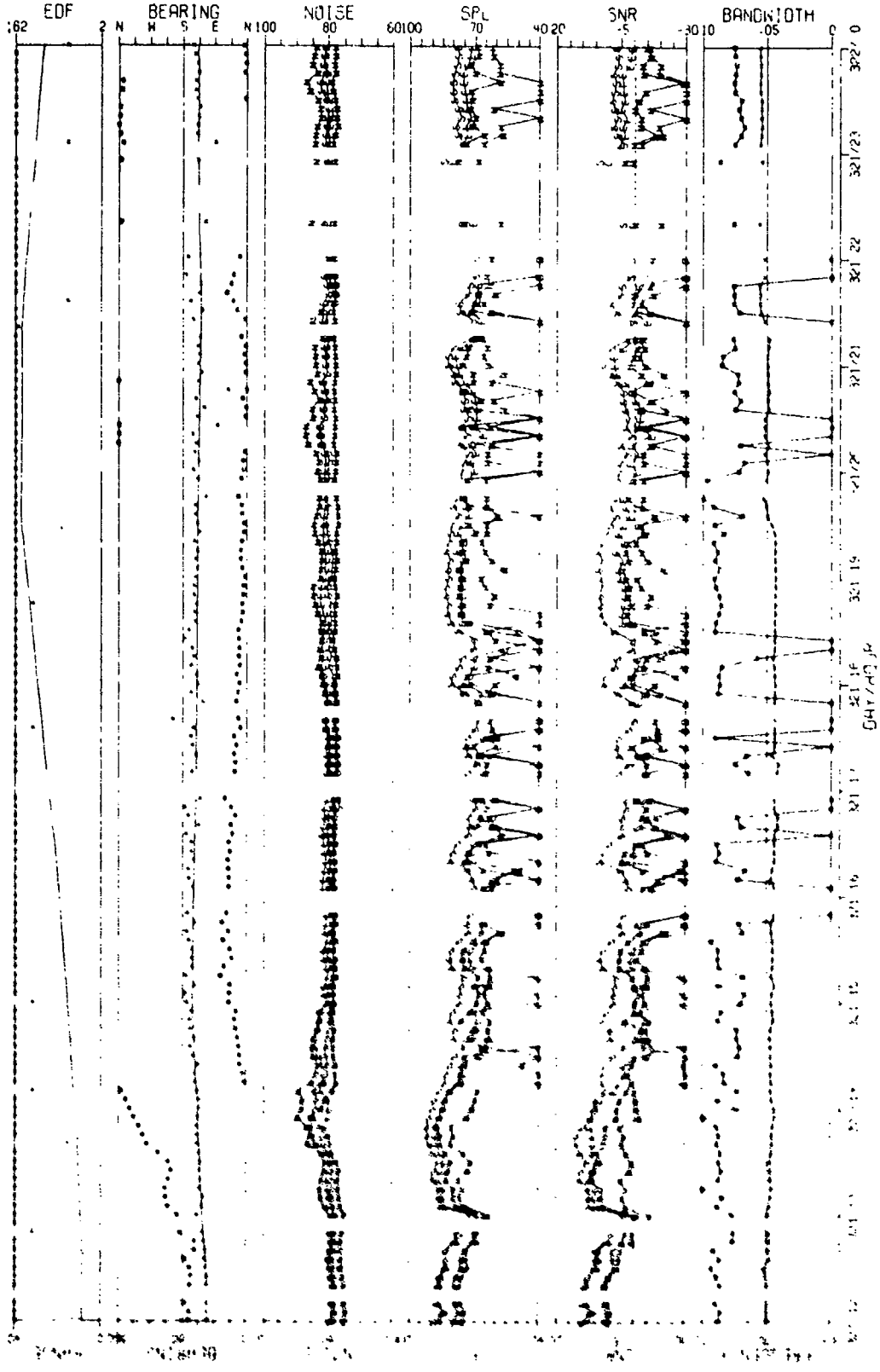

FIGURE [illegible]
[illegible] OBSERVED ON THE MAY SAIN LIMACONS ALONG
[illegible] NOV FIELD EVENT WITH STANDARD RESOLUTION (U)

AS-77-2972

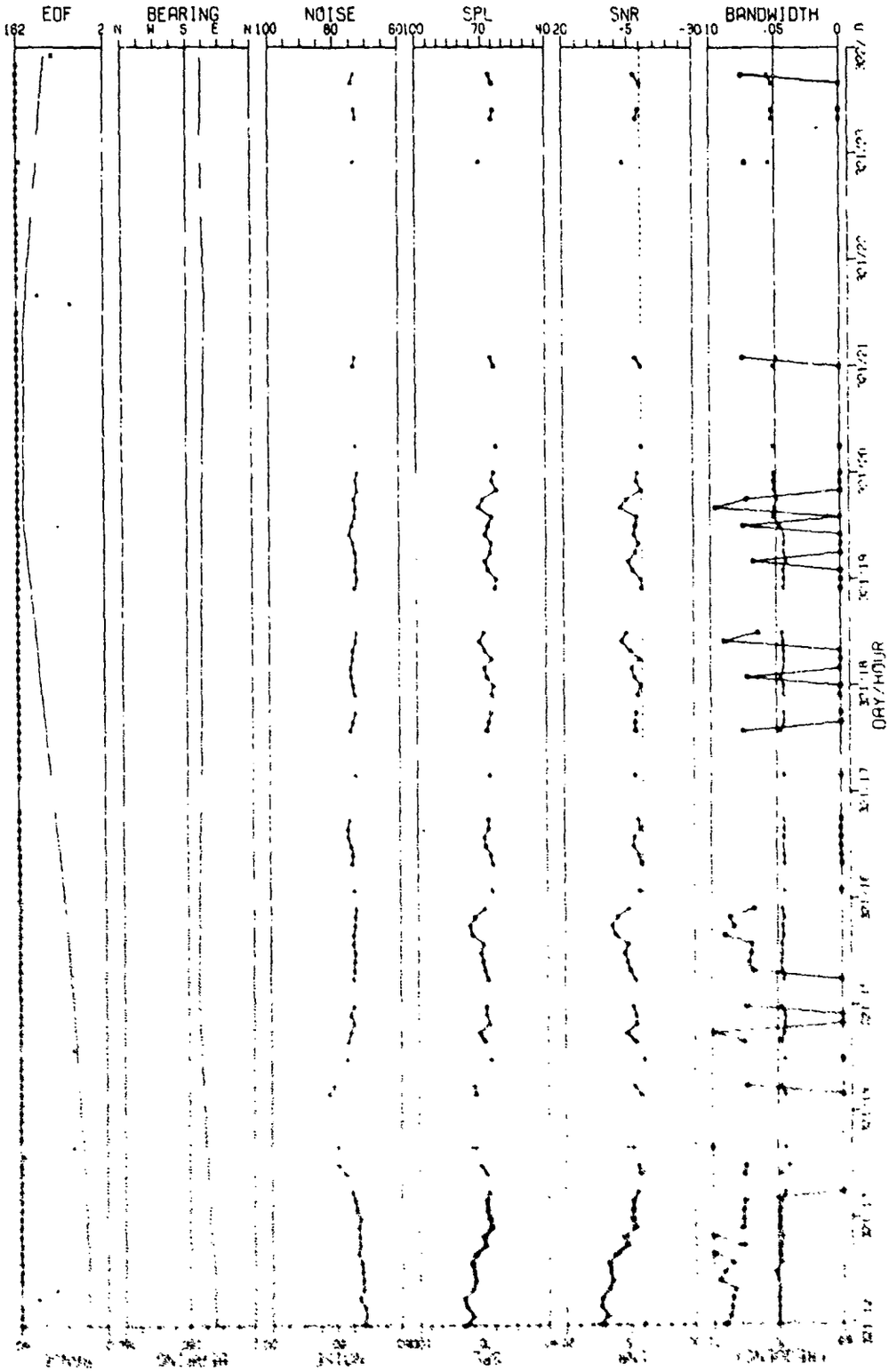

FIGURE 11-46.
OBSERVED VIA THE VERTICAL DIPOLE SENSOR
THE 17 NOV FIELD EVENT WITH STANDARD RESOLUTION TUI

AS-77-2973

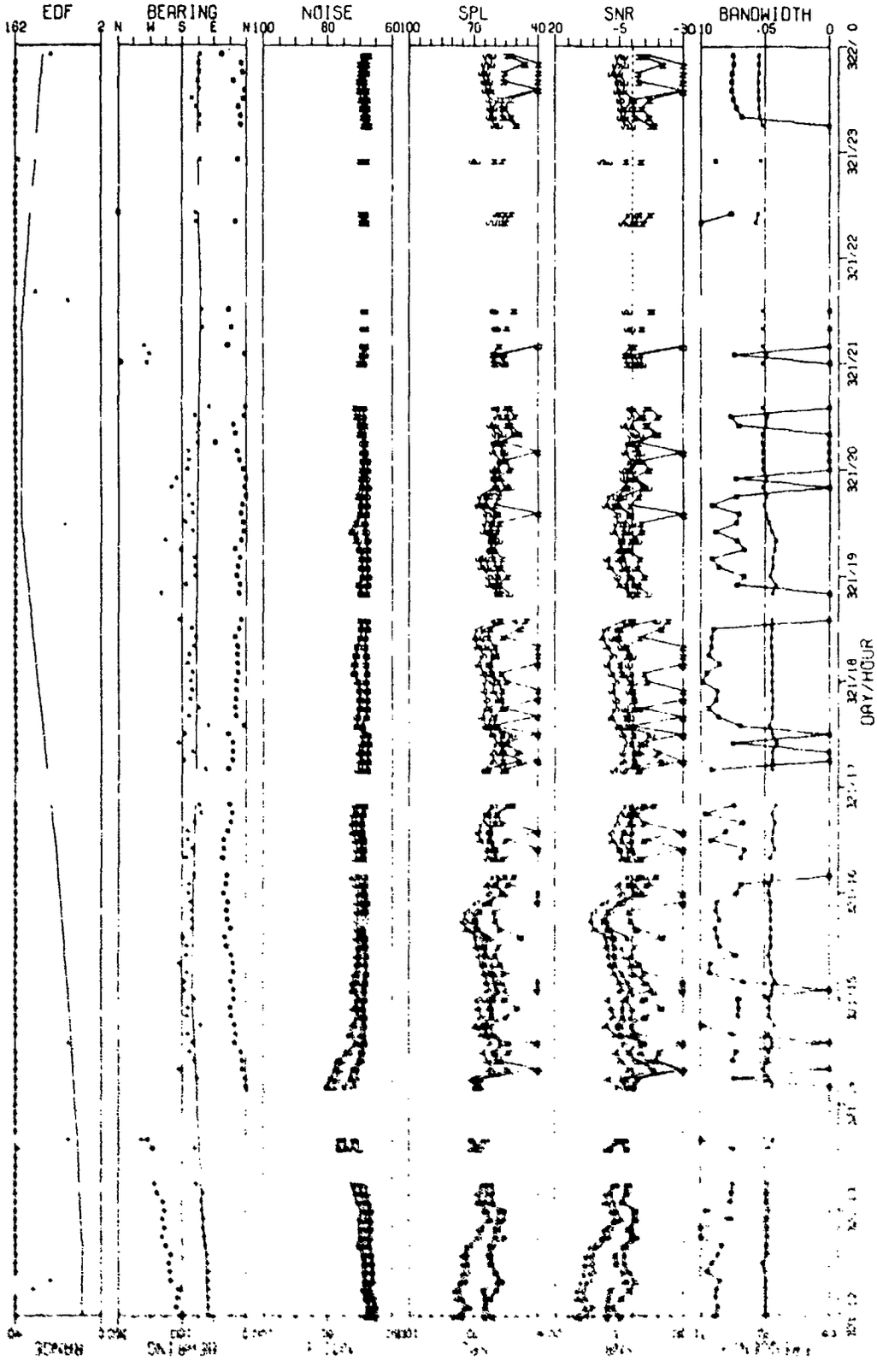

FIGURE 11-47
...LINE MISSION AS OBSERVED VIA THE DIFFERENCED CARDIOIDS SENSOR
...SITE AT DURING THE 17 NOV FIELD EVENT WITH STANDARD RESOLUTION (U)

AS-77-2974

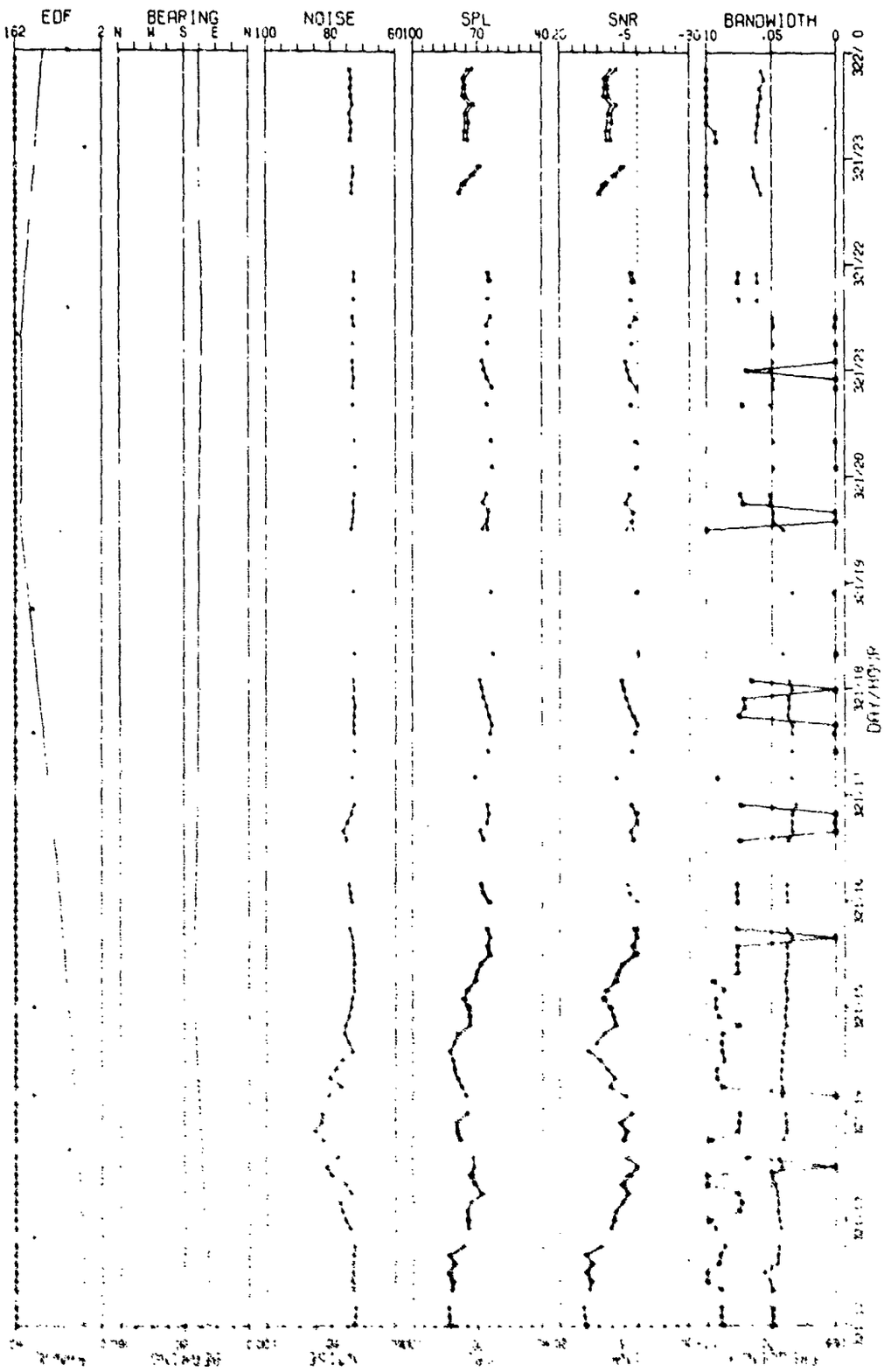

FIGURE 11 OF
OBSERVED AIM THE OMNIDIRECTIONAL SENSOR
FIELD EVENT WITH STANDARD RESOLUTION (UI

AS-77-2975

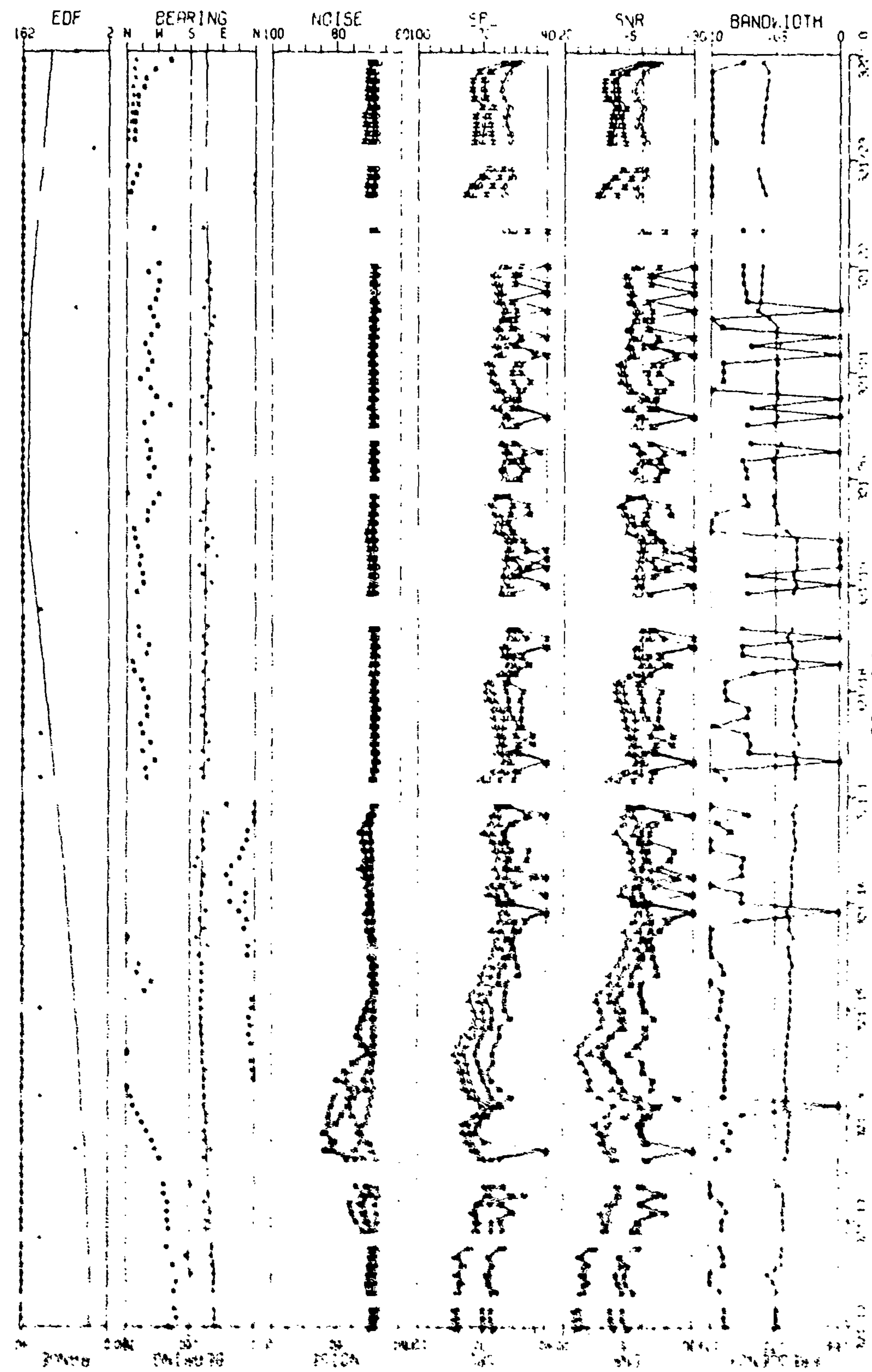

FIGURE 11 [illegible] HISTORY [illegible] OBSERVED [illegible] THE SINGLE CARDIOID SENSOR [illegible] DURING THE 17 NOV FIELD EVENT WITH STANDARD RESOLUTION (U)

AS-77-2976

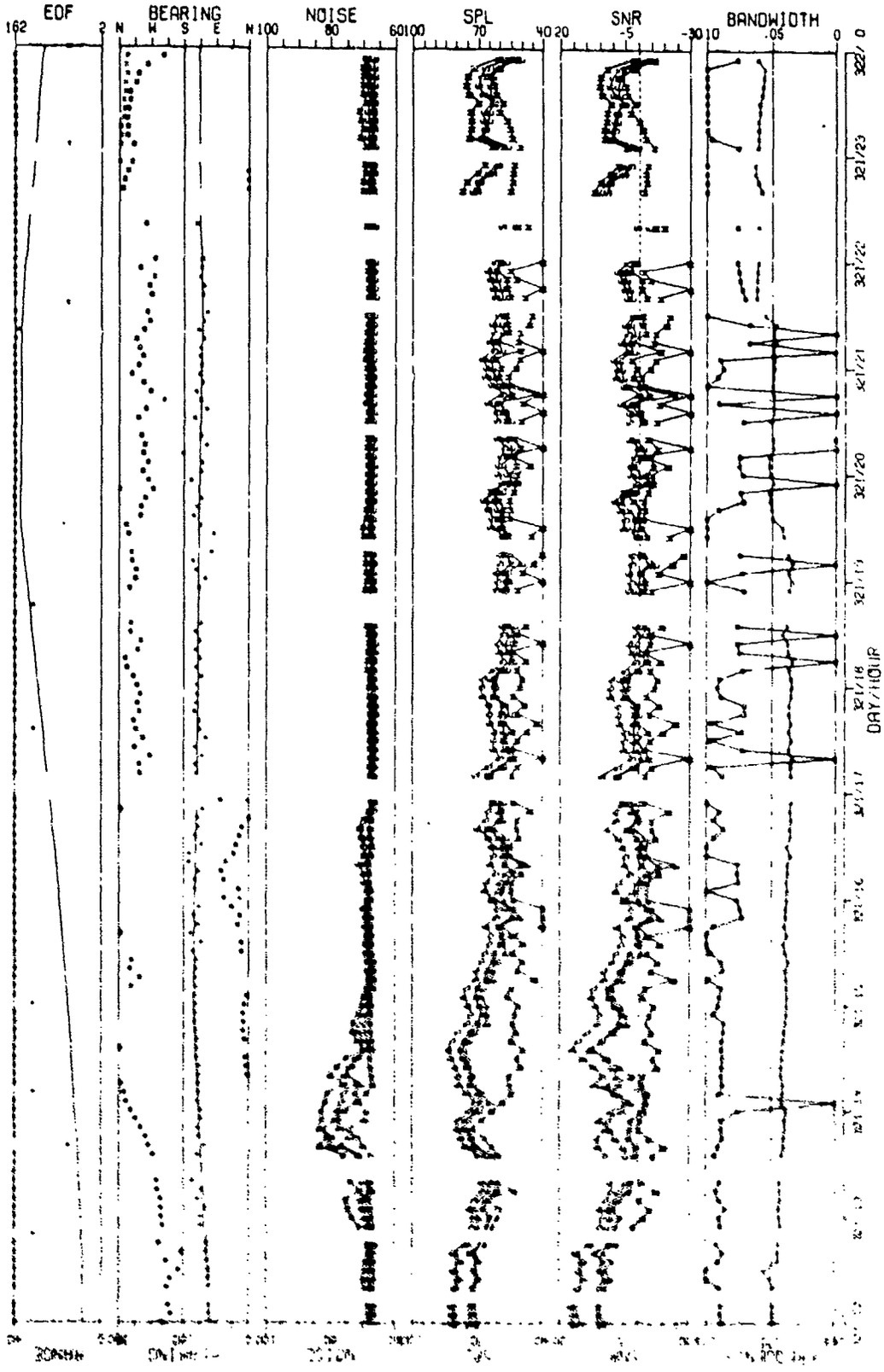

AS-77-2977

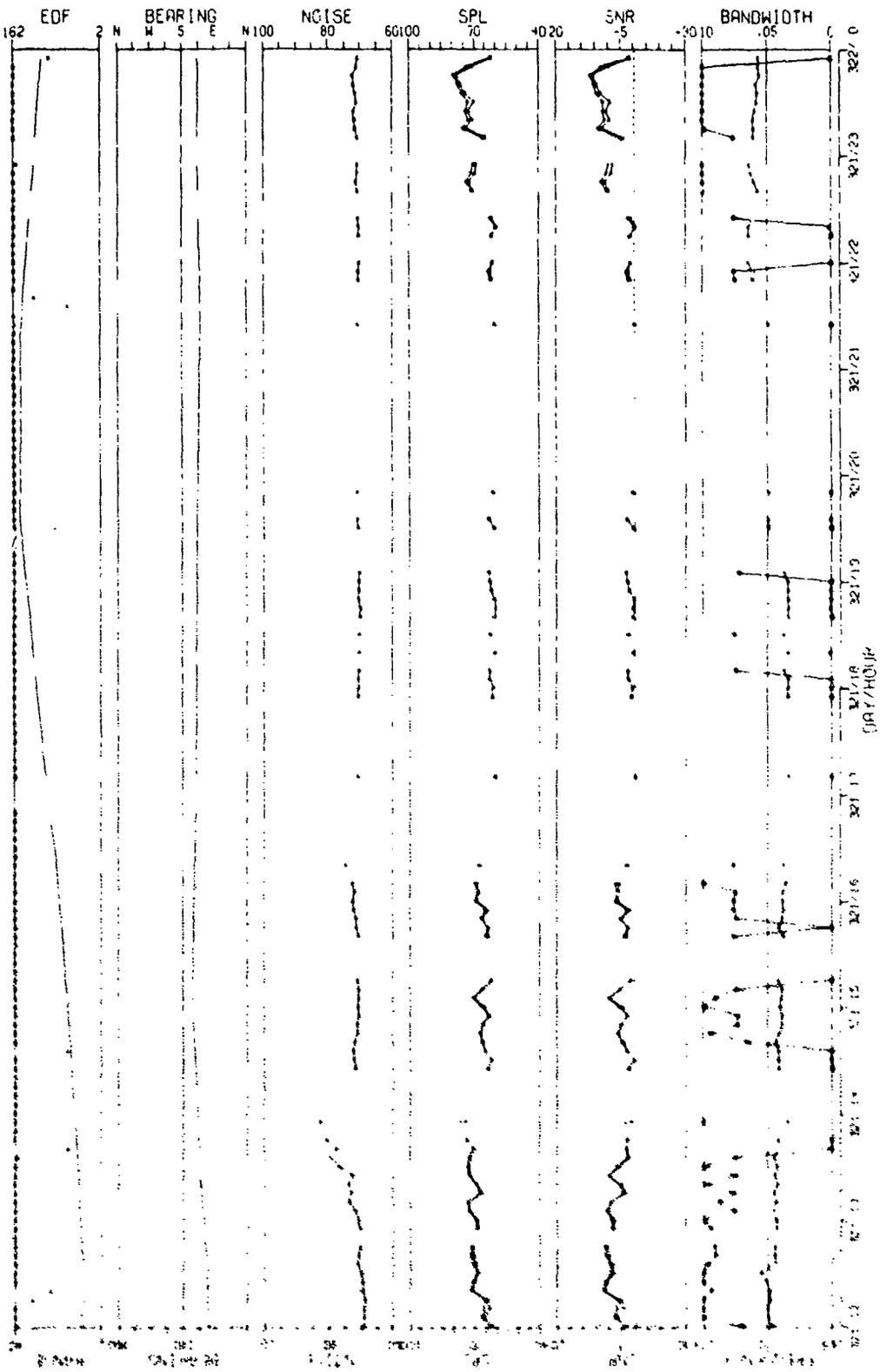
EDF
162
2
BEARING
N
W
S
E
N
NOISE
100
80
60
SPL
100
70
40
SNR
20
-5
-30
BANDWIDTH
10
.05
0
322/0
321/23
321/22
321/21
321/20
321/19
321/18
321/16
DAY/HOUR

AS-77-2978

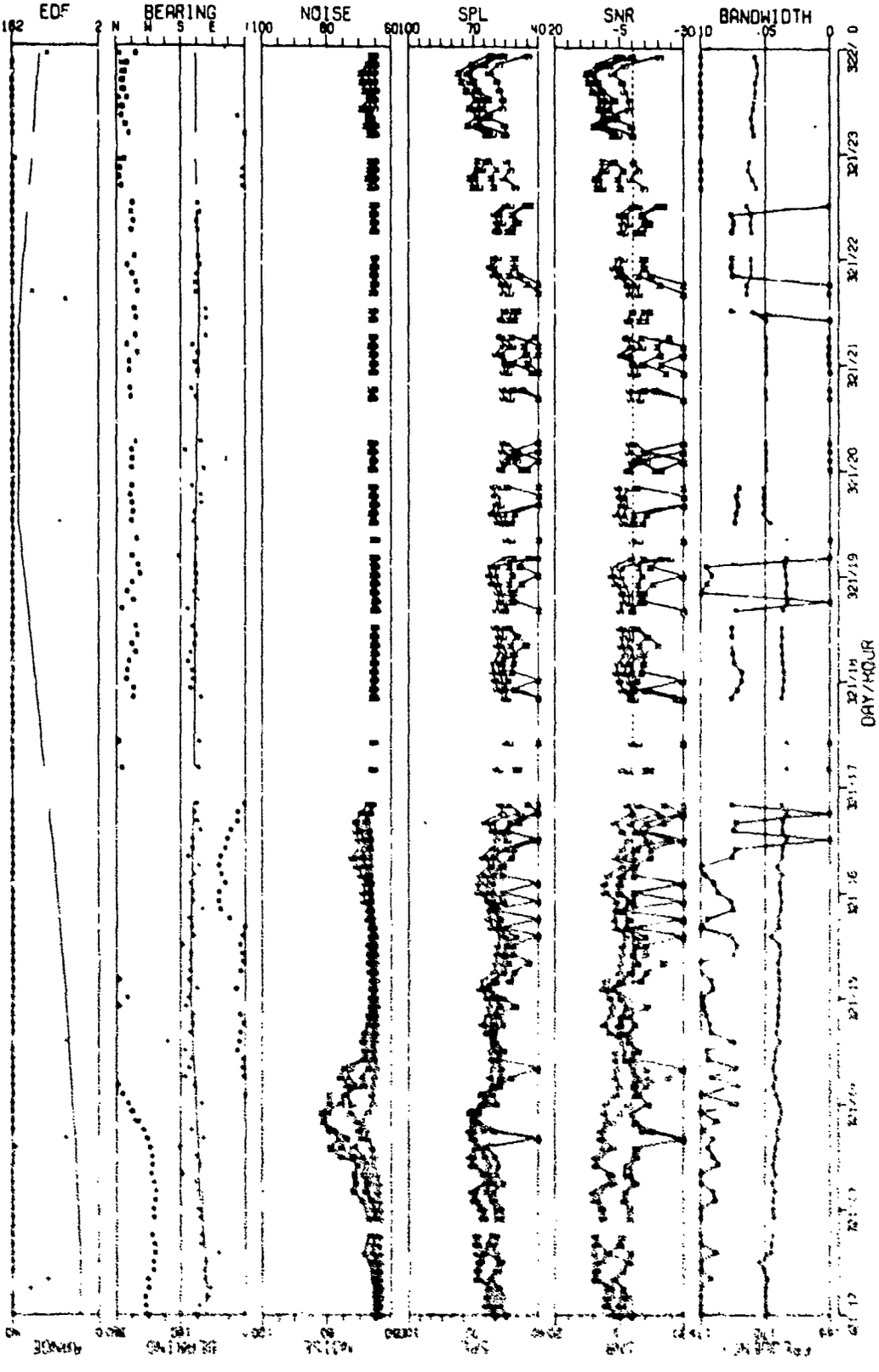

FIGURE 11-52
[illegible] LINE HIS. ORY AS OBSERVED VIA THE DIFFERENCED CARDIOIDS SENSOR
[illegible] SITE AT DURING THE 17 NOV FIELD EVENT WITH STANDARD RESOLUTION (U)

AS-77-2979

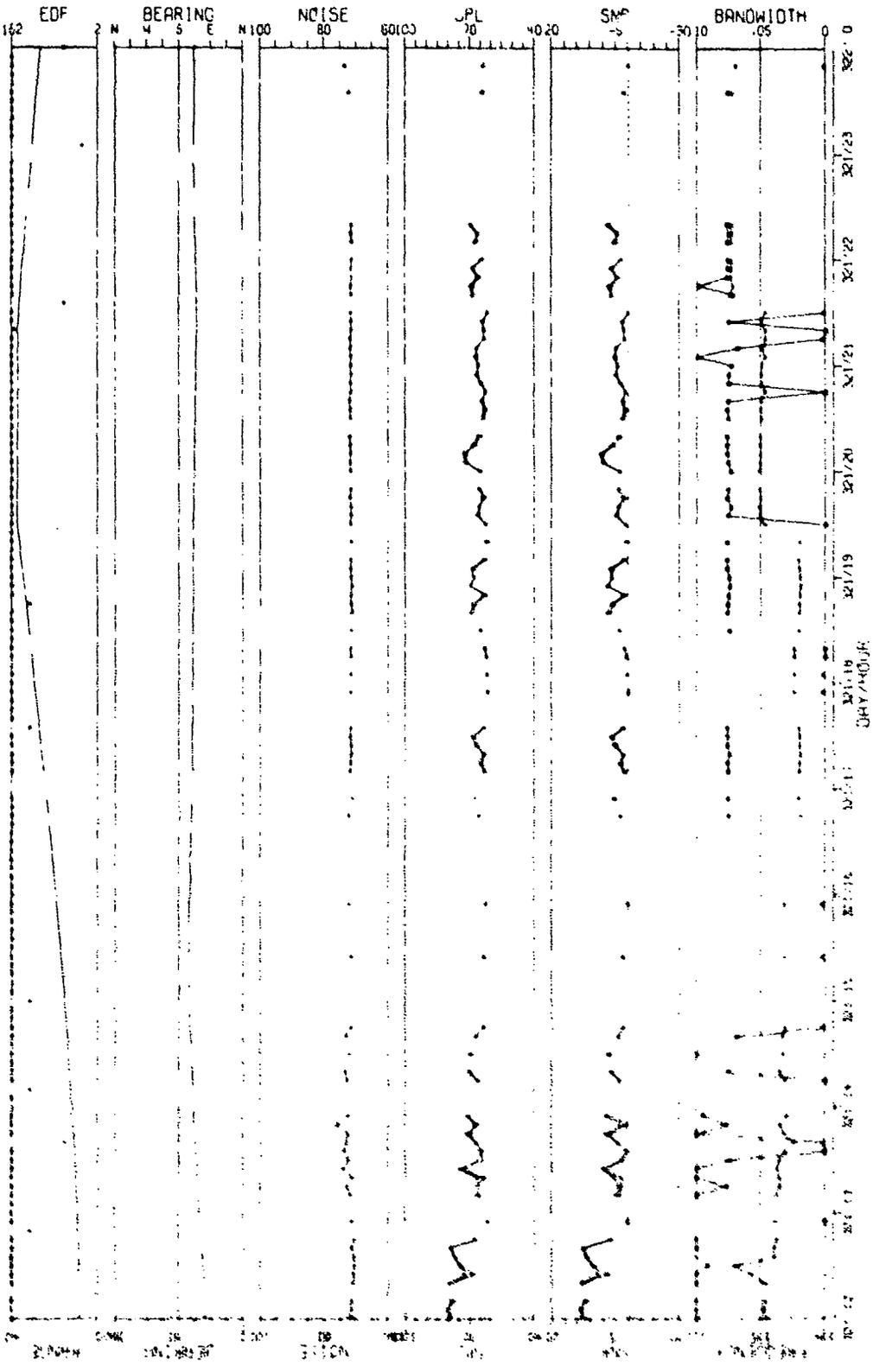

AS-77-2980

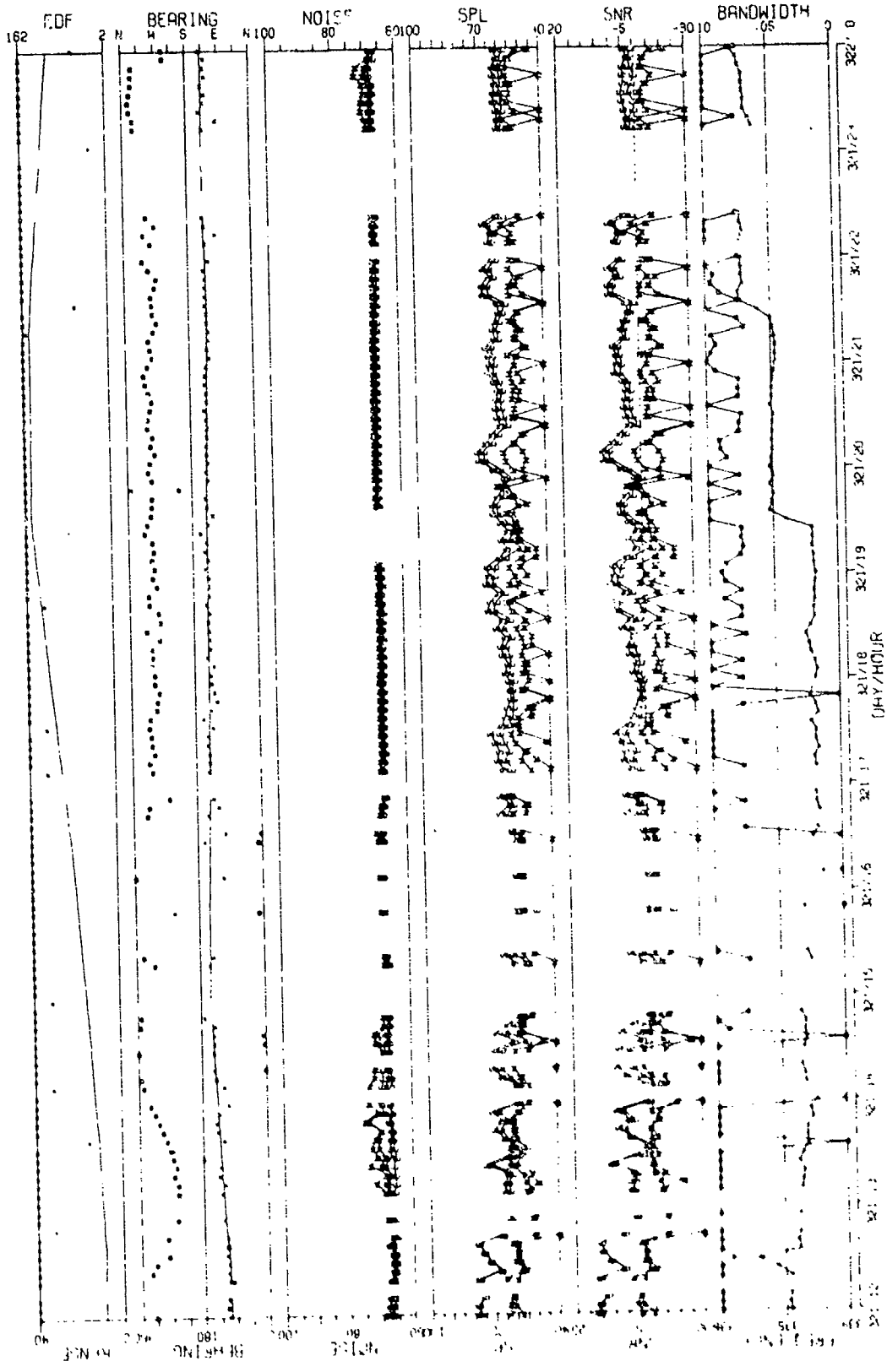

AS-77-2981

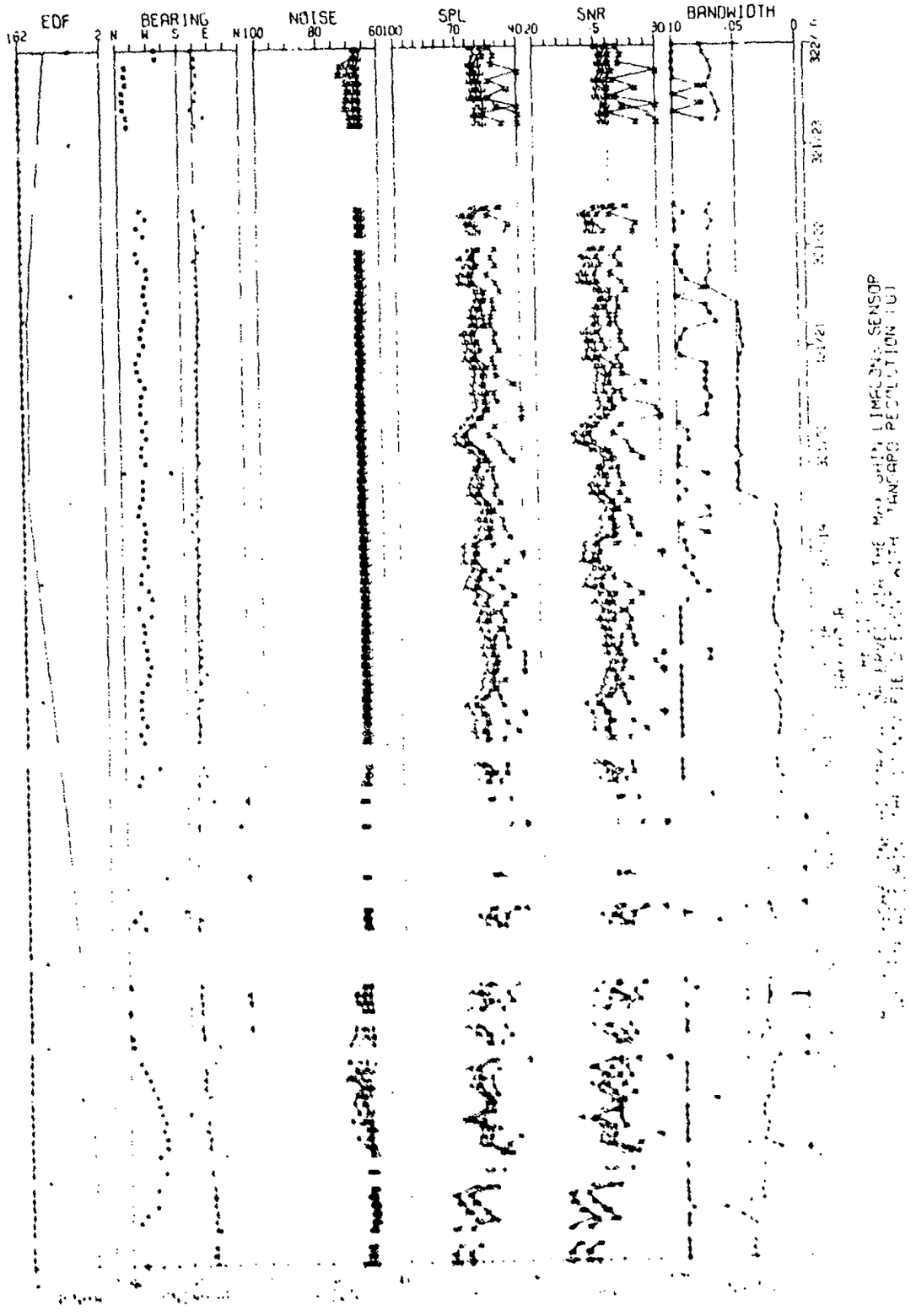

AS-77-2982

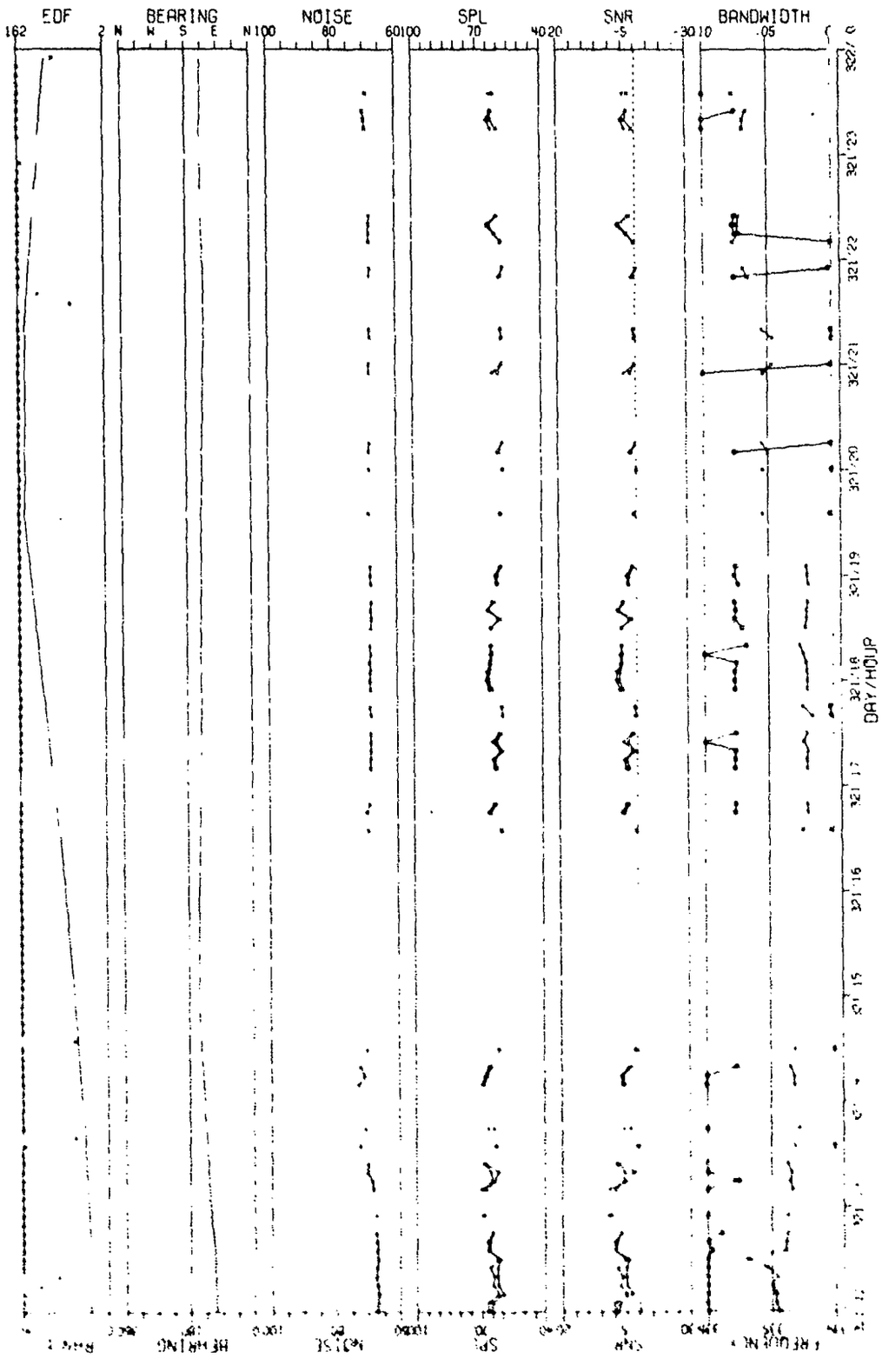

FIGURE II-56
[illegible] LINE HISTORY AS OBSERVED VIA THE VERTICAL DIPOLE SENSOR
[illegible] THE 17 NOV FIELD EVENT WITH STANDARD RESOLUTION (U)

AS-77-2983

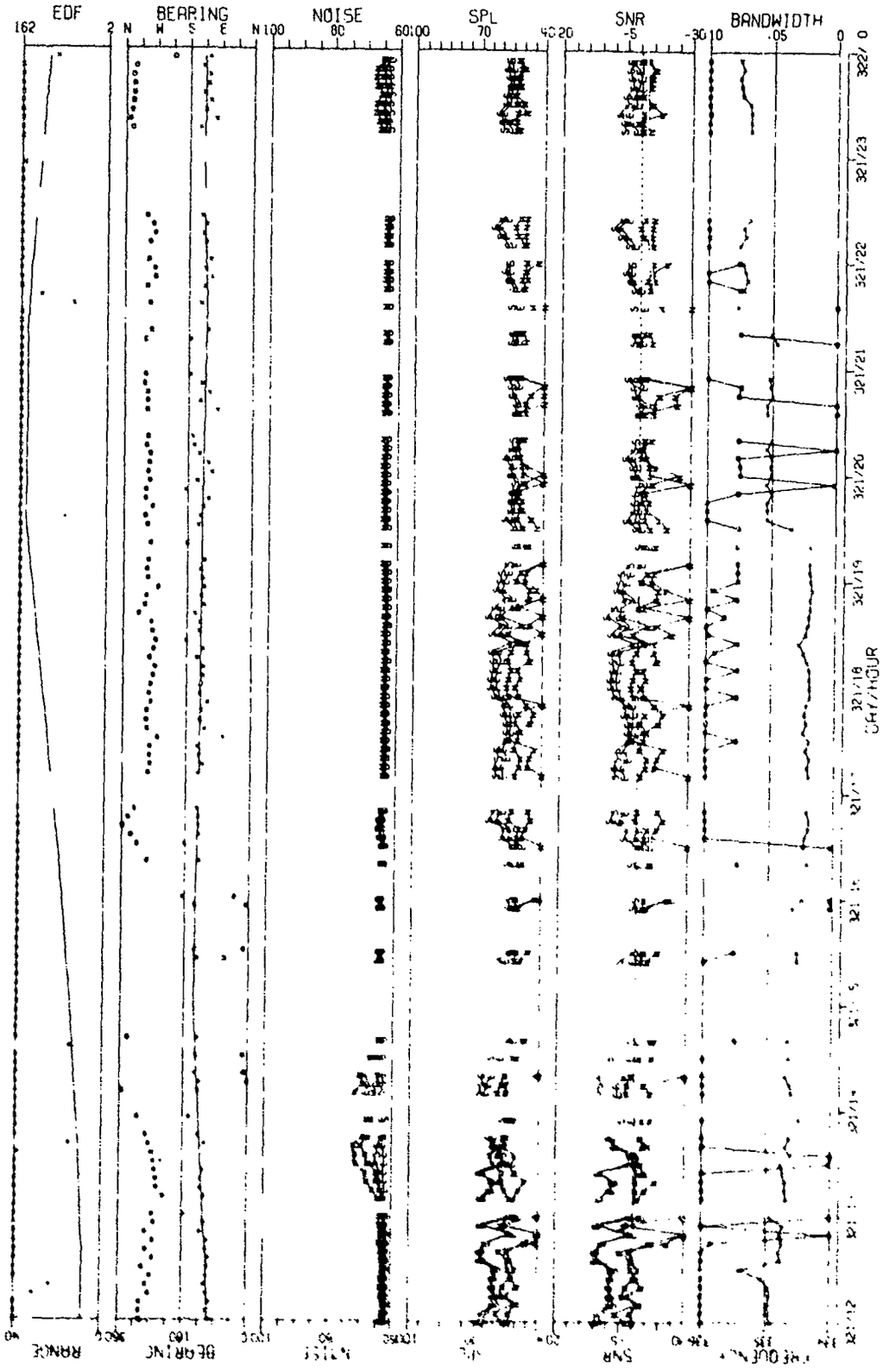

FIGURE II-57
MSS-F-F 325HZ LINE HISTORY AS OBSERVED VIA THE DIFFERENCED CARDIOIDS SENSOR
DURING THE 17 NOV FIELD EVENT WITH STANDARD RESOLUTION (U)

AS-77-2984

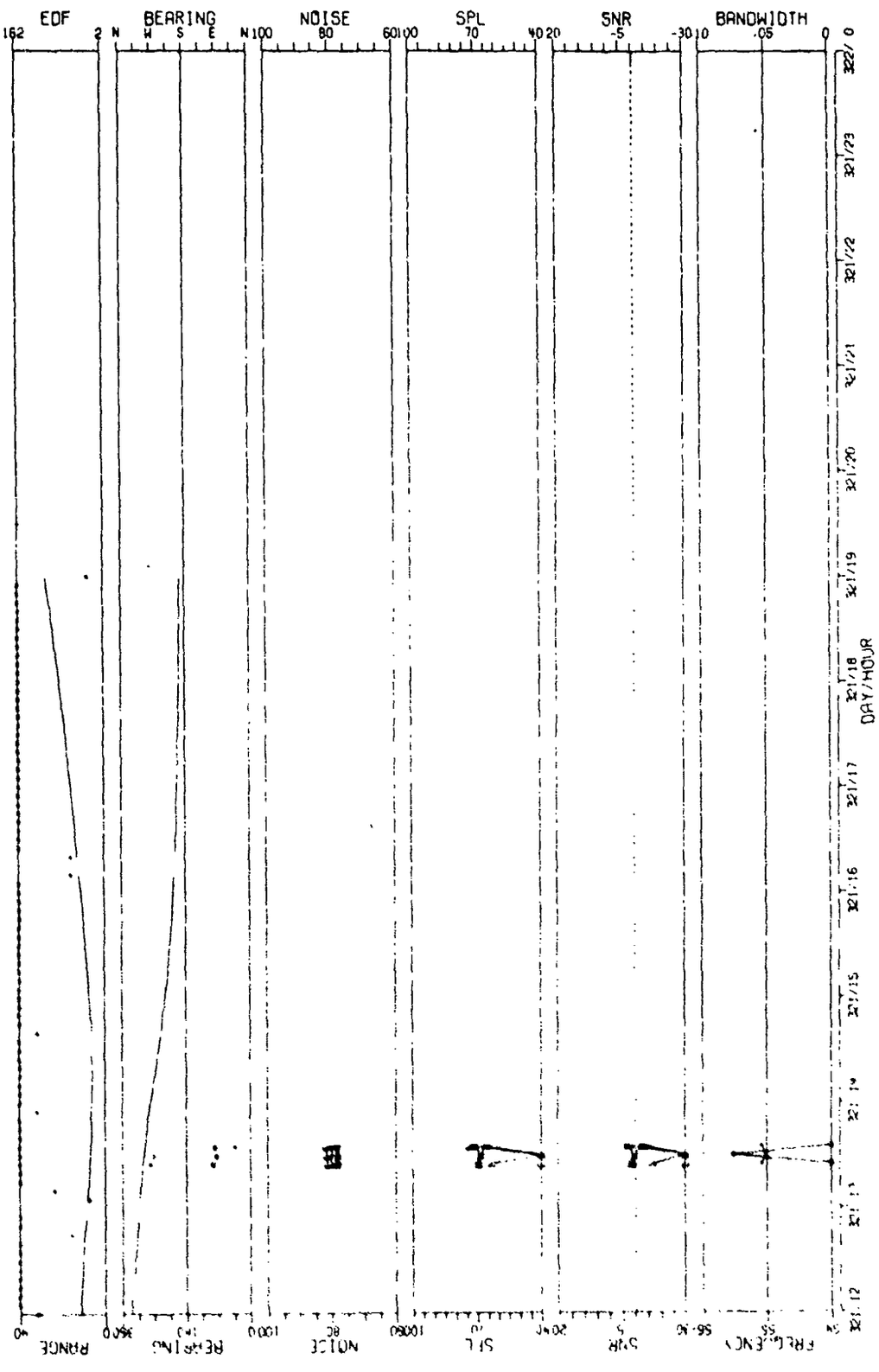

FIGURE 11-59
OBSERVED AIR THE SINGLE CHANNEL SENSOR
THE 17 NOV FIELD EVENT WITH STANDARD RESOLUTION (U)

AS-77-2985

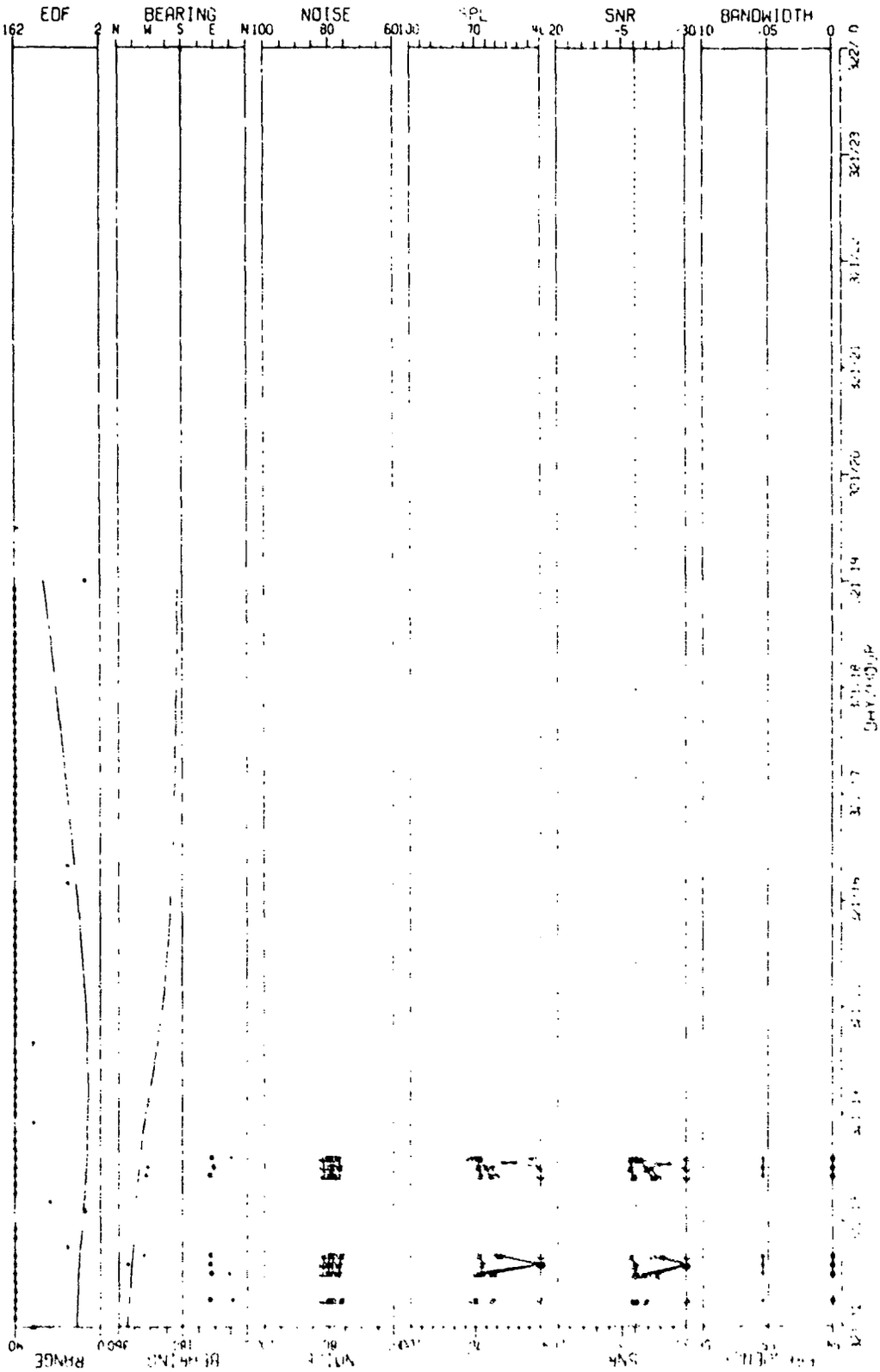
EOF
BEARING
NOISE
SNR
BANDWIDTH
162
2
N
W
S
E
N
100
80
60
30
70
20
-5
-30
10
-05
0

AS-77-2986

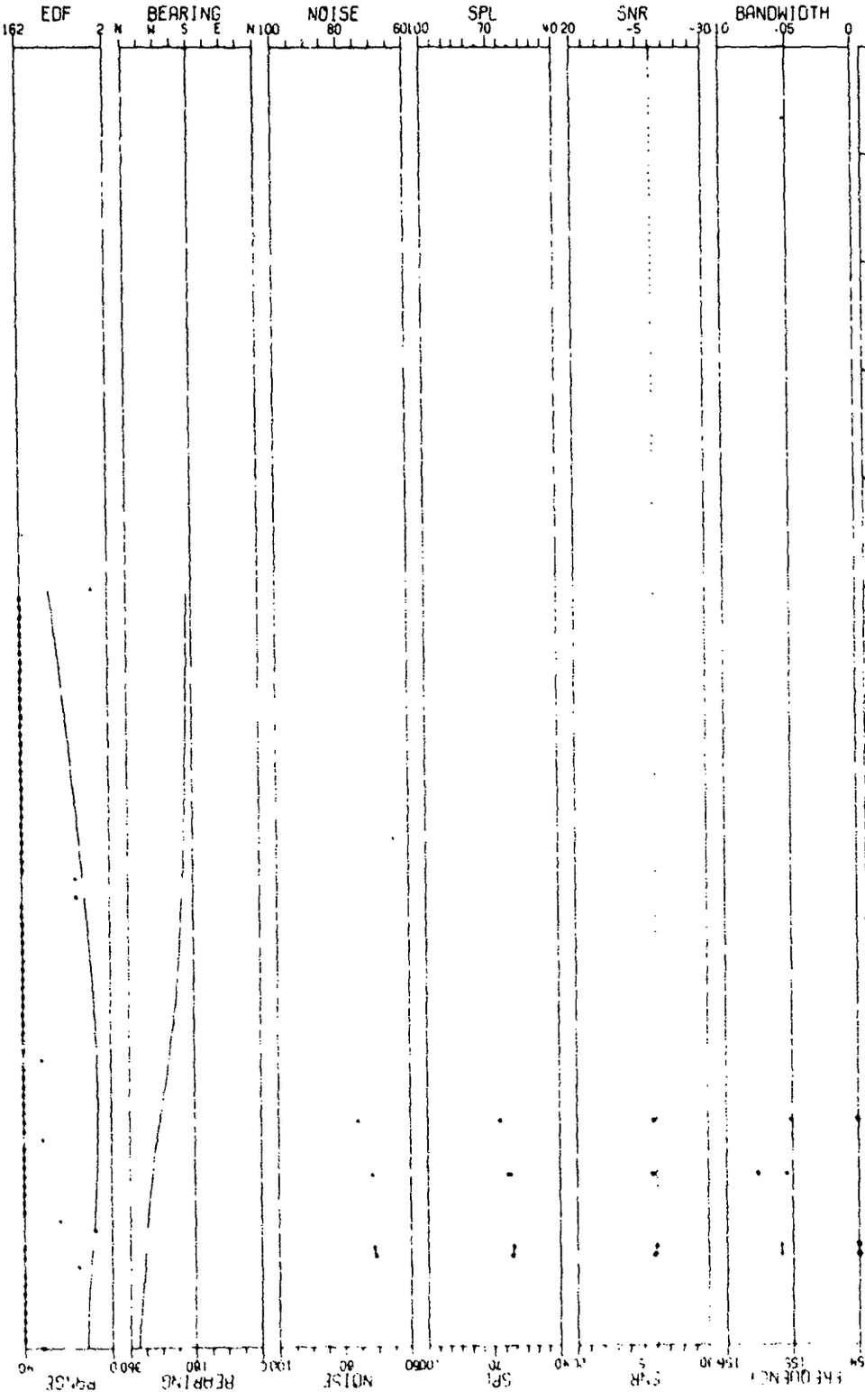

FIGURE 11-60
155-FT 155HZ LINE HISTORY AS OBSERVED VIA THE OMNIDIRECTIONAL SENSOR
AT SITE A2 DURING THE 17 NOV FIELD EVENT WITH STANDARD RESOLUTION FFT

AS-77-2987

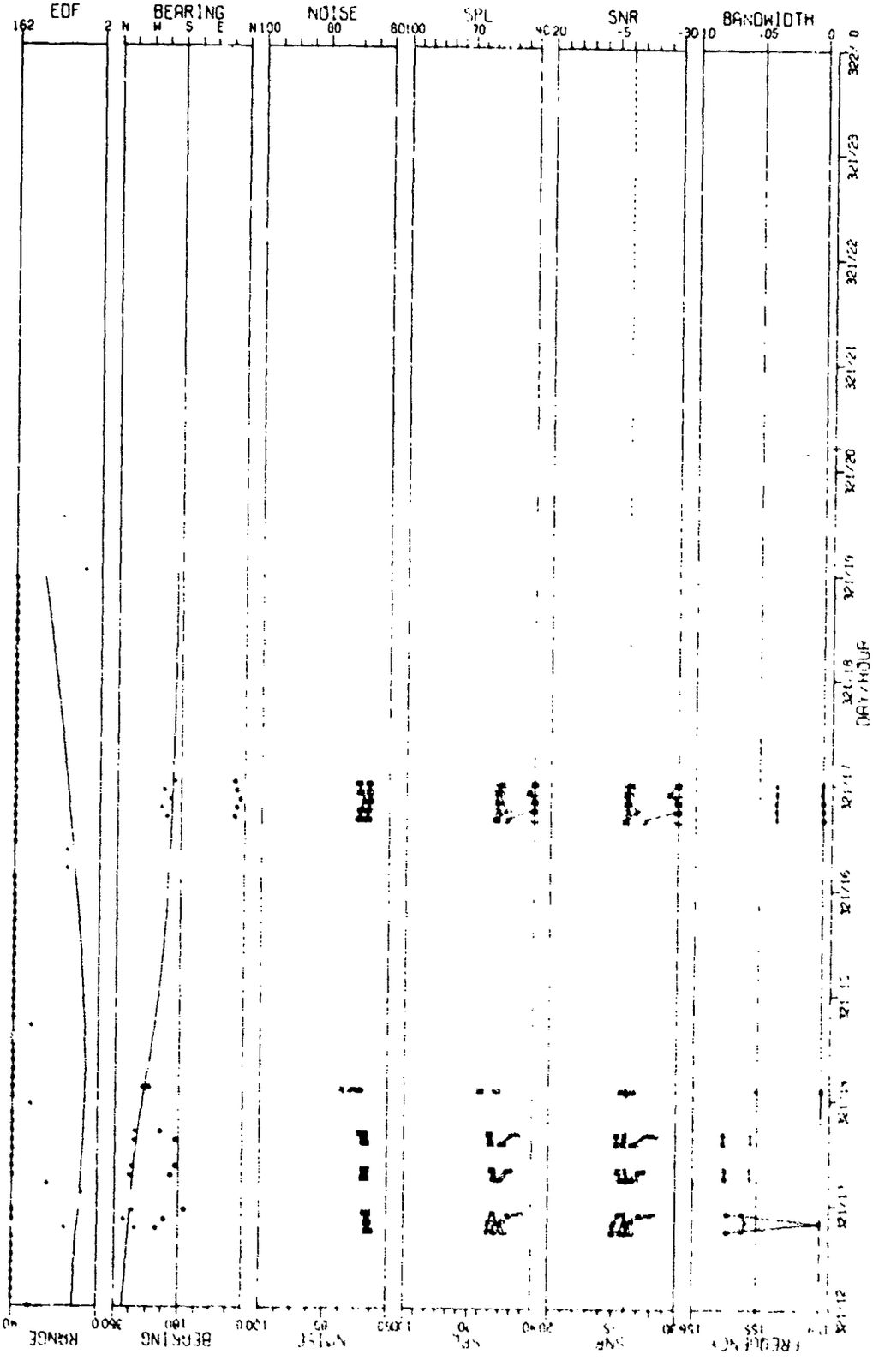

FIGURE II-61
155HZ LINE HISTORY AS OBSERVED VIA THE SINGLE CARDIOIDS SENSOR
AT SITE A2 DURING THE 17 NOV FIELD EVENT WITH STANDARD RESOLUTION (U)

AS-77-2988

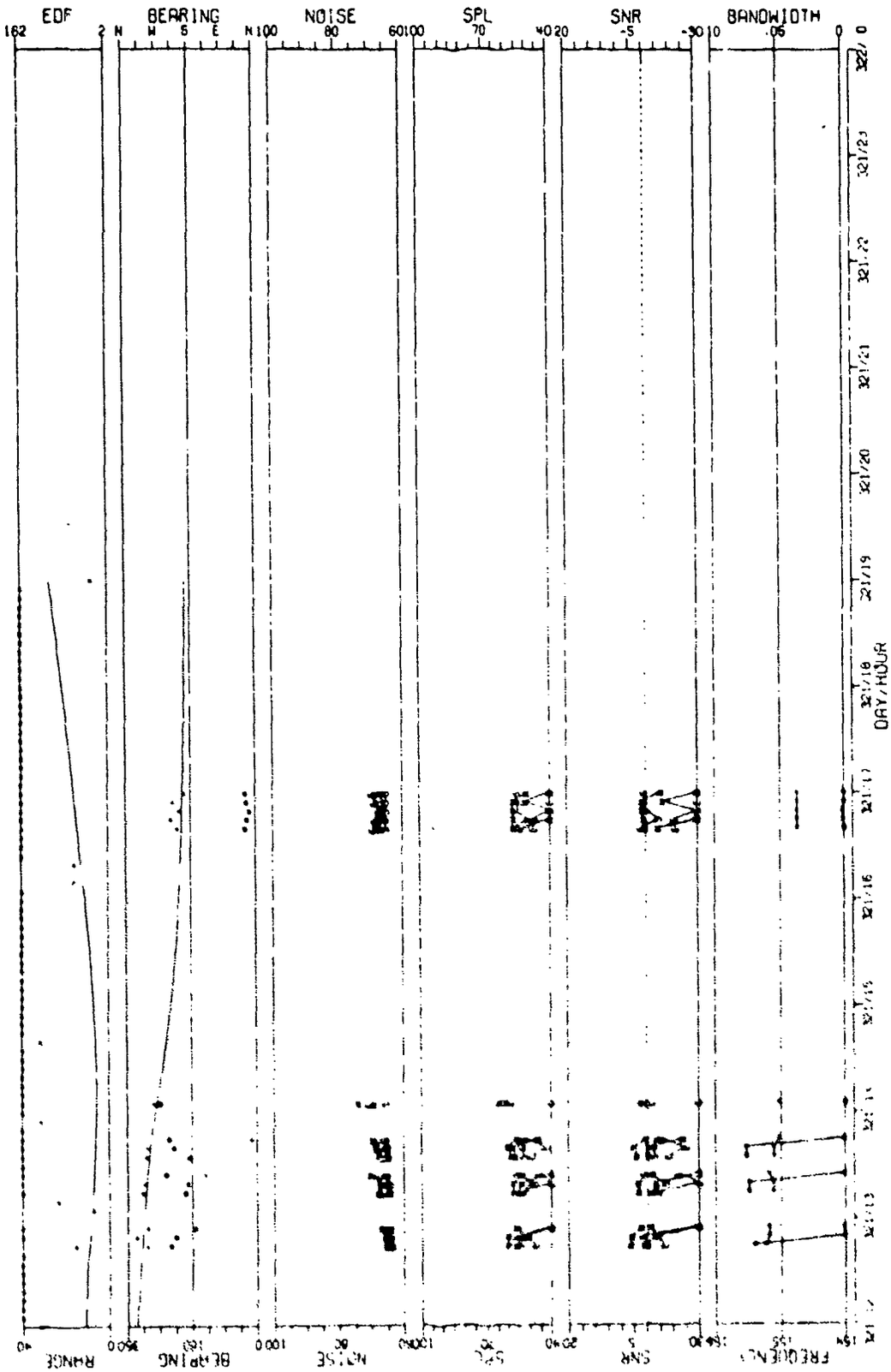

FIGURE 11-62
[illegible] 155HZ LINE HISTORY AS OBSERVED VIA THE MAX GAIN LIMACONS SENSOR
[illegible] SITE AP DURING THE 17 NOV FIELD EVENT WITH STANDARD RESOLUTION (U)

AS-77-2989

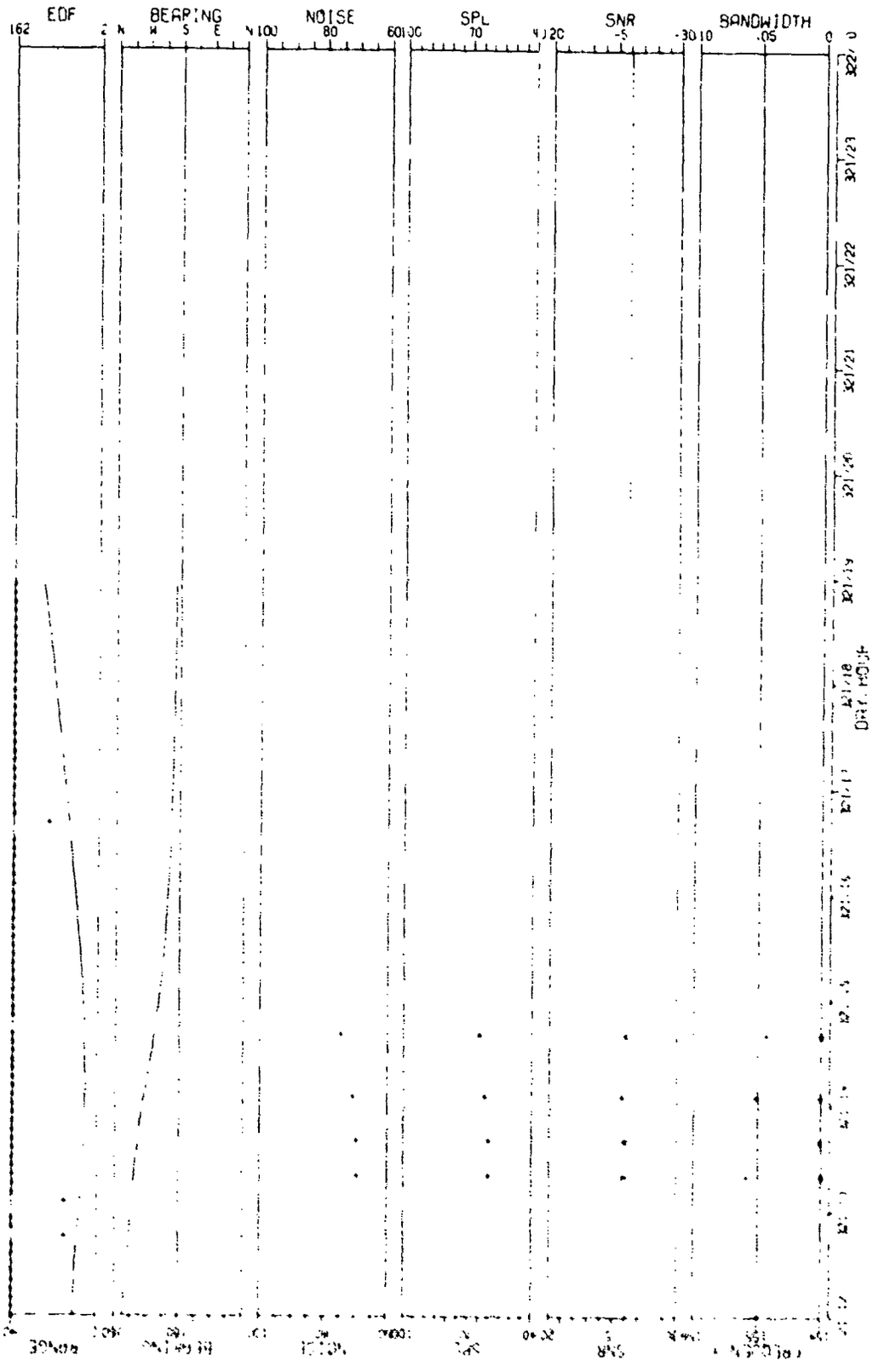

FIGURE 11-63
TRACK LINE HISTORY AS OBSERVED VIA THE VERTICAL DIPOLE SENSOR
AT SITE A2 DURING THE 17 NOV FIELD EVENT WITH STANDARD RESOLUTION (U)

AS-77-2990

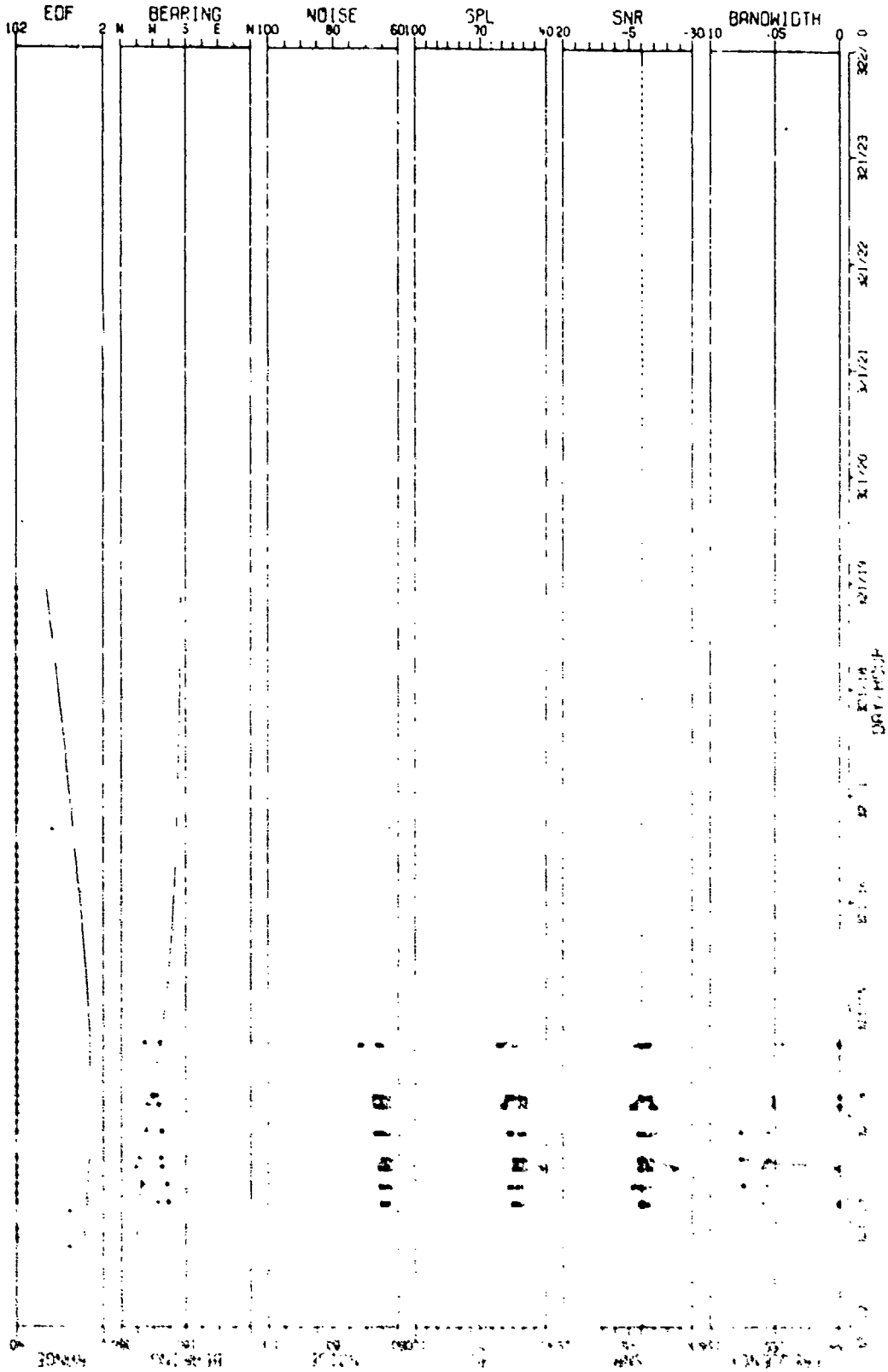
EOF
102
2
BEARING
N
W
S
E
N
NOISE
100
80
60
SPL
100
70
40
SNR
20
-5
-30
BANDWIDTH
10
.05
0

AS-77-2991

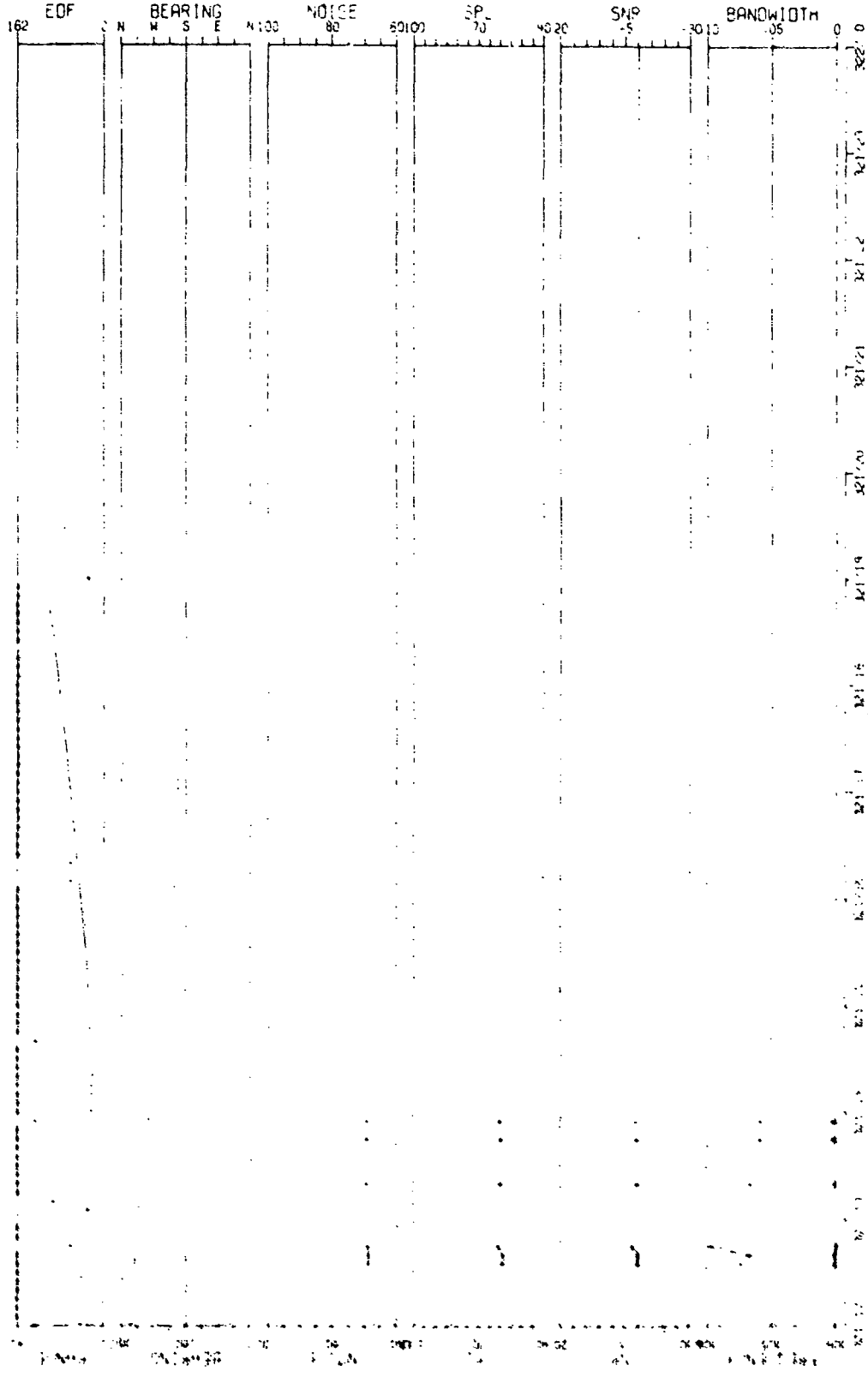
EOF
162
BEARING
N W S E N
NOISE
100 80 60
SP
100 70 40
SNR
20 5 -30
BANDWIDTH
15 05 0

AS-77-2952

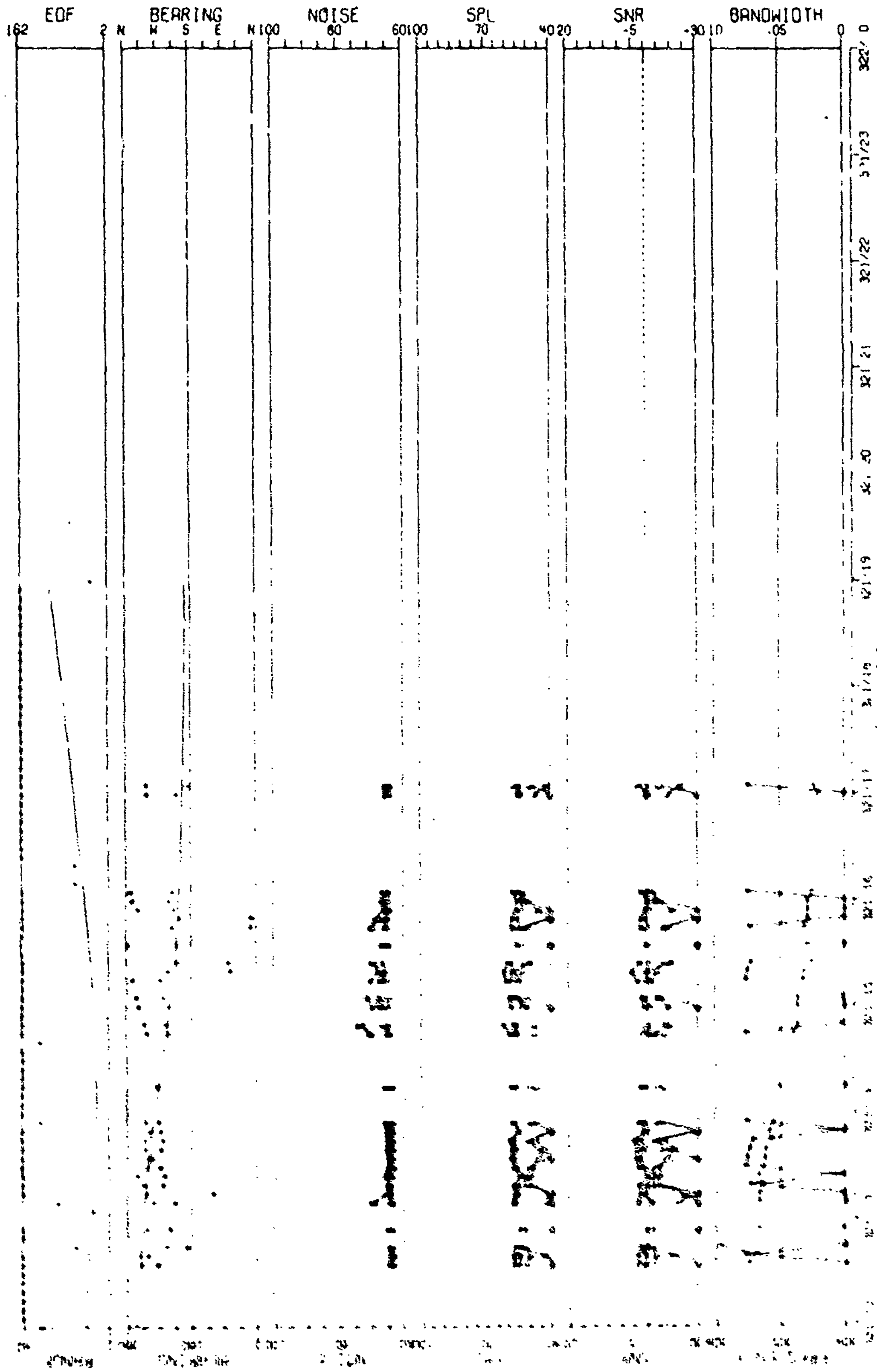

FIGURE 11-66
... HISTORY AS OBSERVED VIA THE SINGLE CARDIOIDS SENSOR
... 17 NOV FIELD EVENT WITH STANDARD RESOLUTION (U)

AS-77-2993

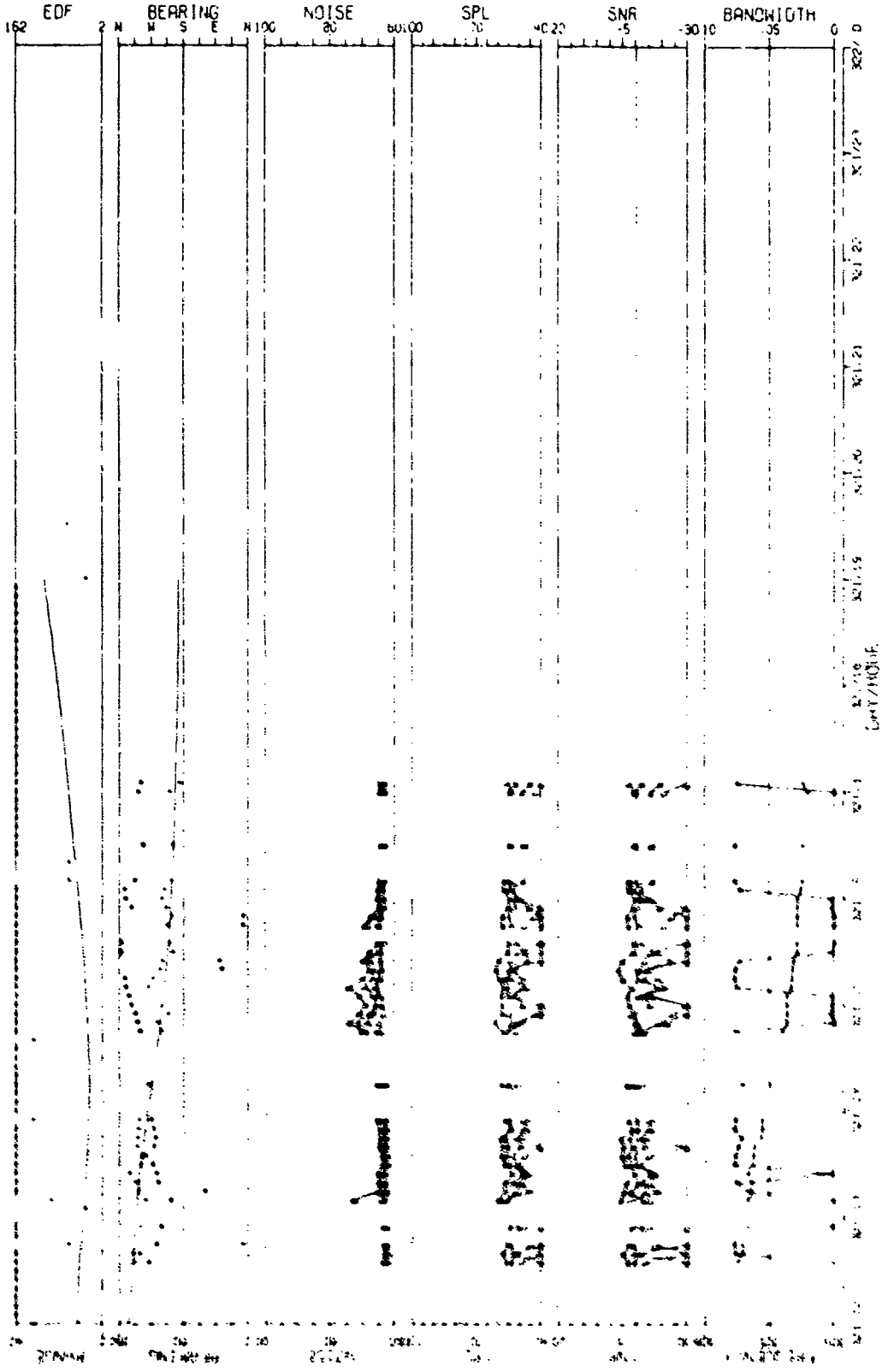

AS-77-2994

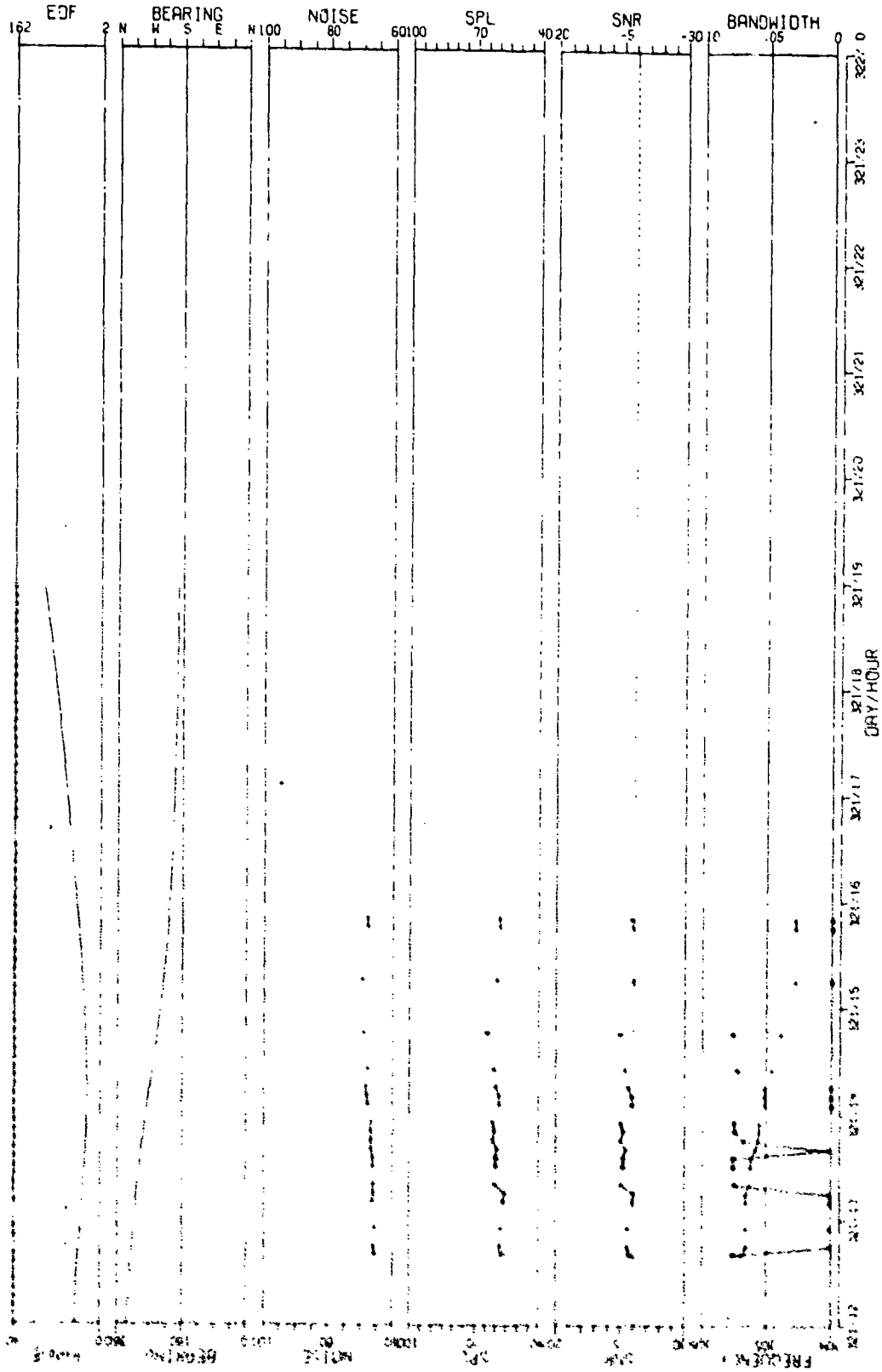

FIGURE 11-65
305HZ LINE HISTORY AS OBSERVED VIA THE VERTICAL DIPOLE SENSOR
A2 DURING THE 13 NOV FIELD EVENT WITH STANDARD RESOLUTION (U)

AS-77-2995

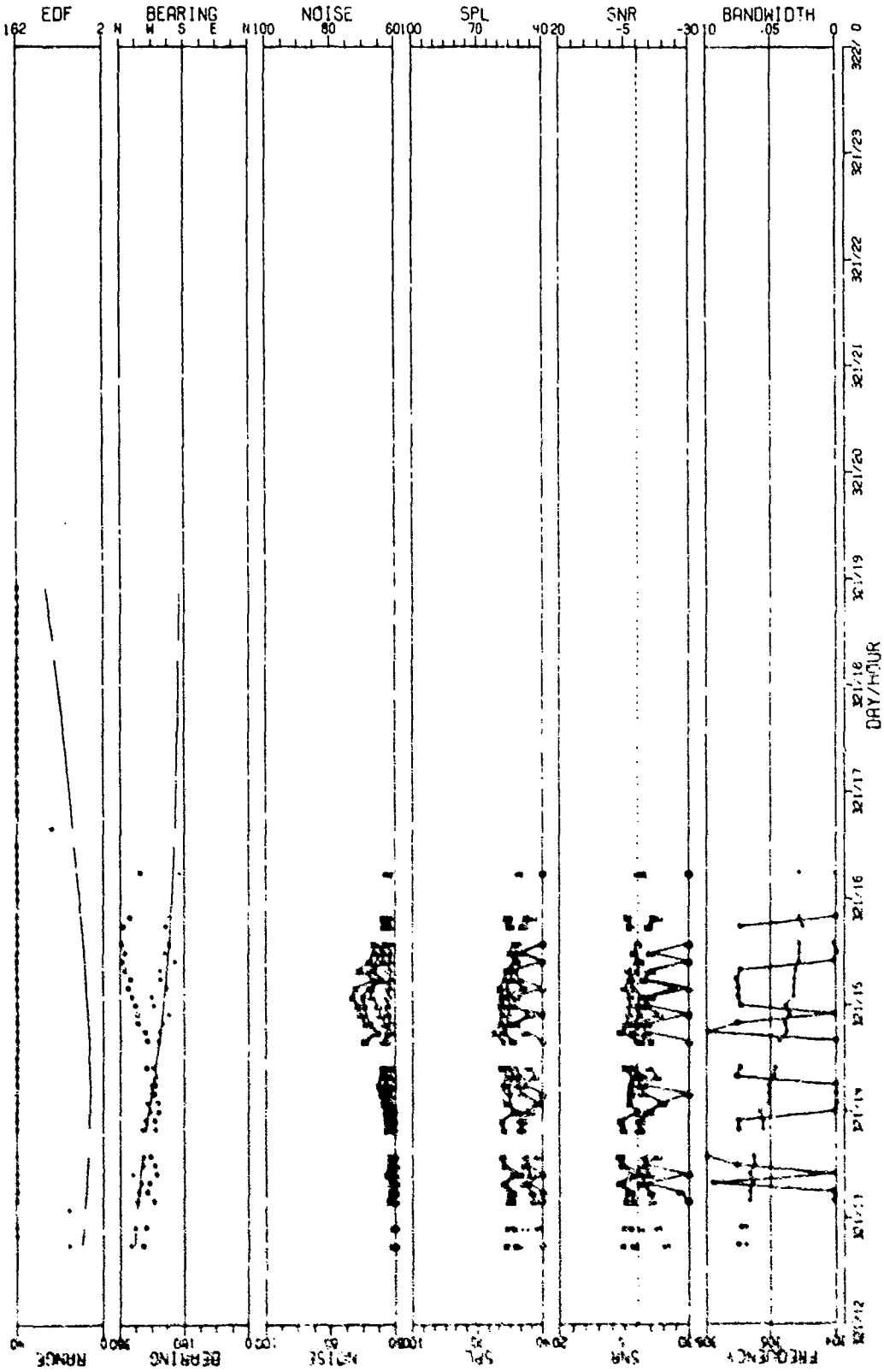

FIGURE II-C)
MSS-FV' 305M2 LINE HISTORY AS OBSERVED VIA THE DIFFERENCED CARDIOIDS SENSOR
AT SITE A2 DURING THE 17 NOV FIELD EVENT WITH STANDARD RESOLUTION (U)

AS-77-2996

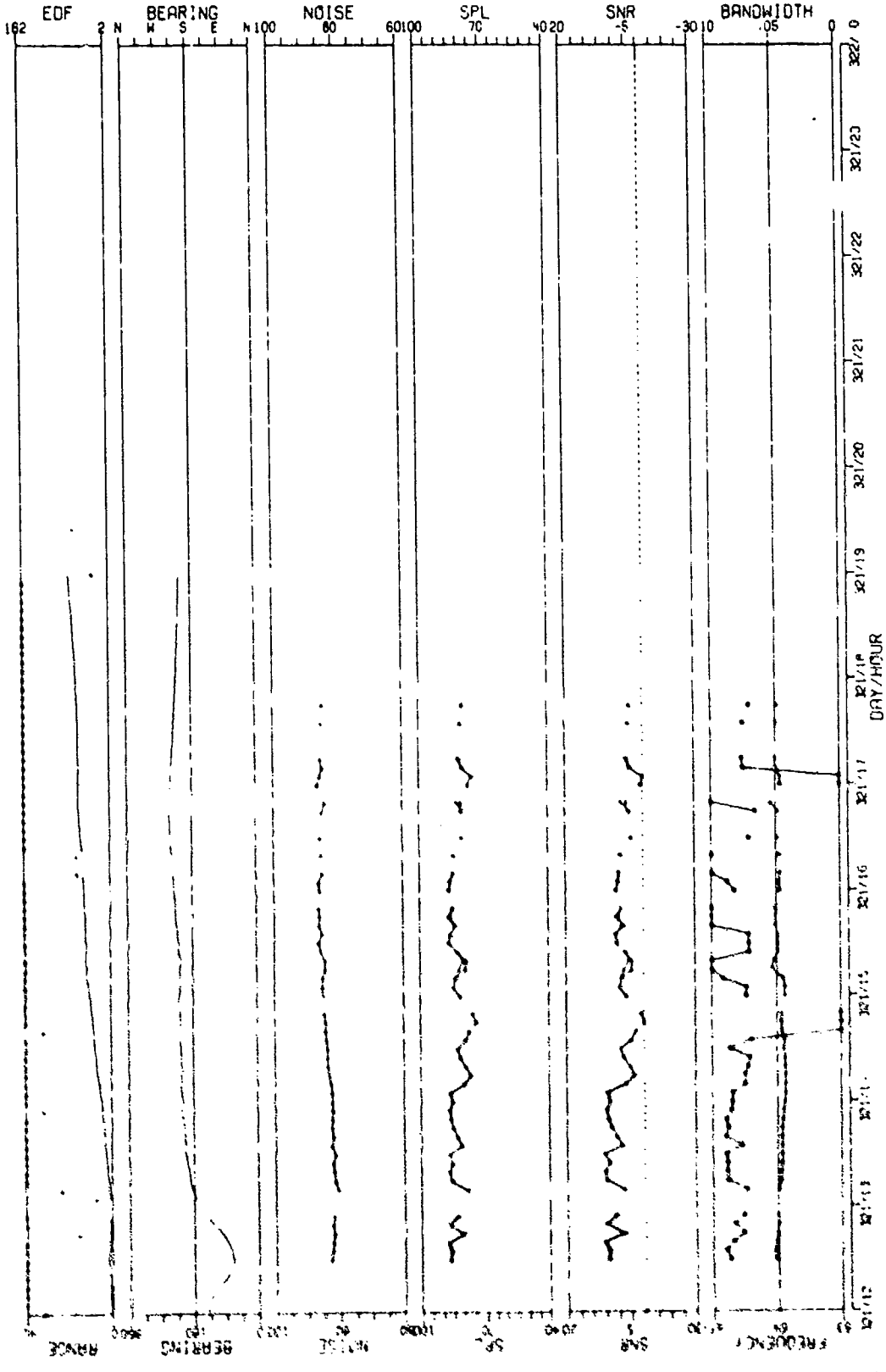

FIGURE II-70
[illegible] LINE HISTORY AS OBSERVED VIA THE OMNIDIRECTIONAL SENSOR
[illegible] THE 17 NOV FIELD EVENT WITH STANDARD RESOLUTION (U)

AS-77-2997

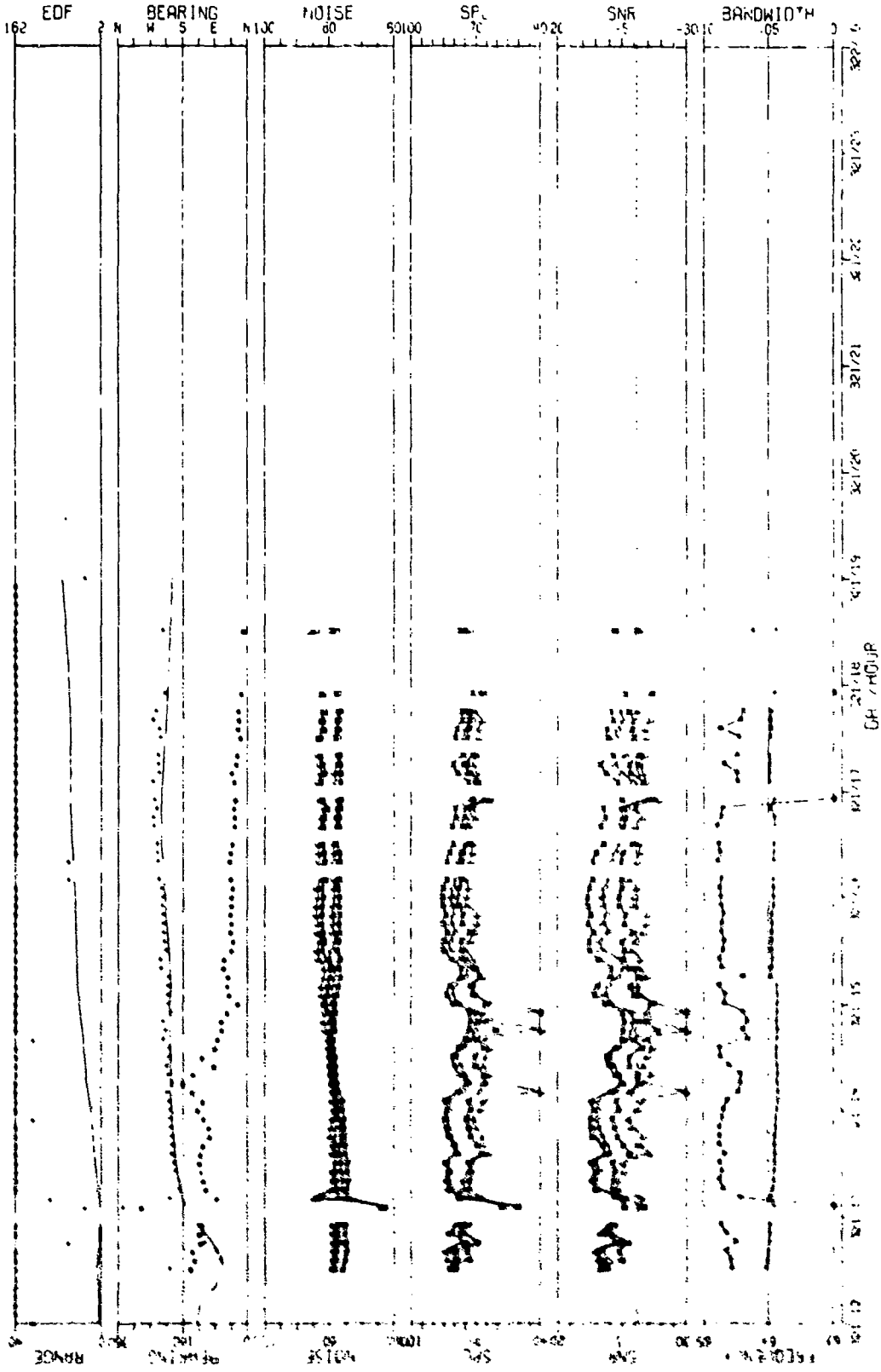

AS-77-2998

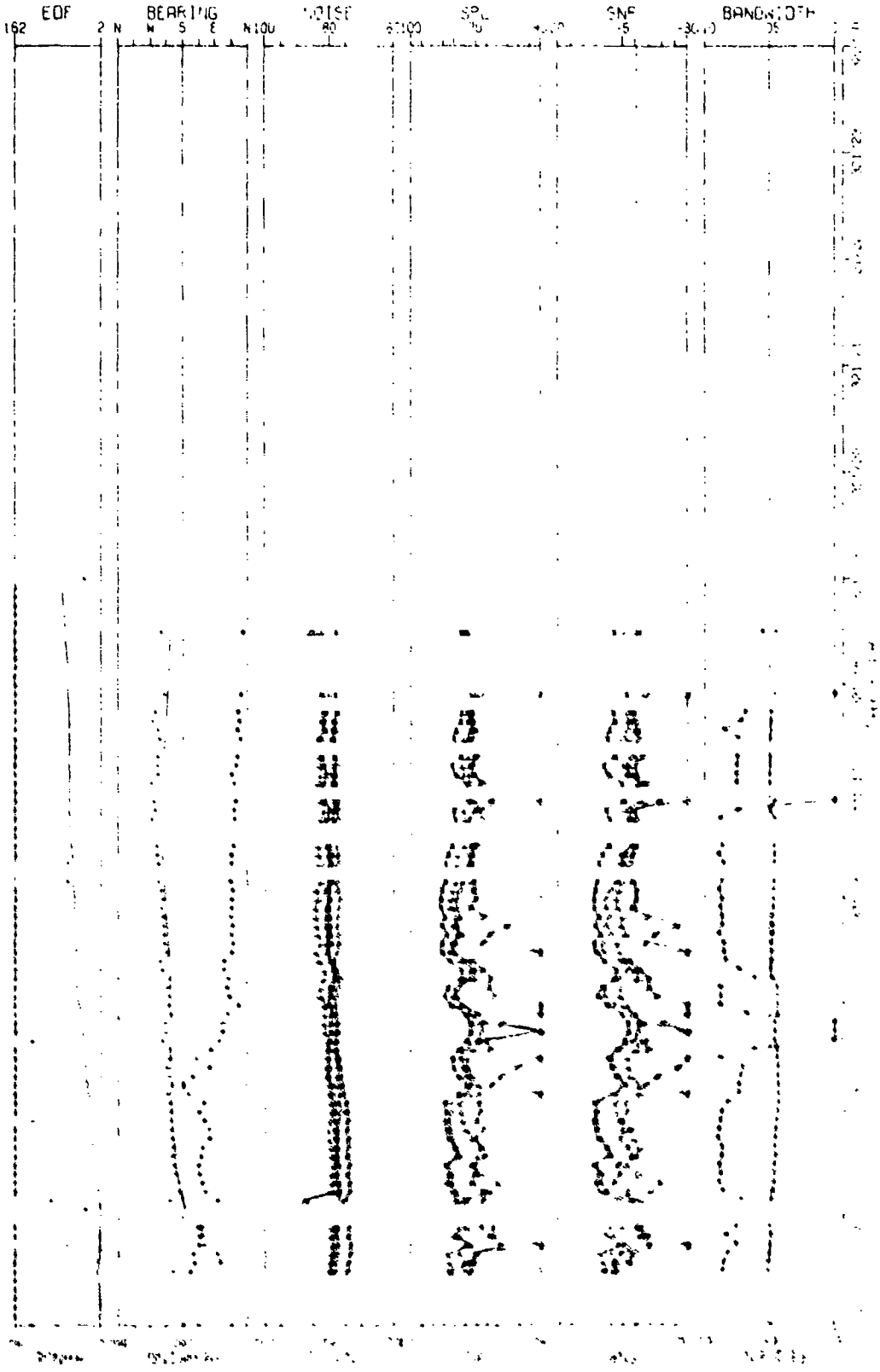

AS-77-2999

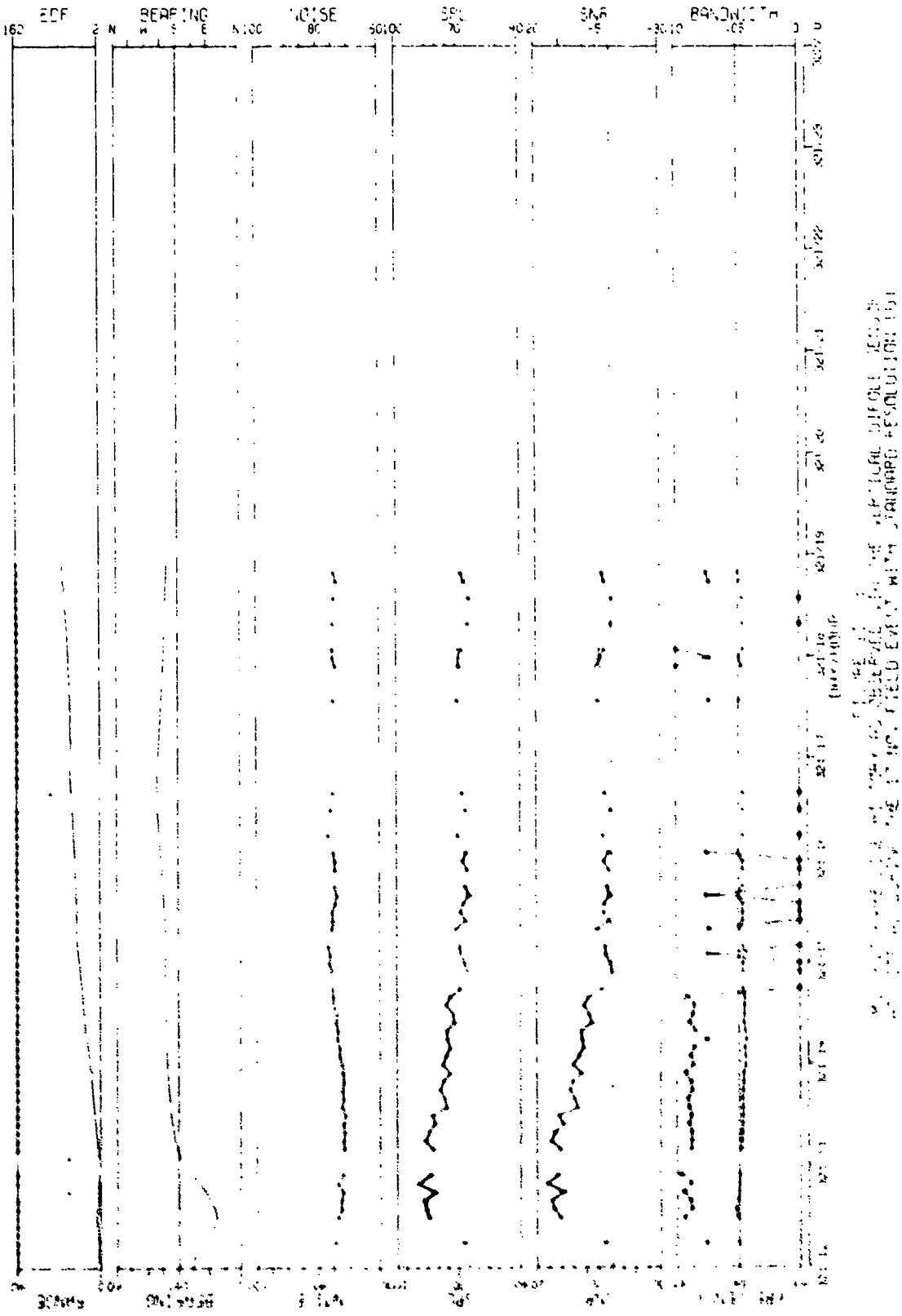

AS-77-3000

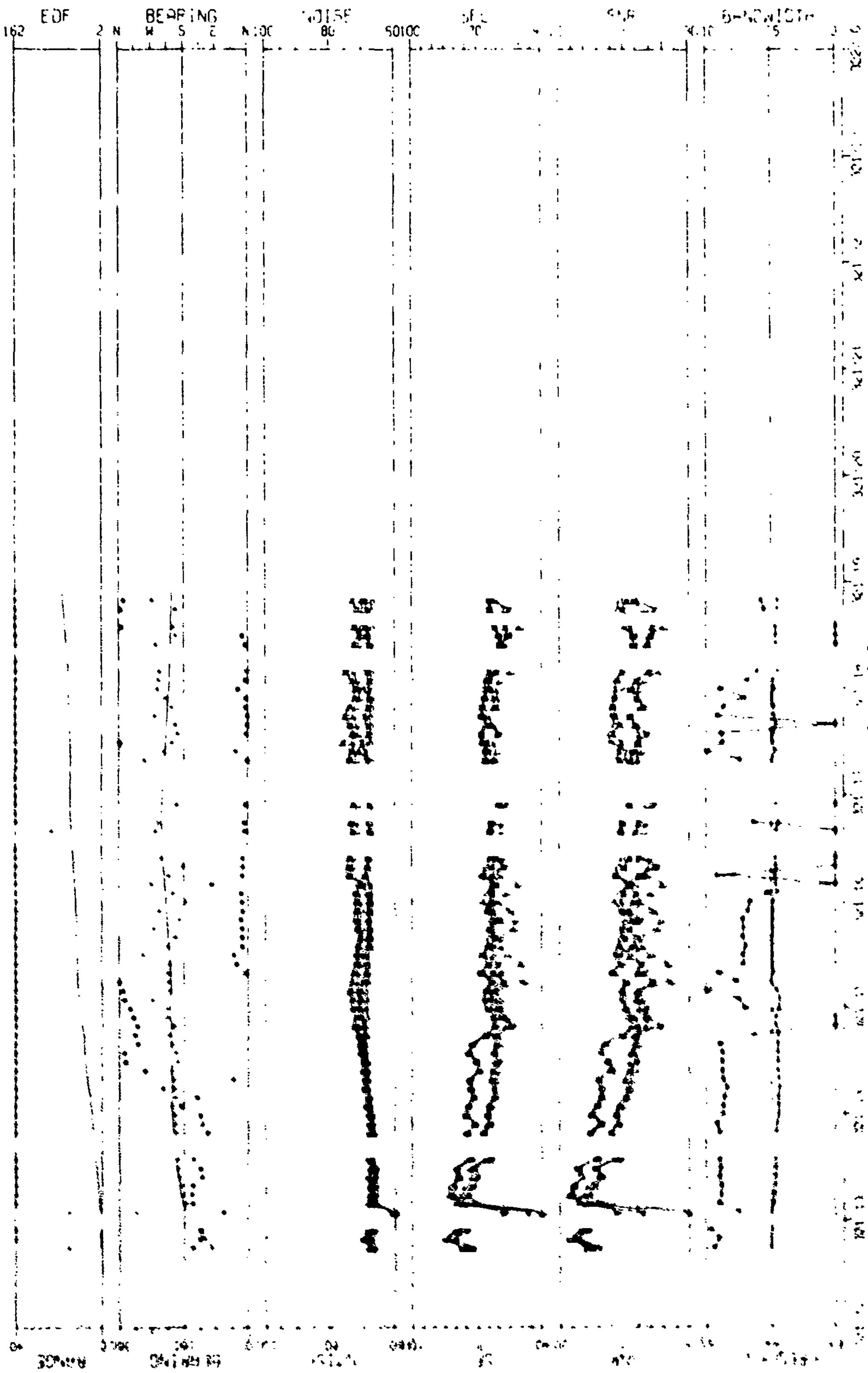

[illegible] HISTORY AS OBSERVED [illegible] THE DIFFERENCED CAPON [illegible] EVENT WITH STANDARD RESOLUTION (U)

AS-77-3001

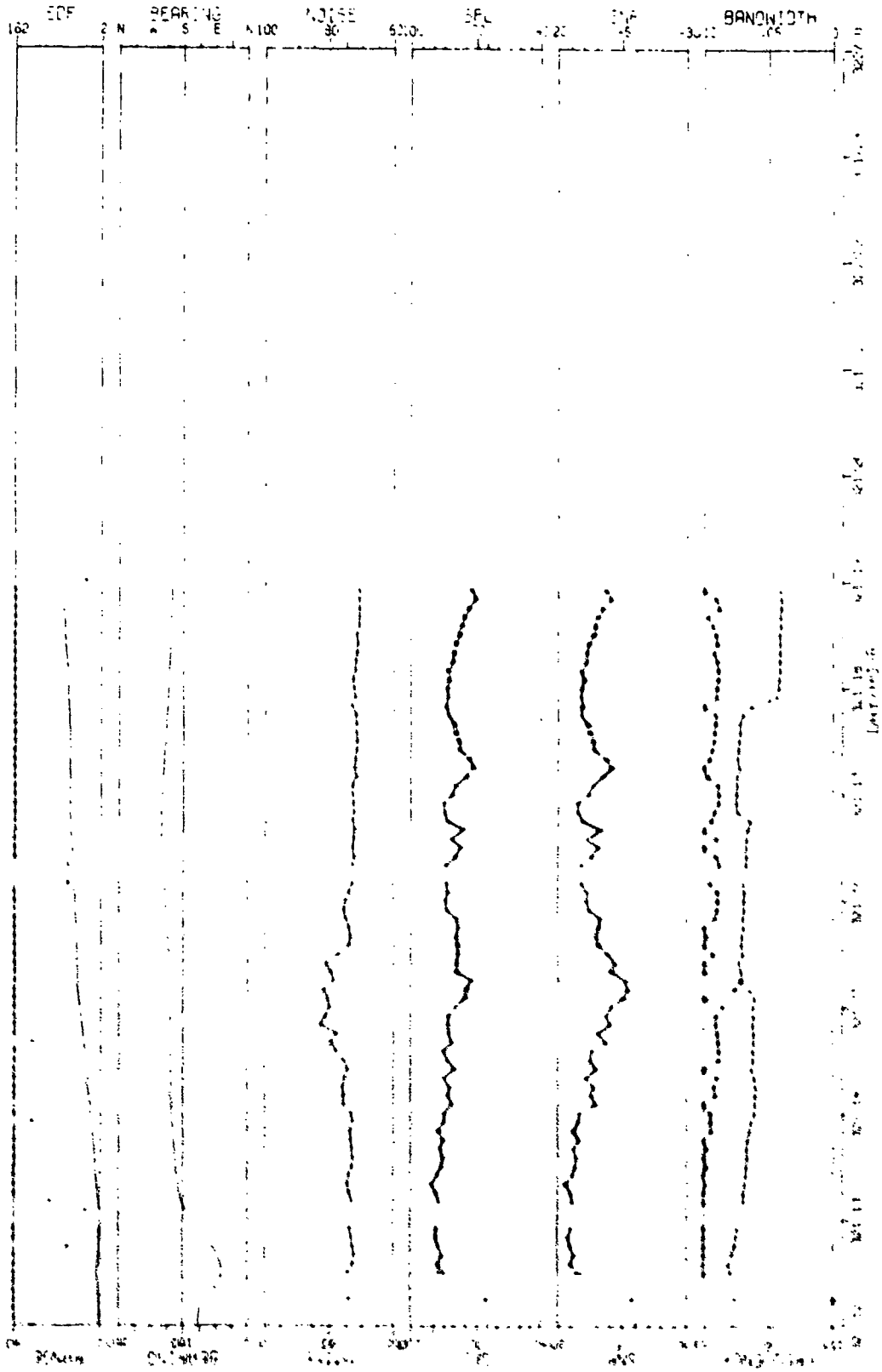

AS-77-3002

AS-77-3003

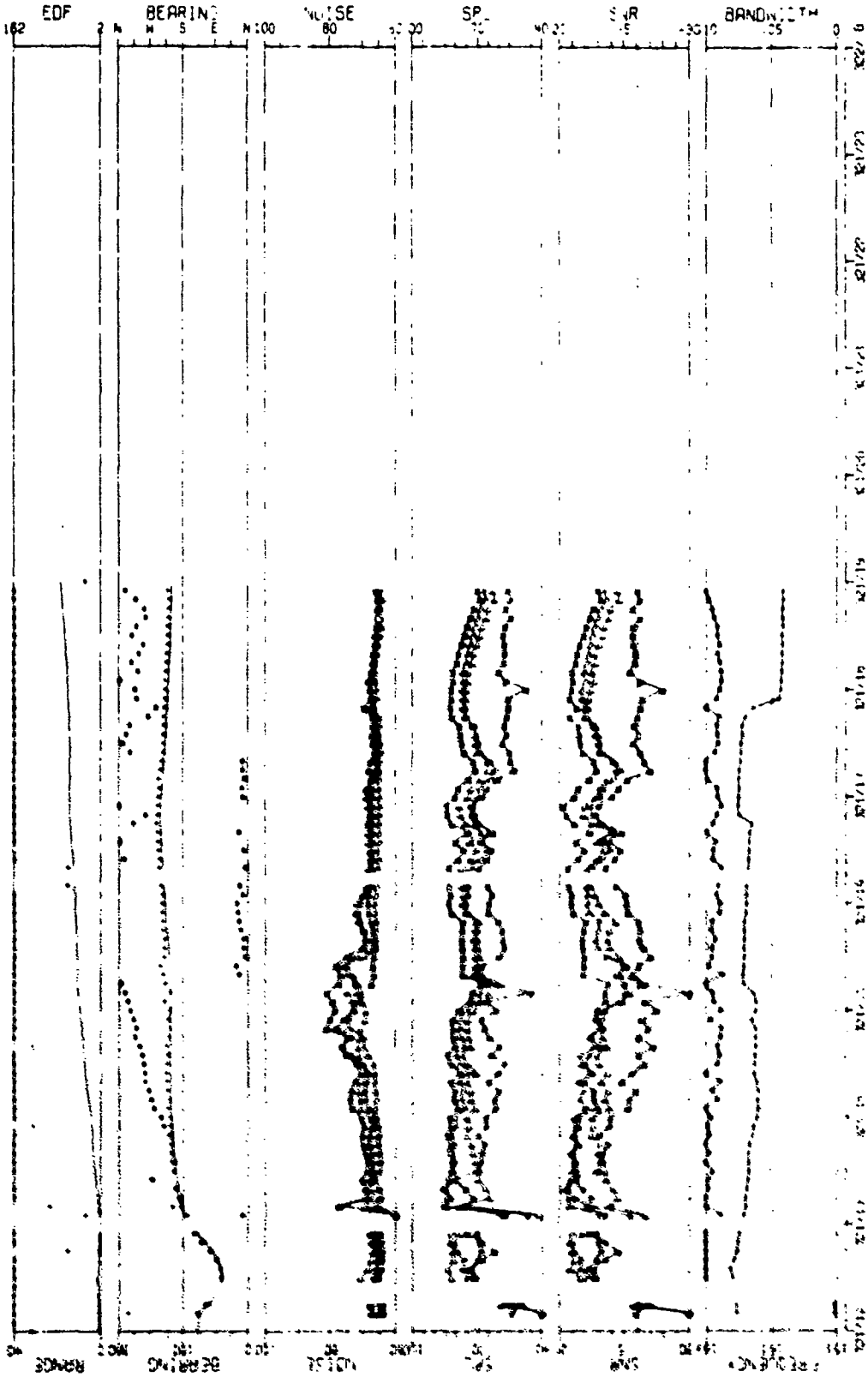

AS-77-3004

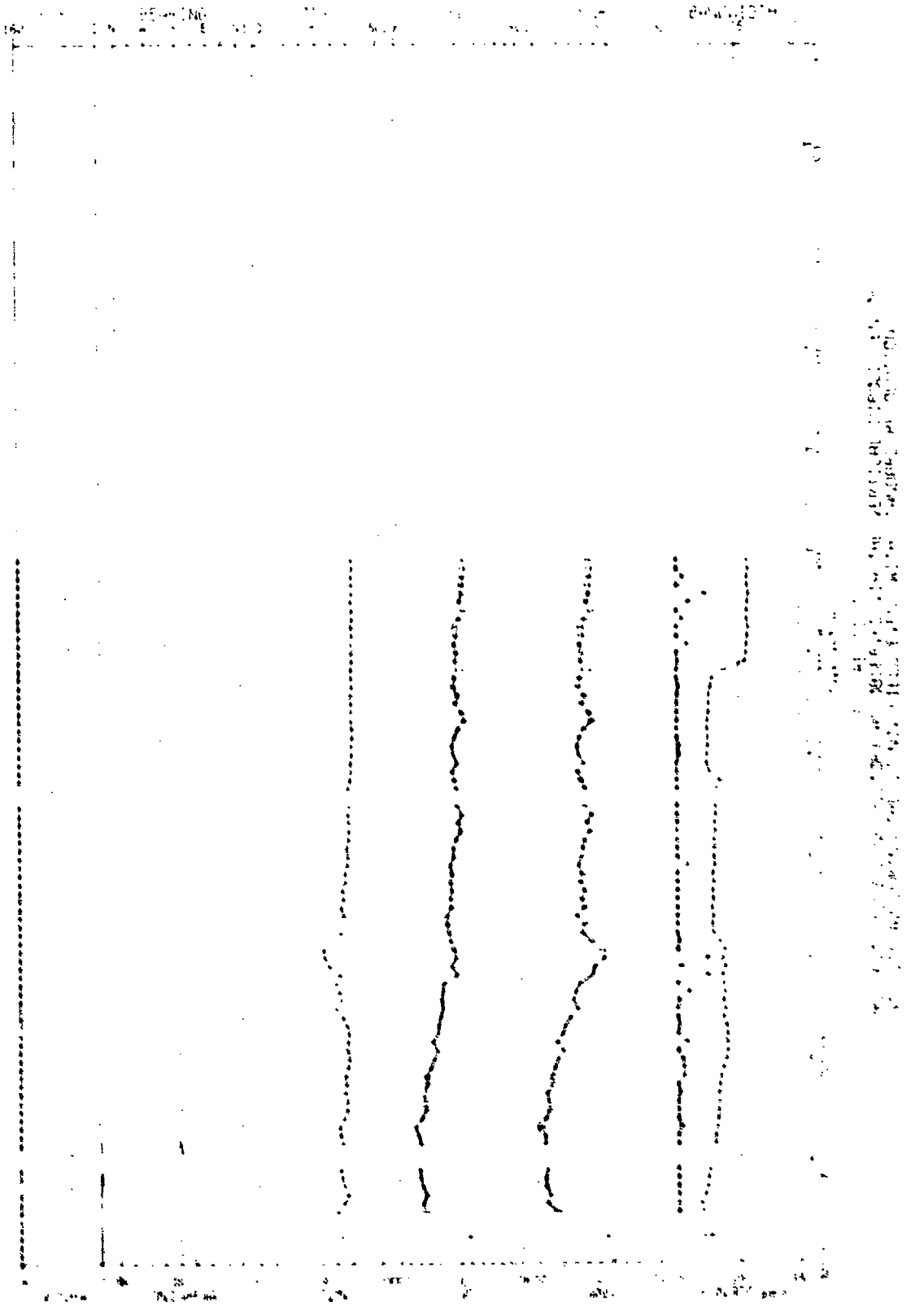

AS-77-3005

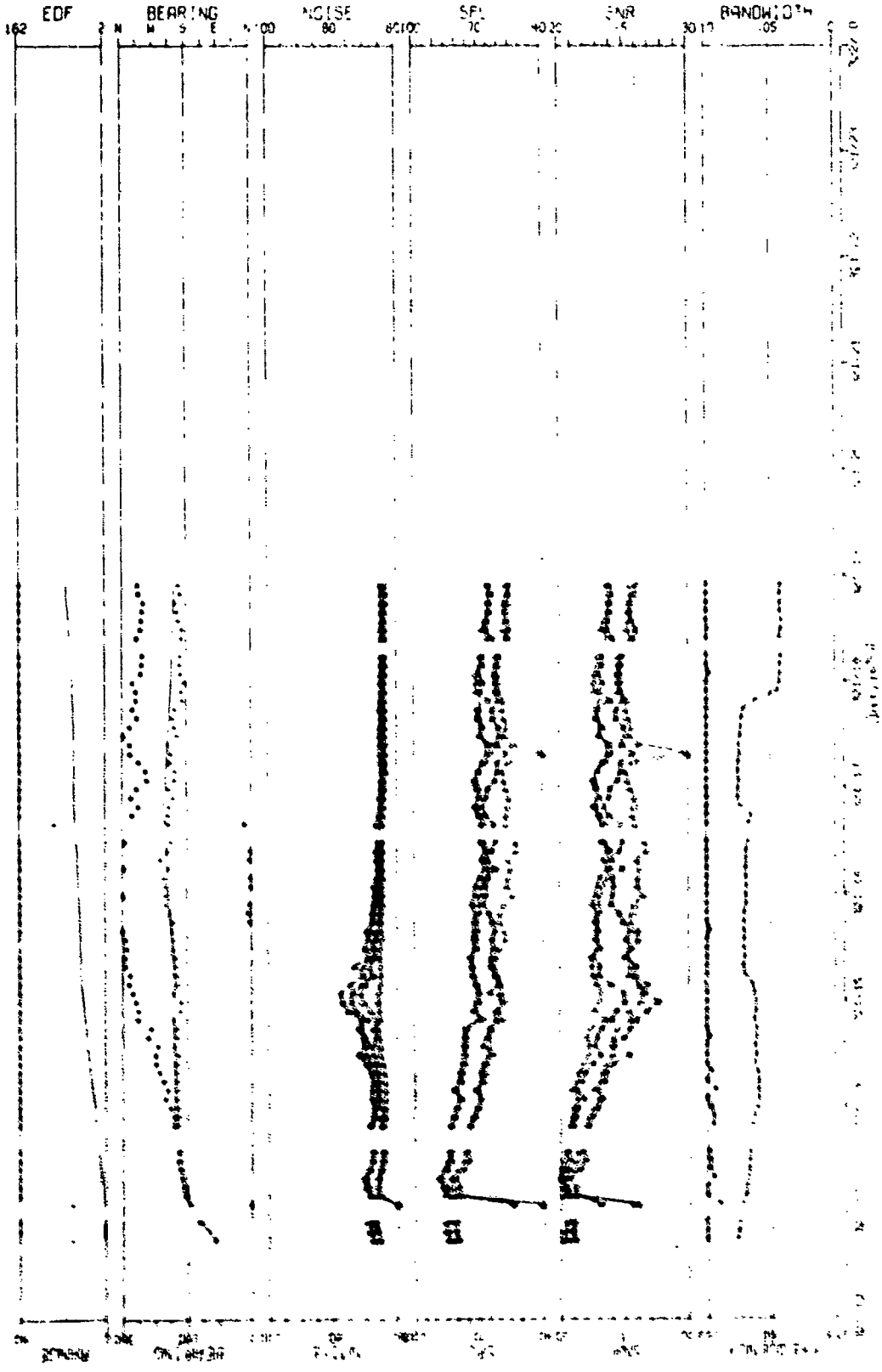

AS-77-3006

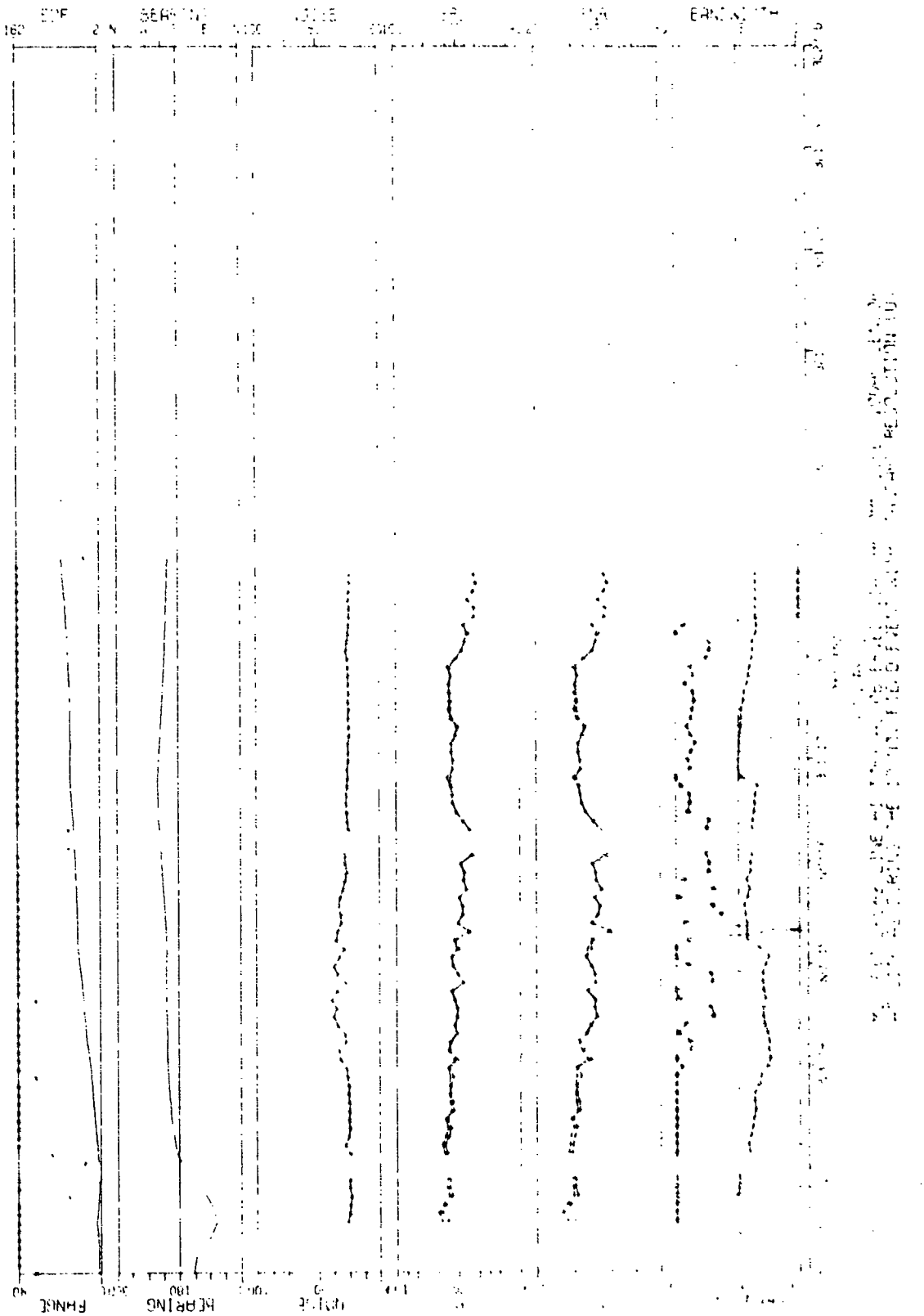

AS-77-3007

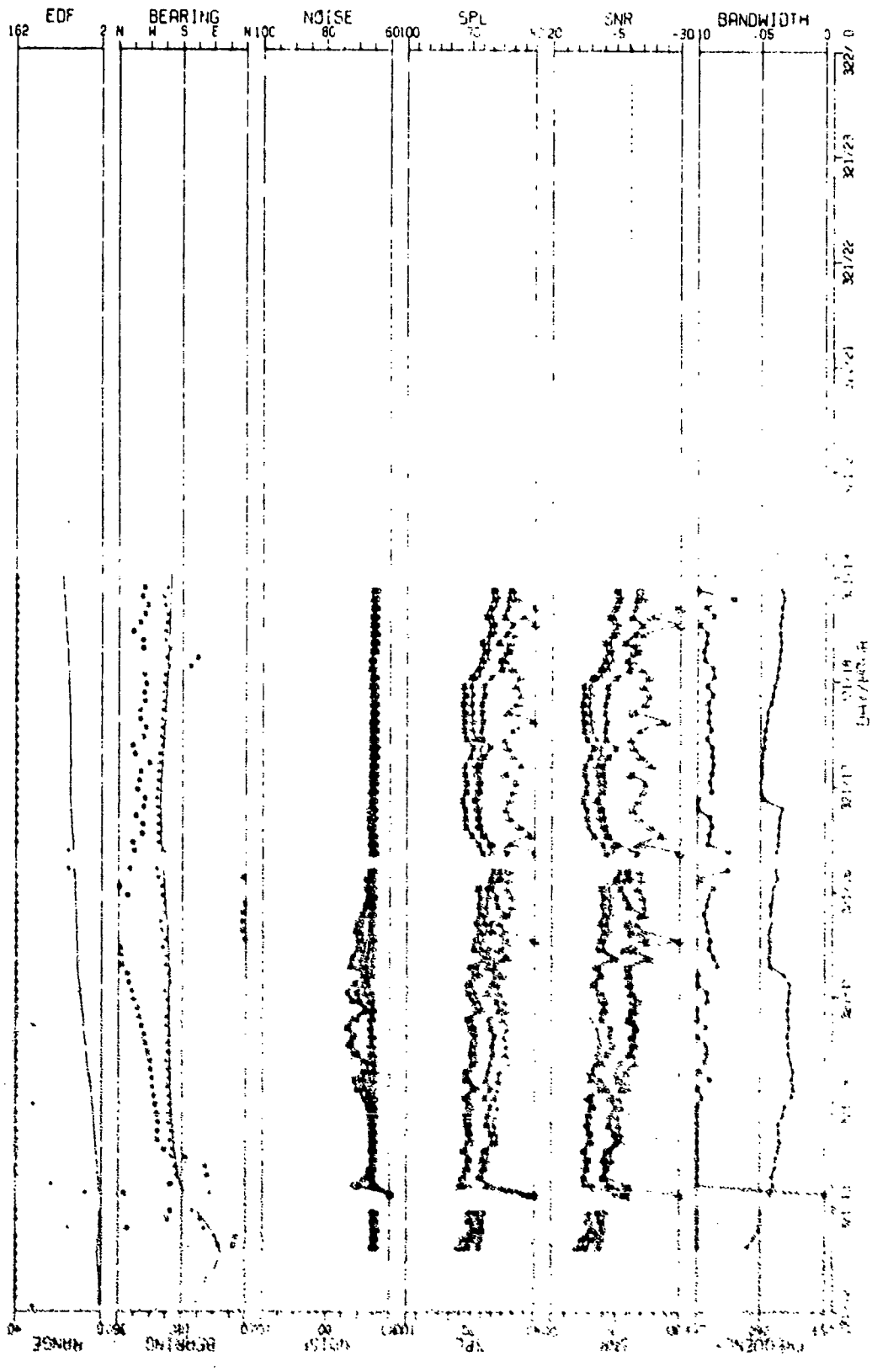
EDF
162
2
BEARING
N W S E N
NOISE
100
80
60
SPL
100
20
SNR
-5
-30
BANDWIDTH
10
.05
0
322/0
321/23
321/22

AS-77-3008

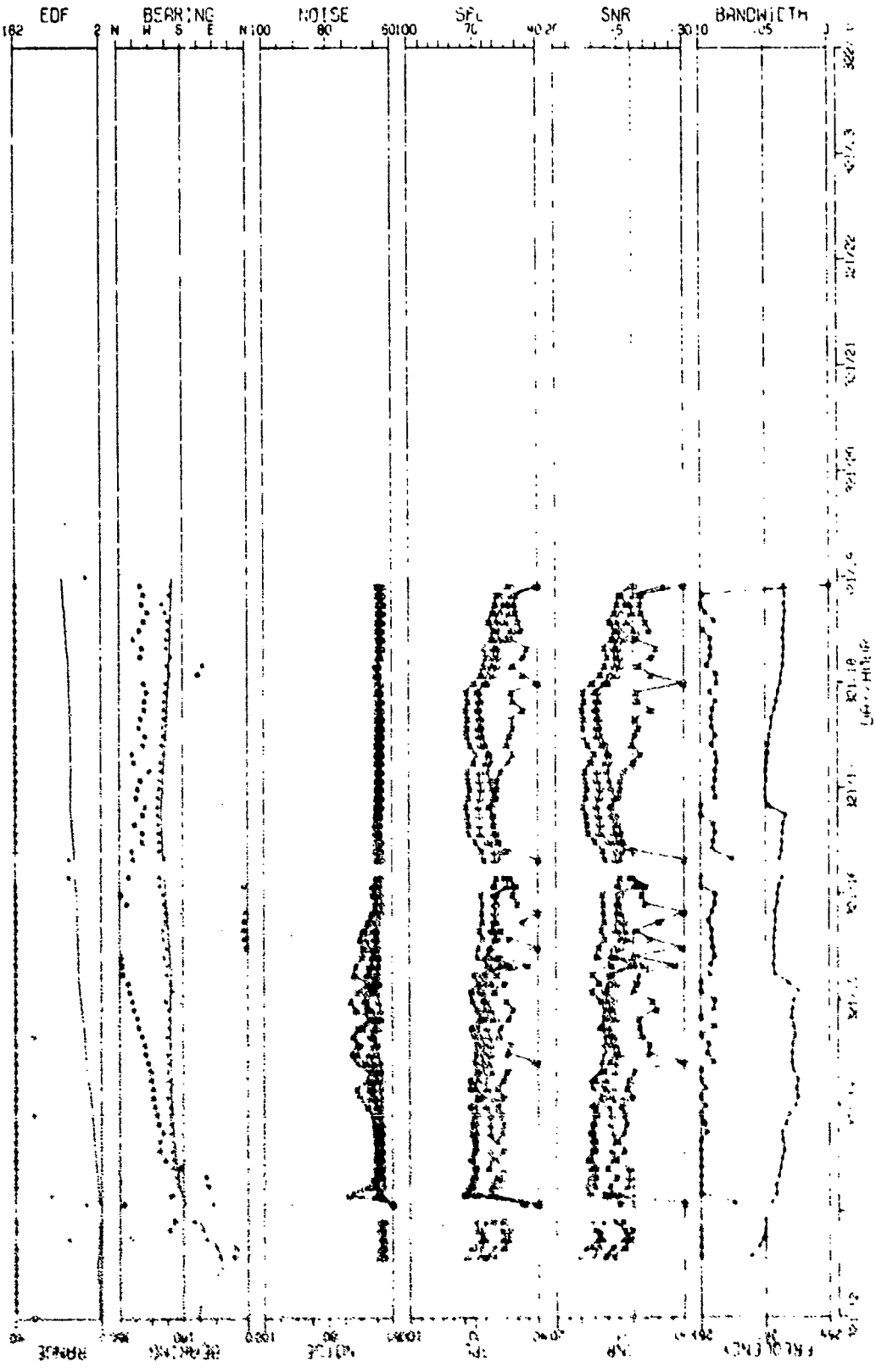

AS-77-3009

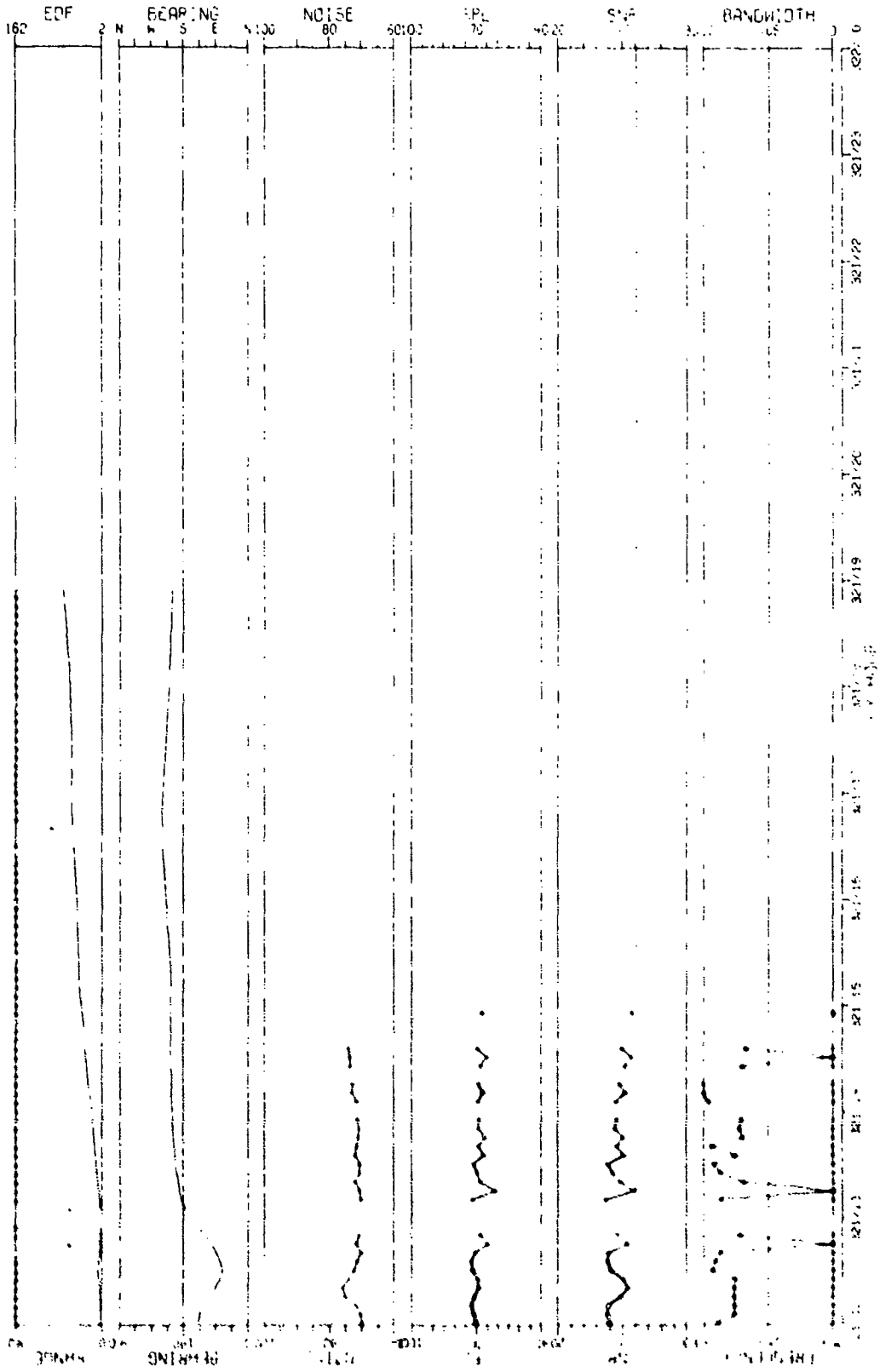

AS-77-3010

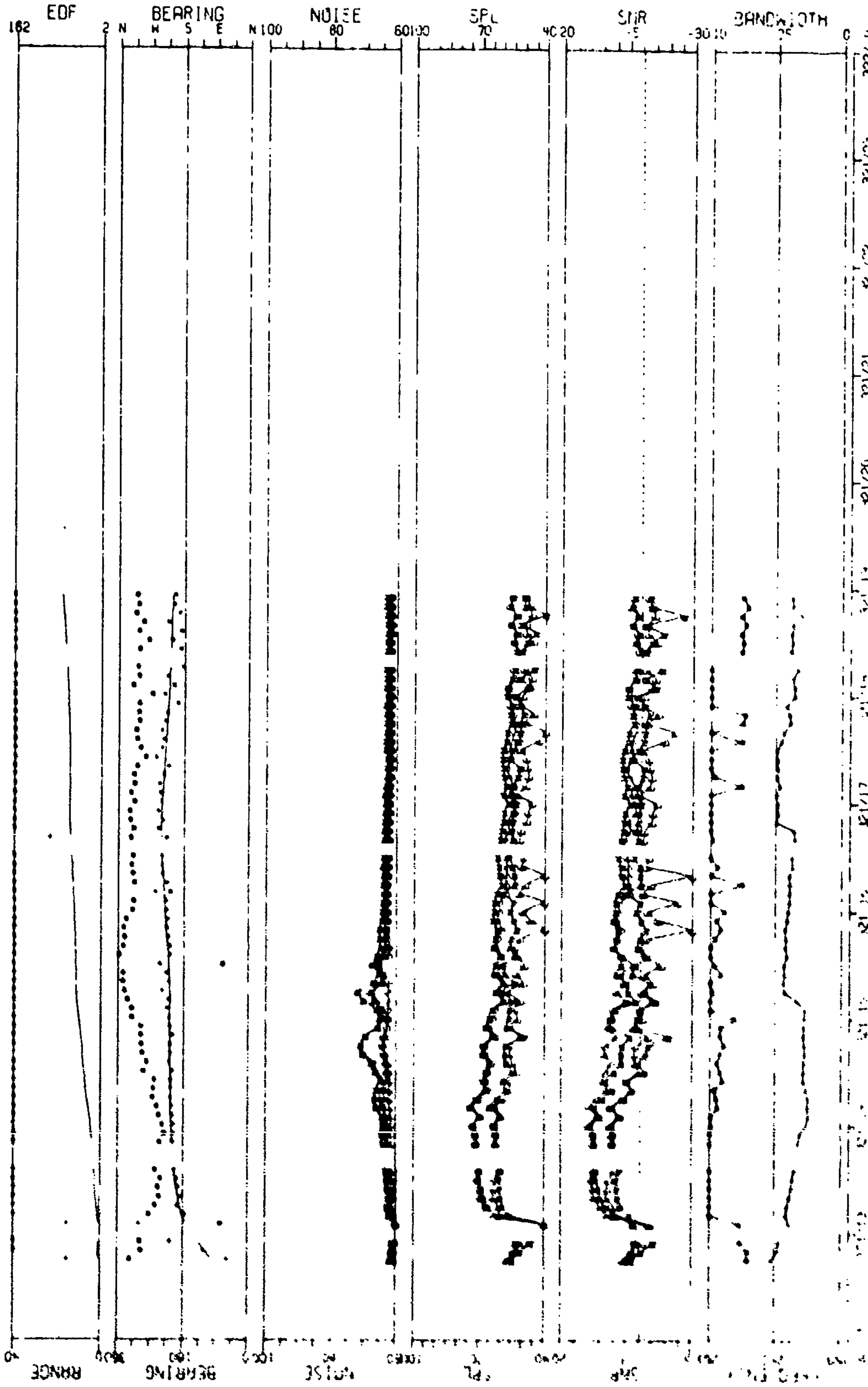

FIGURE II-4
LINE HISTORY AS OBSERVED ON THE DIFFERENCED CARDIOIDS SENSOR AT SITE H2 DURING THE 17 NOV FIELD EVENT WITH STANDARD RESOLUTION (U)

AS-77-3011

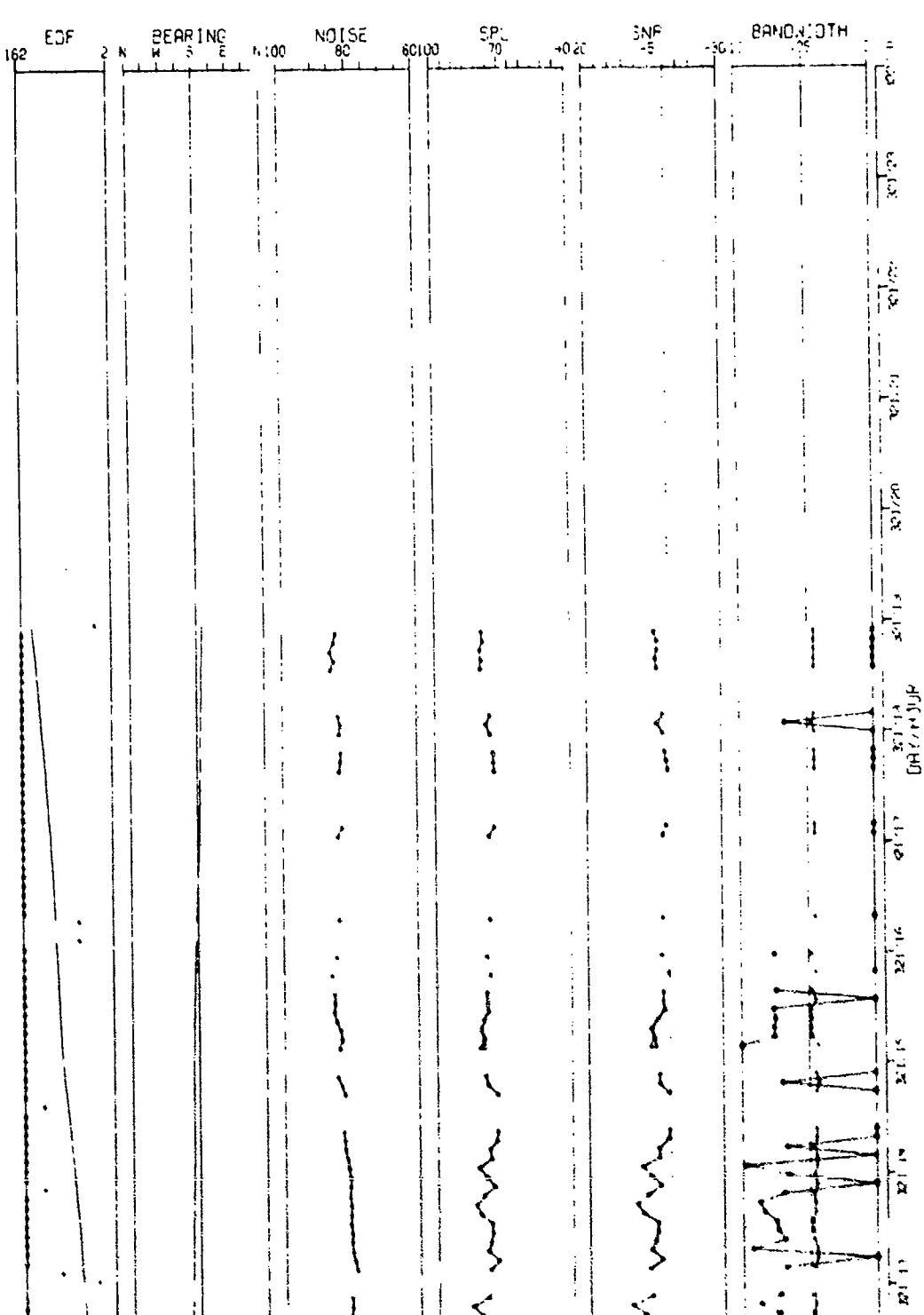
EDF
BEARING
NOISE
SPL
SNR
BANDWIDTH
162
2
N
W
S
E
100
80
60
100
70
+0
-5
-30

AS-77-3012

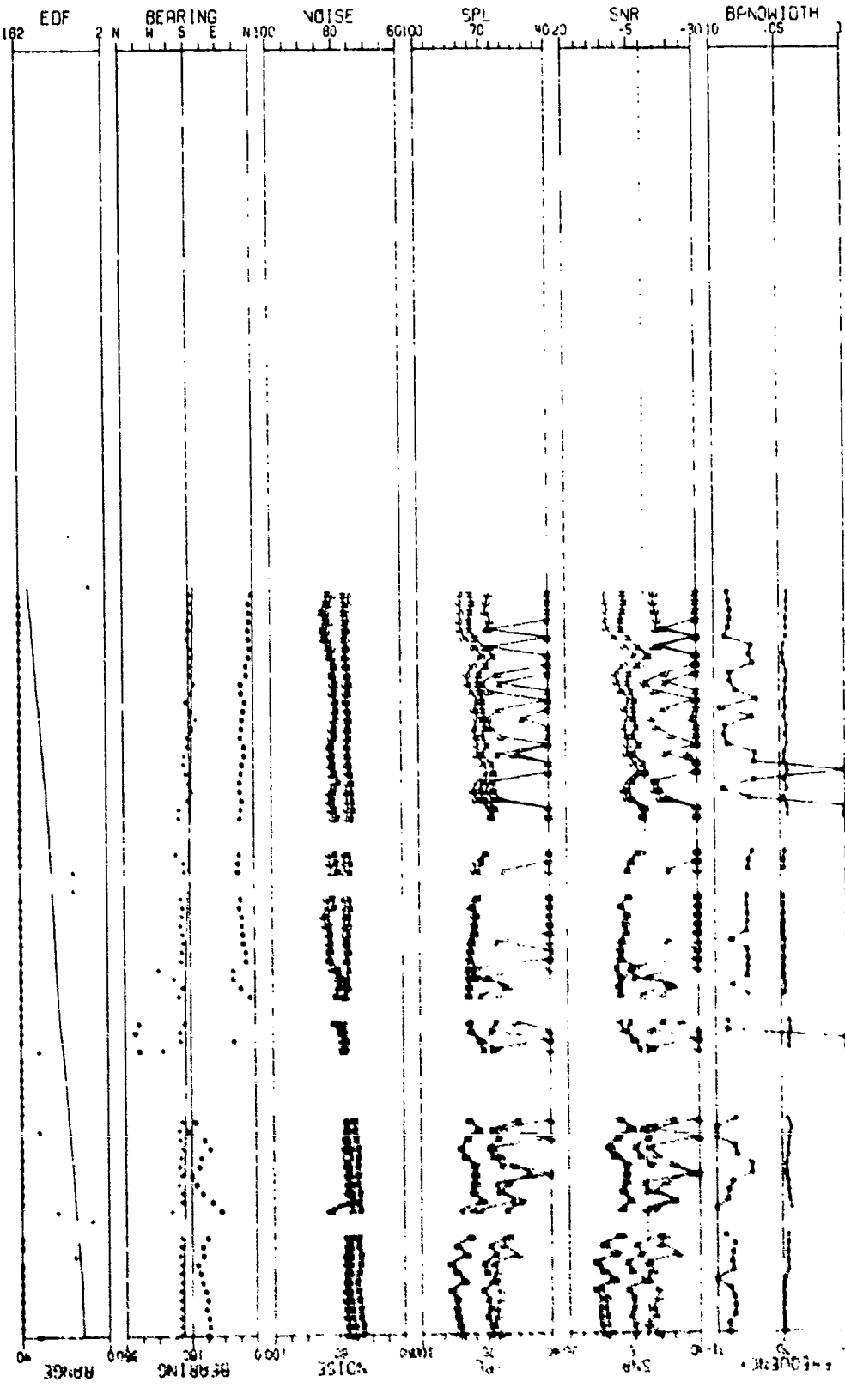

FIGURE 11-10.
HISTORY AS OBSERVED VIA THE SINGLE CARDIOID SENSOR AT SITE A2 DURING THE 17 NOV FIELD EVENT WITH STANDARD RESOLUTION (U)

AS-77-3013

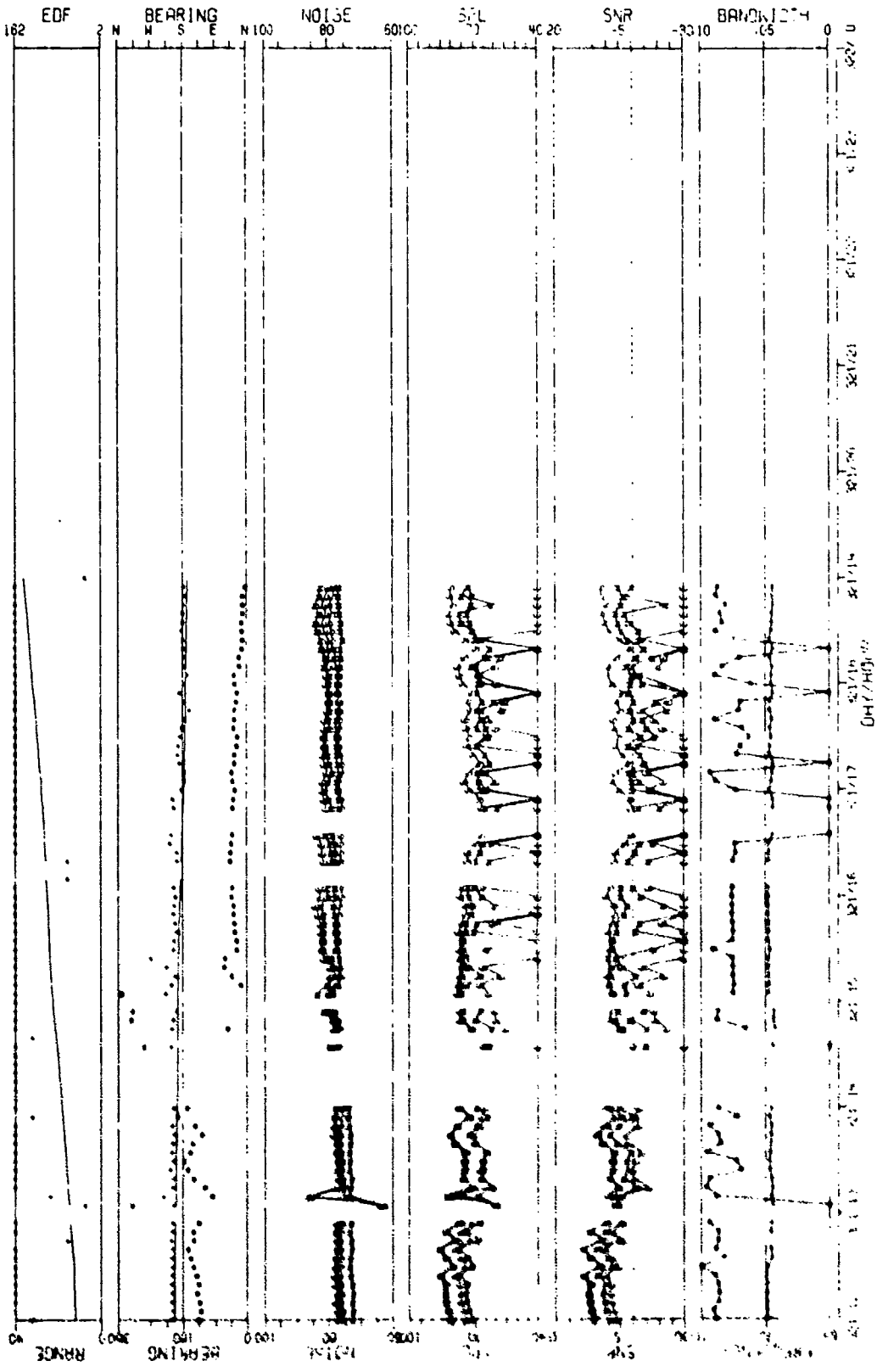

AS-77-3014

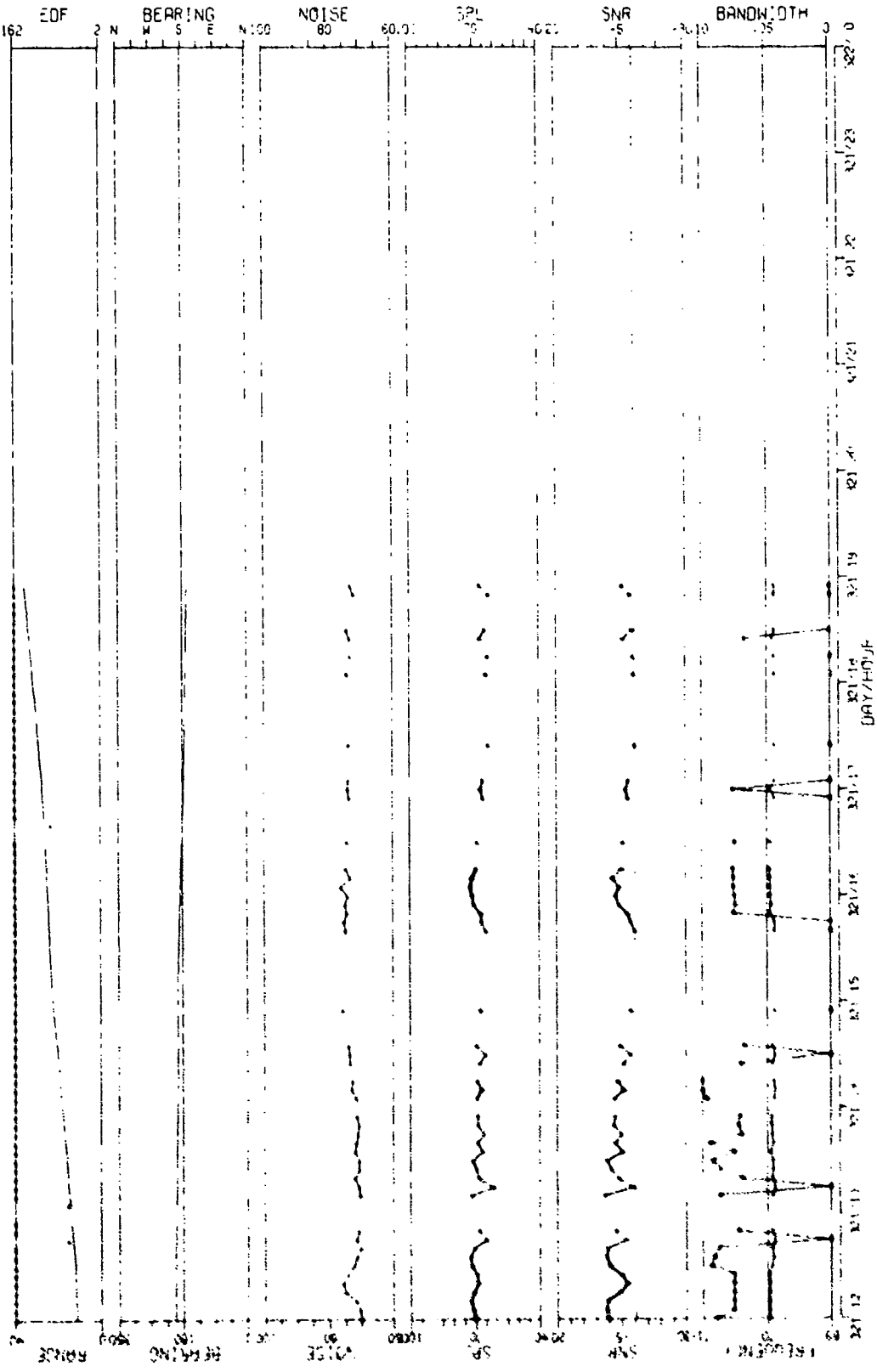

FIGURE 11-29
LOFAR LINE HISTORY AS OBSERVED VIA THE VERTICAL DIPOLE ARRAY
AT SITE A2 DURING THE 17 NOV FIELD EVENT WITH STANDARD RESOLUTION (U)

AS-77-3015

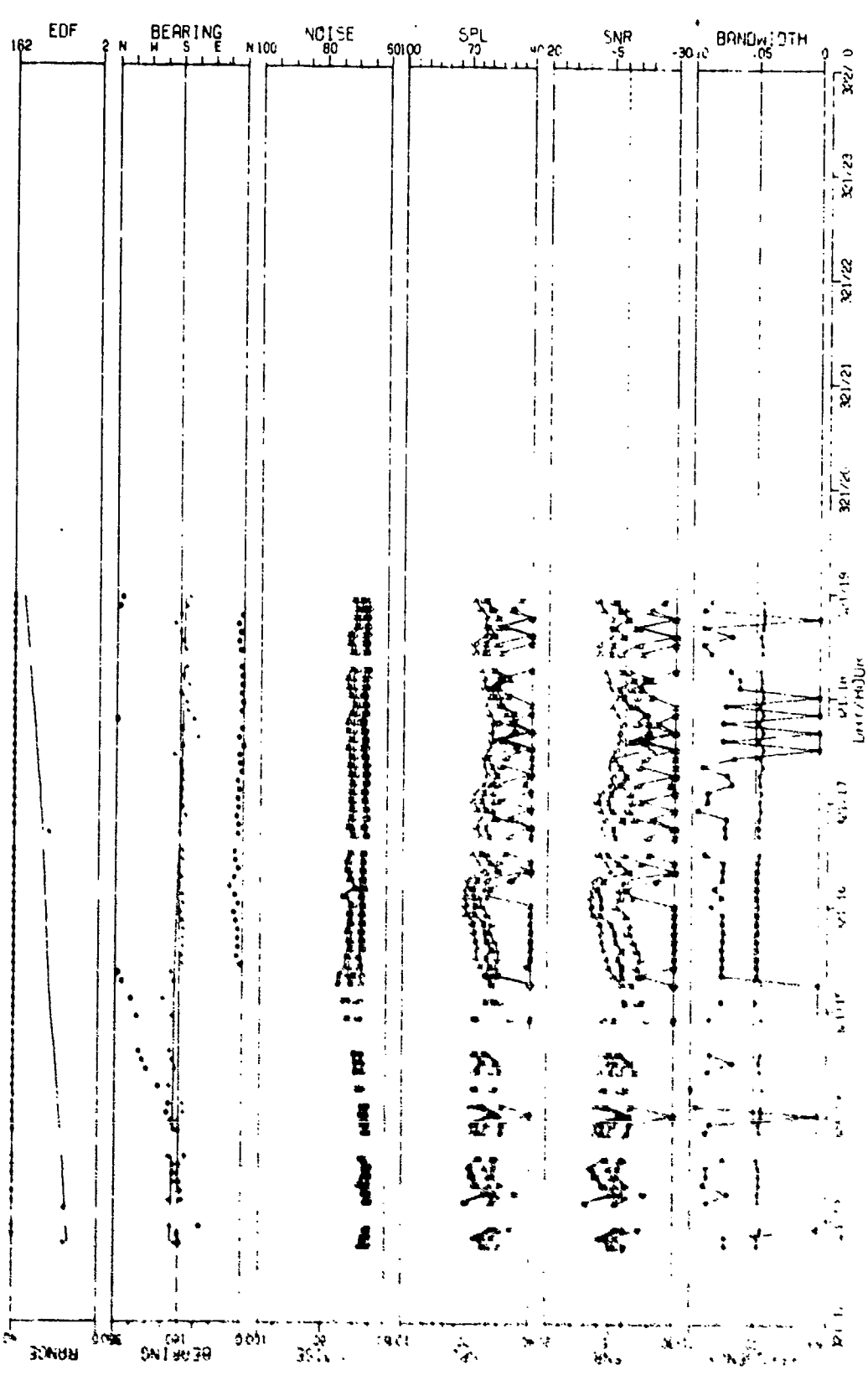
EDF
BEARING
NOISE
SPL
SNR
BANDWIDTH
162
2
N
W
S
E
N 100
80
50 100
70
20
-5
-30
.05
0
321/23
321/22
321/21
321/20
321/19
RANGE
BEARING

AS-77-3016

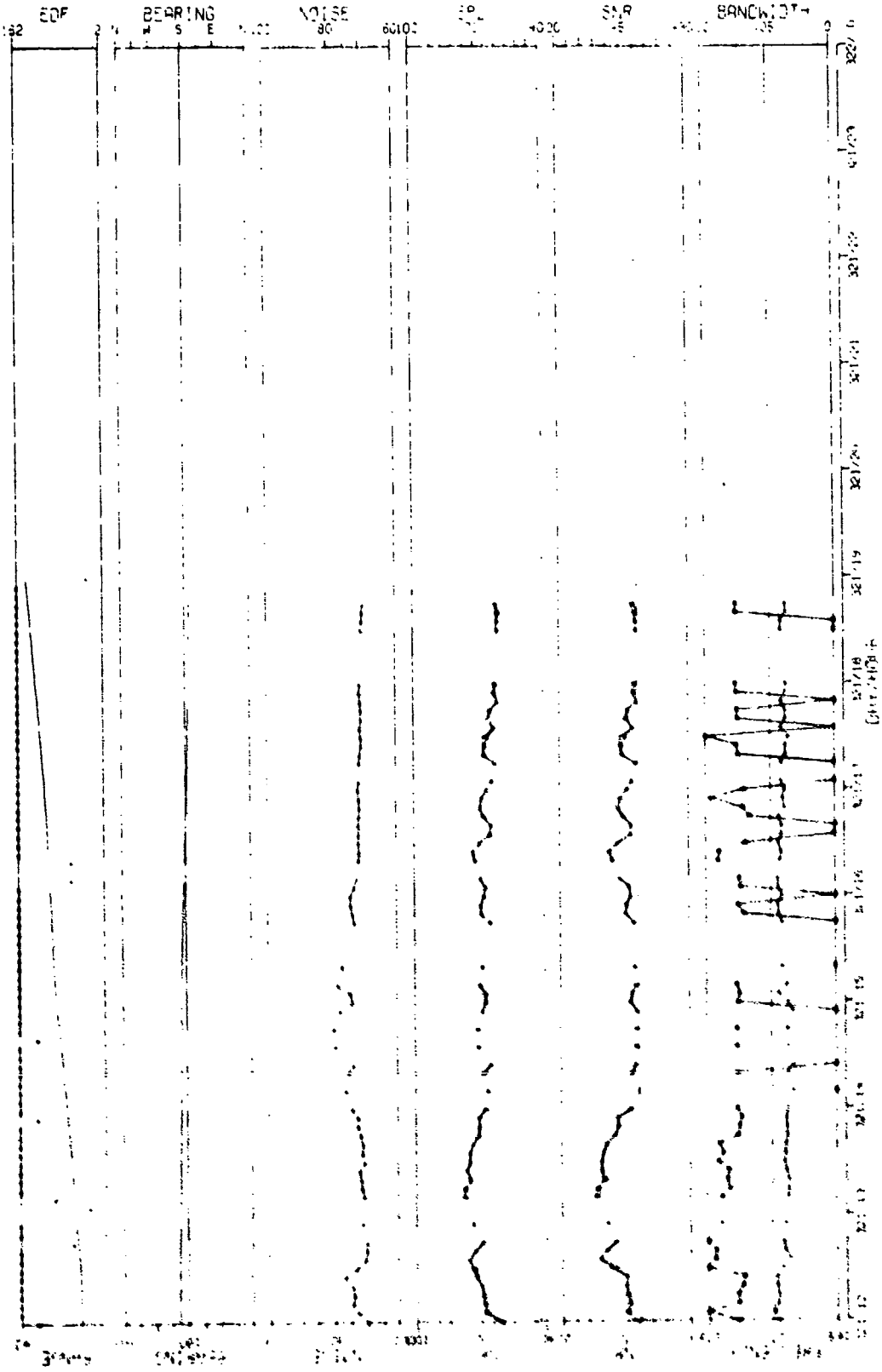

AS-77-3017

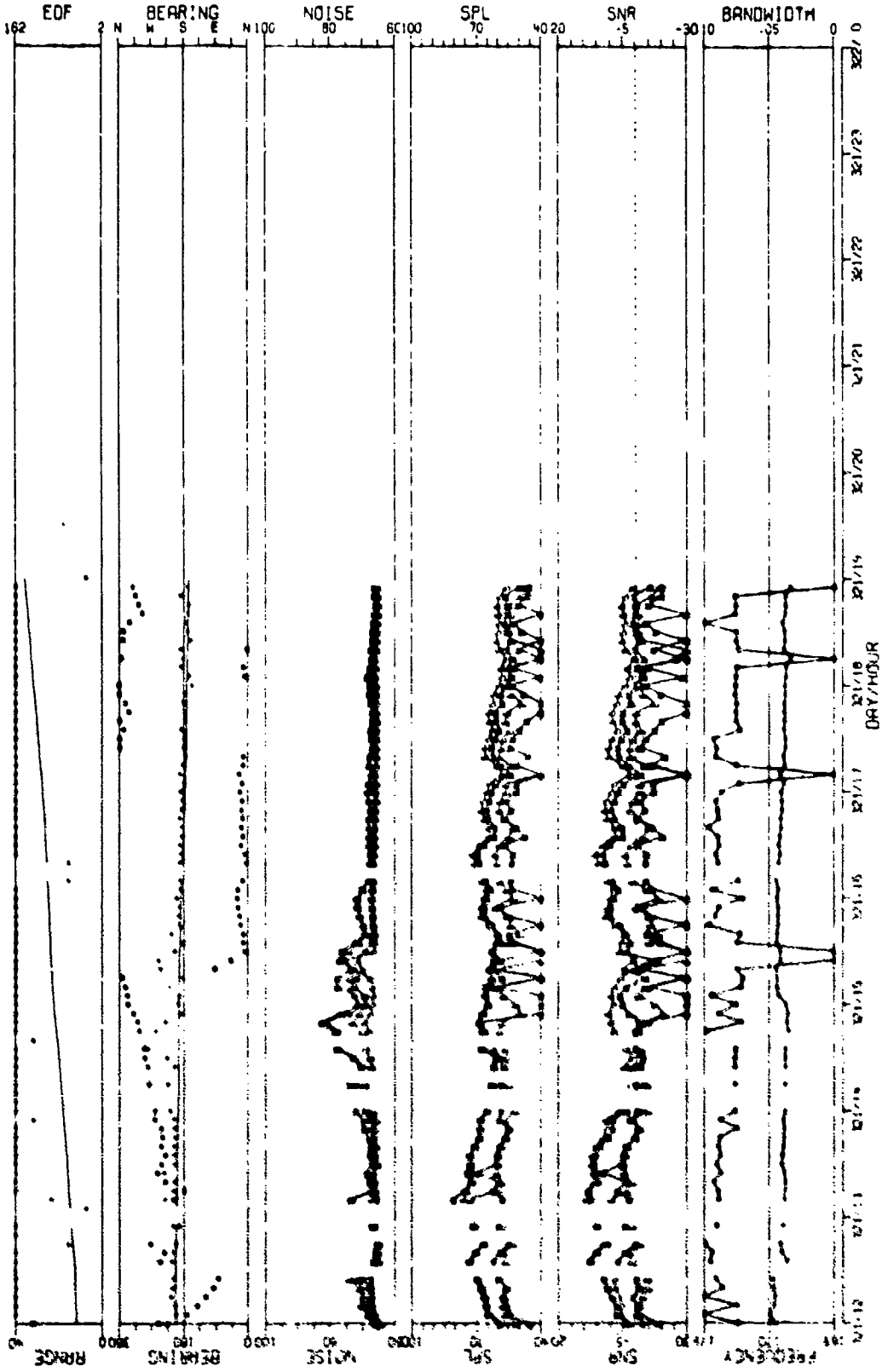

AS-77-3018

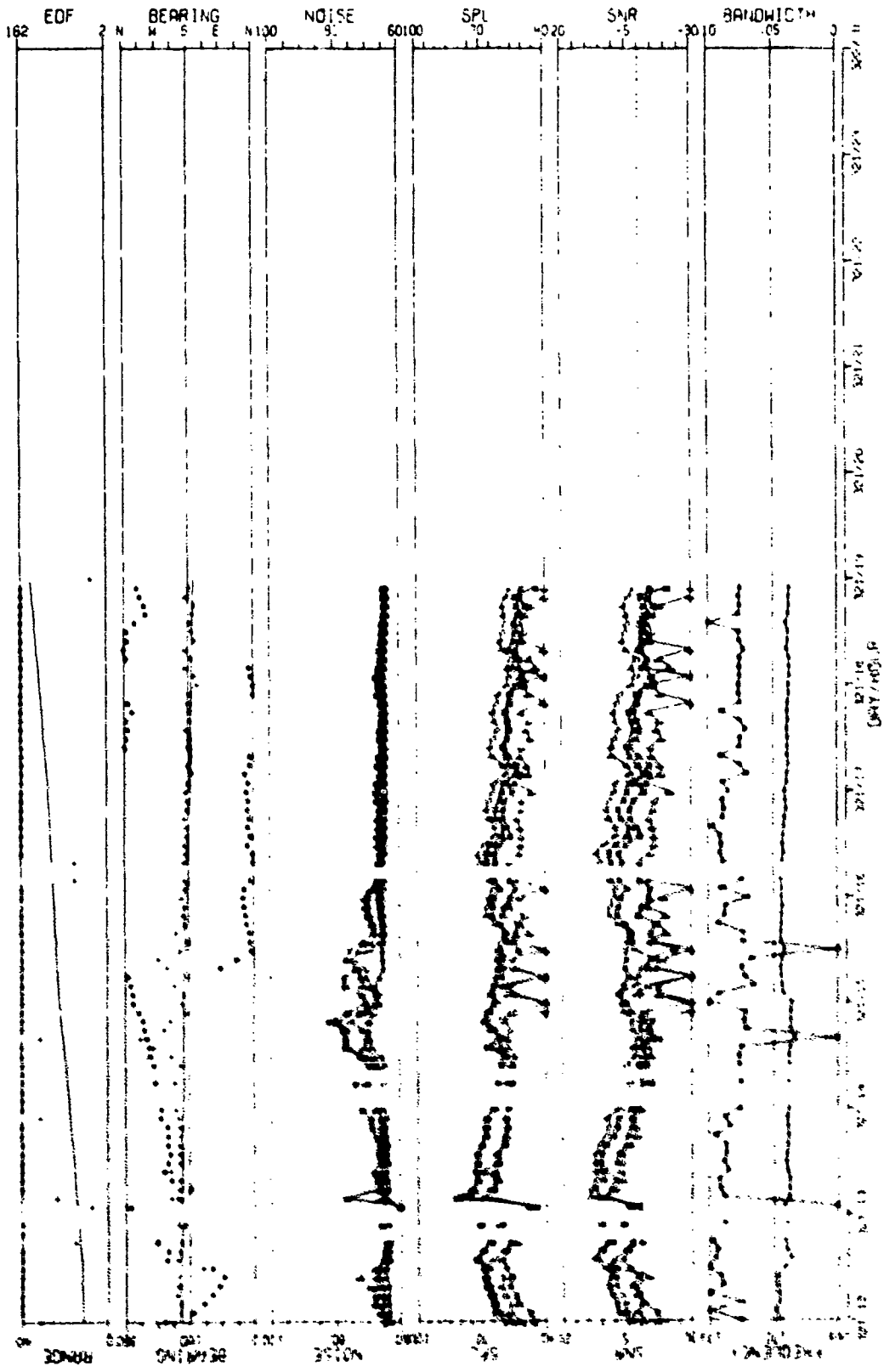

FIGURE II-3c
TIME HISTORY AS OBSERVED VIA THE MAY GAIN LIMACONS SENSOR
OF SIDE NO. 3 DURING THE 17 NOV. FIELD EVENT WITH STANDARD RESOLUTION (U)

AC-77-3019

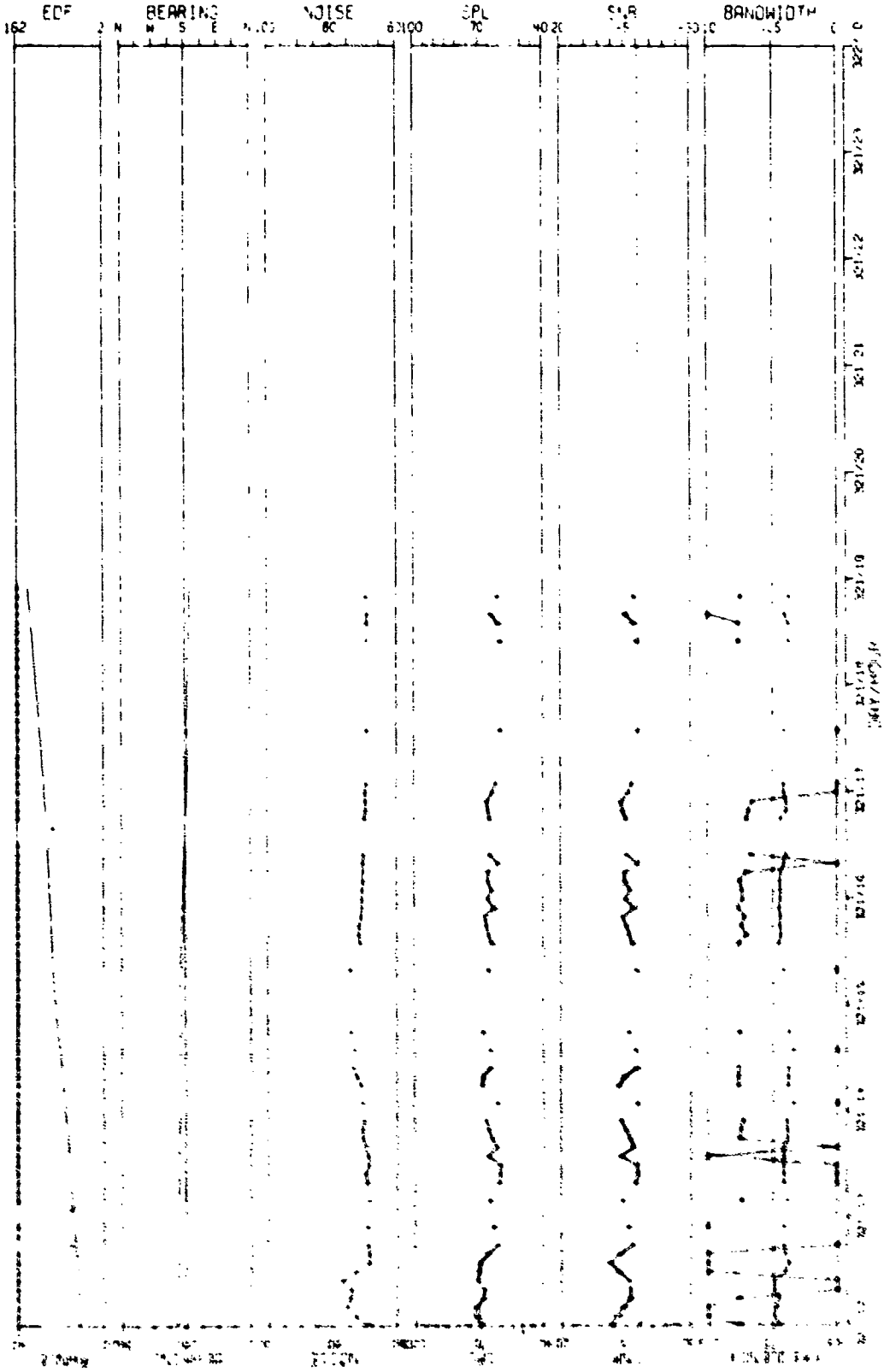

AS-77-3020

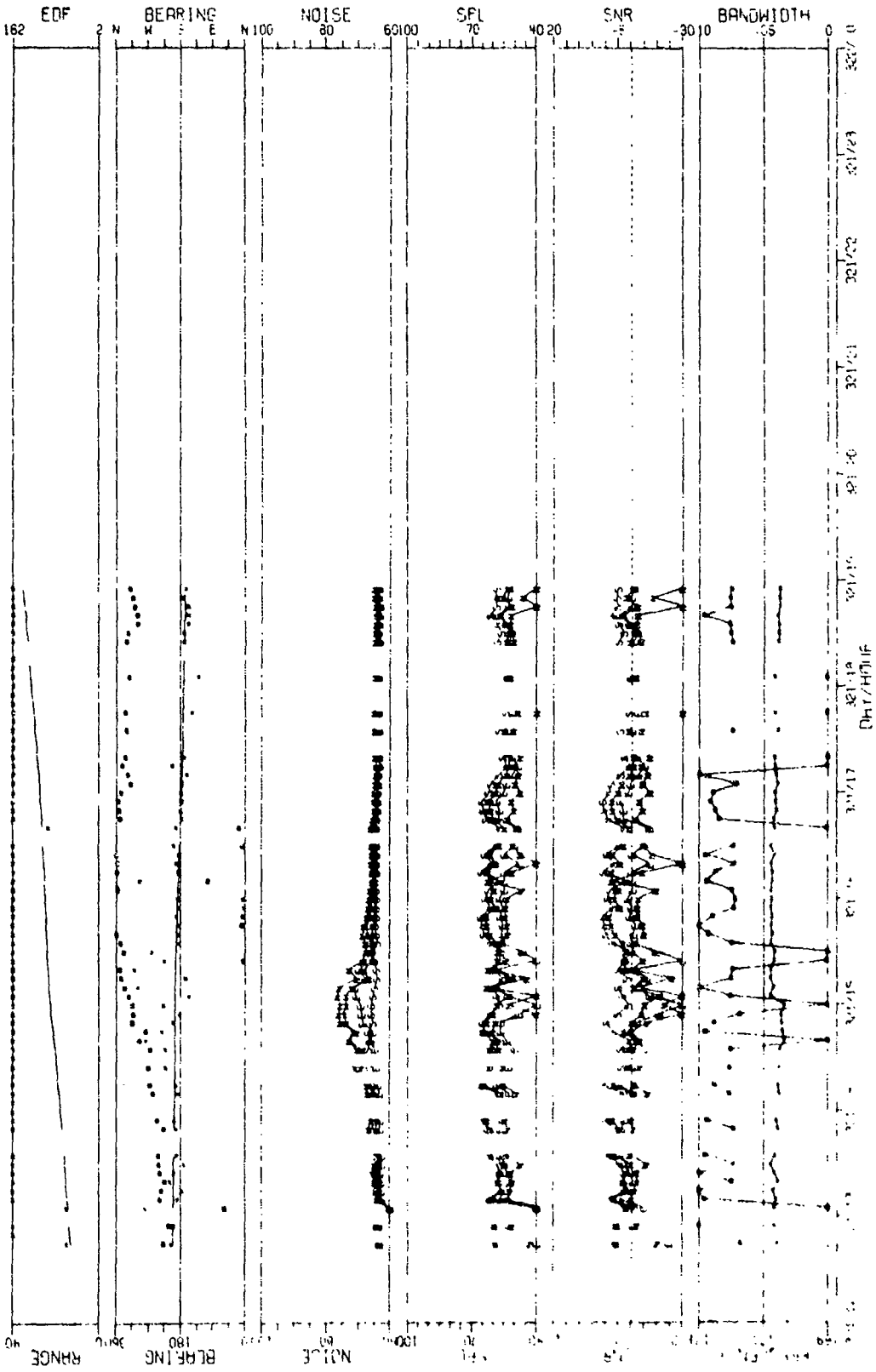

FIGURE II-[illegible]
LINE HISTORY AS OBSERVED VIA THE DIFFERENCED CHARIOTEER SENSOR
DURING THE 17 NOV FIELD EVENT WITH STANDARD RESOLUTION [illegible]

AS-77-3021

AS-77-3022

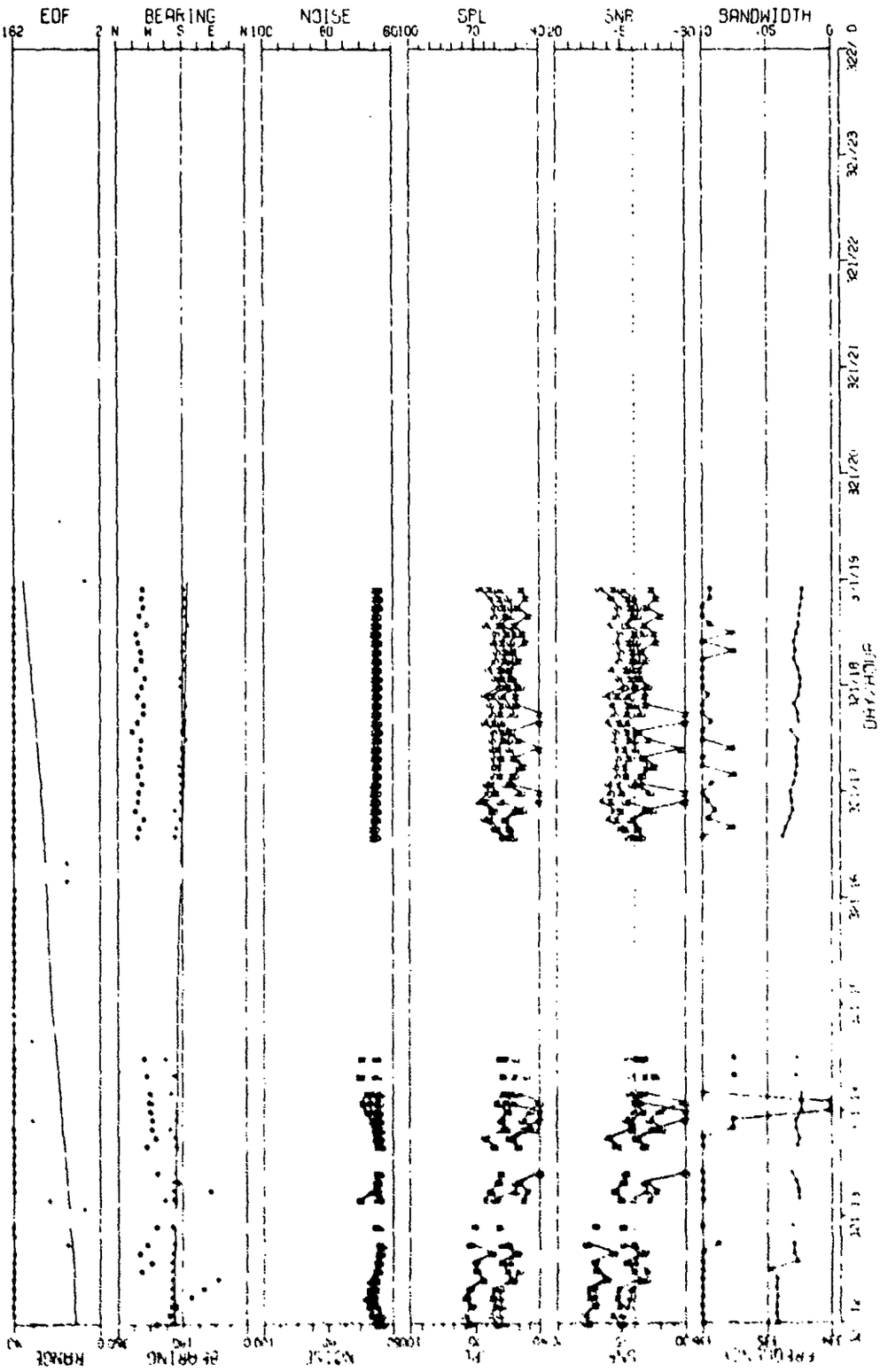

AS-77-3023

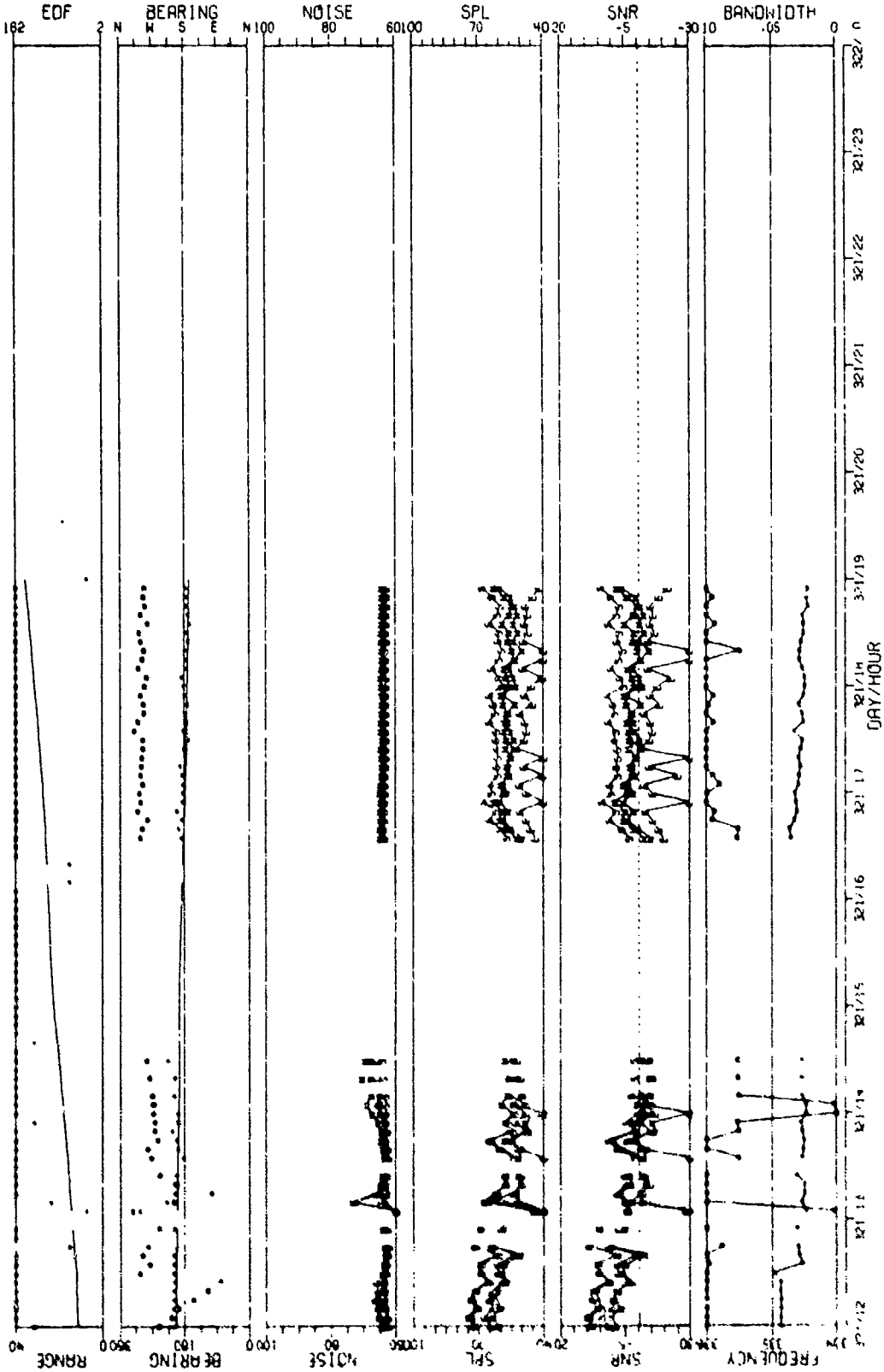

FIGURE II-97
MSS-FVI 335H2 LINE HISTORY AS OBSERVED VIA THE MAX GAIN LIMACONS SENSOR
AT SITE 42 DURING THE 17 NOV FIELD EVENT WITH STANDARD RESOLUTION (U)

AS-77-3024

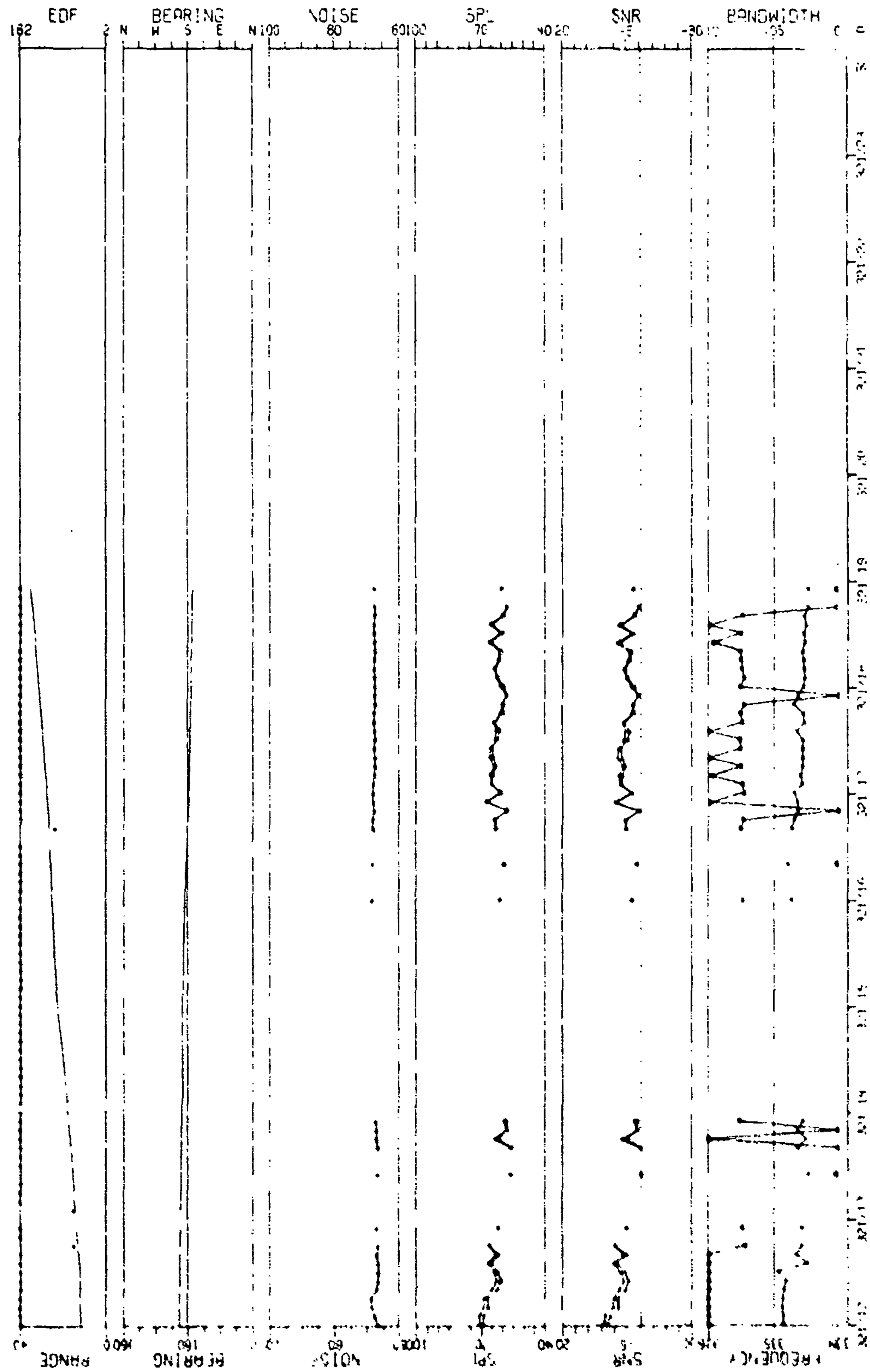

FIGURE II-9A
MSO-F?T 335HZ LINE HISTORY AS OBSERVED VIA THE VERTICAL DIPOLE SENSOR AT SITE A2 DURING THE 17 NOV FIELD EVENT WITH STANDARD RESOLUTION (U)

AS-77-3025

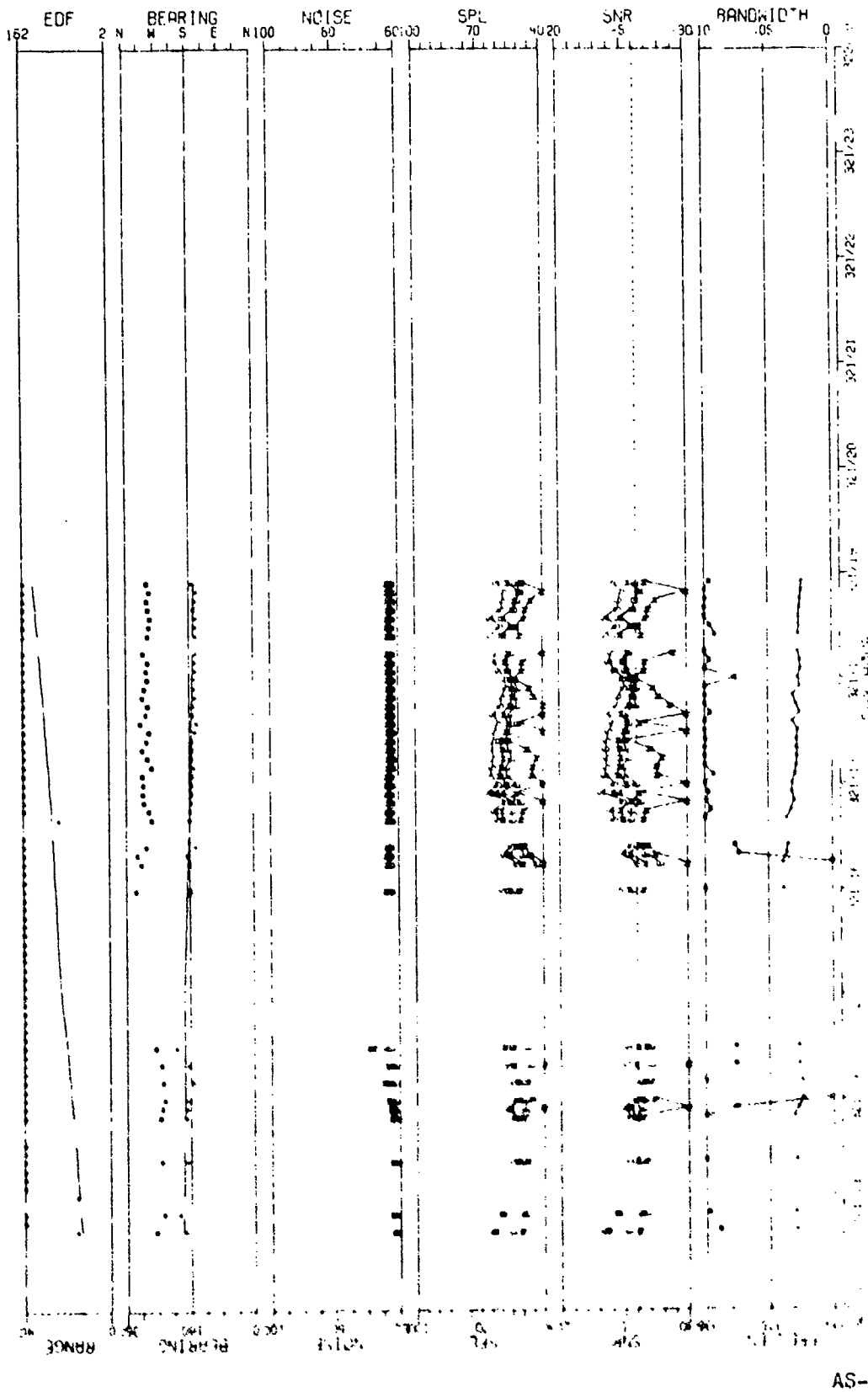
EOF
BEARING
NOISE
SPL
SNR
BANDWIDTH
152
2
N
W
S
E
N100
60
60
00
70
40
20
-5
30
10
.05
0
321/23
321/22
321/21
321/20

AS-77-3026

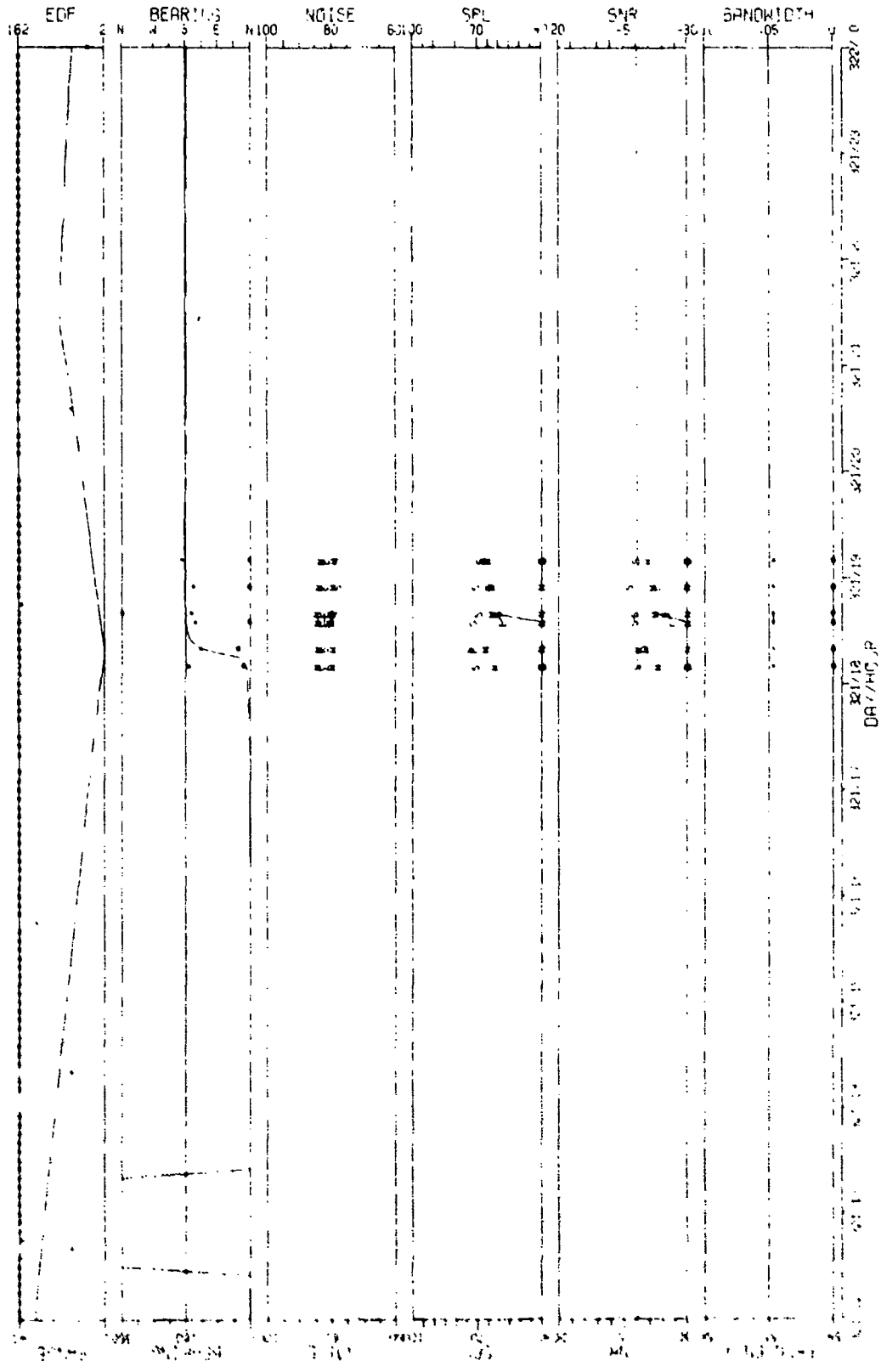

AS-77-3027

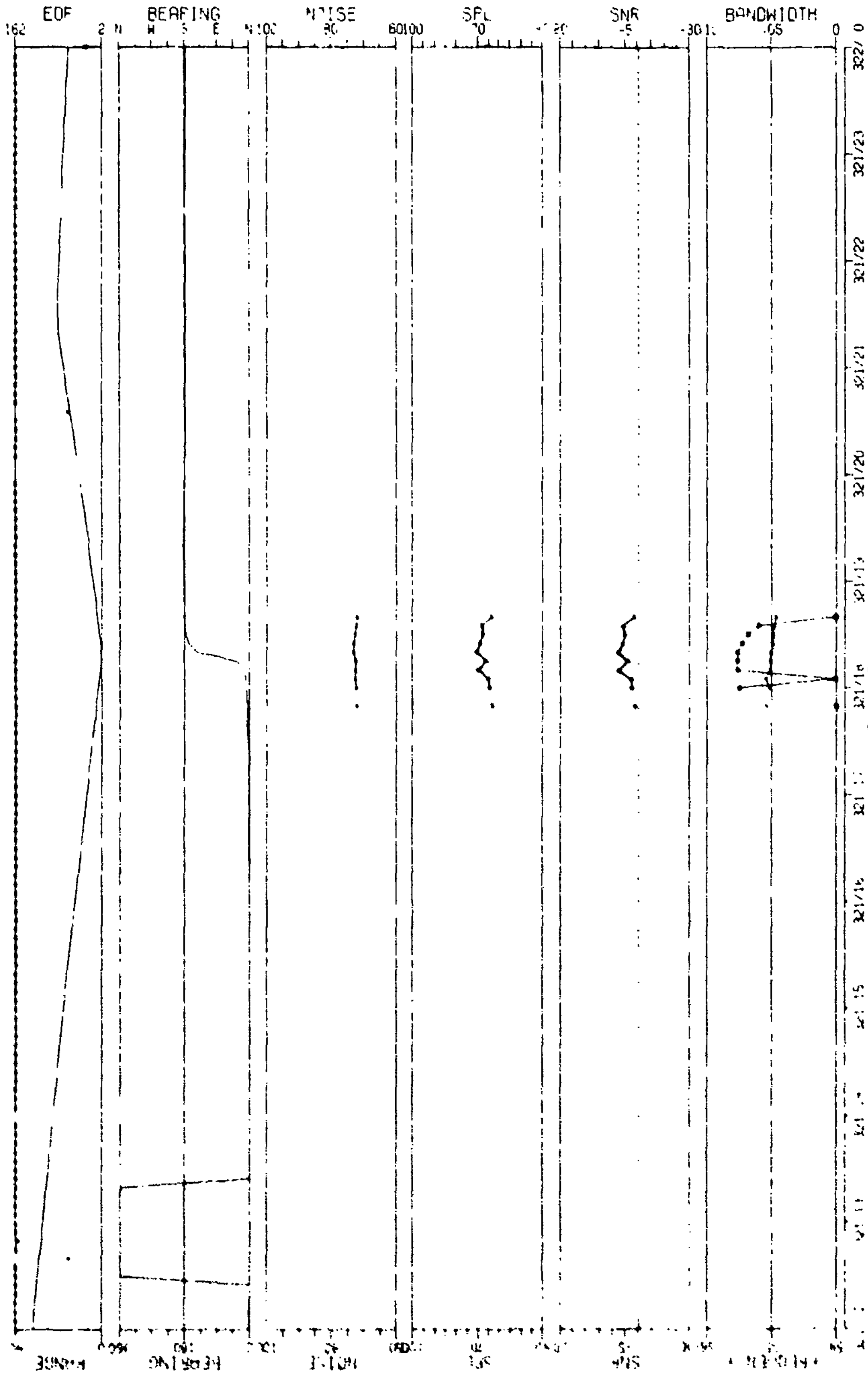

FIGURE II-101
[illegible] LINE HISTORY AS OBSERVED VIA THE VERTICAL DIPOLE SENSOR AT SITE A3 DURING THE 17 NOV FIELD EVENT WITH STANDARD RESOLUTION (U)

AS-77-3028

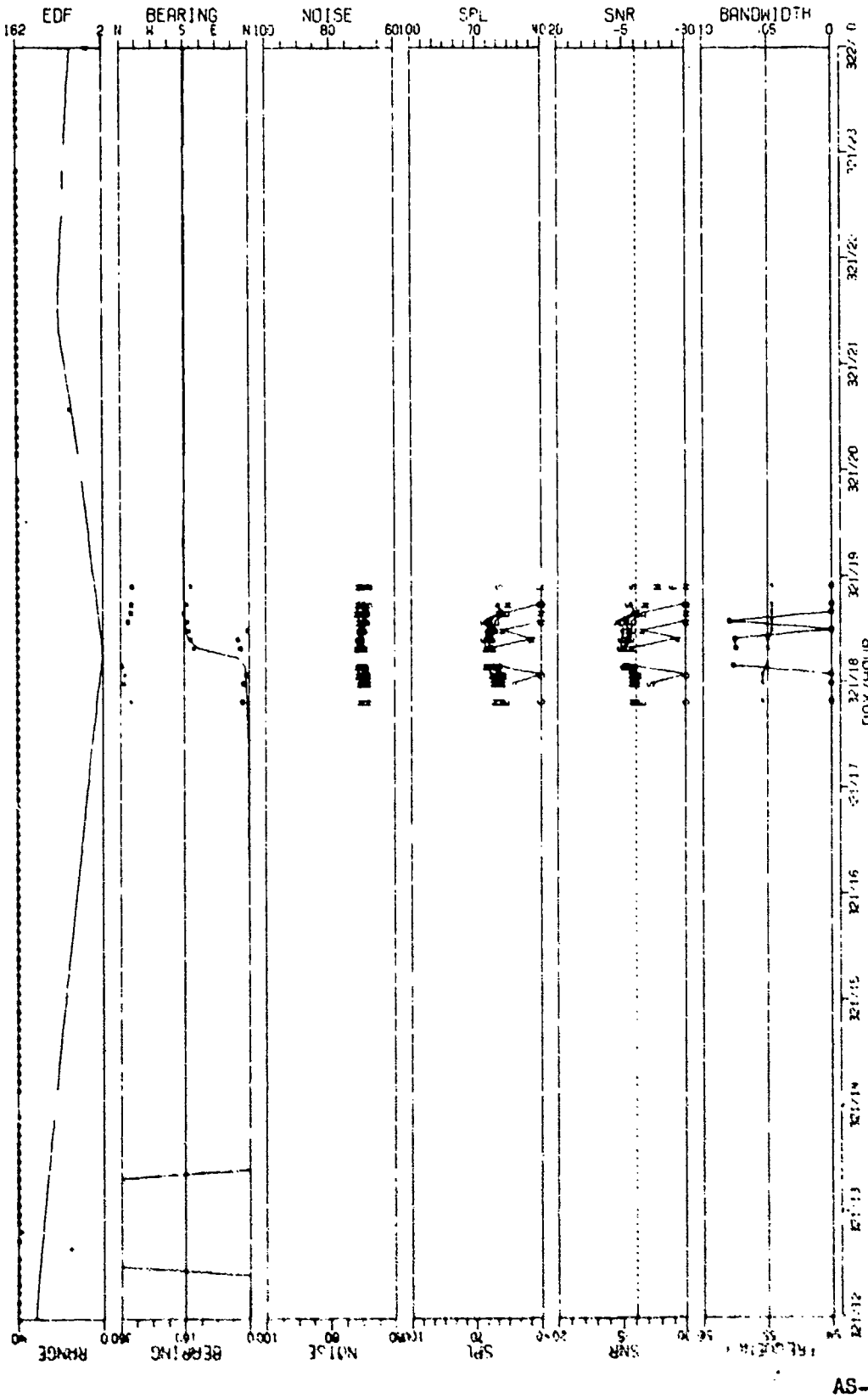

FIGURE 11-102
AS OBSERVED VIA THE DIFFERENCED CARDIOID SENSOR
AT SITE A3 DURING THE 17 NOV FIELD EVENT WITH STANDARD RESOLUTION (U)

AS-77-3029

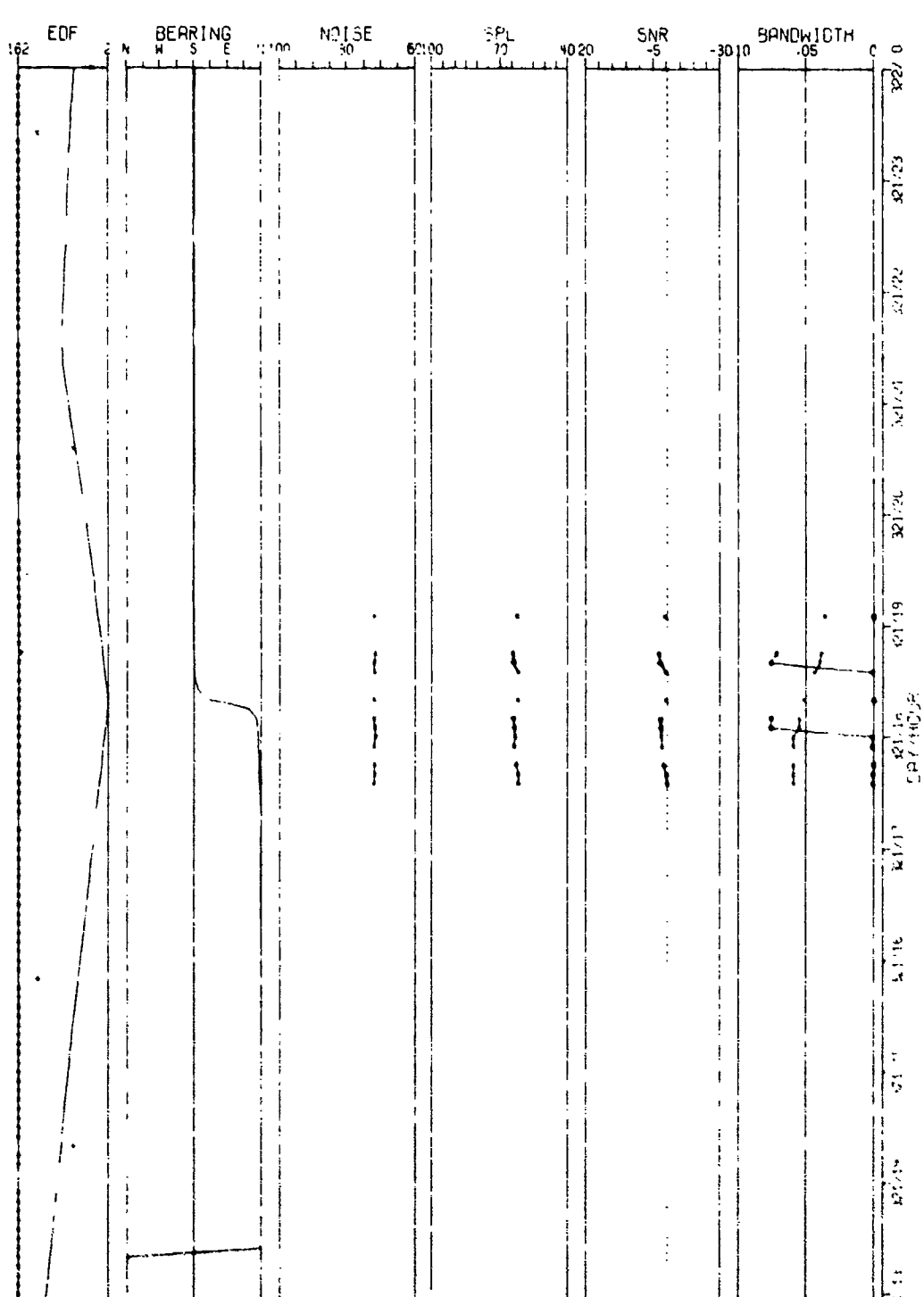

FIGURE 11-103
155H2 LINE HISTORY AS OBSERVED VIA THE OMNIDIRECTIONAL SENSOR
AS COPIED THE 17 NOV FIELD EVENT WITH STANDARD RESOLUTION (U)

AS-77-3030

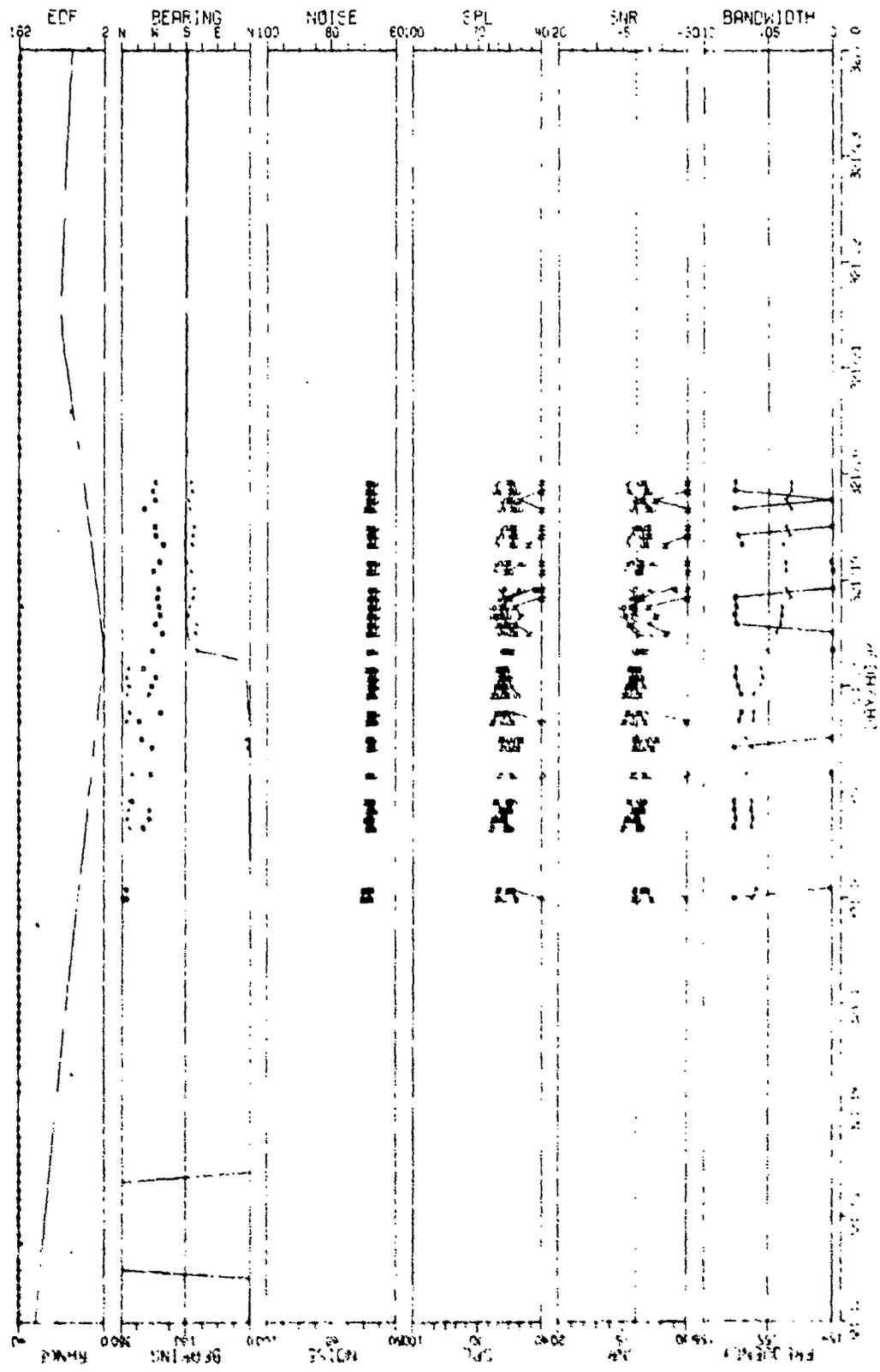

AS-77-3031

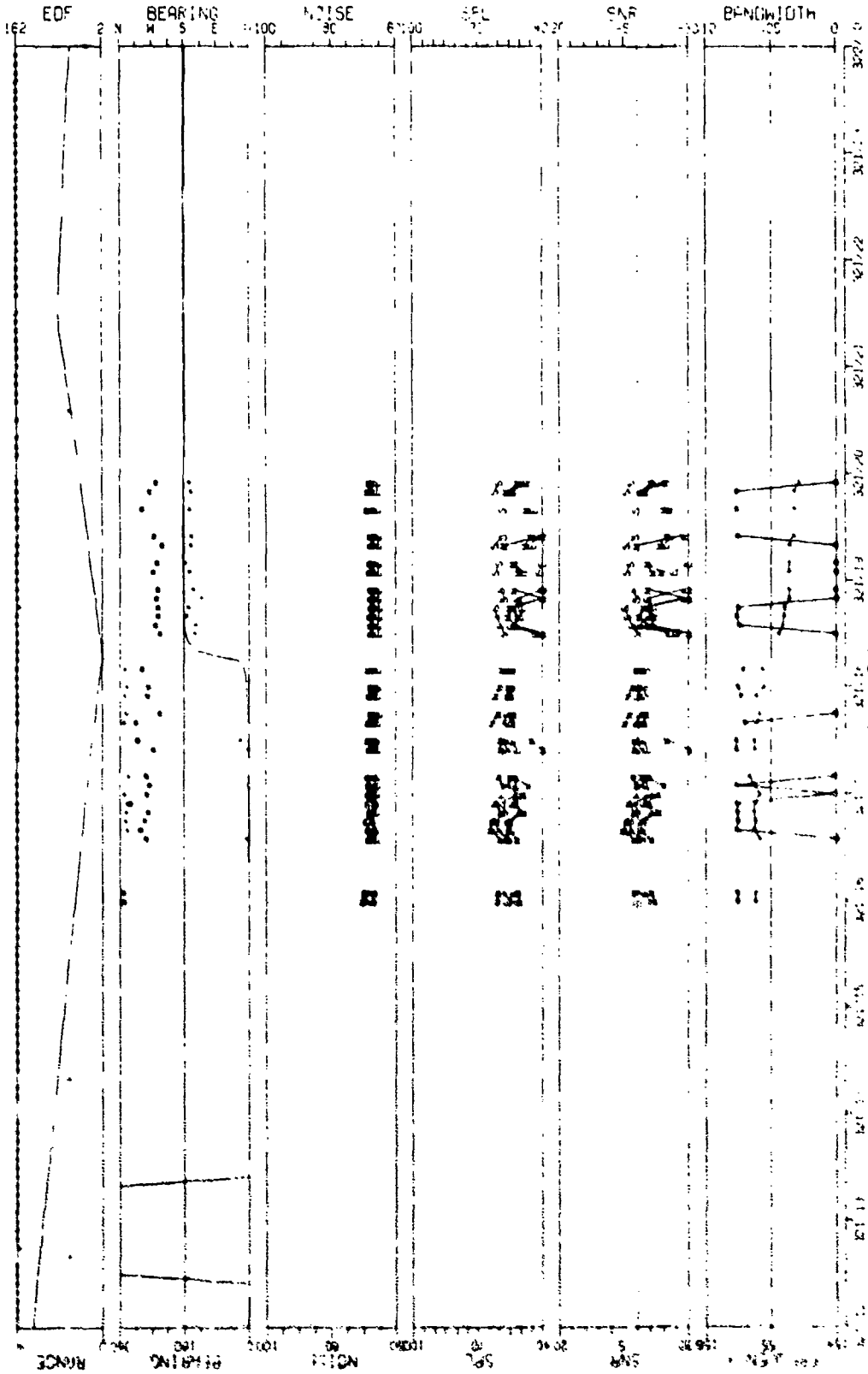
EOF
BEARING
NOISE
SEL
SNR
BANDWIDTH
RANGE
BEARING
NOISE
SEL
SNR
BANDWIDTH

AS-77-3032

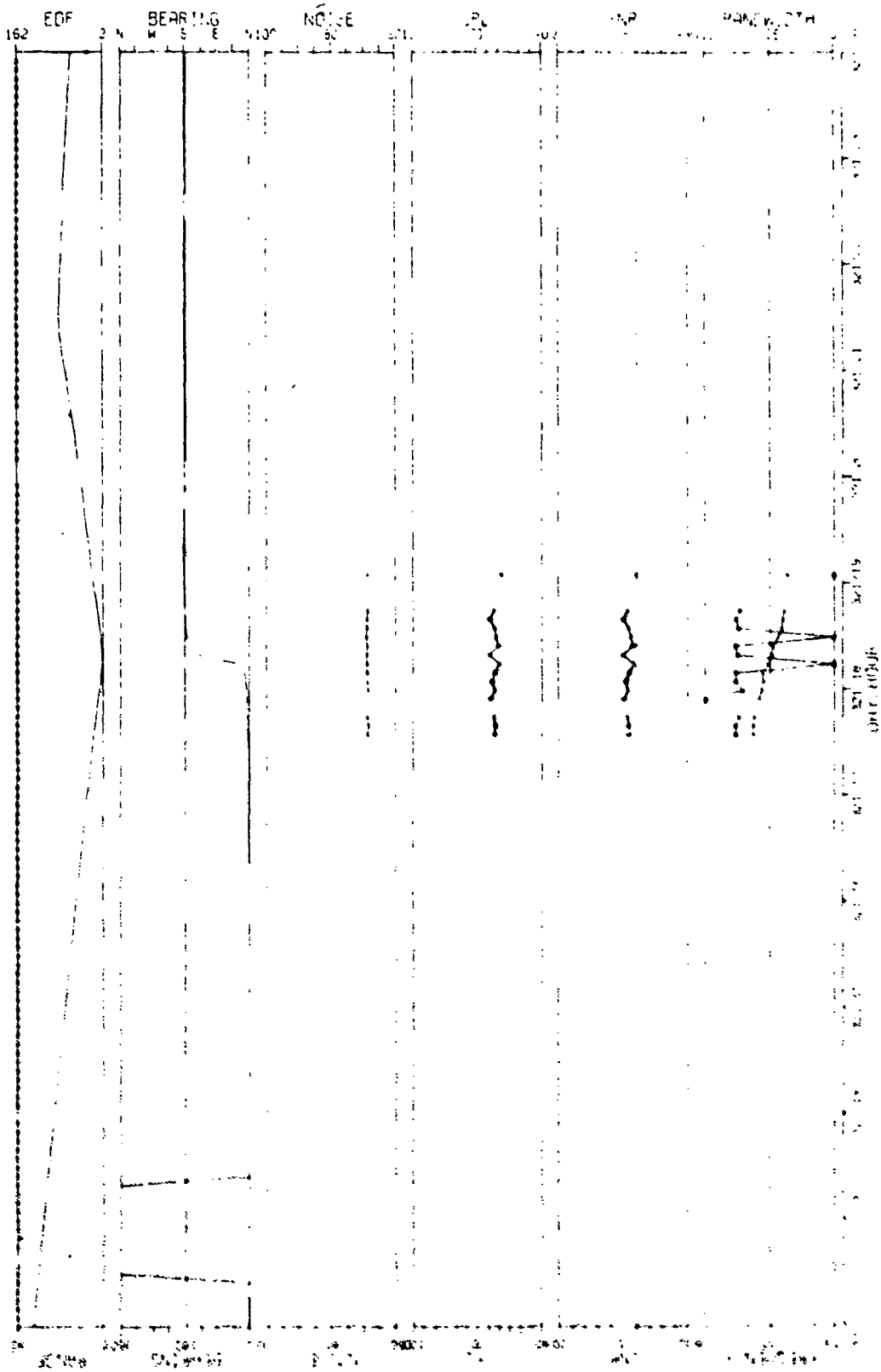

AS-77-3033

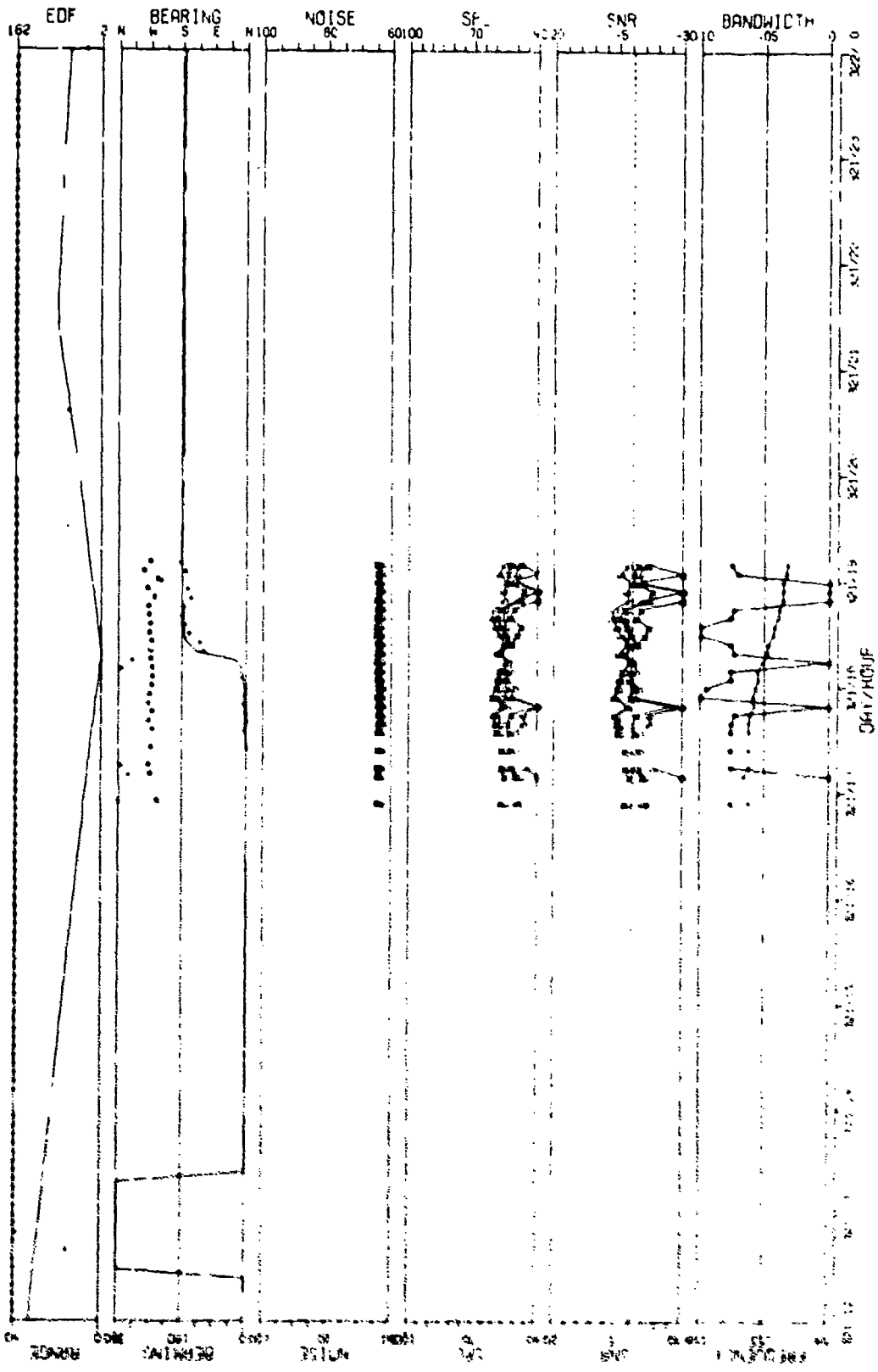

AS-77-3034

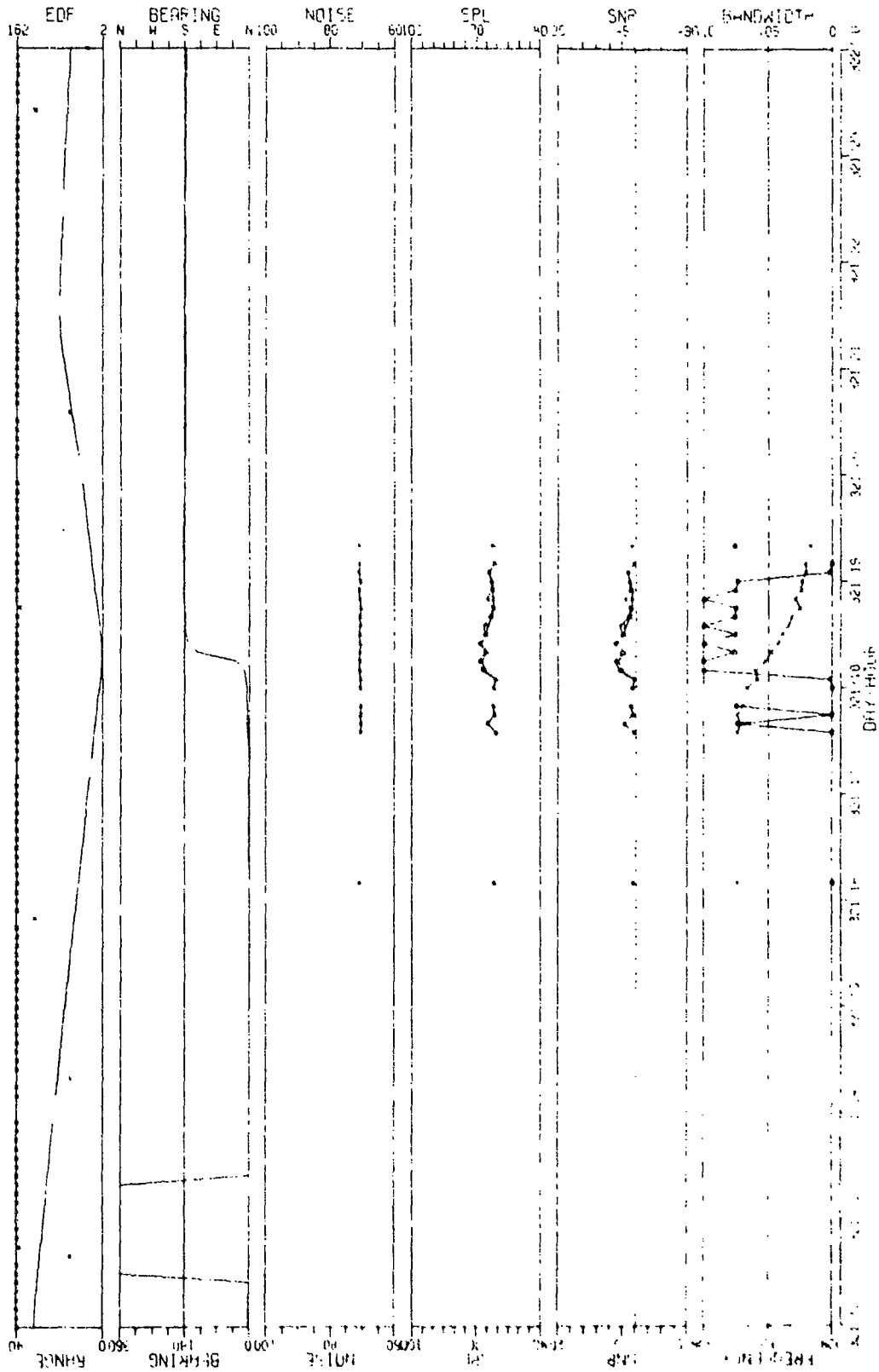

FIGURE 11-105

AS-77-3035

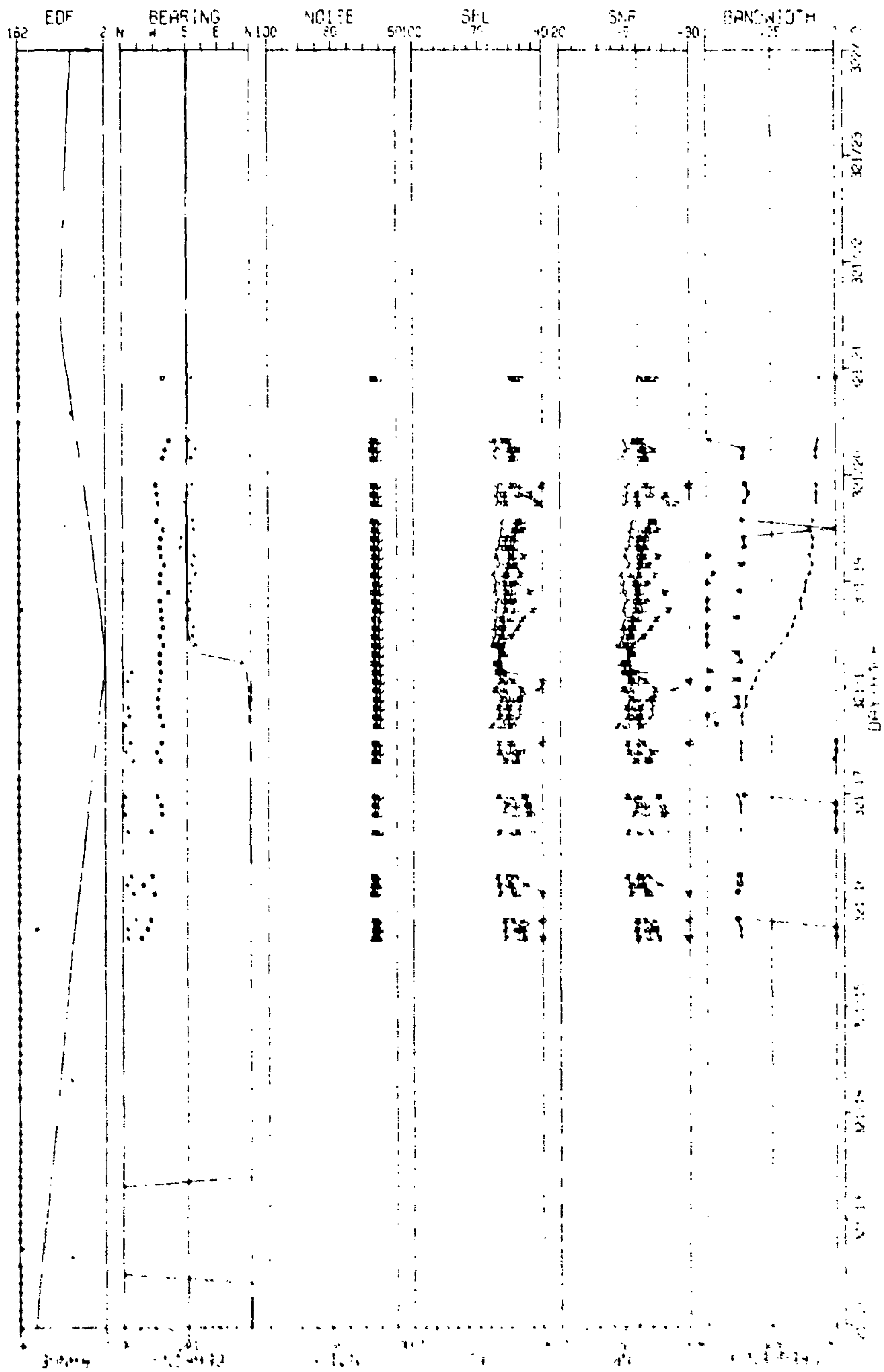

AS-77-3036

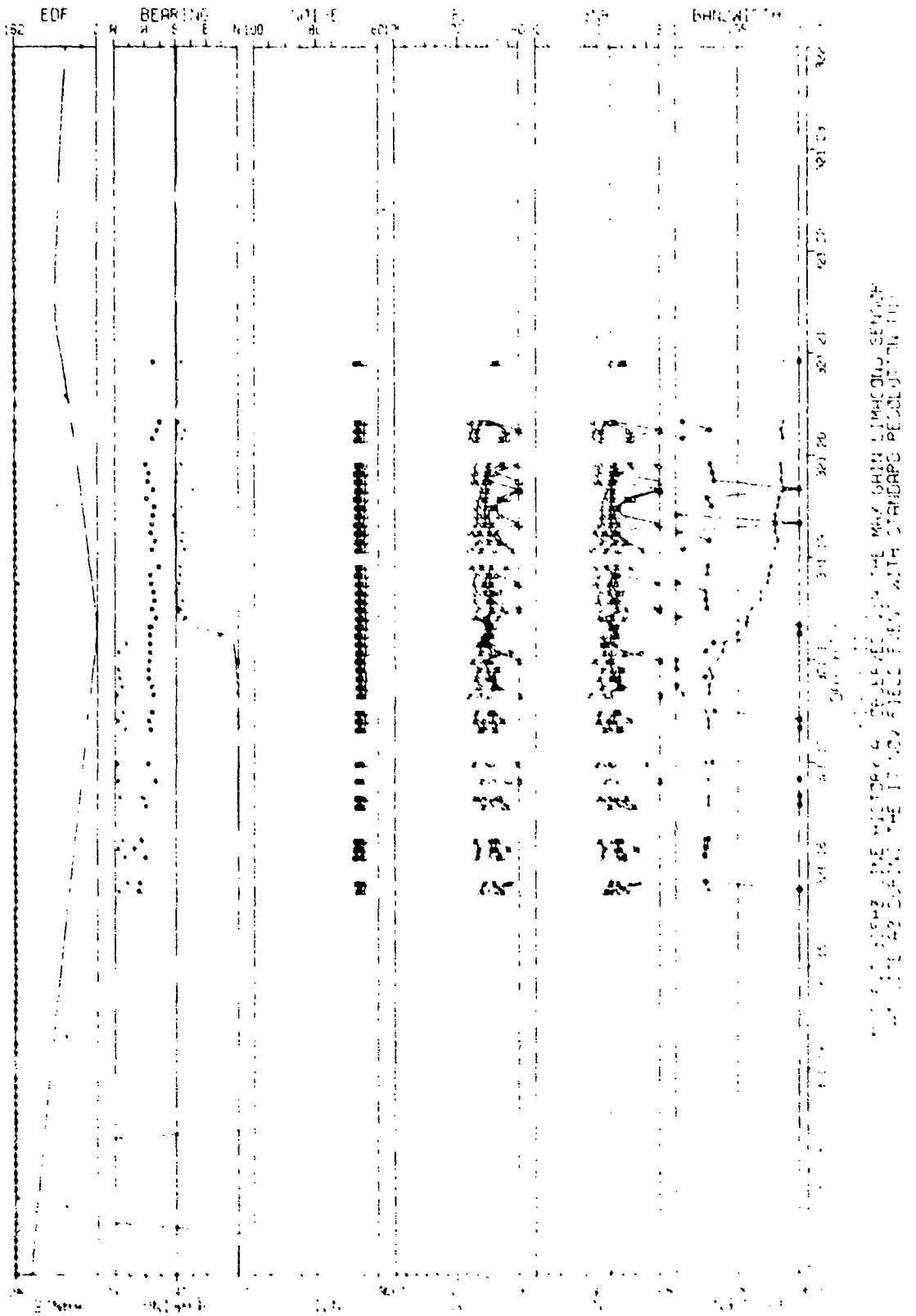

AS-77-3037

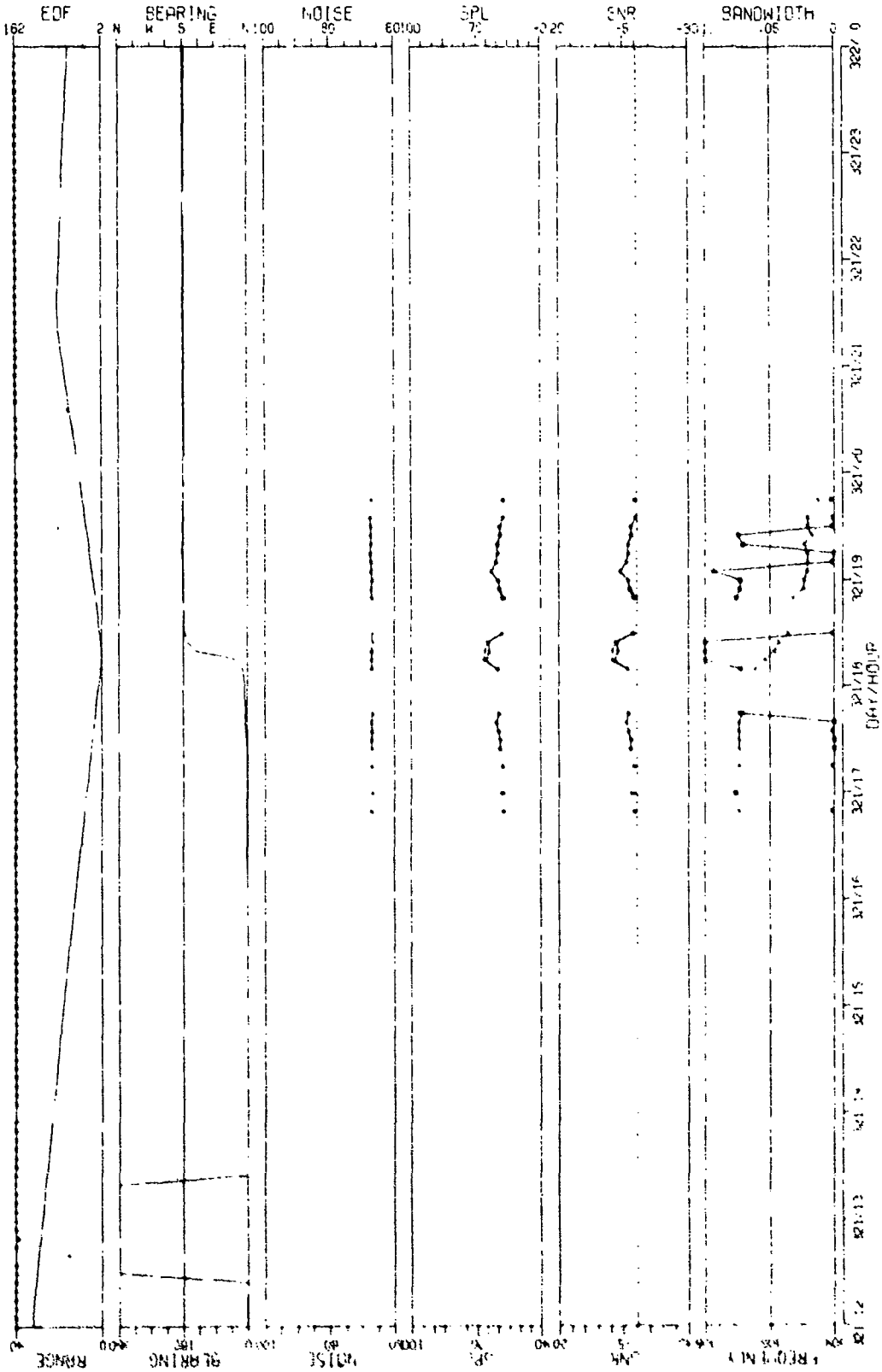

AS-77-3038

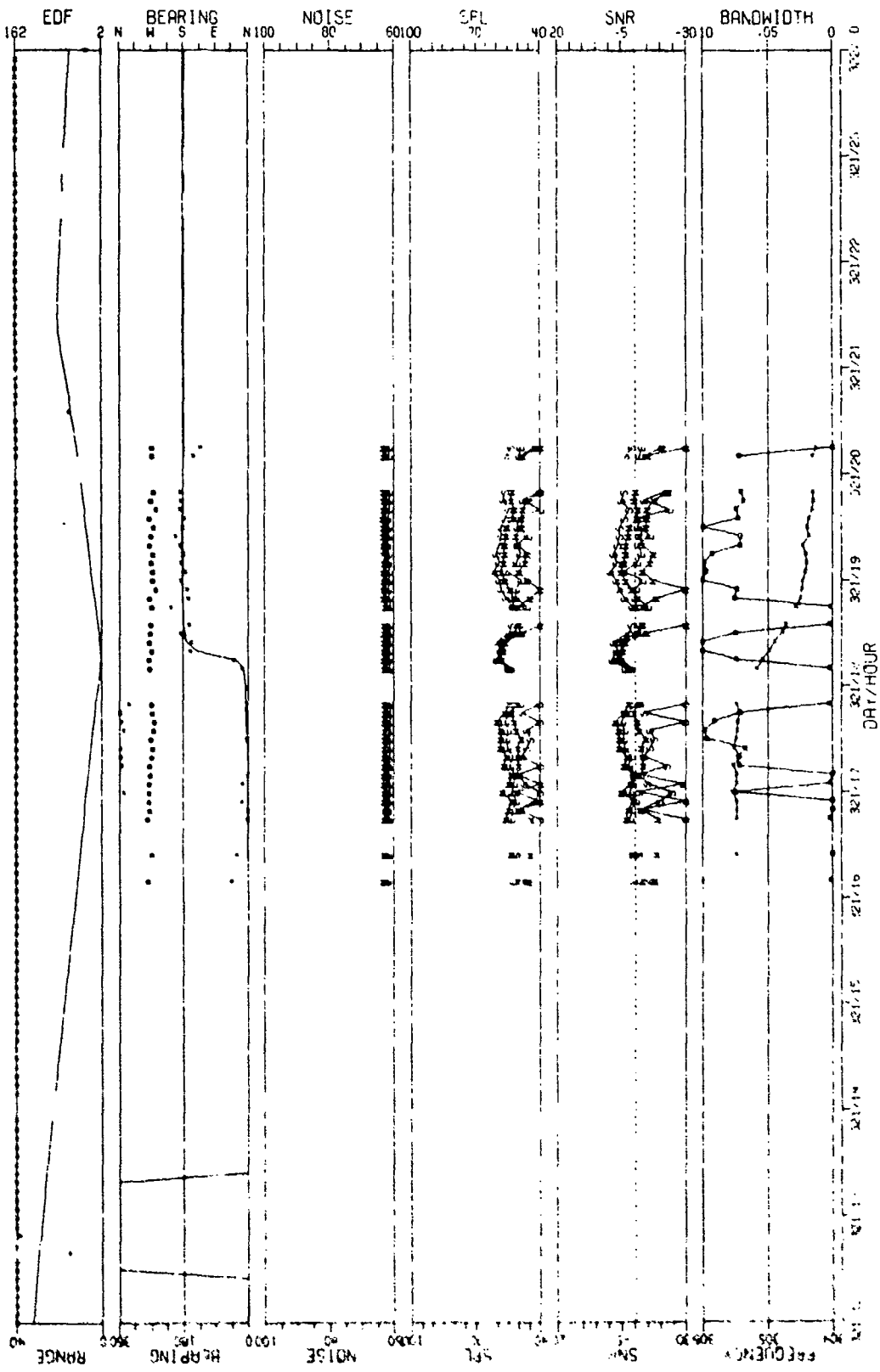

FIGURE II-112
[illegible] TIME HISTORY AS OBSERVED VIA THE DIFFERENCED CARDIOIDS SENSOR
[illegible] DURING THE 17 NOV FIELD EVENT WITH STANDARD RESOLUTION (U)

AS-77-3039

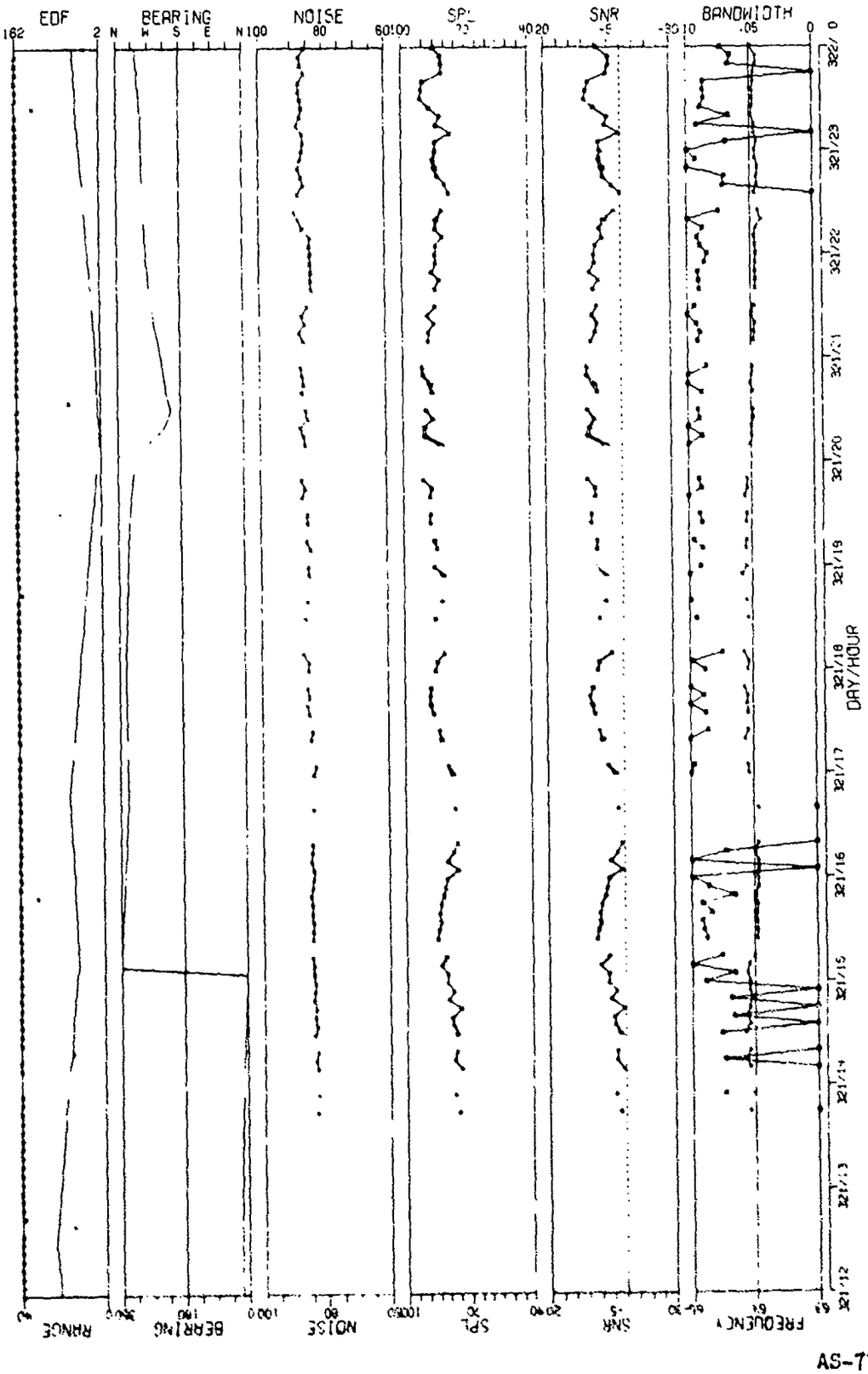

FIGURE 11-113
OBSERVED VIA THE OMNIDIRECTIONAL SENSOR
DURING THE 17 NOV FIELD EVENT WITH STANDARD RESOLUTION FOR

AS-77-3040

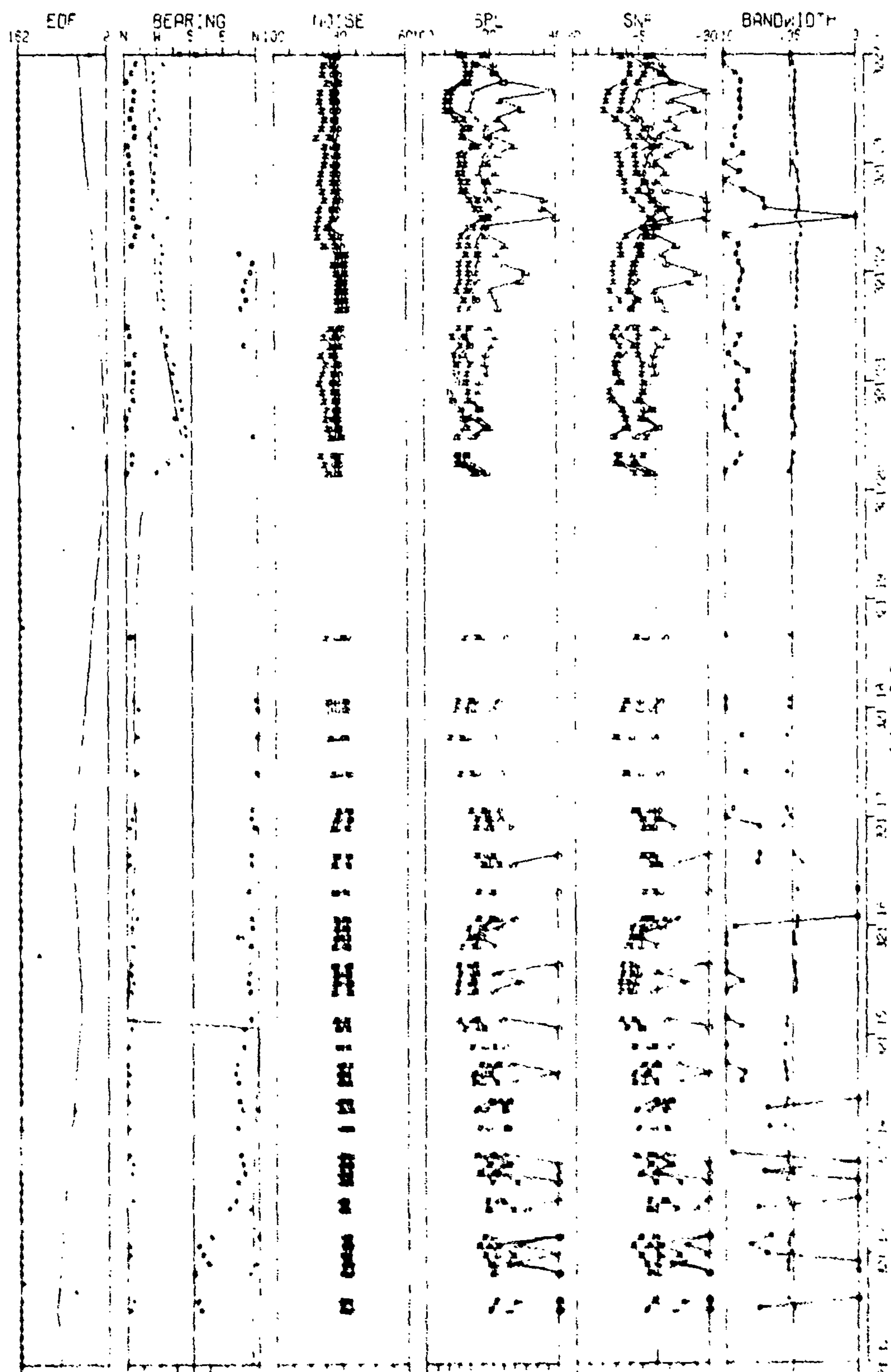

FIGURE II-1.4
MSG-FVT 6NHZ LINE HISTORY AS OBSERVED VIA THE SINGLE CARDIOID SENSOR AT SITE A3 DURING THE 17 NOV FIELD EVENT WITH STANDARD RESOLUTION (U)

AS-77-3041

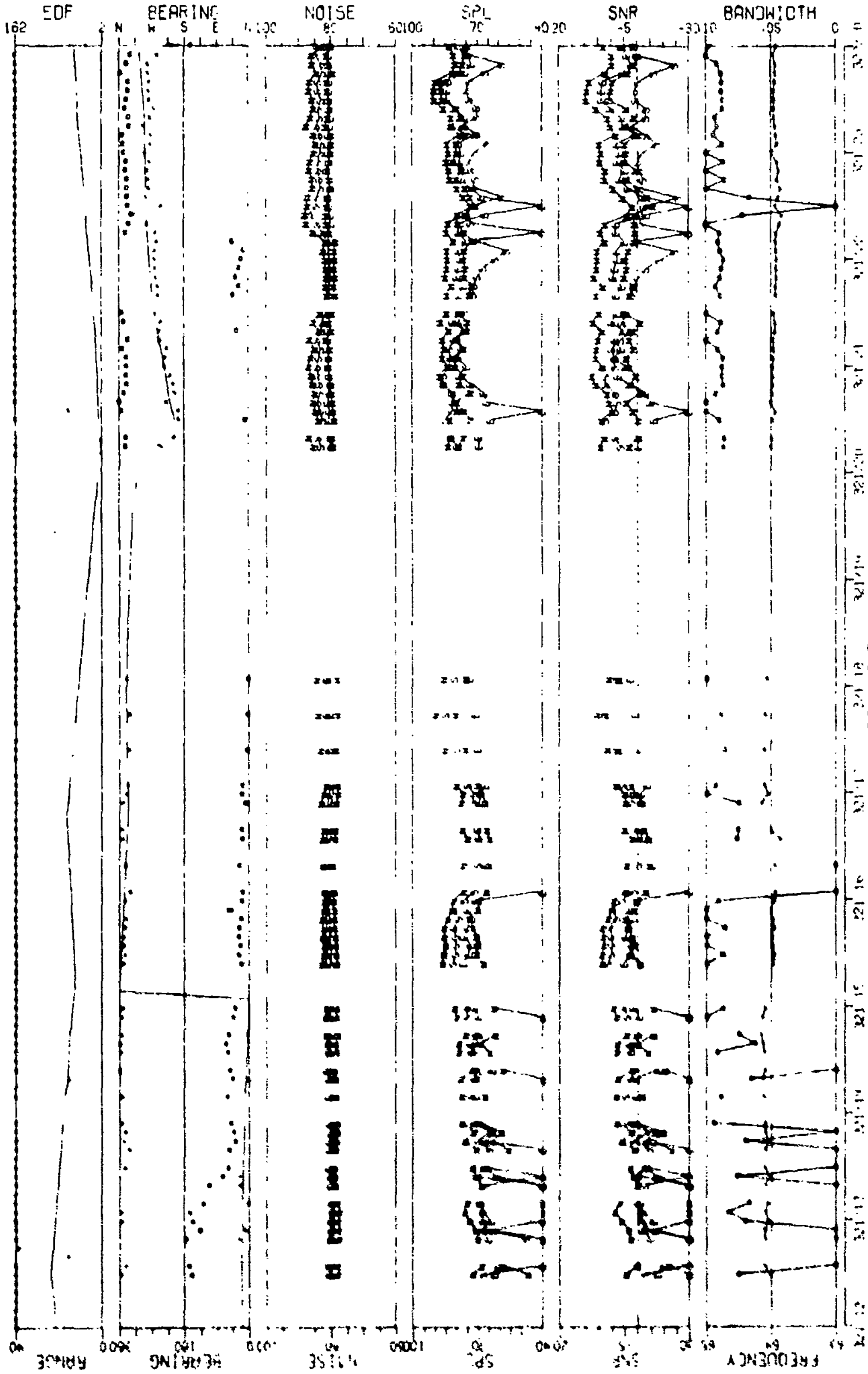

FIGURE II-1[illegible]
MSS (F?) 64HZ LINE HISTORY AS OBSERVED VIA THE MAX GAIN LIMACONS SENSOR AT SITE A3 DURING THE 17 NOV FIELD EVENT WITH STANDARD RESOLUTION (U)

AS-77-3042

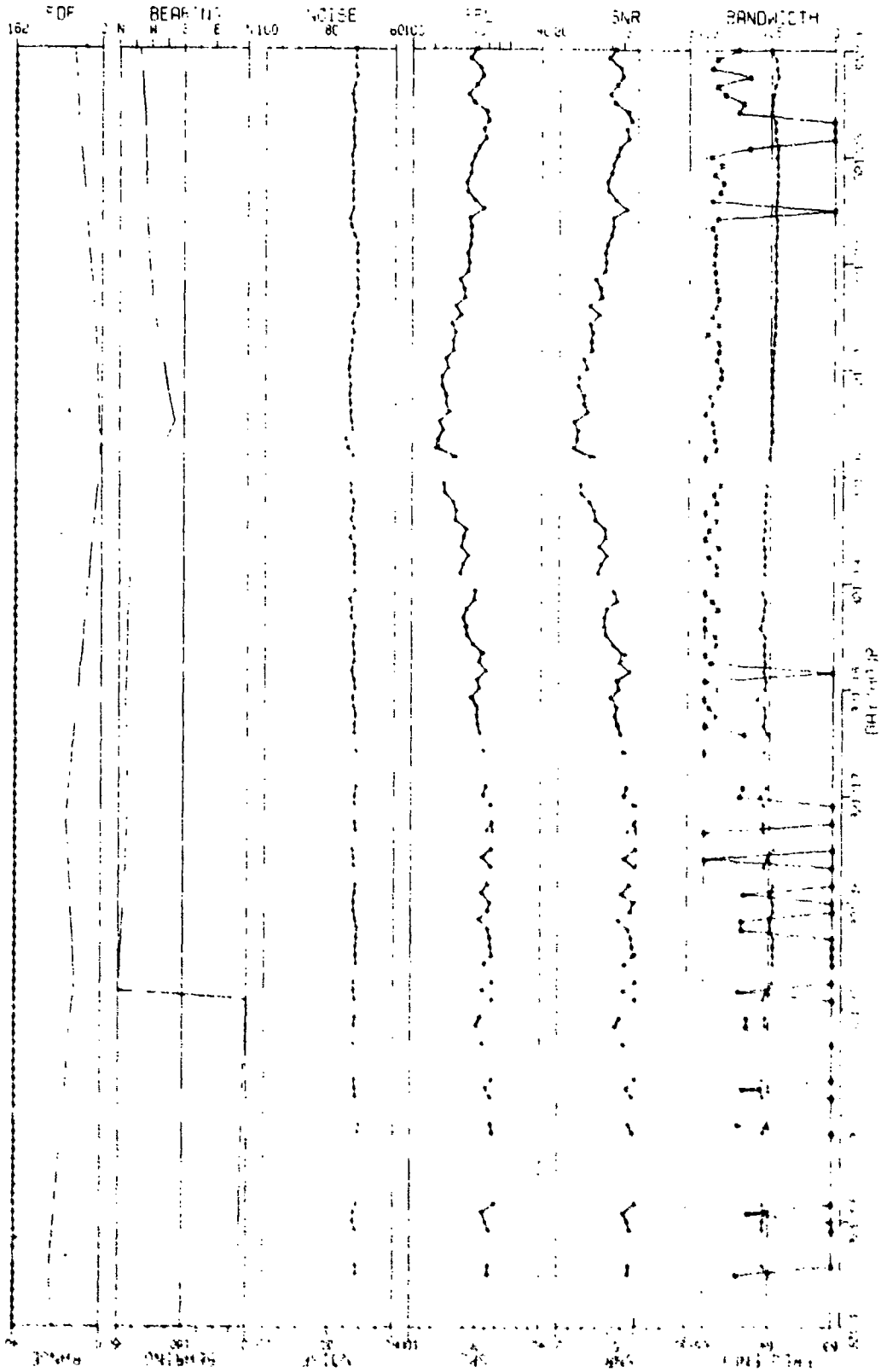

AS-77-3043

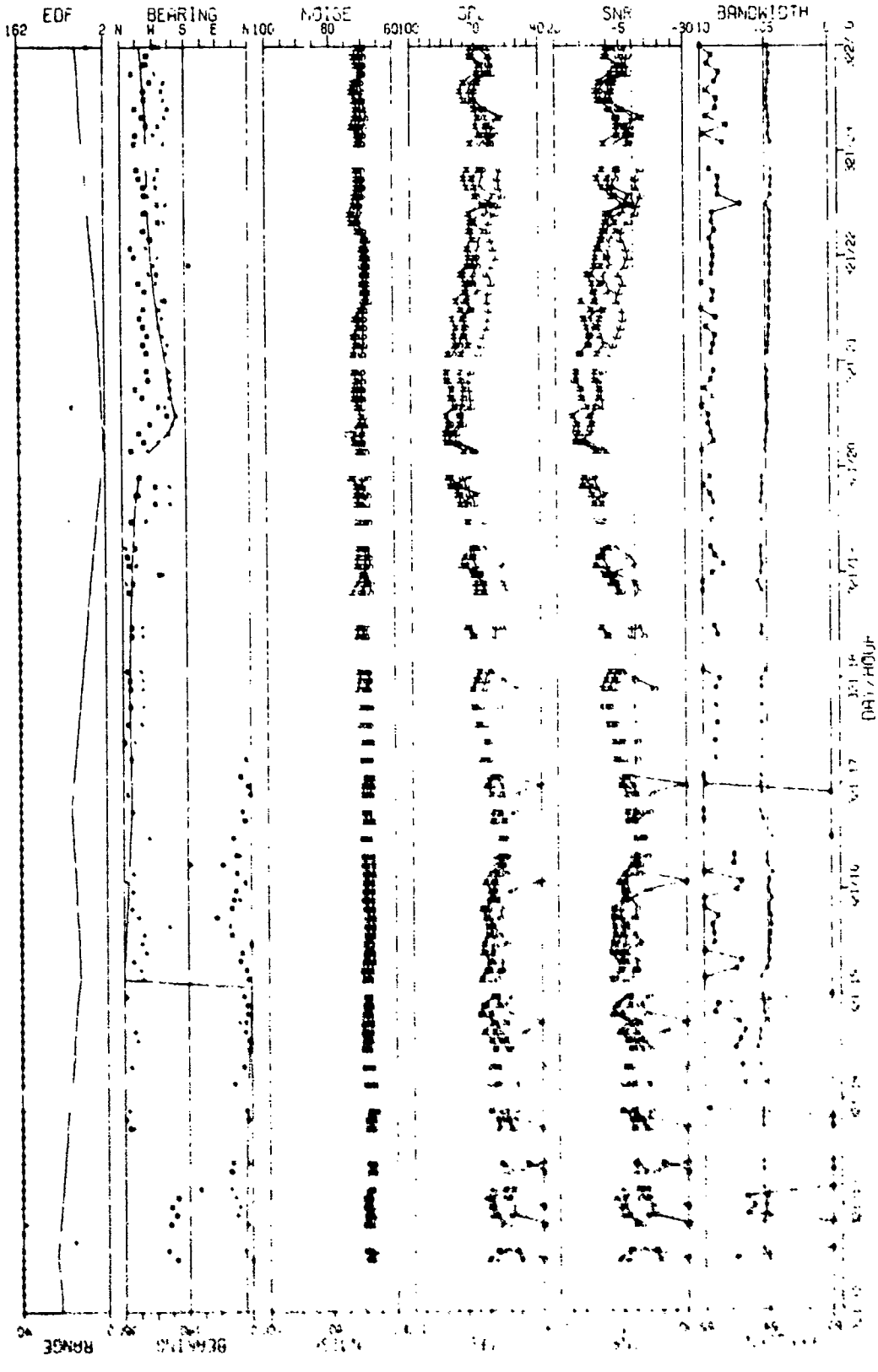

AS-77-3044

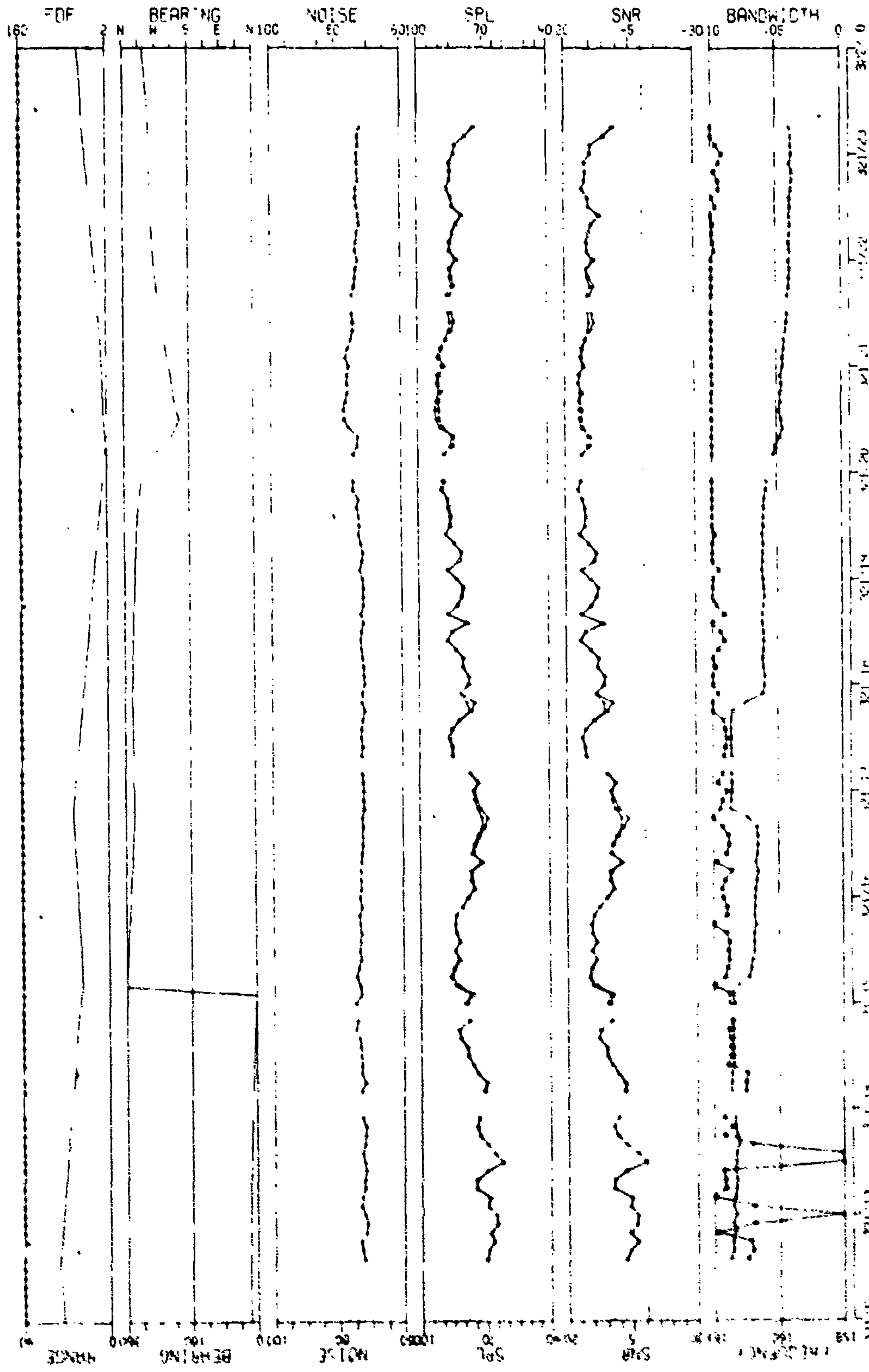

FIGURE II-11[illegible]
[illegible] 160HZ LINE HISTORY AS OBSERVED [illegible] THE OMNIDIRECTIONAL SENSOR
[illegible] SITE [illegible] DURING THE 17 NOV FIELD EVENT WITH STANDARD RESOLUTION [illegible]

AS-77-3045

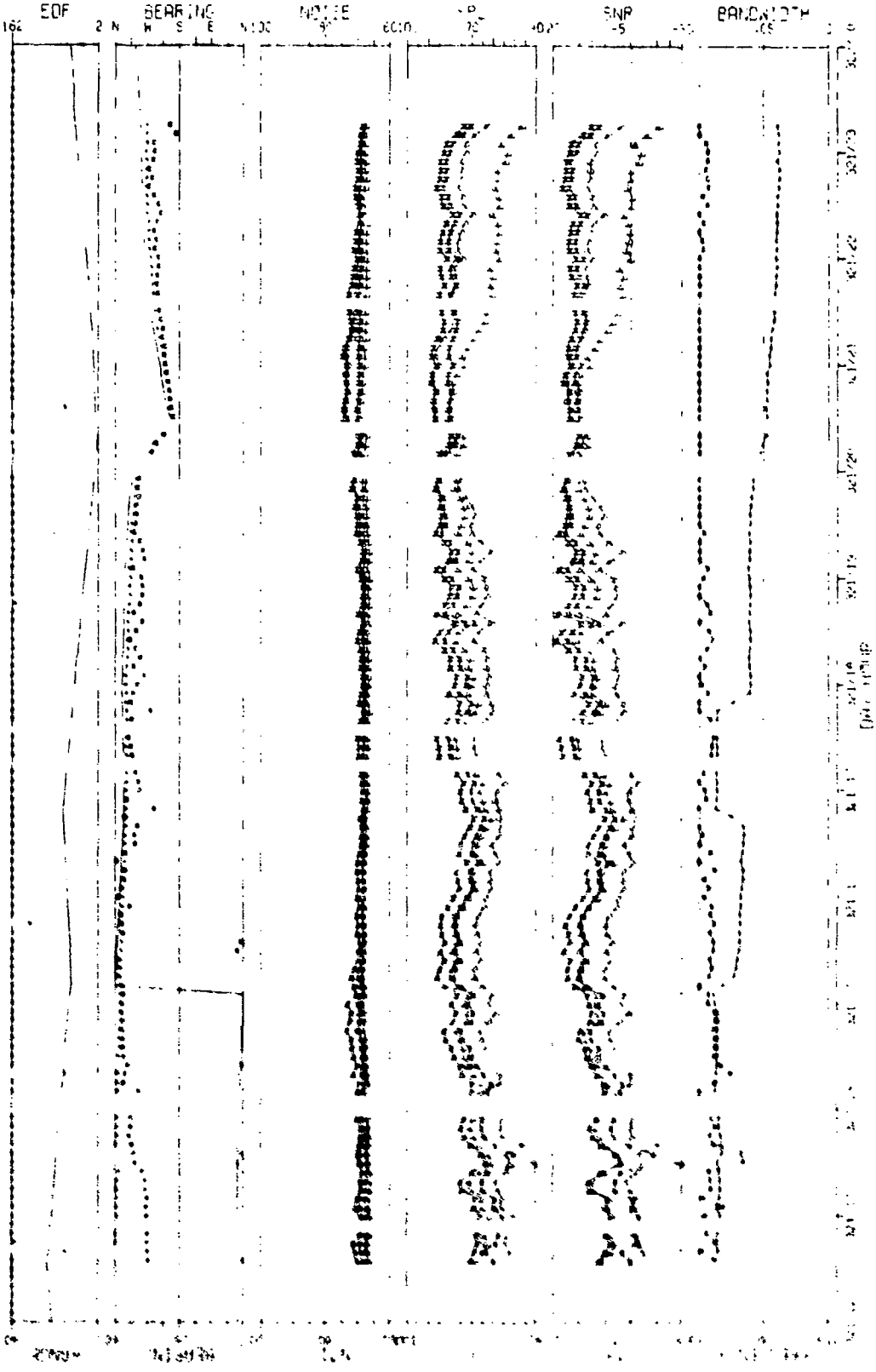

AS-77-3046

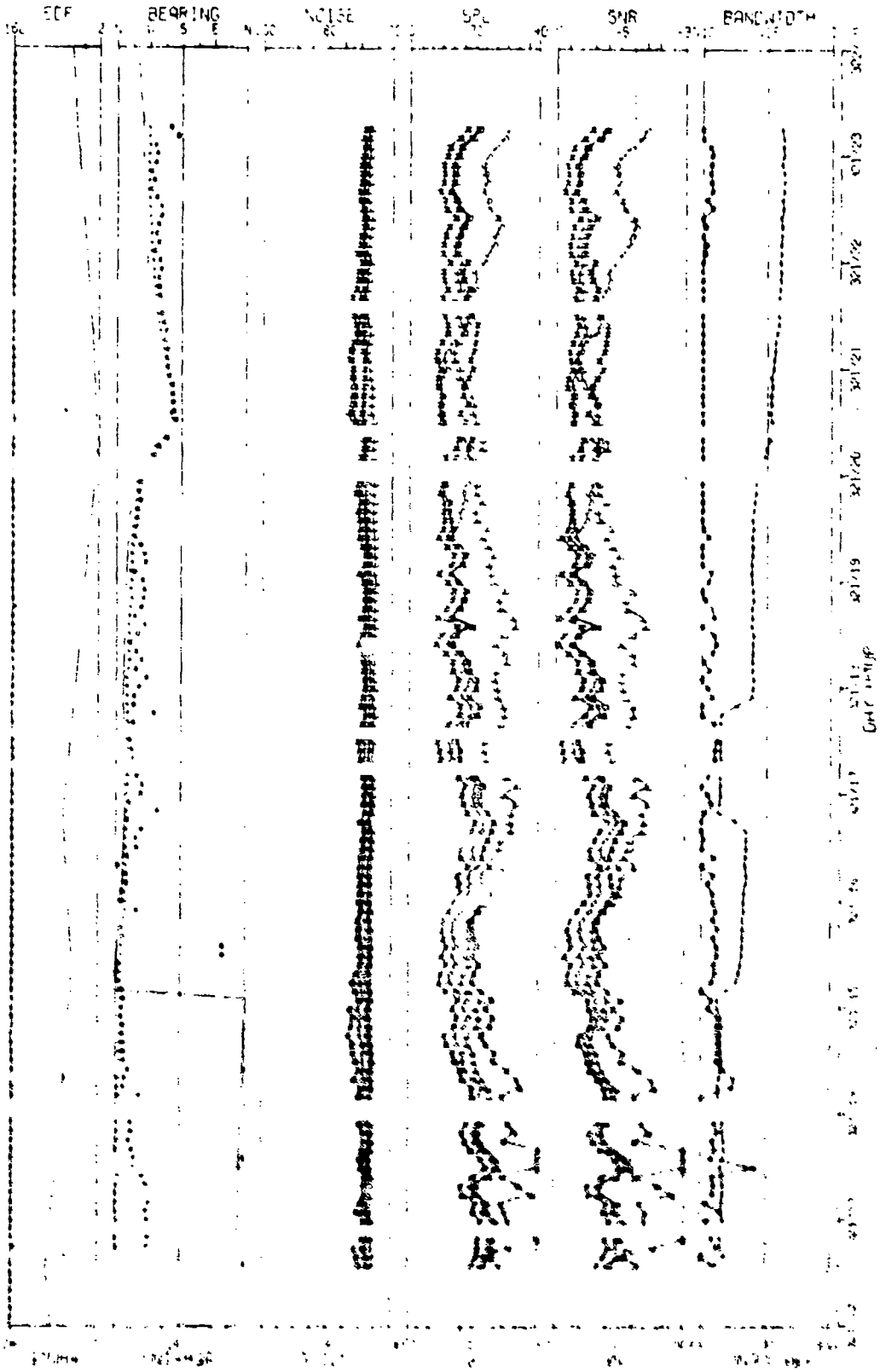

AS-77-3047

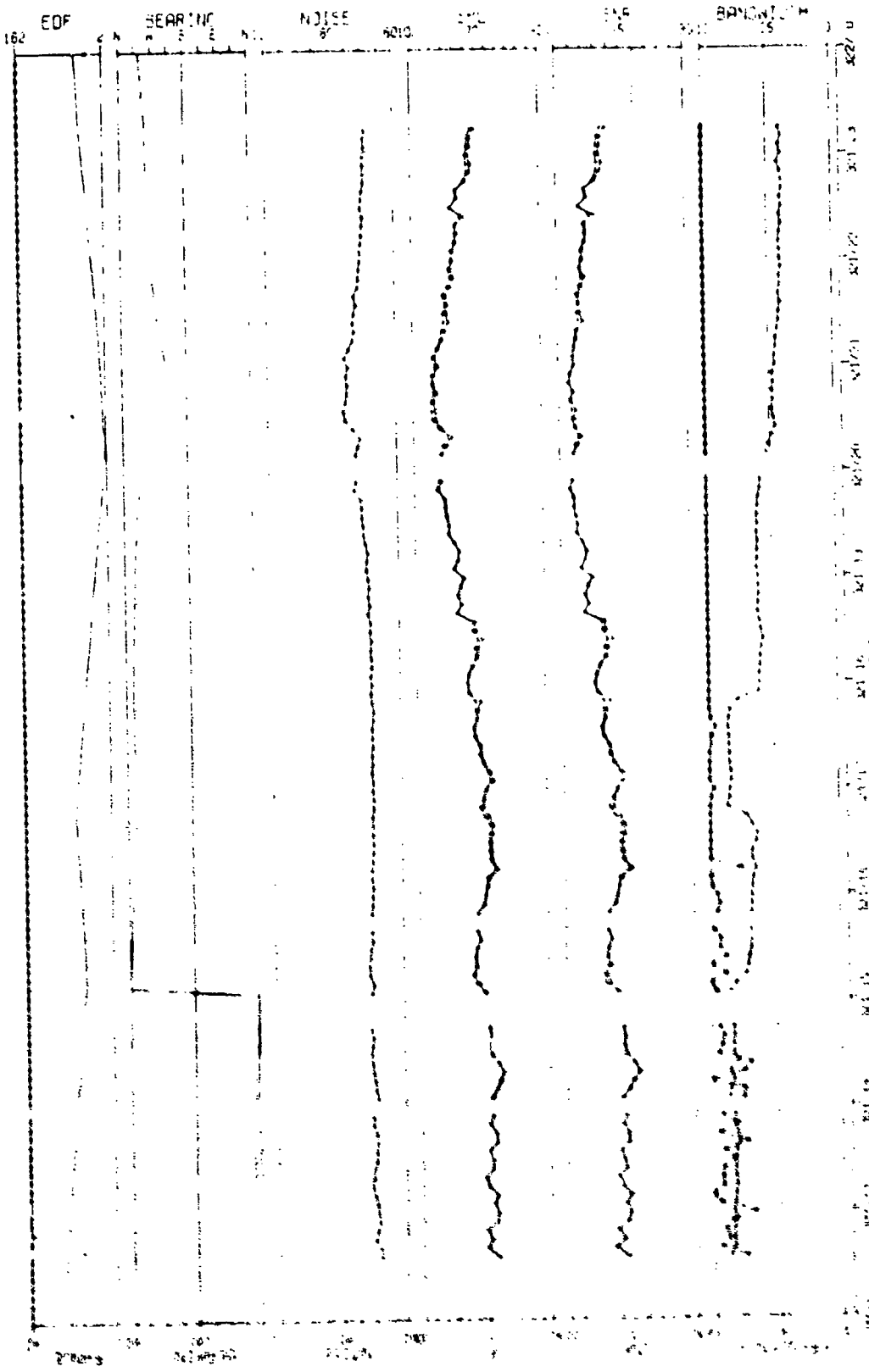

AS-77-3046

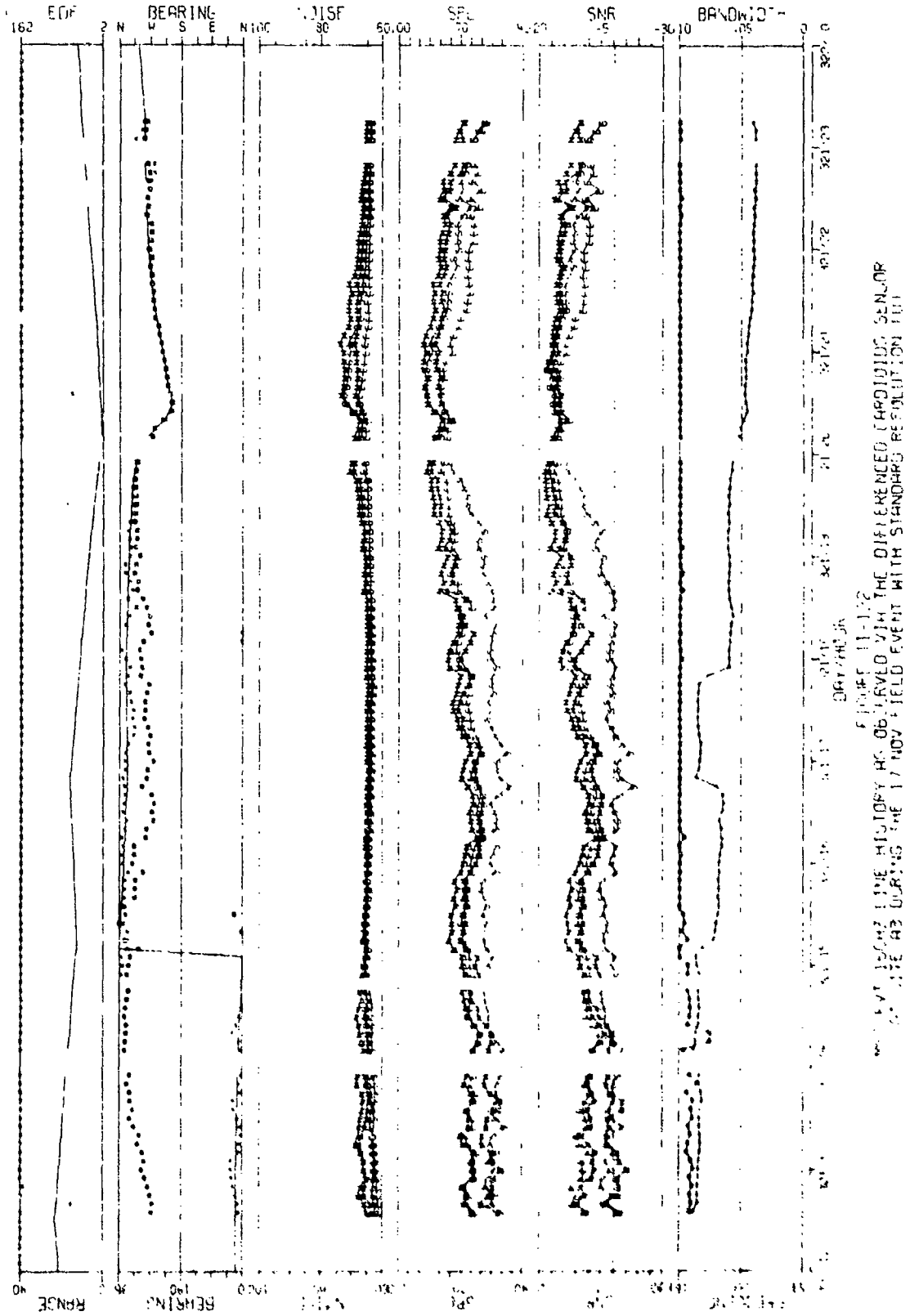

AS-77-3049

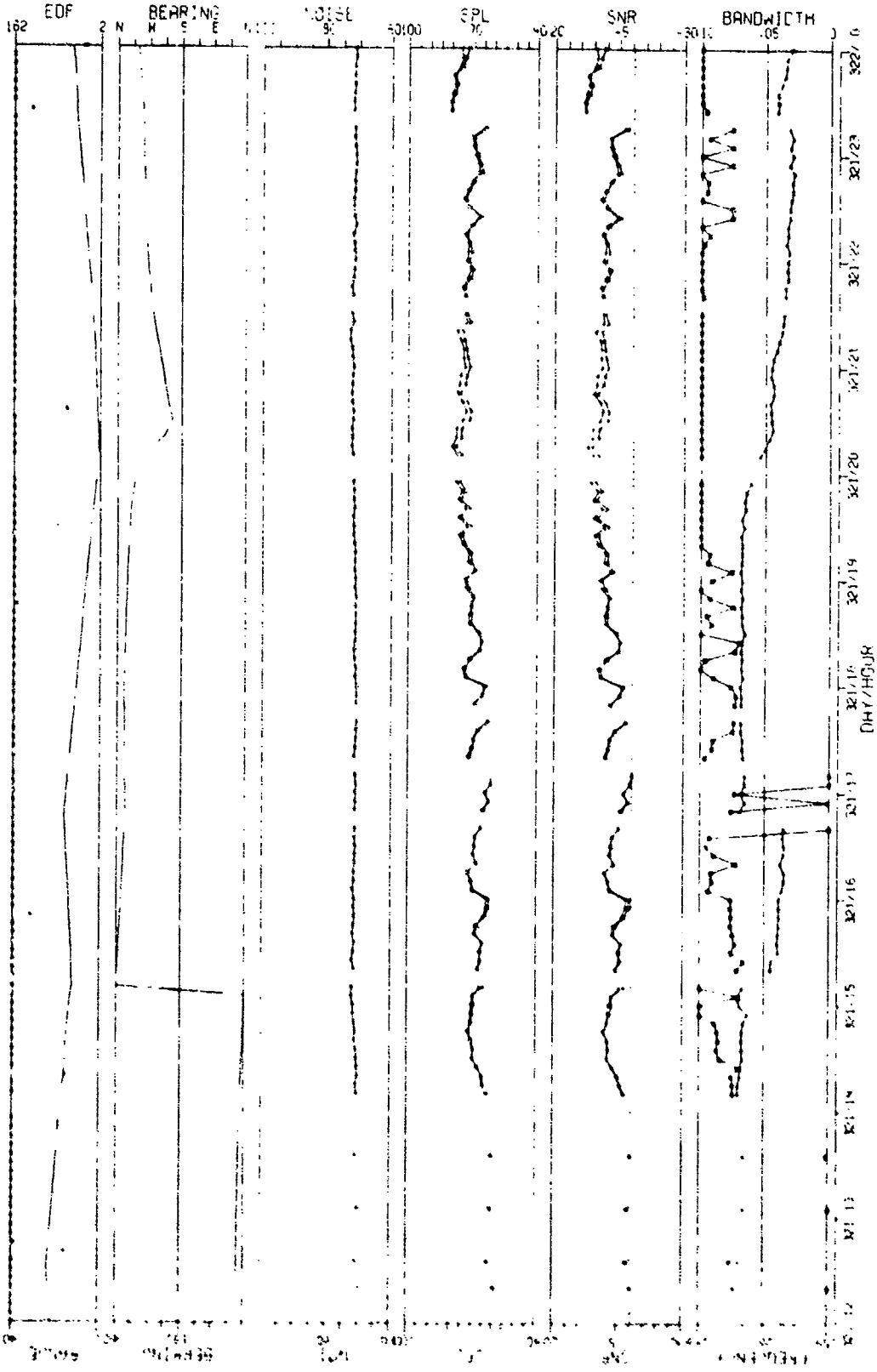

AS-77-3050

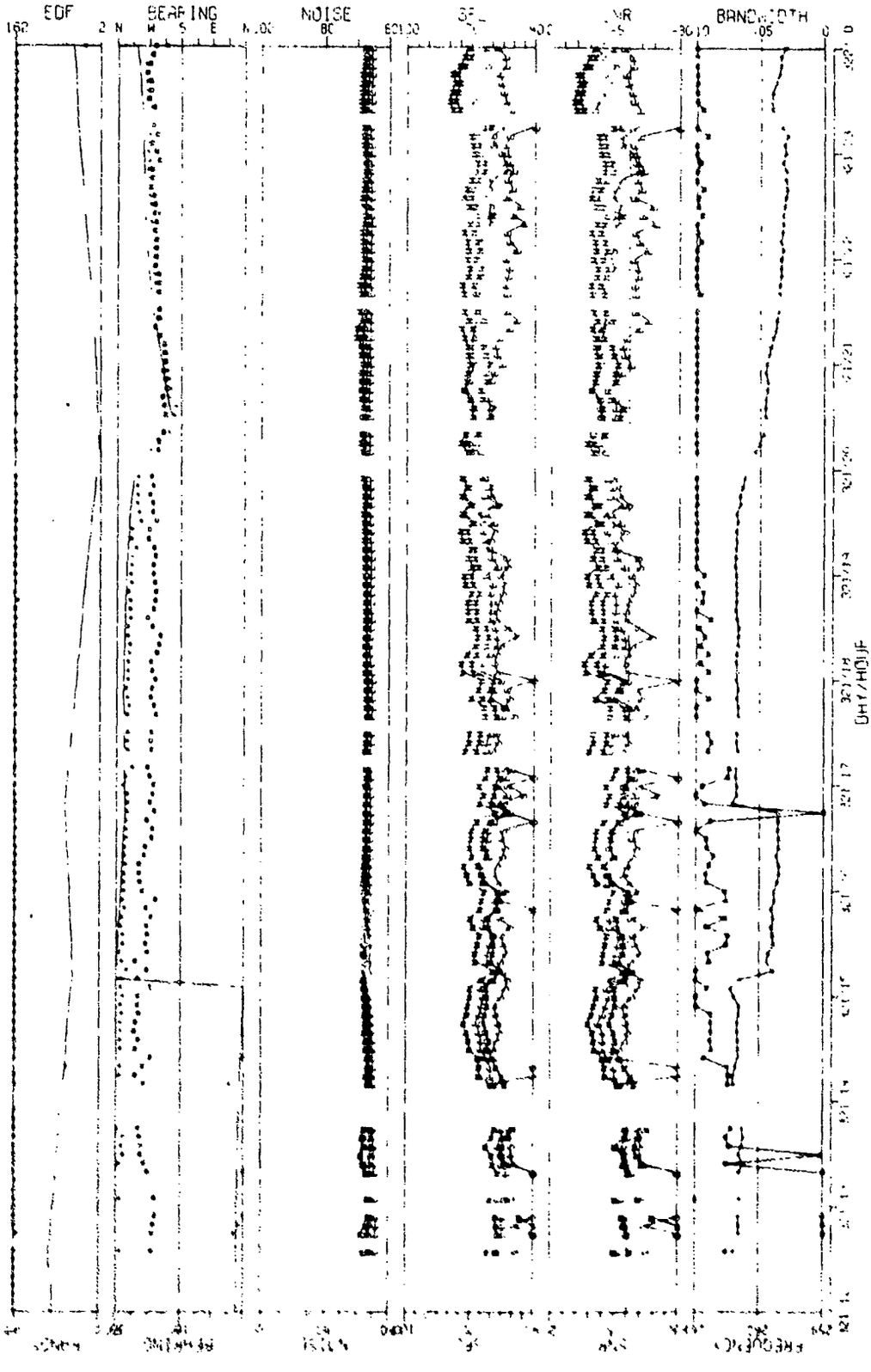

AS-77-3051

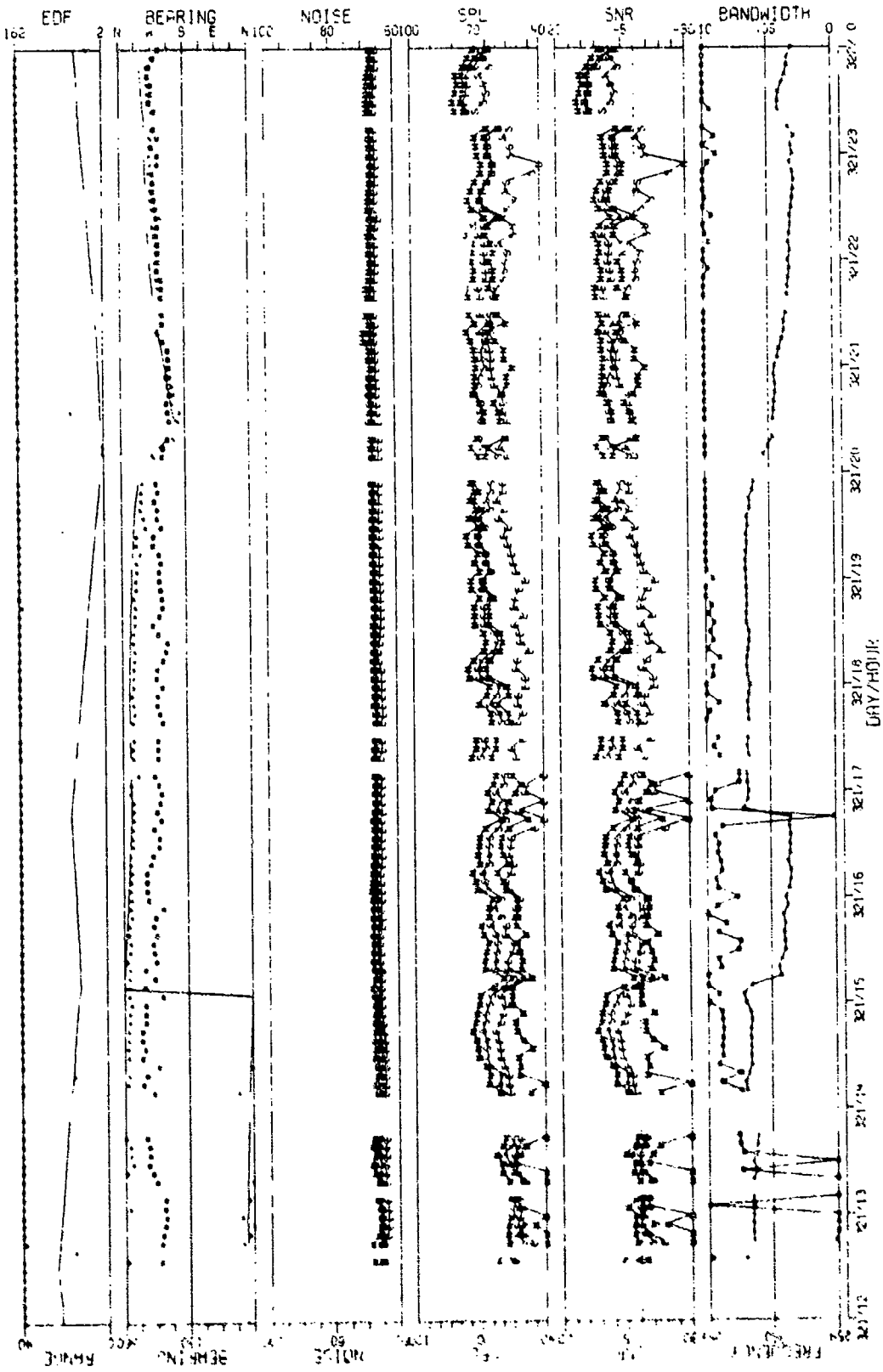

AS-77-3052

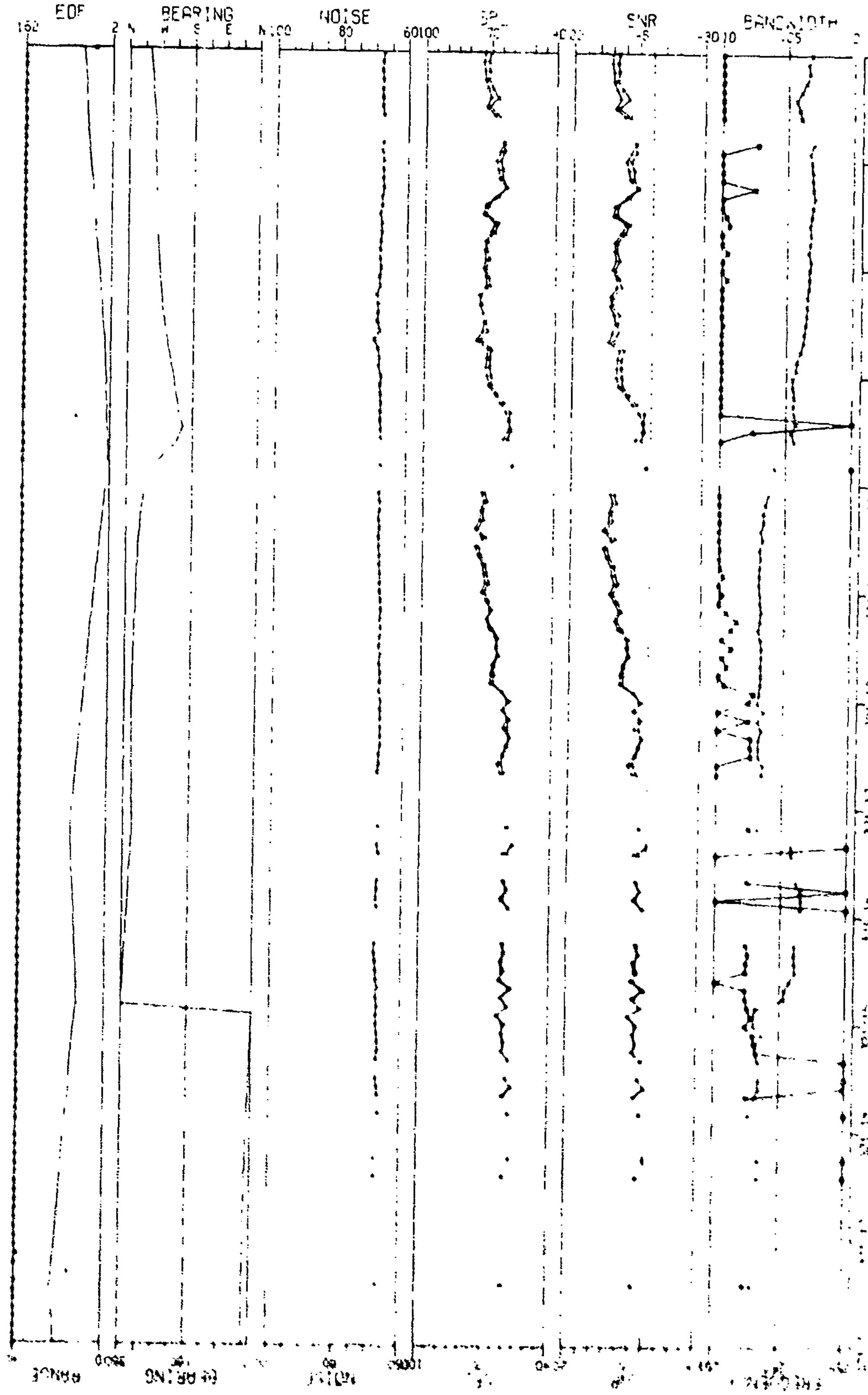

FIGURE [illegible]
MSS EVT 260HZ LINE HISTORY AS OBSERVED VIA THE VERTICAL DIPOLE SENSOR AT SITE A3 DURING THE 17 NOV FIELD EVENT WITH STANDARD RESOLUTION (U)

AS-77-3053

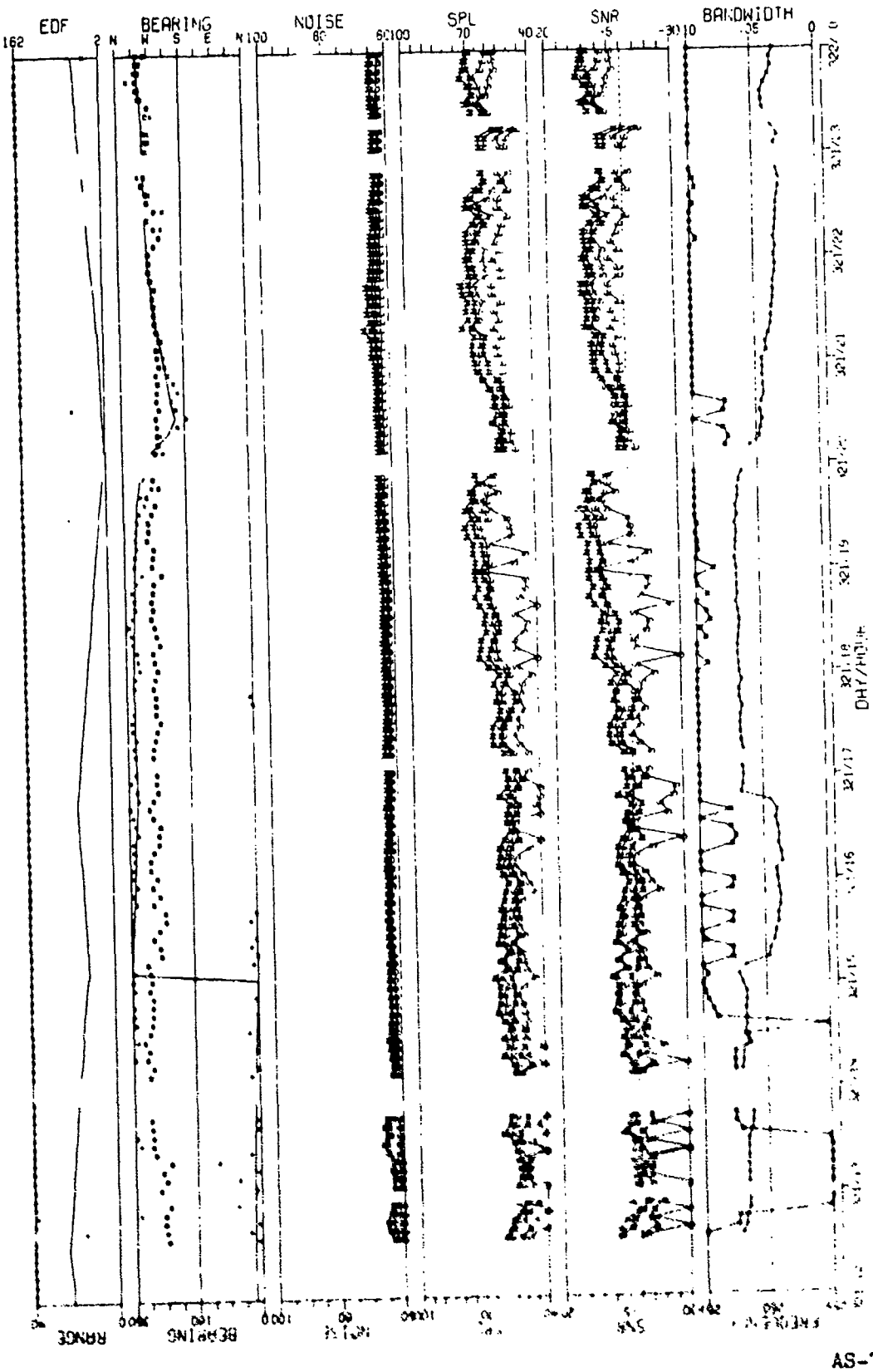

FIGURE 11-127
OBSERVED VIH THE DIFFERENCED CARDIOIDS SENSOR
DURING THE 17 NOV FIELD EVENT WITH STANDARD RESOLUTION (U)

AS-77-3054

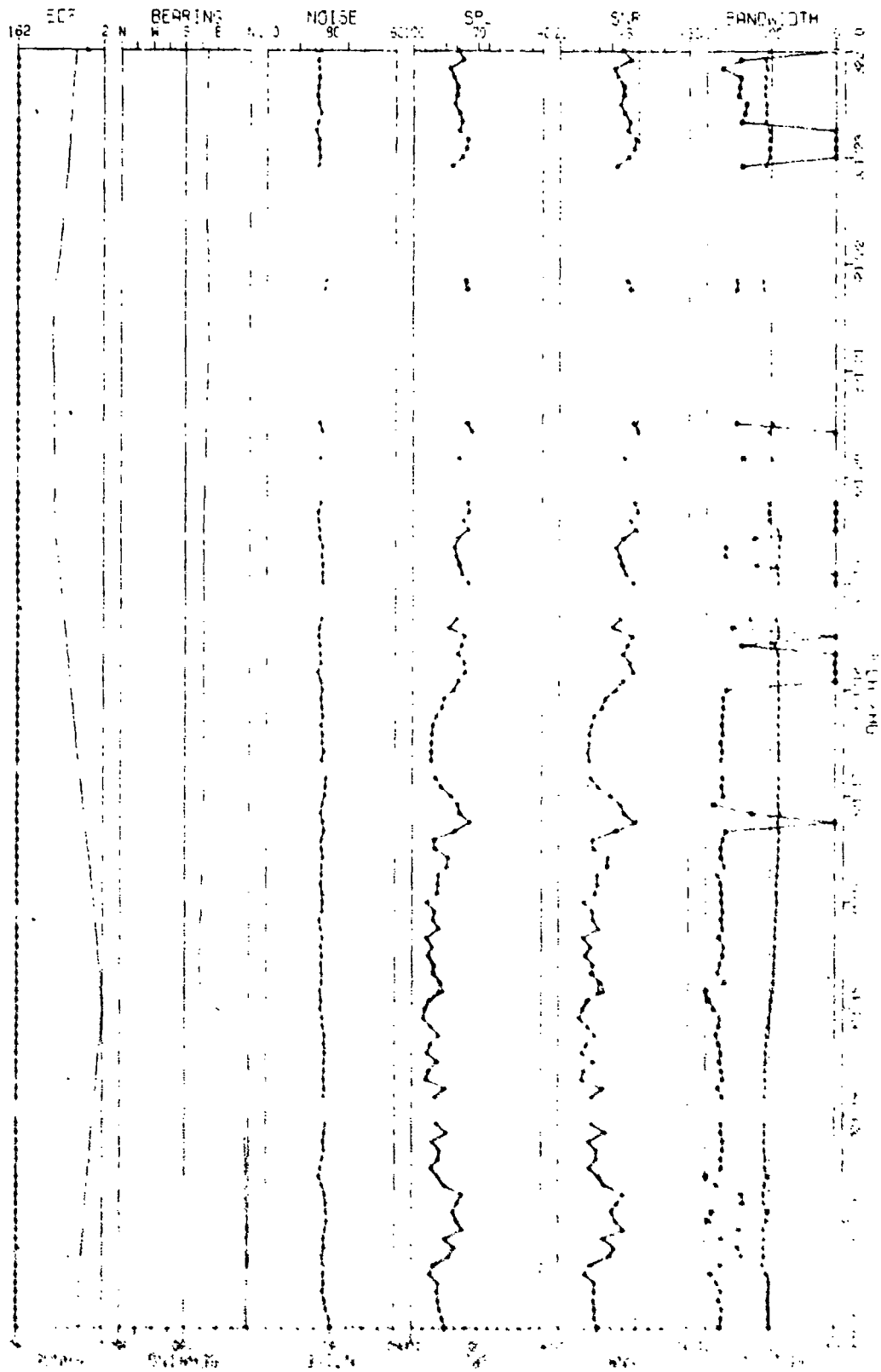

AS-77-3055

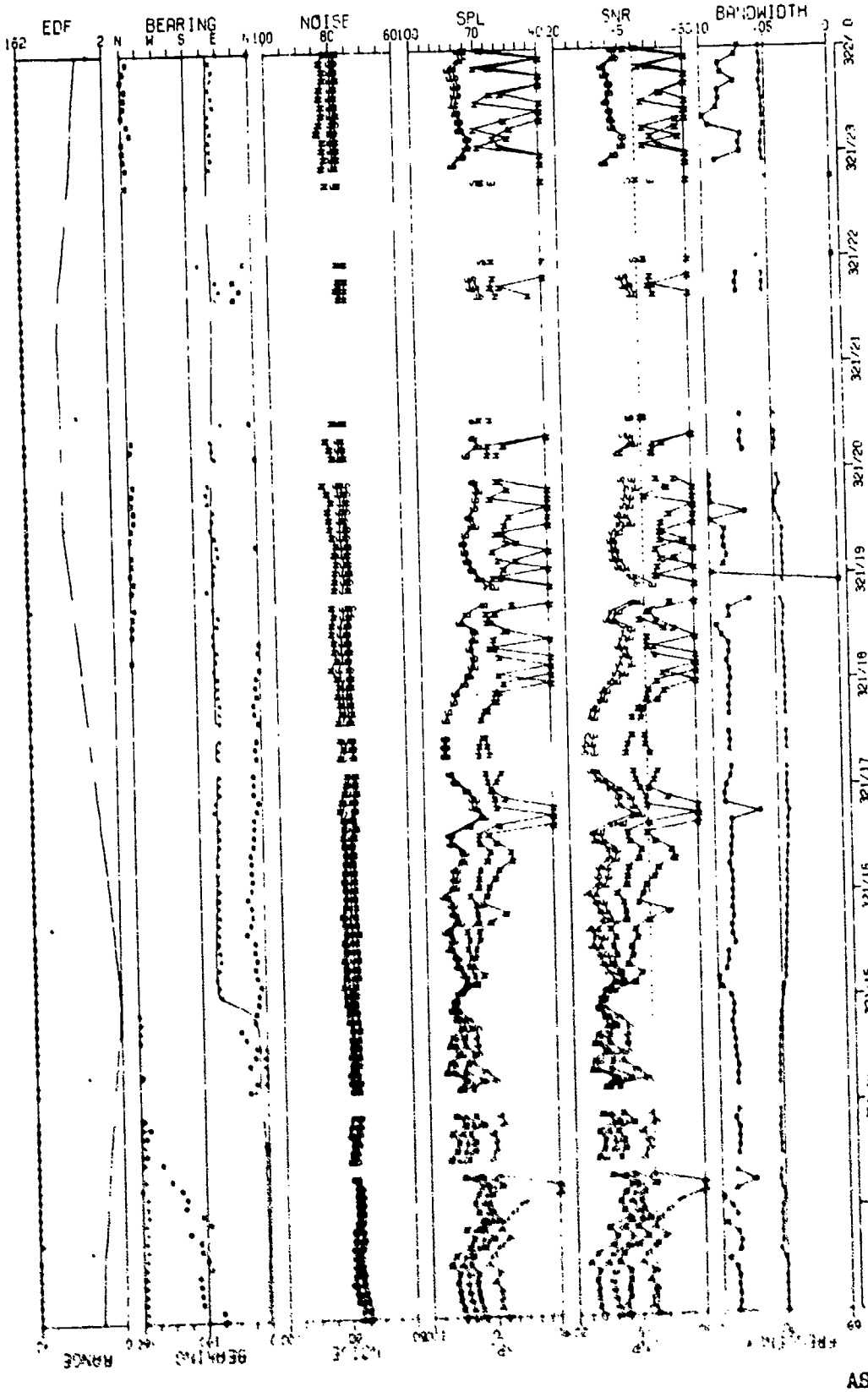

FIGURE 11-129
MSS-FVT 70HZ LINE HISTORY AS OBSERVED VIA THE SINGLE CARDIOIDS SENSOR
AT SITE A3 DURING THE 17 NOV FIELD EVENT WITH STANDARD RESOLUTION (U)

AS-77-3056

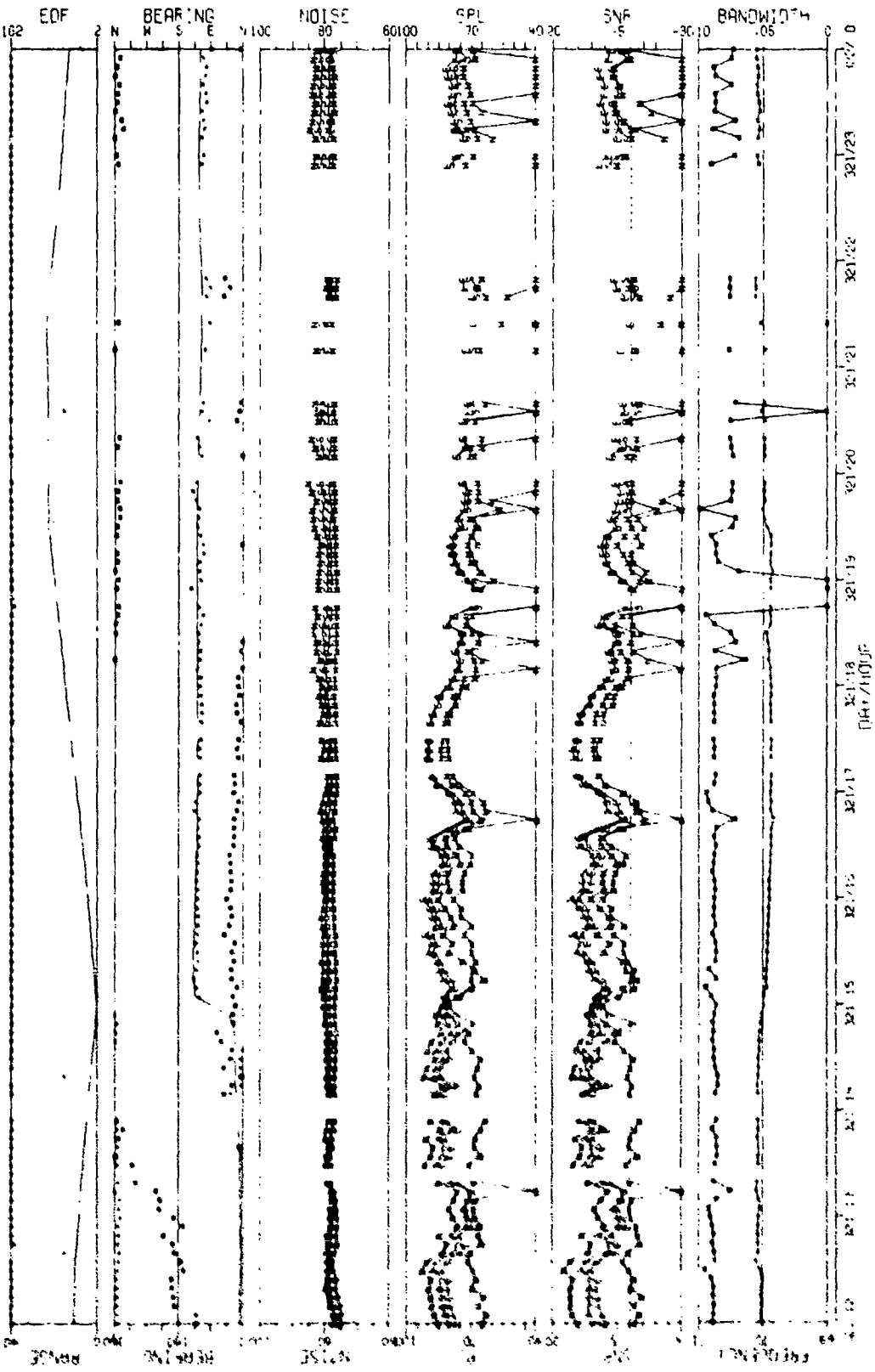

FIGURE II-130
MS-[illegible] 7GHZ LINE HISTORY AS OBSERVED VIA THE MAX GAIN LIMACONS SENSOR
AT SITE A3 DURING THE 17 NOV FIELD EVENT WITH STANDARD RESOLUTION TUI

AS-77-3057

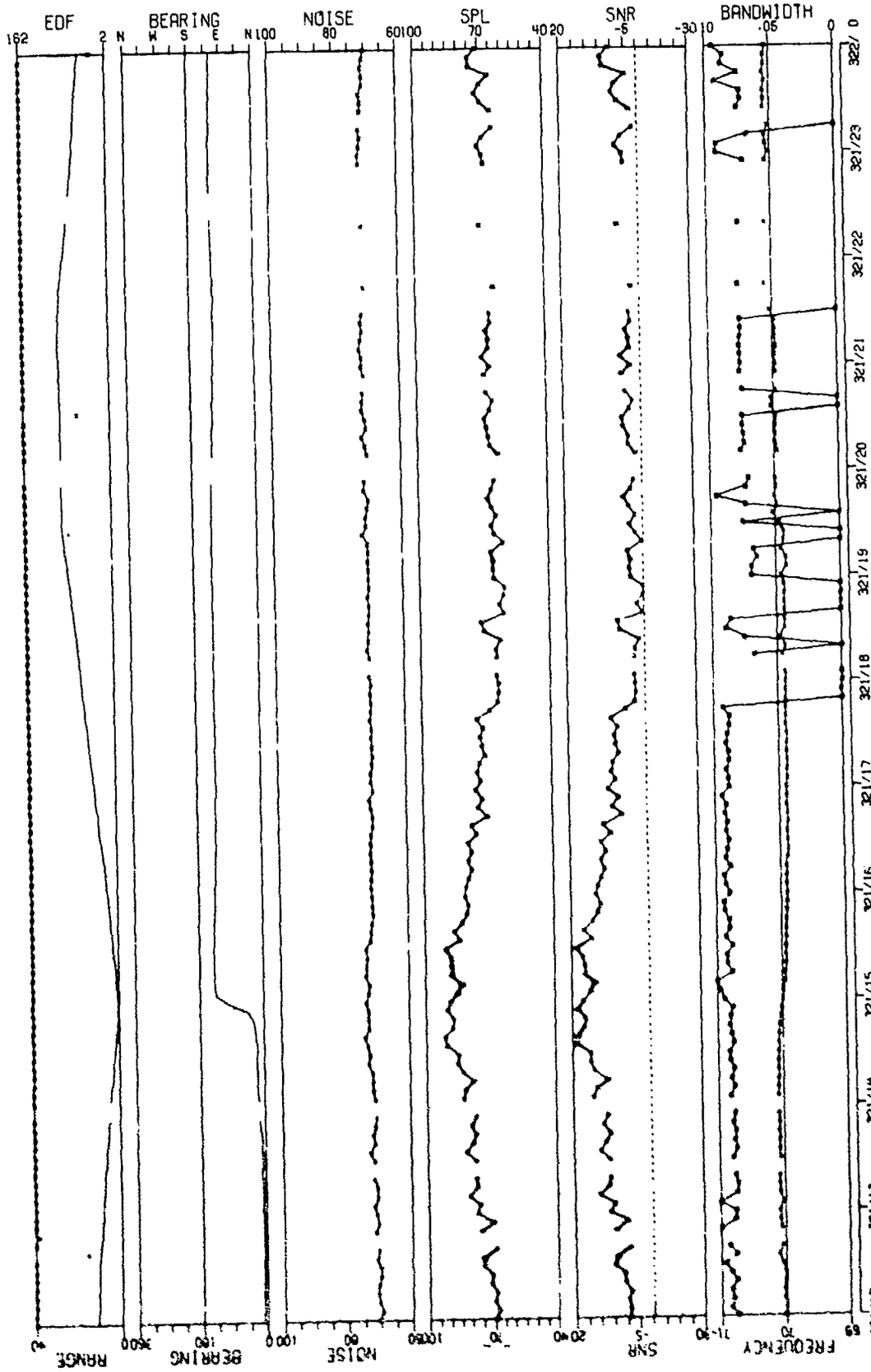

FIGURE 11-131
MSS-FVT 70HZ LINE HISTORY AS OBSERVED VIA THE VERTICAL DIPOLE SENSOR AT SITE A3 DURING THE 17 NOV FIELD EVENT WITH STANDARD RESOLUTION (U)

AS-77-3058

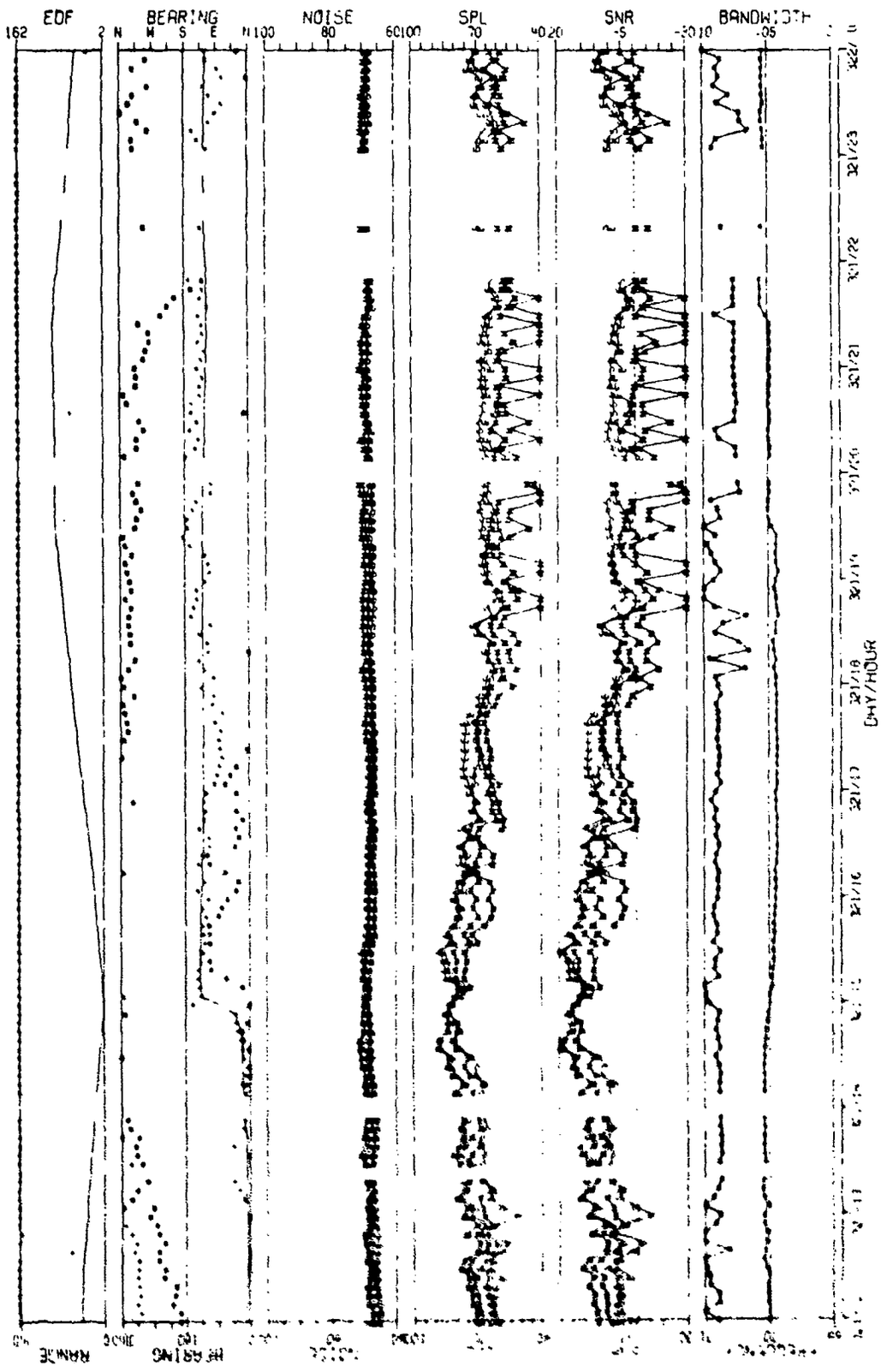

FIGURE 11-132
[illegible] 20HZ LINE HISTORY AS OBSERVED VIA THE DIFFERENCED CARDIOIDS SENSOR
[illegible] THE 17 NOV FIELD EVENT WITH STANDARD RESOLUTION (U)

AS-77-3059

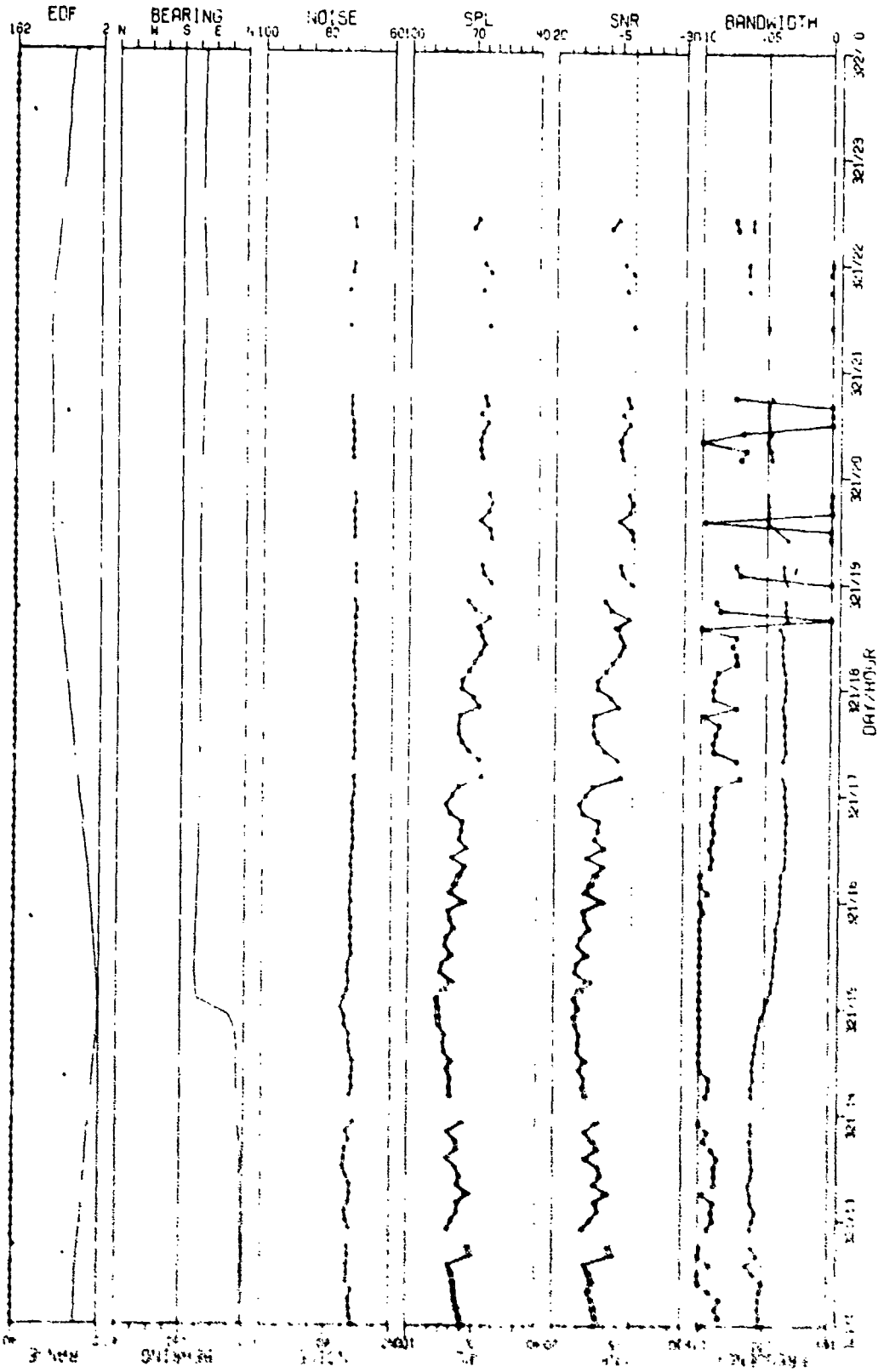

AS-77-3060

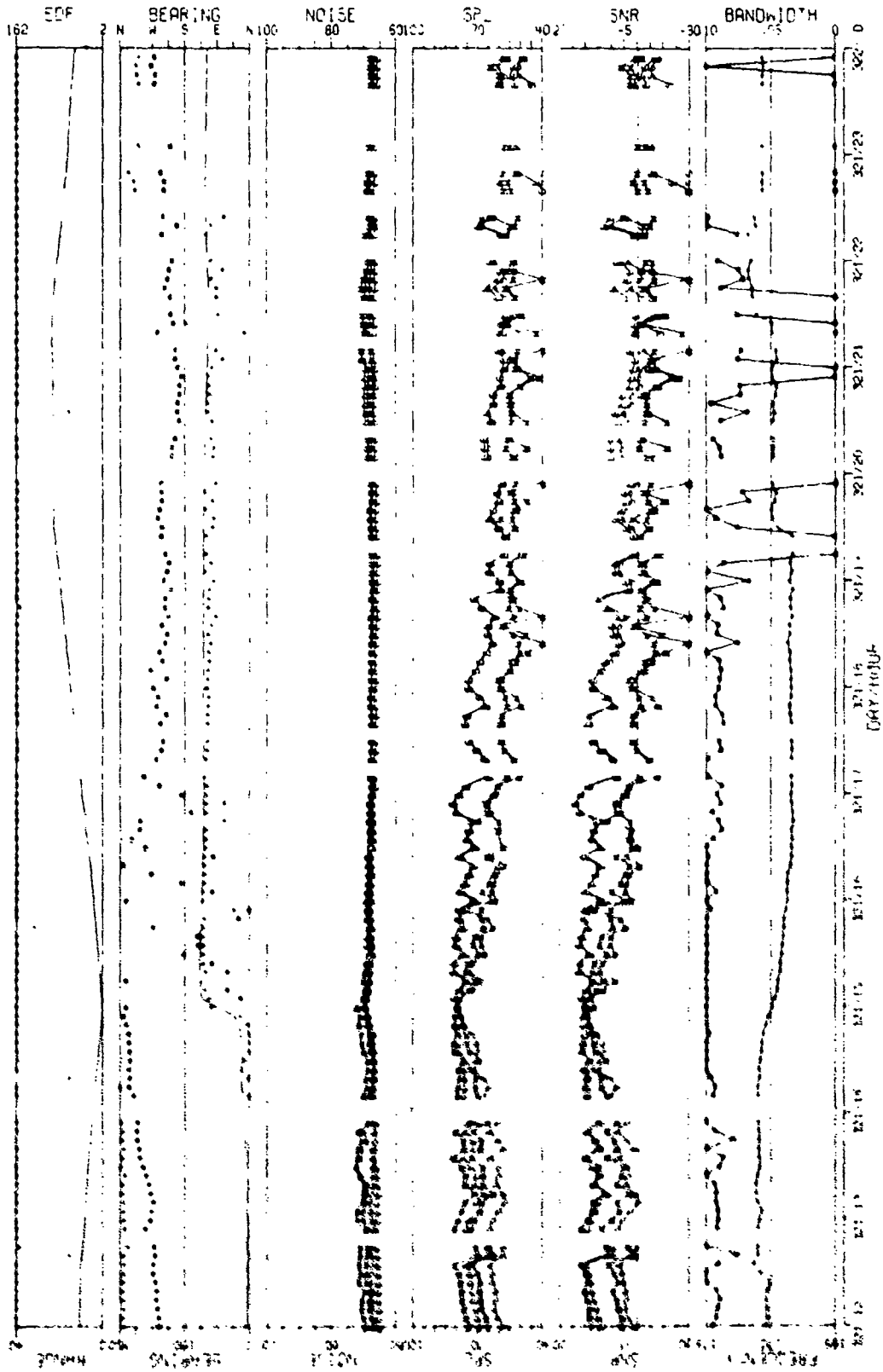

AS-77-3061

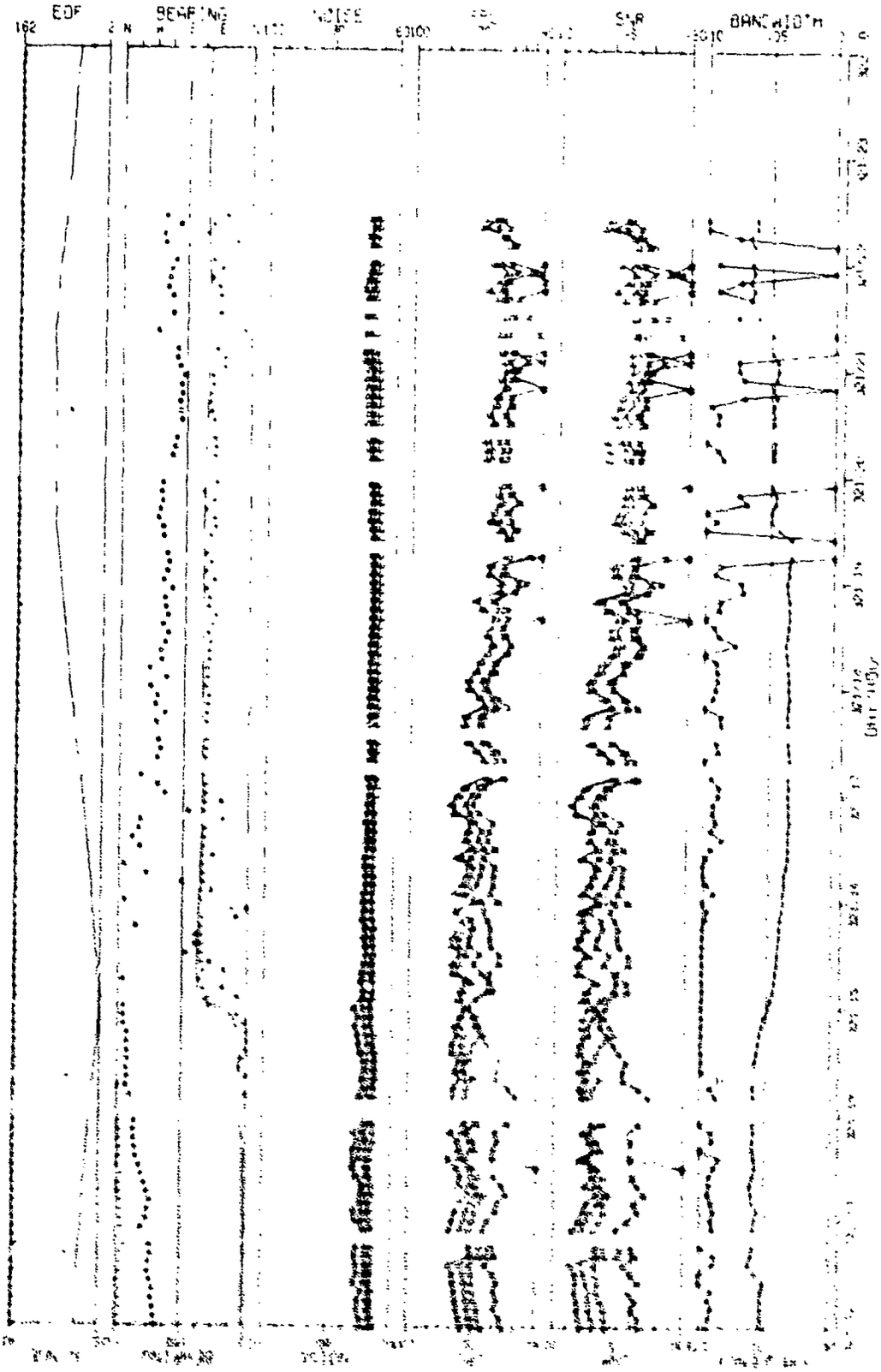

AS-77-3062

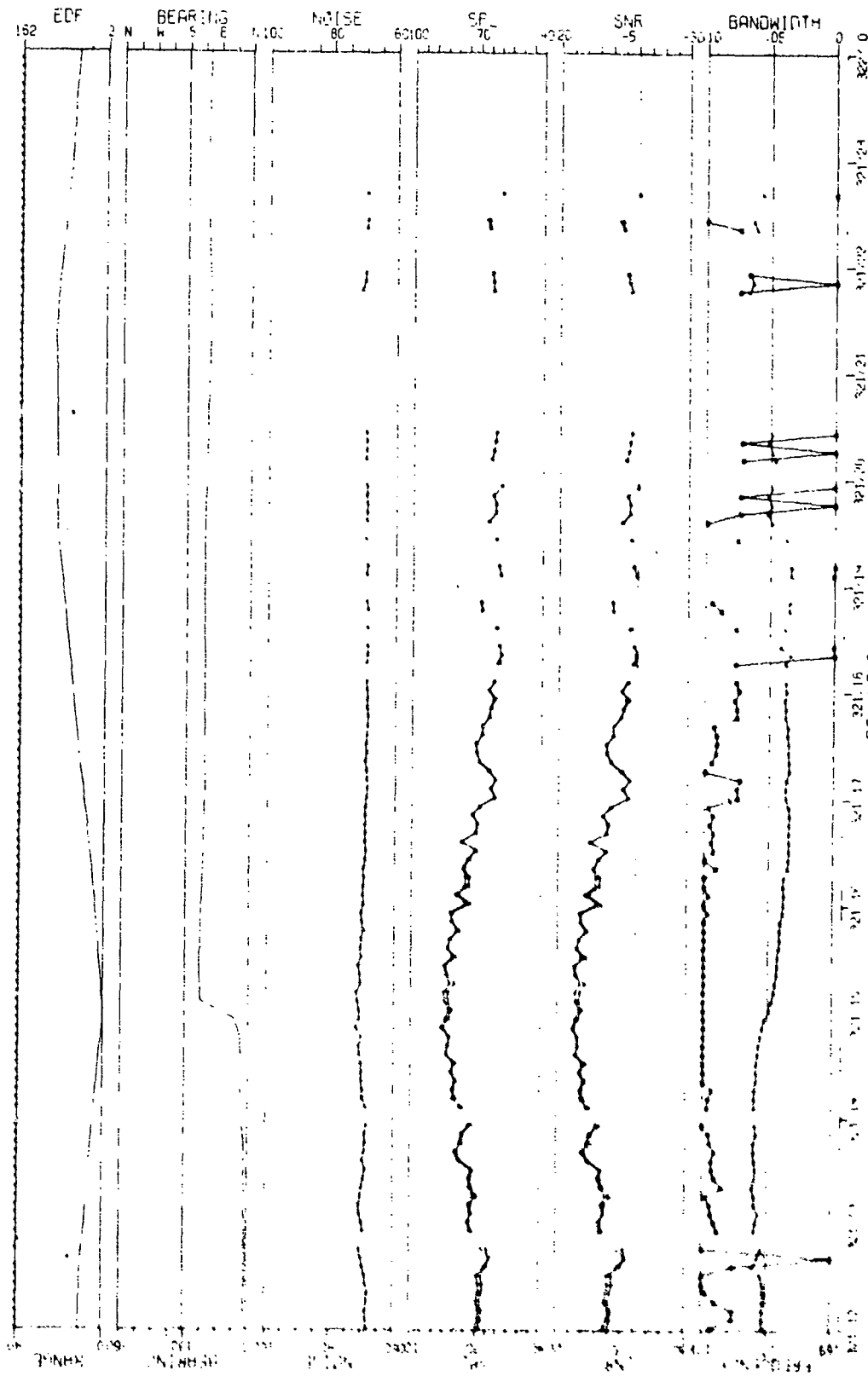

FIGURE 11-136
[illegible] LINE HISTORY AS OBSERVED VIA THE VERTICAL DIPOLE SENSOR
AT [illegible] AS DURING THE 17 NOV FIELD EVENT WITH STANDARD RESOLUTION (U)

AS-77-3063

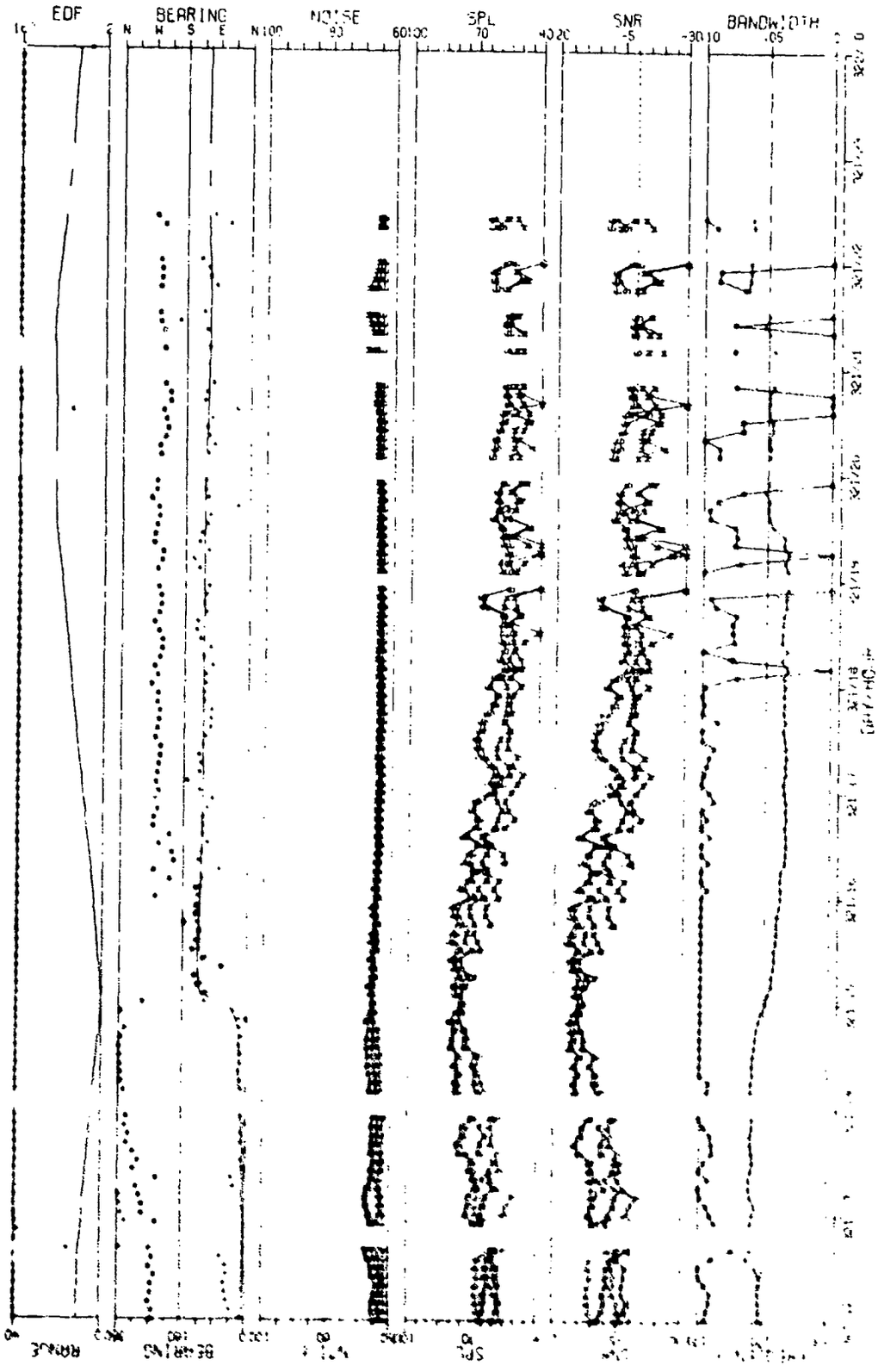

AS-77-3064

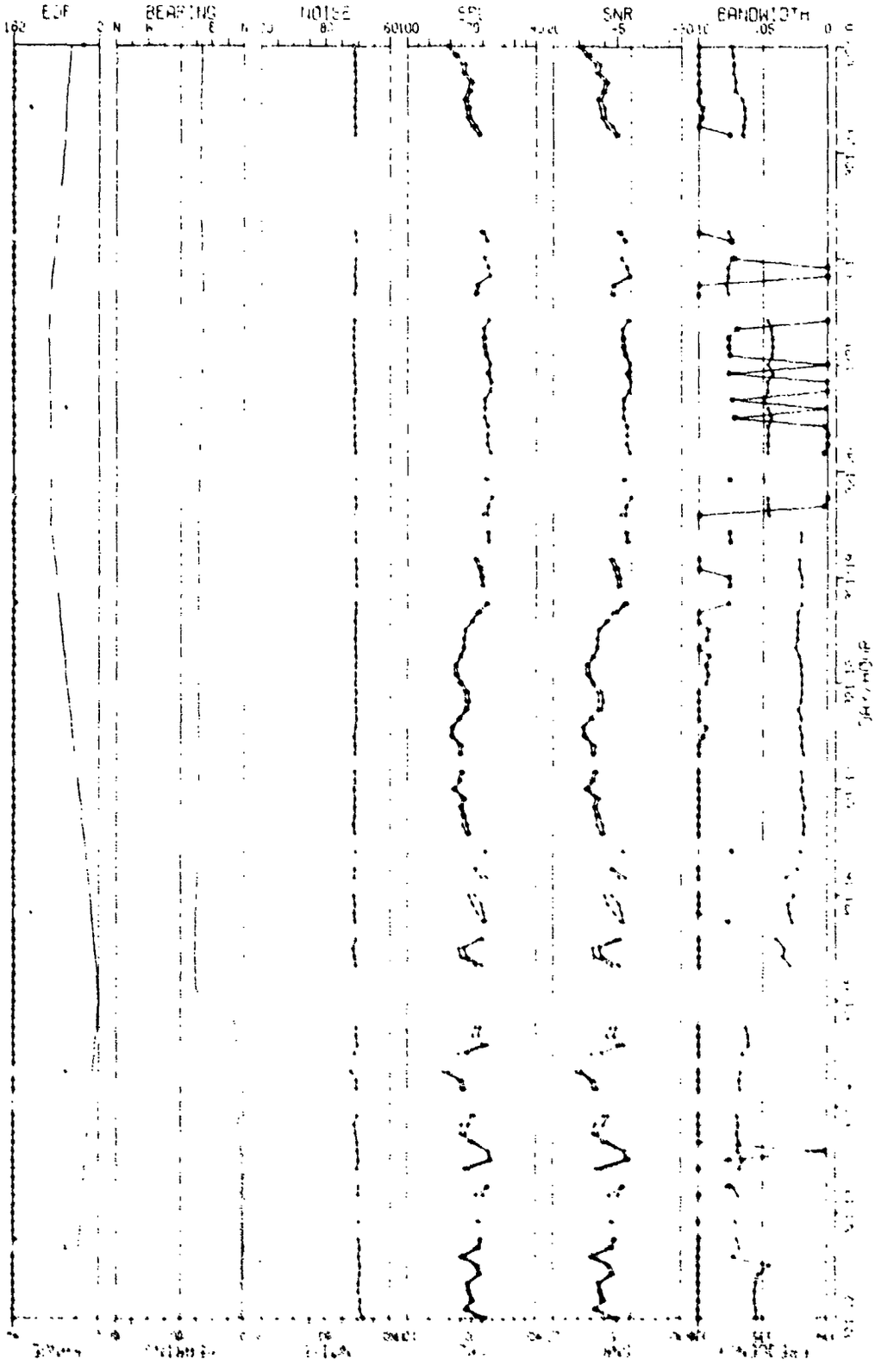

AS-77-3065

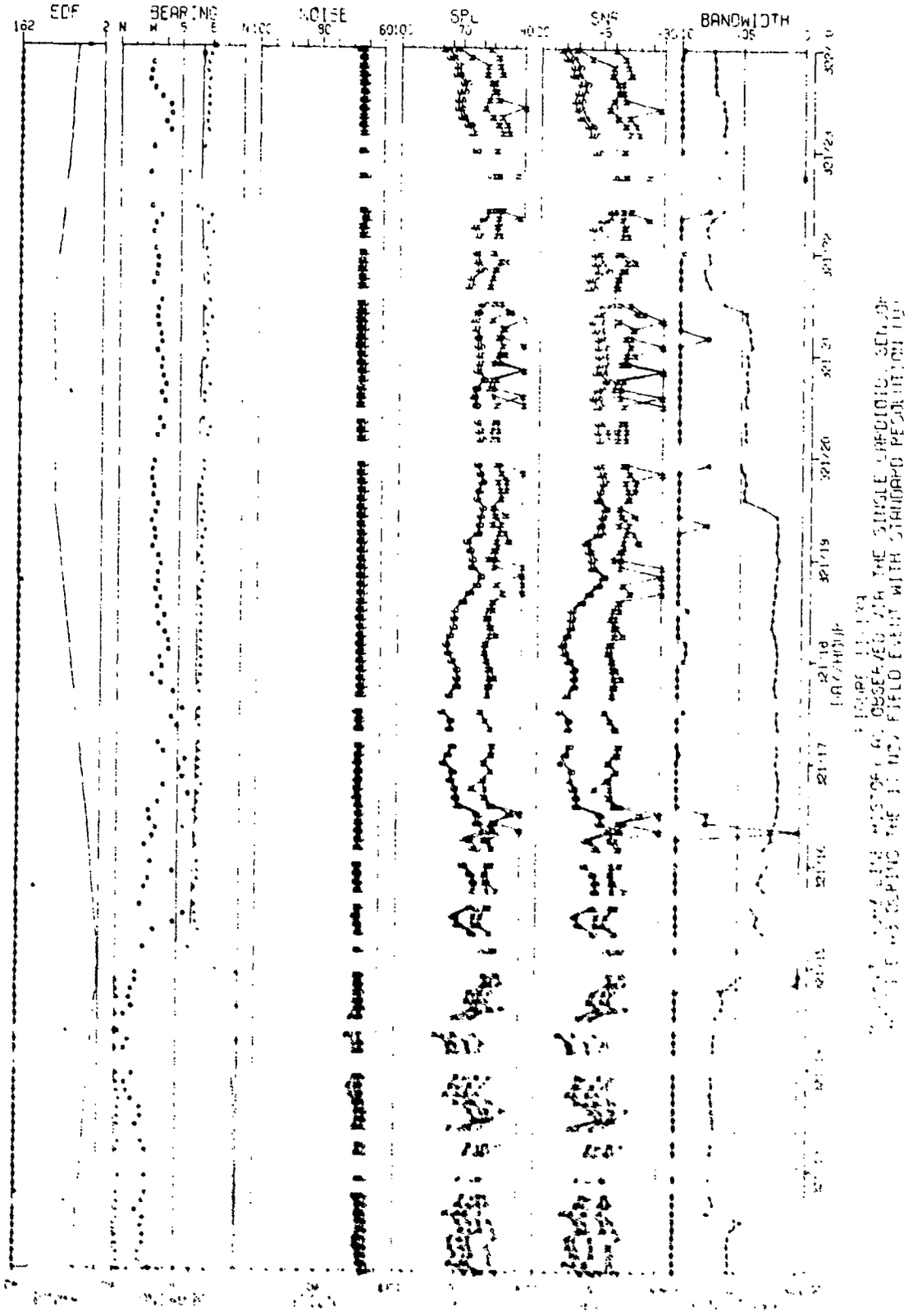

AS-77-3066

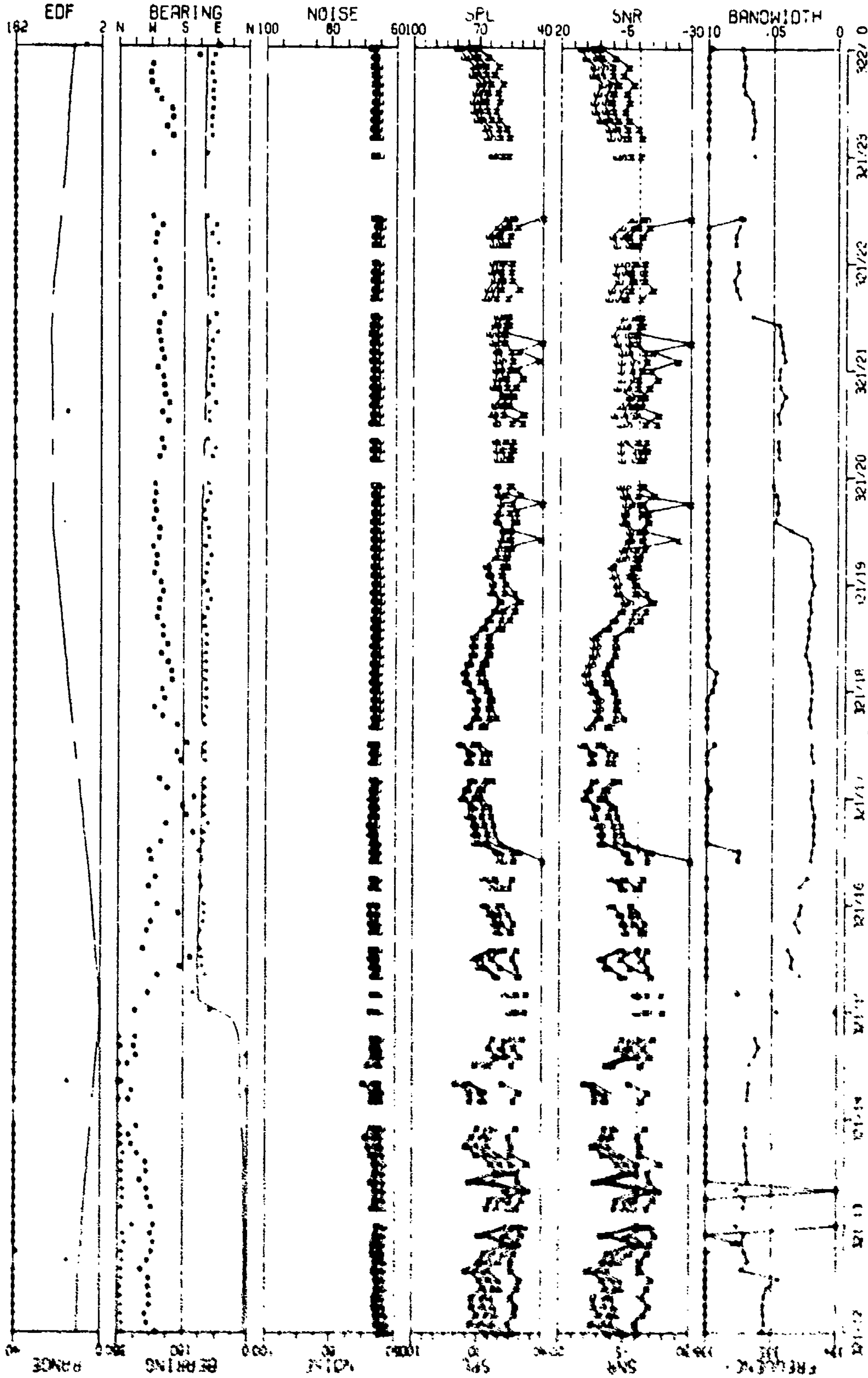

FIGURE 11-140
MSS-FVT 135HZ LINE HISTORY AS OBSERVED VIA THE MAX GAIN LIMACONS SENSOR AT SITE A3 DURING THE 17 NOV FIELD EVENT WITH STANDARD RESOLUTION (U)

A3-77-3067

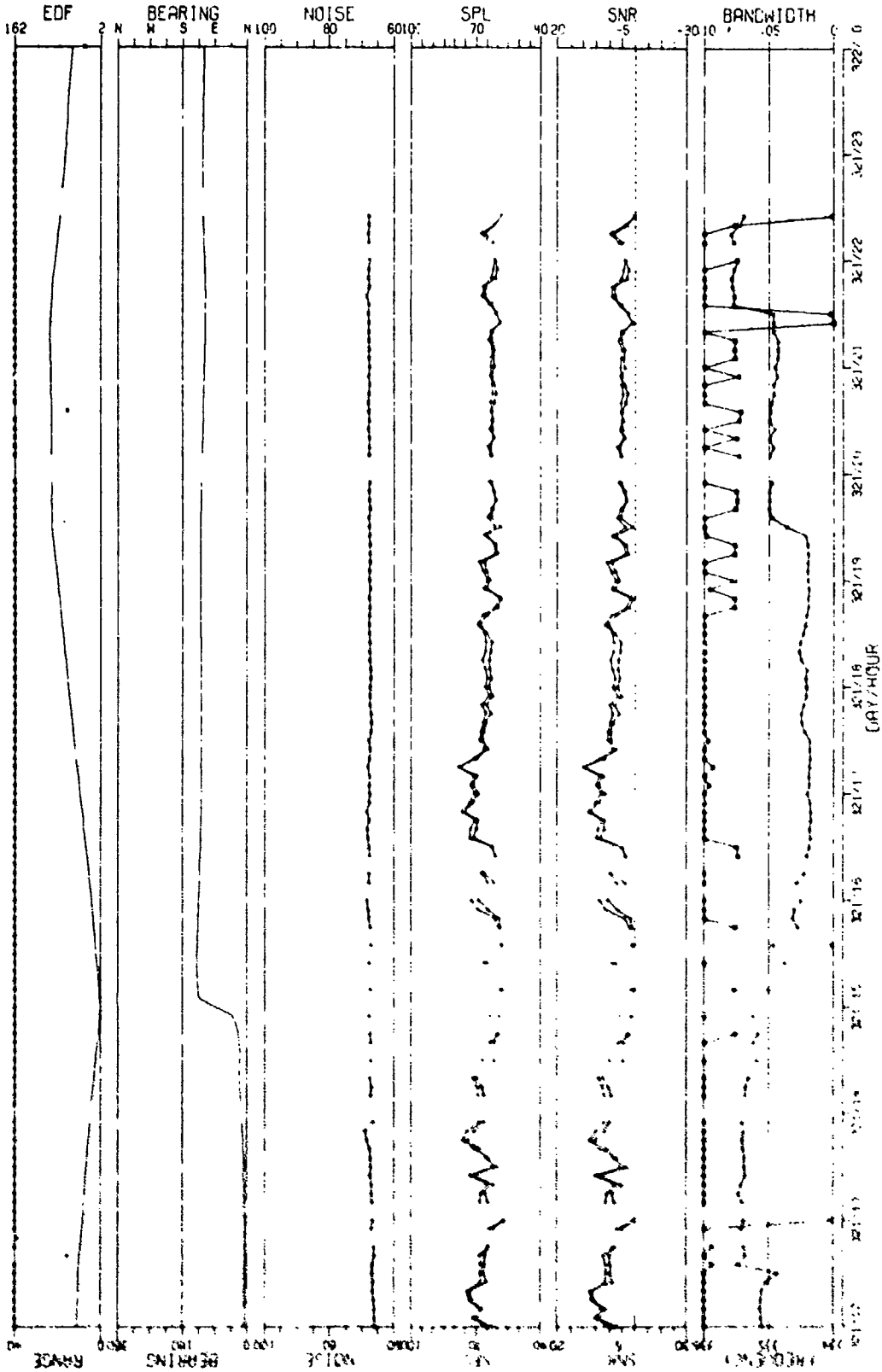

FIGURE 11 [illegible]
[illegible] 35HZ LINE HISTORY AS OBSERVED WITH THE VERTICAL DIPOLE SENSOR
AT SITE 44 DURING THE 17 NOV FIELD EVENT WITH STANDARD RESOLUTION (U)

AS-77-3068

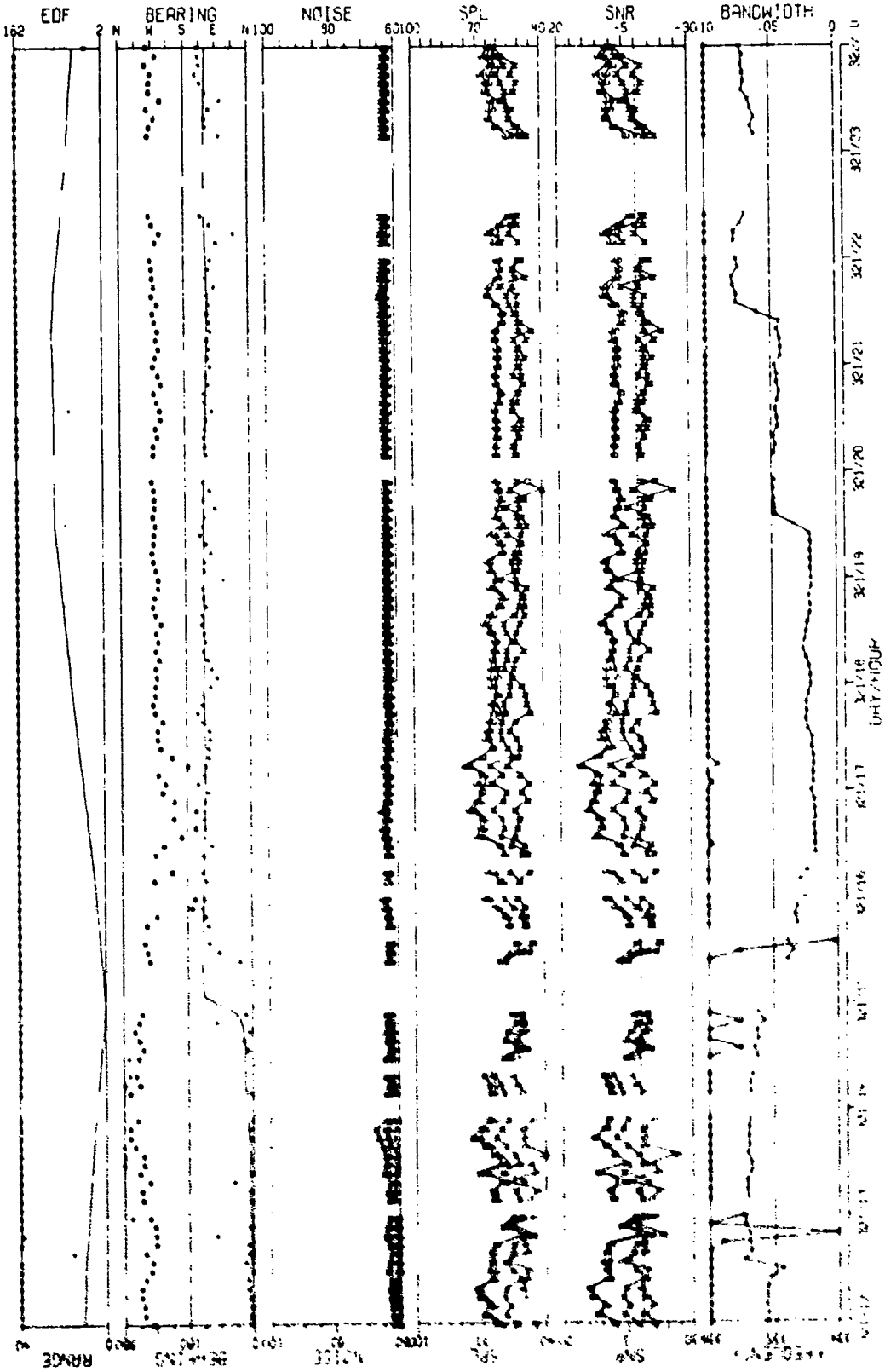

FIGURE II-142
RESULTS OF 335HZ LINE HISTORY AS OBSERVED VIA THE DIFFERENCED CARDIOIDS SENSOR AT SITE A1 DURING THE 17 NOV FIELD EVENT WITH STANDARD RESOLUTION (U)

AS-77-3069

(The reverse of this page is blank.)

APPENDIX C

PROPAGATION LOSS versus RANGE CURVES (U)

(FIGURES II-143 - II-150)

(The reverse of this page is blank.)

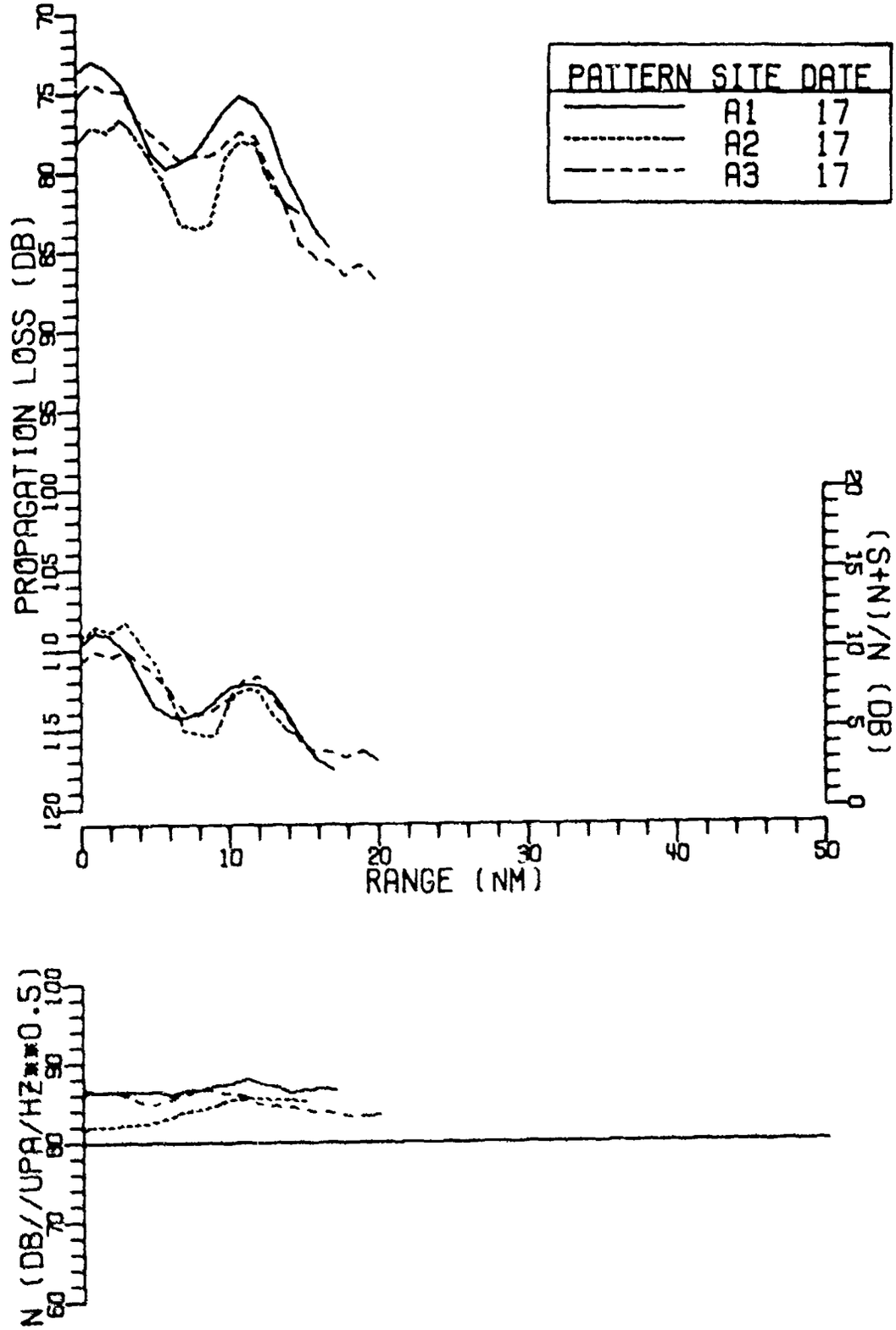

FIGURE II-143
MSS-FVT NEAR BOTTOM OMNIDIRECTIONAL SENSOR
PROPAGATION LOSS RESULTS FOR 64HZ AT 162DB (U)

AS-77-30

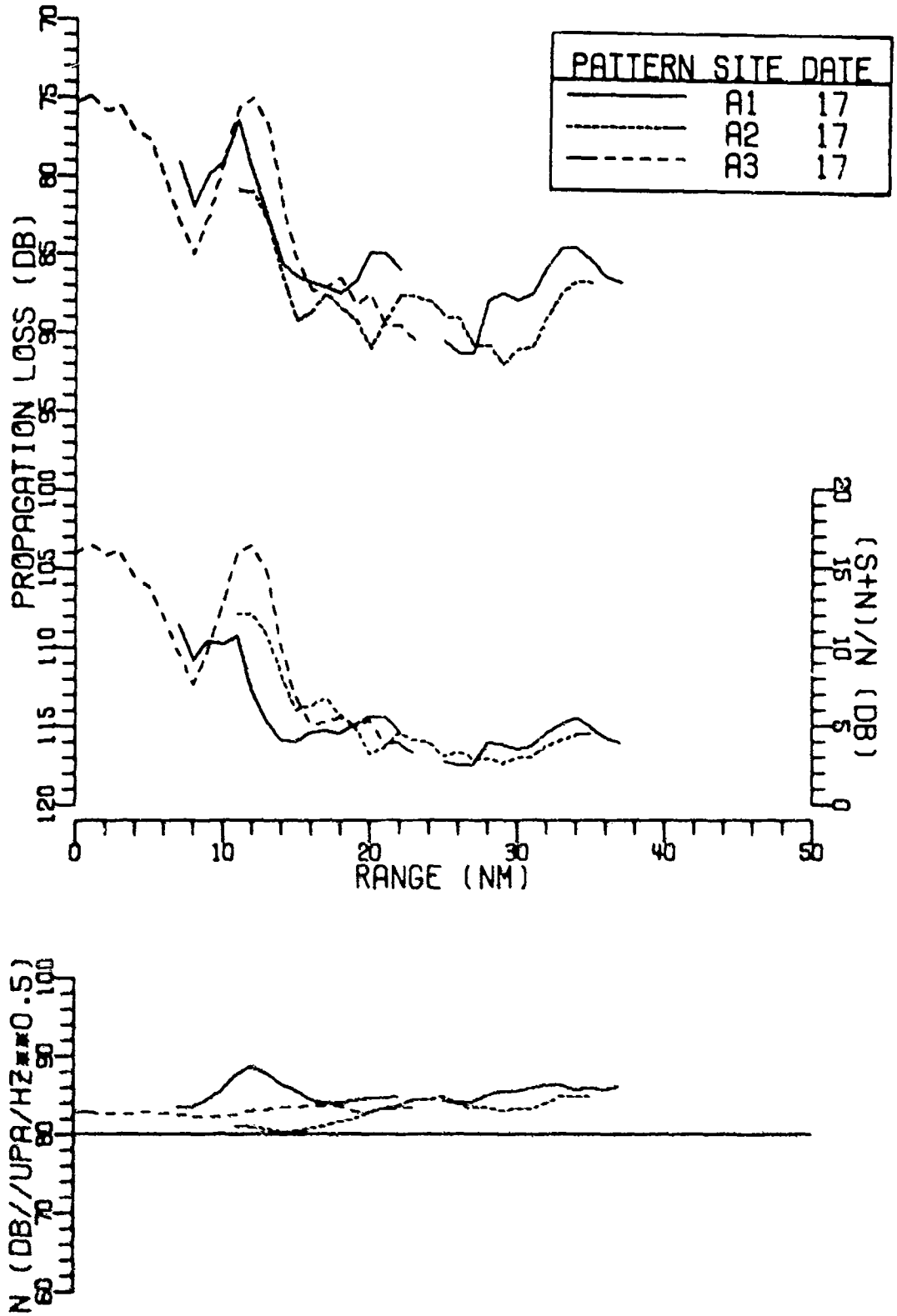

FIGURE II-144
MSS-FVT NEAR BOTTOM OMNIDIRECTIONAL SENSOR
PROPAGATION LOSS RESULTS FOR 70HZ AT 166DB (U)

AS-77-3071

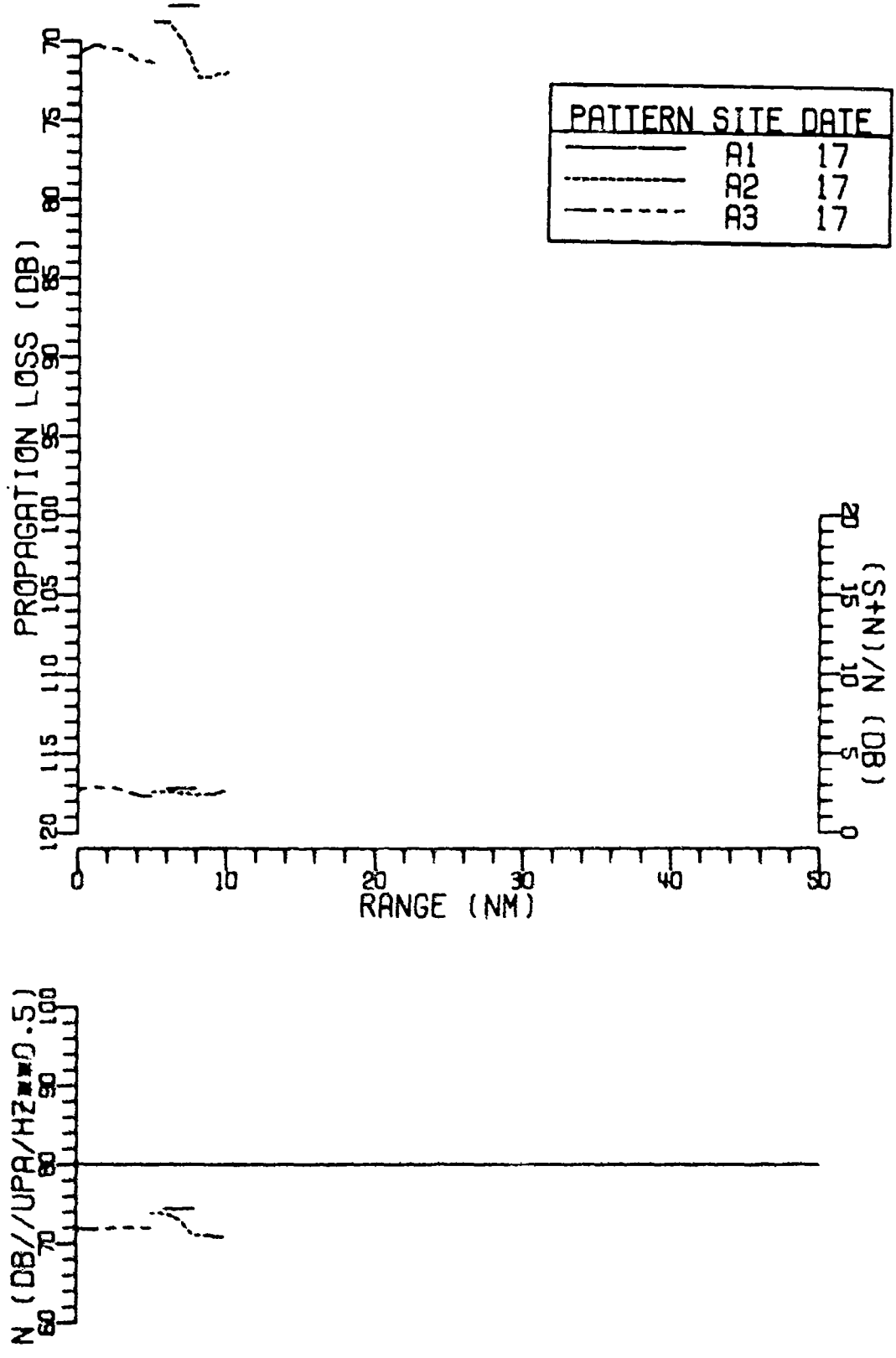

FIGURE II-145
MSS-FVT NEAR BOTTOM OMNIDIRECTIONAL SENSOR
PROPAGATION LOSS RESULTS FOR 155HZ AT 134DB (U)

AS-77-307

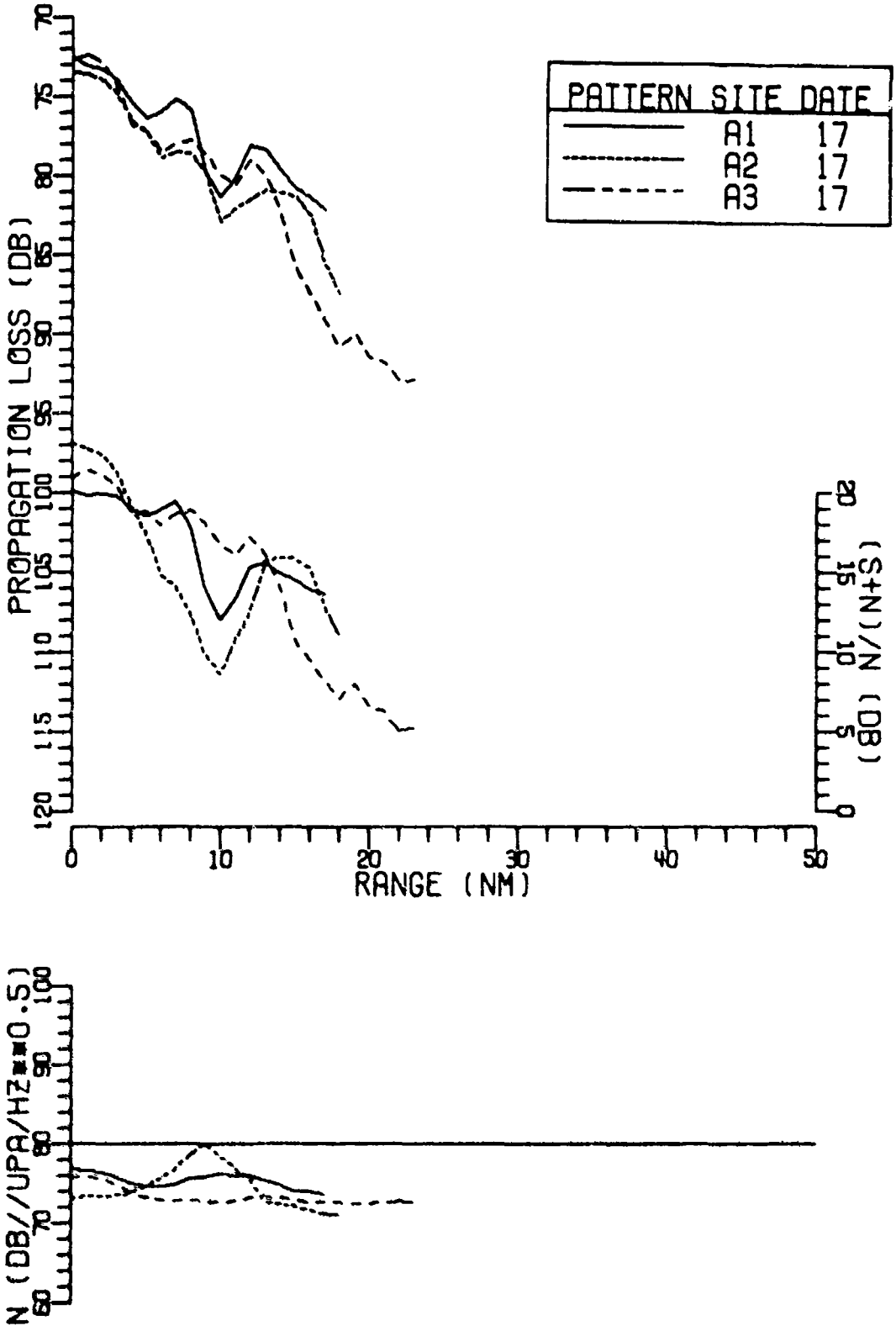

FIGURE II-146
MSS-FVT NEAR BOTTOM OMNIDIRECTIONAL SENSOR
PROPAGATION LOSS RESULTS FOR 160HZ AT 161DB (U)

AS-77-3073

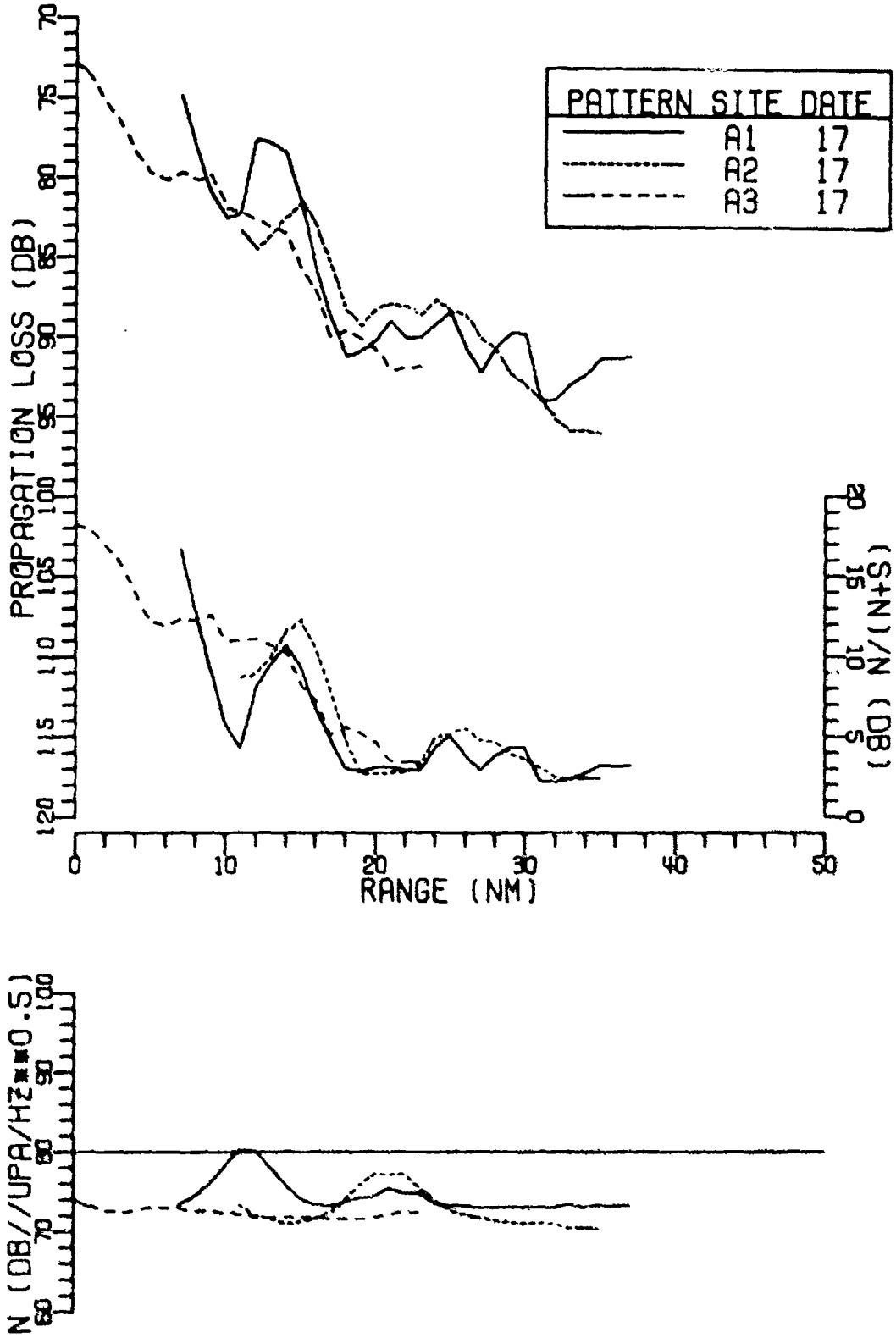

FIGURE II-147
MSS-FVT NEAR BOTTOM OMNIDIRECTIONAL SENSOR
PROPAGATION LOSS RESULTS FOR 170HZ AT 156DB (U)

AS-77-3

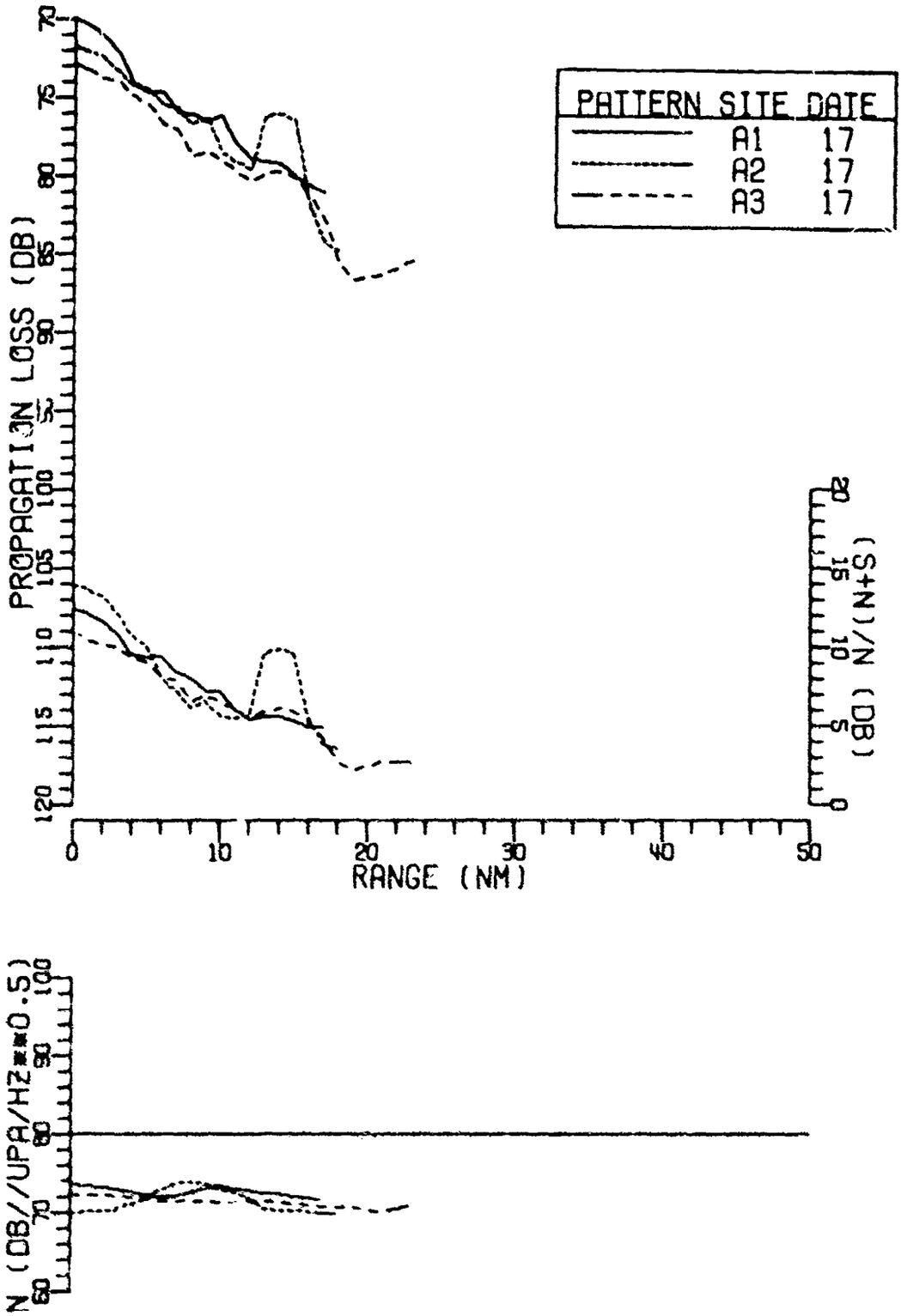

FIGURE II-148
MSS-FVT NEAR BOTTOM OMNIDIRECTIONAL SENSOR
PROPAGATION LOSS RESULTS FOR 260HZ AT 1470B (U)

AS-77-3075

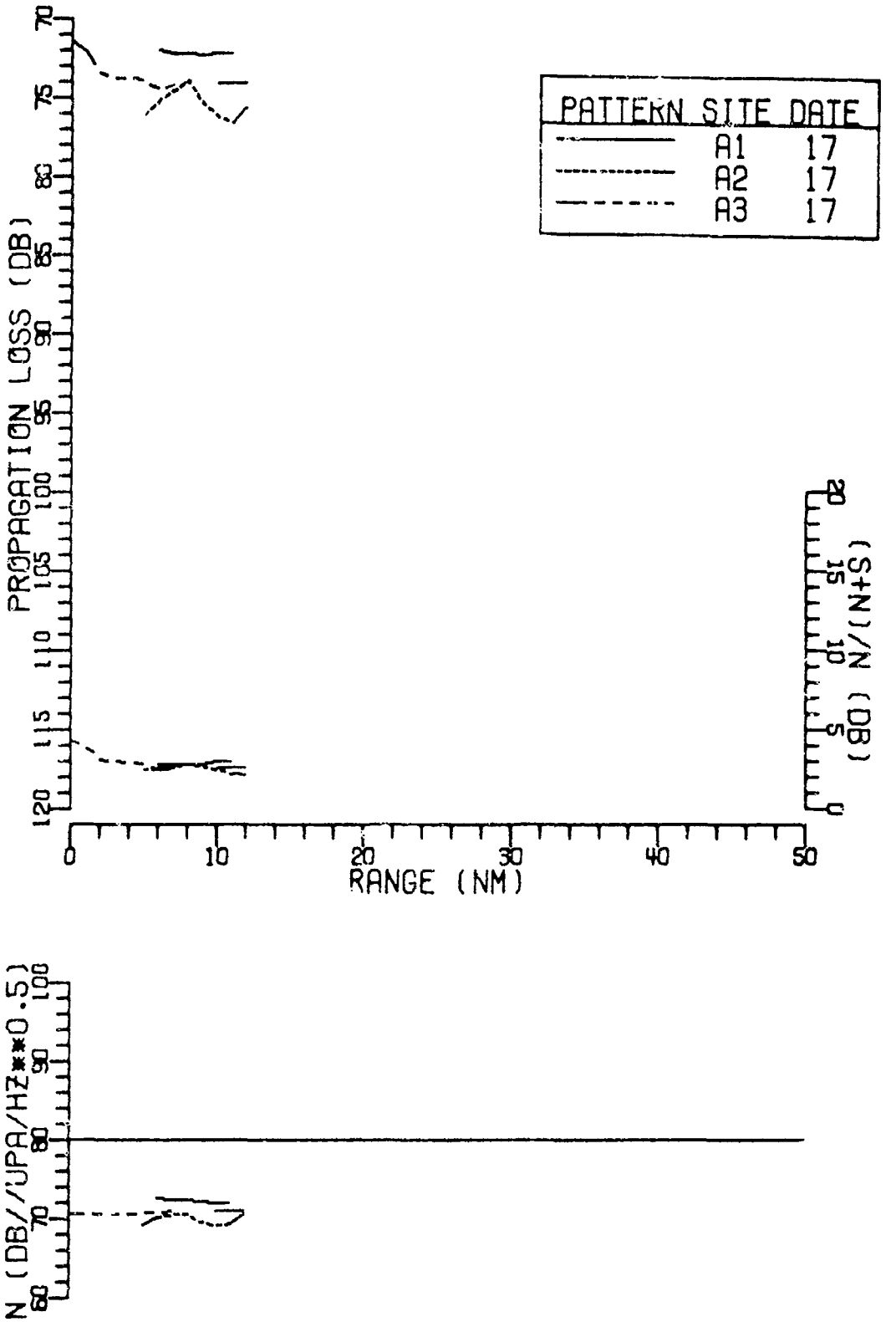

FIGURE II-149
MSS-FVT NEAR BOTTOM OMNIDIRECTIONAL SENSOR
PROPAGATION LOSS RESULTS FOR 305HZ AT 136DB (U)

AS-77-30

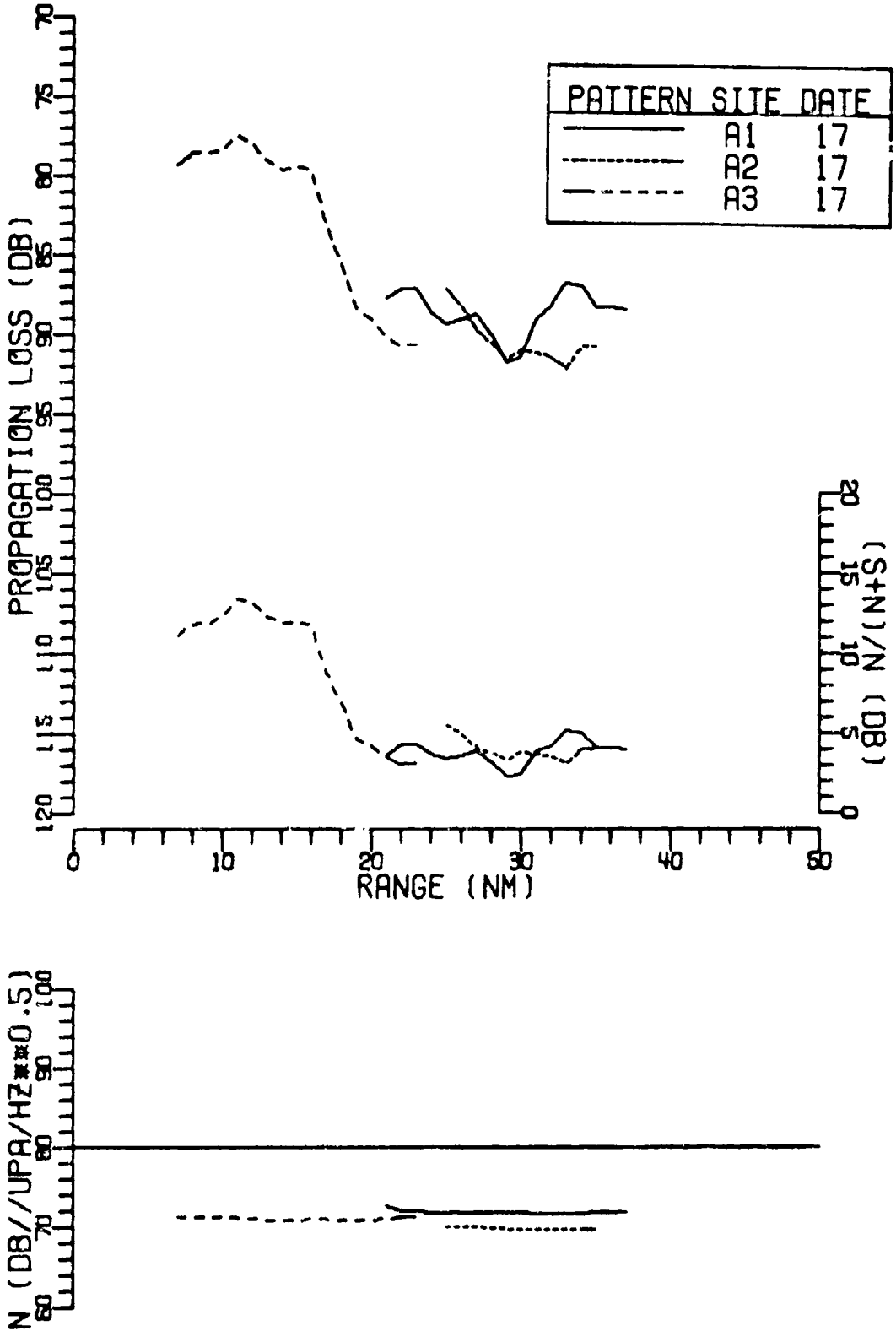

FIGURE II-150
MSS-FVT NEAR BOTTOM OMNIDIRECTIONAL SENSOR
PROPAGATION LOSS RESULTS FOR 335HZ AT 154DB (U)

AS-77-3077

APPENDIX D

ARRAY GAIN versus RANGE CURVES (U)

(FIGURES II-151 - II-182)

(The reverse of this page is blank.)

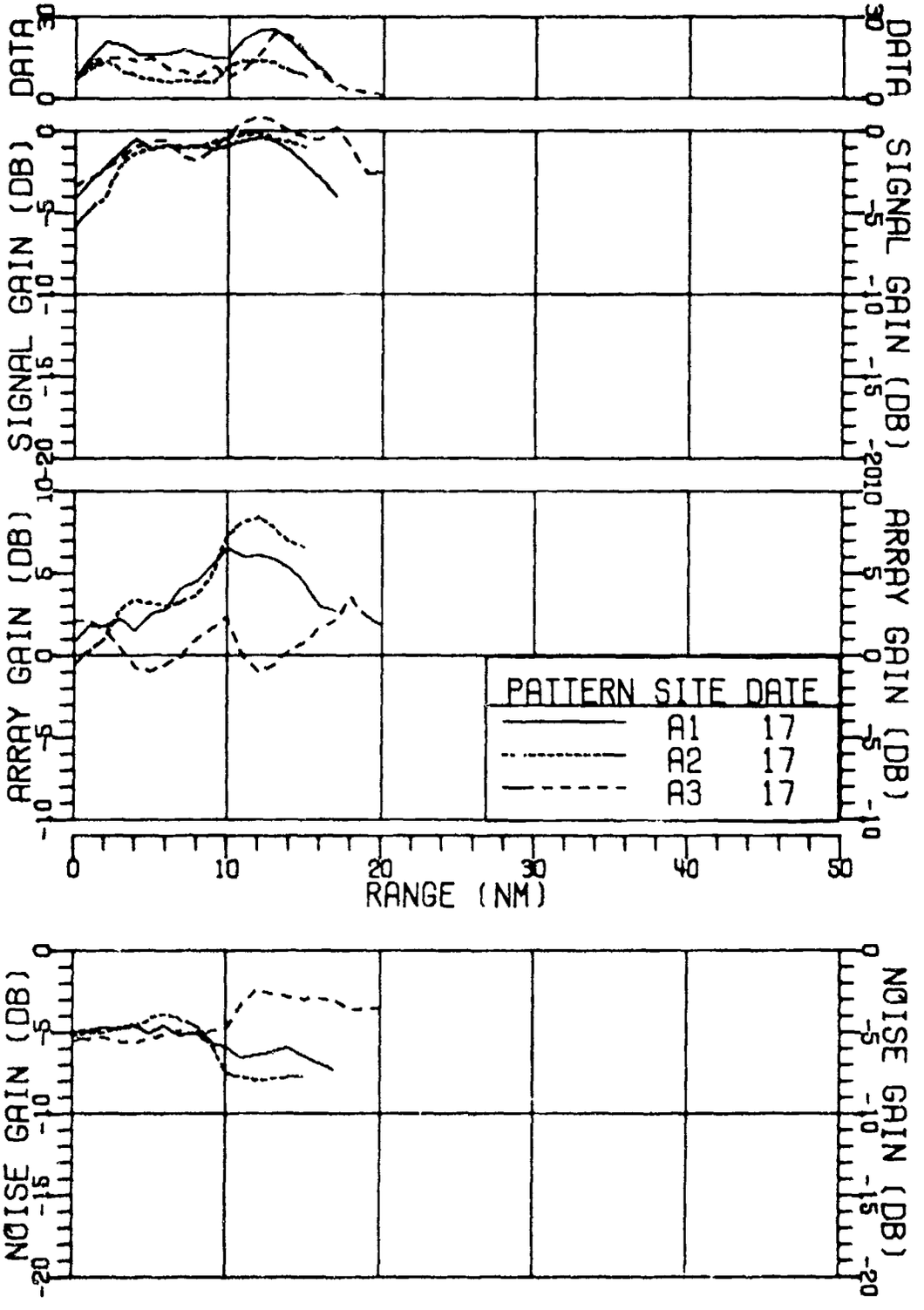

FIGURE II-151
MSS-FVT NEAR BOTTOM SINGLE CARDIOIDS SENSOR
ARRAY GAIN RESULTS FOR 64HZ AT 162DB (U)

AS-77-

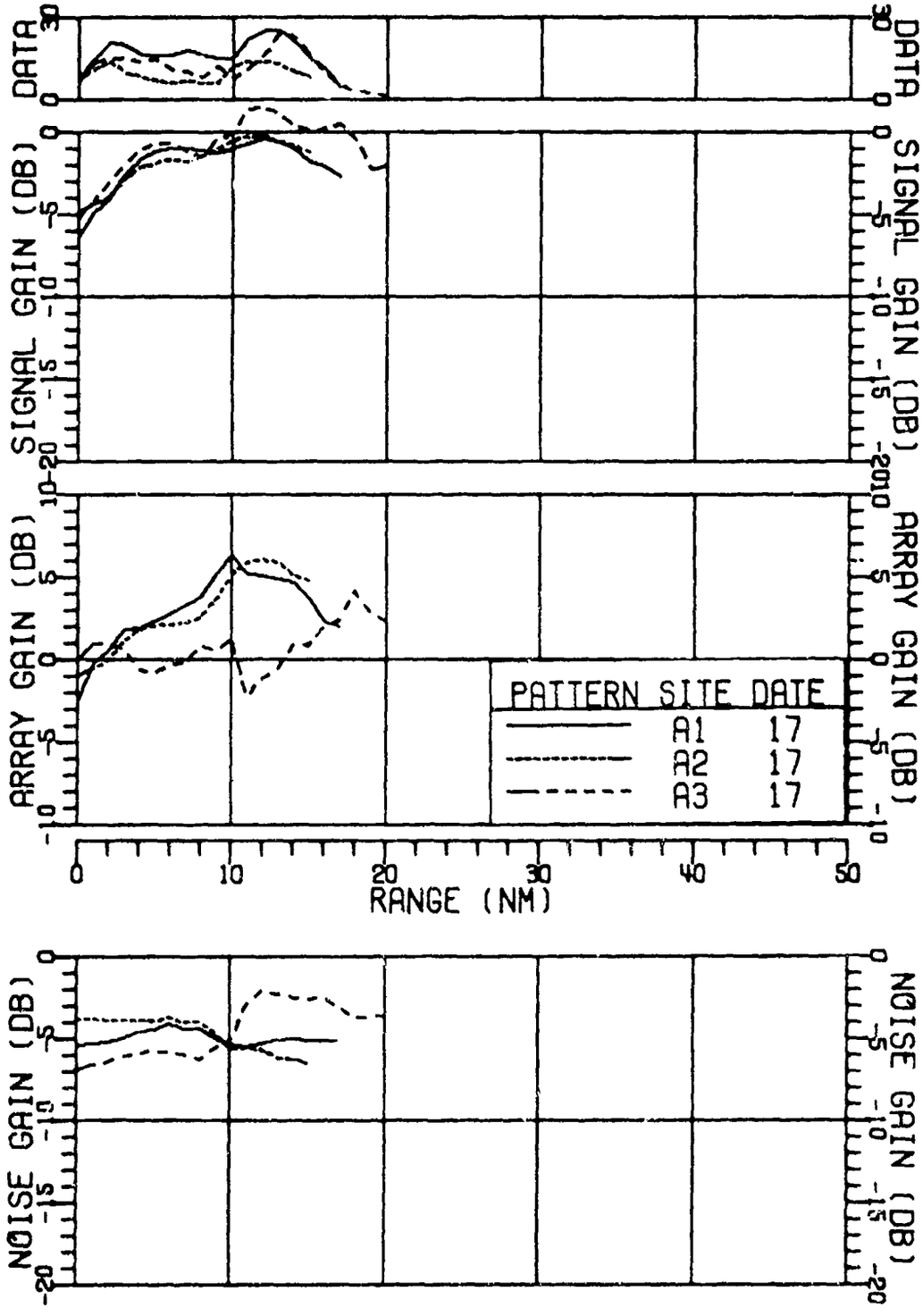

FIGURE II-152
MSS-FVT NEAR BOTTOM MAX GAIN LIMACONS SENSOR
ARRAY GAIN RESULTS FOR 64HZ AT 162DB (U)

AS-77-3079

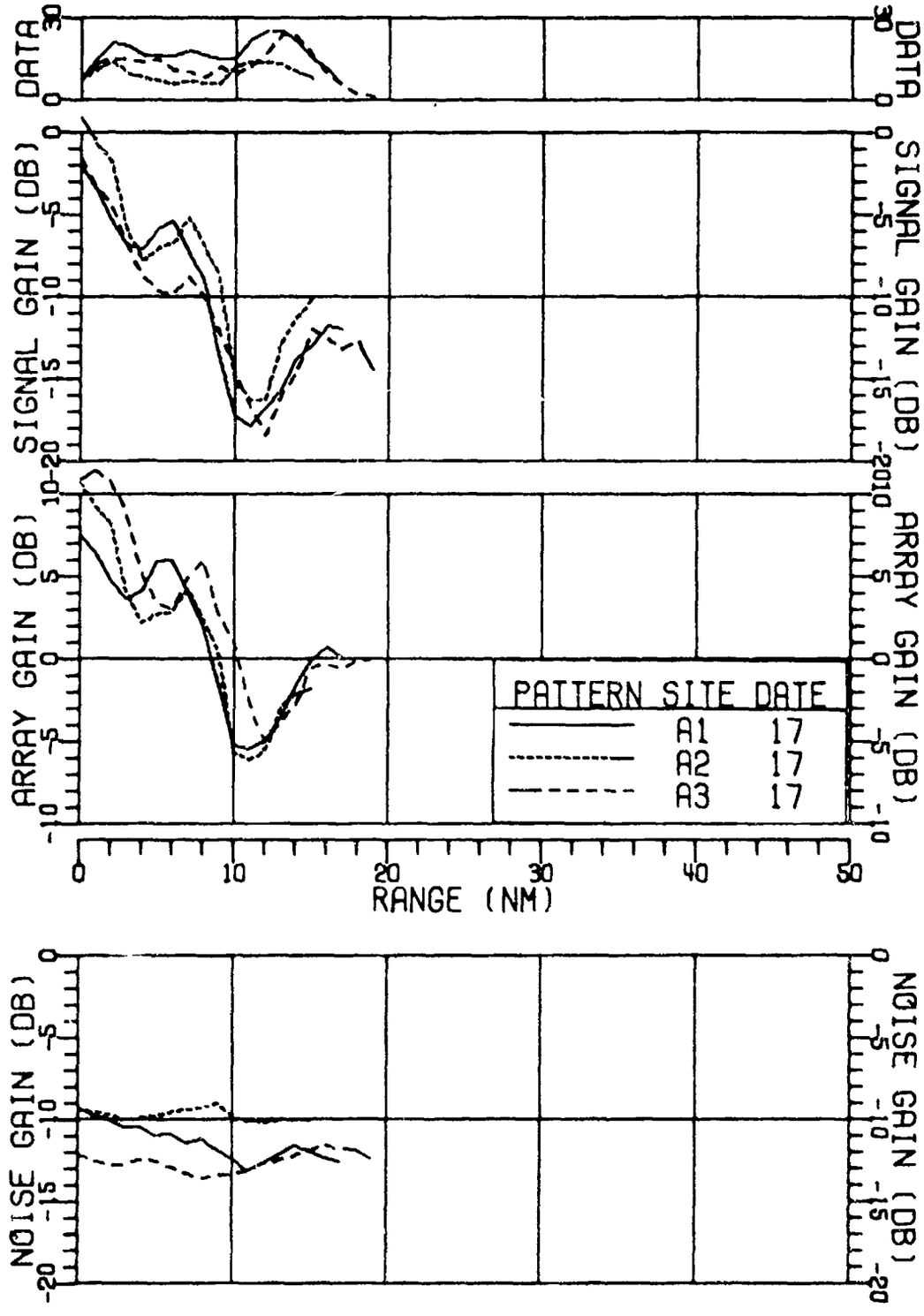

FIGURE II-153
MSS-FVT NEAR BOTTOM VERTICAL DIPOLE SENSOR
ARRAY GAIN RESULTS FOR 64HZ AT 162DB (U)

AS-77-3

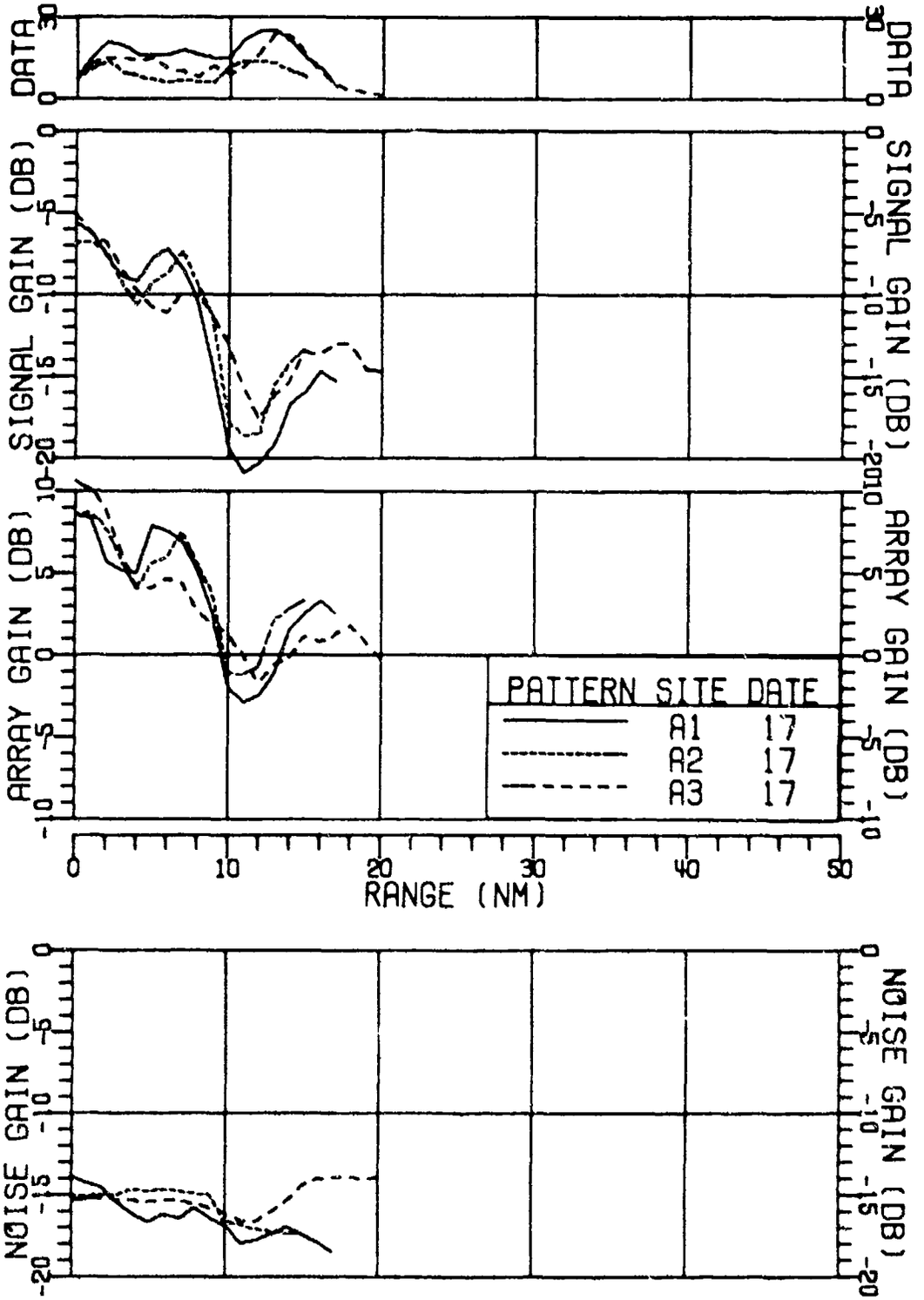

FIGURE II-154
MSS-FVT NEAR BOTTOM DIFFERENCED CARDIOIDS SENSOR
ARRAY GAIN RESULTS FOR 64HZ AT 162DB (U)

AS-77-3081

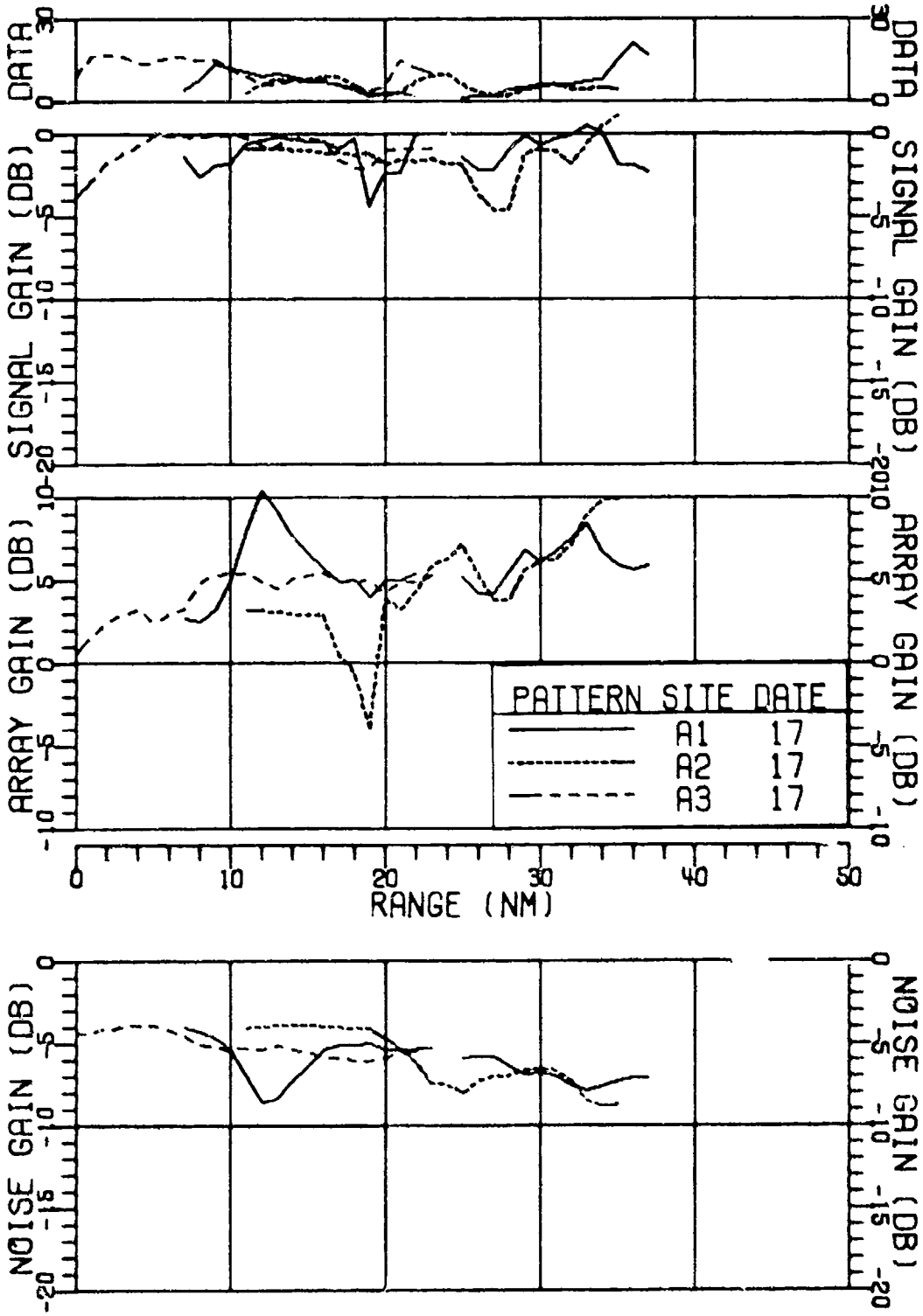

FIGURE II-155
MSS-FVT NEAR BOTTOM SINGLE CARDIOIDS SENSOR
ARRAY GAIN RESULTS FOR 70HZ AT 166DB (U)

AS-77-308

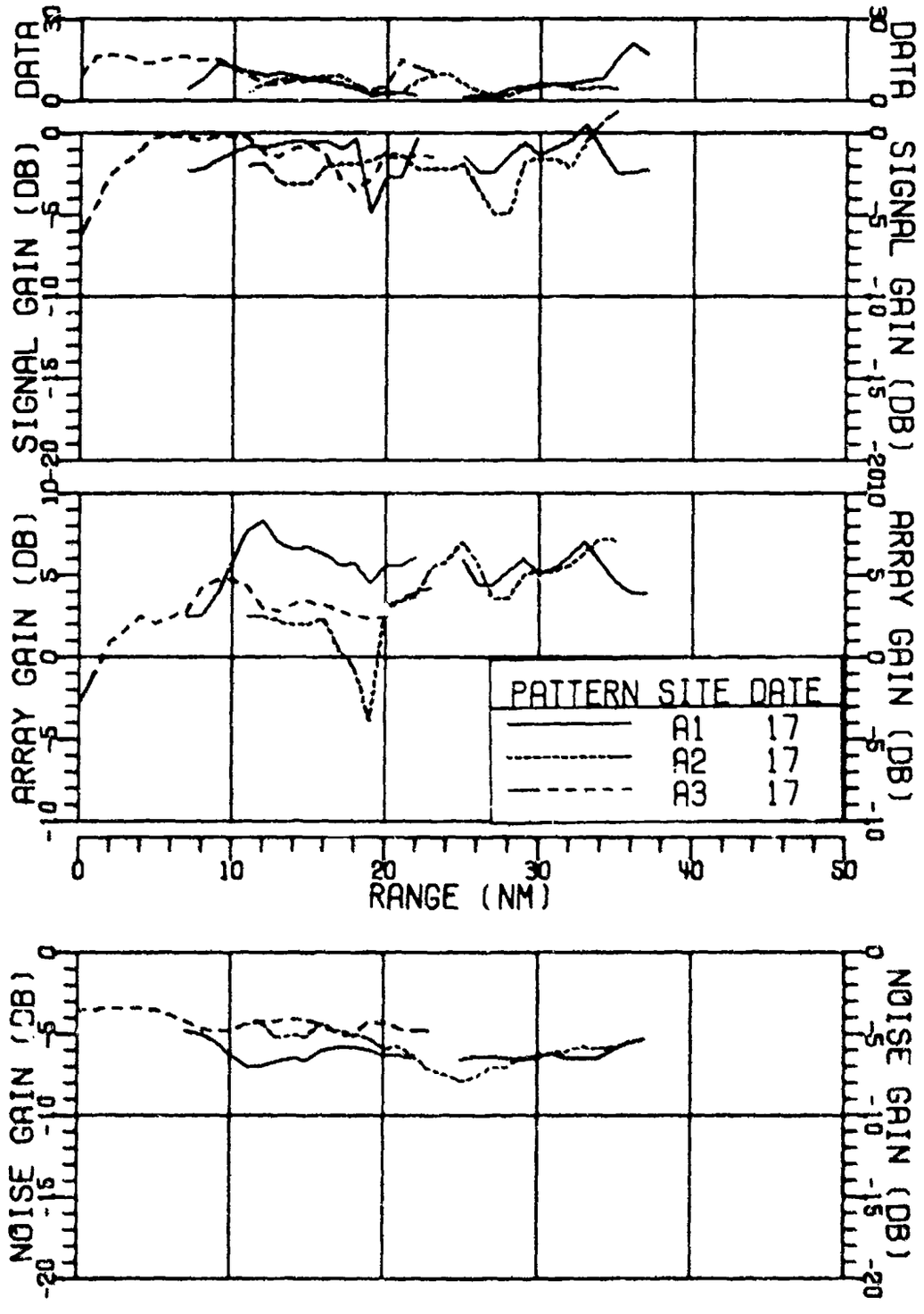

FIGURE II-156
MSS-FVT NEAR BOTTOM MAX GAIN LIMACONS SENSOR
ARRAY GAIN RESULTS FOR 70HZ AT 166DB (U)

AS-77-3083

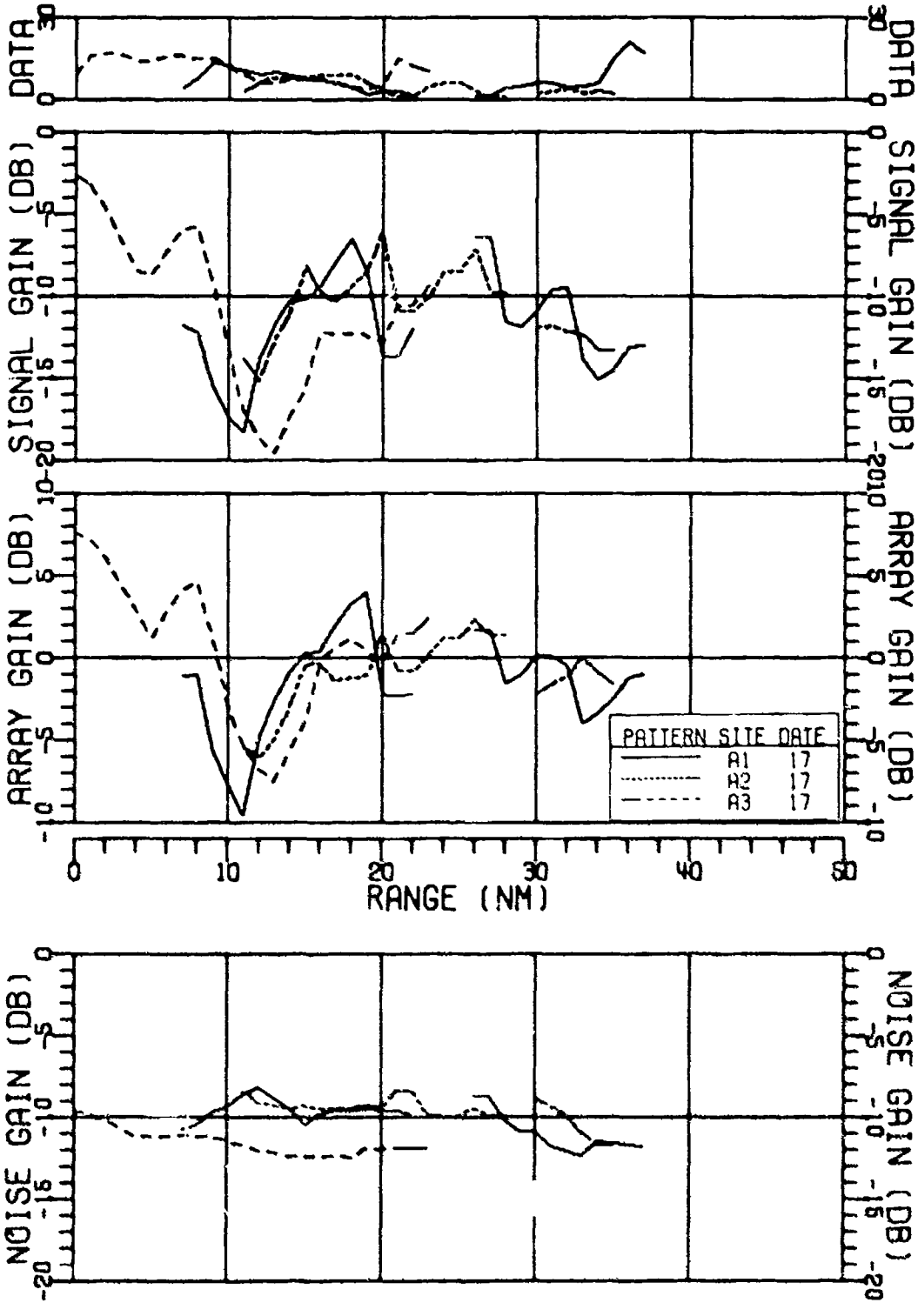

FIGURE II-157
MSS-FVT NEAR BOTTOM VERTICAL DIPOLE SENSOR
ARRAY GAIN RESULTS FOR 70HZ AT 166DB (U)

AS-77-308

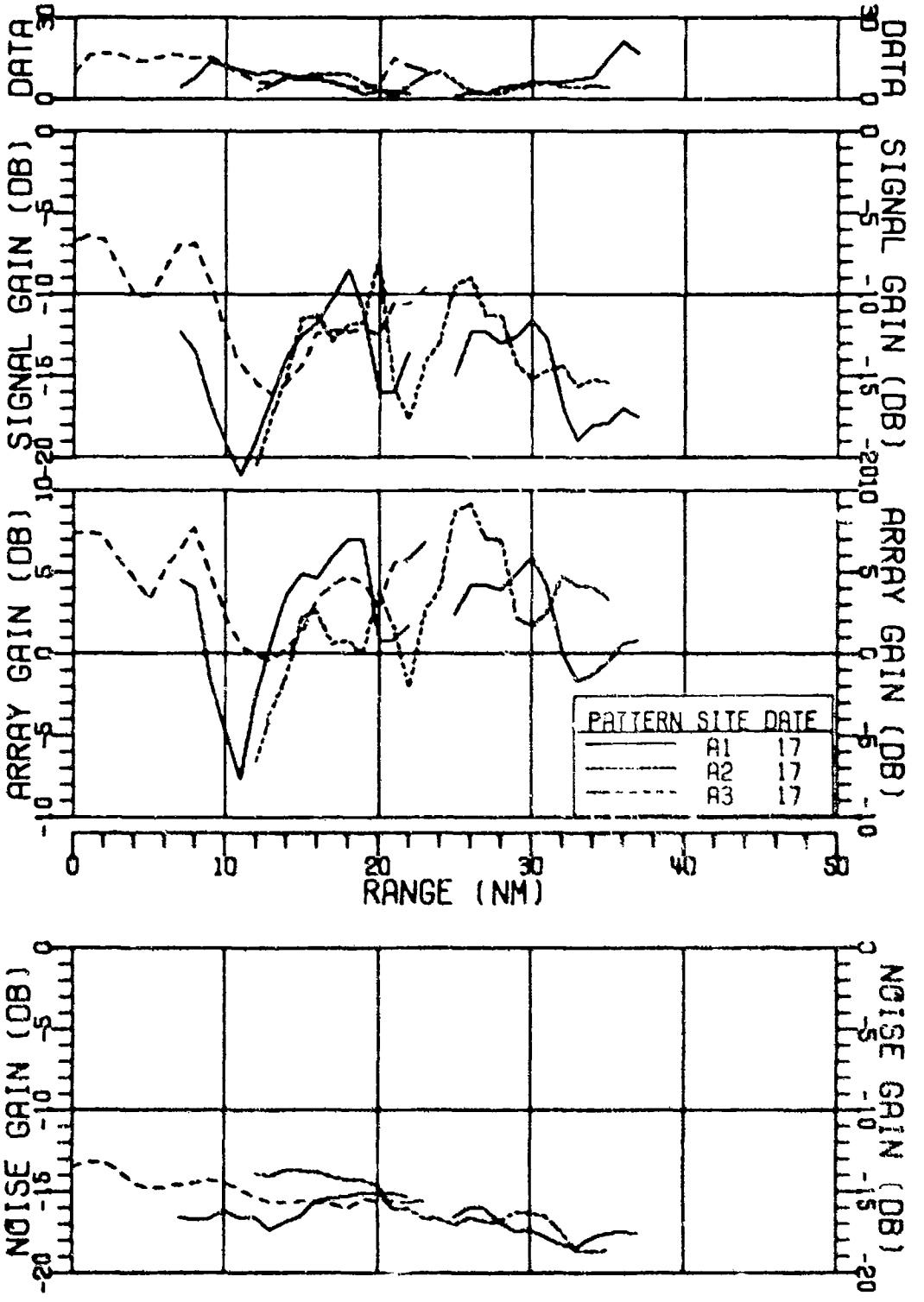

FIGURE II-158
MSS-FVT NEAR BOTTOM DIFFERENCED CARDIOIDS SENSOR ARRAY GAIN RESULTS FOR 70HZ AT 166DB (U)

AS-77-3085

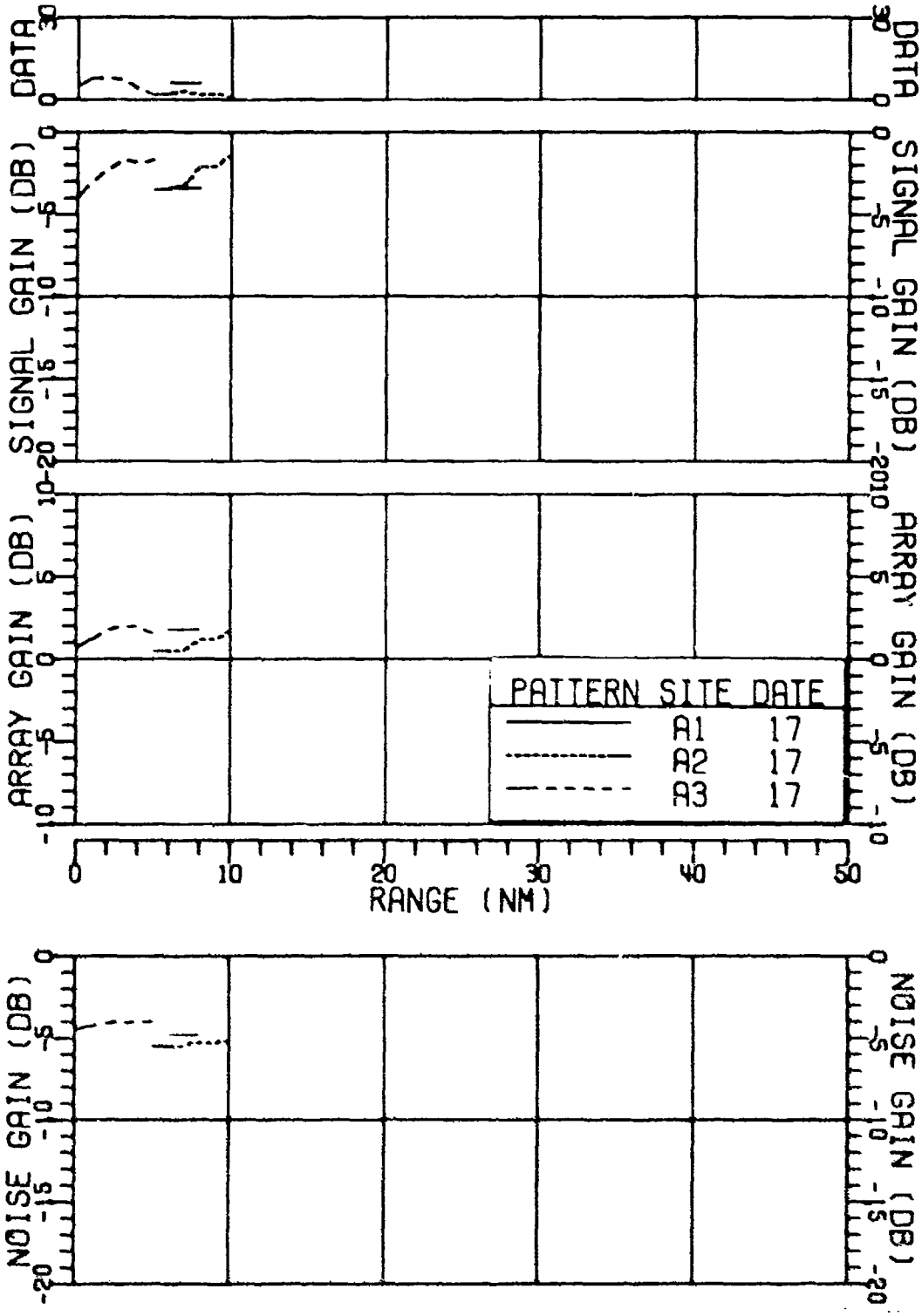

FIGURE II-159
MSS-FVT NEAR BOTTOM SINGLE CARDIOIDS SENSOR
ARRAY GAIN RESULTS FOR 155HZ AT 134DB (U)

AS-77-3(

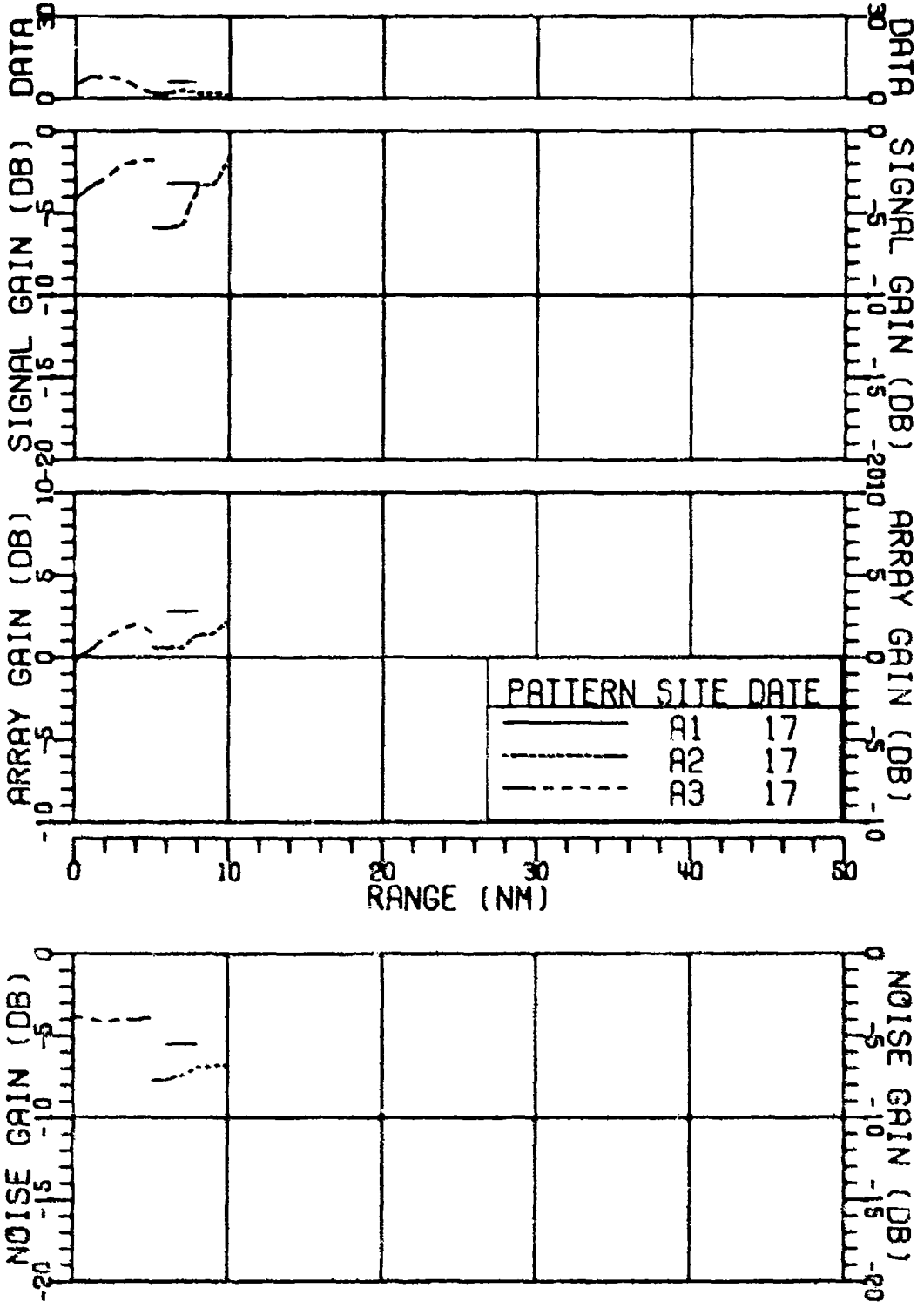

FIGURE II-160
MSS-FVT NEAR BOTTOM MAX GAIN LIMACONS SENSOR
ARRAY GAIN RESULTS FOR 155HZ AT 134DB (U)

AS-77-3087

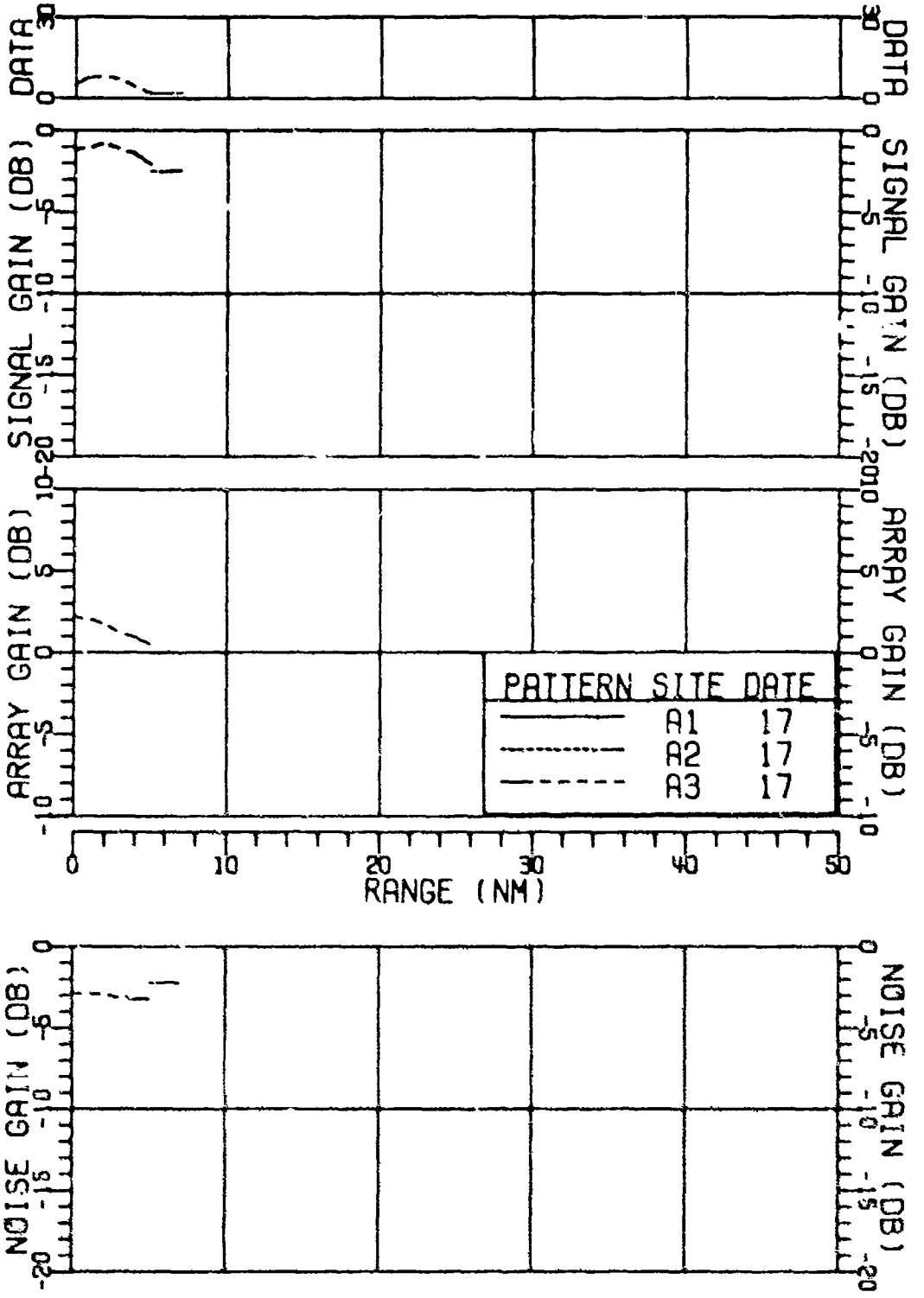

FIGURE II-161
MSS-FVT NEAR BOTTOM VERTICAL DIPOLE SENSOR
ARRAY GAIN RESULTS FOR 155HZ AT 134DB (U)

AS-77-[illegible]

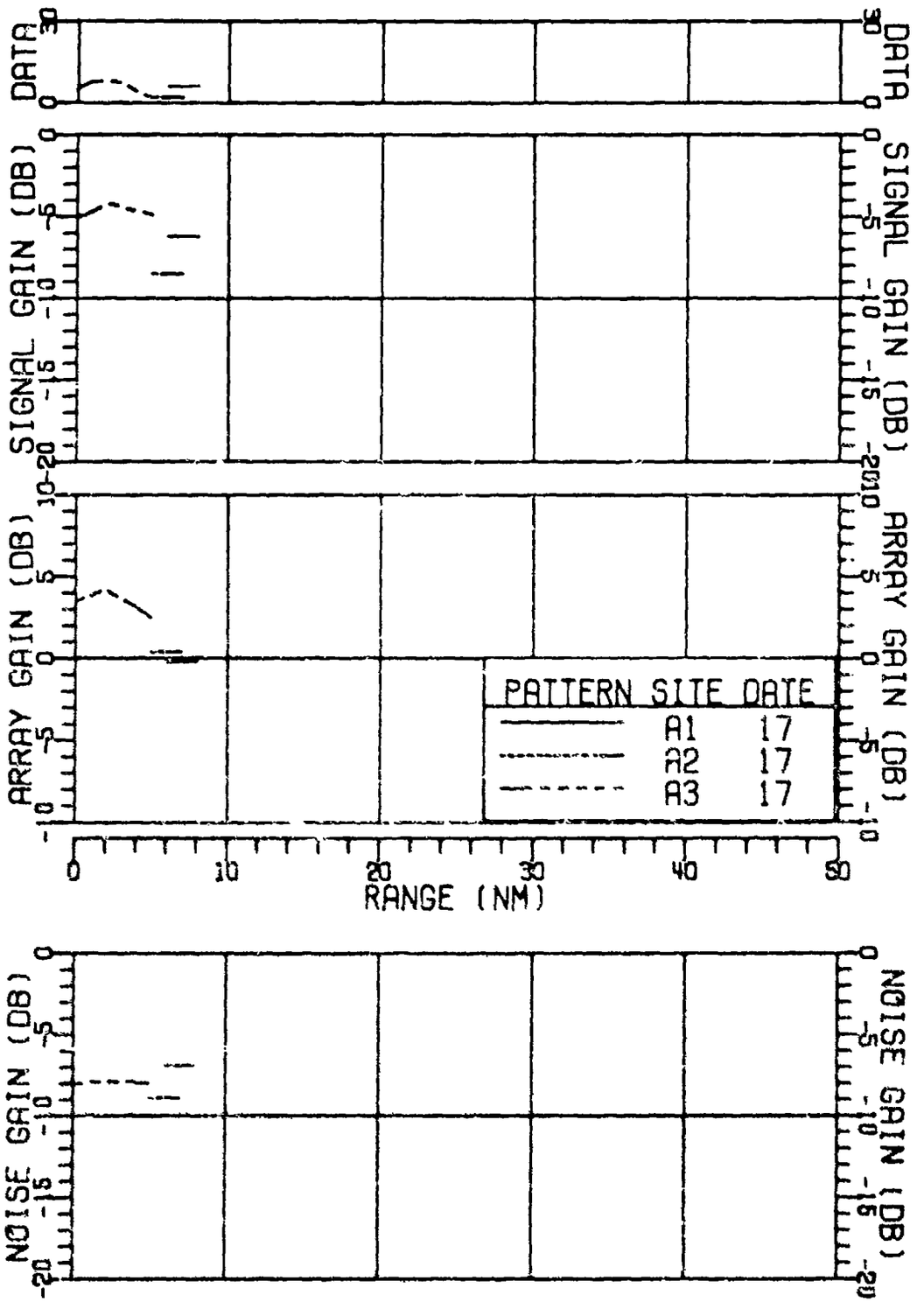

FIGURE II-162
MSS-FVT NEAR BOTTOM DIFFERENCED CARDIOIDS SENSOR
ARRAY GAIN RESULTS FOR 155HZ AT 134DB (U)

AS-77-3089

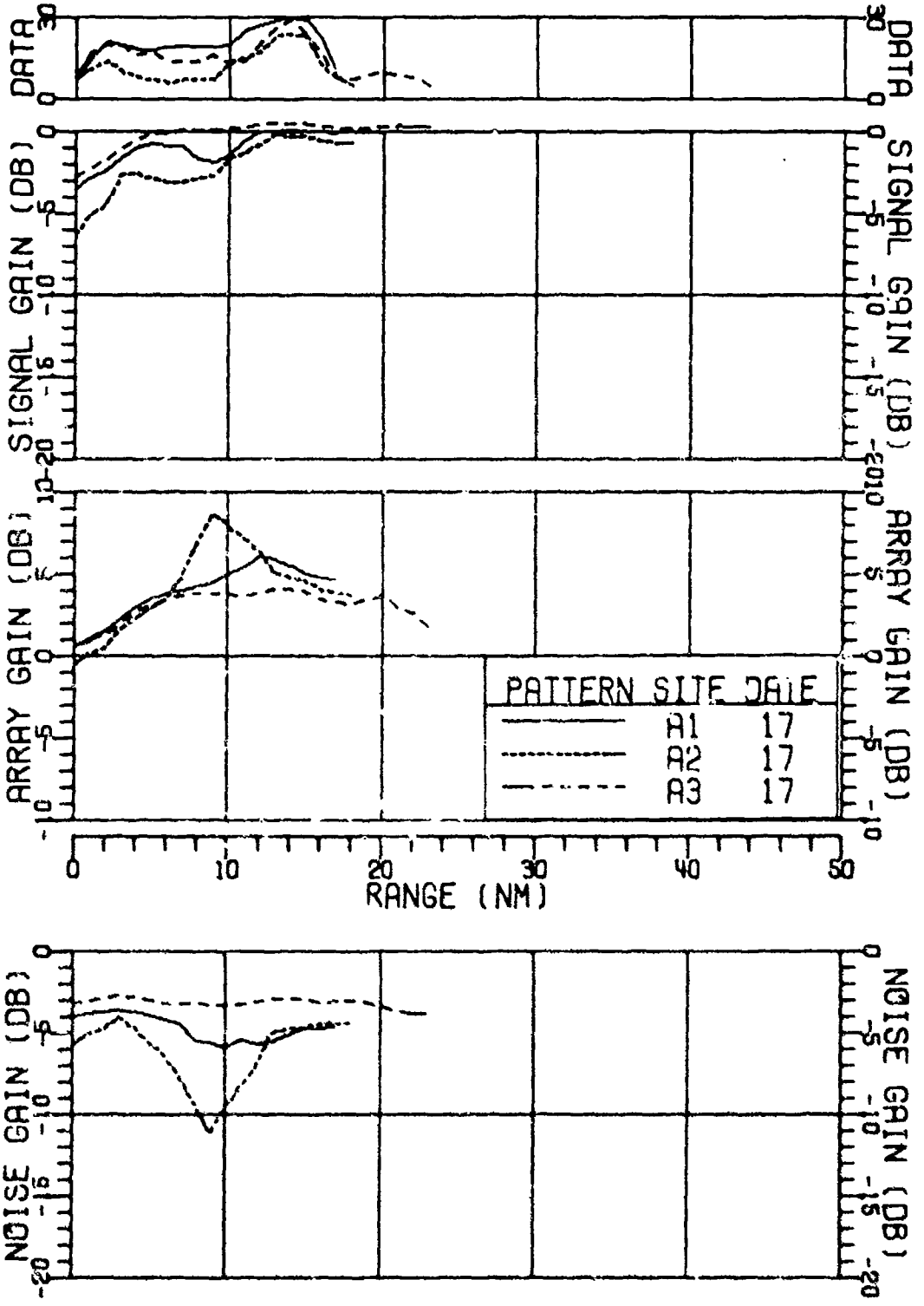

FIGURE II-163
MSS-FVT NEAR BOTTOM SINGLE CARDIOIDS SENSOR
ARRAY GAIN RESULTS FOR 160HZ AT 161DB (U)

AS-77-309

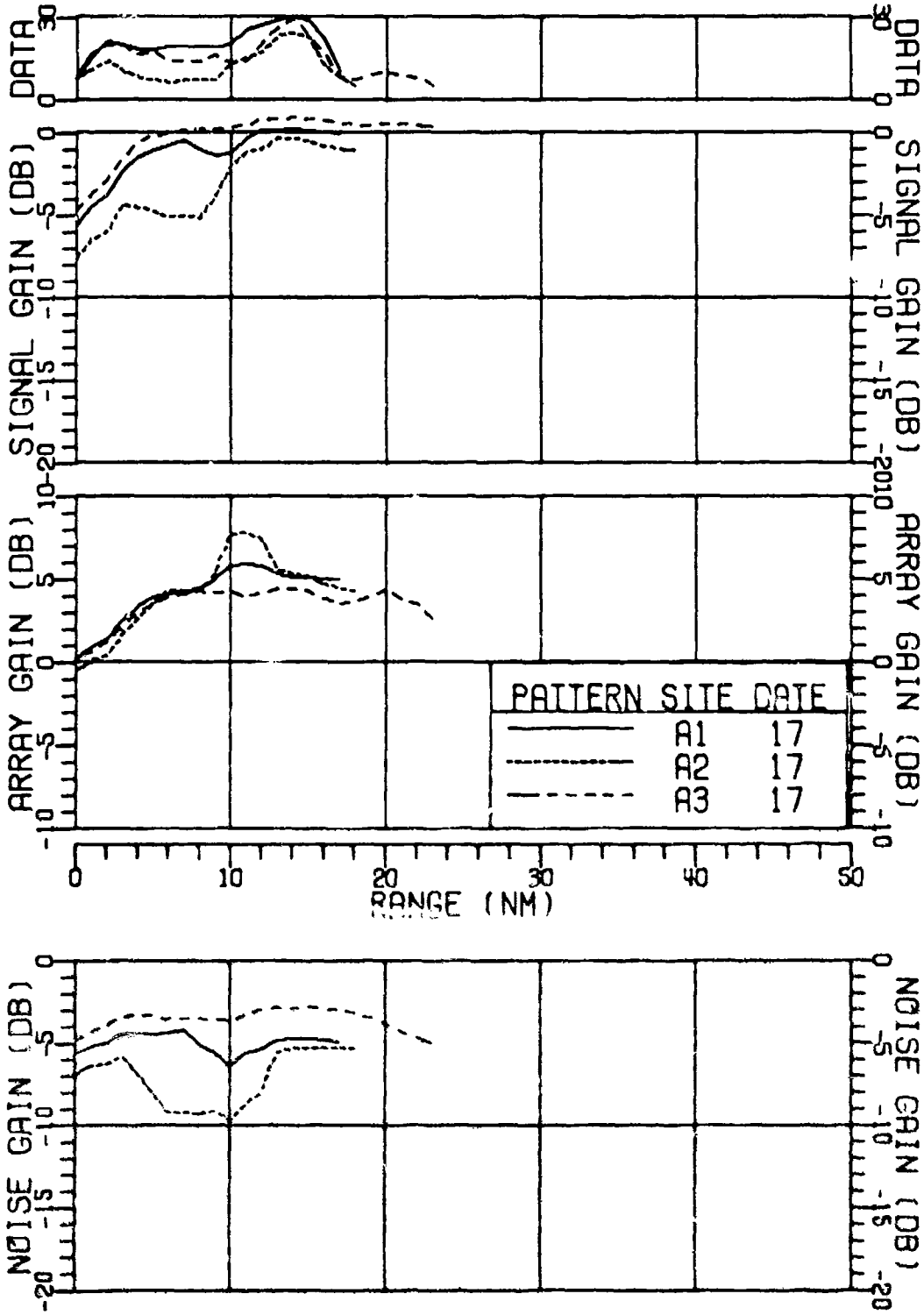

FIGURE II-164
MSS-FVT NEAR BOTTOM MAX GAIN LIMACONS SENSOR
ARRAY GAIN RESULTS FOR 160HZ AT 161DB (U)

AS-77-3091

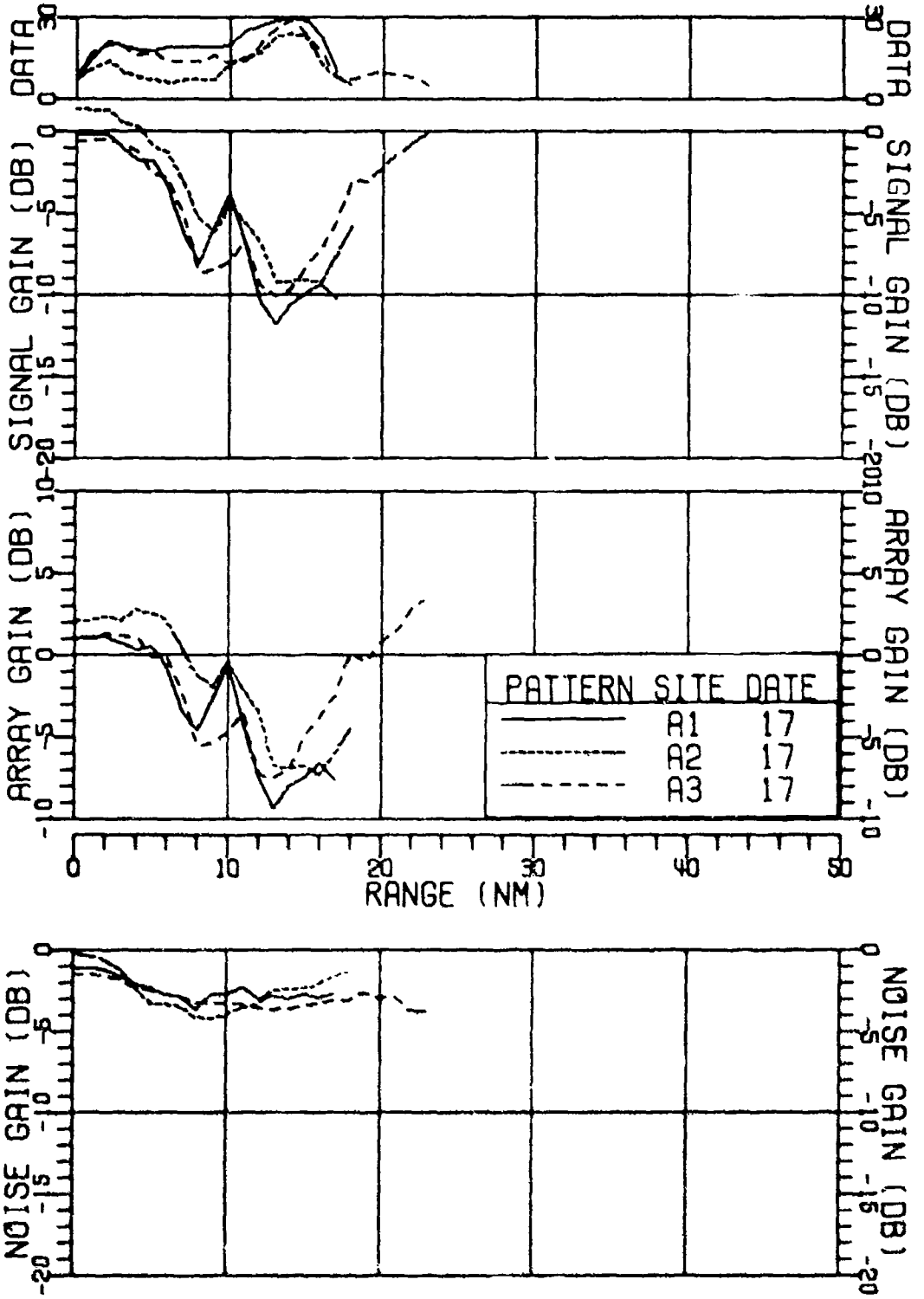

FIGURE II-165
MSS-FVT NEAR BOTTOM VERTICAL DIPOLE SENSOR
ARRAY GAIN RESULTS FOR 160HZ AT 161DB (U)

AS-77-309

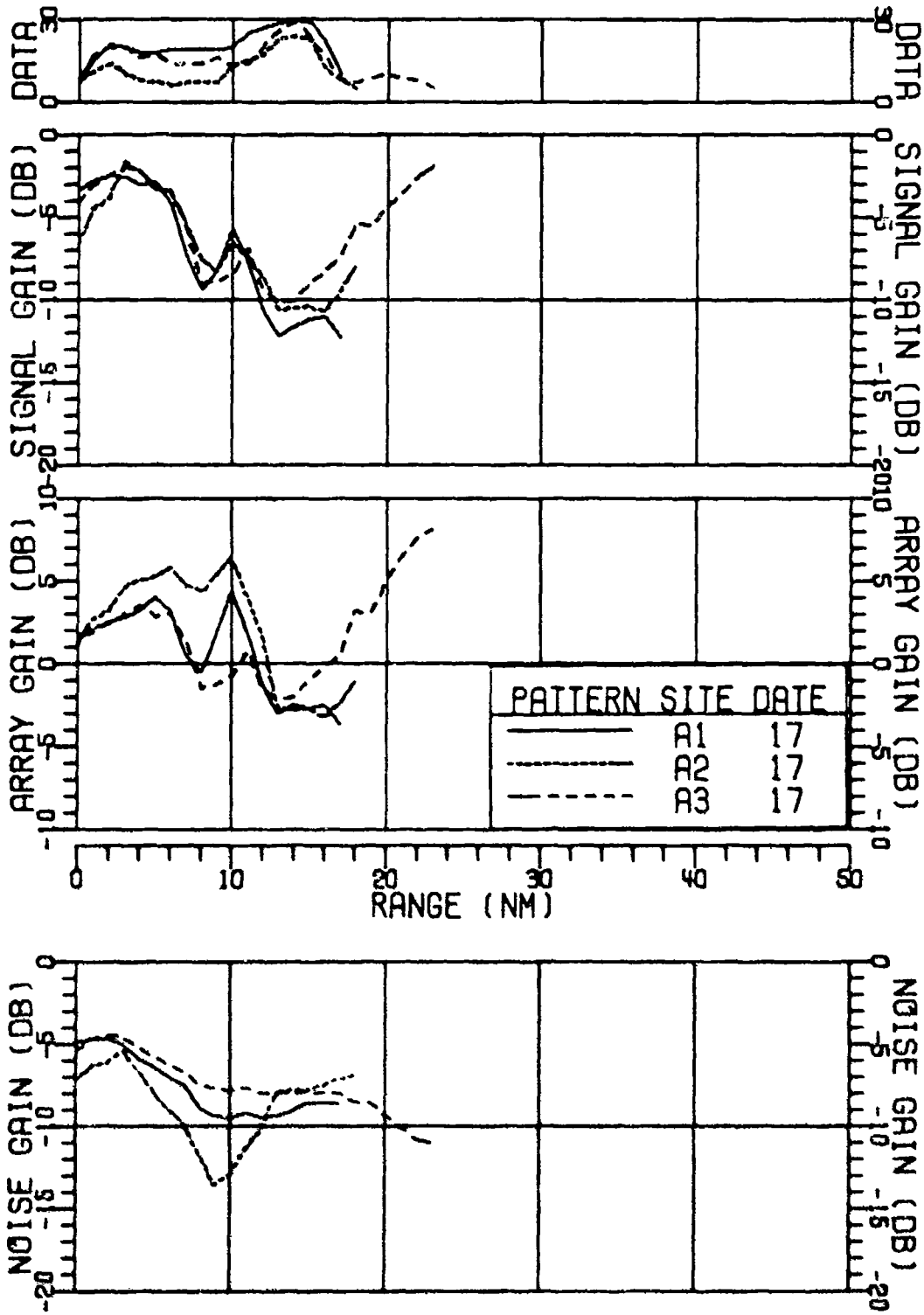

FIGURE II-166
MSS-FVT NEAR BOTTOM DIFFERENCED CARDIOIDS SENSOR ARRAY GAIN RESULTS FOR 160HZ AT 161DB (U)

AS-77-3093

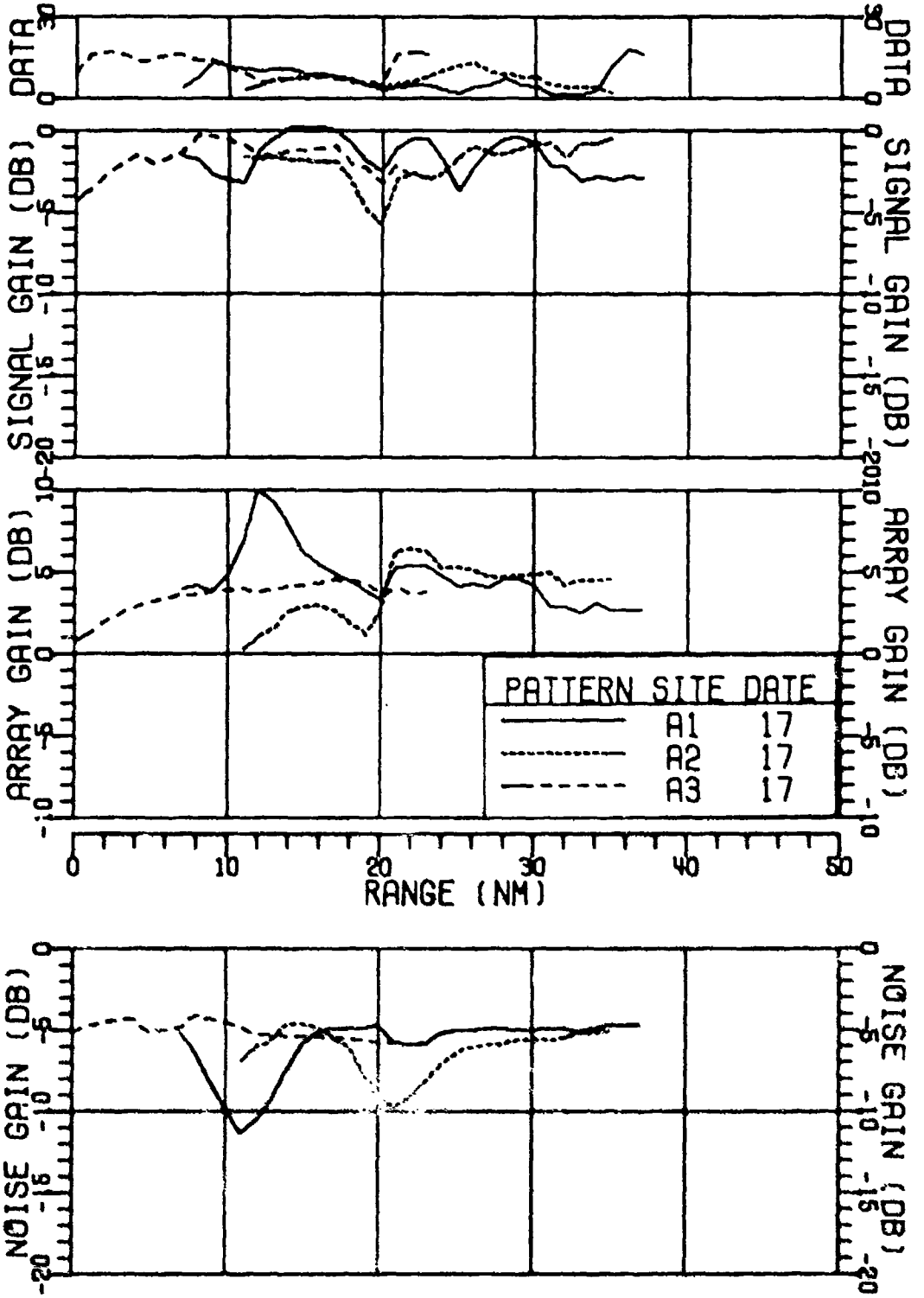

FIGURE II-167
MSS-FVT NEAR BOTTOM SINGLE CARDIOIDS SENSOR
ARRAY GAIN RESULTS FOR 170HZ AT 156DB (U)

AS-77-3094

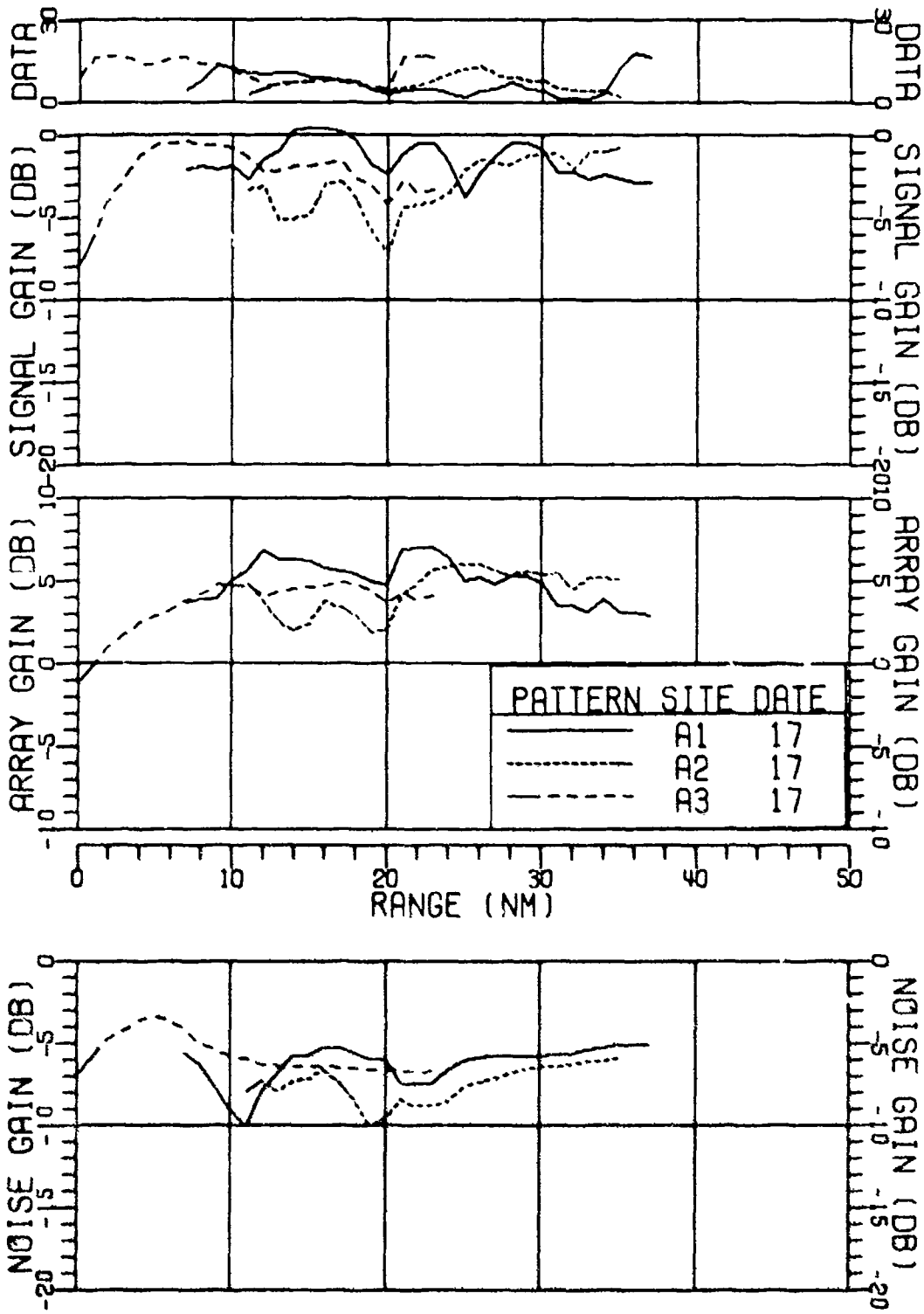

FIGURE II-168
MSS-FVT NEAR BOTTOM MAX GAIN LIMACONS SENSOR
ARRAY GAIN RESULTS FOR 170HZ AT 156DB (U)

AS-77-3095

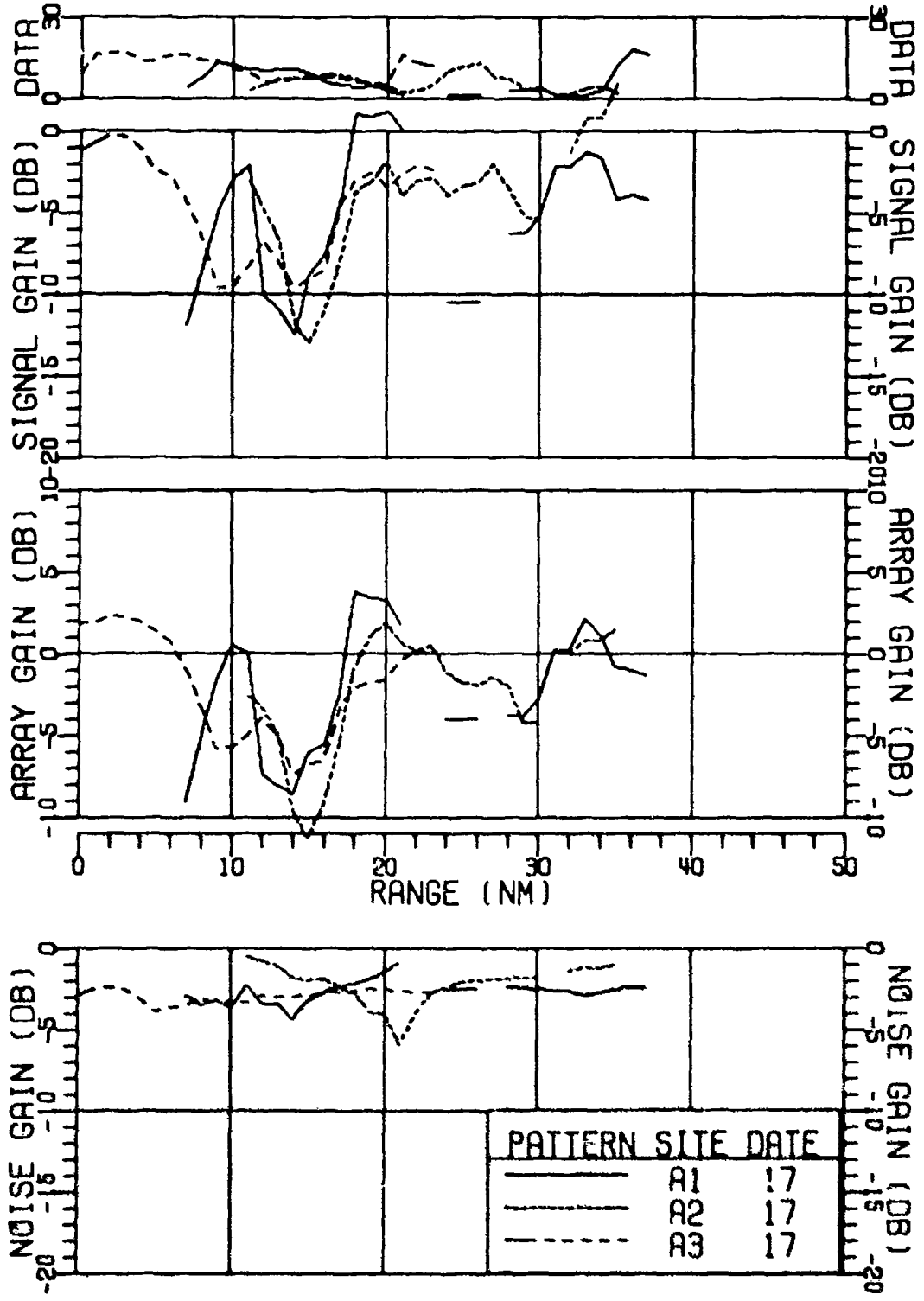

FIGURE II-169
MSS-FVT NEAR BOTTOM VERTICAL DIPOLE SENSOR
ARRAY GAIN RESULTS FOR 170HZ AT 156DB (U)

AS-77-3096

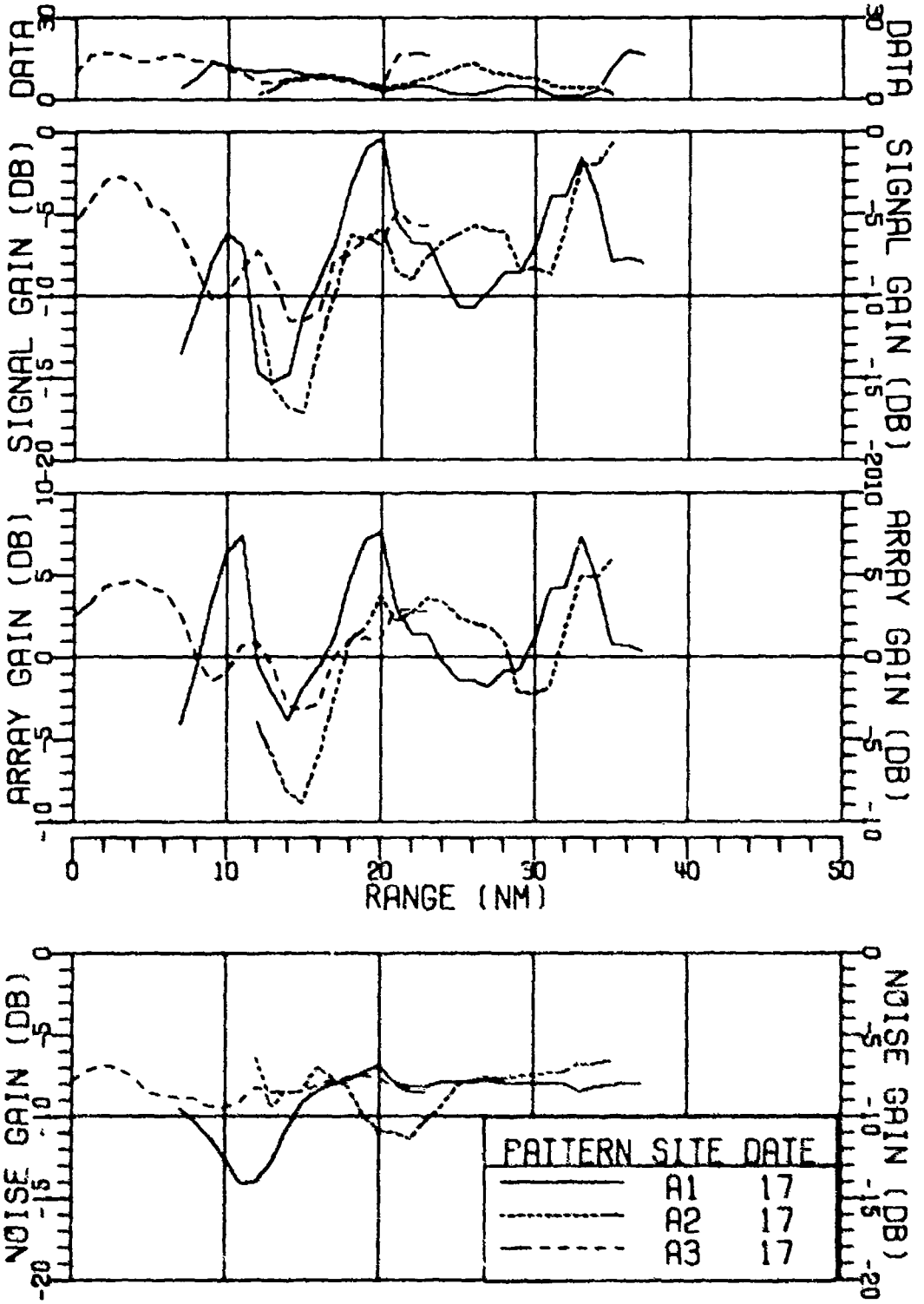

FIGURE II-170
MSS-FVT NEAR BOTTOM DIFFERENCED CARDIOIDS SENSOR
ARRAY GAIN RESULTS FOR 170HZ AT 156DB (U)

AS-77-3097

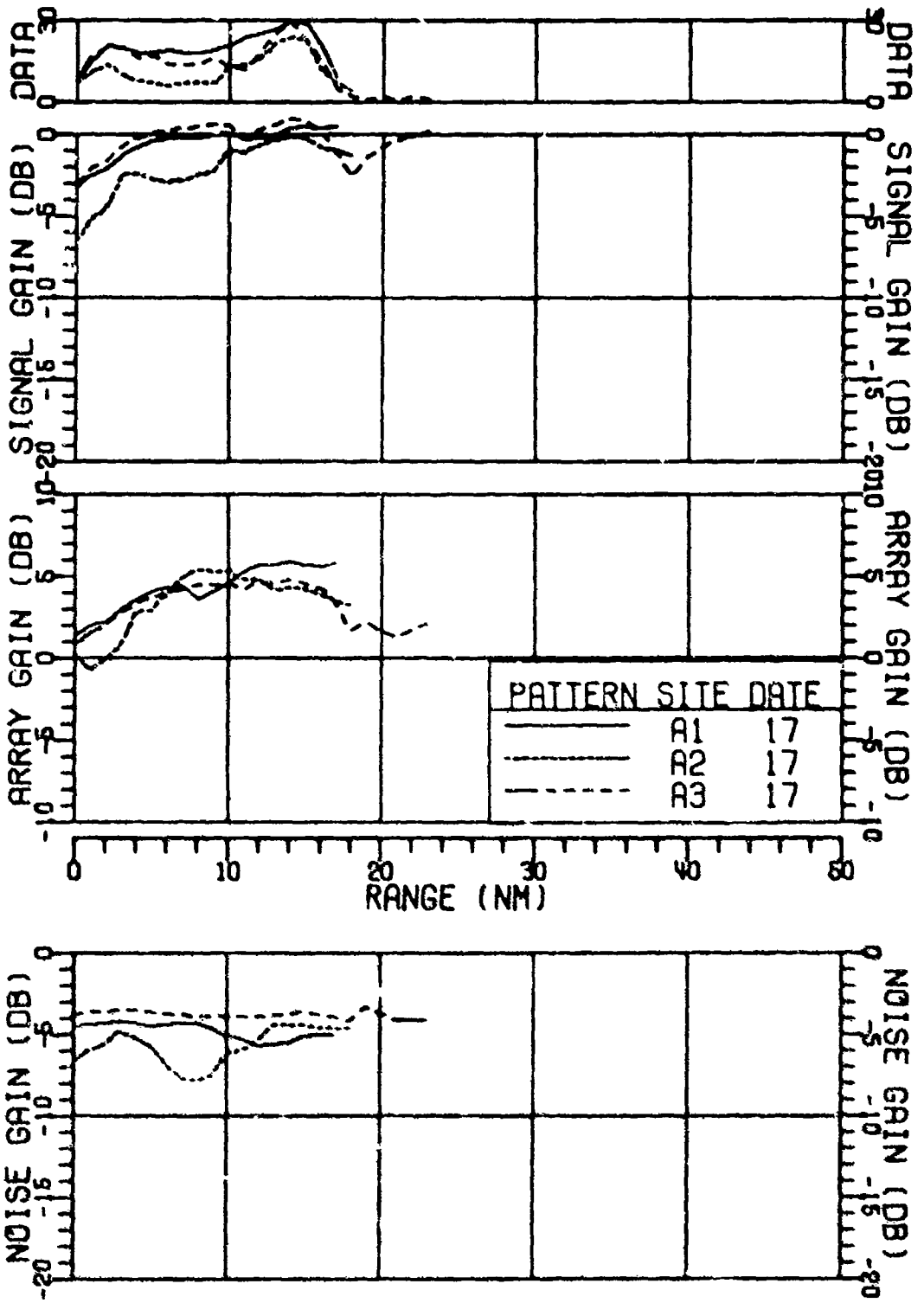

FIGURE II-171
MSS-FVT NEAR BOTTOM SINGLE CARDIOIDS SENSOR
ARRAY GAIN RESULTS FOR 260HZ AT 147DB (U)

AS-77-3098

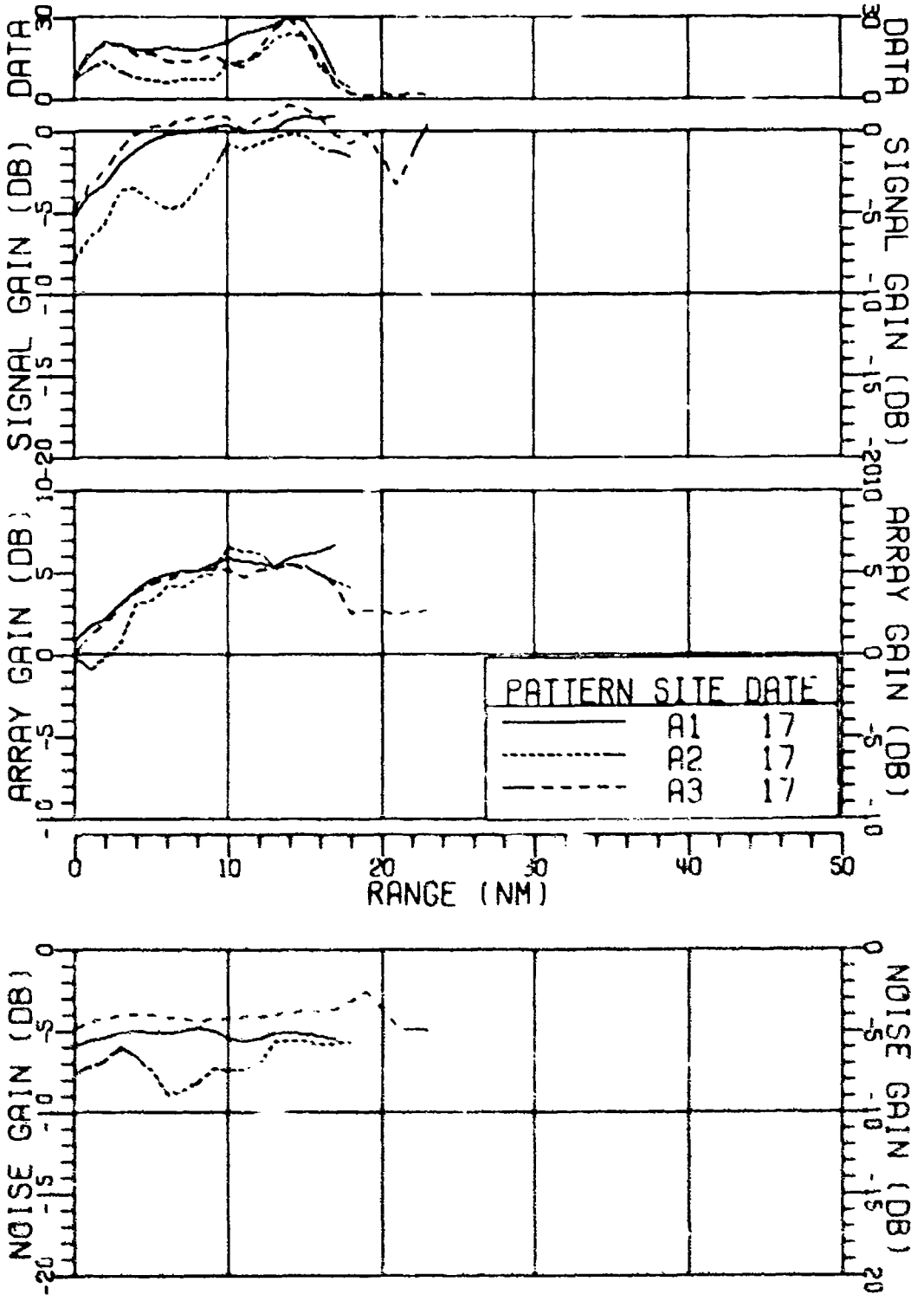

FIGURE II-172
MSS-FVT NEAR BOTTOM MAX GAIN LIMACONS SENSOR
ARRAY GAIN RESULTS FOR 260HZ AT 147DB (U)

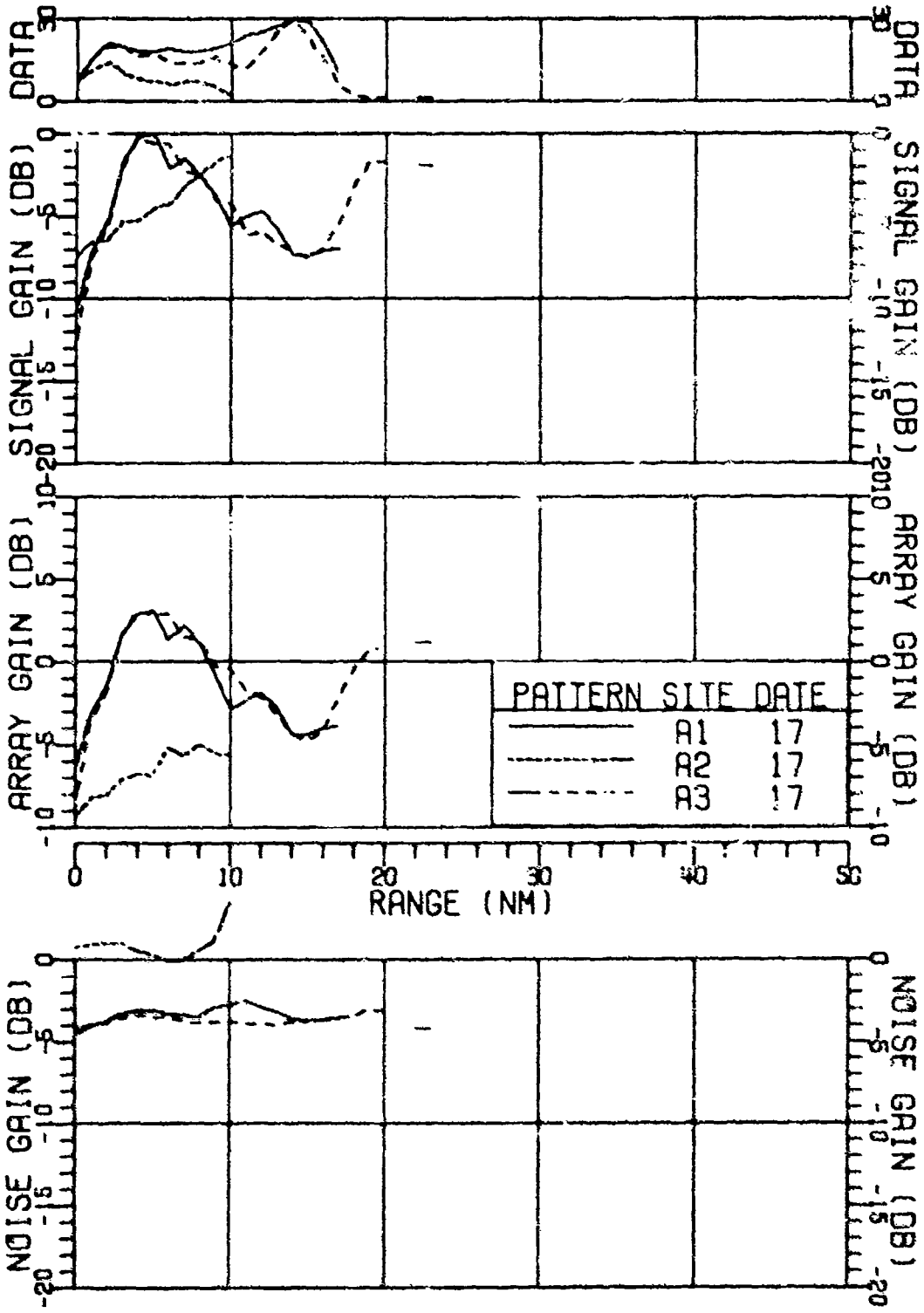

FIGURE II-173
MSS-FVT NEAR BOTTOM VERTICAL DIPOLE SENSOR
ARRAY GAIN RESULTS FOR 260HZ AT 147DB (U)

AS-77-3100

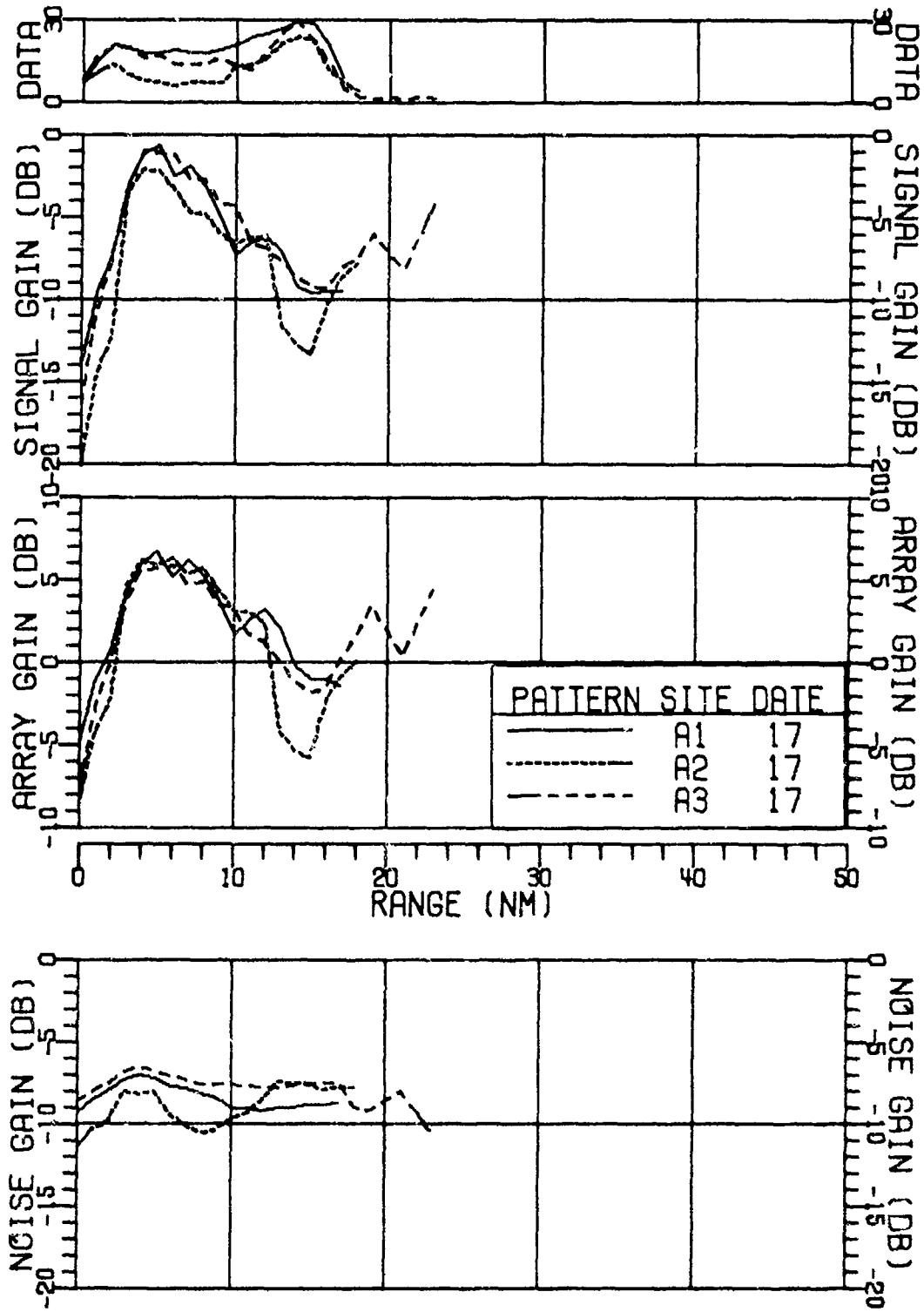

FIGURE II-174
MSS-FVT NEAR BOTTOM DIFFERENCED CARDIOIDS SENSOR
ARRAY GAIN RESULTS FOR 260HZ AT 147DB (U)

AS-77-3101

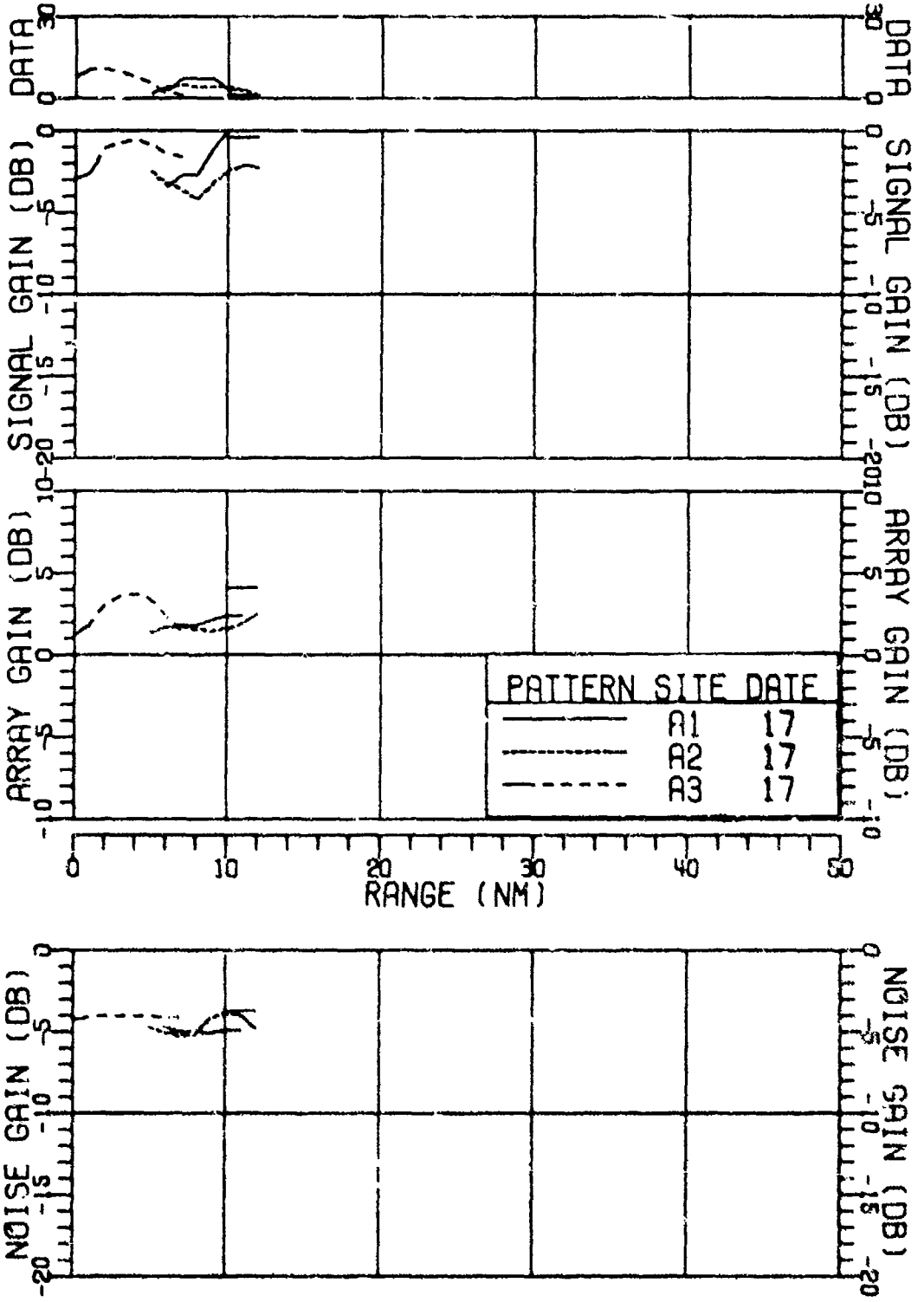

FIGURE II-175
MSS-FVT NEAR BOTTOM SINGLE CARDIOIDS SENSOR
ARRAY GAIN RESULTS FOR 305HZ AT 136DB (U)

AS-77-310

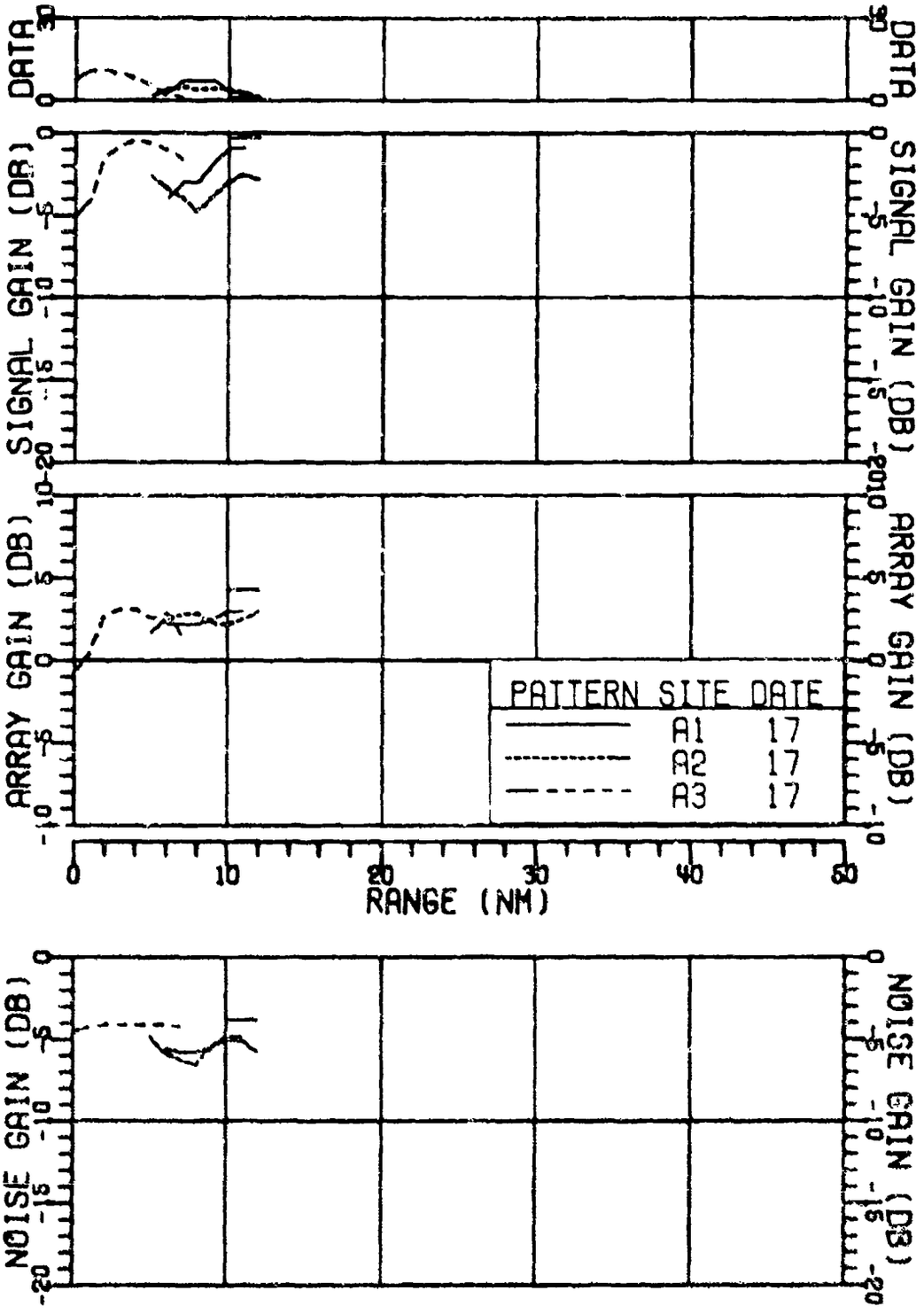

FIGURE II-176
MSS-FVT NEAR BOTTOM MAX GAIN LIMACONS SENSOR
ARRAY GAIN RESULTS FOR 305HZ AT 136DB (U)

AS-77-3103

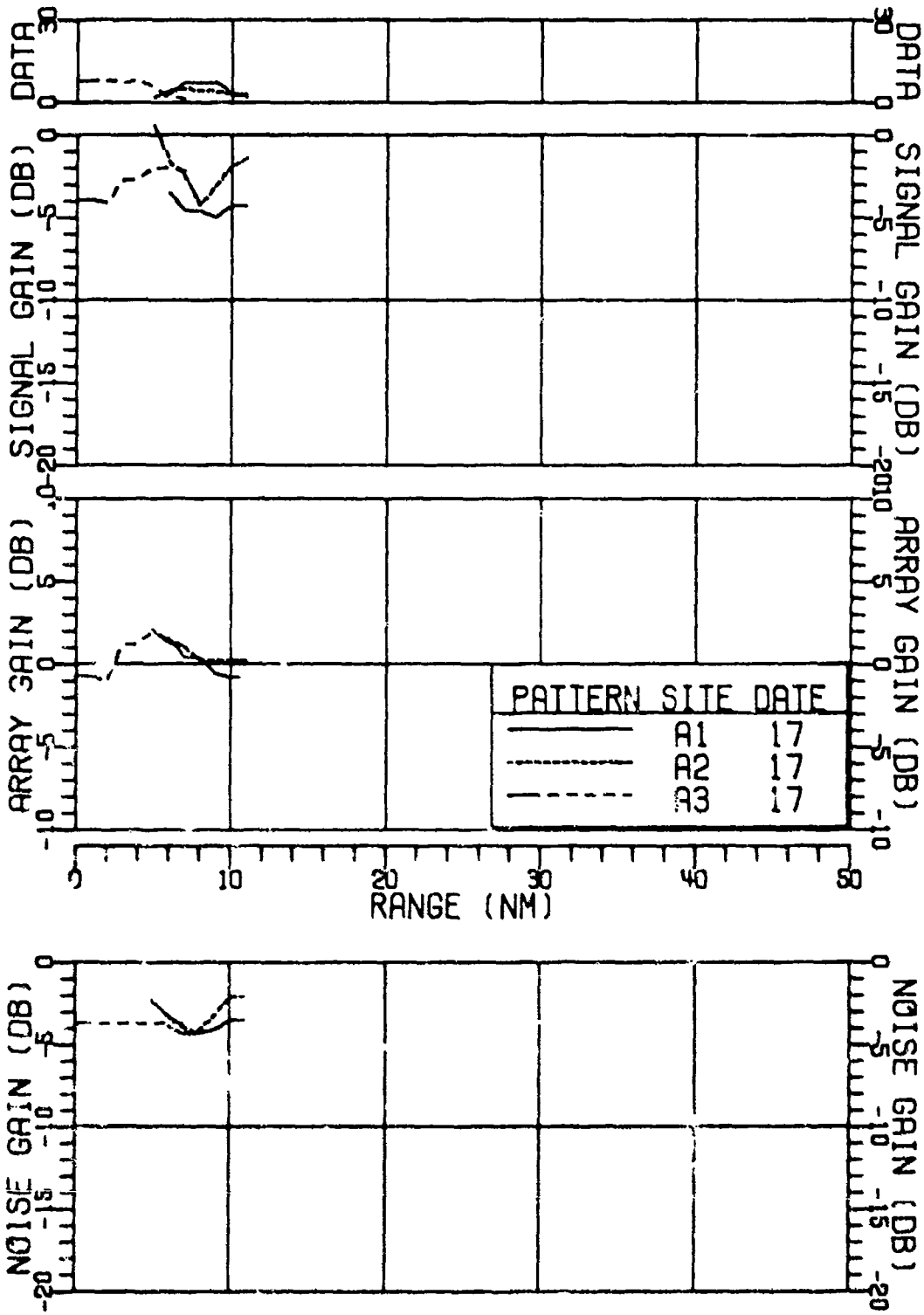

FIGURE II-177
MSS-FVT NEAR BOTTOM VERTICAL DIPOLE SENSOR
ARRAY GAIN RESULTS FOR 305HZ AT 136DB (U)

AS-77-3104

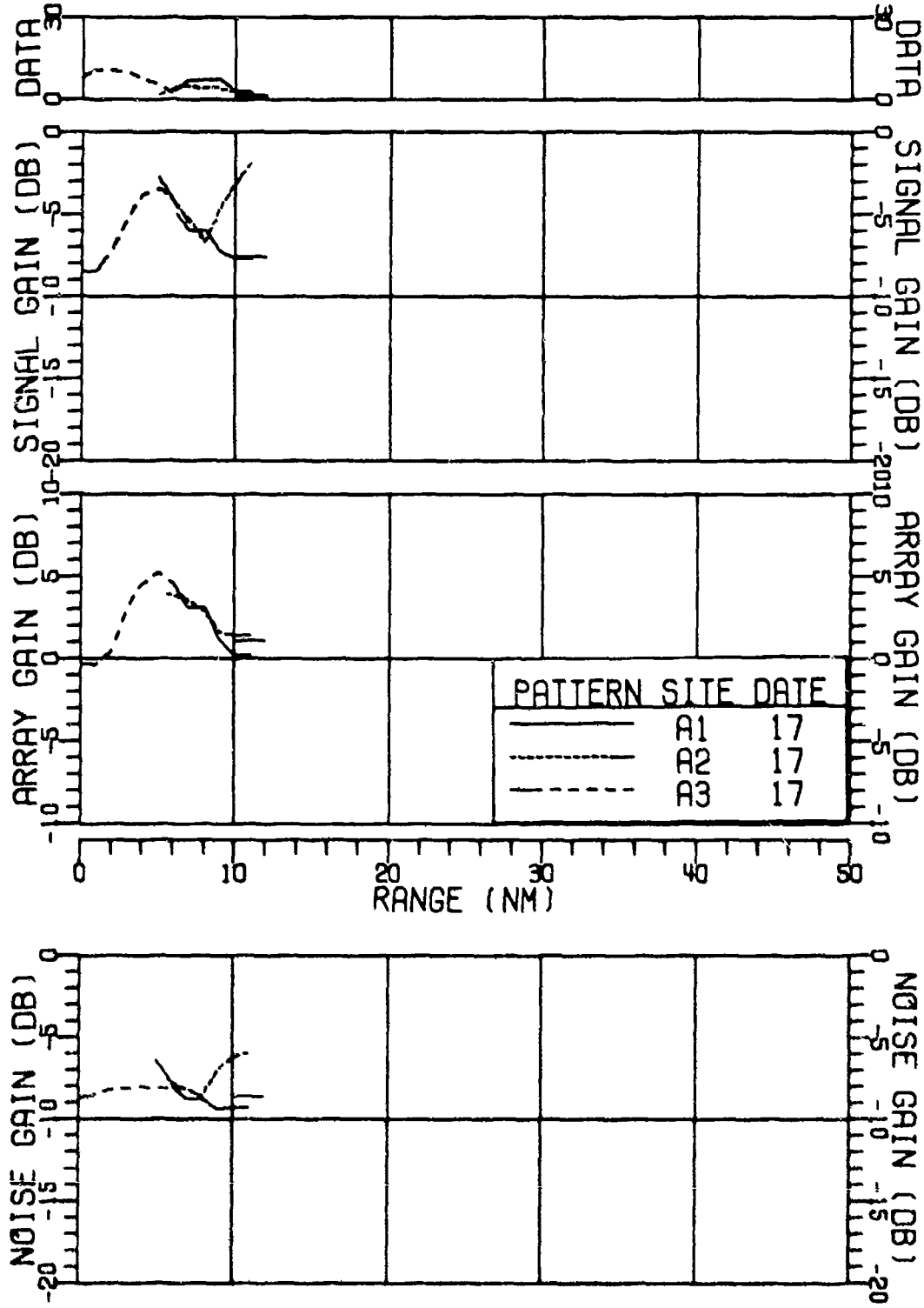

FIGURE II-178
MSS-FVT NEAR BOTTOM DIFFERENCED CARDIOIDS SENSOR
ARRAY GAIN RESULTS FOR 305HZ AT 136DB (U)

AS-77-3105

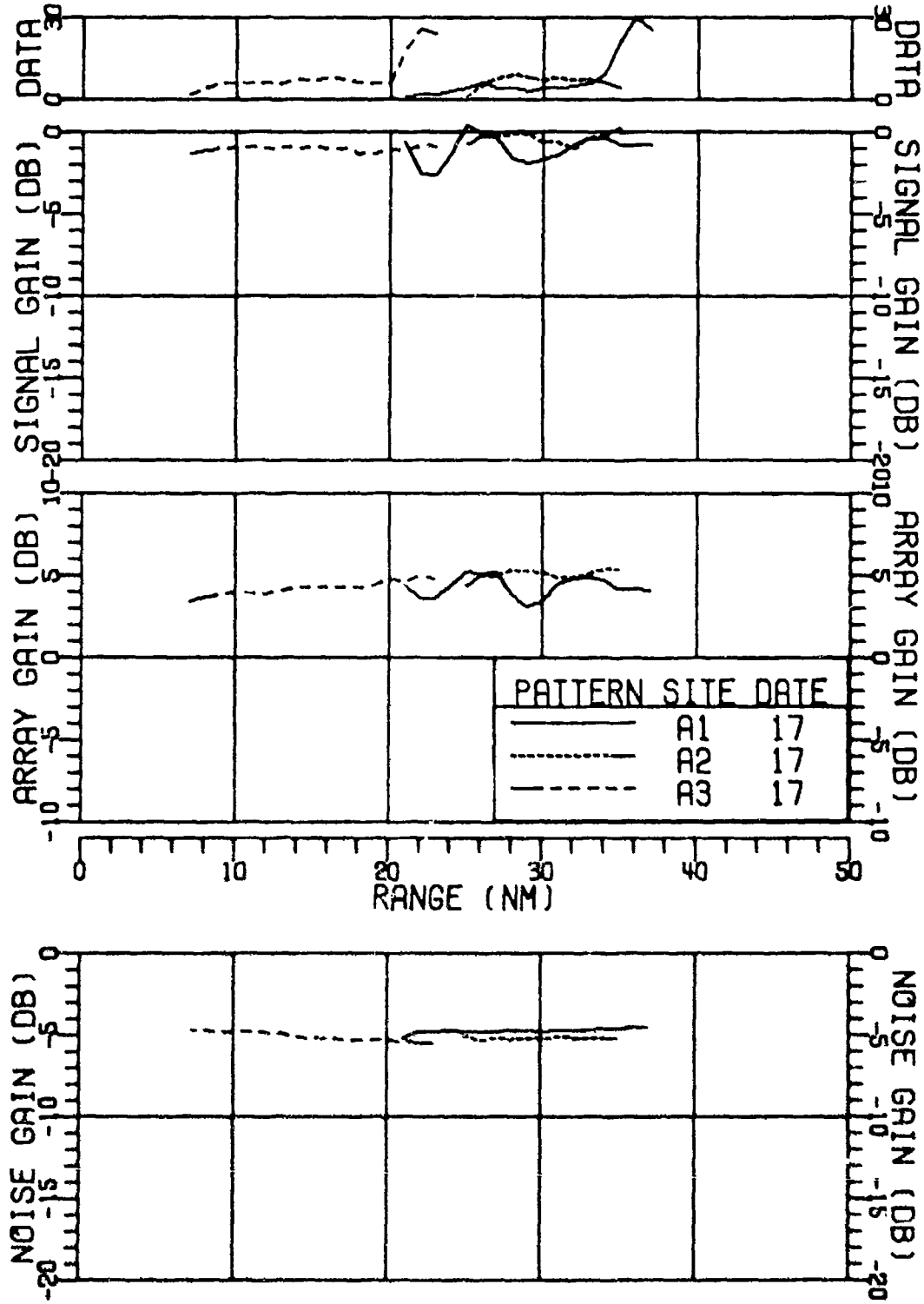

FIGURE II-179
MSS-FVT NEAR BOTTOM SINGLE CARDIOIDS SENSOR
ARRAY GAIN RESULTS FOR 335HZ AT 154DB (U)

AS-77-3106

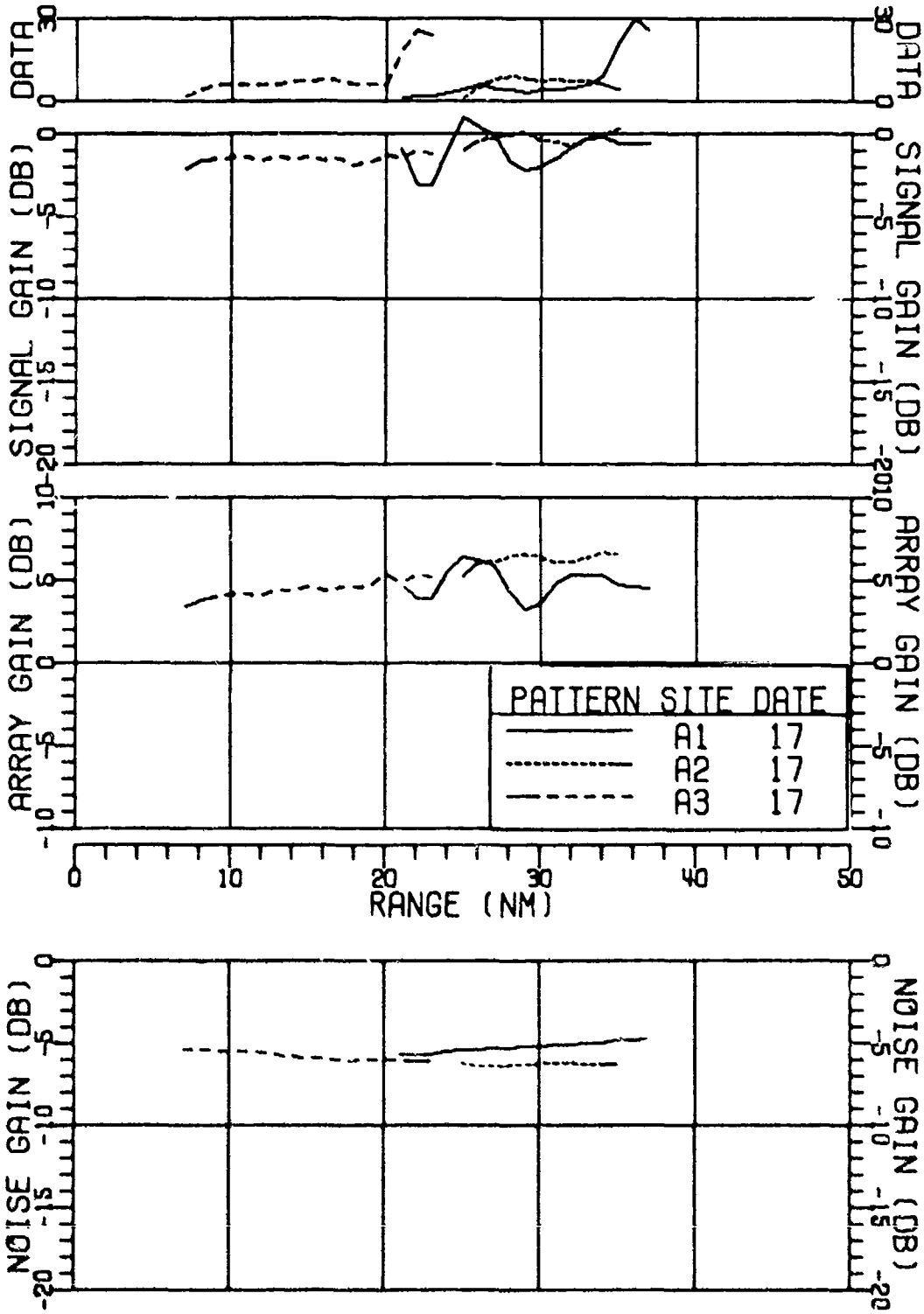

FIGURE II-180
MSS-FVT NEAR BOTTOM MAX GAIN LIMACONS SENSOR
ARRAY GAIN RESULTS FOR 335HZ AT 154DB (U)

AS-77-3107

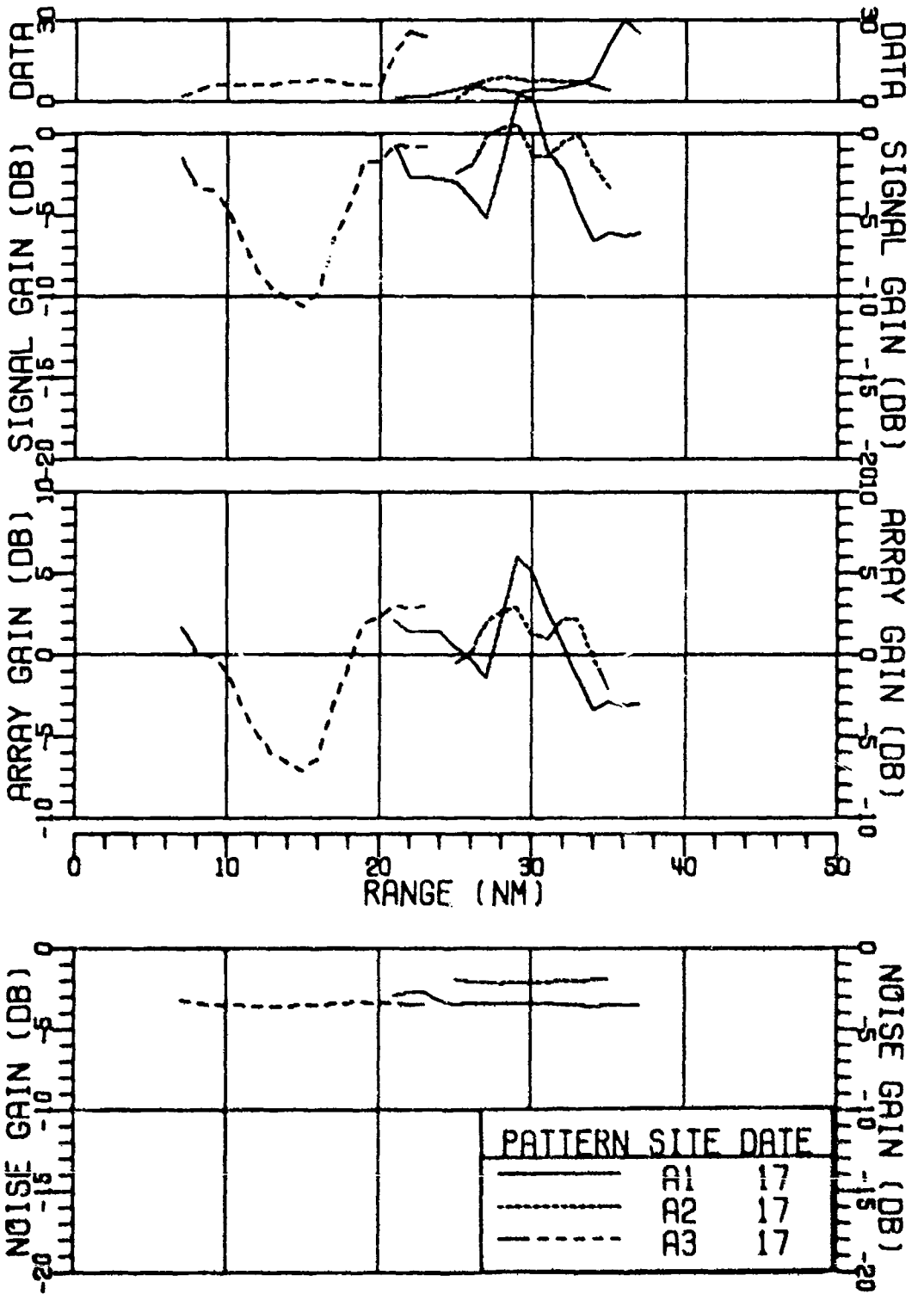

FIGURE II-181
MSS-FVT NEAR BOTTOM VERTICAL DIPOLE SENSOR
ARRAY GAIN RESULTS FOR 335HZ AT 154DB (U)

AS-77-3108

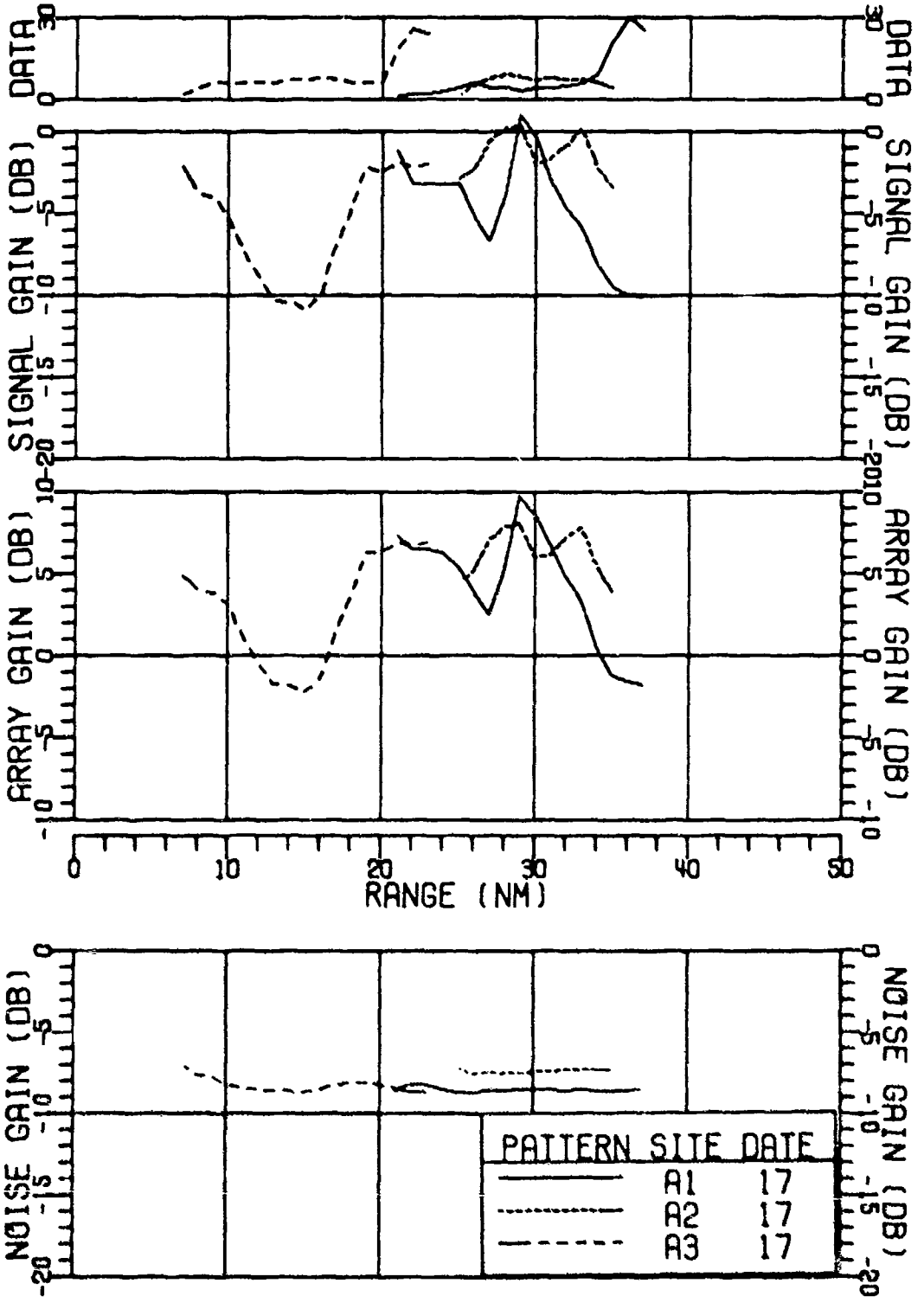

FIGURE II-182
MSS-FVT NEAR BOTTOM DIFFERENCED CARDIOIDS SENSOR ARRAY GAIN RESULTS FOR 335HZ AT 154DB (U)

AS-77-3109

APPENDIX E

PERCENTAGE DETECTION versus RANGE CURVES (U)

(FIGURES II-183 - II-225)

(The reverse of this page is blank.)

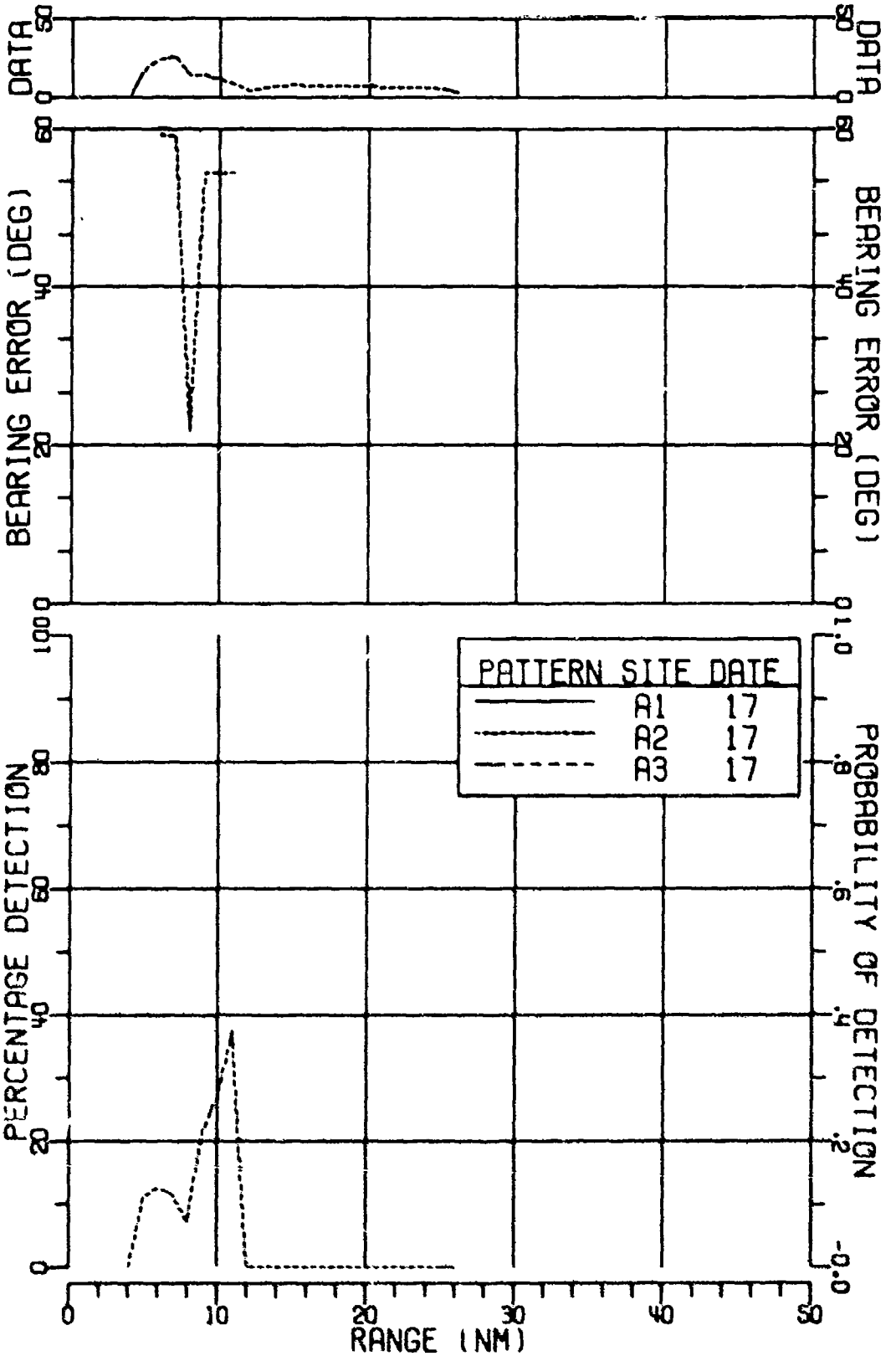

FIGURE II-183
MSS-FVT NEAR BOTTOM MAX GAIN LIMACONS SENSOR
DETECTION RESULTS FOR 55HZ AT 141DB (U)

AS-77-3110

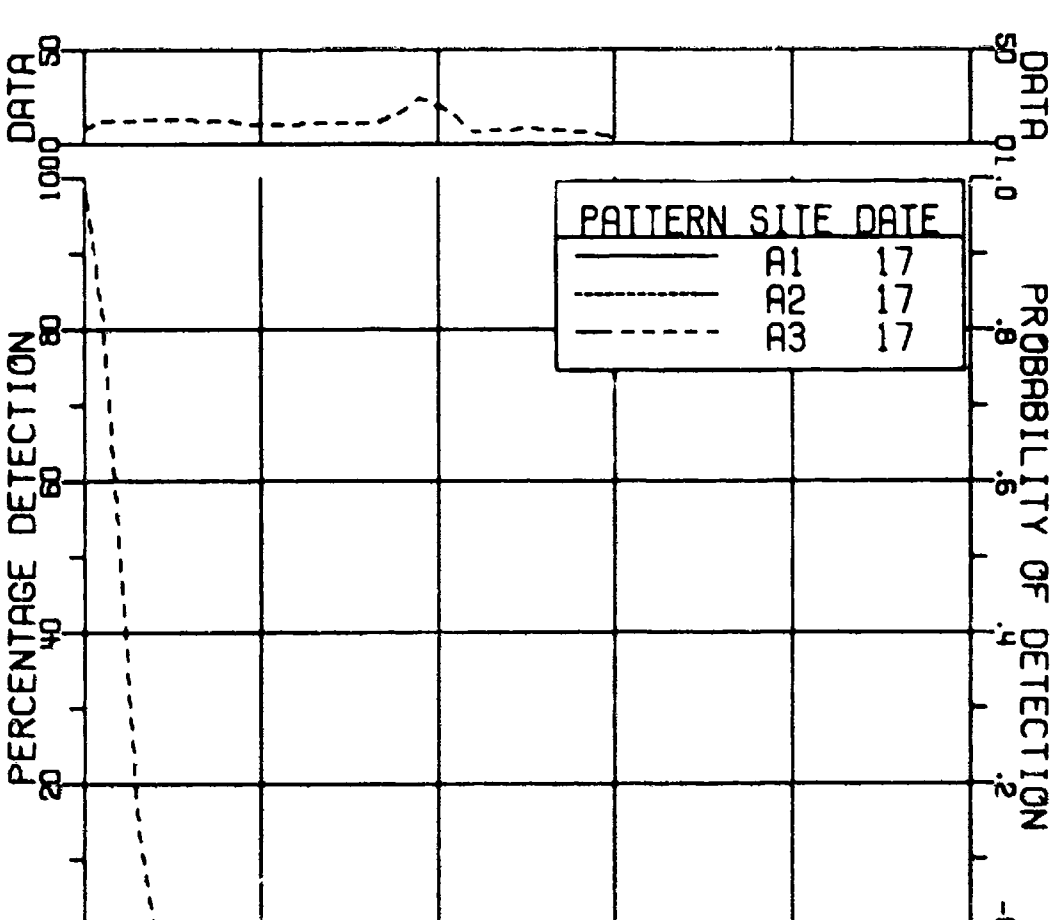

FIGURE II-184
MSS-FVT NEAR BOTTOM VERTICAL DIPOLE SENSOR
DETECTION RESULTS FOR 55HZ AT 141DB (U)

AS-77-3111

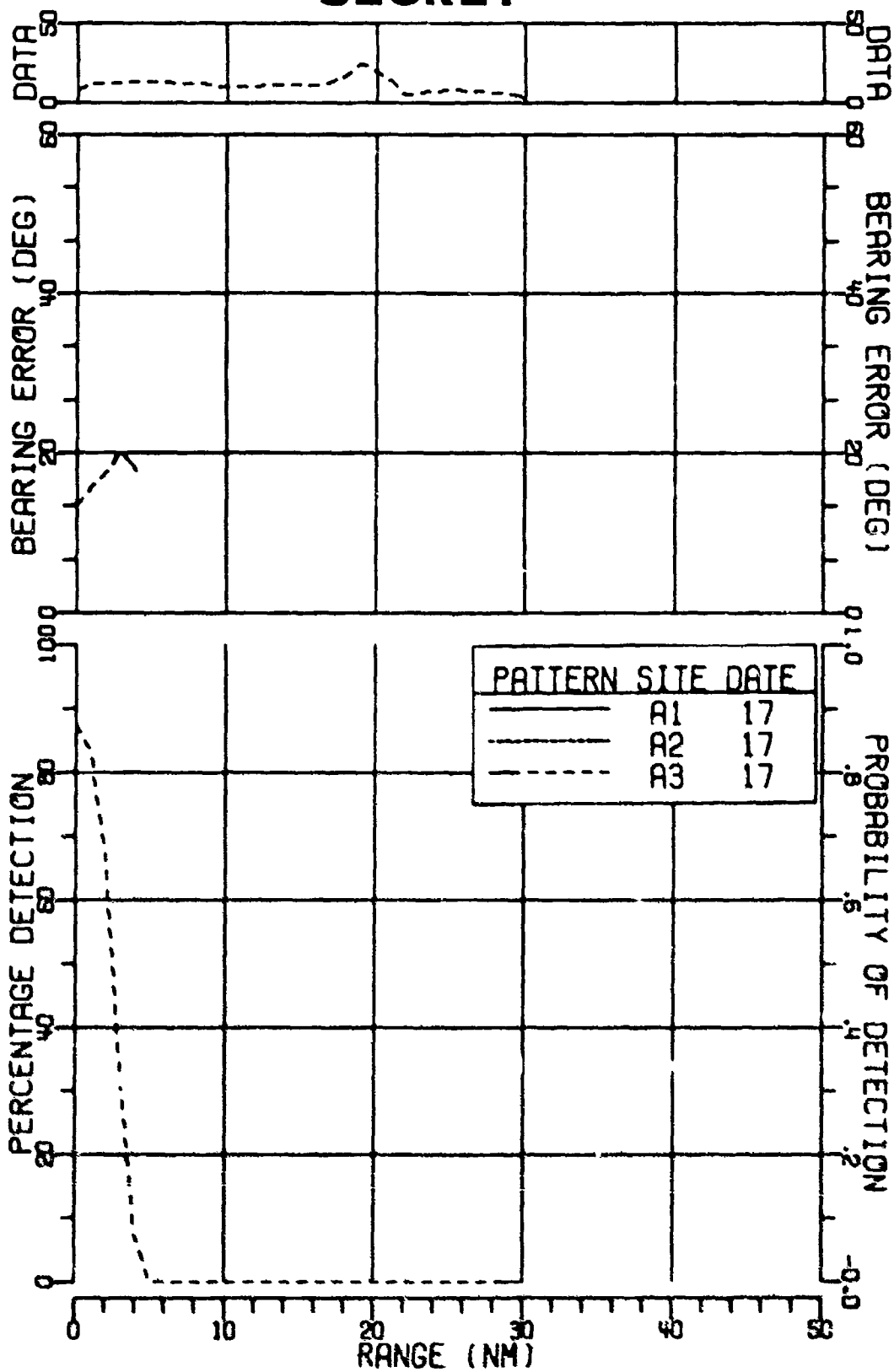

FIGURE II-185
MSS-FVT NEAR BOTTOM DIFFERENCED CARDIOIDS SENSOR
DETECTION RESULTS FOR 55HZ AT 141DB (U)

AS-77-3112

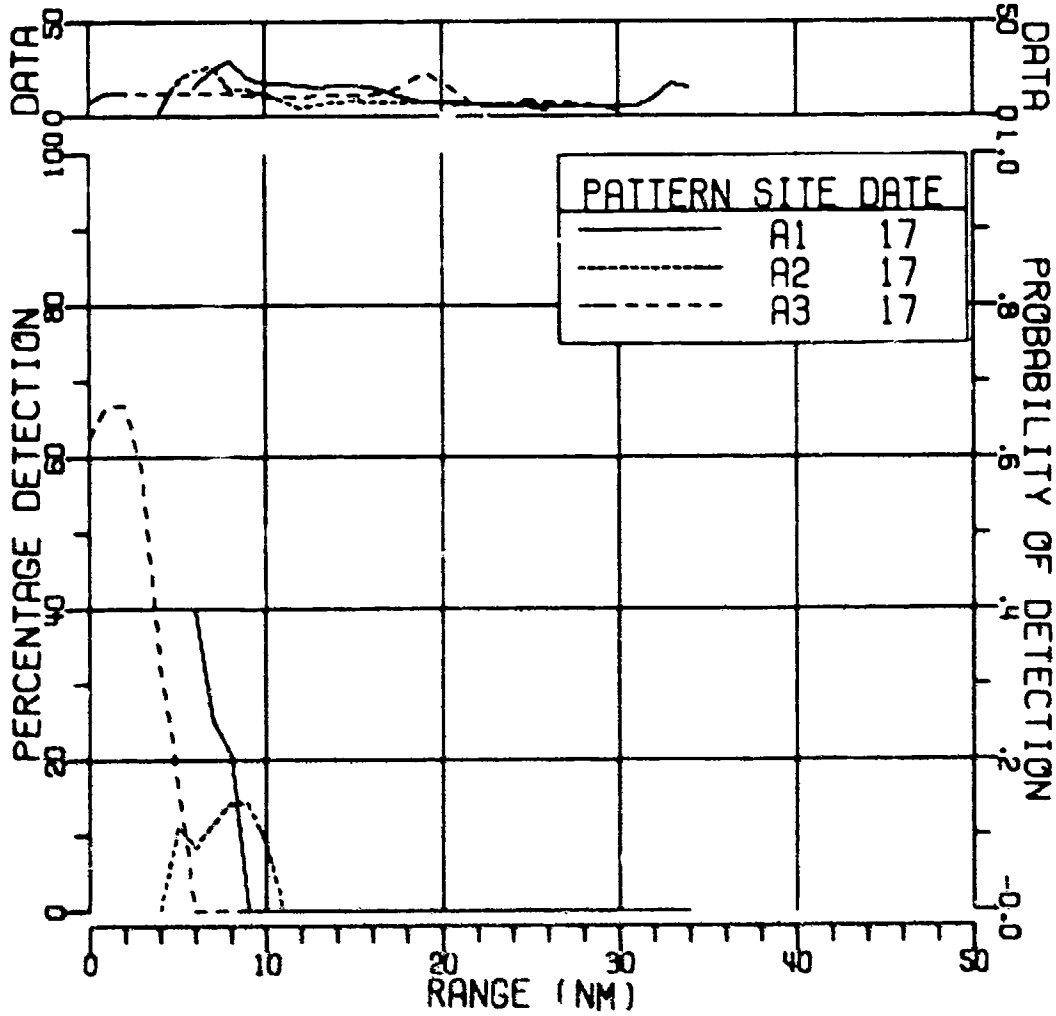

FIGURE II-186
MSS-FVT NEAR BOTTOM OMNIDIRECTIONAL SENSOR
DETECTION RESULTS FOR 155HZ AT 1340B (U)

AS-77-3113

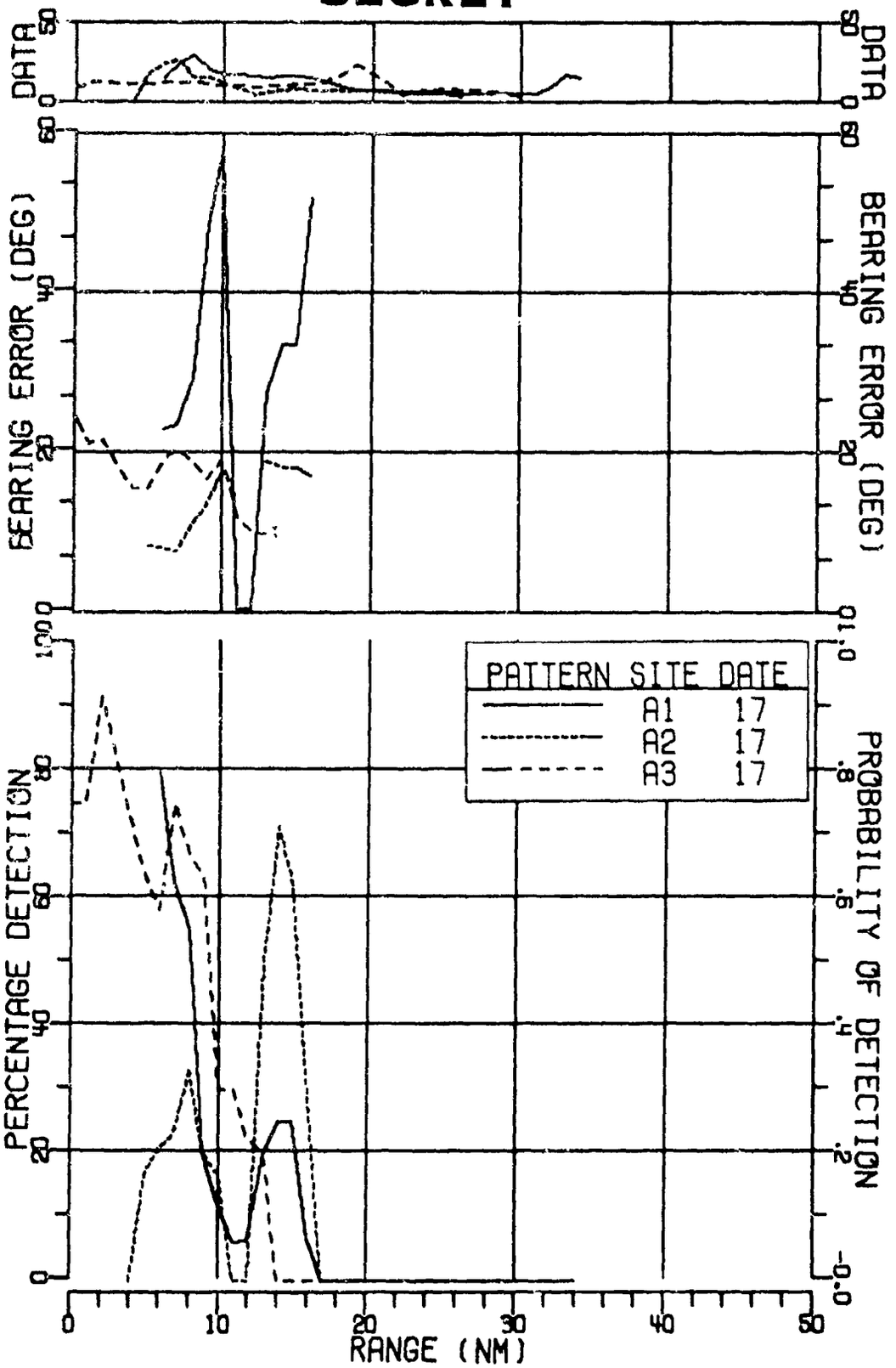

FIGURE II-187
MSS-FVT NEAR BOTTOM SINGLE CARDIOIDS SENSOR
DETECTION RESULTS FOR 155HZ AT 134DB (U)

AS-77-3114

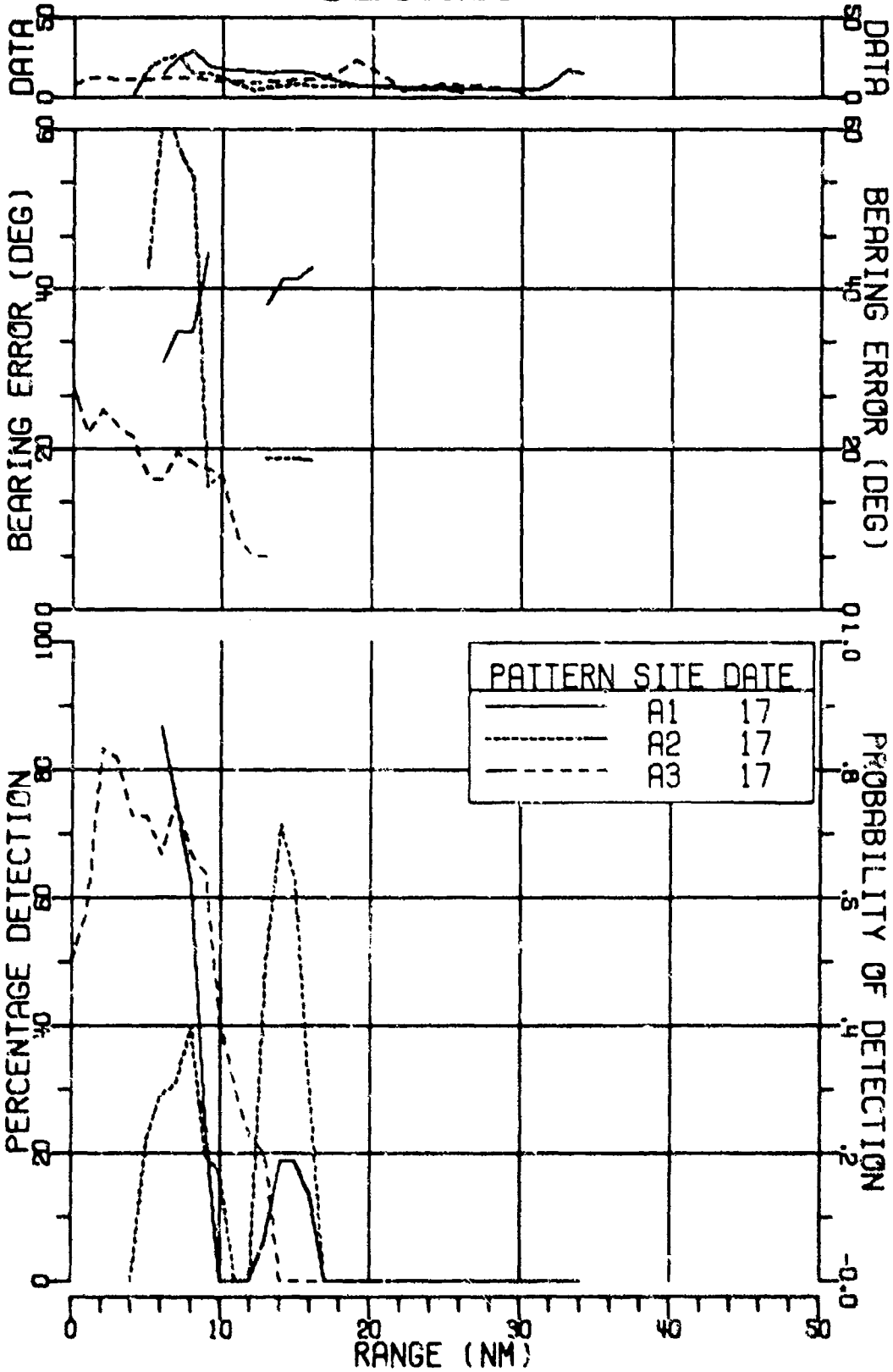

FIGURE II-188
MSS-FVT NEAR BOTTOM MAX GAIN LIMACONS SENSOR
DETECTION RESULTS FOR 155HZ AT 134DB (U)

AS-77-3115

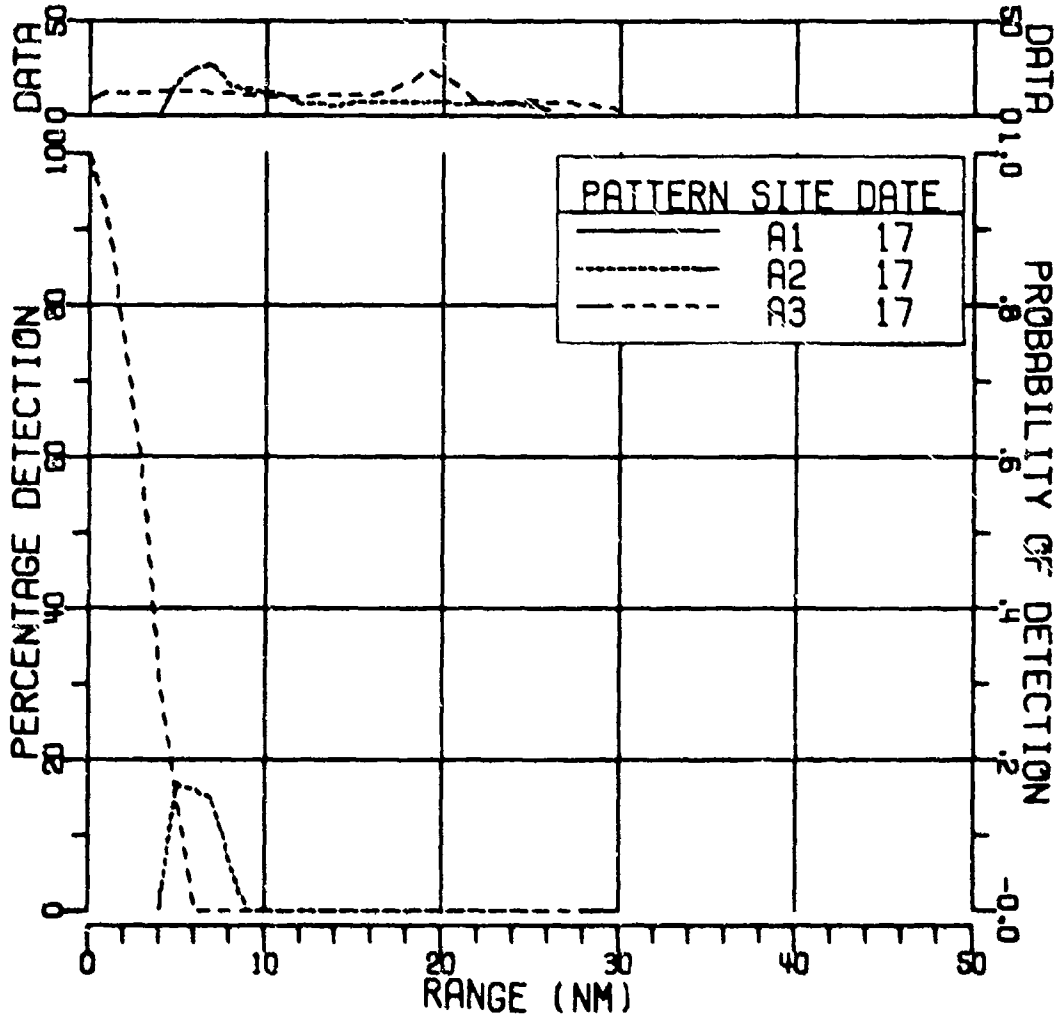

FIGURE II-189
MSS-FVT NEAR BOTTOM VERTICAL DIPOLE SENSOR
DETECTION RESULTS FOR 155HZ AT 134DB (U)

AS-77-3116

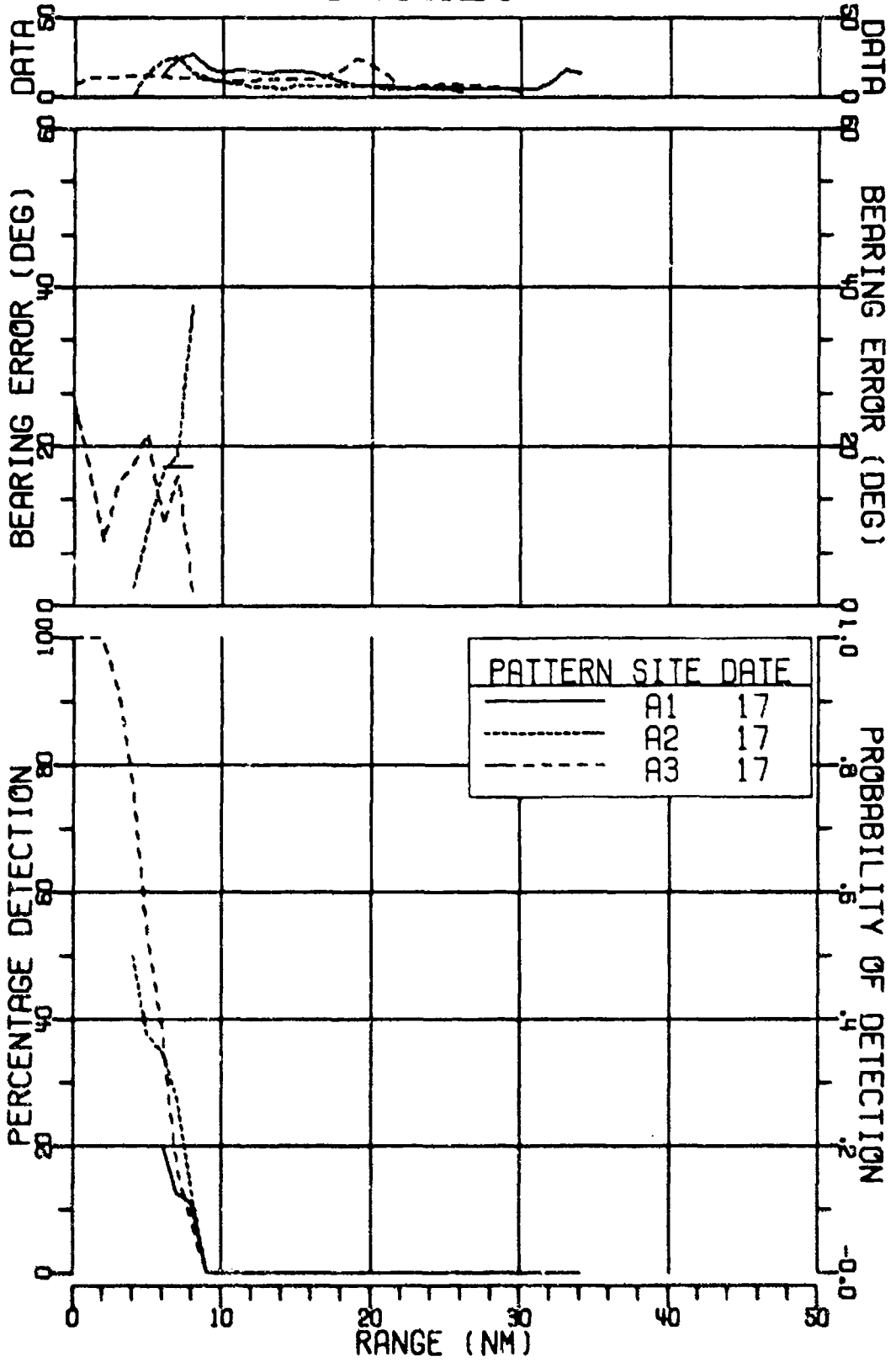

FIGURE II-190
MSS-FVT NEAR BOTTOM DIFFERENCED CARDIOIDS SENSOR
DETECTION RESULTS FOR 155HZ AT 134DB (U)

AS-77-3117

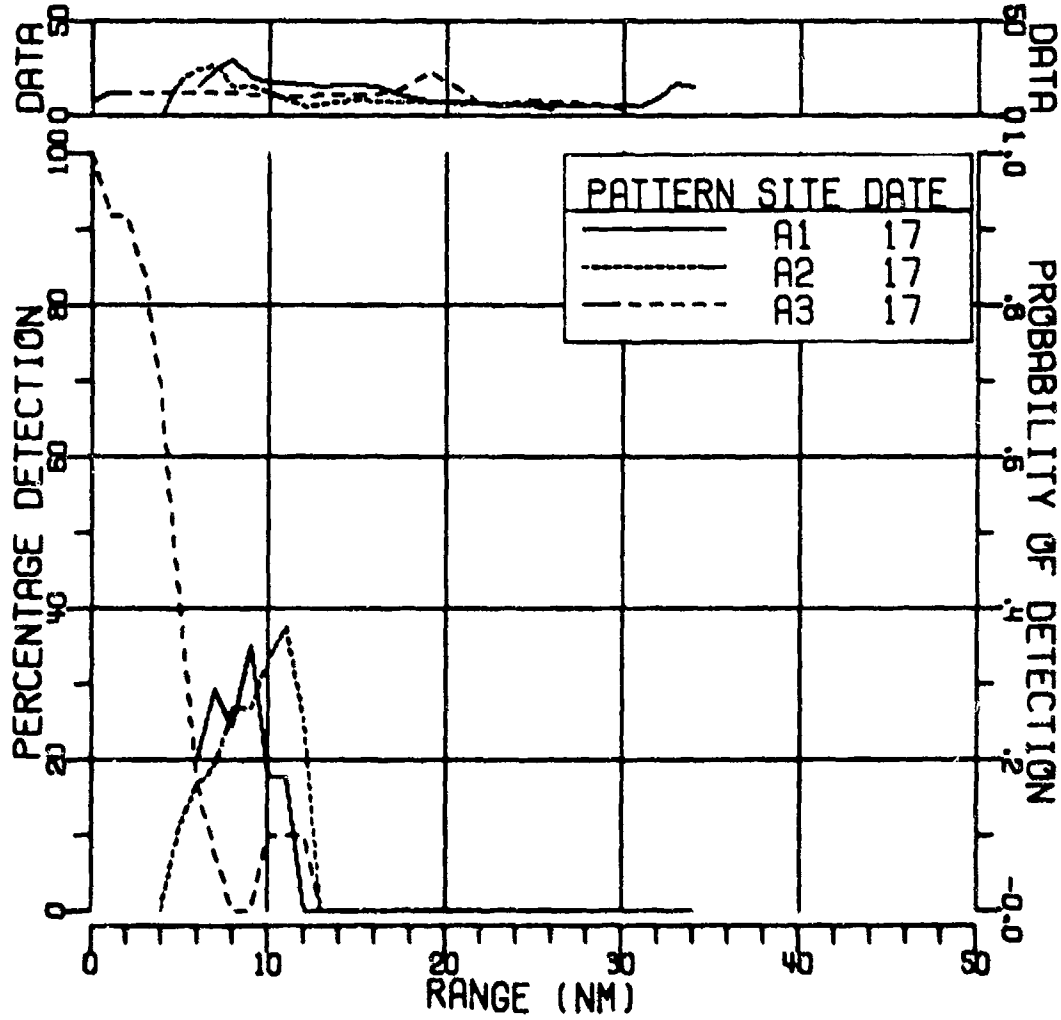

FIGURE II-191
MSS-FVT NEAR BOTTOM OMNIDIRECTIONAL SENSOR
DETECTION RESULTS FOR 305HZ AT 136DB (U)

AS-77-3118

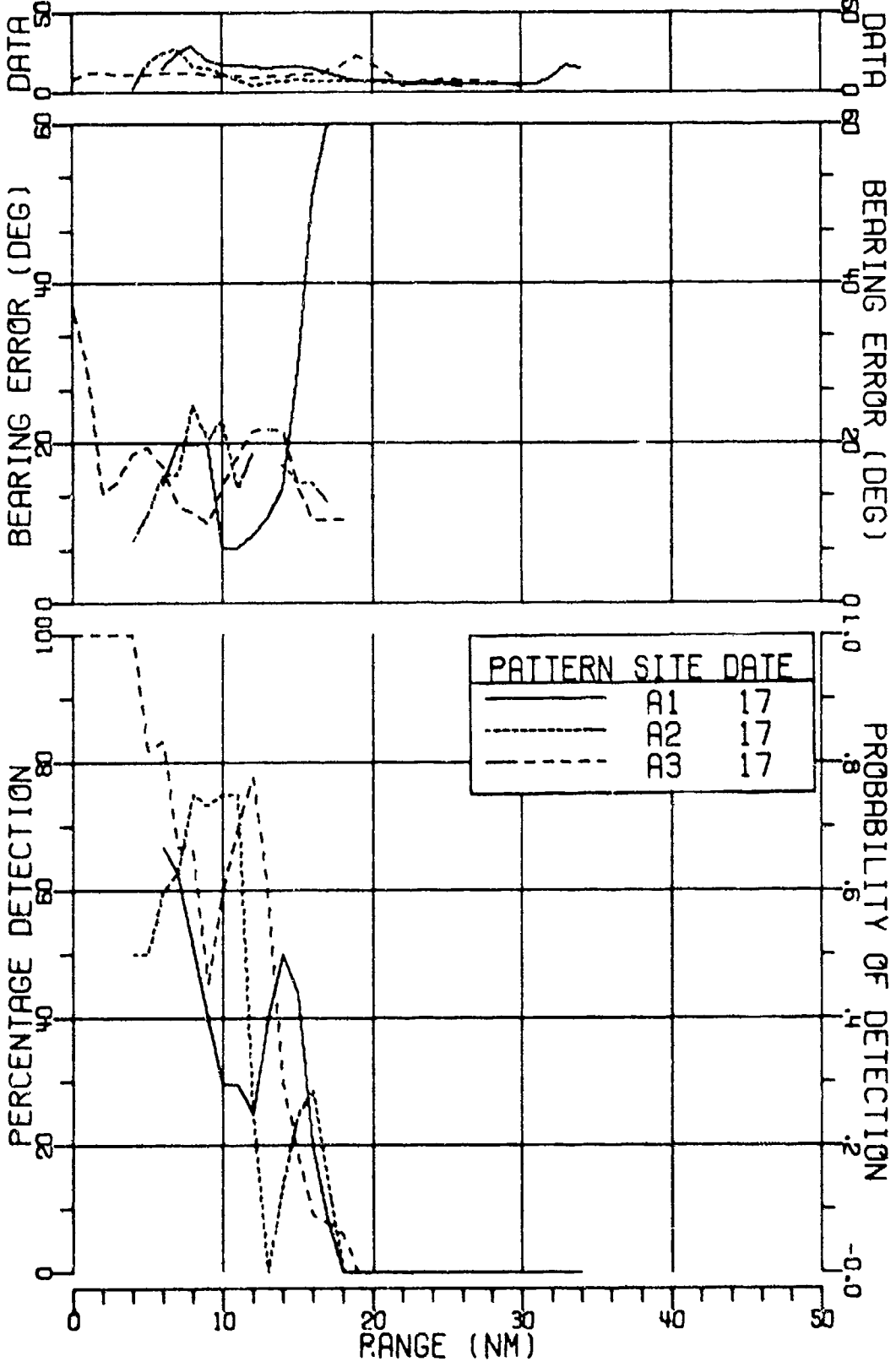

FIGURE II-192
MSS-FVT NEAR BOTTOM SINGLE CARDIOIDS SENSOR
DETECTION RESULTS FOR 305HZ AT 136DB (U)

AS-77-3119

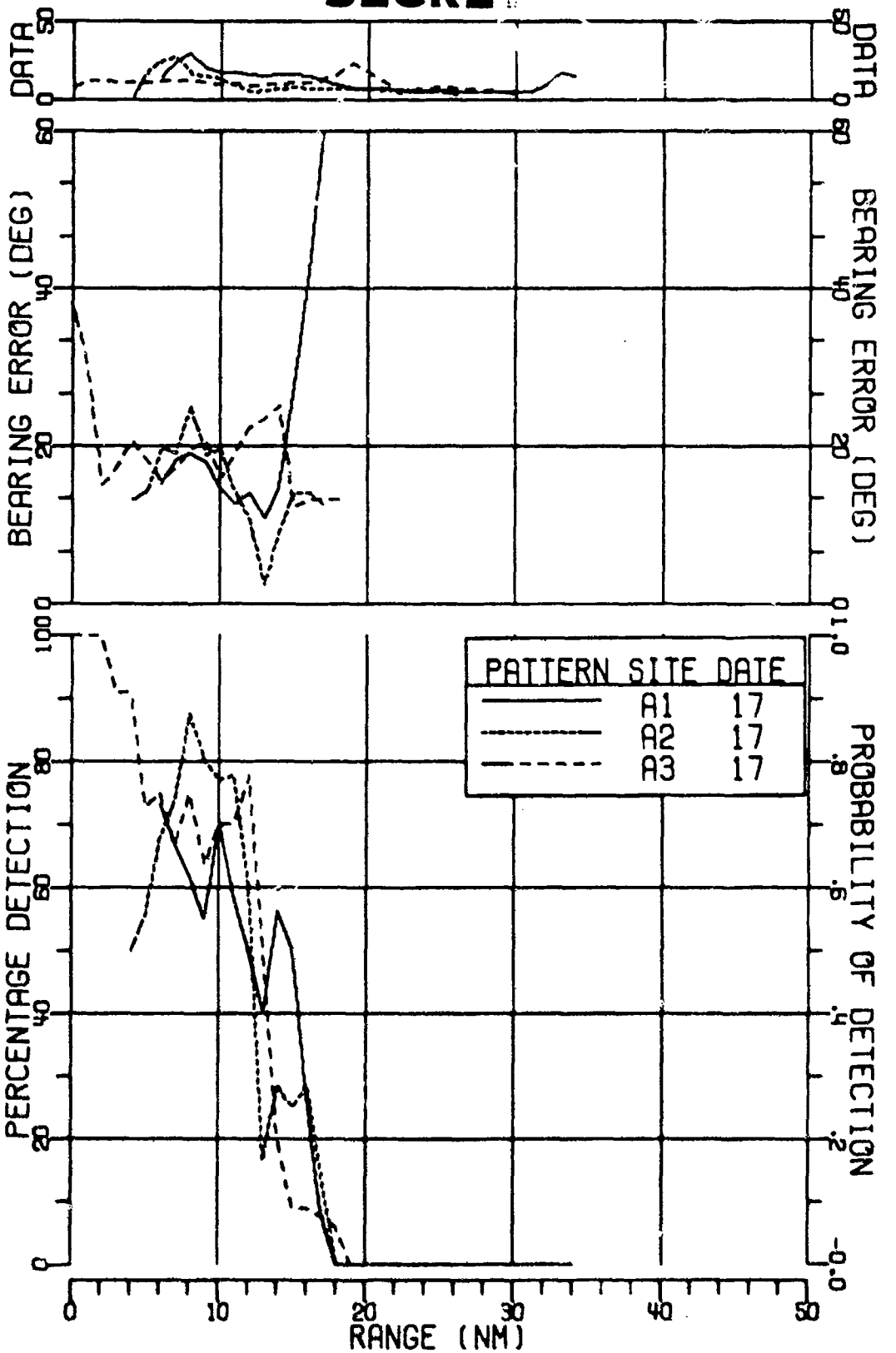

FIGURE II-193
MSS-FVT NEAR BOTTOM MAX GAIN LIMACONS SENSOR
DETECTION RESULTS FOR 305HZ AT 136DB (U)

AS-77-3120

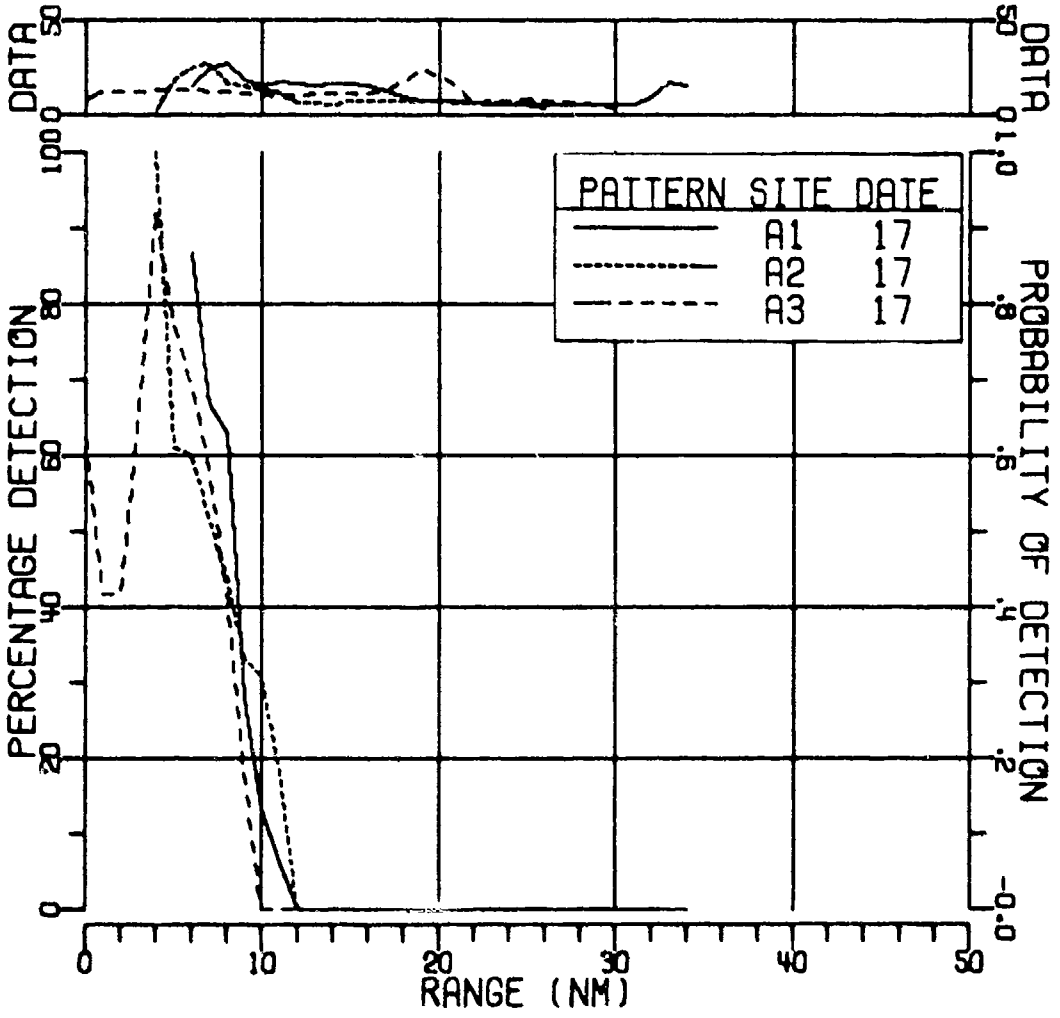

FIGURE II-194
MSS-FVT NEAR BOTTOM VERTICAL DIPOLE SENSOR
DETECTION RESULTS FOR 305HZ AT 136DB (U)

AS-77-3121

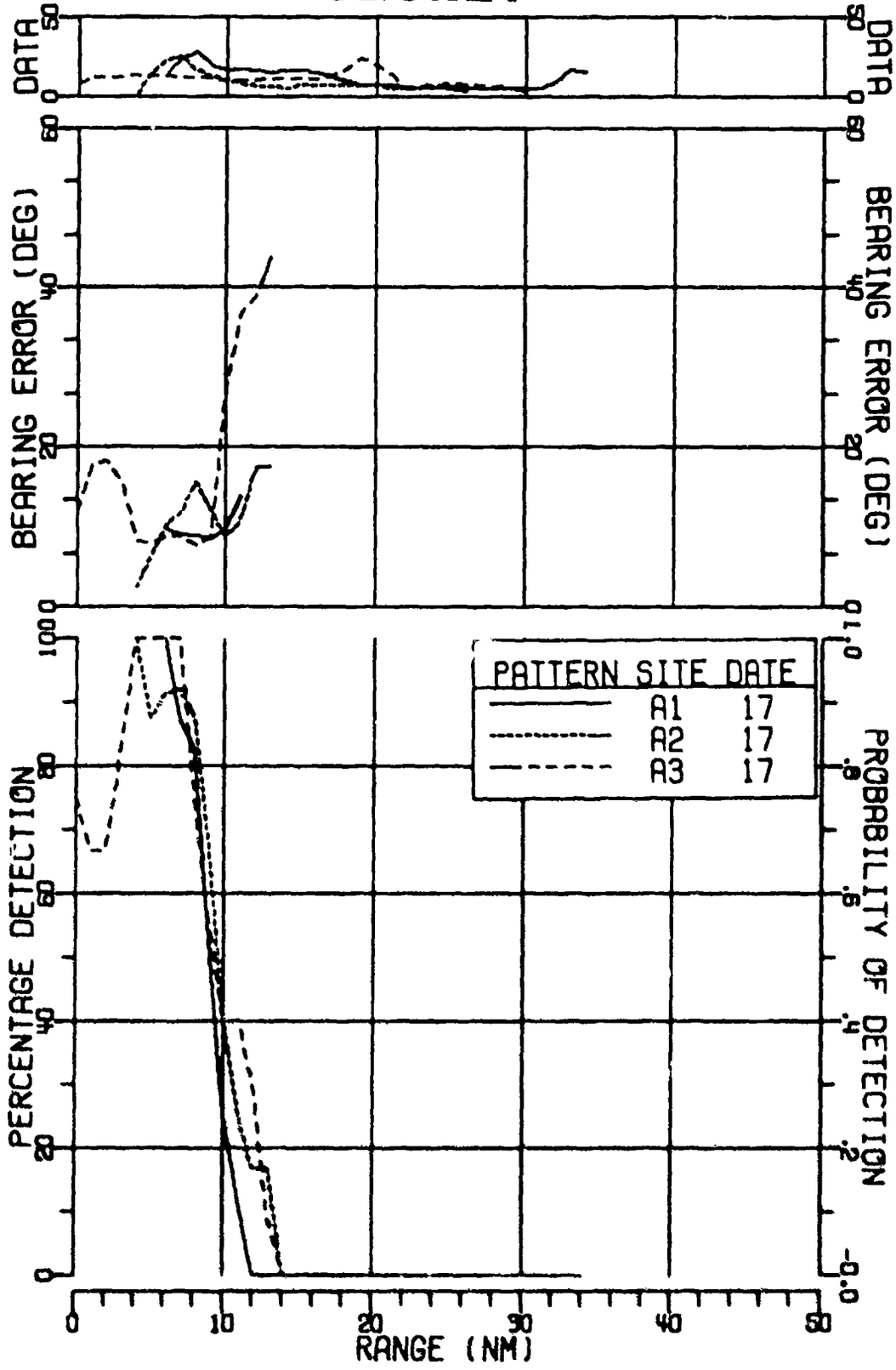

FIGURE II-195
MSS-FVT NEAR BOTTOM DIFFERENCED CARDIOIDS SENSOR
DETECTION RESULTS FOR 305HZ AT 136DB (U)

AS-77-3122

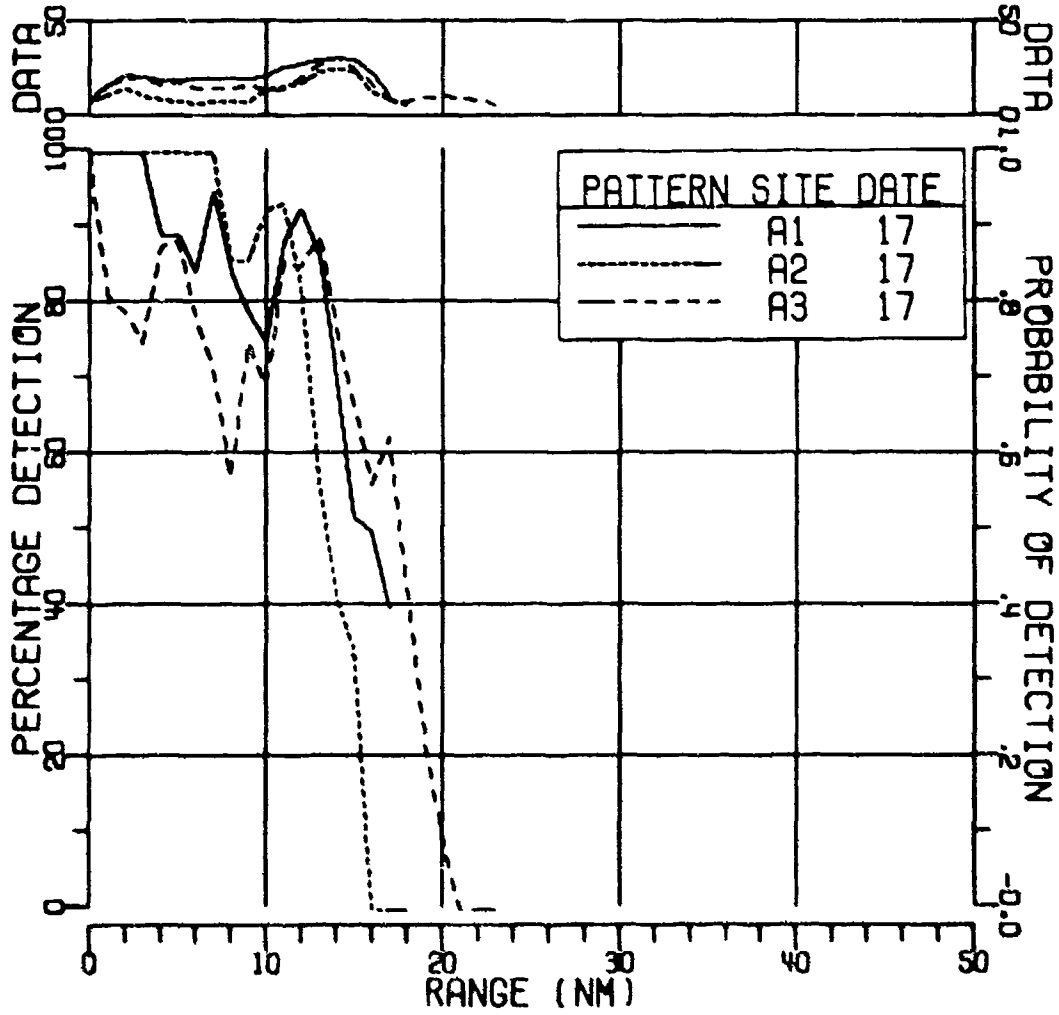

FIGURE II-196
MSS-FVT NEAR BOTTOM OMNIDIRECTIONAL SENSOR
DETECTION RESULTS FOR 64HZ AT 162DB (U)

AS-77-3123

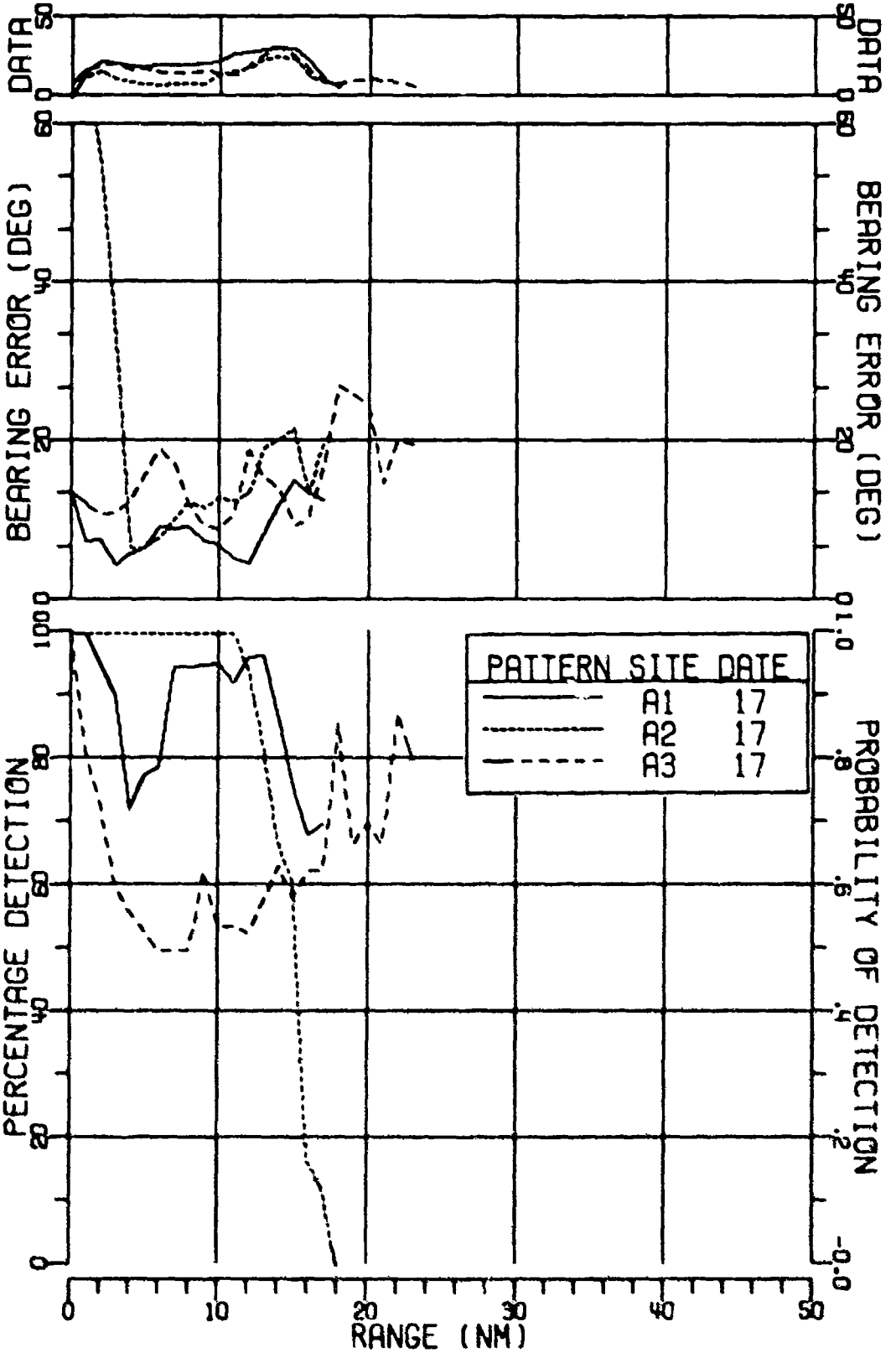

FIGURE II-197
MSS-FVT NEAR BOTTOM SINGLE CARDIOIDS SENSOR
DETECTION RESULTS FOR 64HZ AT 162DB (U)

AS-77-3124

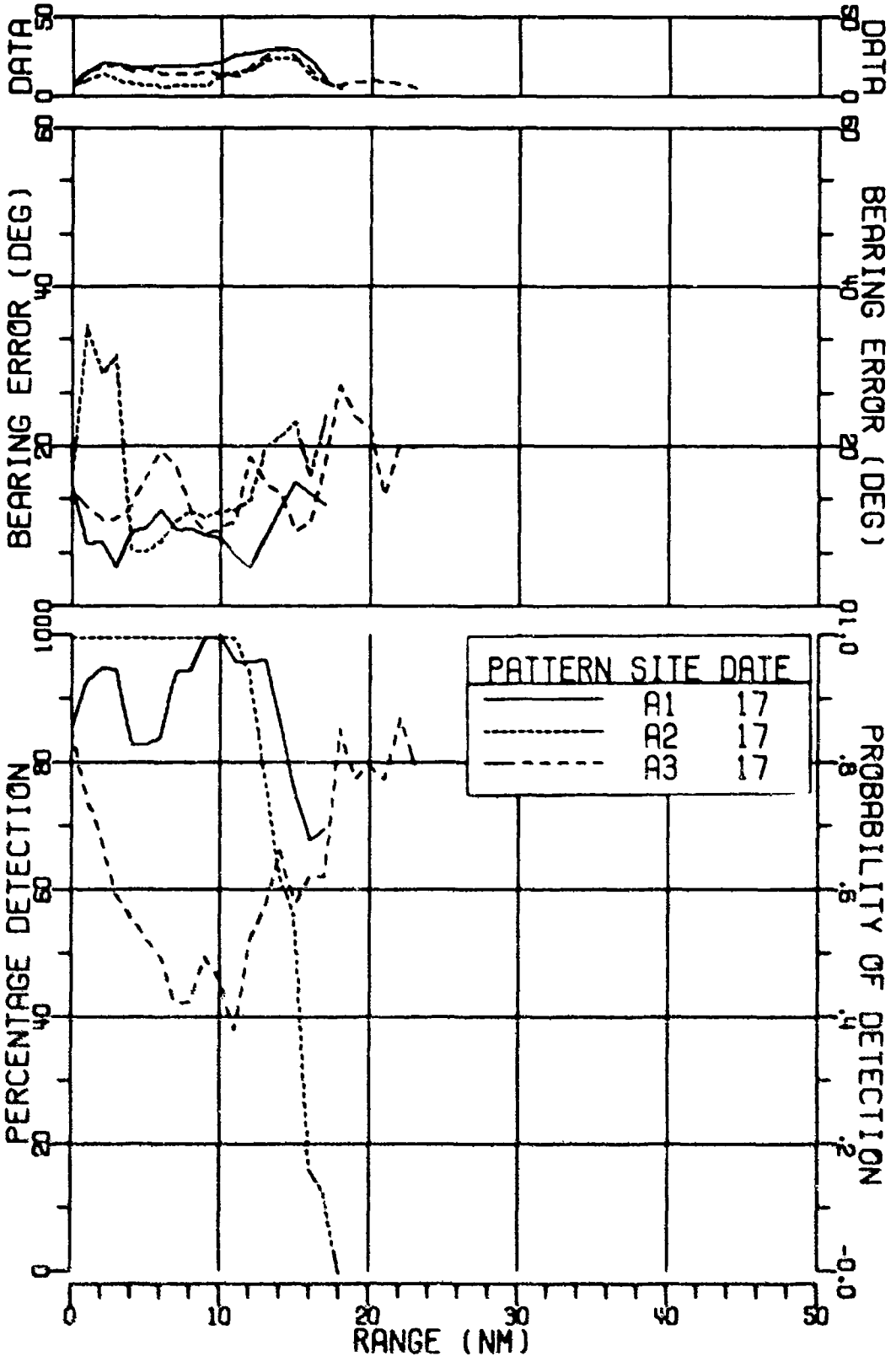

FIGURE II-198
MSS-FVT NEAR BOTTOM MAX GAIN LIMACONS SENSOR
DETECTION RESULTS FOR 64HZ AT 162DB (U)

AS-77-3125

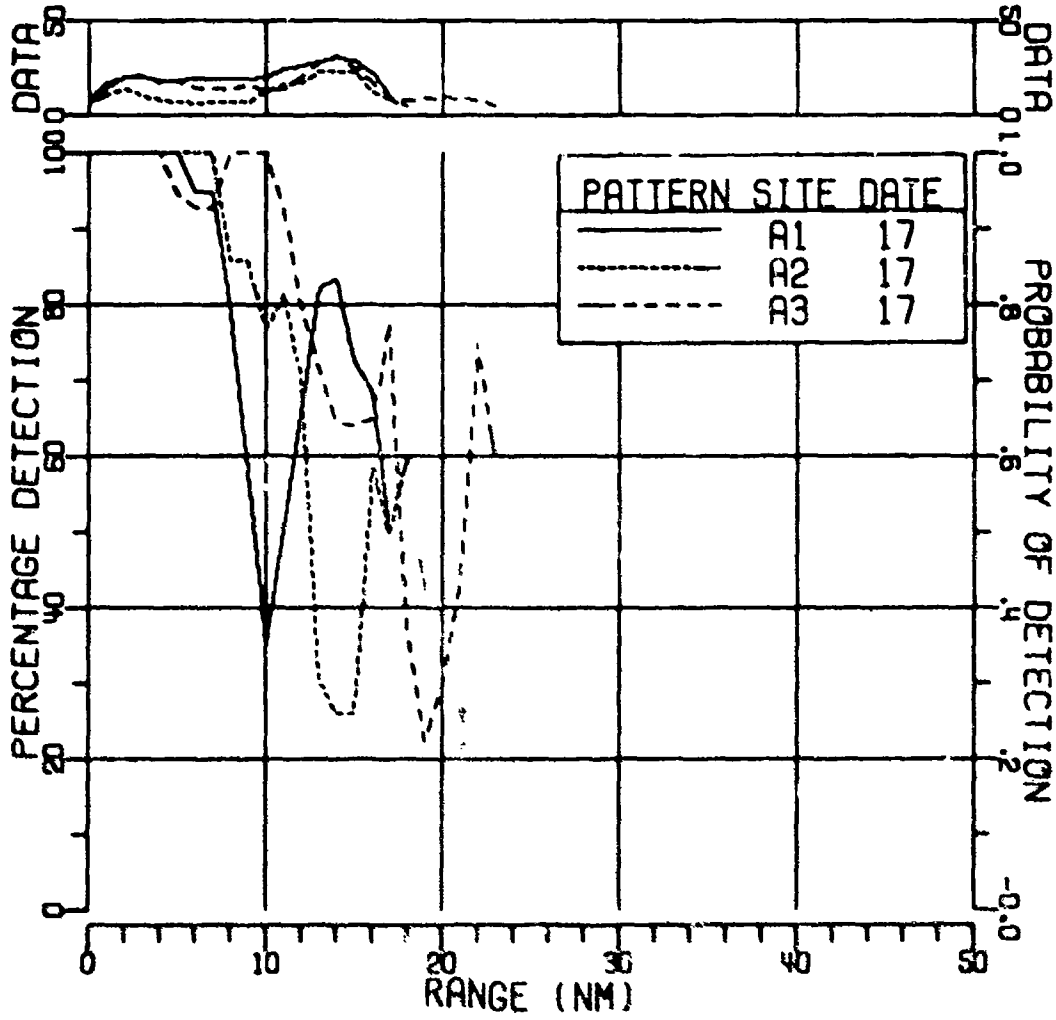

FIGURE II-199
MSS-FVT NEAR BOTTOM VERTICAL DIPOLE SENSOR
DETECTION RESULTS FOR 64HZ AT 162DB (U)

AS-77-3126

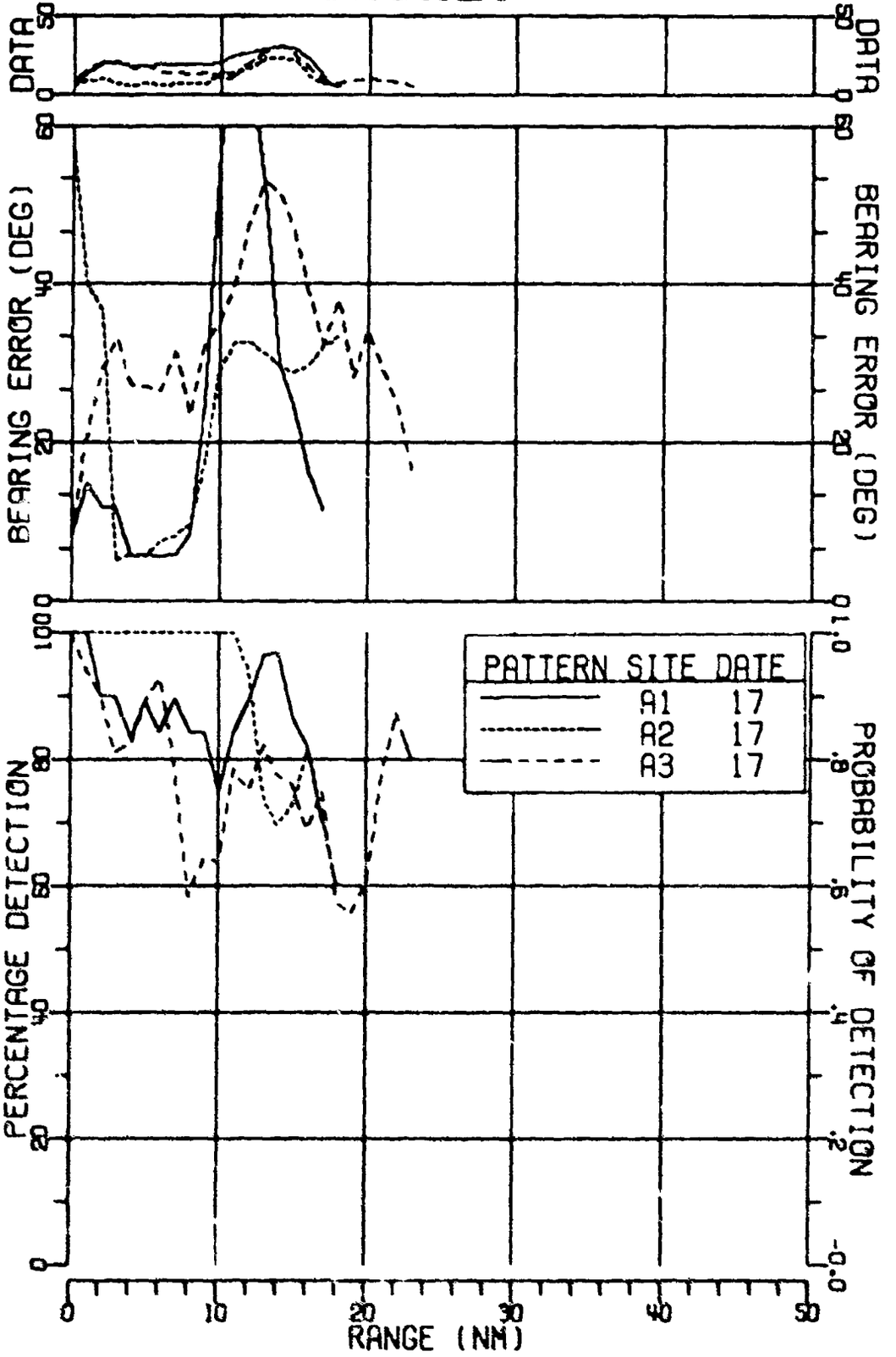

FIGURE II-200
MSS-FVT NEAR BOTTOM DIFFERENCED CARDIOIDS SENSOR
DETECTION RESULTS FOR 64HZ AT 162DB (U)

AS-77-3127

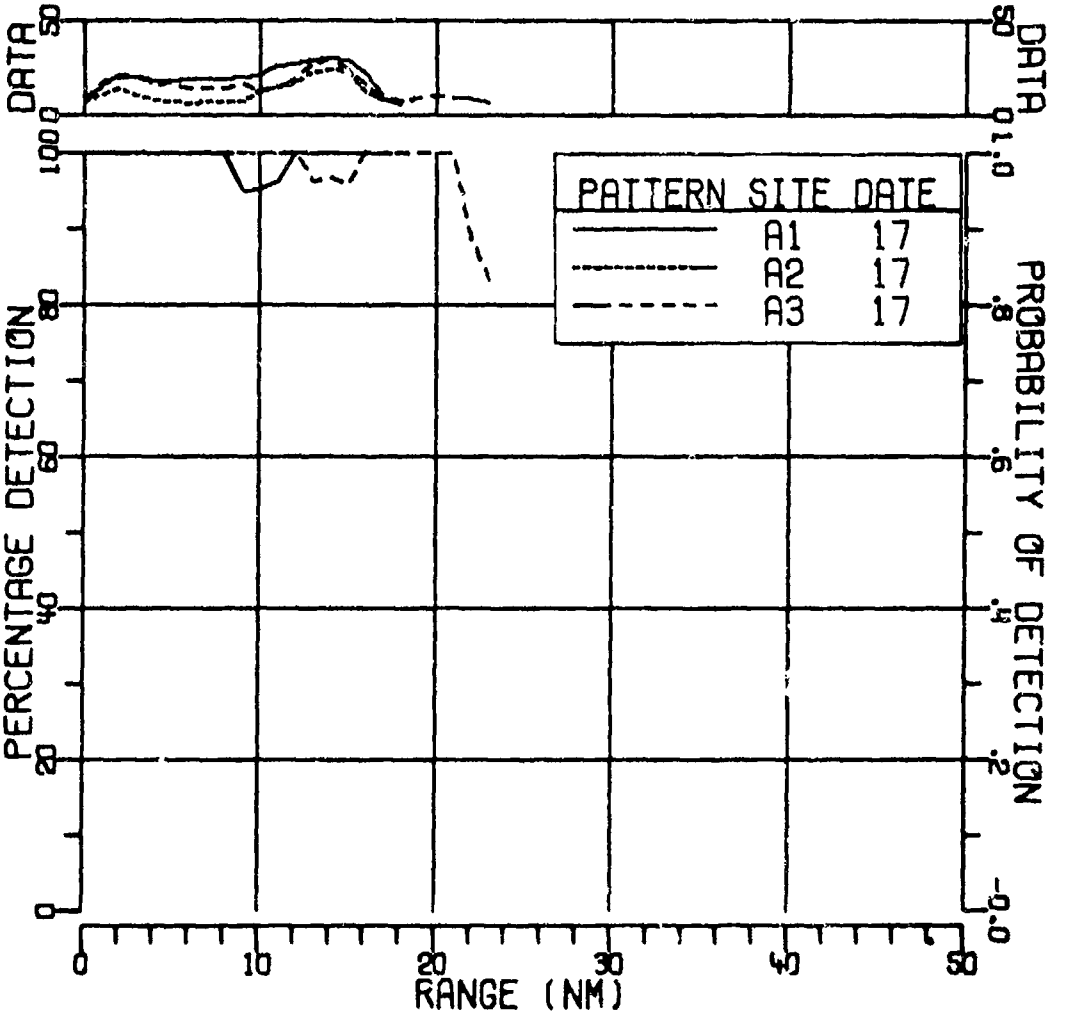

FIGURE II-201
MSS-FVT NEAR BOTTOM OMNIDIRECTIONAL SENSOR
DETECTION RESULTS FOR 160HZ AT 161DB (U)

AS-77-3128

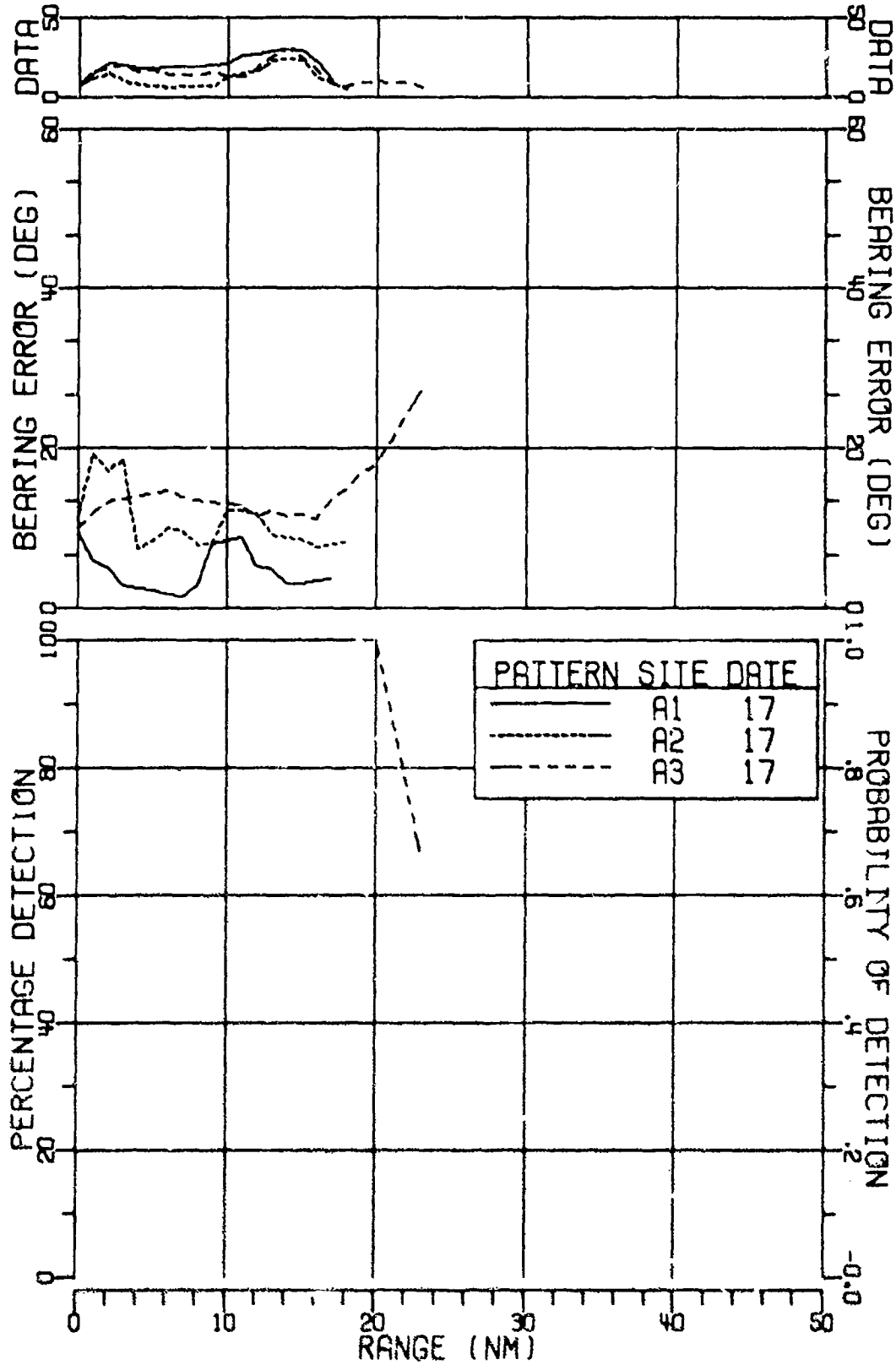

FIGURE II-202
MSS-FVT NEAR BOTTOM SINGLE CARDIOIDS SENSOR
DETECTION RESULTS FOR 160HZ AT 161DB (U)

AS-77-3129

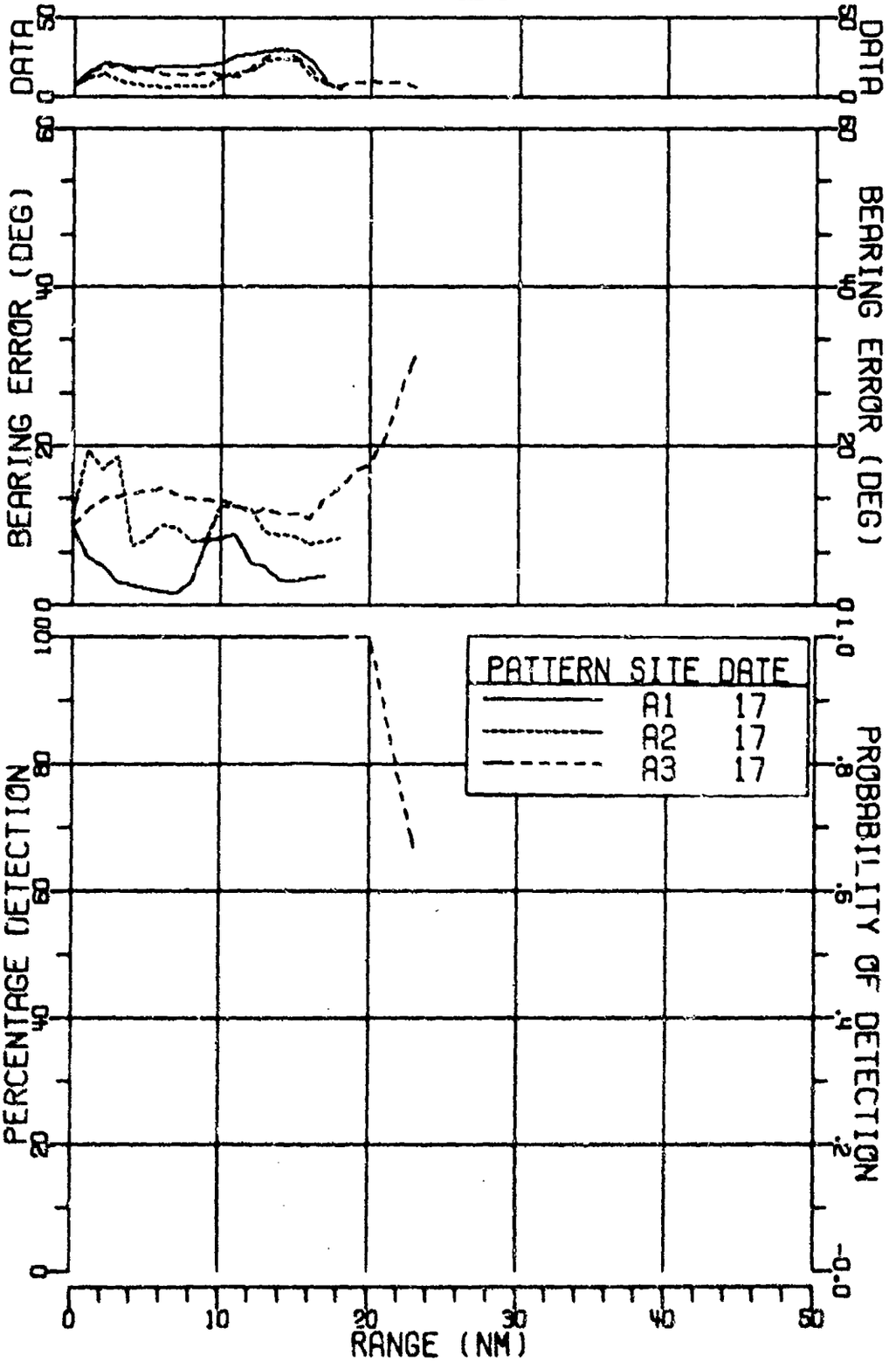

FIGURE II-203
MSS-FVT NEAR BOTTOM MAX GAIN LIMACONS SENSOR
DETECTION RESULTS FOR 160HZ AT 161DB (U)

AS-77-3130

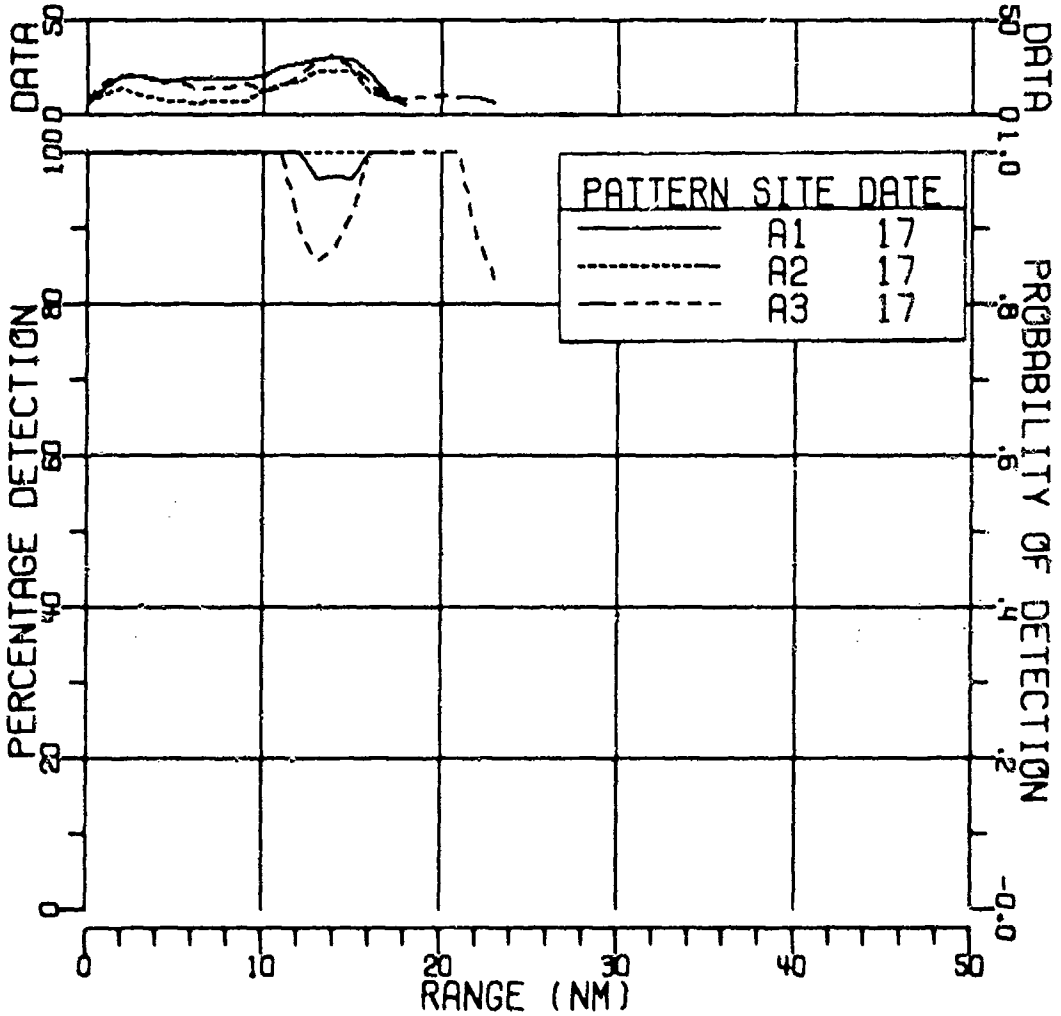

FIGURE II-204
MSS-FVT NEAR BOTTOM VERTICAL DIPOLE SENSOR
DETECTION RESULTS FOR 160HZ AT 161DB (U)

AS-77-3131

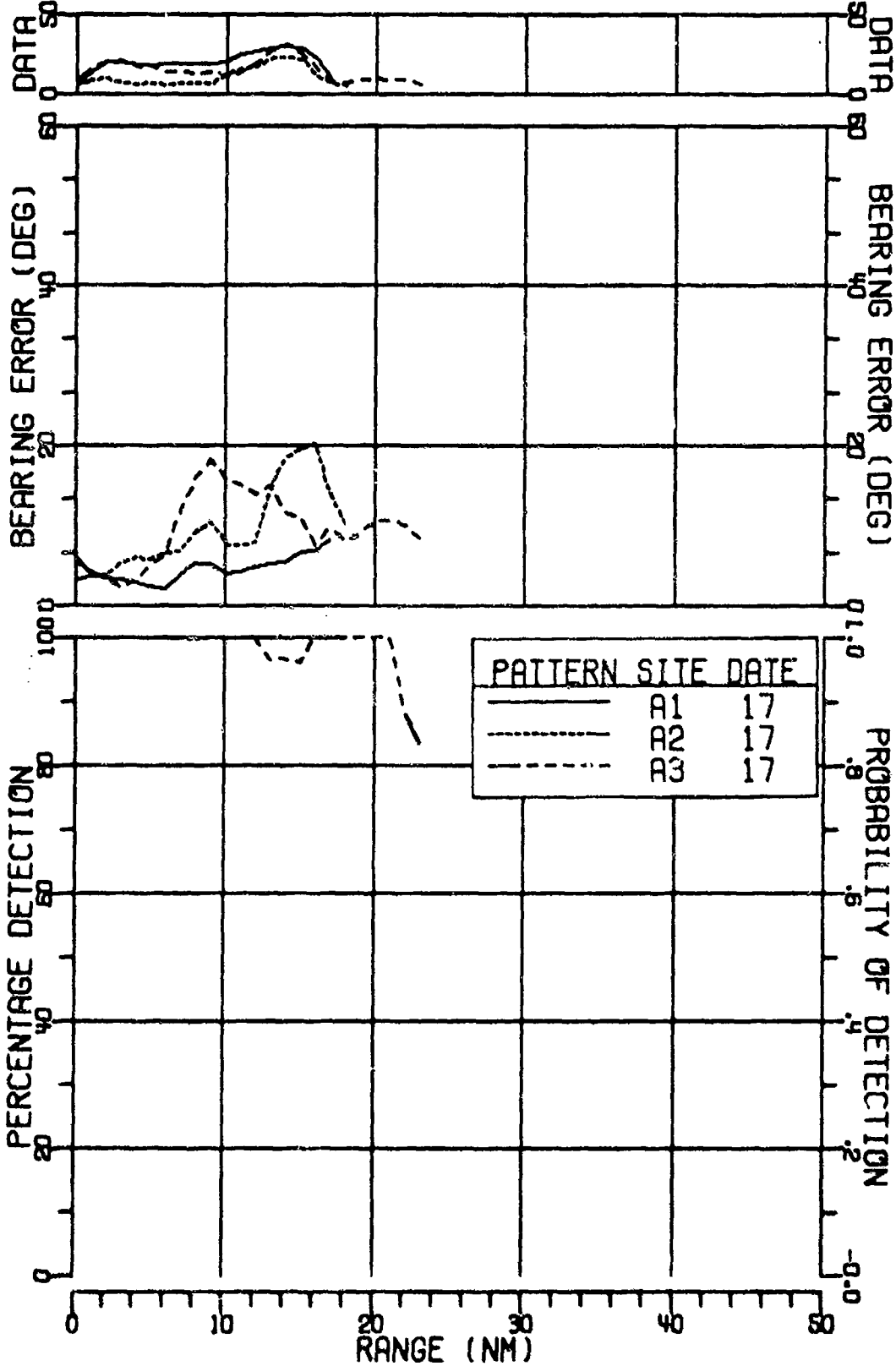

FIGURE II-205
MSS-FVT NEAR BOTTOM DIFFERENCED CARDIOIDS SENSOR DETECTION RESULTS FOR 160HZ AT 161DB (U)

AS-77-3132

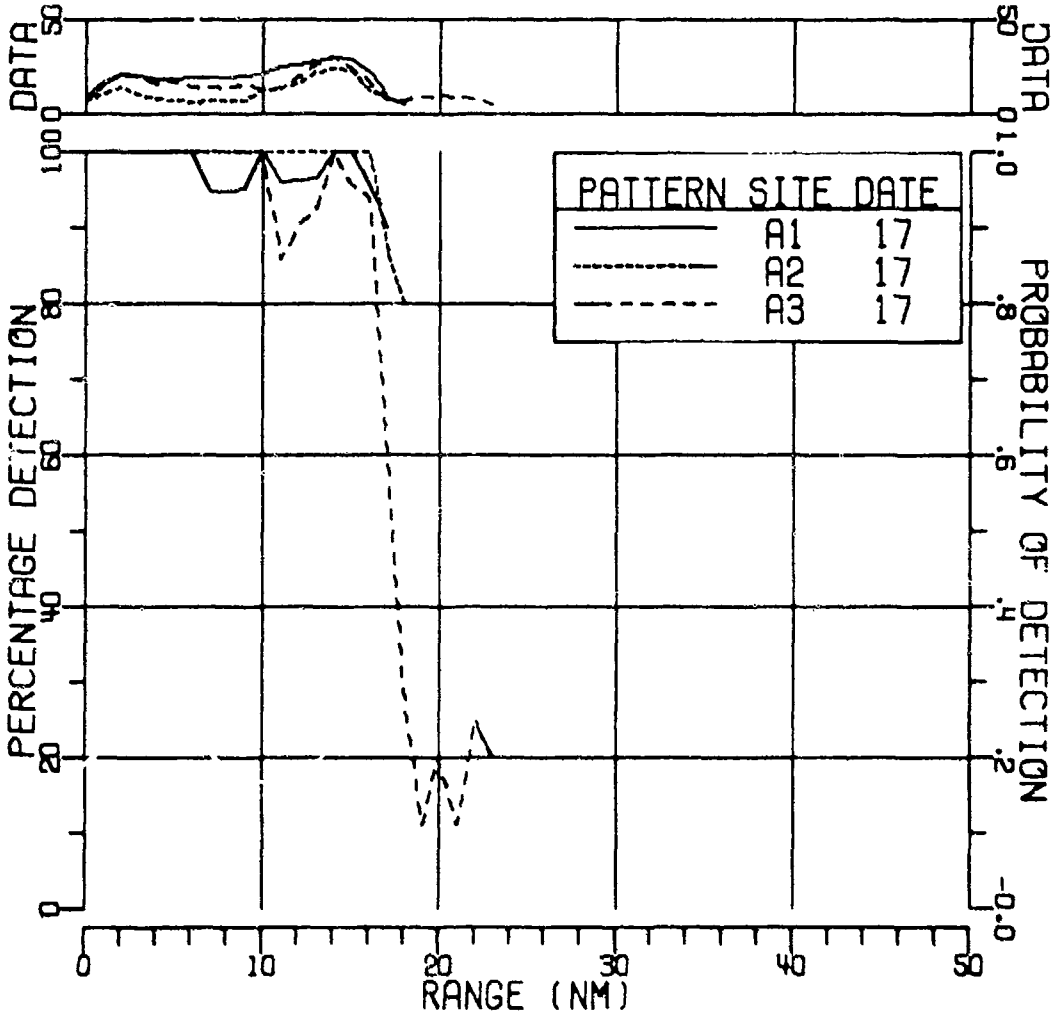

FIGURE II-206
MSS-FVT NEAR BOTTOM OMNIDIRECTIONAL SENSOR
DETECTION RESULTS FOR 260HZ AT 147DB (U)

AS-77-3133

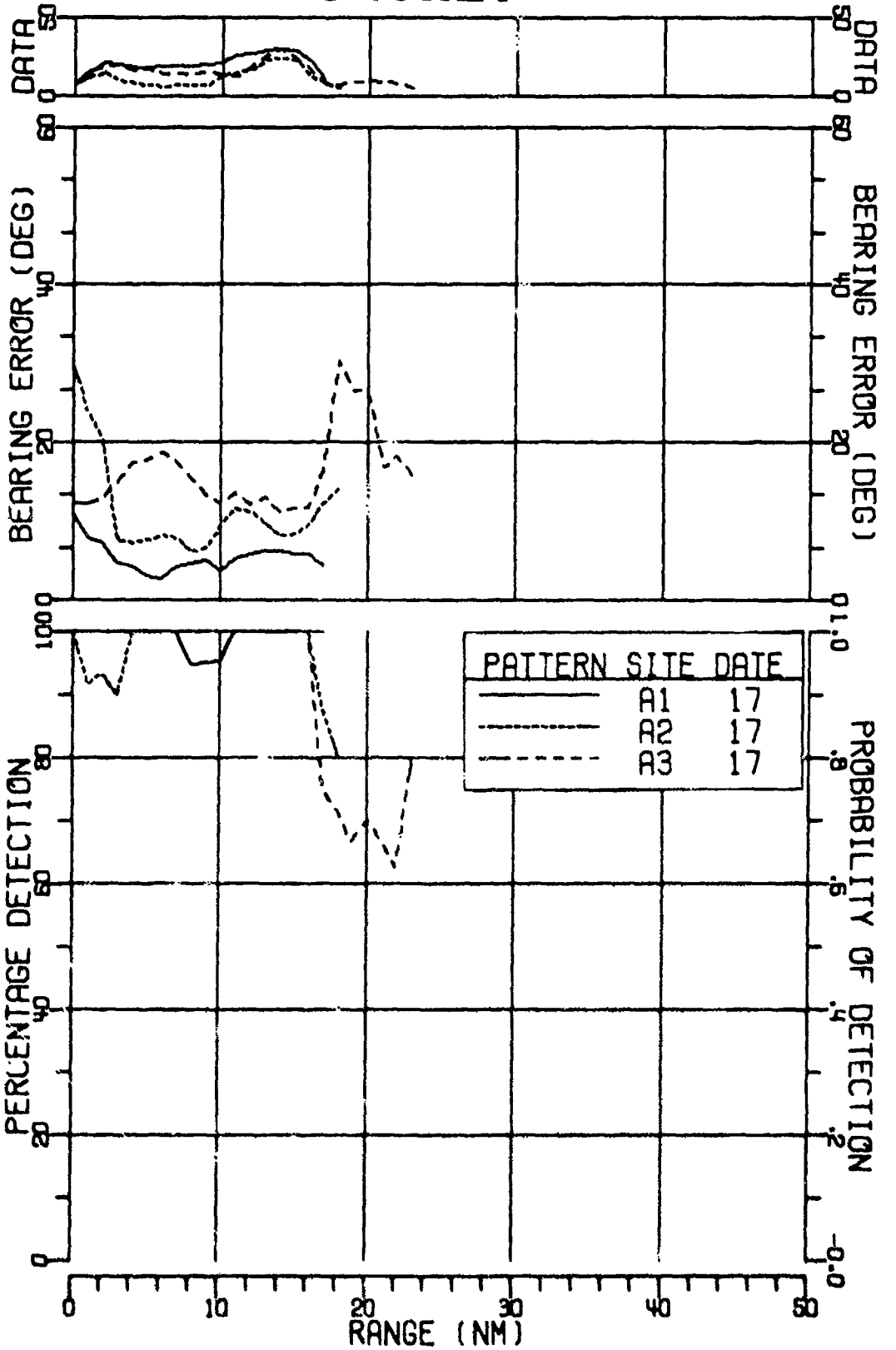

FIGURE II-207
MSS-FVT NEAR BOTTOM SINGLE CARDIOIDS SENSOR
DETECTION RESULTS FOR 260HZ AT 147DB (U)

AS-77-3134

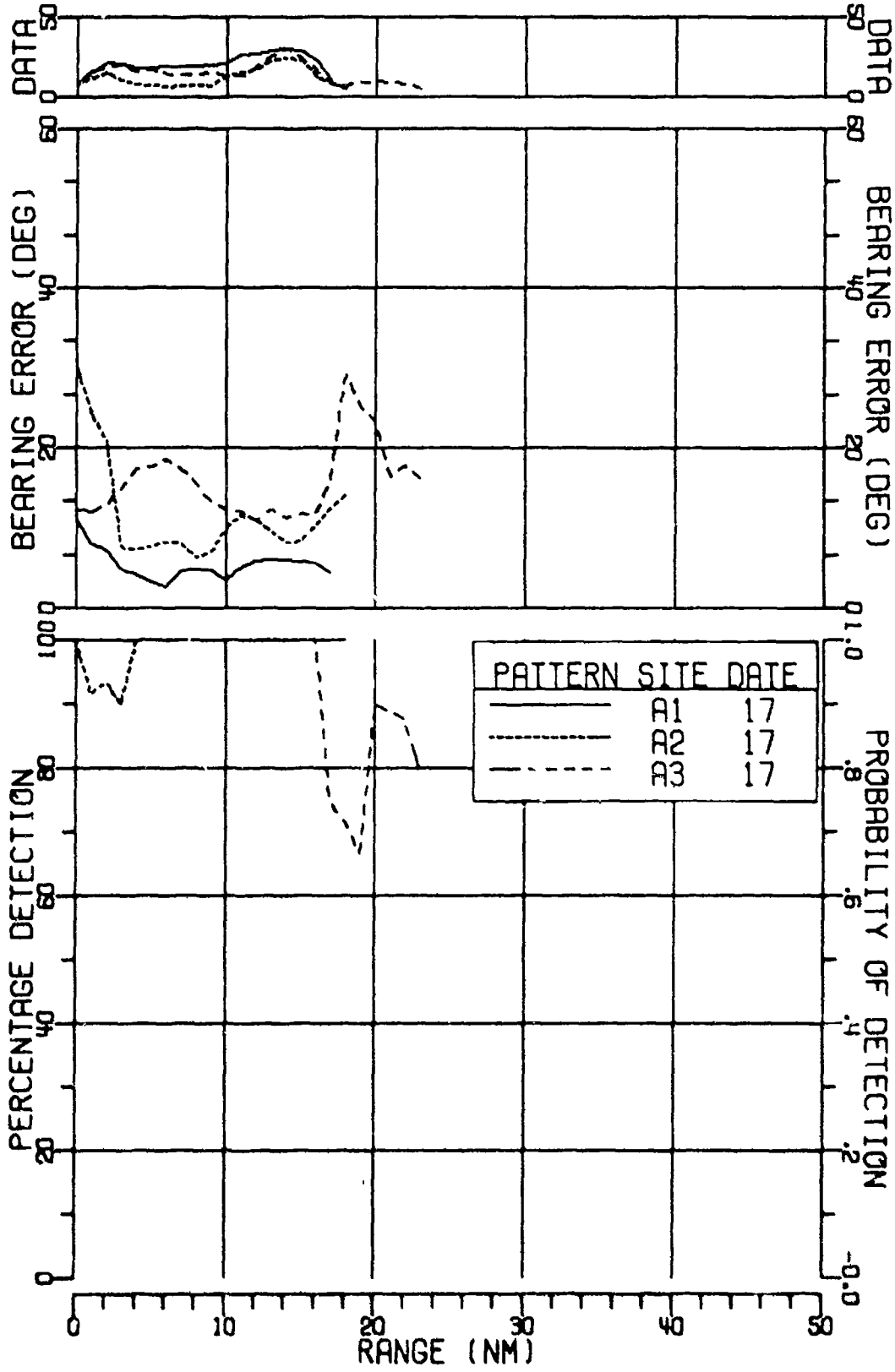

FIGURE II-208
MSS-FVT NEAR BOTTOM MAX GAIN LIMACONS SENSOR
DETECTION RESULTS FOR 260HZ AT 147DB (U)

AS-77-3135

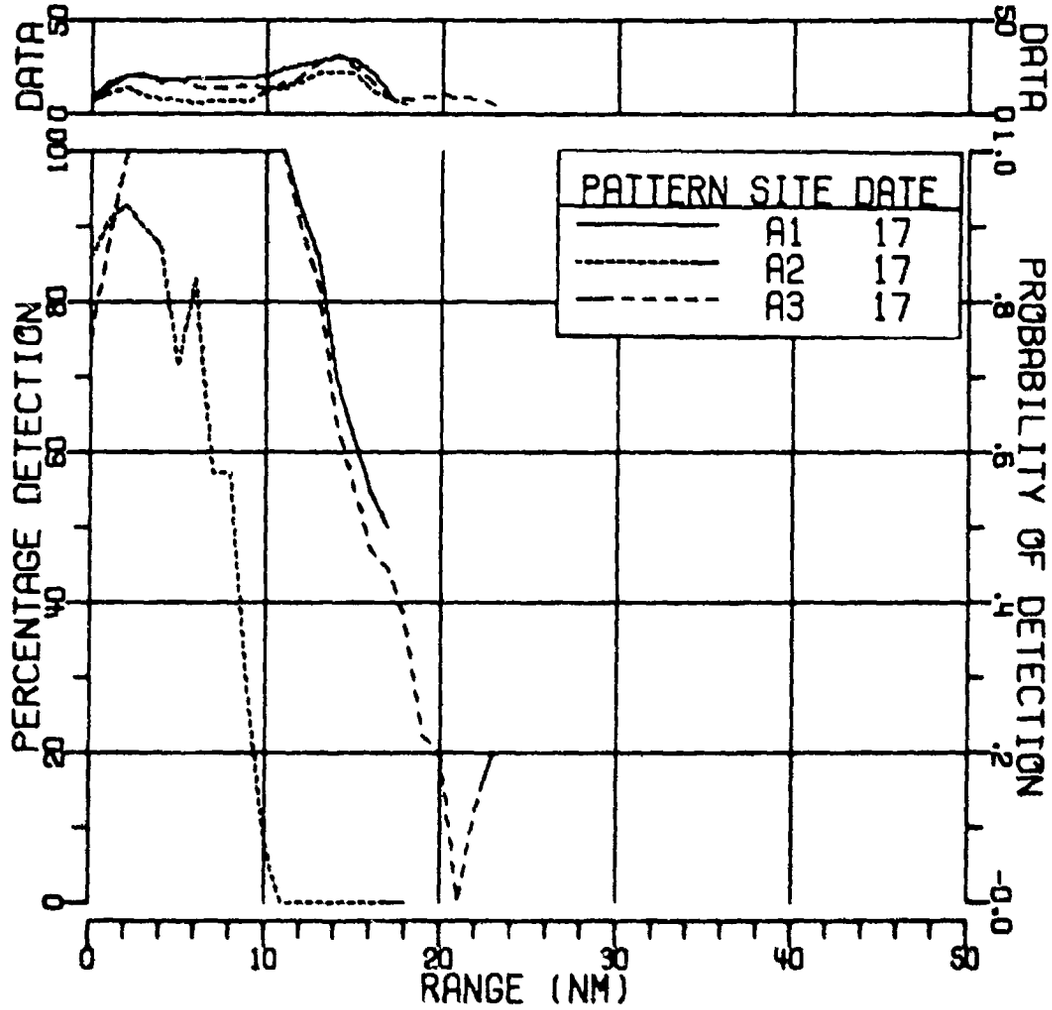

FIGURE II-209
MSS-FVT NEAR BOTTOM VERTICAL DIPOLE SENSOR
DETECTION RESULTS FOR 260HZ AT 147DB (U)

AS-77-3136

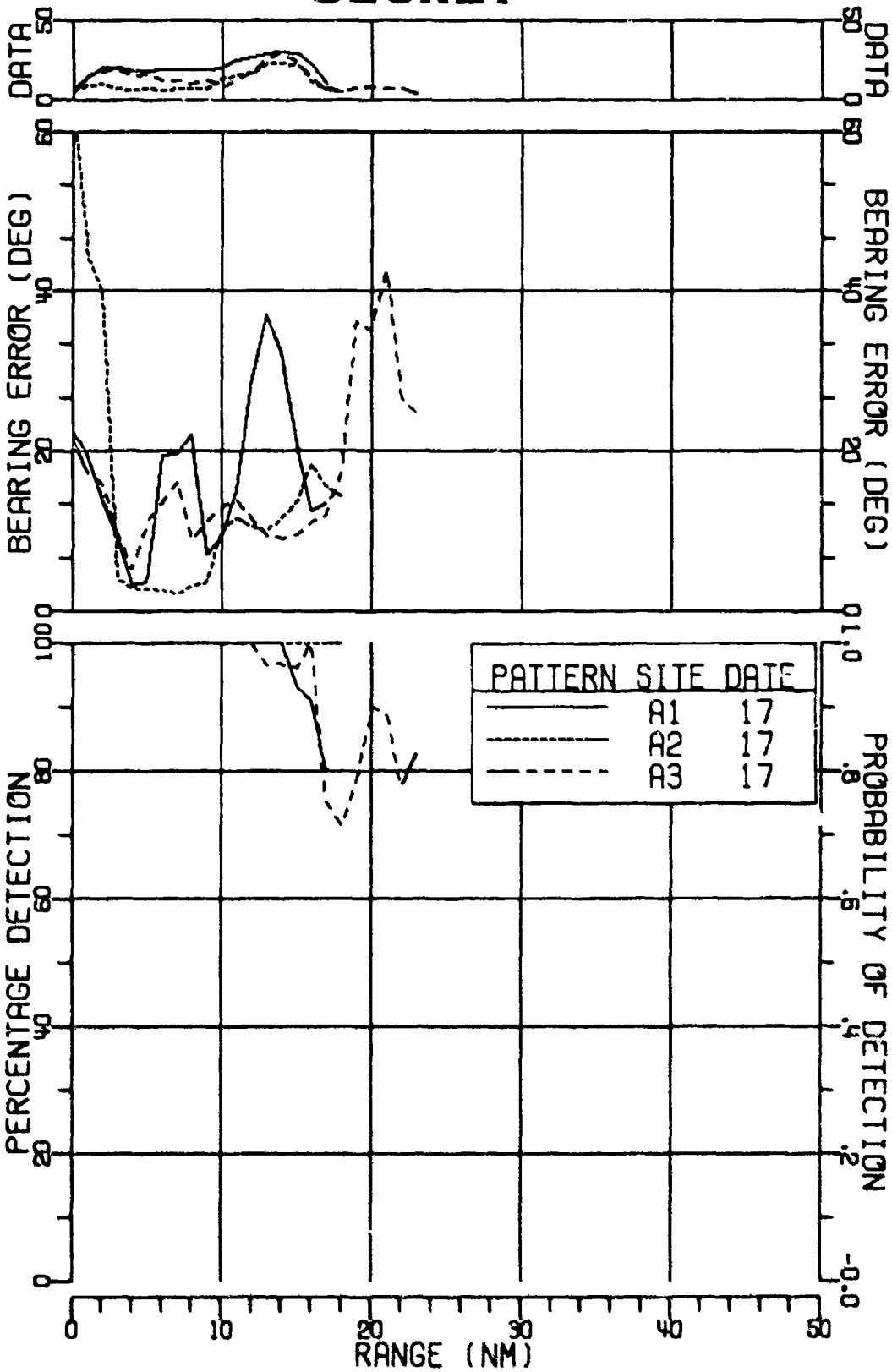

FIGURE II-210
MSS-FVT NEAR BOTTOM DIFFERENCED CARDIOIDS SENSOR
DETECTION RESULTS FOR 260HZ AT 147DB (U)

AS-77-3137

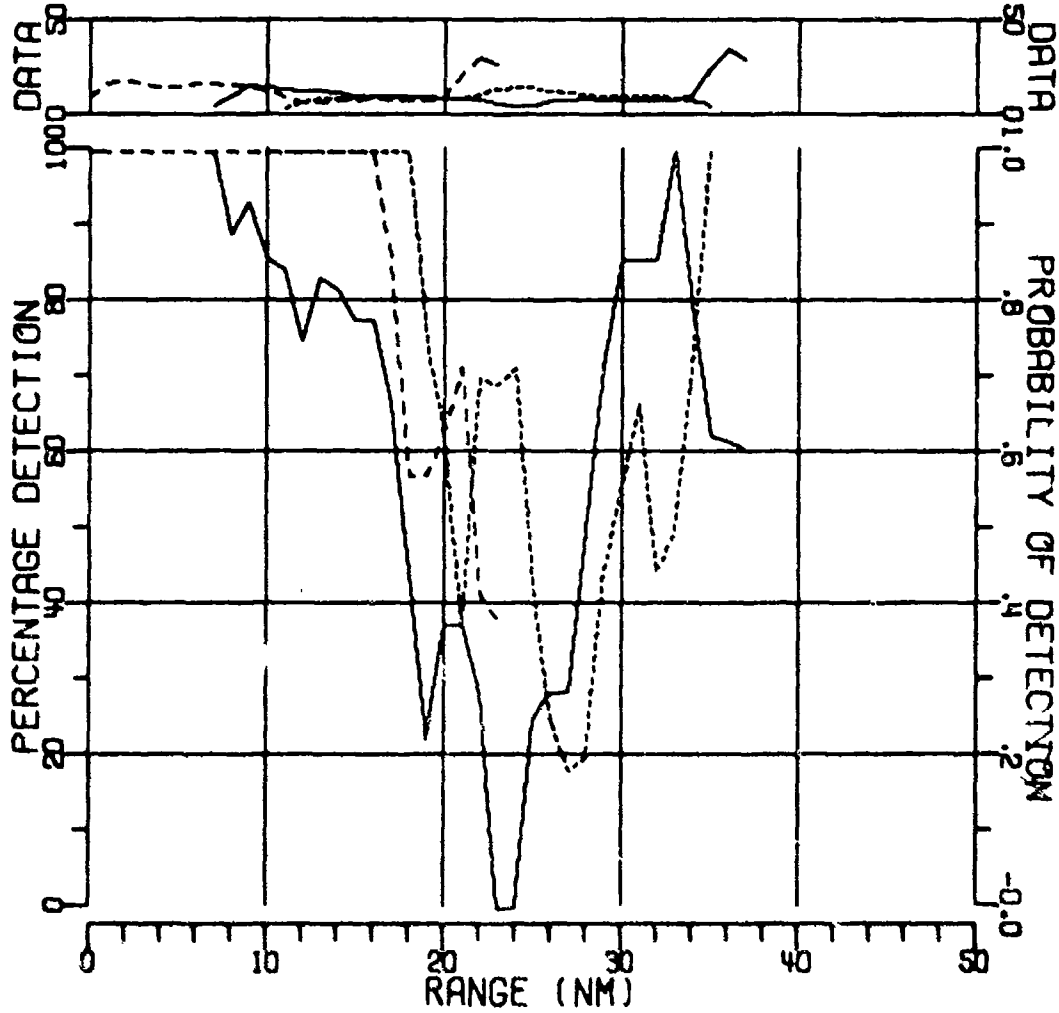

FIGURE II-211
MSS-FVT NEAR BOTTOM OMNIDIRECTIONAL SENSOR
DETECTION RESULTS FOR 70HZ AT 166DB (U)

PATTERN	SITE	DATE
———	A1	17
.....	A2	17
- - - - -	A3	17

AS-77-3138

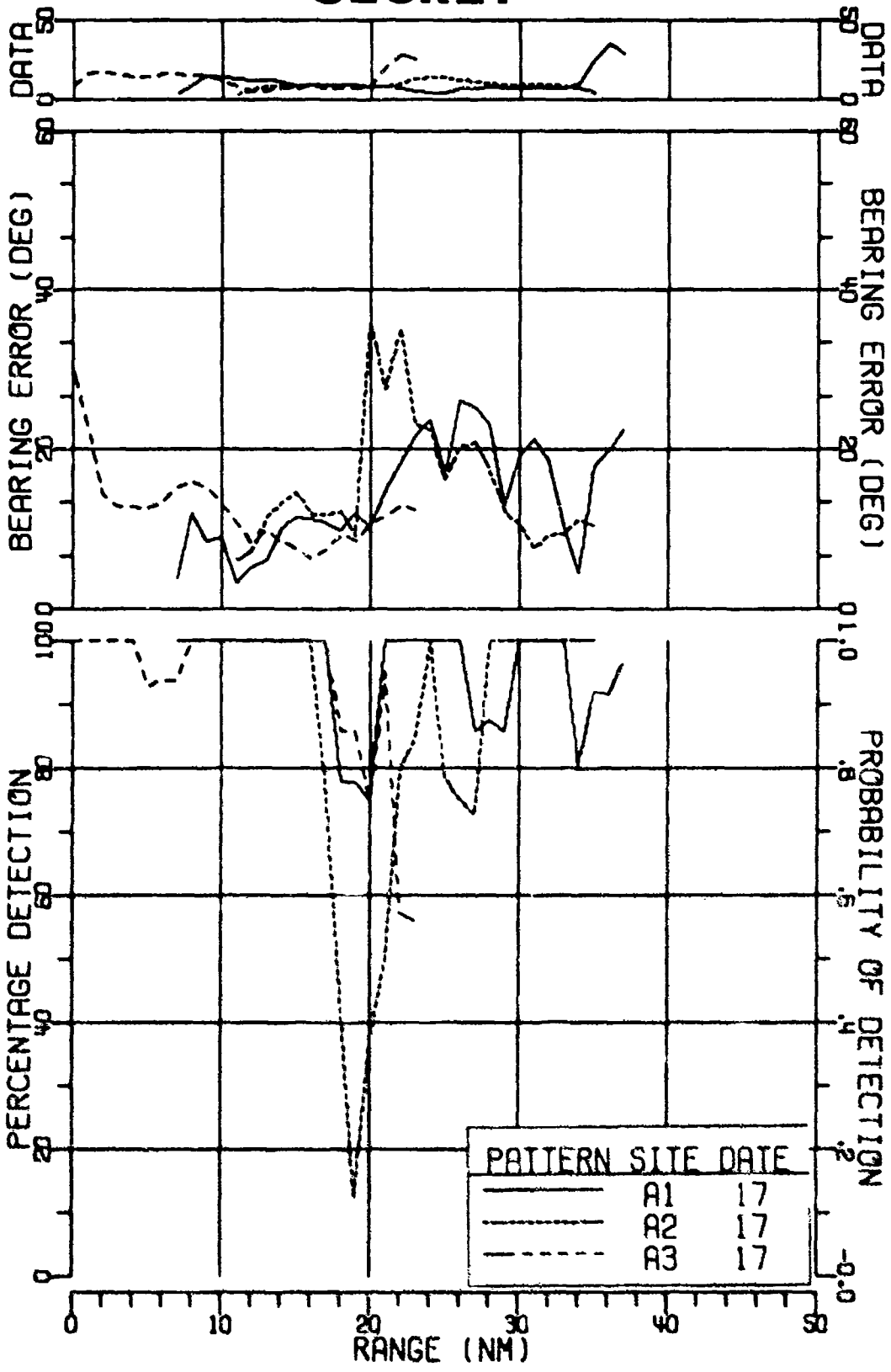

FIGURE II-212
MSS-FVT NEAR BOTTOM SINGLE CARDIOIDS SENSOR
DETECTION RESULTS FOR 70HZ AT 166DB (U)

AS-77-3139

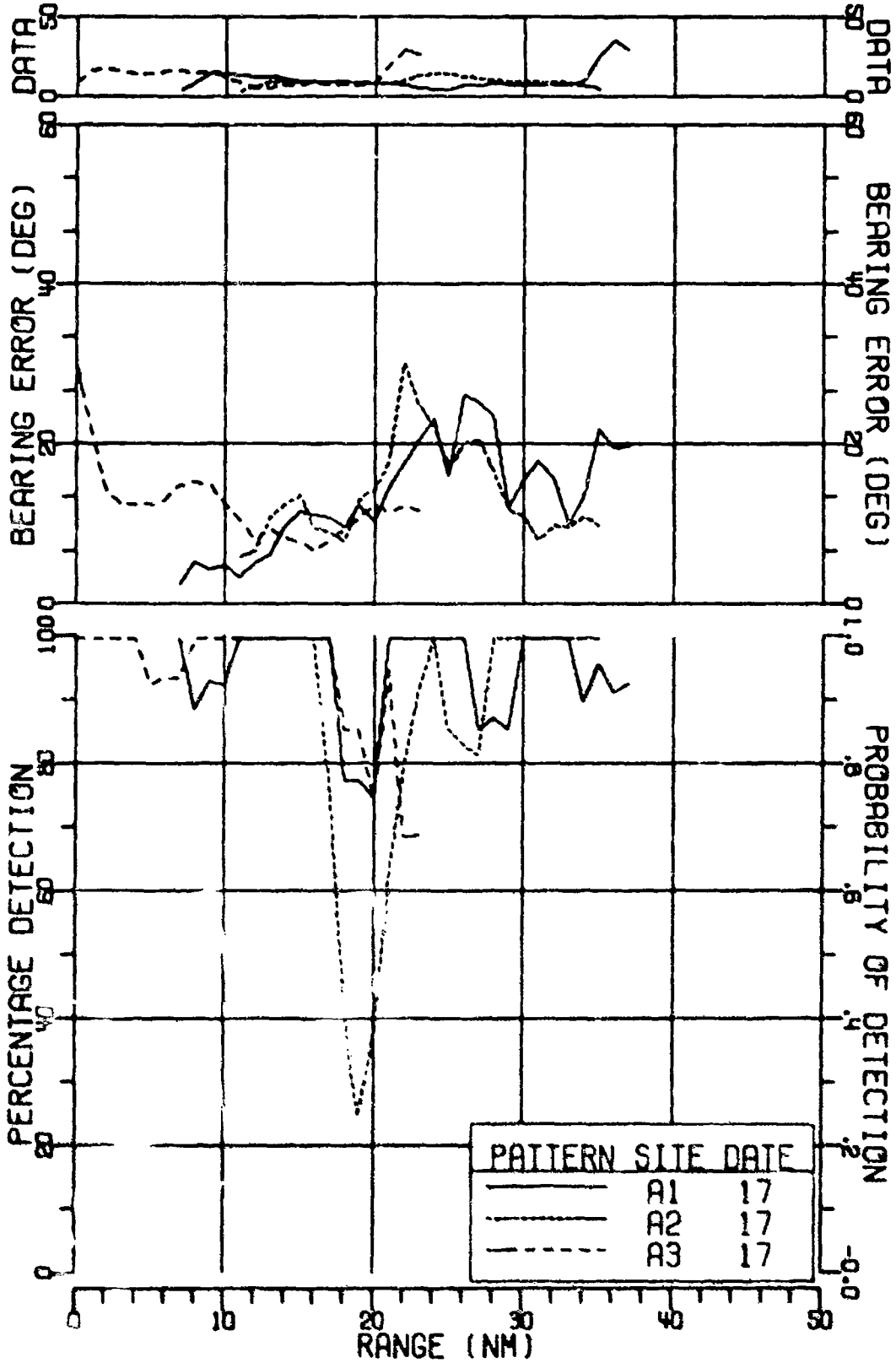

FIGURE II-213
MSS-FVT NEAR BOTTOM MAX GAIN LIMACONS SENSOR
DETECTION RESULTS FOR 70HZ AT 166DB (U)

AS-77-3140

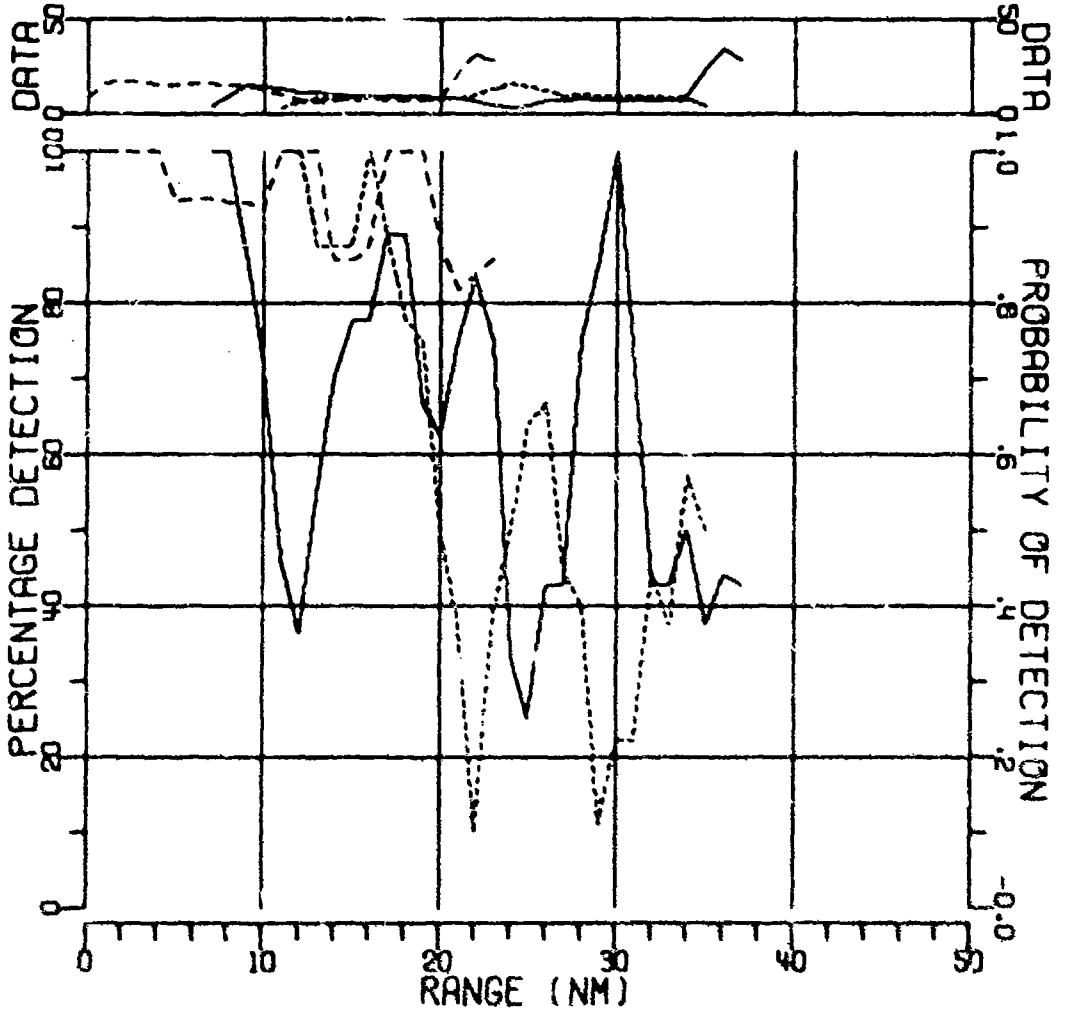

FIGURE II-214
MSS-FVT NEAR BOTTOM VERTICAL DIPOLE SENSOR
DETECTION RESULTS FOR 70HZ AT 166DB (U)

PATTERN	SITE	DATE
———	A1	17
.....	A2	17
- - - - - -	A3	17

AS-77-3141

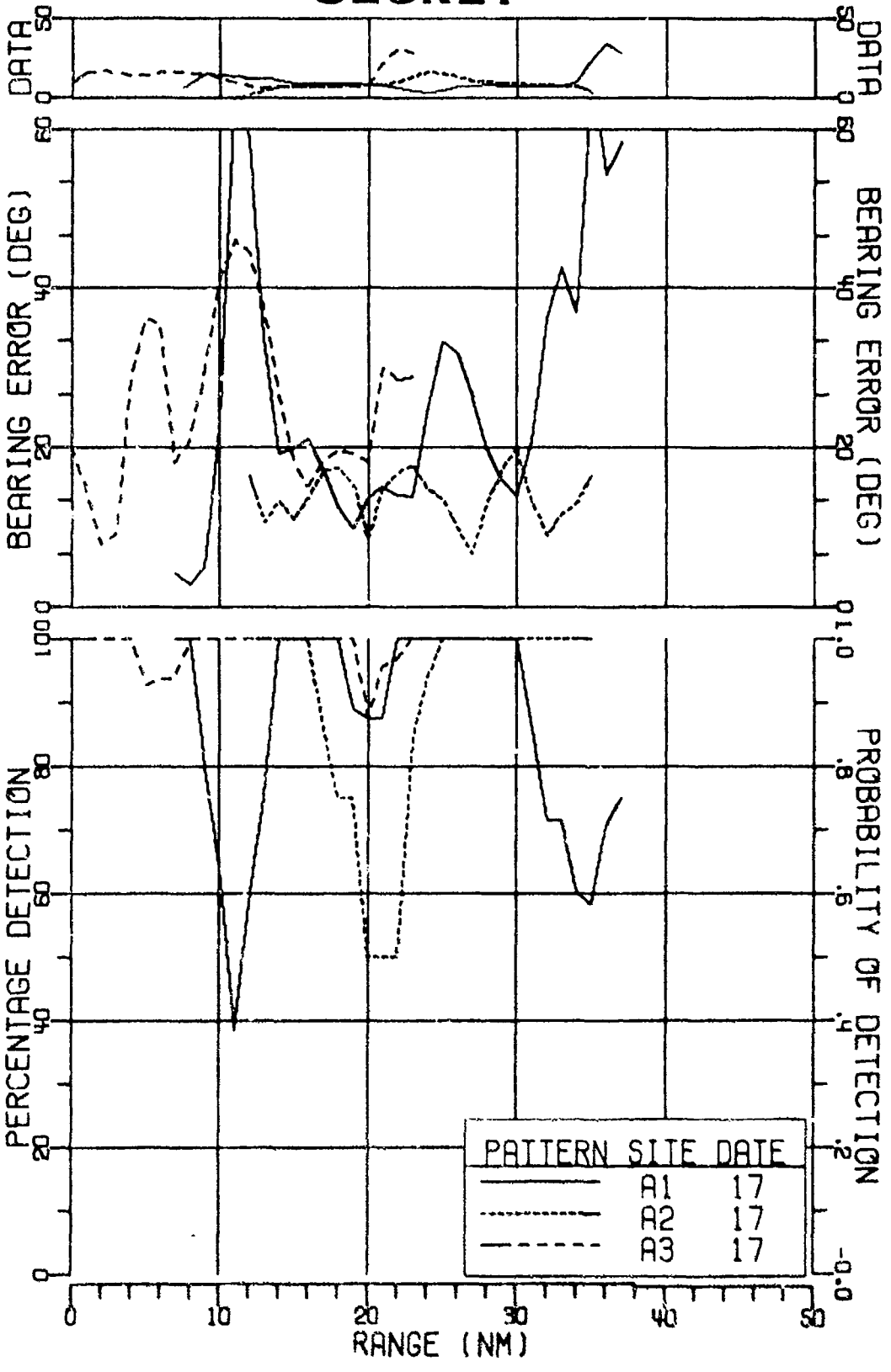

FIGURE II-215
MSS-FVT NEAR BOTTOM DIFFERENCED CARDIOIDS SENSOR
DETECTION RESULTS FOR 70HZ AT 166DB (U)

AS-77-3142

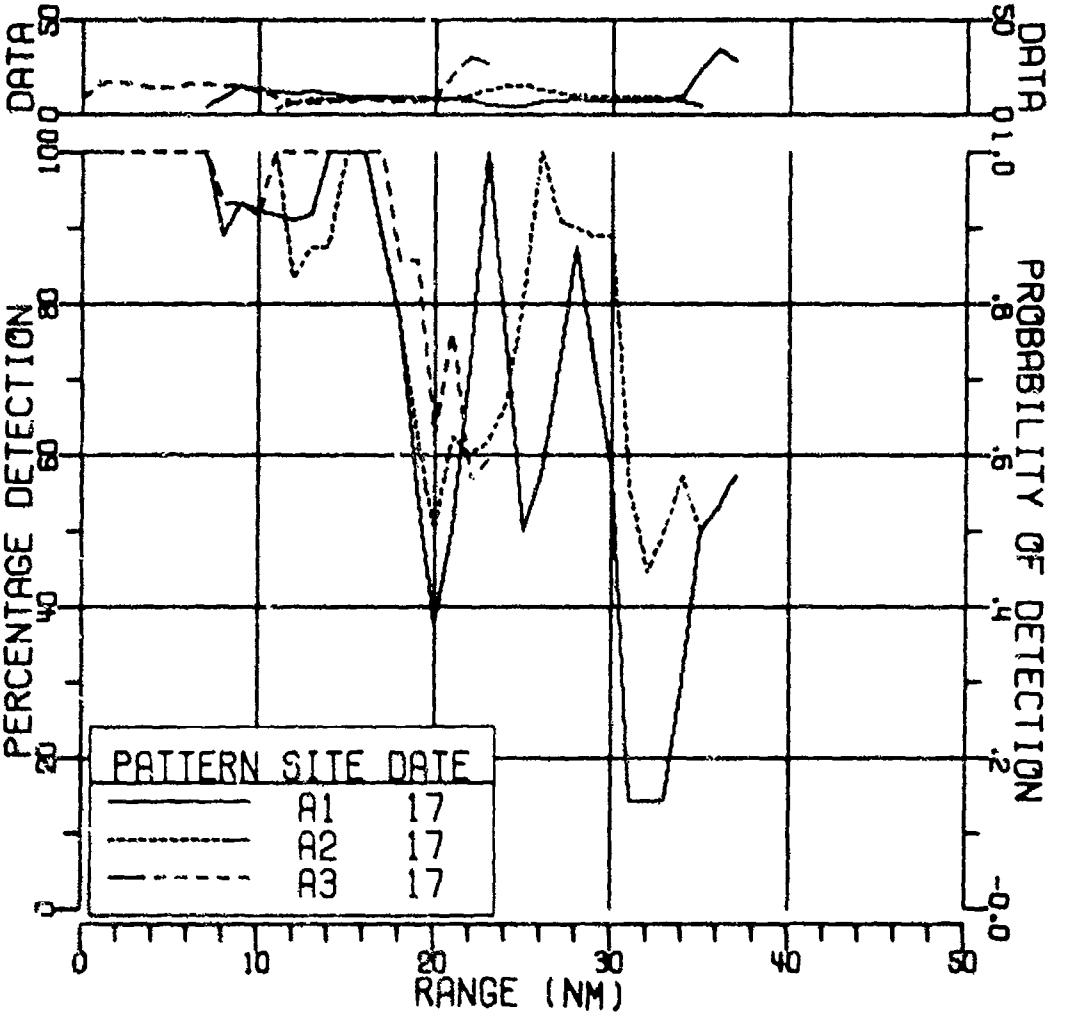

FIGURE II-216
NSS-FVT NEAR BOTTOM OMNIDIRECTIONAL SENSOR
DETECTION RESULTS FOR 170HZ AT 156DB (U)

AS-77-3143

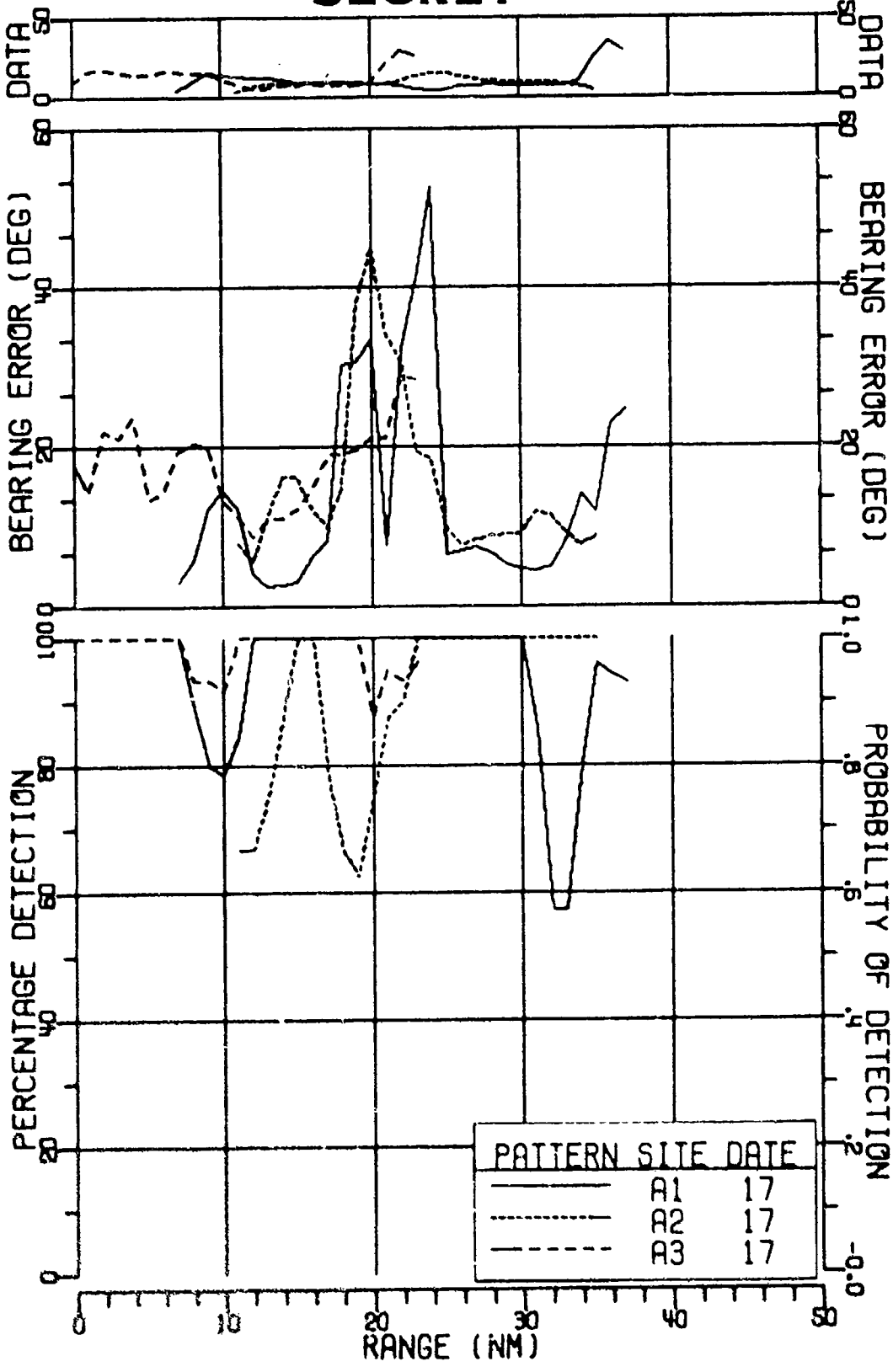

FIGURE II-217
MSS-FVT NEAR BOTTOM SINGLE CARDIOIDS SENSOR
DETECTION RESULTS FOR 170HZ AT 156DB (U)

AS-77-3144

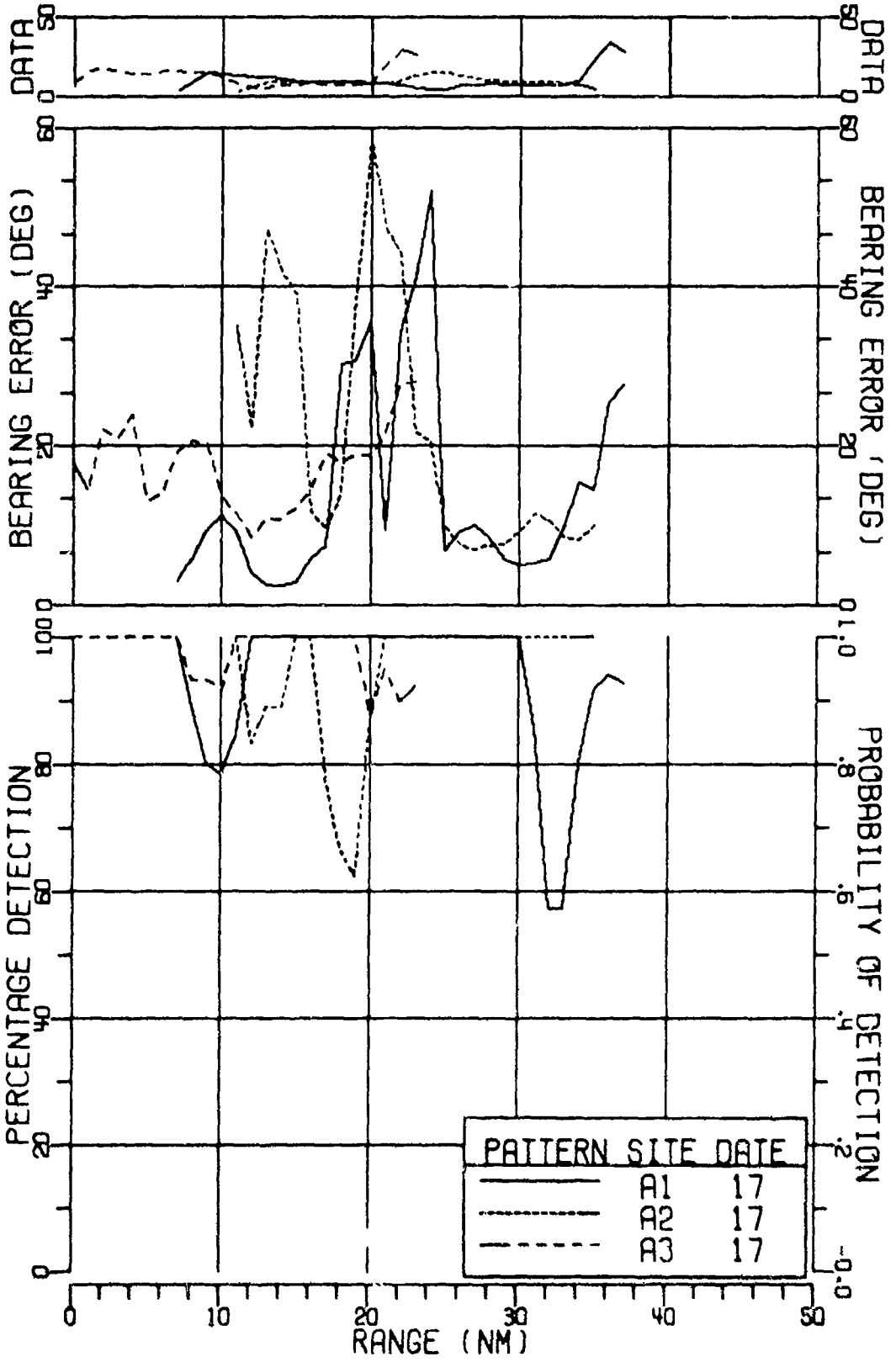

FIGURE II-218
MSS-FVT NEAR BOTTOM MAX GAIN LIMACONS SENSOR
DETECTION RESULTS FOR 170HZ AT 156DB (U)

AS-77-3145

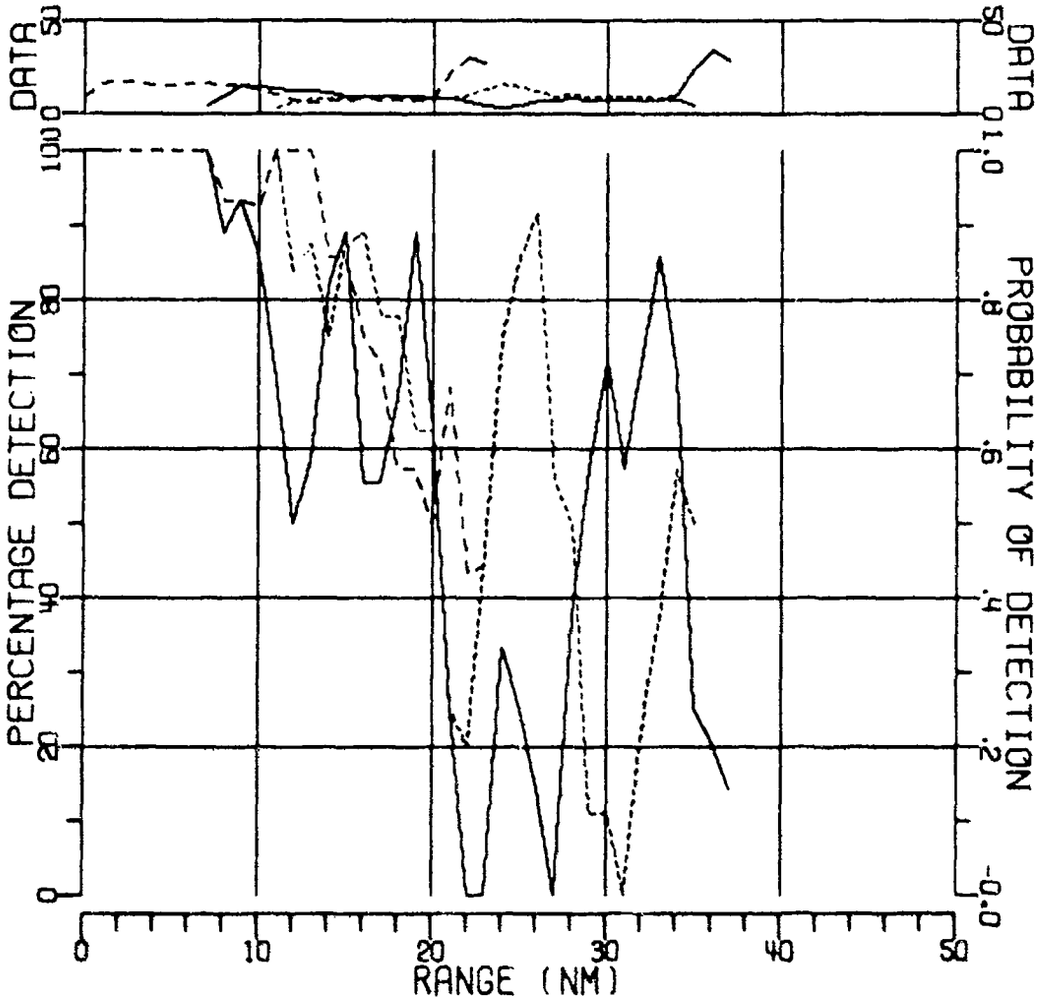

FIGURE II-219
MSS-FVT NEAR BOTTOM VERTICAL DIPOLE SENSOR
DETECTION RESULTS FOR 17OHZ AT 156DB (U)

PATTERN	SITE	DATE
———	A1	17
·····	A2	17
— - - - -	A3	17

AS-77-3146

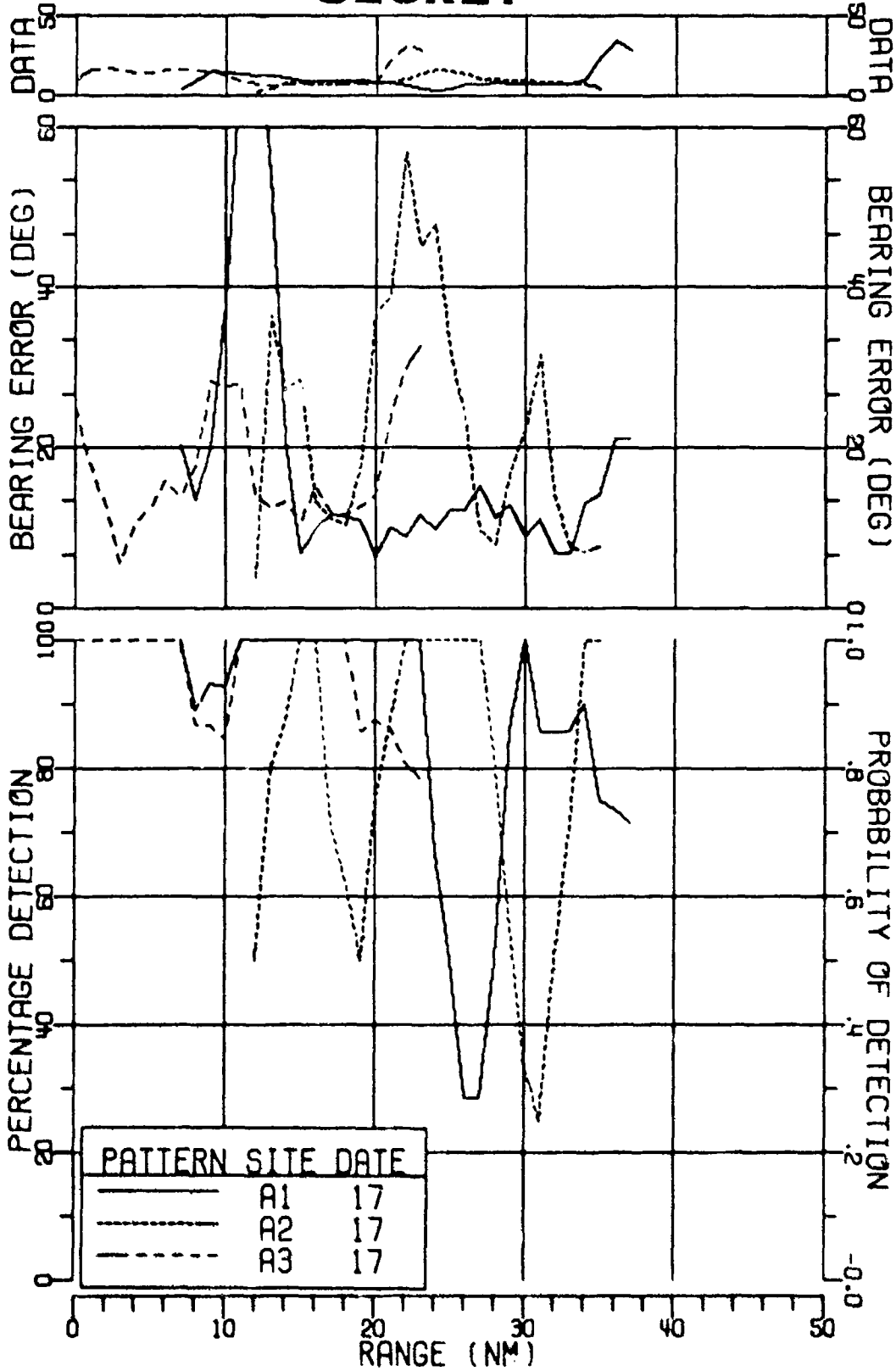

FIGURE II-220
MSS-FVT NEAR BOTTOM DIFFERENCED CARDIOIDS SENSOR DETECTION RESULTS FOR 170HZ AT 156DB (U)

AS-77-3147

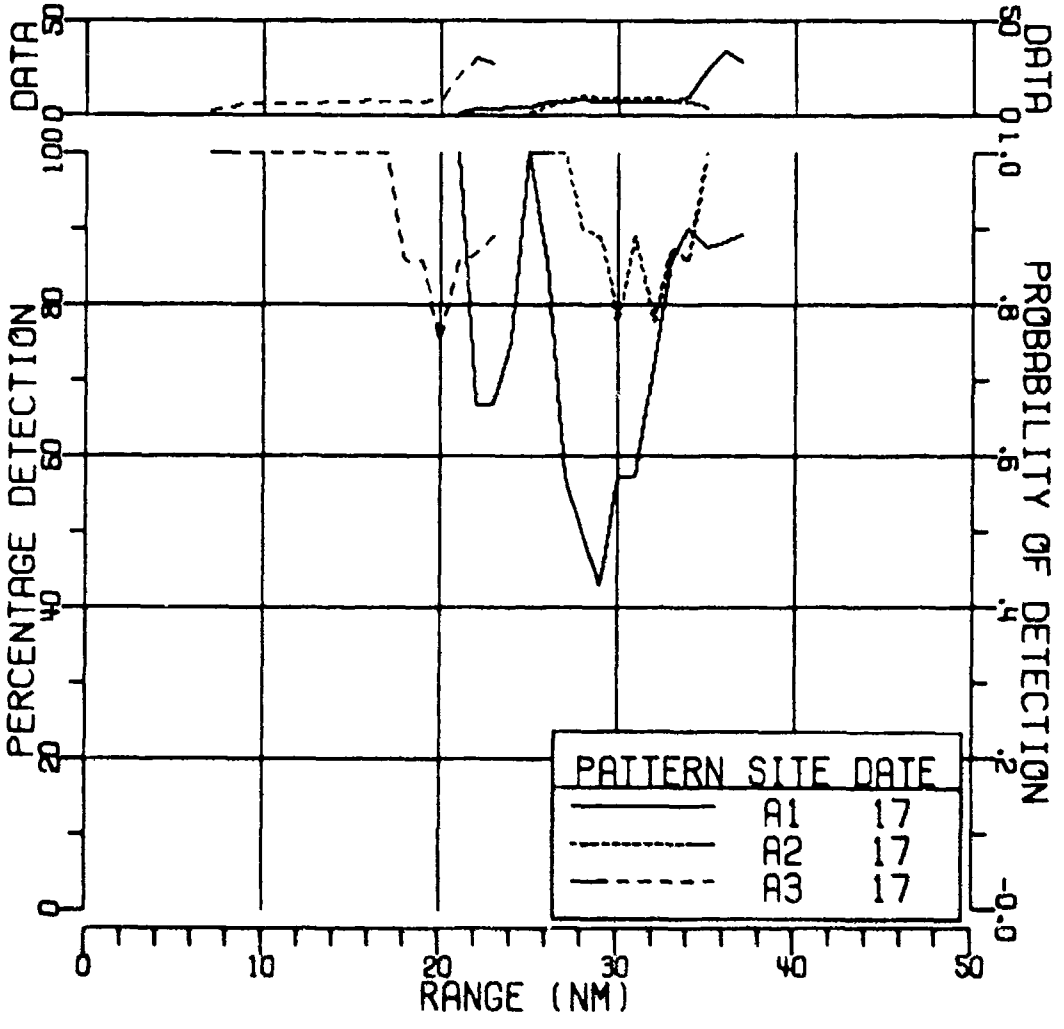

FIGURE II-221
MSS-FVT NEAR BOTTOM OMNIDIRECTIONAL SENSOR
DETECTION RESULTS FOR 335HZ AT 154DB (U)

AS-77-3148

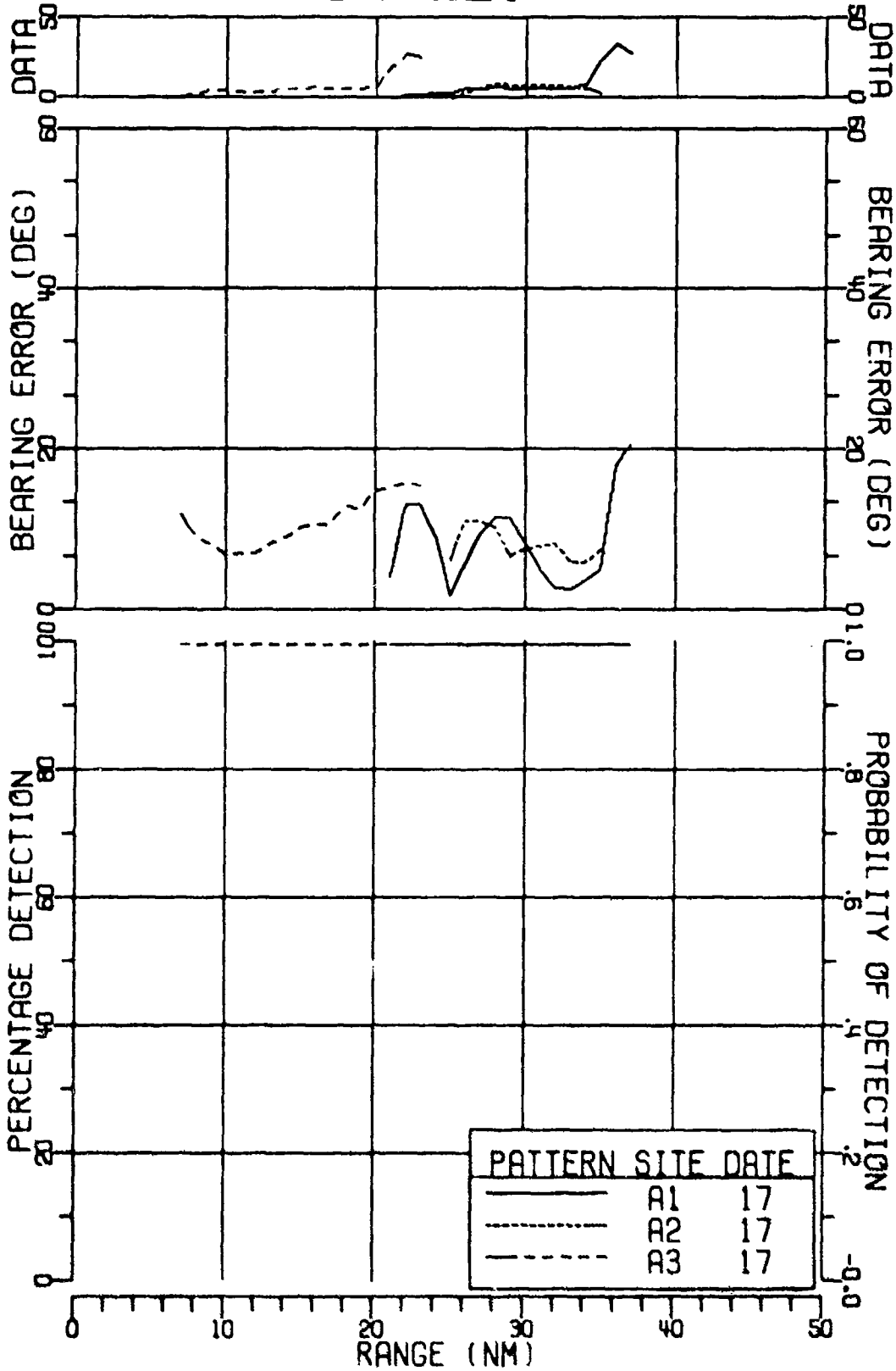

FIGURE II-222
MSS-FVT NEAR BOTTOM SINGLE CARDIOIDS SENSOR
DETECTION RESULTS FOR 335HZ AT 154DB (U)

AS-77-3149

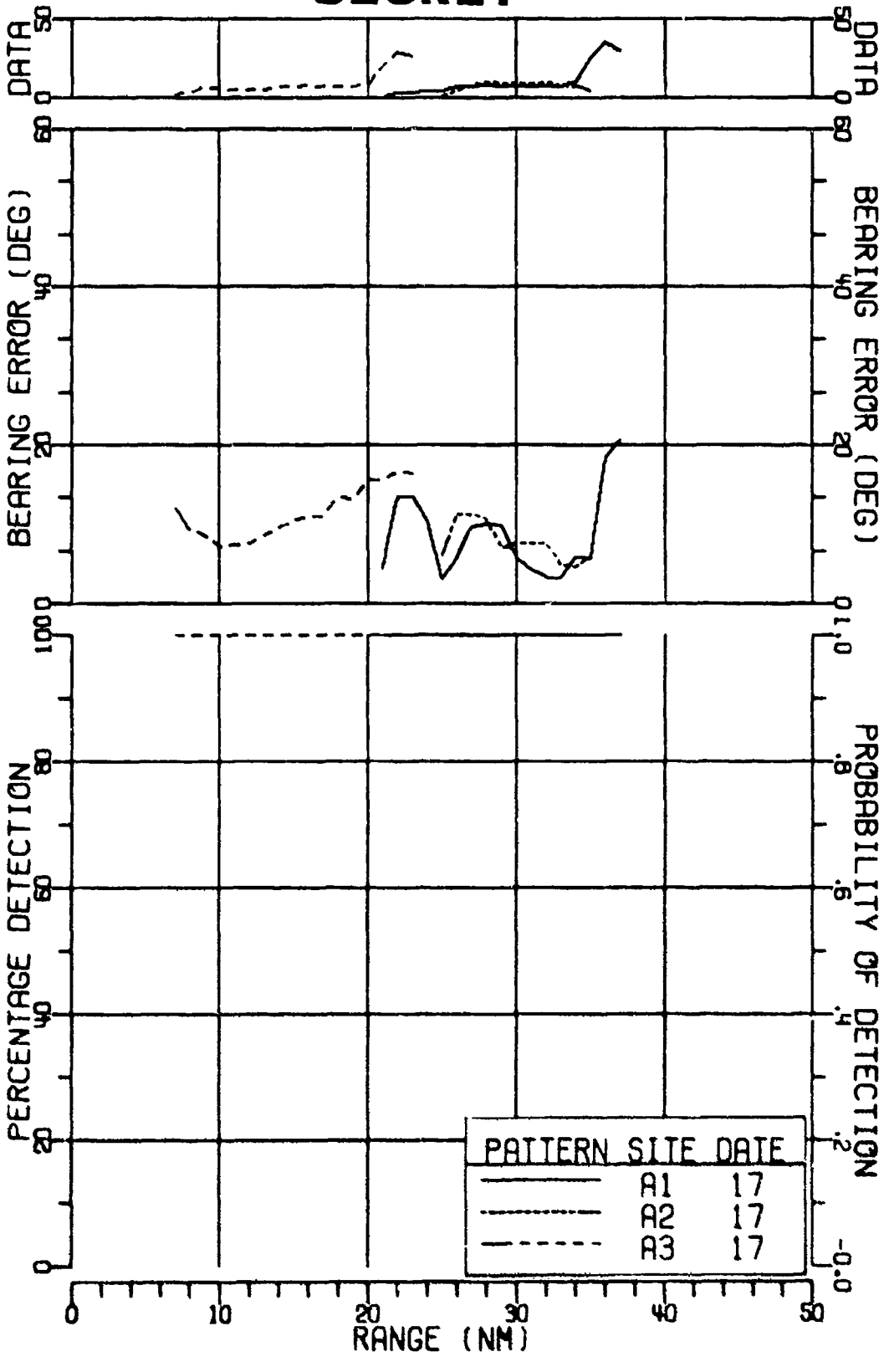

FIGURE II-223
MSS-FVT NEAR BOTTOM MAX GAIN LIMACONS SENSOR
DETECTION RESULTS FOR 335HZ AT 154DB (U)

AS-77-3150

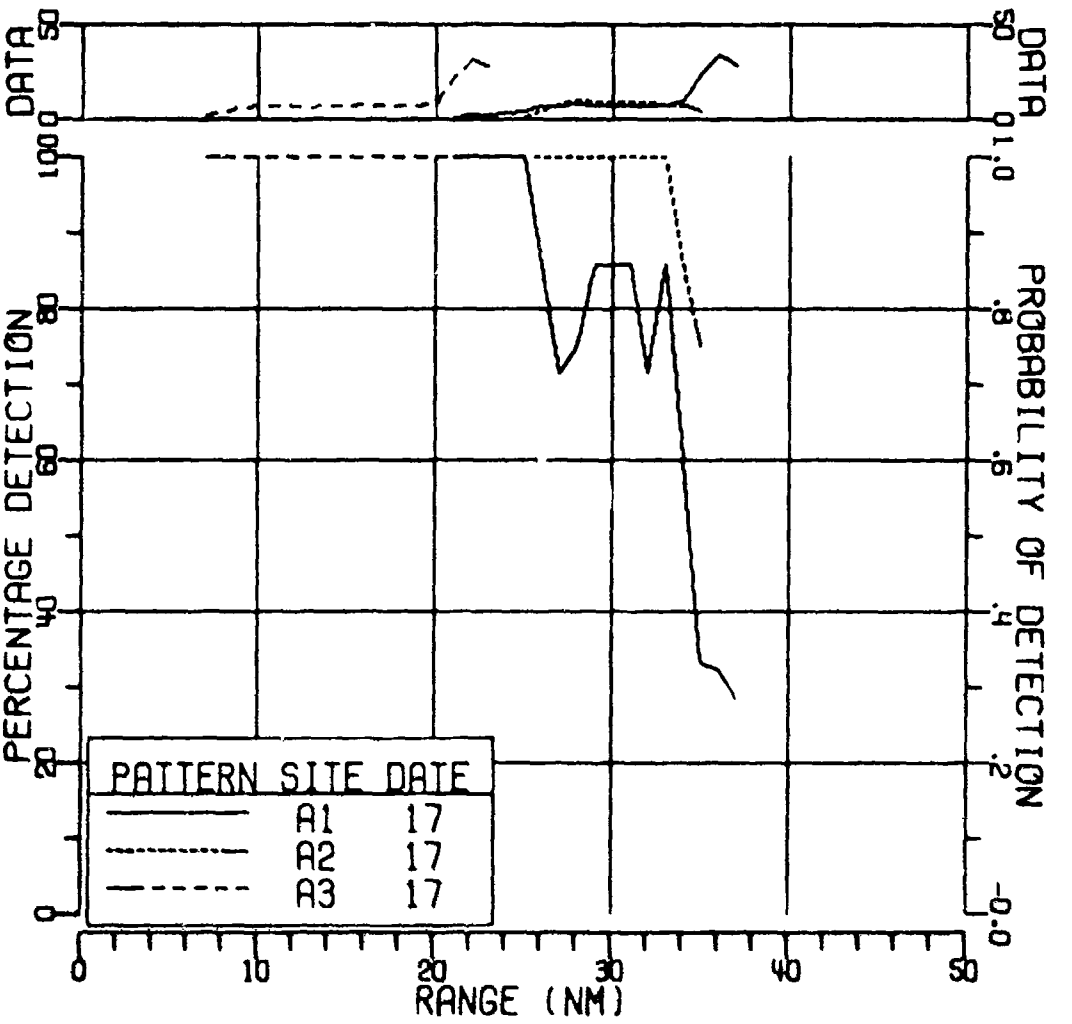

FIGURE II-224
MSS-FVT NEAR BOTTOM VERTICAL DIPOLE SENSOR
DETECTION RESULTS FOR 335HZ AT 154DB (U)

AS-77-3151

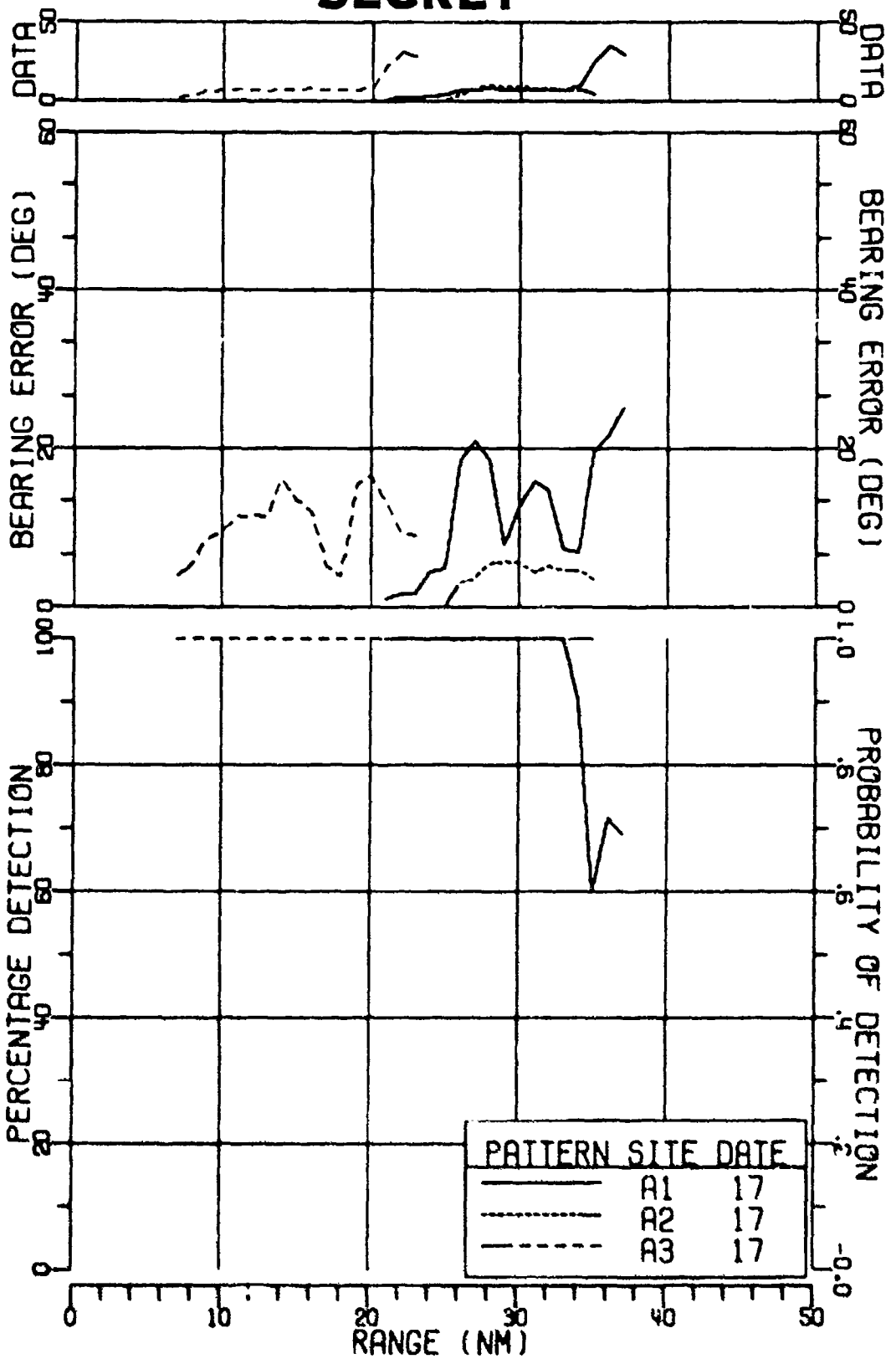

FIGURE II-225
MSS-FVT NEAR BOTTOM DIFFERENCED CARDIOIDS SENSOR DETECTION RESULTS FOR 335HZ AT 154DB (U)

AS-77-3152

(The reverse of this page is blank.)

APPENDIX F

BEARING ERROR versus SIGNAL-TO-NOISE RATIO CURVES (U)

(FIGURES II-226 - II-251)

(The reverse of this page is blank.)

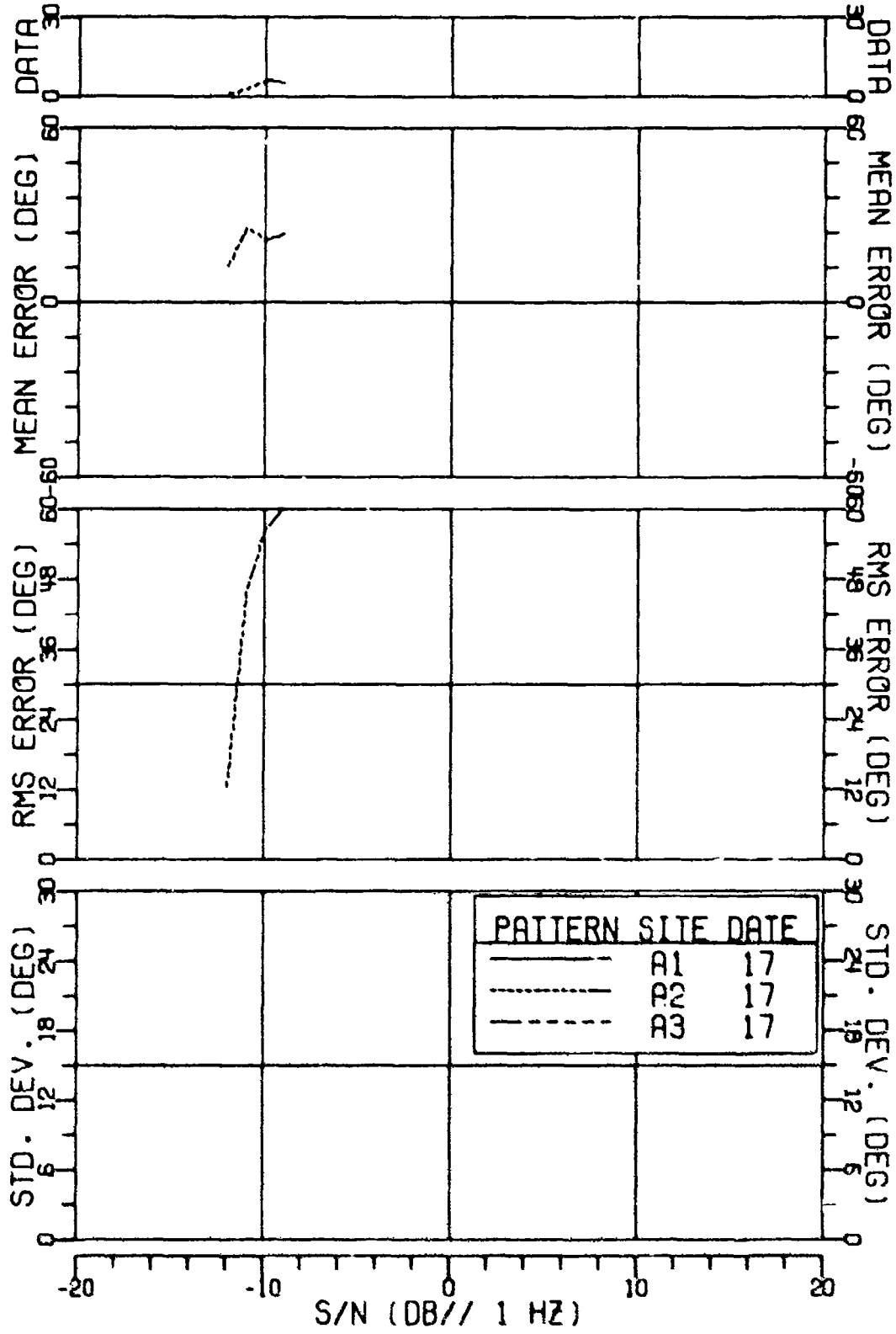

FIGURE II-226
MSS-FVT NEAR BOTTOM MAX GAIN LIMACONS SENSOR
BEARING ERROR RESULTS FOR 55HZ AT 141DB (U)

S-77-3153

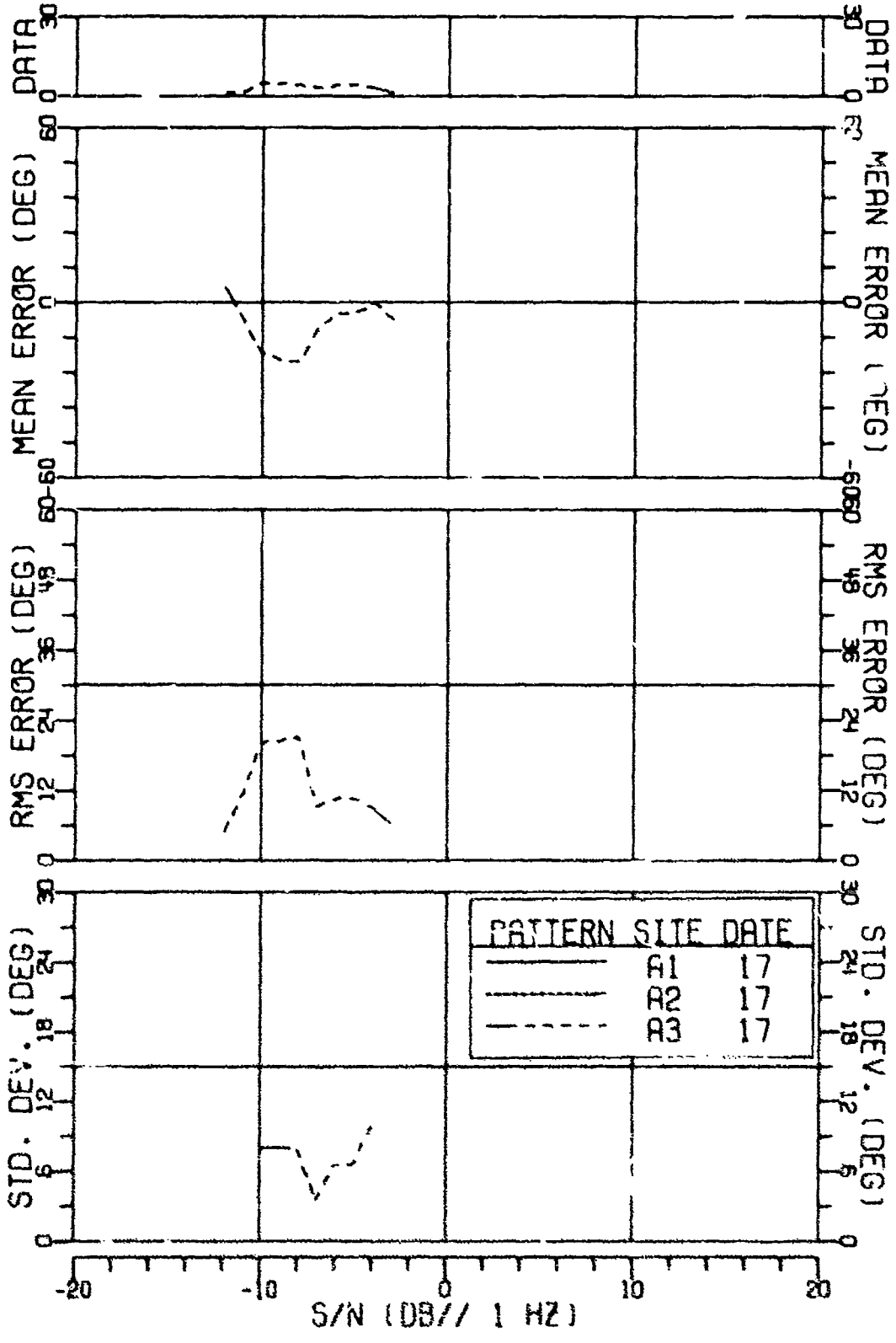

FIGURE II-227
MSS-FVT NEAR BOTTOM DIFFERENCED CARDICIDS SENSOR
BEARING ERROR RESULTS FOR 55HZ AT 141DB (U)

AS-77-3154

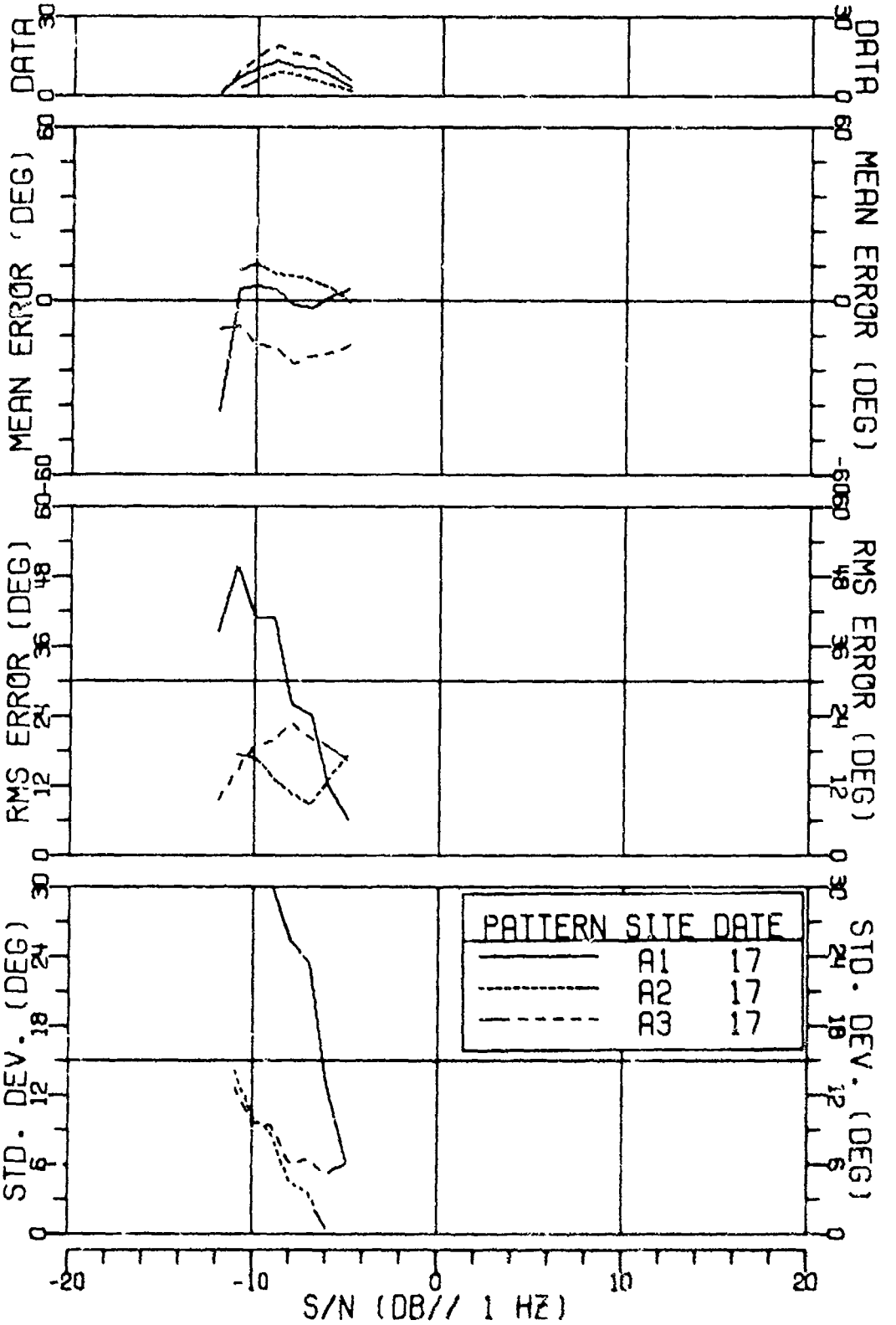

FIGURE II-228
MSS-FVT NEAR BOTTOM SINGLE CARDIOIDS SENSOR
BEARING ERROR RESULTS FOR 155HZ AT 134DB (U)

AS-77-3155

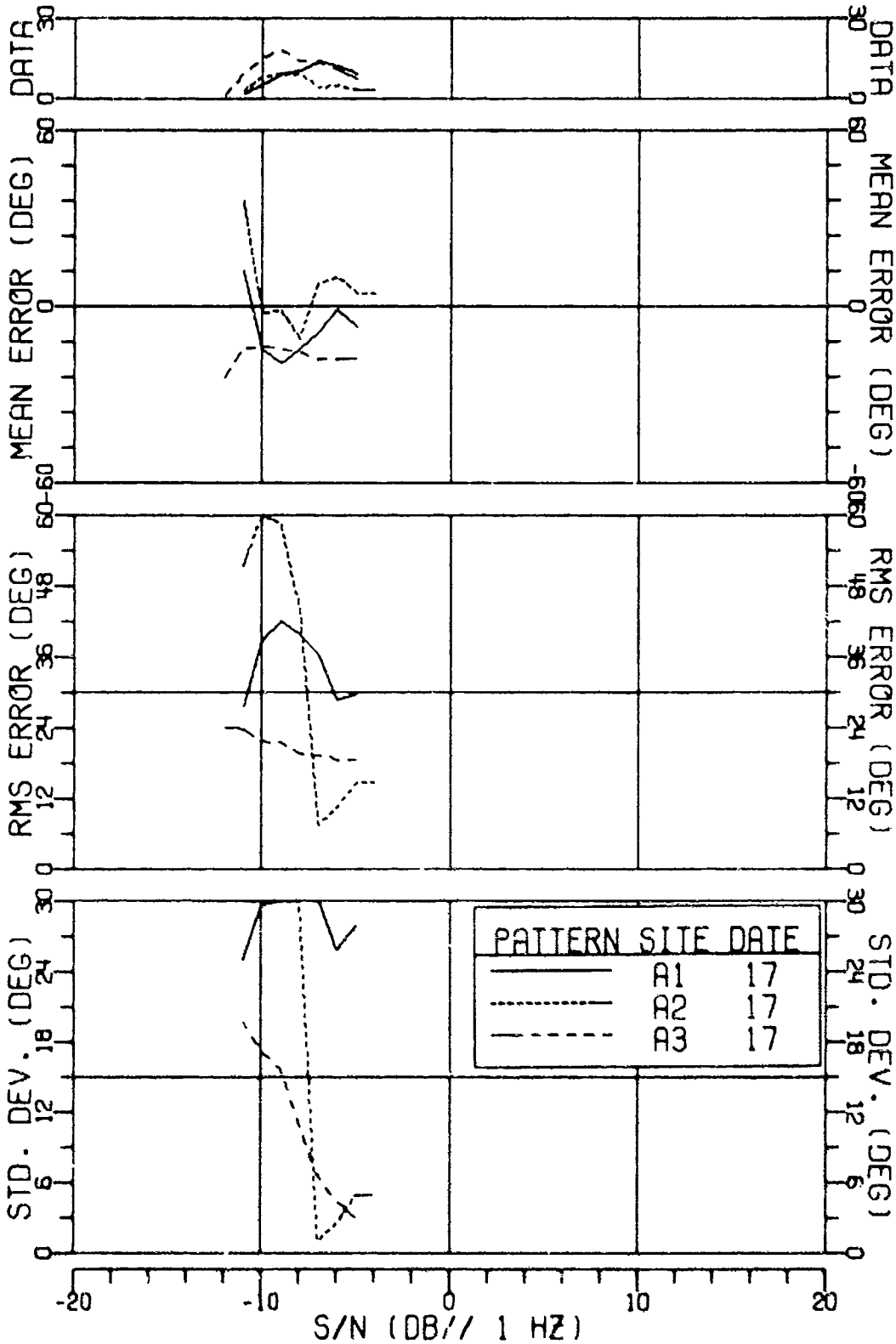

FIGURE II-229
MSS-FVT NEAR BOTTOM MAX GAIN LIMACONS SENSOR
BEARING ERROR RESULTS FOR 155HZ AT 134DB (U)

AS-77-3156

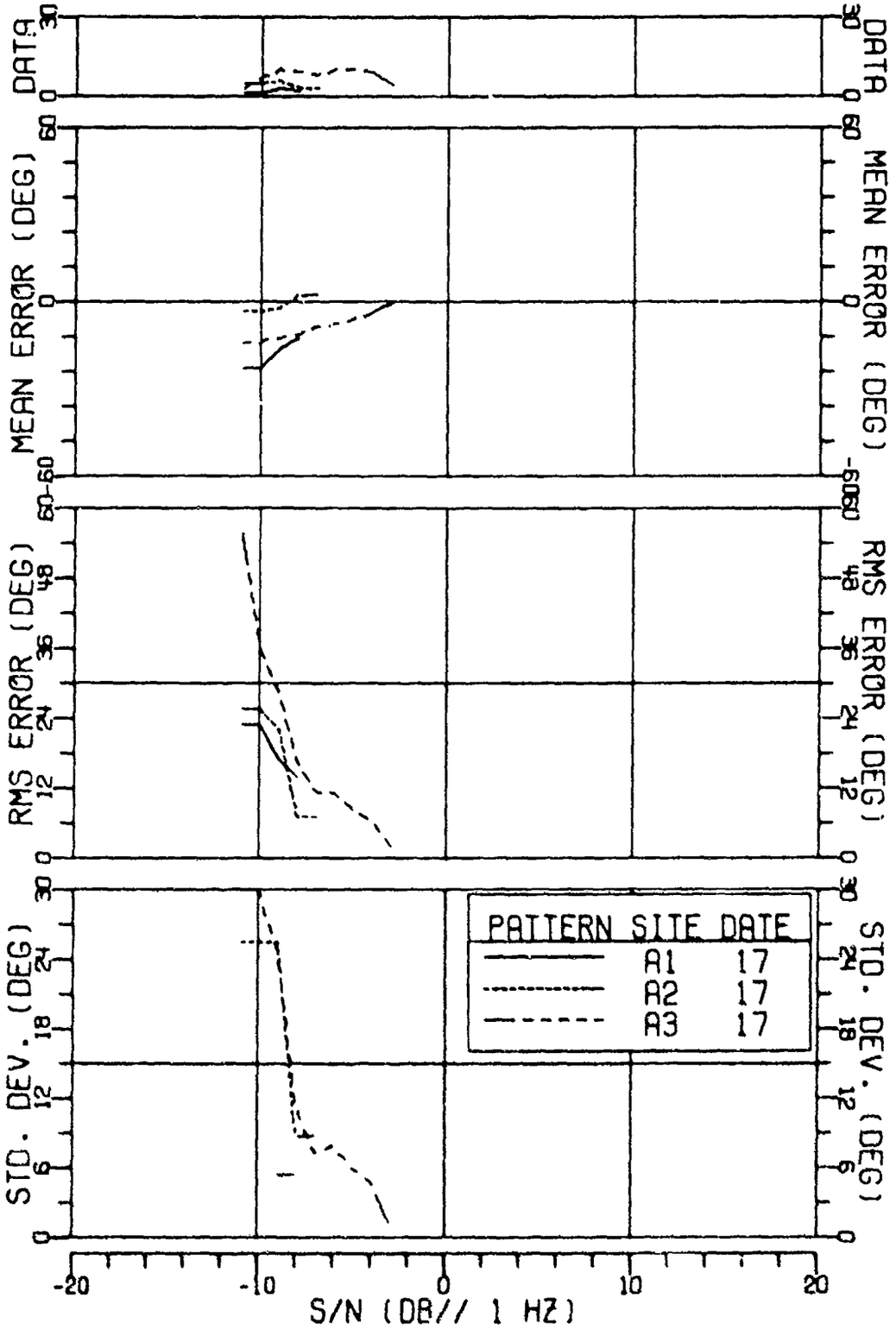

FIGURE II-230
MSS-FVT NEAR BOTTOM DIFFERENCED CARDIOIDS SENSOR BEARING ERROR RESULTS FOR 155HZ AT 134DB (U)

AS-77-3157

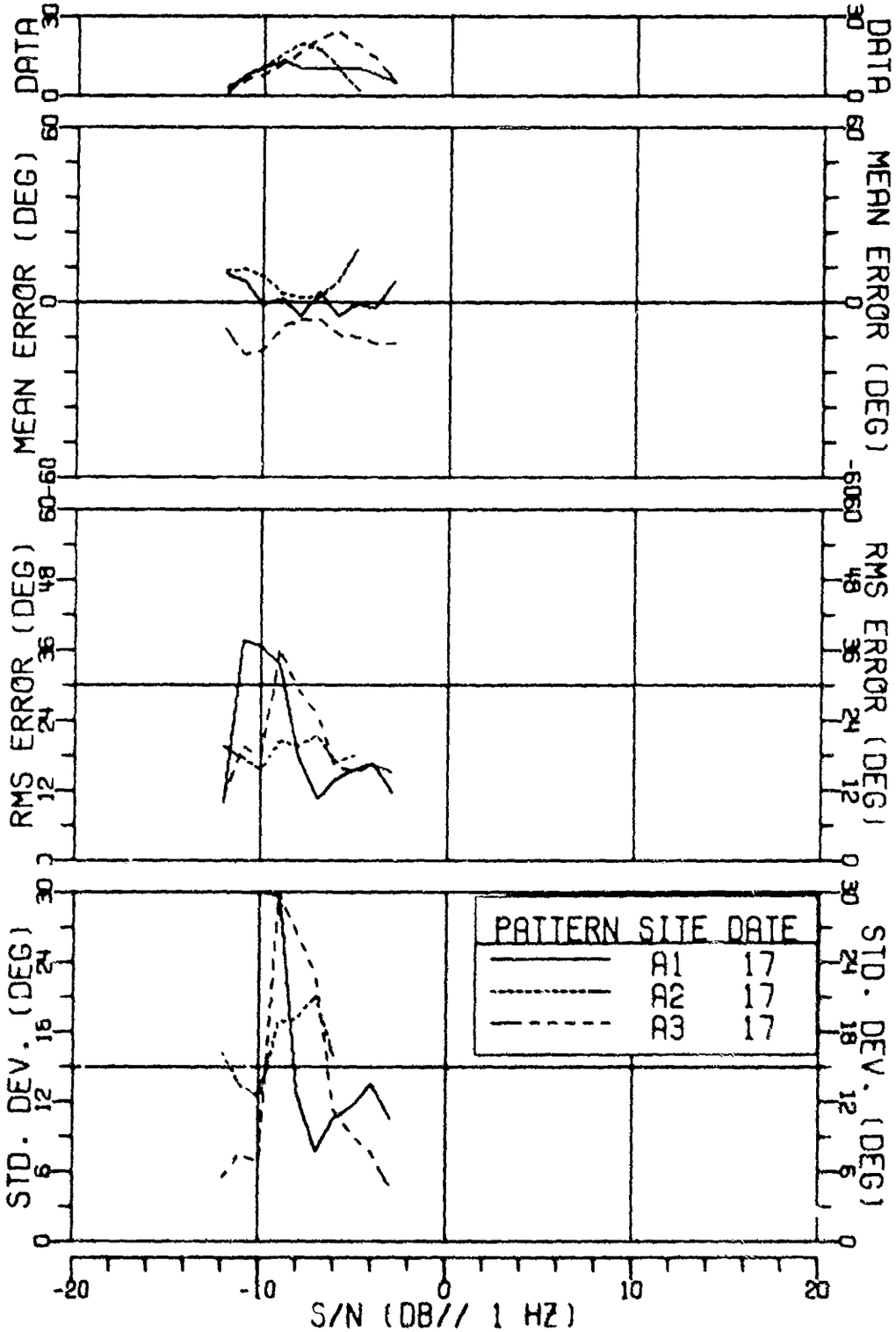

FIGURE II-231
MSS-FVT NEAR BOTTOM SINGLE CARDIOIDS SENSOR
BEARING ERROR RESULTS FOR 305 HZ AT 136DB (U)

AS-77-3158

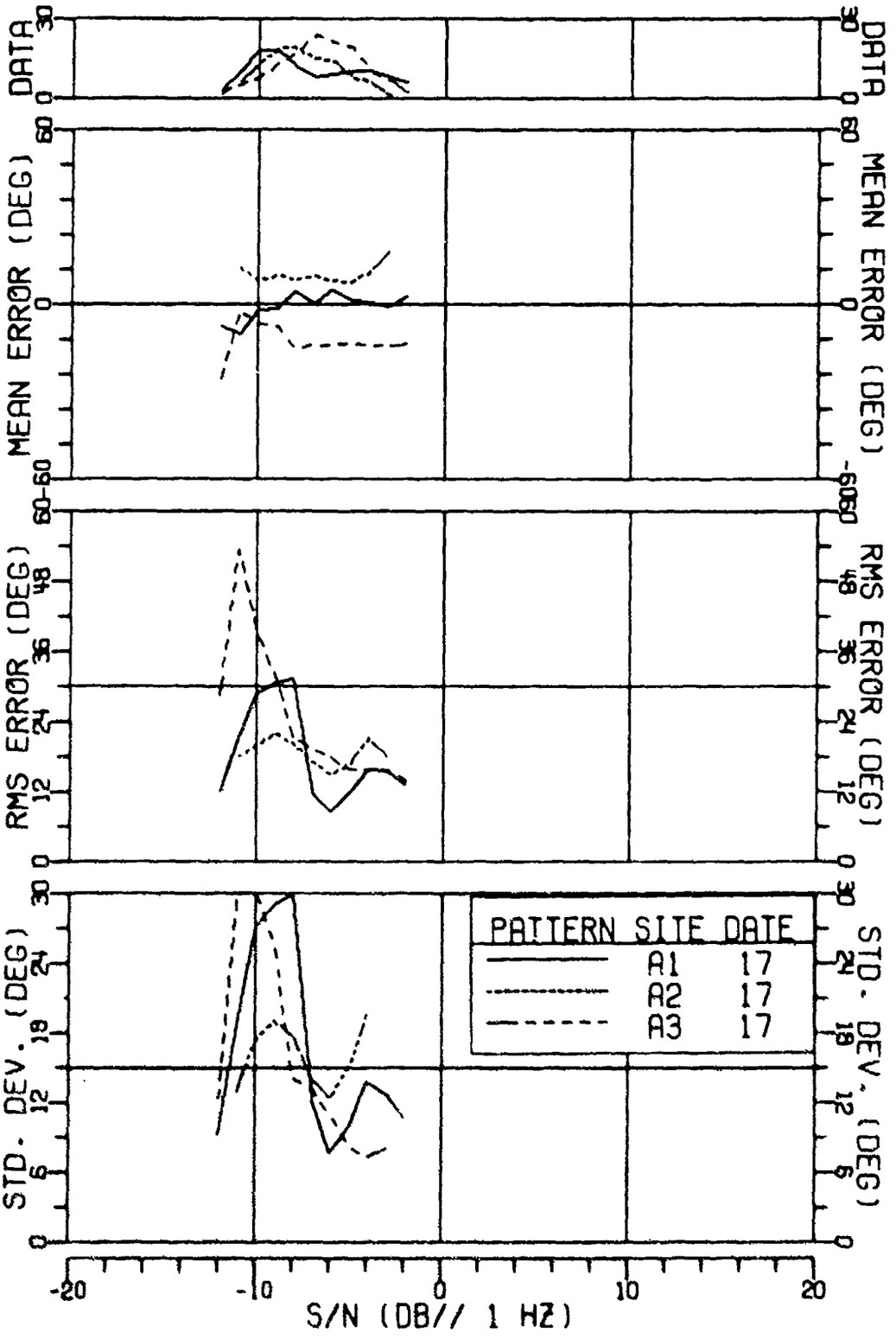

FIGURE II-232
MSS-FVT NEAR BOTTOM MAX GAIN LIMACONS SENSOR
BEARING ERROR RESULTS FOR 305 HZ AT 136DB (U)

AS-77-3159

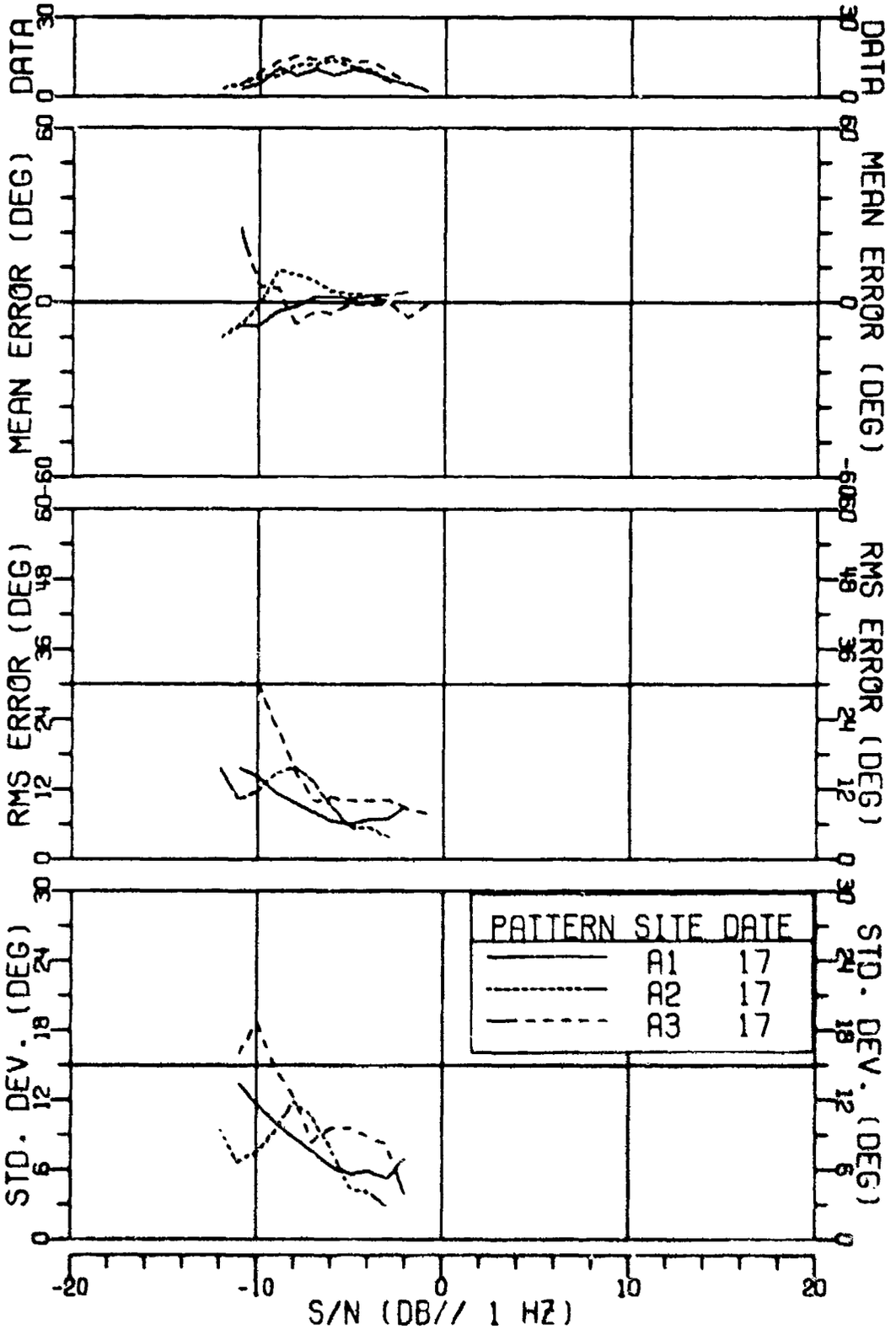

FIGURE II-233
MSS-FVT NEAR BOTTOM DIFFERENCED CARDIOIDS SENSOR BEARING ERROR RESULTS FOR 305HZ AT 136DB (U)

AS-77-3160

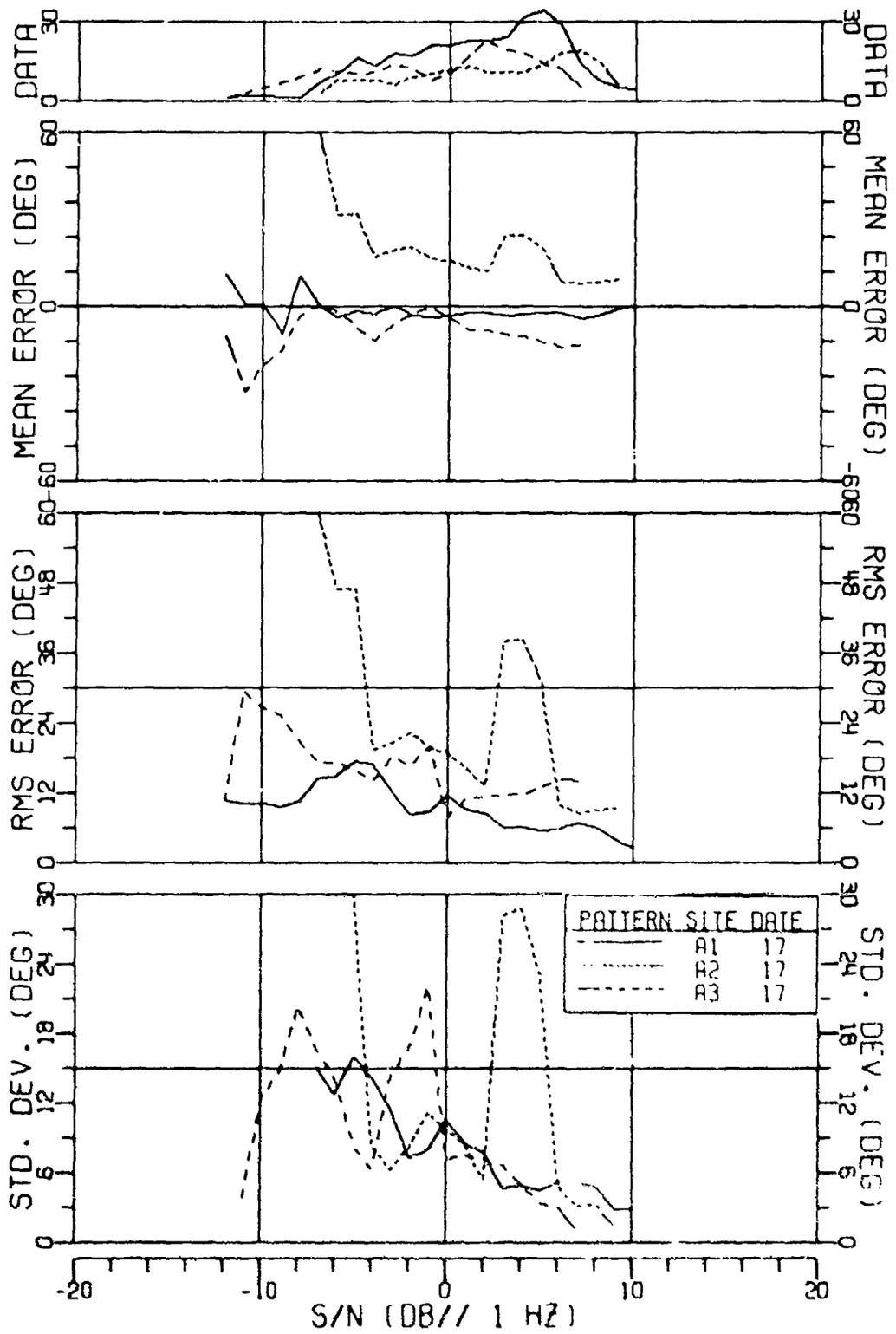

FIGURE II-234
MSS-FVT NEAR BOTTOM SINGLE CARDIOIDS SENSOR
BEARING ERROR RESULTS FOR 64HZ AT 162DB (U)

AS-77-3161

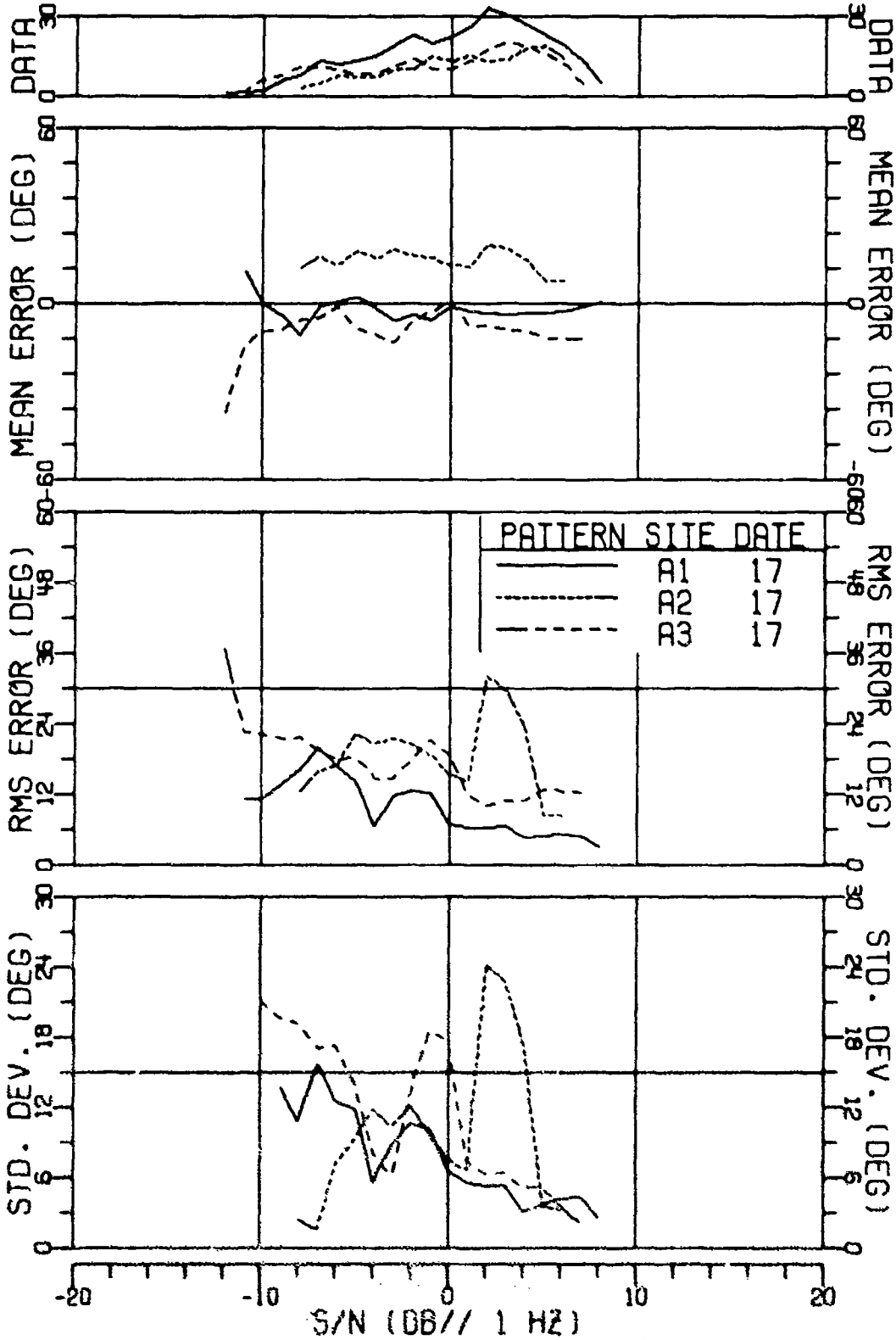

FIGURE II-235
MSS-FVT NEAR BOTTOM MAX GAIN LIMACONS SENSOR
BEARING ERROR RESULTS FOR 64HZ AT 162DB (U)

AS-77-3162

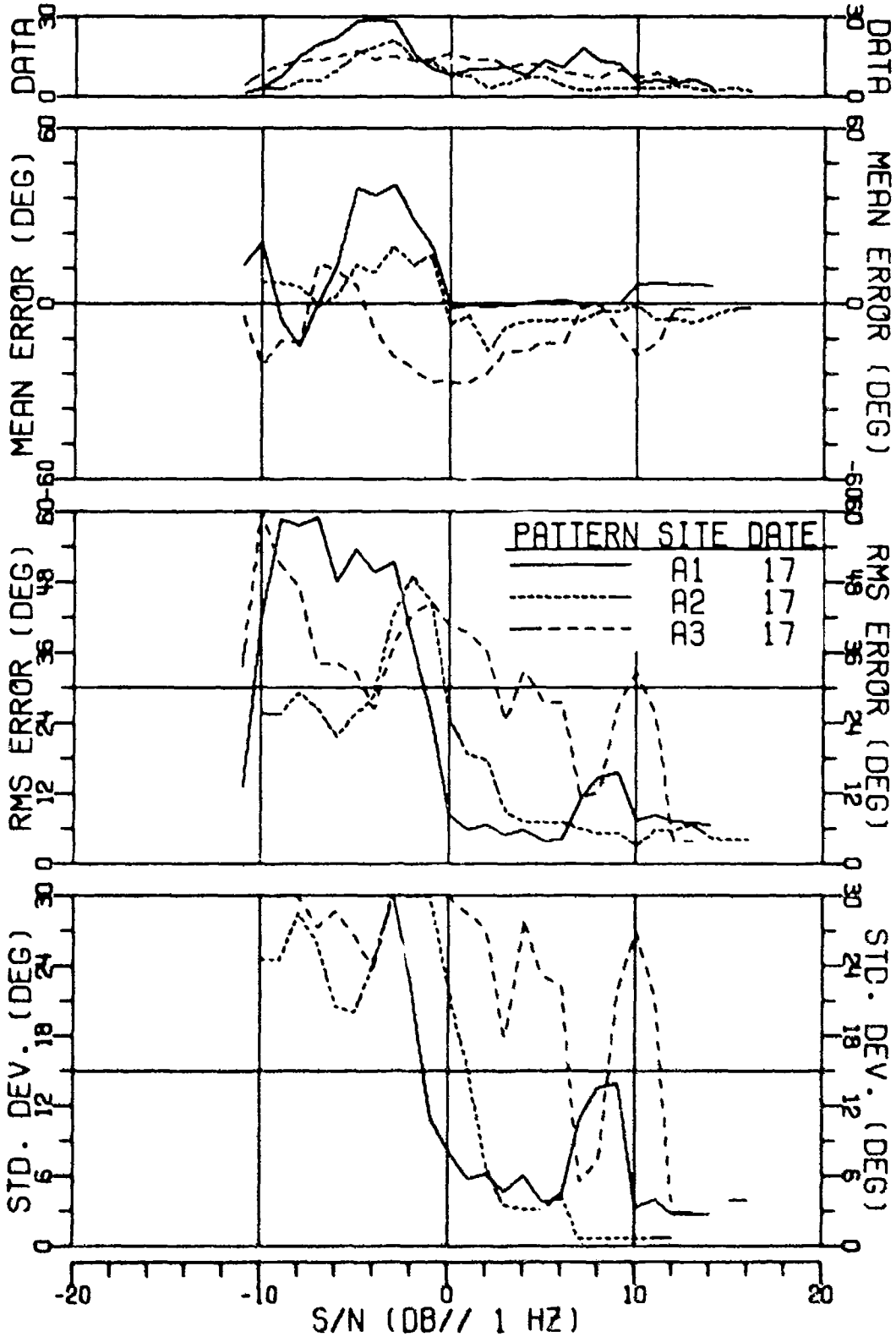

FIGURE II-236
MSS-FVT NEAR BOTTOM DIFFERENCED CARDIOIDS SENSOR
BEARING ERROR RESULTS FOR 64HZ AT 162DB (U)

AS-77-3163

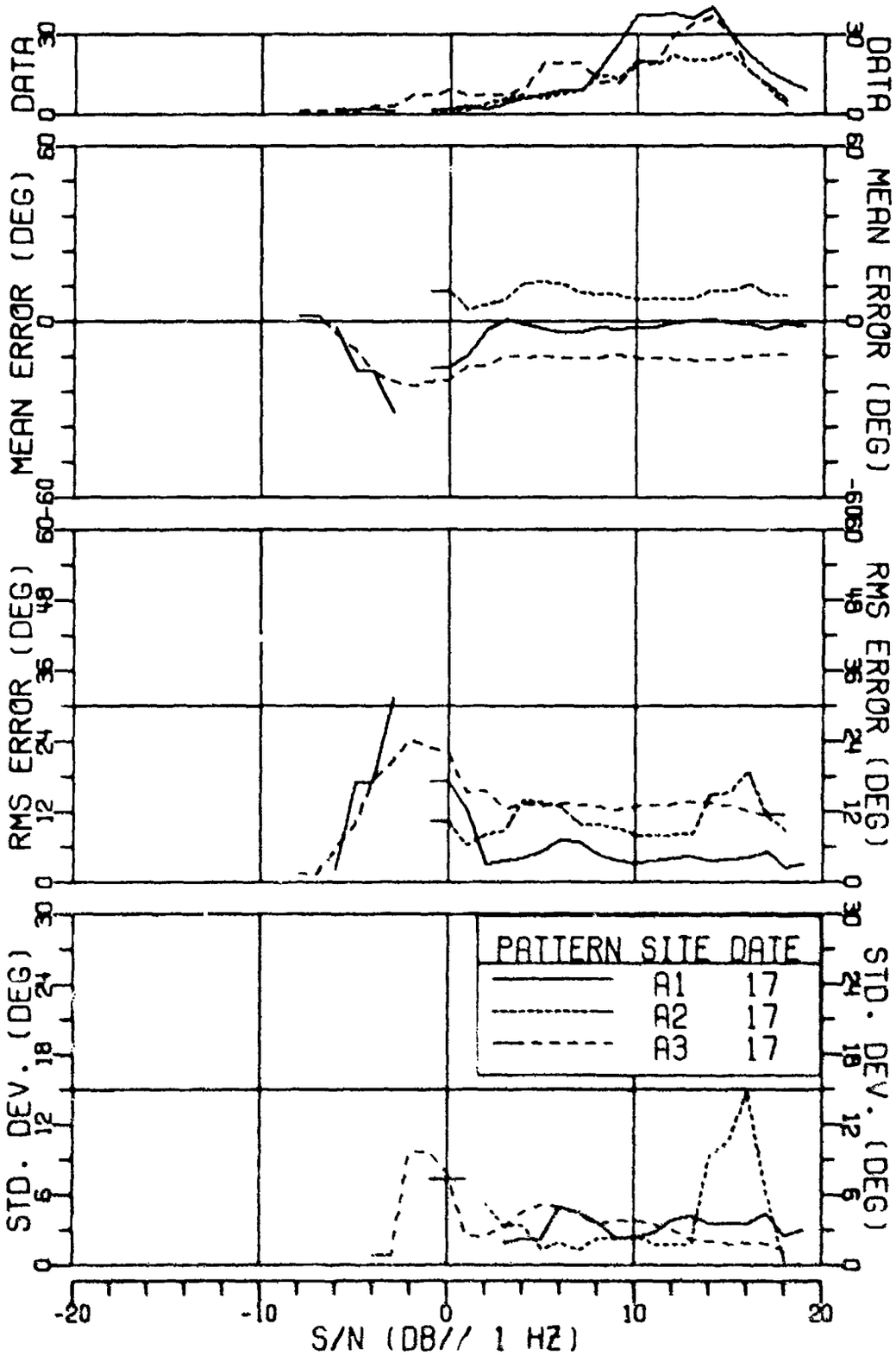

FIGURE II-237
MSS-FVT NEAR BOTTOM SINGLE CARDIOIDS SENSOR
BEARING ERROR RESULTS FOR 160HZ AT 161DB (U)

AS-77-3164

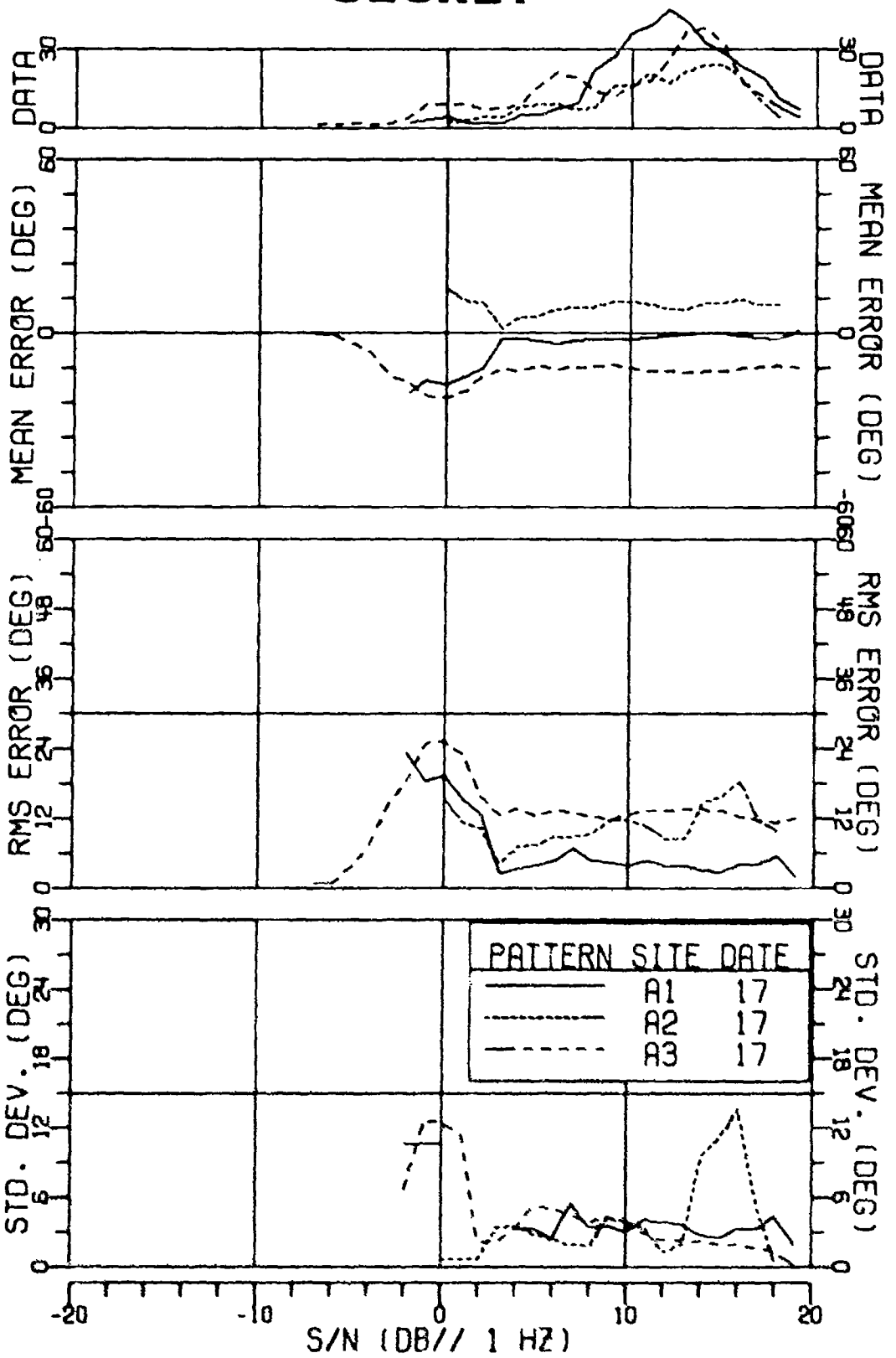

FIGURE II-238
MSS-FVT NEAR BOTTOM MAX GAIN LIMACONS SENSOR
BEARING ERROR RESULTS FOR 160HZ AT 161DB (U)

AS-77-3165

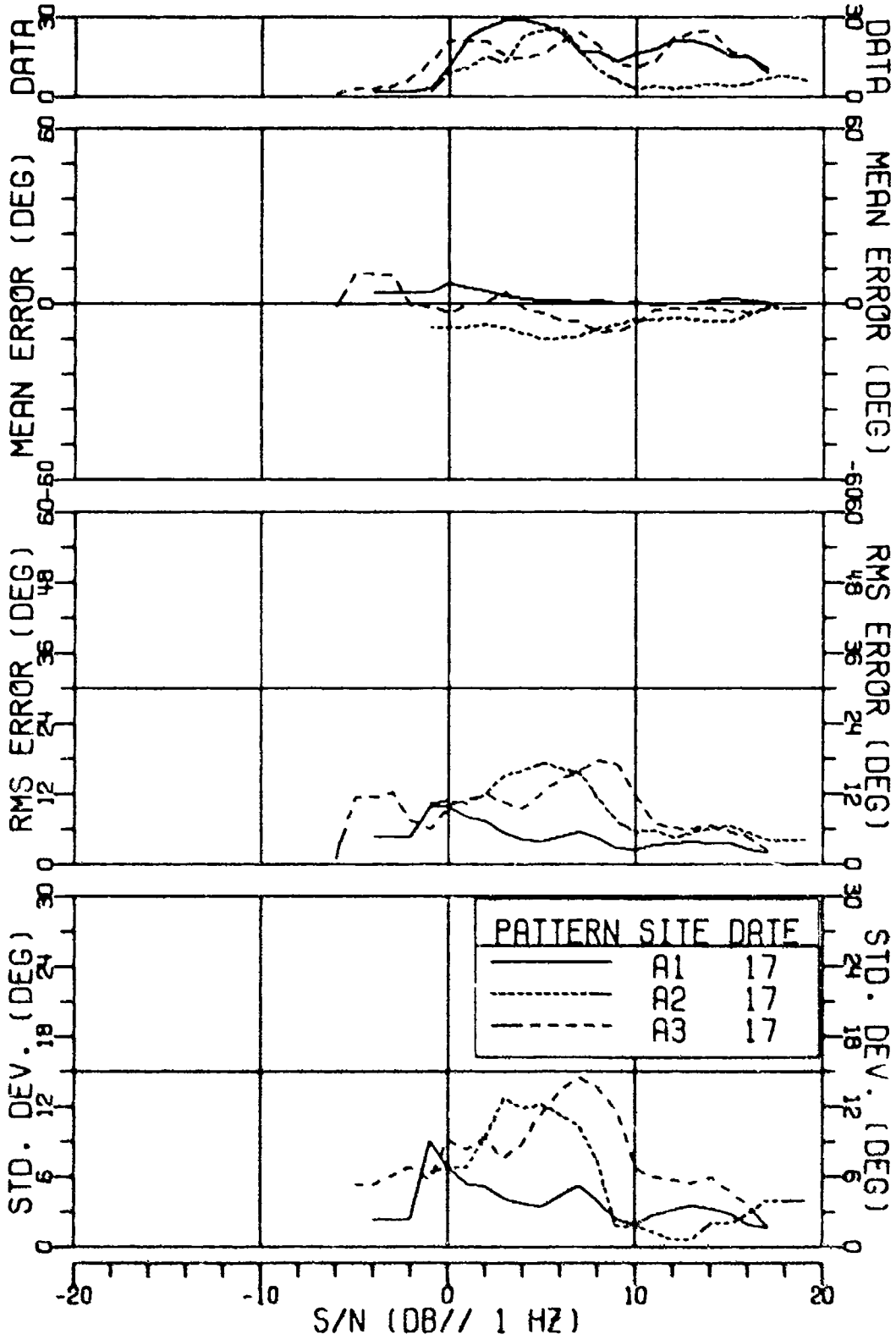

FIGURE II-239
MSS-FVT NEAR BOTTOM DIFFERENCED CARDIOIDS SENSO
BEARING ERROR RESULTS FOR 160HZ AT 161DB (U)

AS-77-3166

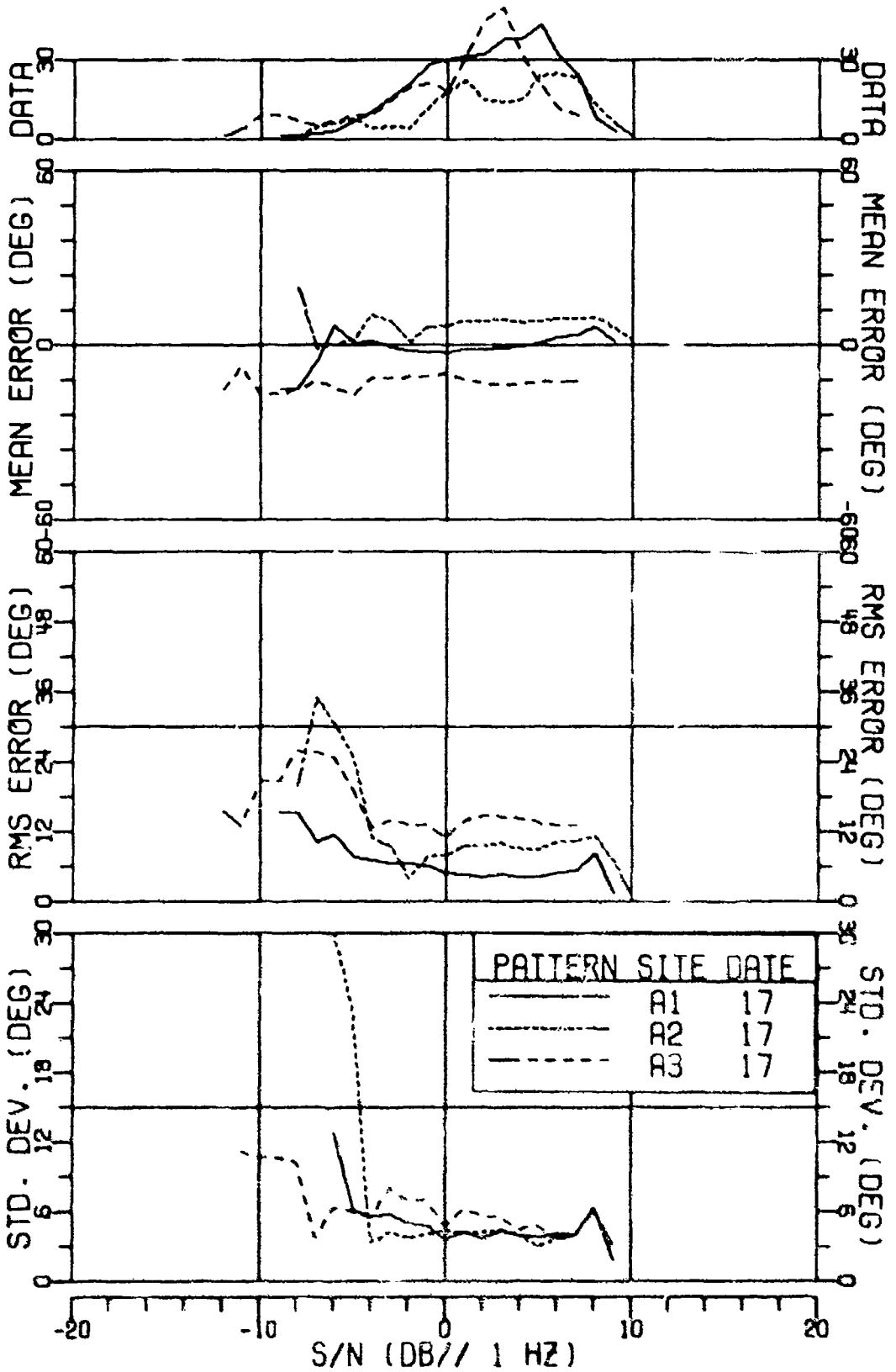

FIGURE II-240
MSS-FVT NEAR BOTTOM SINGLE CARDIOIDS SENSOR
BEARING ERROR RESULTS FOR 260HZ AT 147DB (U)

AS-77-3167

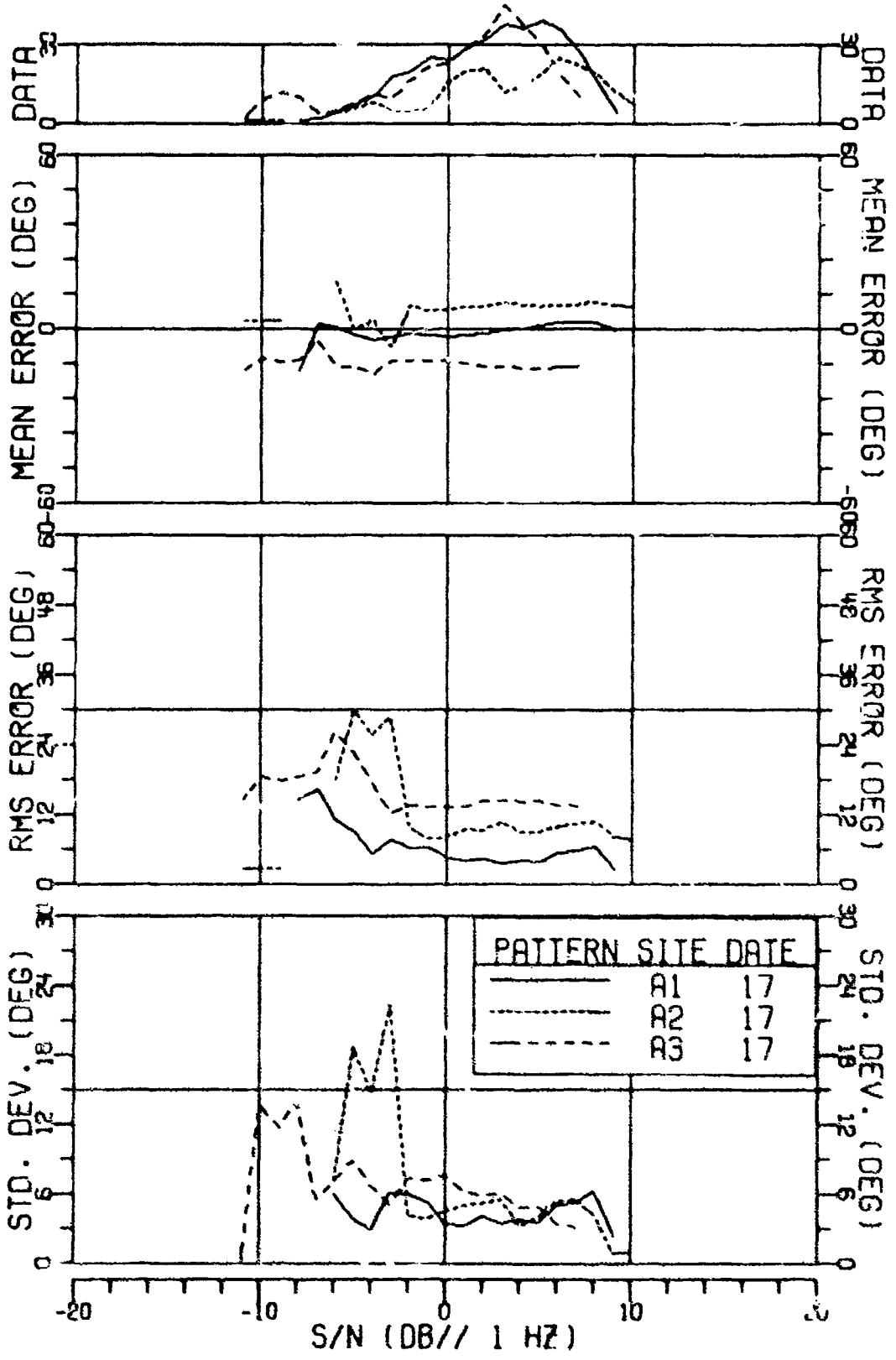

FIGURE II-241
MSS-FVT NEAR BOTTOM MAX GAIN LIMACONS SENSOR
BEARING ERROR RESULTS FOR 260HZ AT 147DB (U)

AS-77-3168

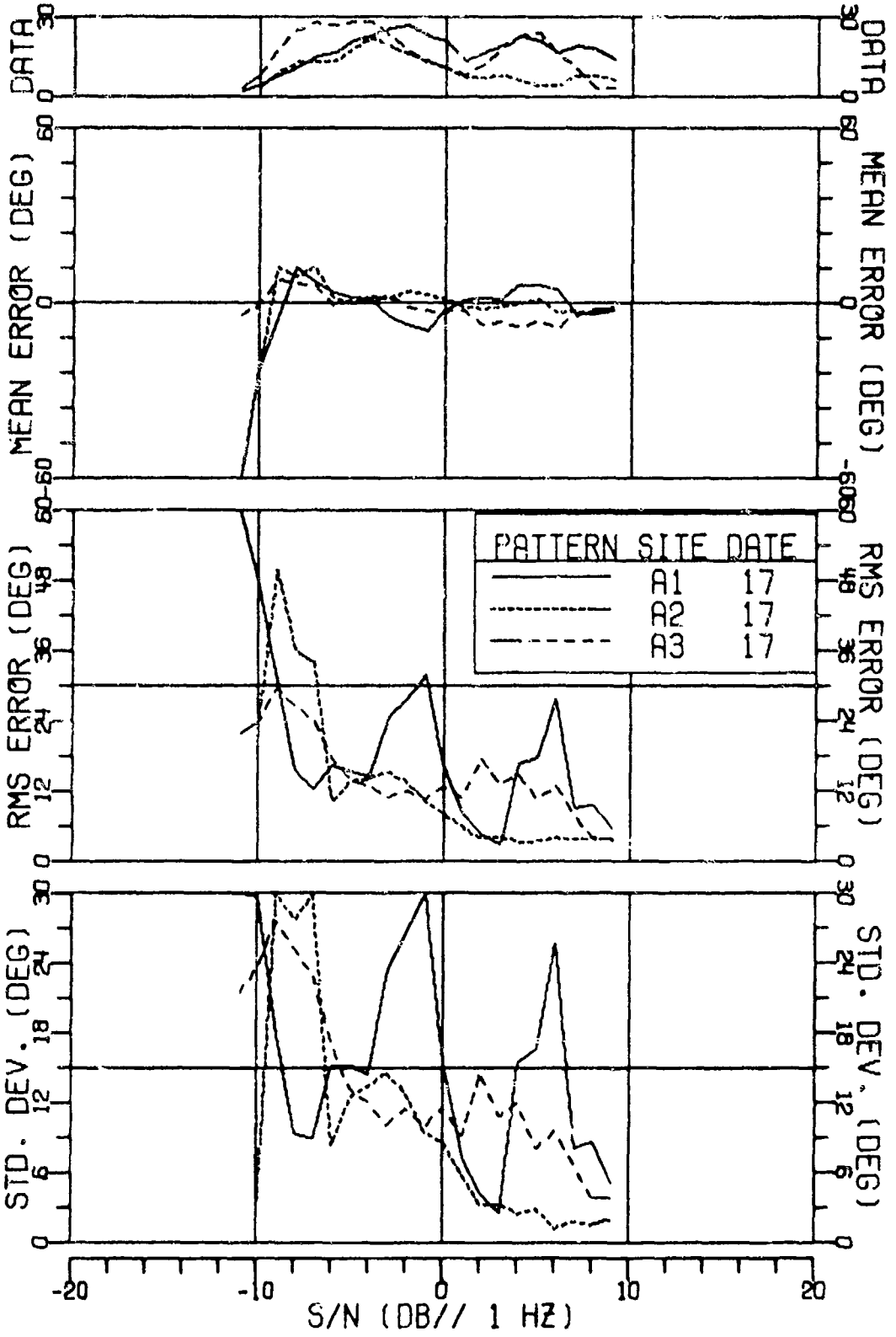

FIGURE II-242
MSS-FVT NEAR BOTTOM DIFFERENCED CARDIOIDS SENSOR BEARING ERROR RESULTS FOR 260HZ AT 147DB (U)

AS-77-3169

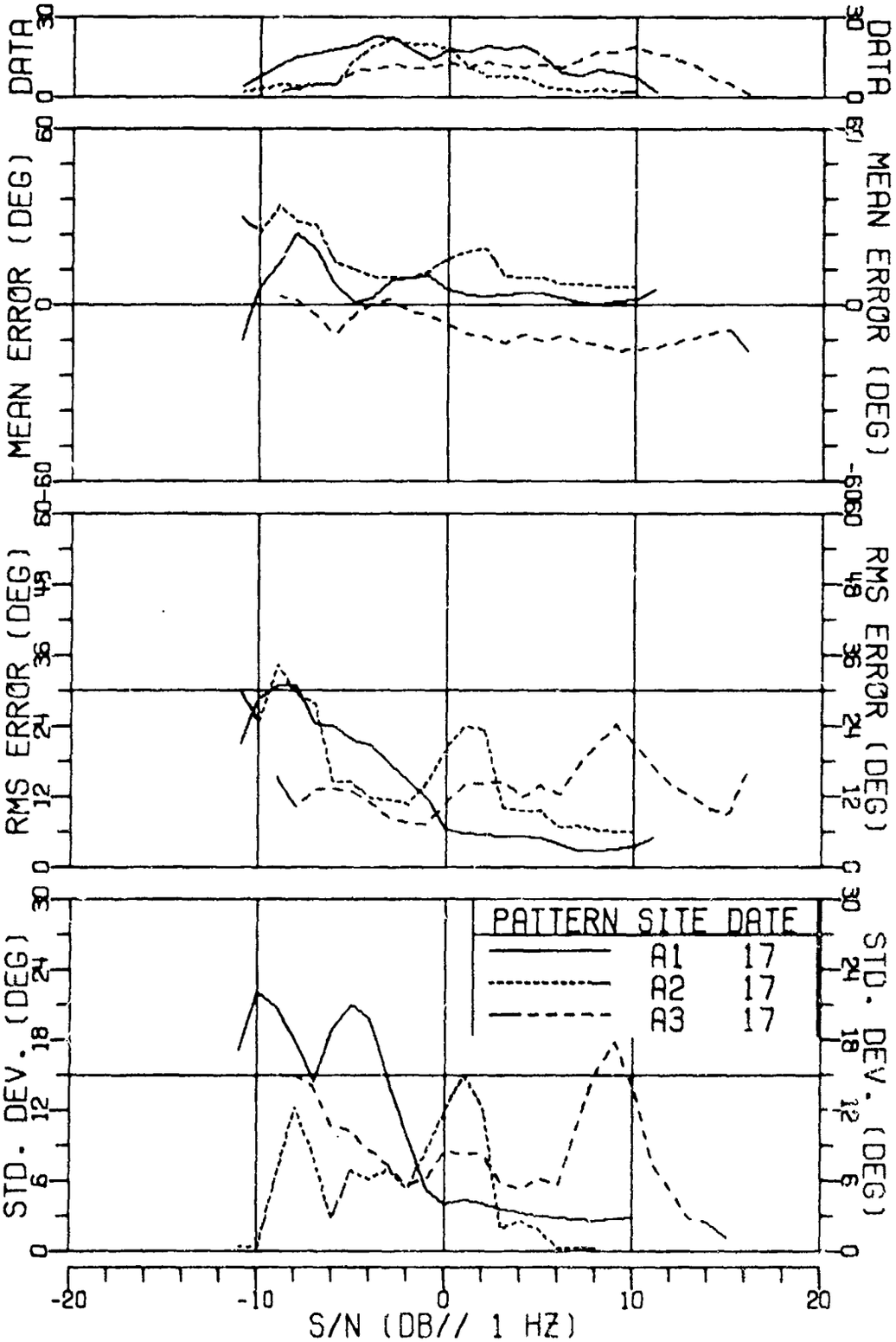

FIGURE II-243
MSS-FVT NEAR BOTTOM SINGLE CARDIOIDS SENSOR
BEARING ERROR RESULTS FOR 70HZ AT 166DB (U)

AS-77-3170

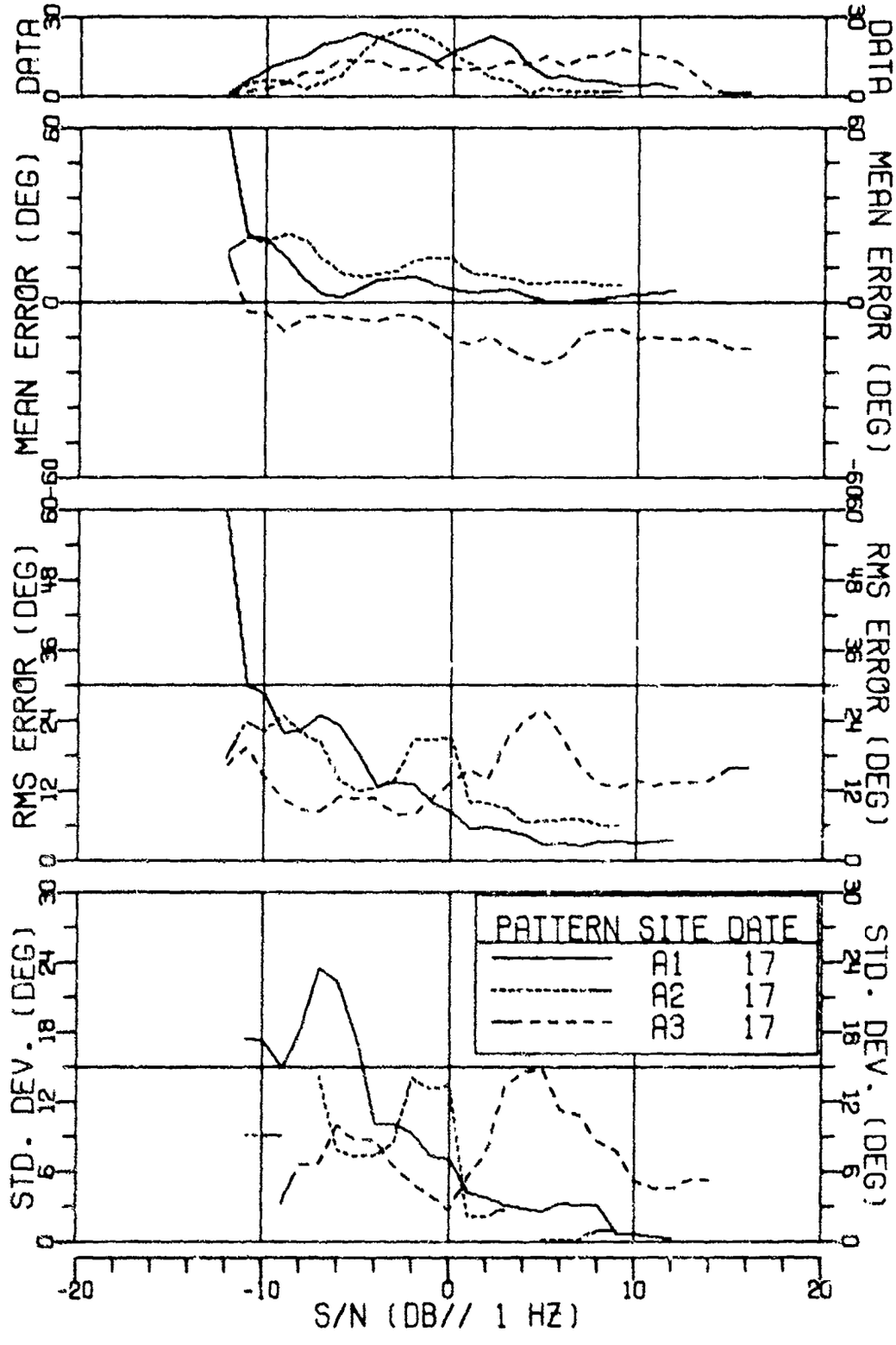

FIGURE II-244
MSS-FVT NEAR BOTTOM MAX GAIN LIMACONS SENSOR
BEARING ERROR RESULTS FOR 70HZ AT 166DB (U)

AS-77-3171

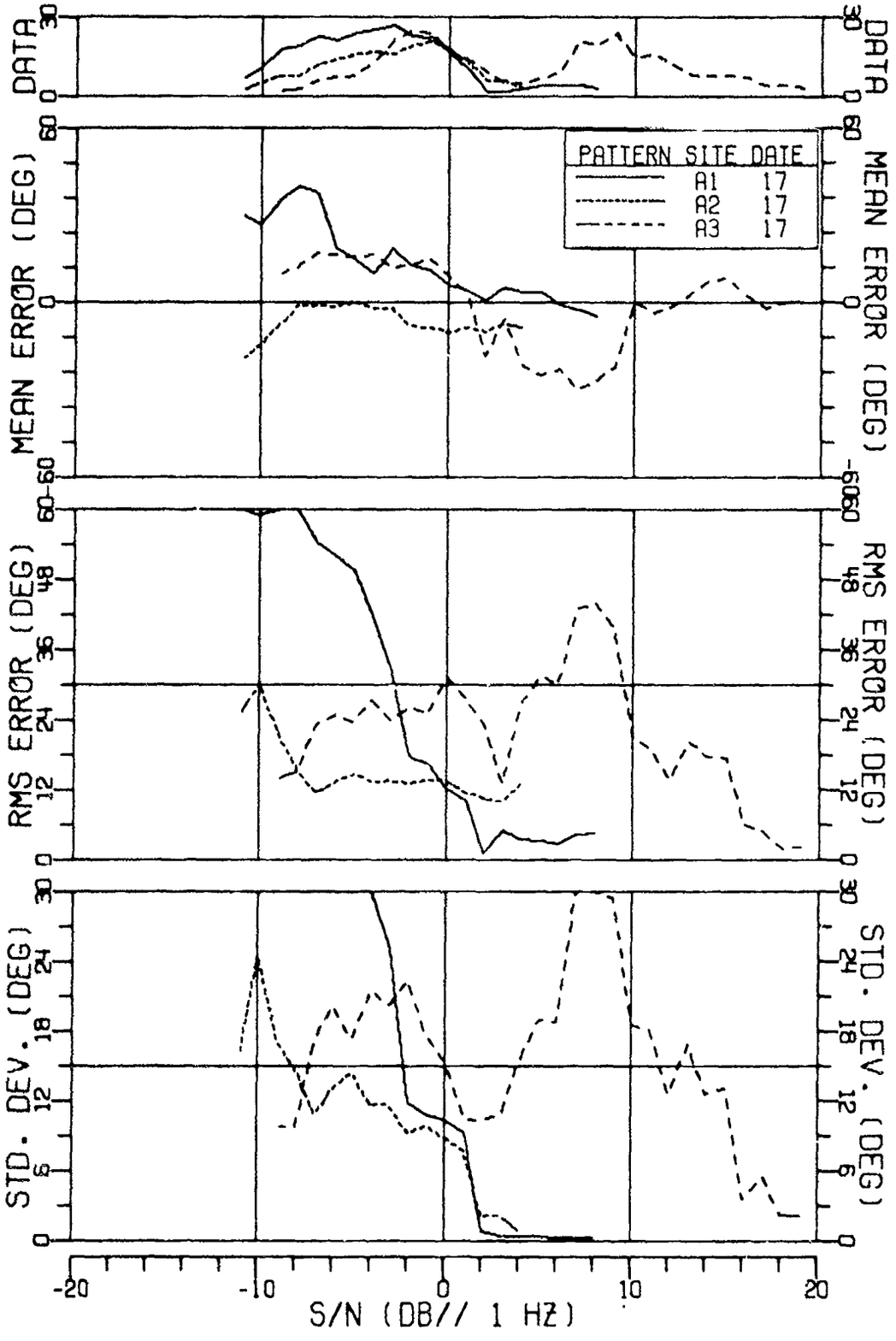

FIGURE II-245
MSS-FVT NEAR BOTTOM DIFFERENCED CARDIOIDS SENSOR BEARING ERROR RESULTS FOR 70HZ AT 166DB (U)

AS-77-3172

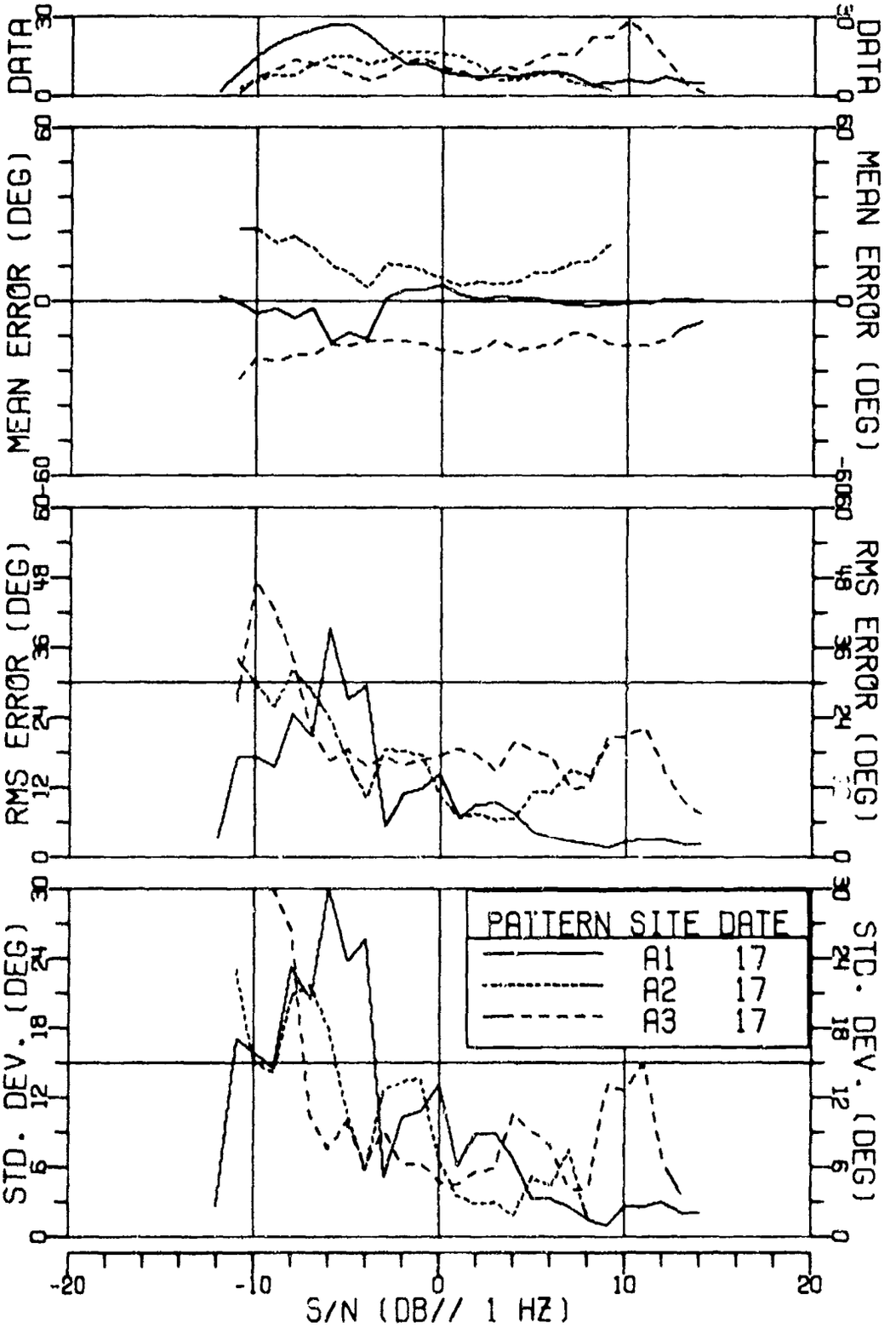

FIGURE II-246
MSS-FVT NEAR BOTTOM SINGLE CARDIOIDS SENSOR
BEARING ERROR RESULTS FOR 170HZ AT 156DB (U)

AS-77-3173

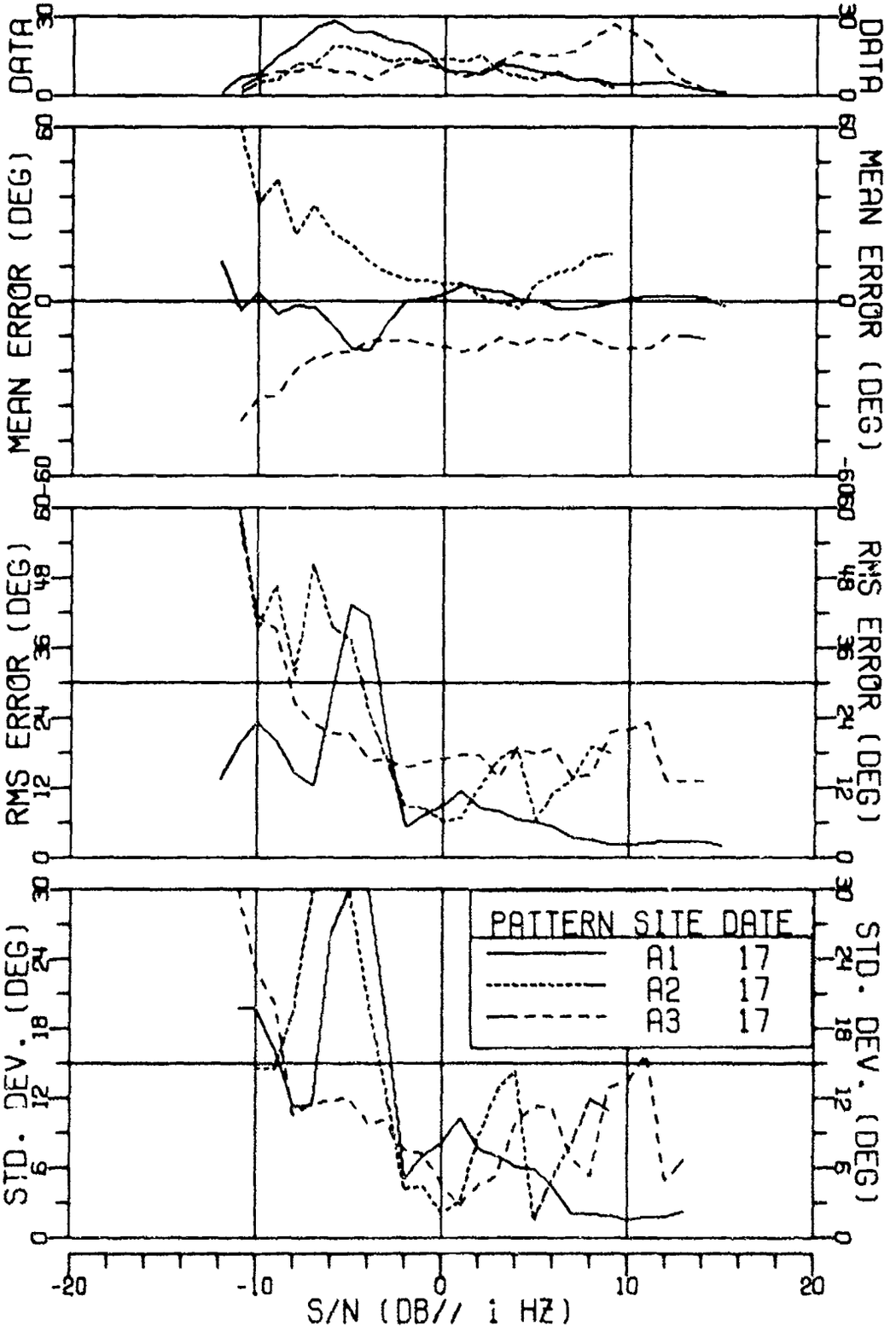

FIGURE II-247
MSS-FVT NEAR BOTTOM MAX GAIN LIMACONS SENSOR
BEARING ERROR RESULTS FOR 170HZ AT 1560 (U)

AS-77-3174

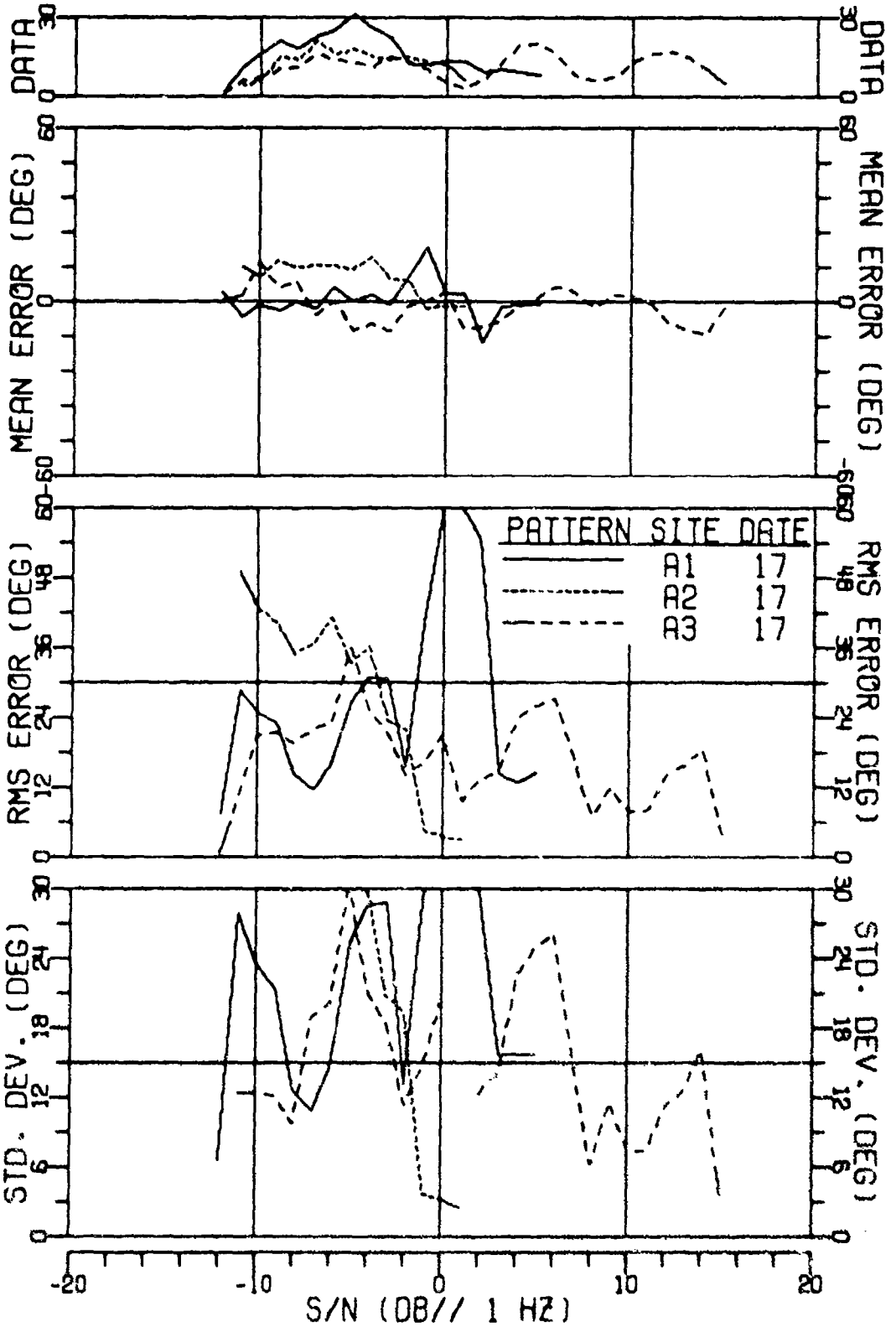

FIGURE II-248
MSS-FVT NEAR BOTTOM DIFFERENCED CARDIOIDS SENSOR BEARING ERROR RESULTS FOR 170HZ AT 156DB (U)

AS-77-3175

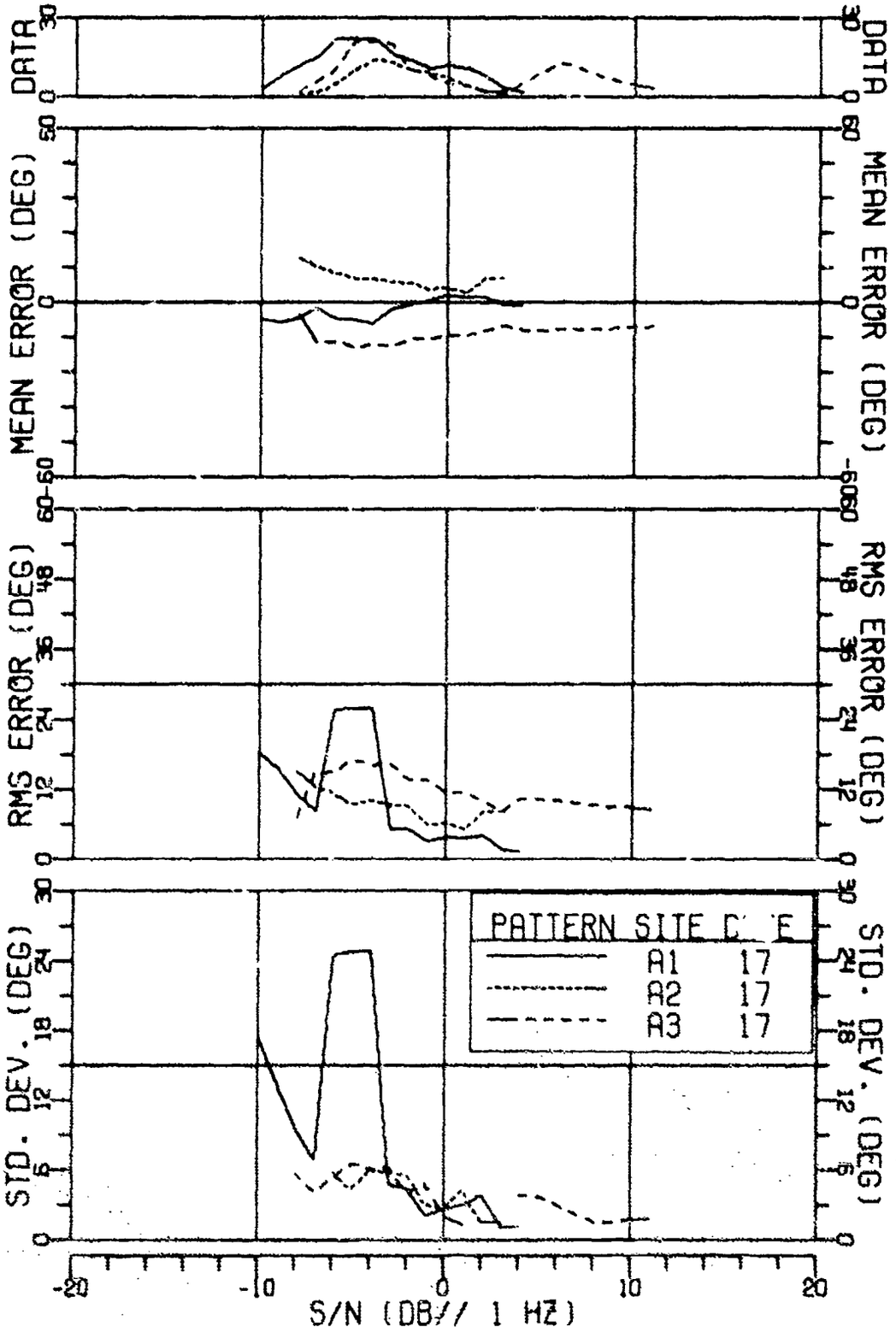

FIGURE II-249
MSS-FVT NEAR BOTTOM SINGLE CARDIOIDS SENSOR
BEARING ERROR RESULTS FOR 335HZ AT 154DB (U)

AS-77-3176

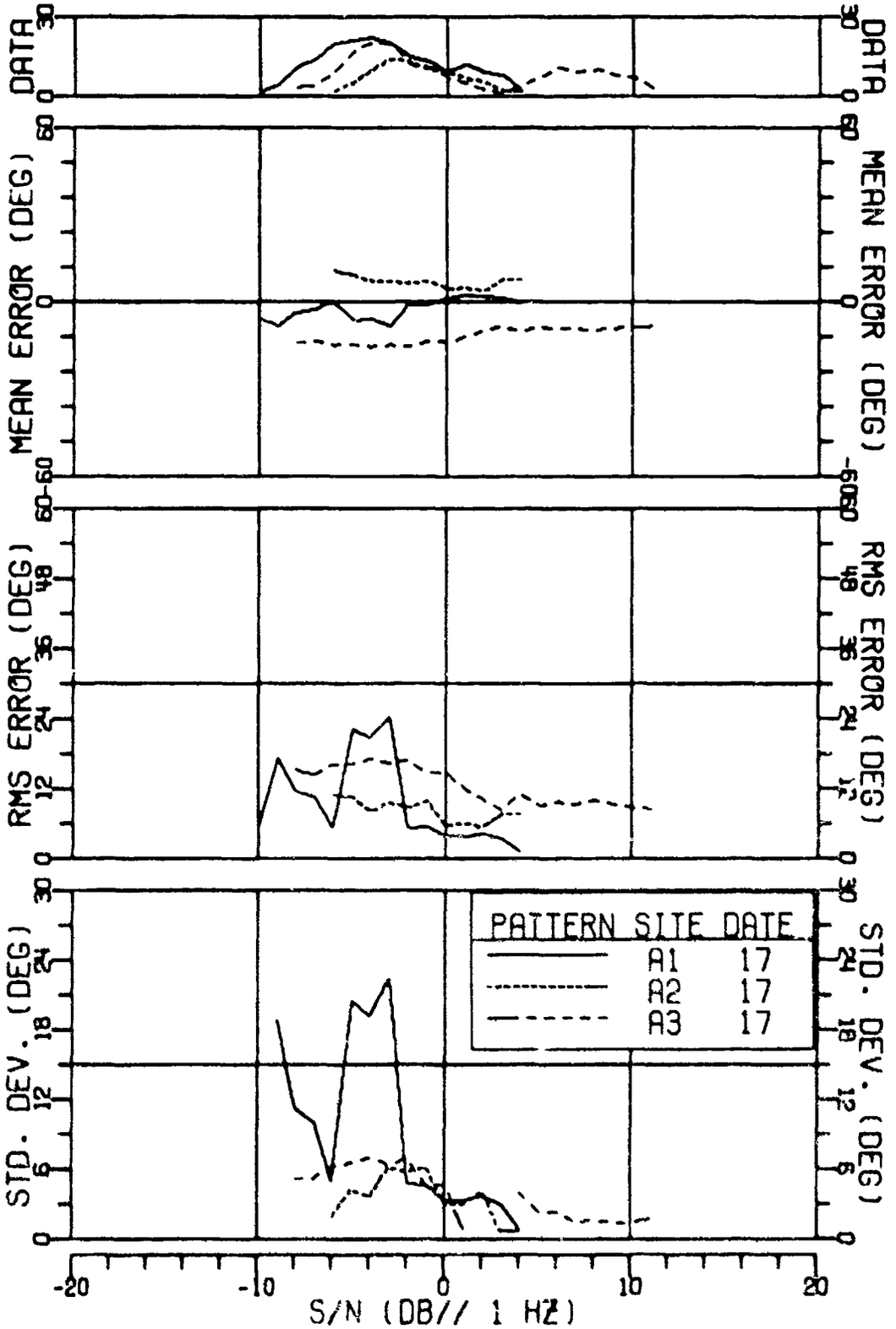

FIGURE II-250
MSS-FVT NEAR BOTTOM MAX GAIN LIMACONS SENSOR
BEARING ERROR RESULTS FOR 335HZ AT 154DB (U)

AS-77-3177

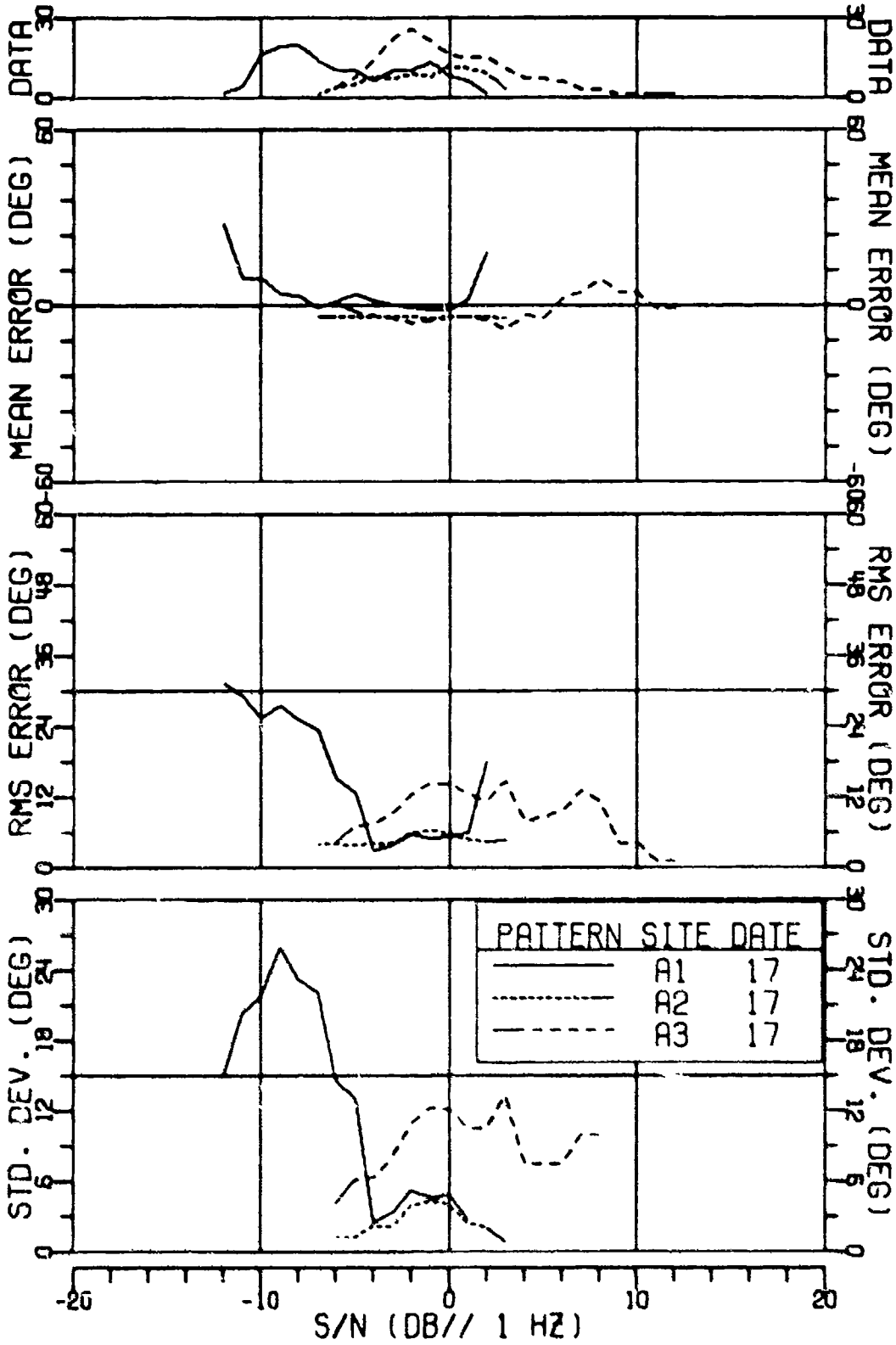

FIGURE II-251
MSS-FVT NEAR BOTTOM DIFFERENCED CARDIOIDS SENSOR BEARING ERROR RESULTS FOR 335HZ AT 154DB (U)

AS-77-3178

APPENDIX G

SIGNAL-TO-NOISE RATIO versus RANGE CURVES (U)

(FIGURES II-252 - II-294)

(The reverse of this page is blank.)

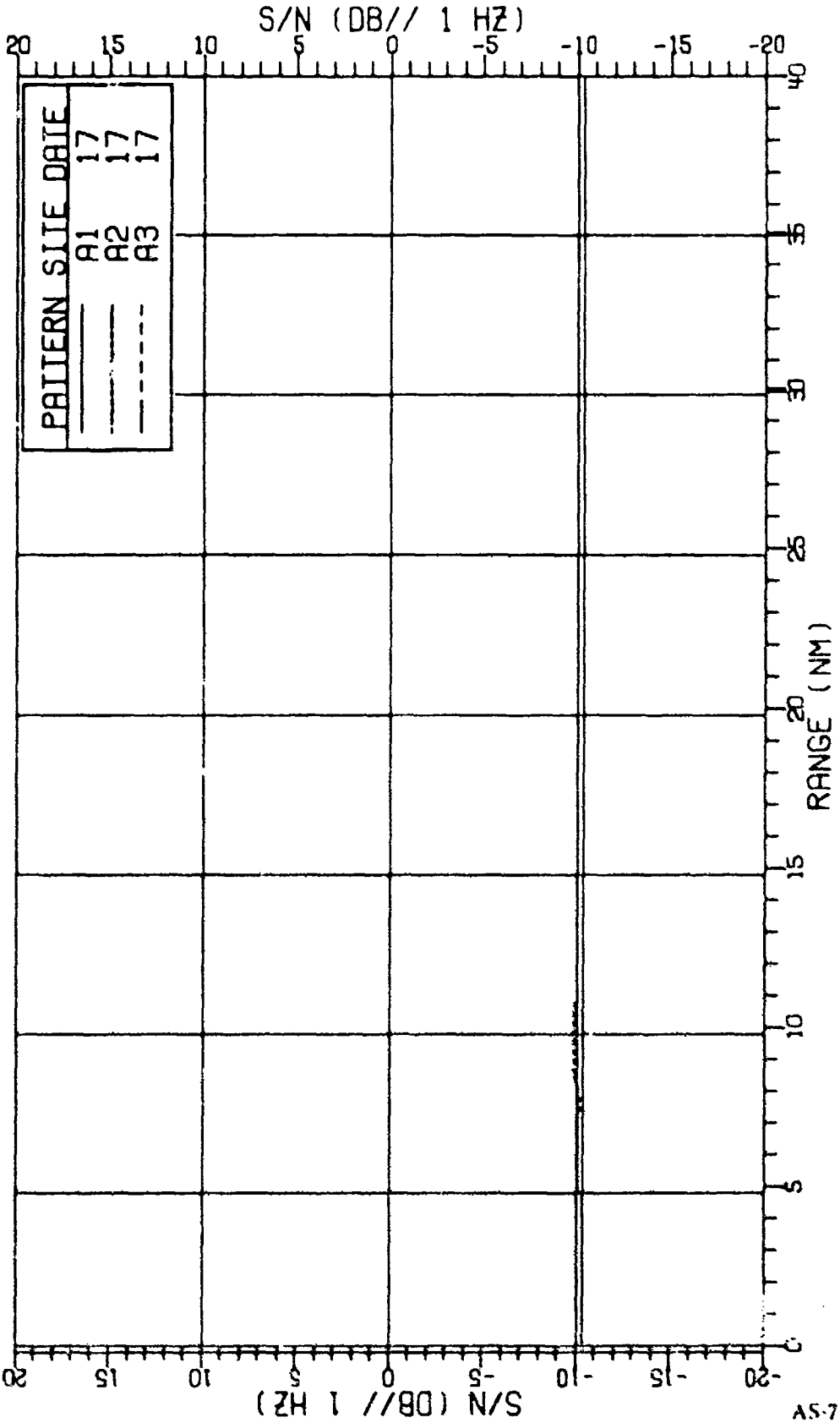

FIGURE II-252
MSS-FVT NEAR BOTTOM MAX GAIN LIMACONS SENSOR
SIGNAL-TO-NOISE RESULTS FOR 5SHZ AT 141DB (U)

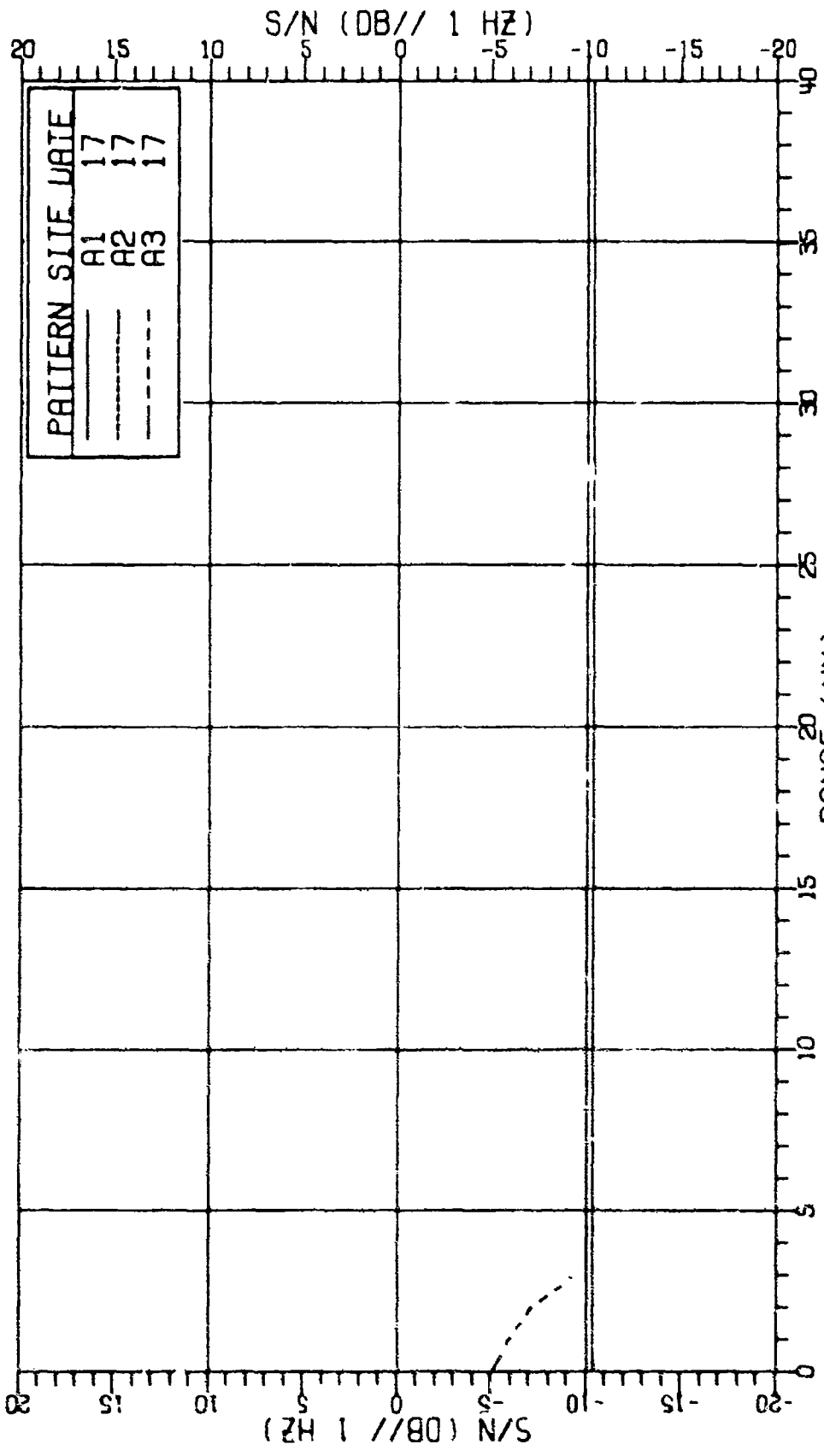

FIGURE II-253
MSS-FVT NEAR BOTTOM VERTICAL DIPOLE SENSOR
SIGNAL-TO-NOISE RESULTS FOR 55HZ AT 141DB (U)

AS-77-3180

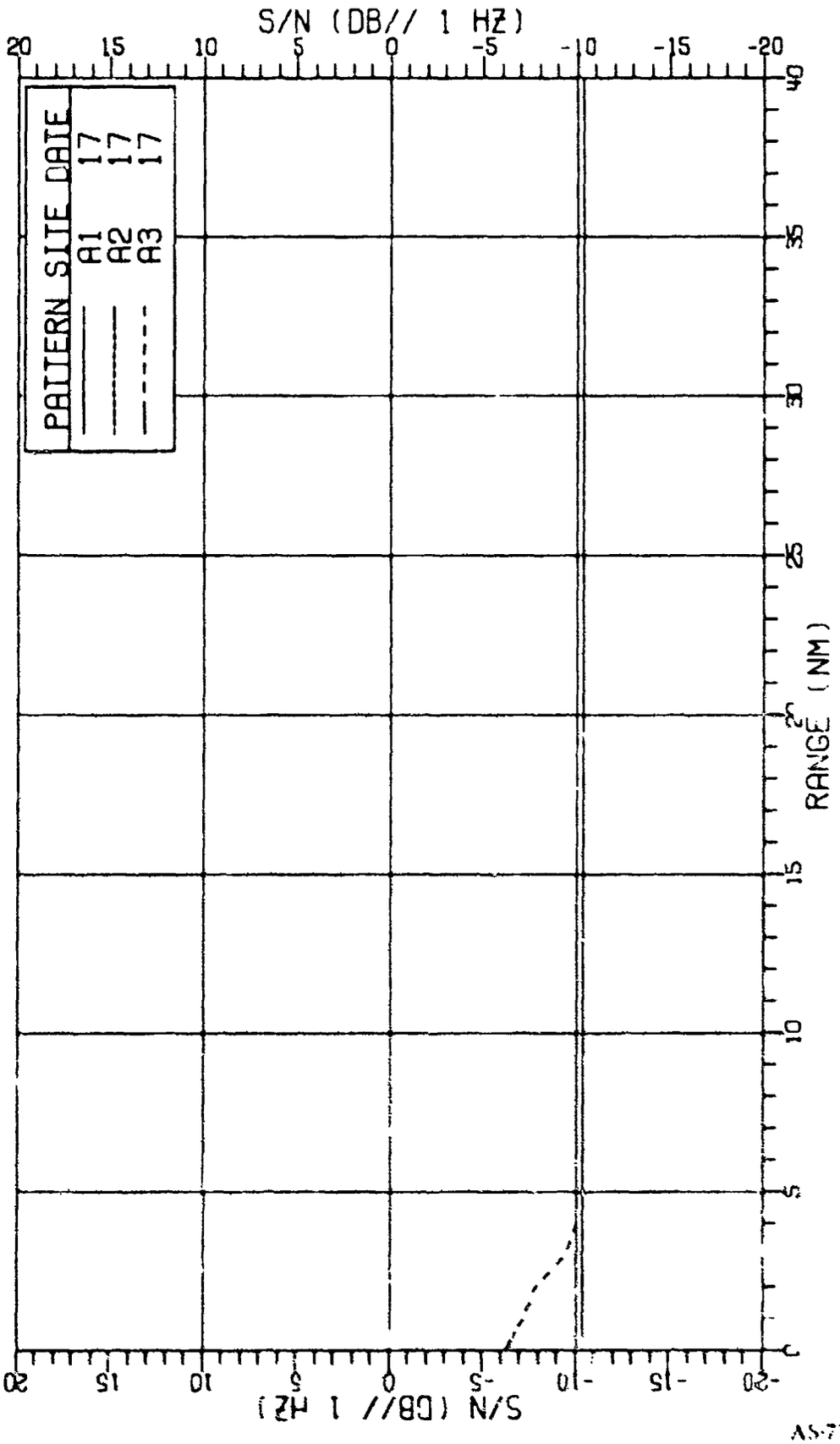

FIGURE II-254
MSS-FVT NEAR BOTTOM DIFFERENCED CARDIOIDS SENSOR
SIGNAL-TO-NOISE RESULTS FOR 55HZ AT 14.1DB (U)

AS-77-3181

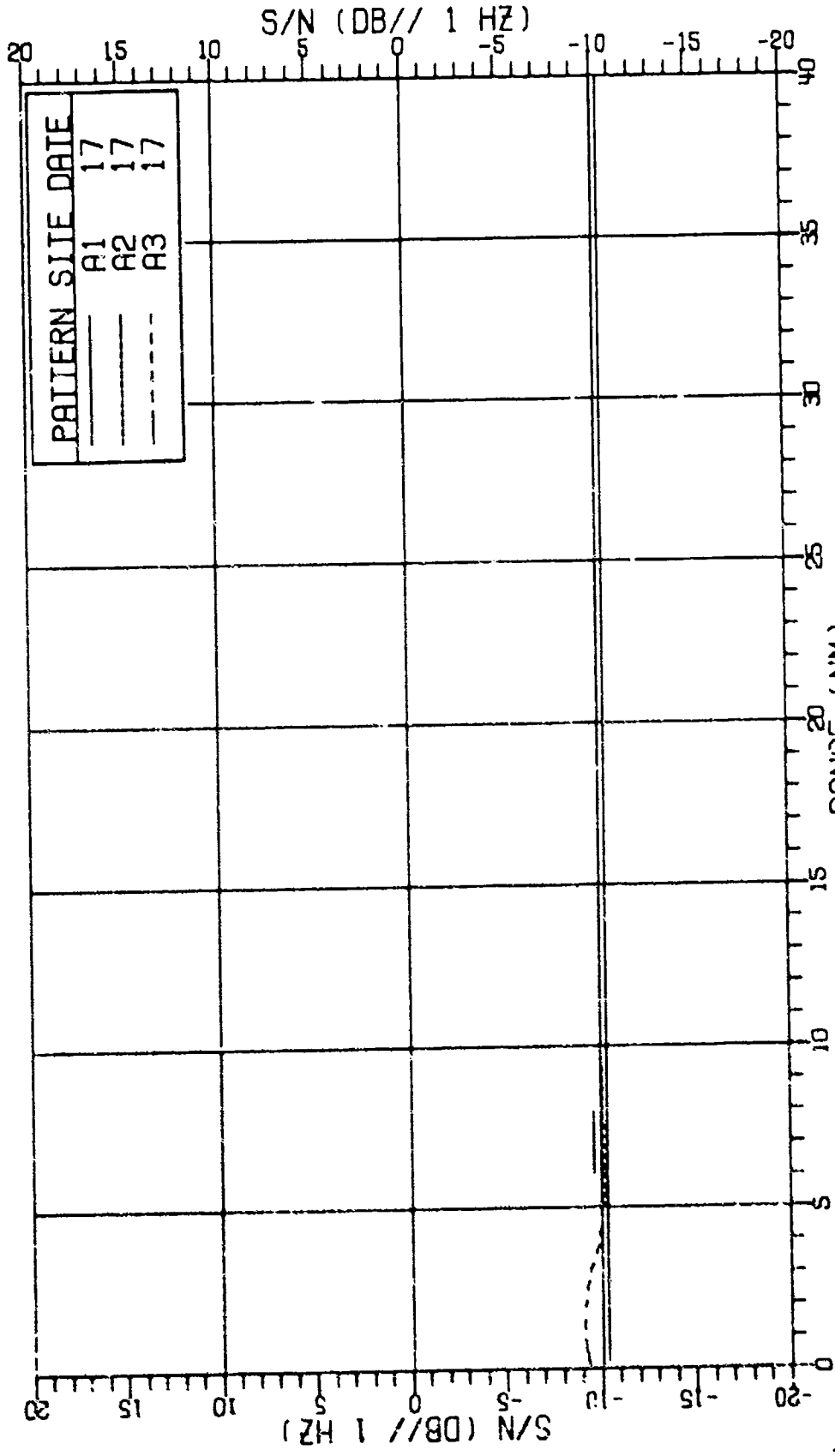

FIGURE II-255
MSS-FVT NEAR BOTTOM OMNIDIRECTIONAL SENSOR
SIGNAL-TO-NOISE RESULTS FOR 155HZ AT 134DB (U)

AS-77-3182

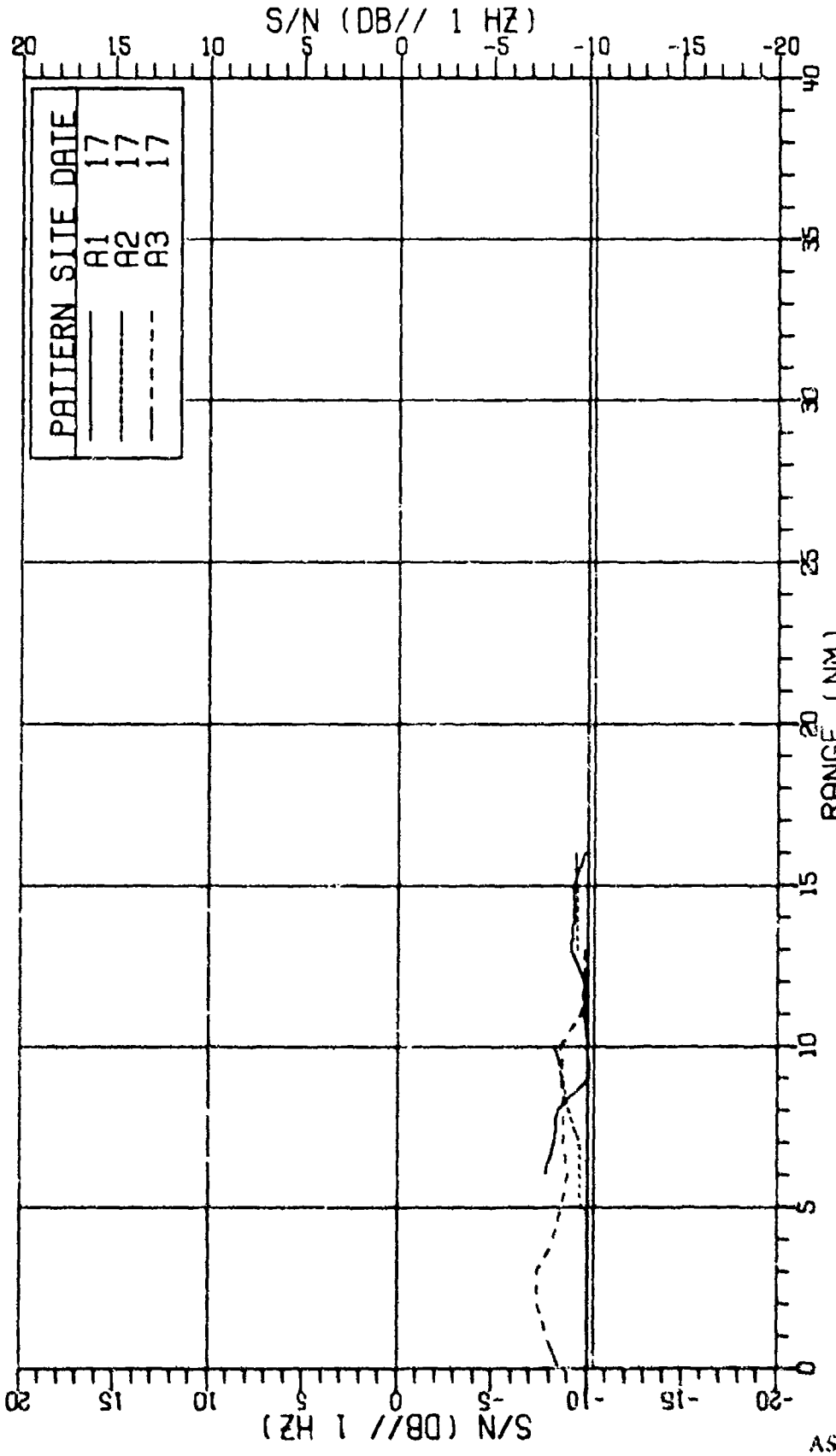

FIGURE II-256
MSS-FVT NEAR BOTTOM SINGLE CARDIOIDS SENSOR
SIGNAL-TO-NOISE RESULTS FOR 155HZ AT 134DB (U)

AS-77-3183

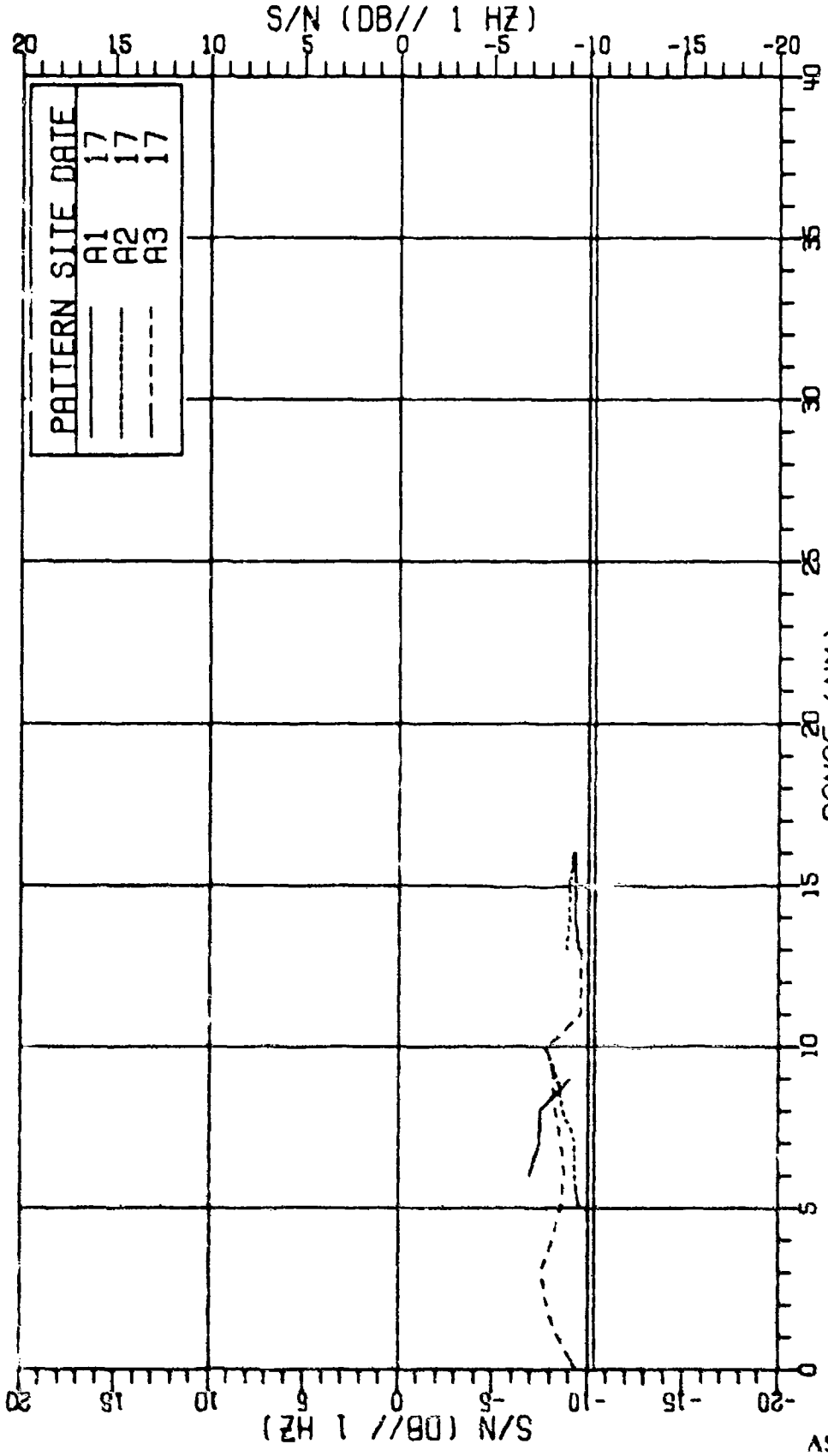

FIGURE II-25
MSS-FVT NEAR BOTTOM MAX GAIN LIMACONS SENSOR
SIGNAL-TO-NOISE RESULTS FOR 155HZ AT 134DB (U)

AS-77-3184

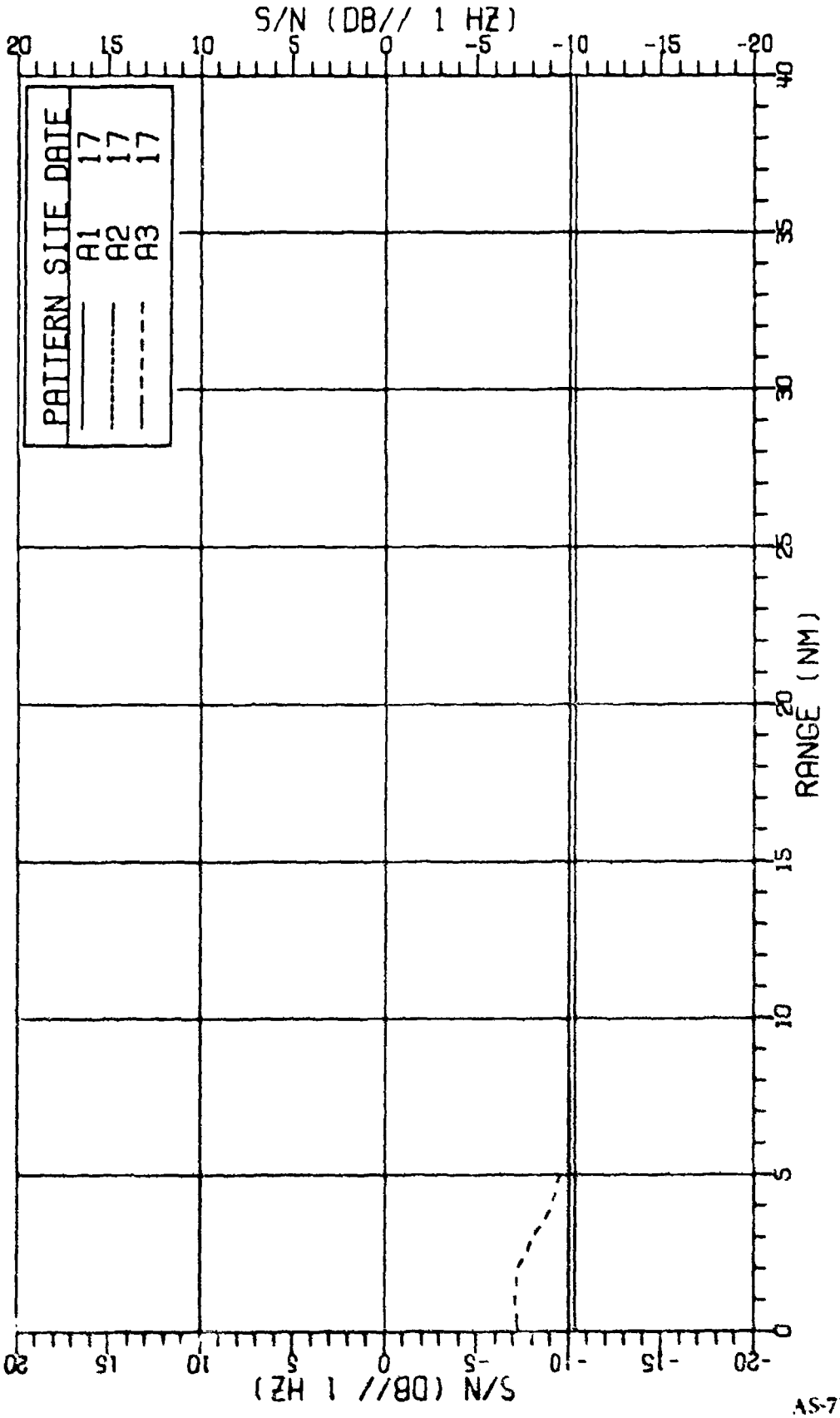

FIGURE II-258
MSS-FVT NEAR BOTTOM VERTICAL DIPOLE SENSOR
SIGNAL-TO-NOISE RESULTS FOR 155HZ AT 134DB (U)

AS-77-3185

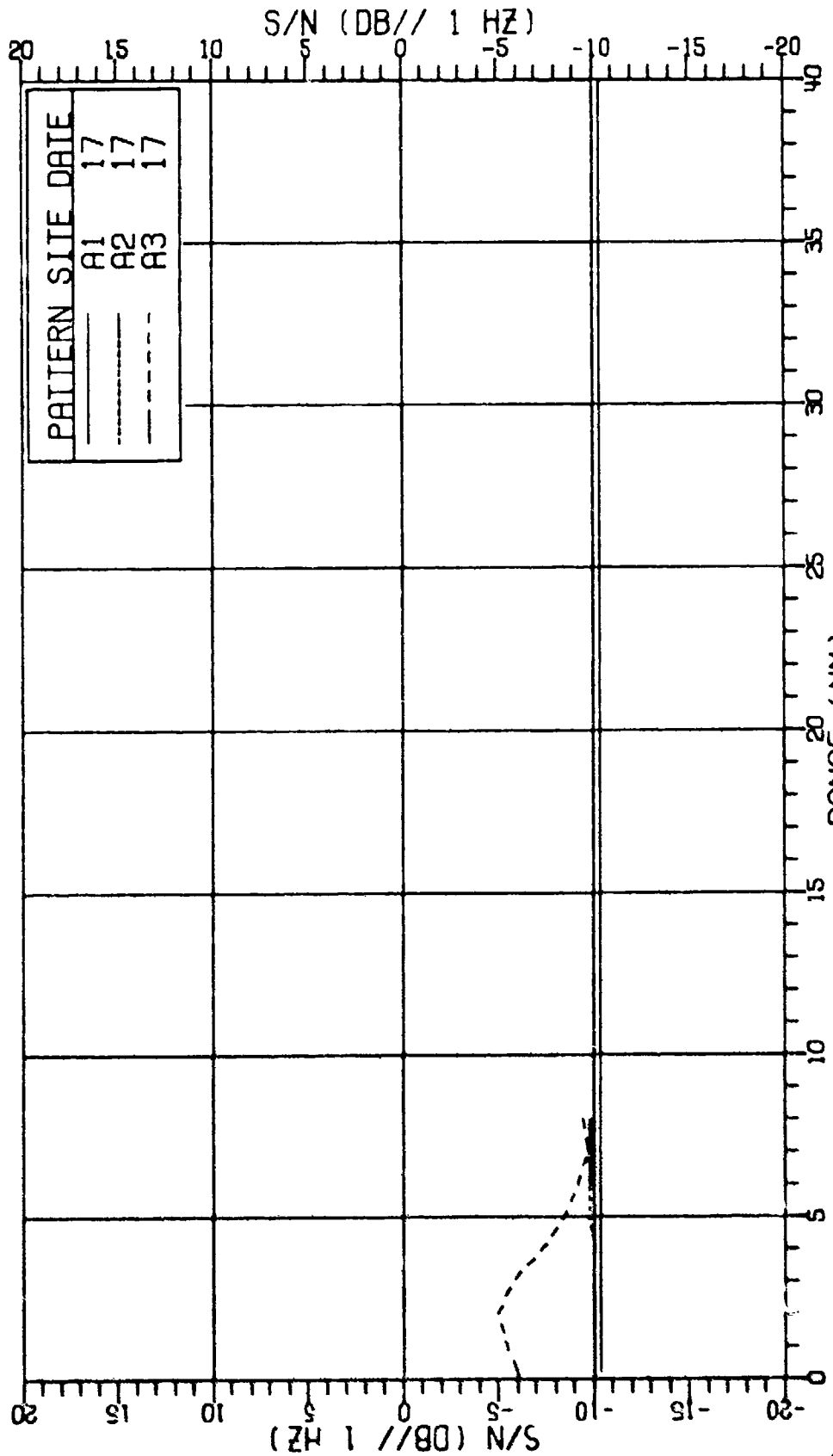

FIGURE II-259
MSS-FVT NEAR BOTTOM DIFFERENCED CARDIOIDS SENSOR
SIGNAL-TO-NOISE RESULTS FOR 155HZ AT 134DB (U)

AS-77-3186

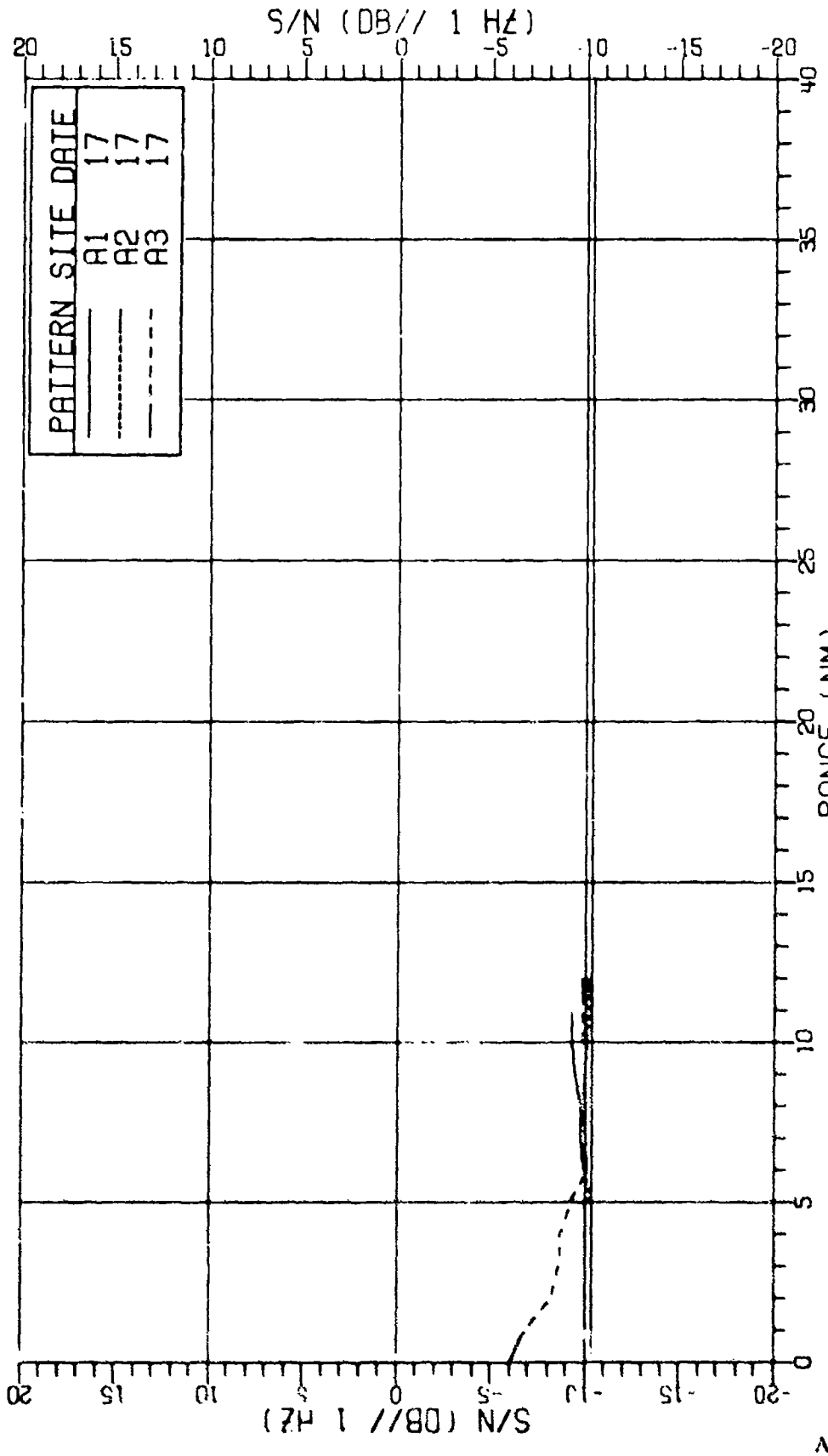

FIGURE II-260
MSS-FVT NEAR BOTTOM OMNIDIRECTIONAL SENSOR
SIGNAL-TO-NOISE RESULTS FOR 305HZ AT 136DB (U)

AS-77-3187

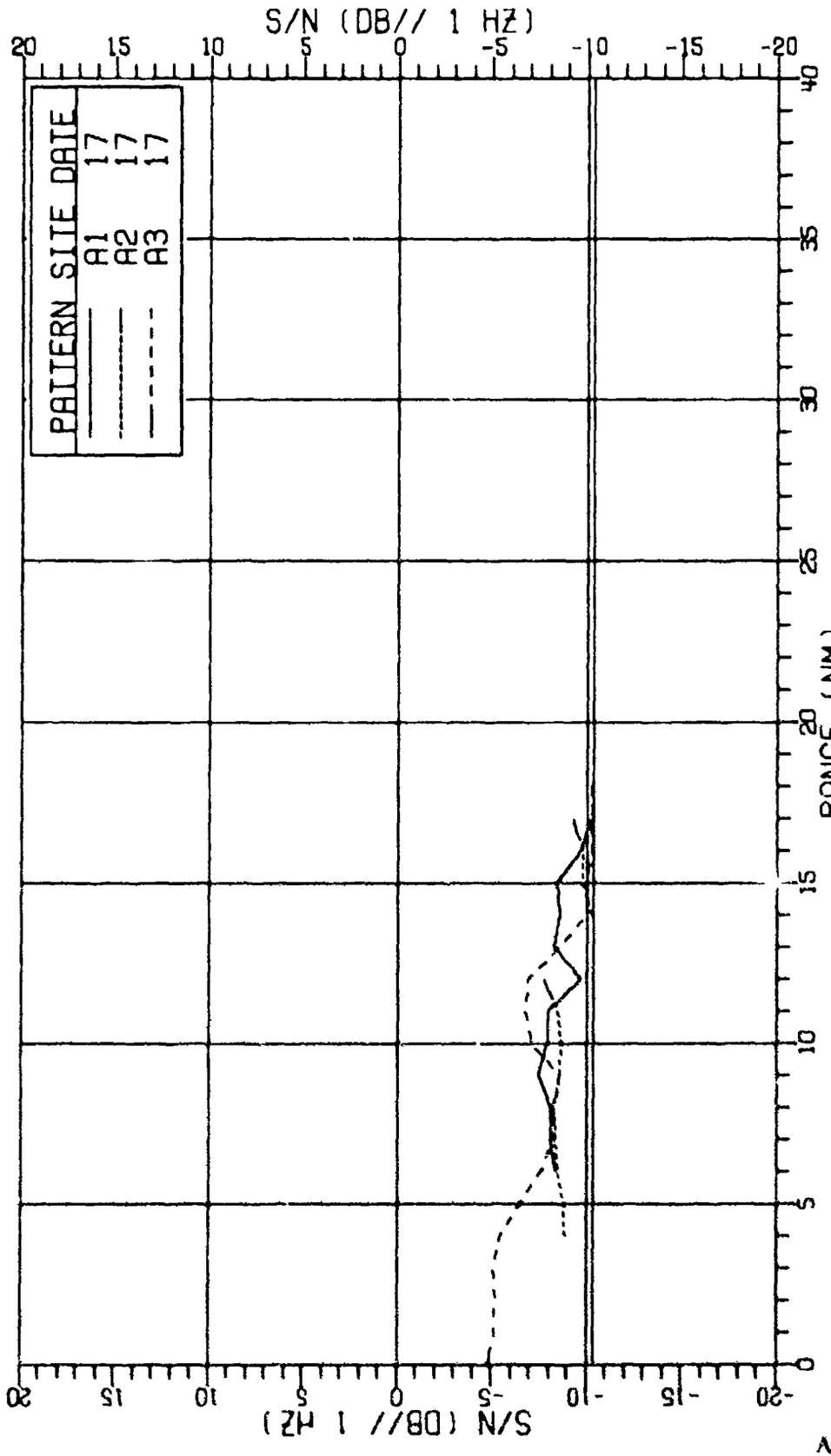

FIGURE II-261
MSS-FVT NEAR BOTTOM SINGLE CARDIOIDS SENSOR
SIGNAL-TO-NOISE RESULTS FOR 30SHZ AT 136DB (U)

AS-77-3188

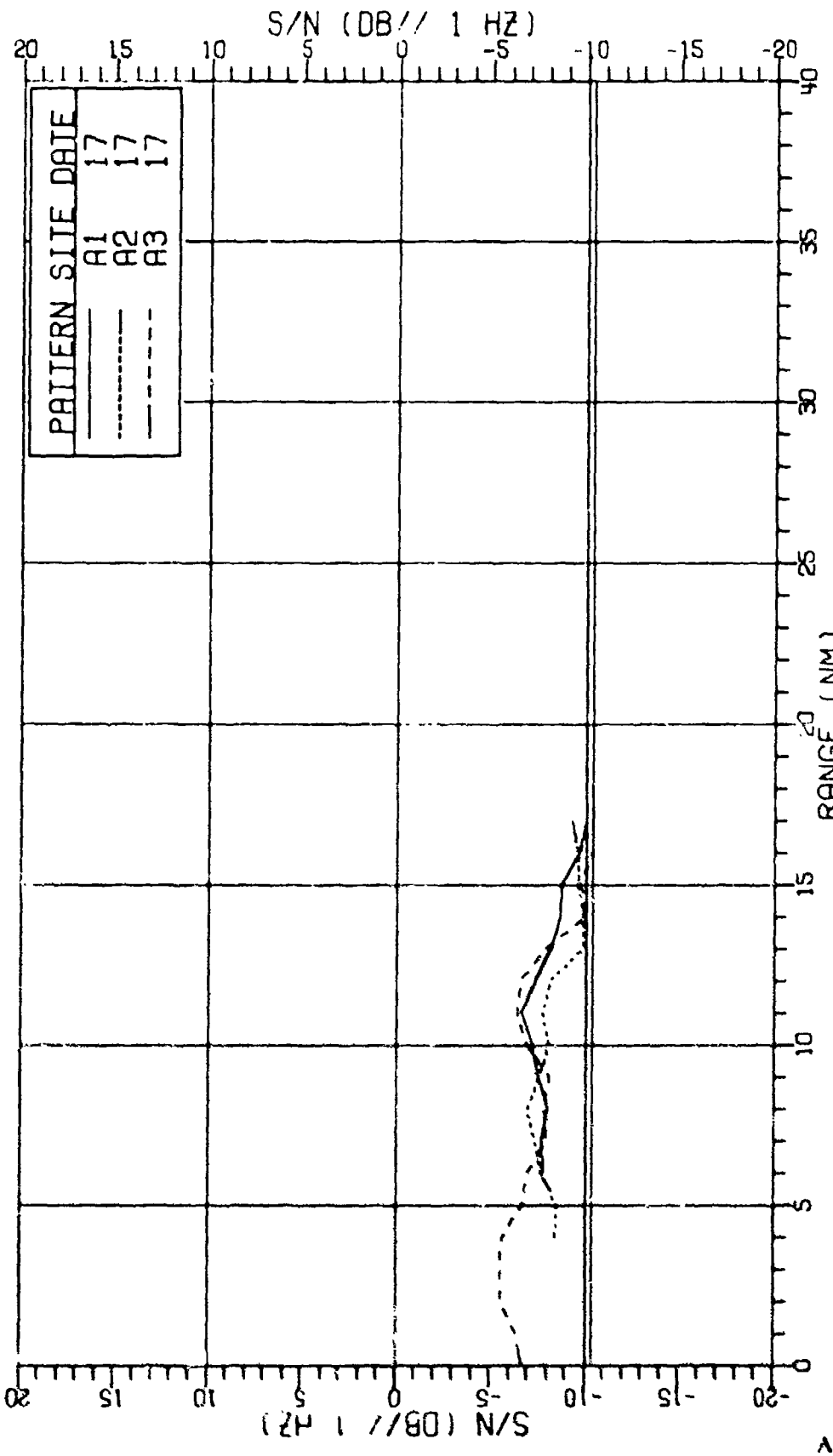

FIGURE II-262
MSS-FVT NEAR BOTTOM MAX GAIN LIMACONS SENSOR
SIGNAL-TO-NOISE RESULTS FOR 305HZ AT 136DB (U)

AS-77-3189

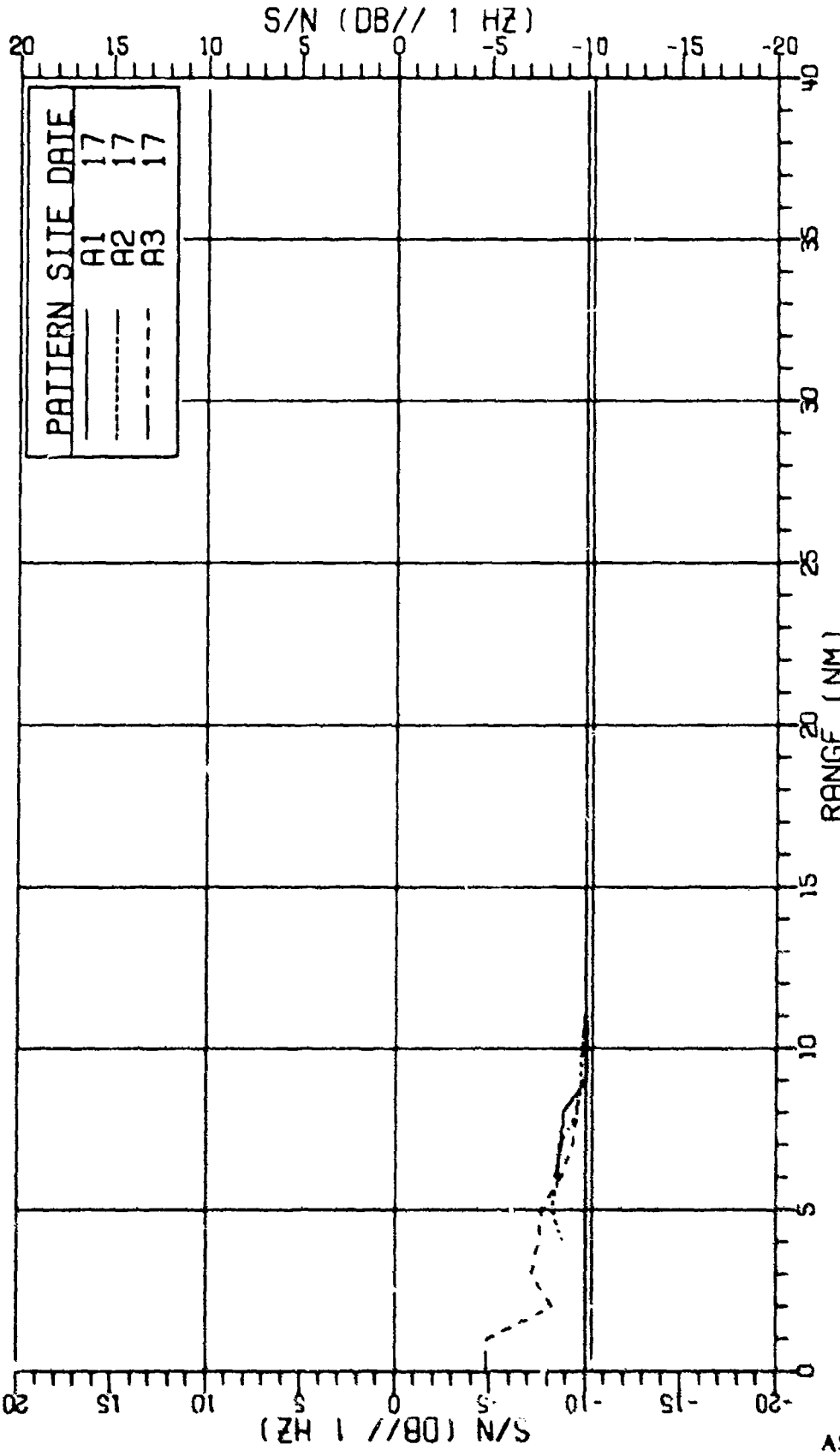

FIGURE II-263
MSS-FVT NEAR BOTTOM VERTICAL DIPOLE SENSOR
SIGNAL-TO-NOISE RESULTS FOR 30SHZ AT 136DB (U)

AS-77-3190

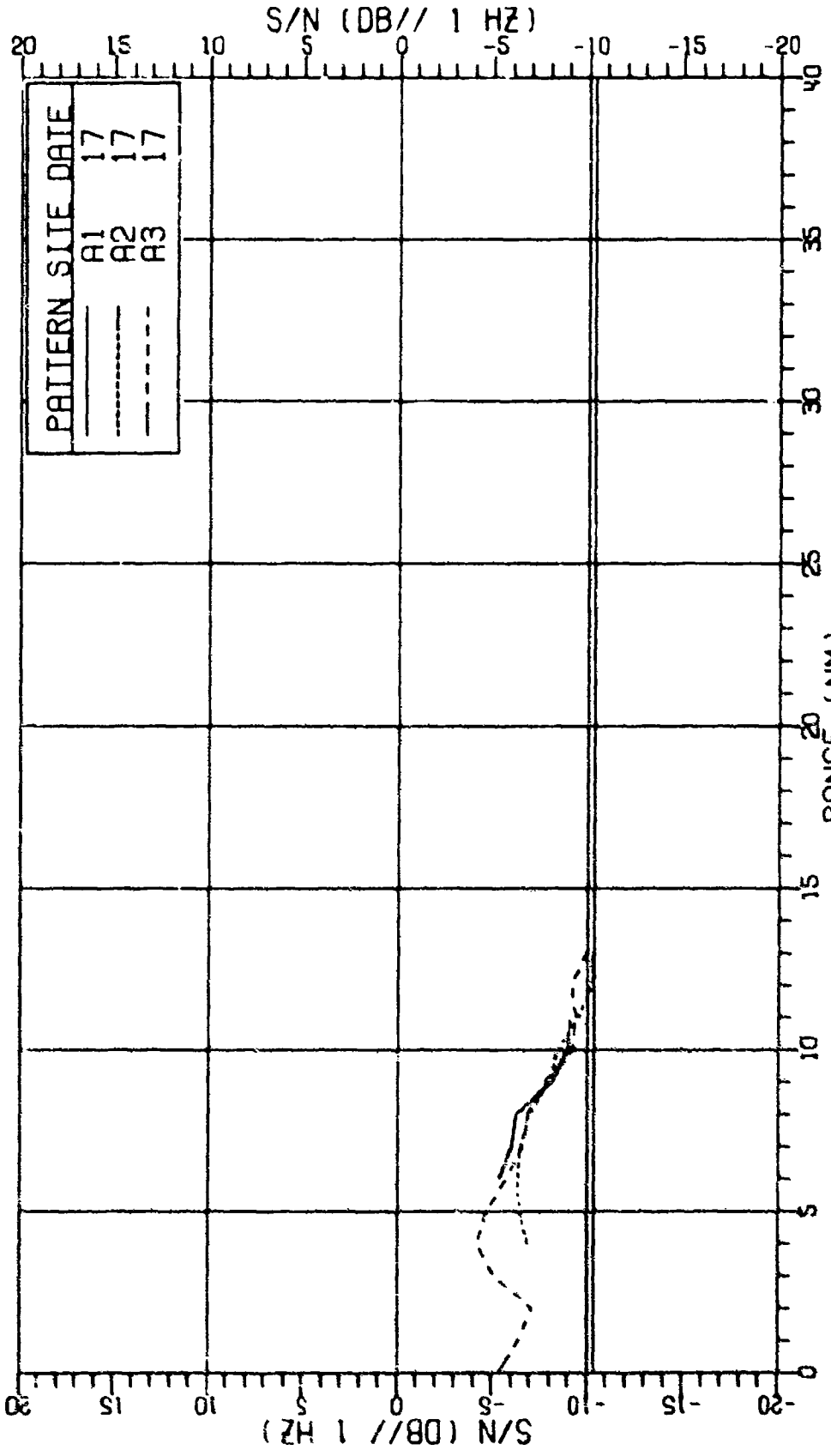

FIGURE II-264
MSS-FVT NEAR BOTTOM DIFFERENCED CARDIOIDS SENSOR
SIGNAL-TO-NOISE RESULTS FOR 305HZ AT 136DB (U)

AS-77-3191

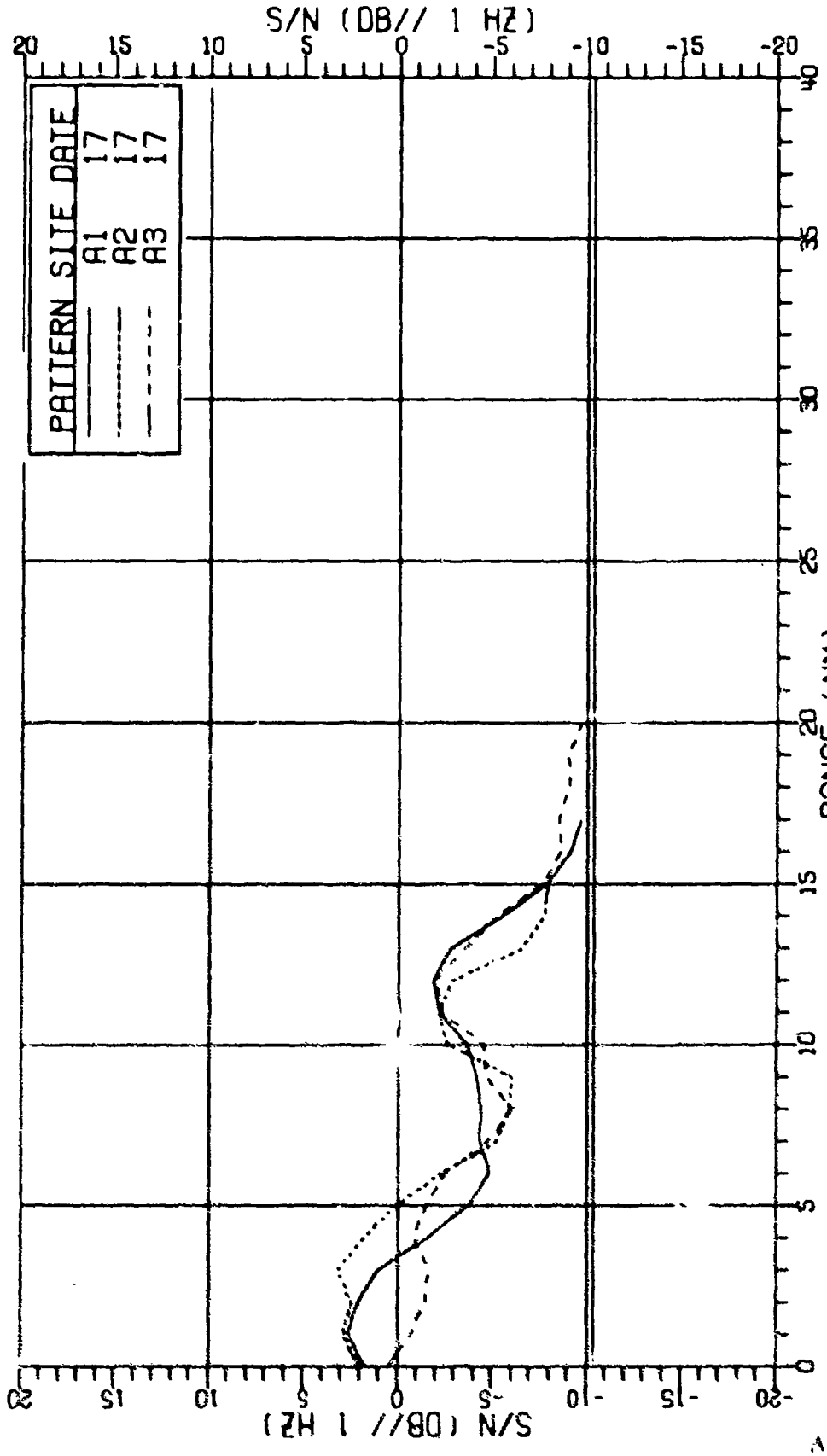

FIGURE II-265
MSS-FVT NEAR BOTTOM OMNIDIRECTIONAL SENSOR
SIGNAL-TO-NOISE RESULTS FOR 64HZ AT 1620B (U)

AS-77-3192

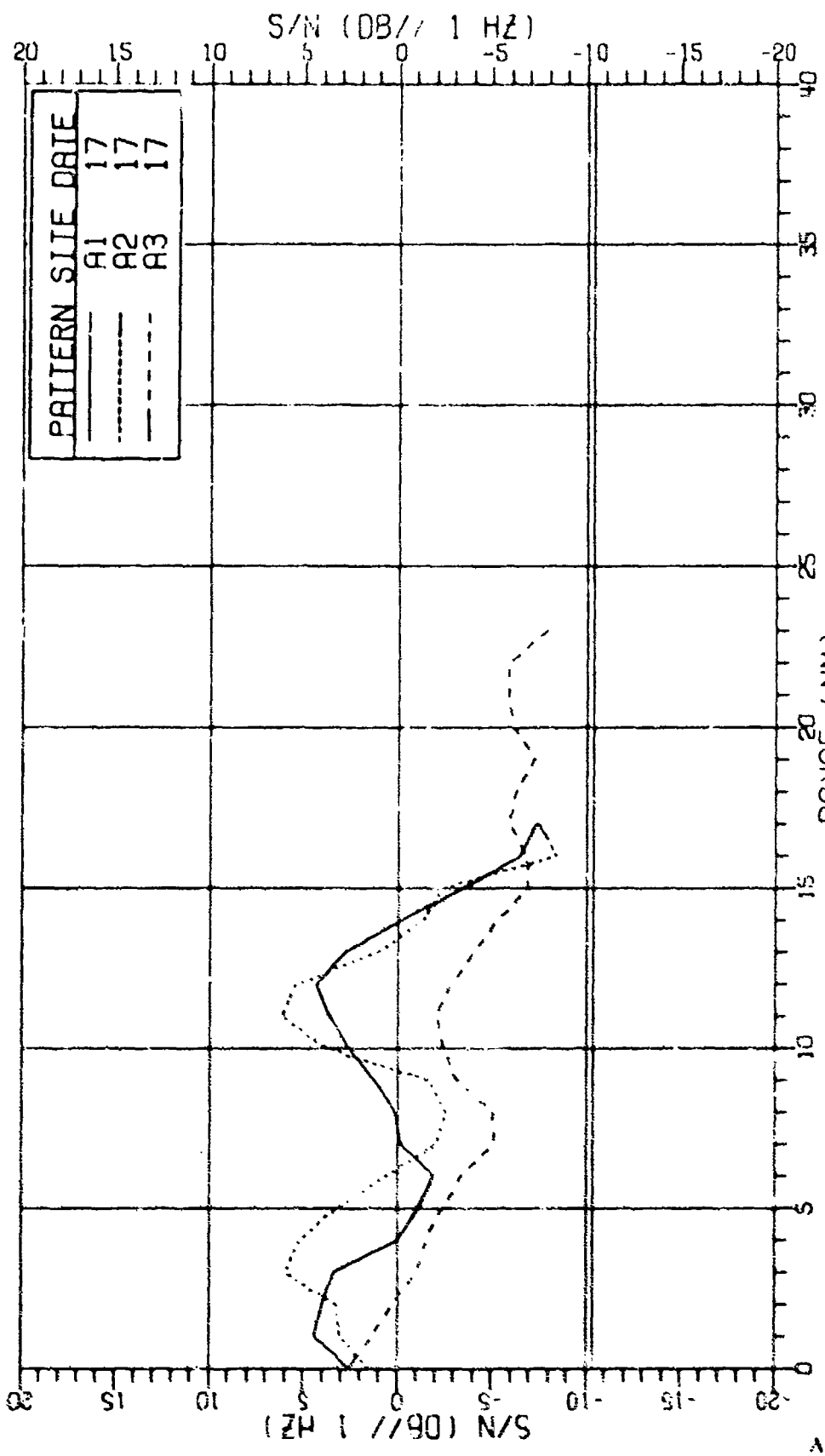

FIGURE II-266
MSS-FVT NEAR BOTTOM SINGLE CARDIOIDS SENSOR
SIGNAL-TO-NOISE RESULTS FOR 64HZ AT 1620B (U)

AS-77-3193

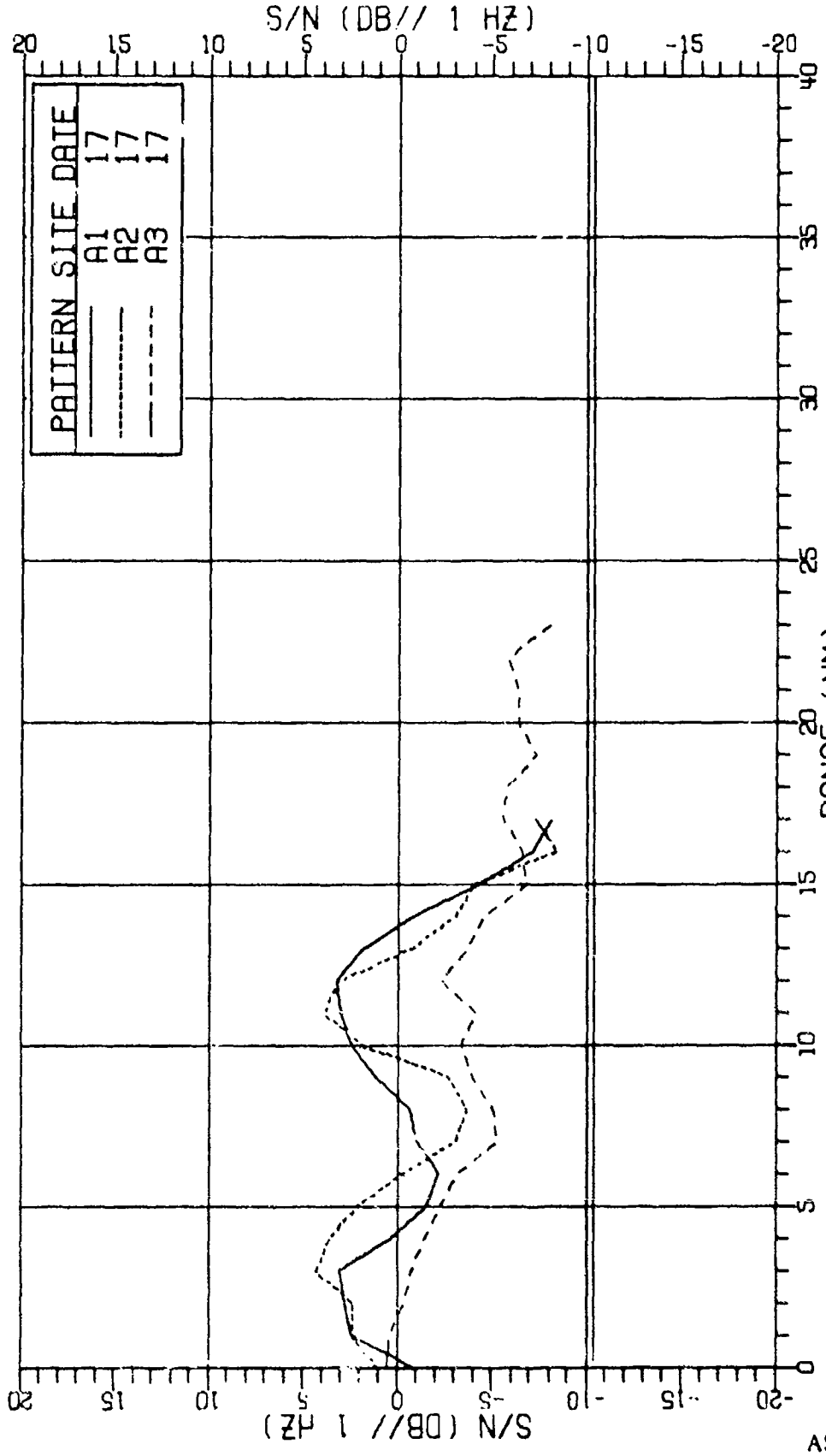

FIGURE II-267
MSS-FVT NEAR BOTTOM MAX GAIN LIMACONS SENSOR
SIGNAL-TO-NOISE RESULTS FOR 64HZ AT 152DB (U)

AS-77-3194

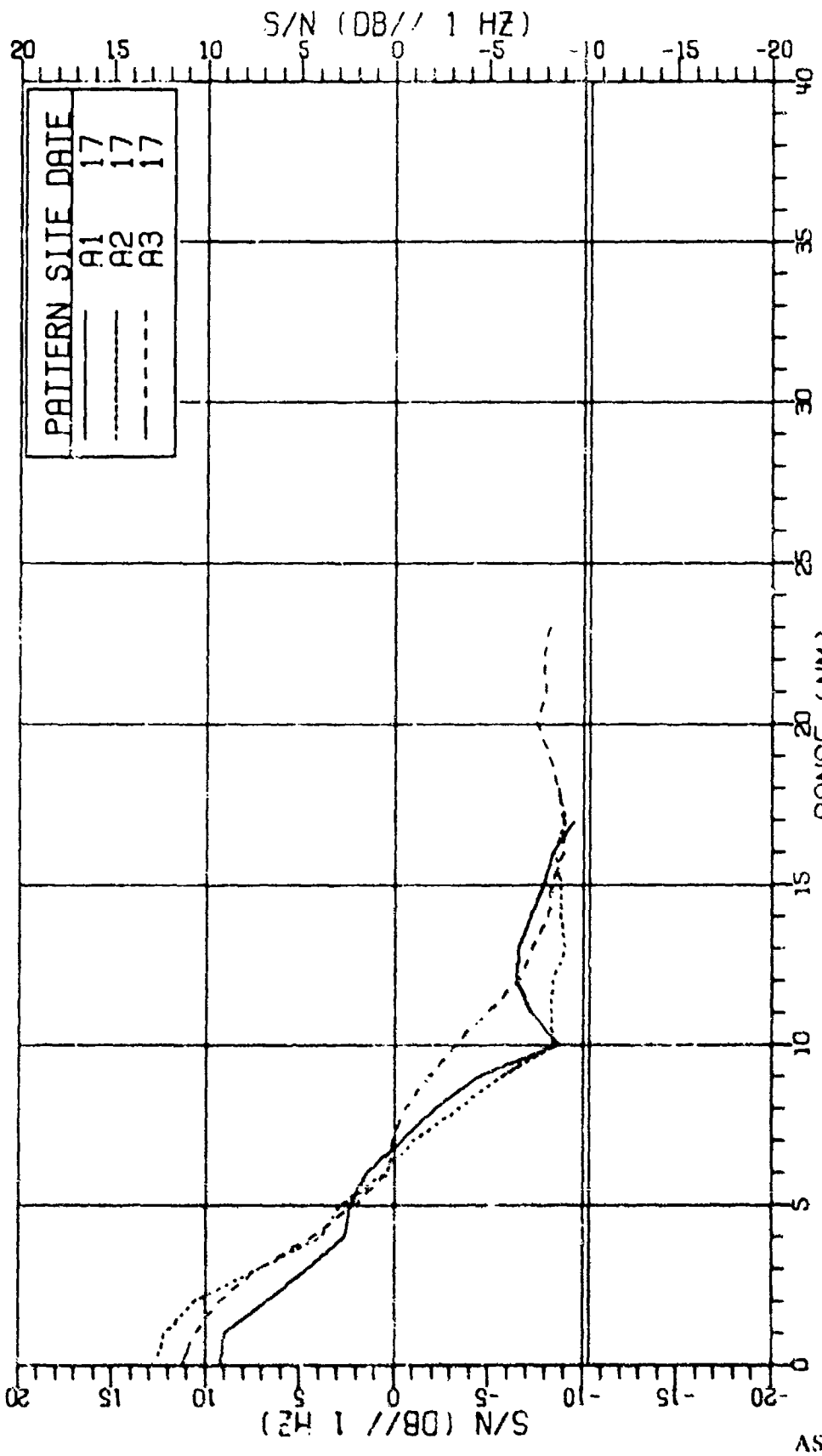

FIGURE II-268
MSS-FVT NEAR BOTTOM VERTICAL DIPOLE SENSOR
SIGNAL-TO-NOISE RESULTS FOR 64HZ AT 162DB (U)

AS-77-3195

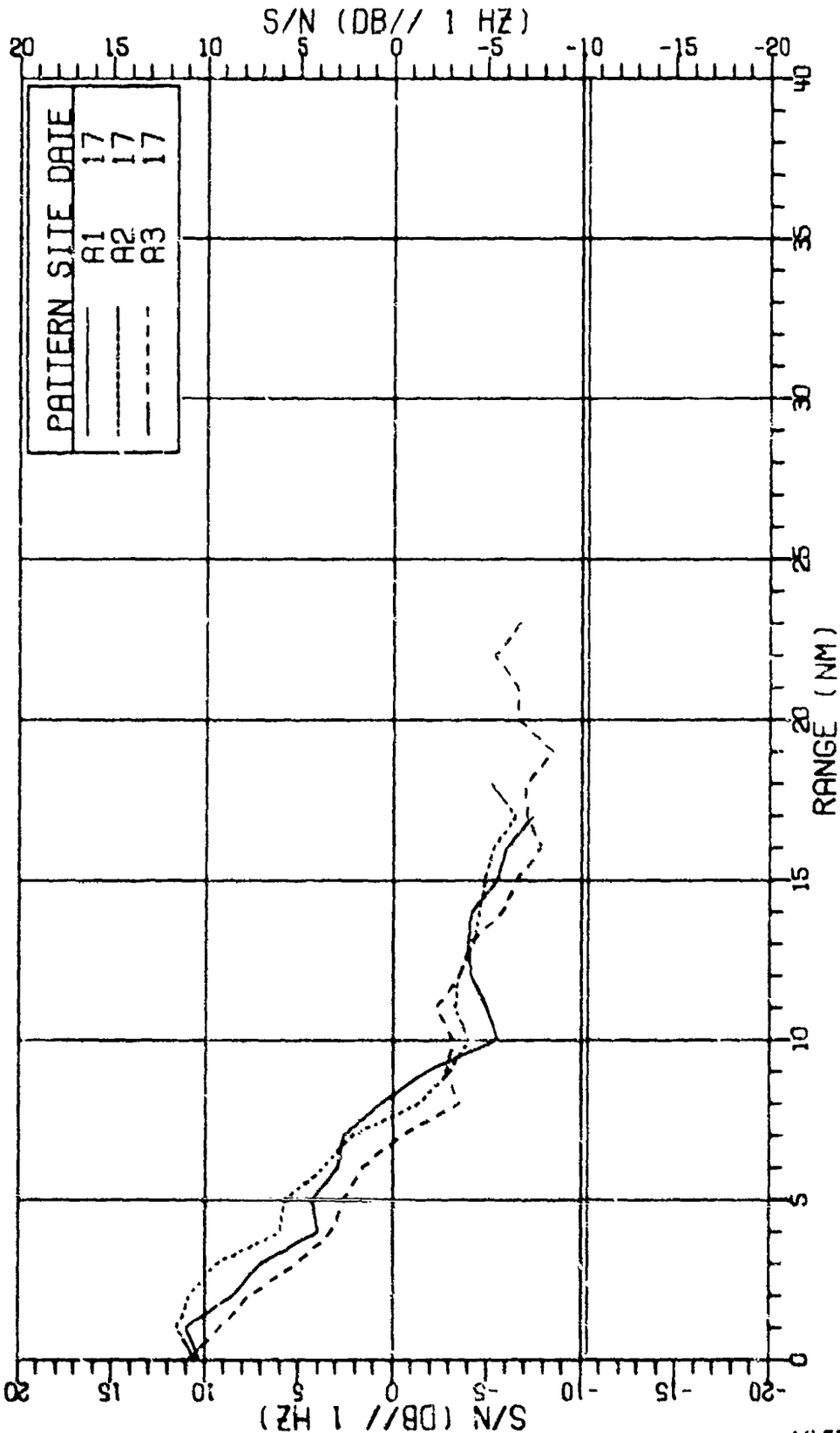

FIGURE II-269
MSS-FVT NEAR BOTTOM DIFFERENCED CARDIOIDS SENSOR
SIGNAL-TO-NOISE RESULTS FOR 64HZ AT 162DB (U)

AS-77-3196

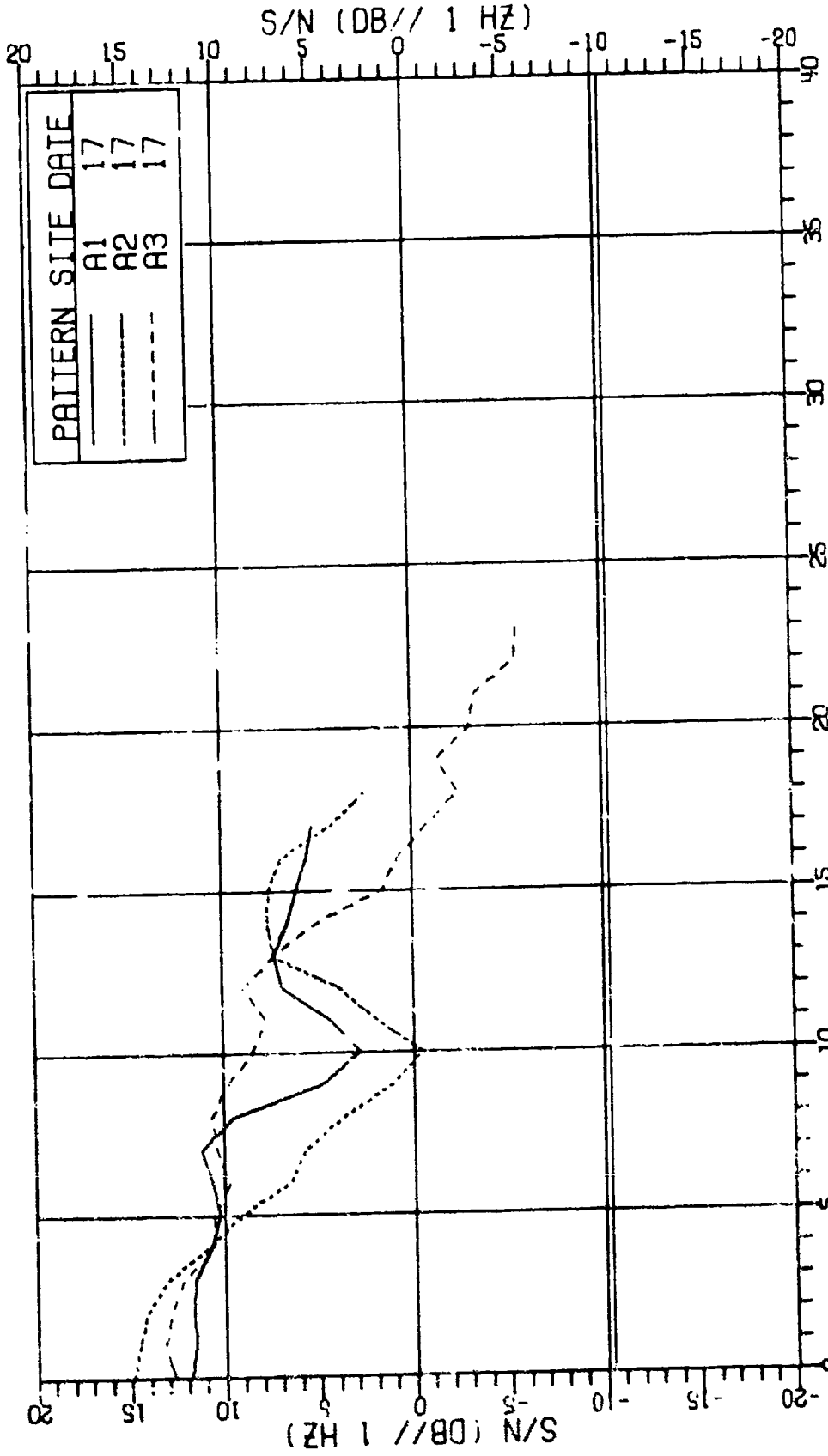

FIGURE II-270
MSS-FVT NEAR BOTTOM OMNIDIRECTIONAL SENSOR
SIGNAL-TO-NOISE RESULTS FOR 160HZ AT 161DB (U)

AS-77-3197

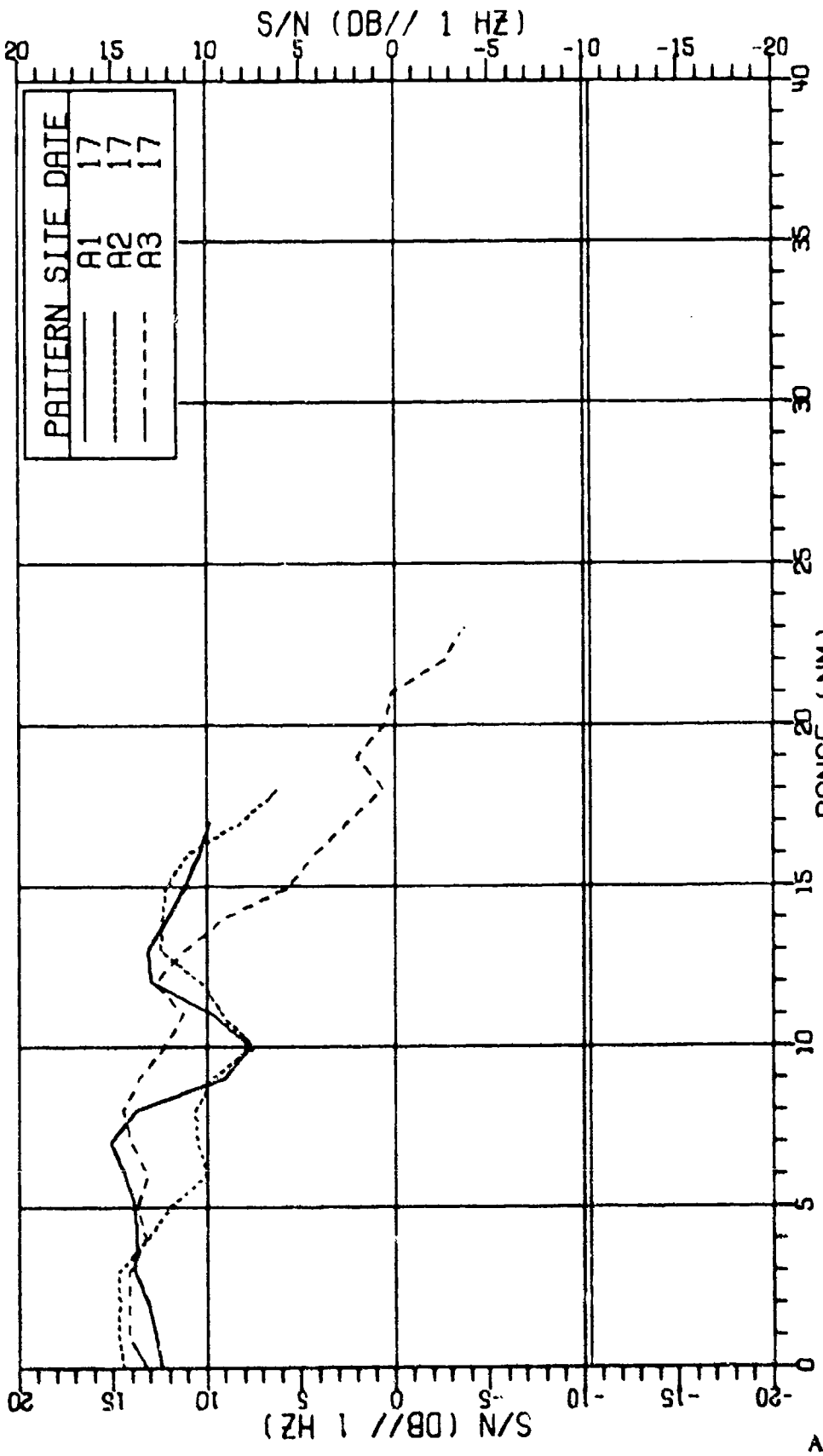

FIGURE II-271
MSS-FVT NEAR BOTTOM SINGLE CARDIOIDS SENSOR
SIGNAL-TO-NOISE RESULTS FOR 160HZ AT 161DB (U)

AS-77-3198

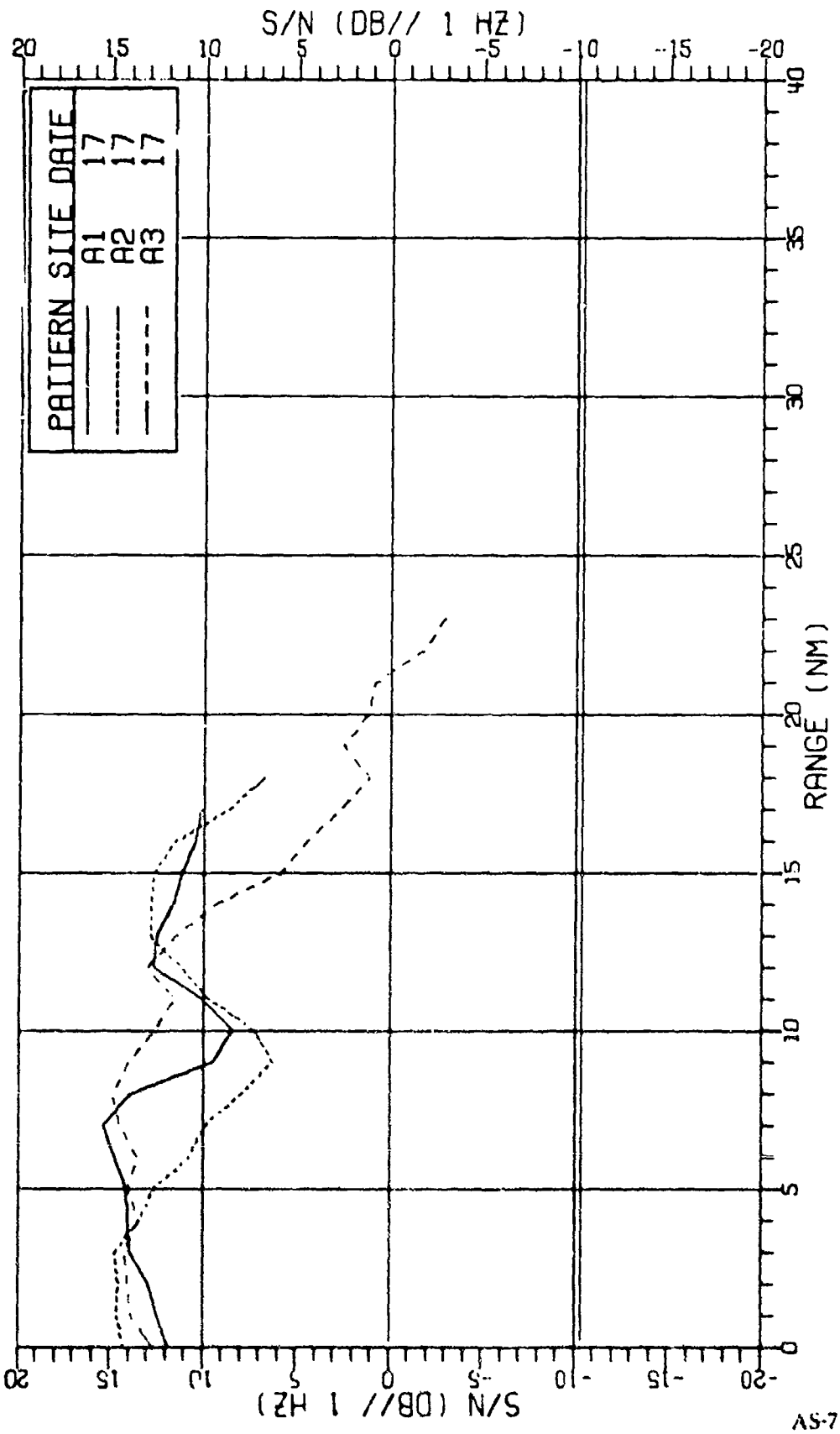

FIGURE II-272
MSS-FVT NEAR BOTTOM MAX GAIN LIMACONS SENSOR
SIGNAL-TO-NOISE RESULTS FOR 160HZ AT 161DB (U)

AS-77-3199

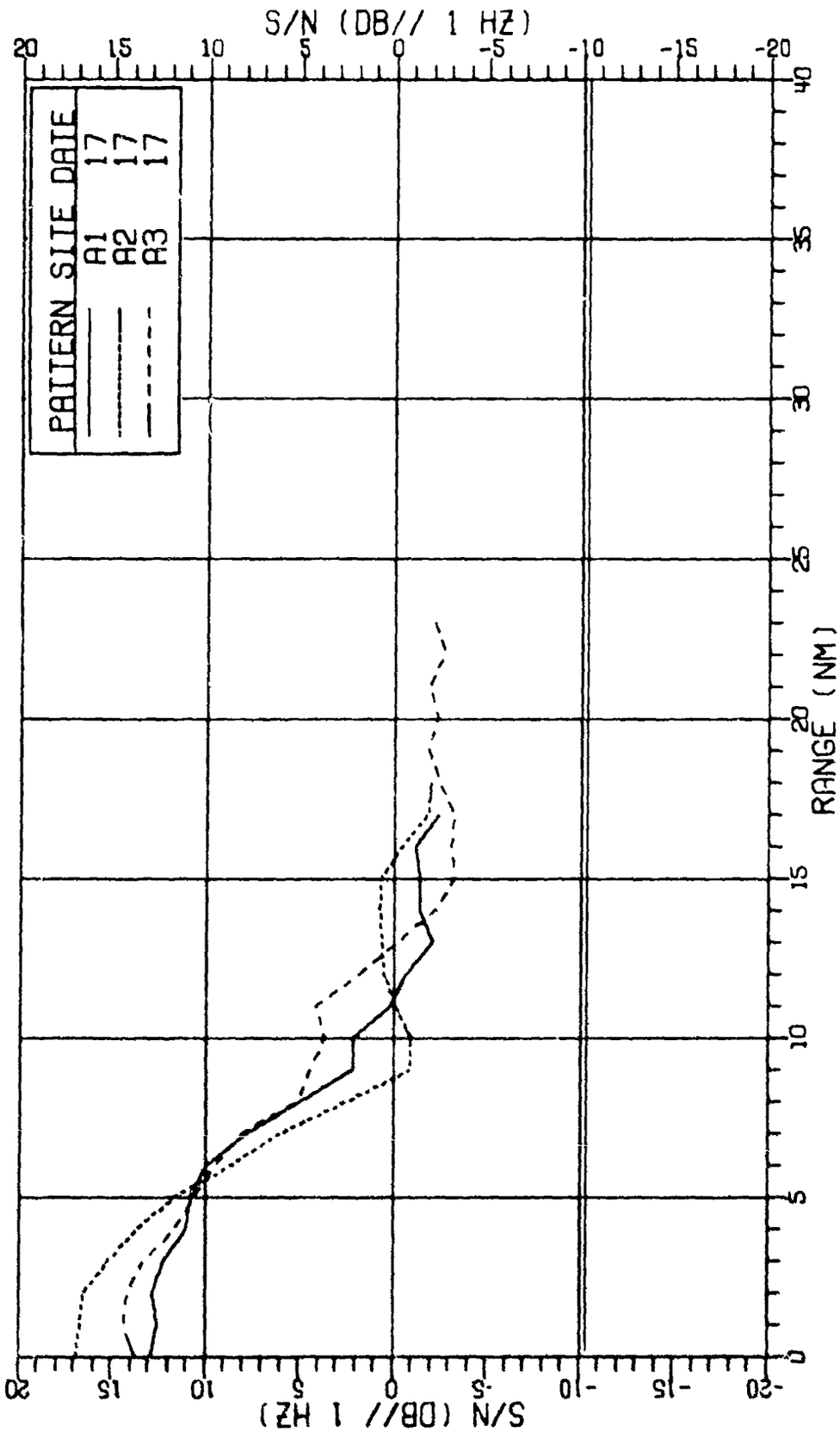

FIGURE II-273
MSS-FVT NEAR BOTTOM VERTICAL DIPOLE SENSOR
SIGNAL-TO-NOISE RESULTS FOR 160HZ AT 161DB (U)

AC-77-3200

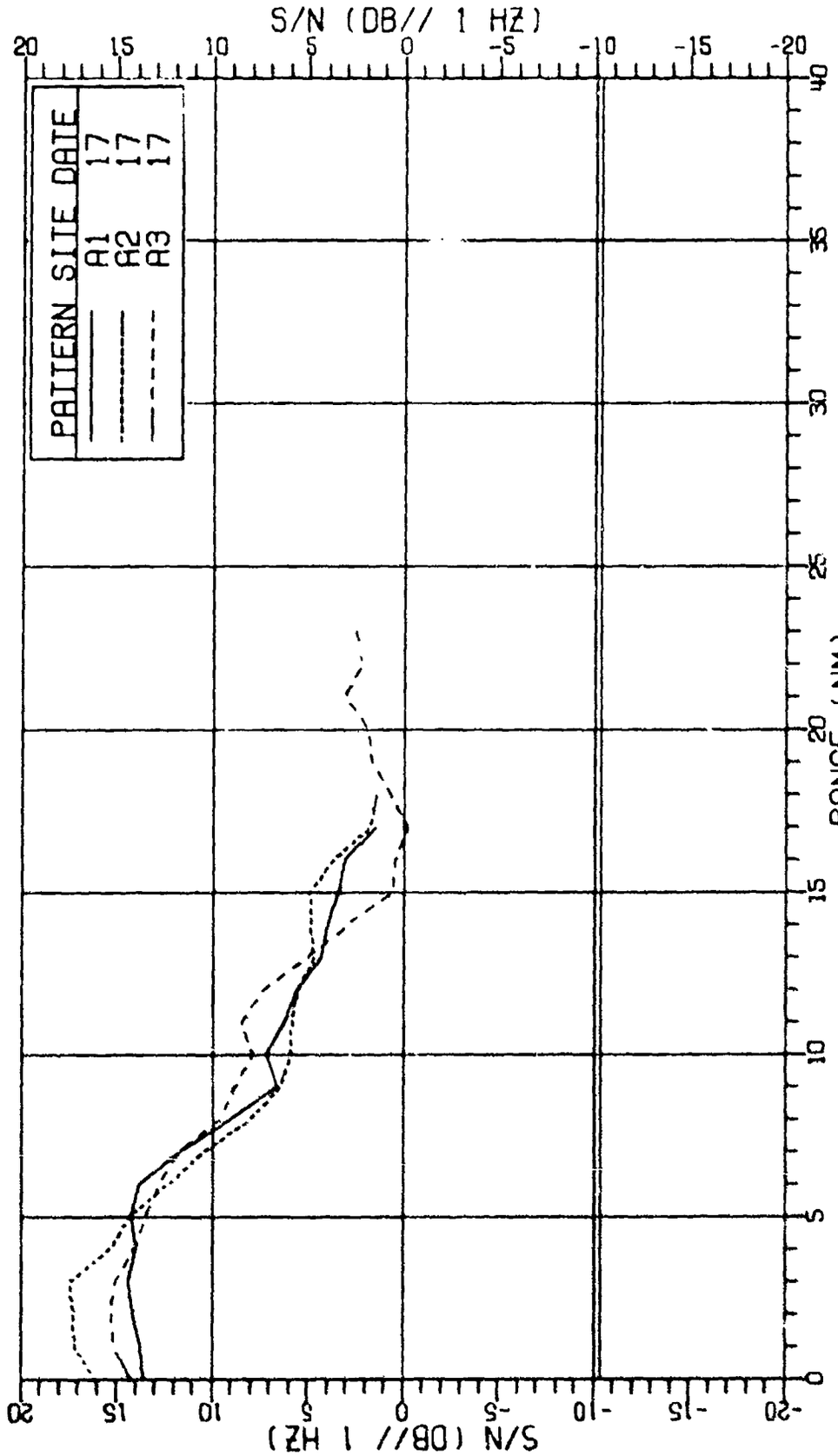

FIGURE II-274
MSS-FVT NEAR BOTTOM DIFFERENCED CARDIOIDS SENSOR
SIGNAL-TO-NOISE RESULTS FOR 160HZ AT 161DB (U)

AS-77-3201

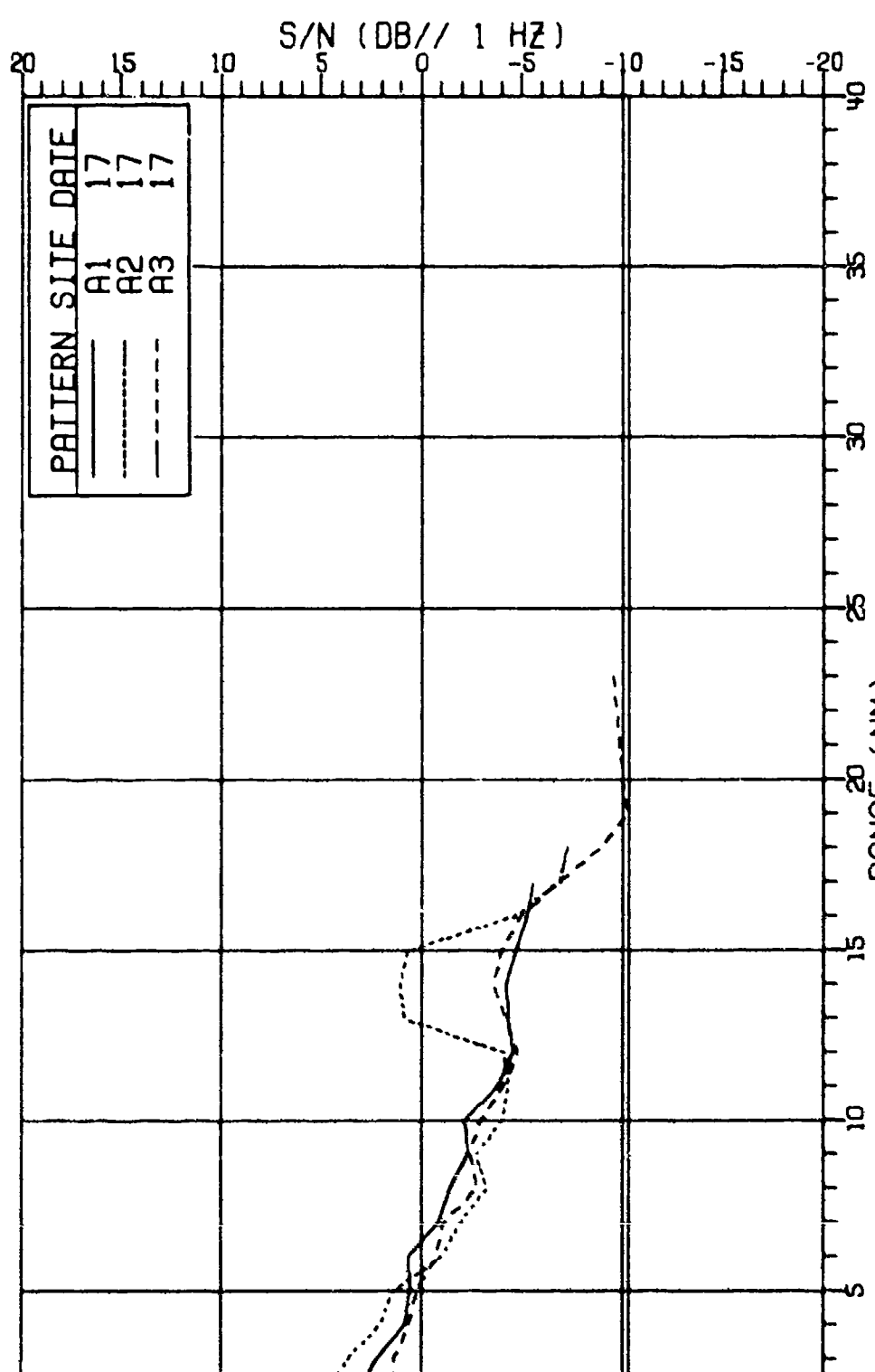

FIGURE II-275
MSS-FVT NEAR BOTTOM OMNIDIRECTIONAL SENSOR
SIGNAL-TO-NOISE RESULTS FOR 260HZ AT 1470B (U)

AS-77-3202

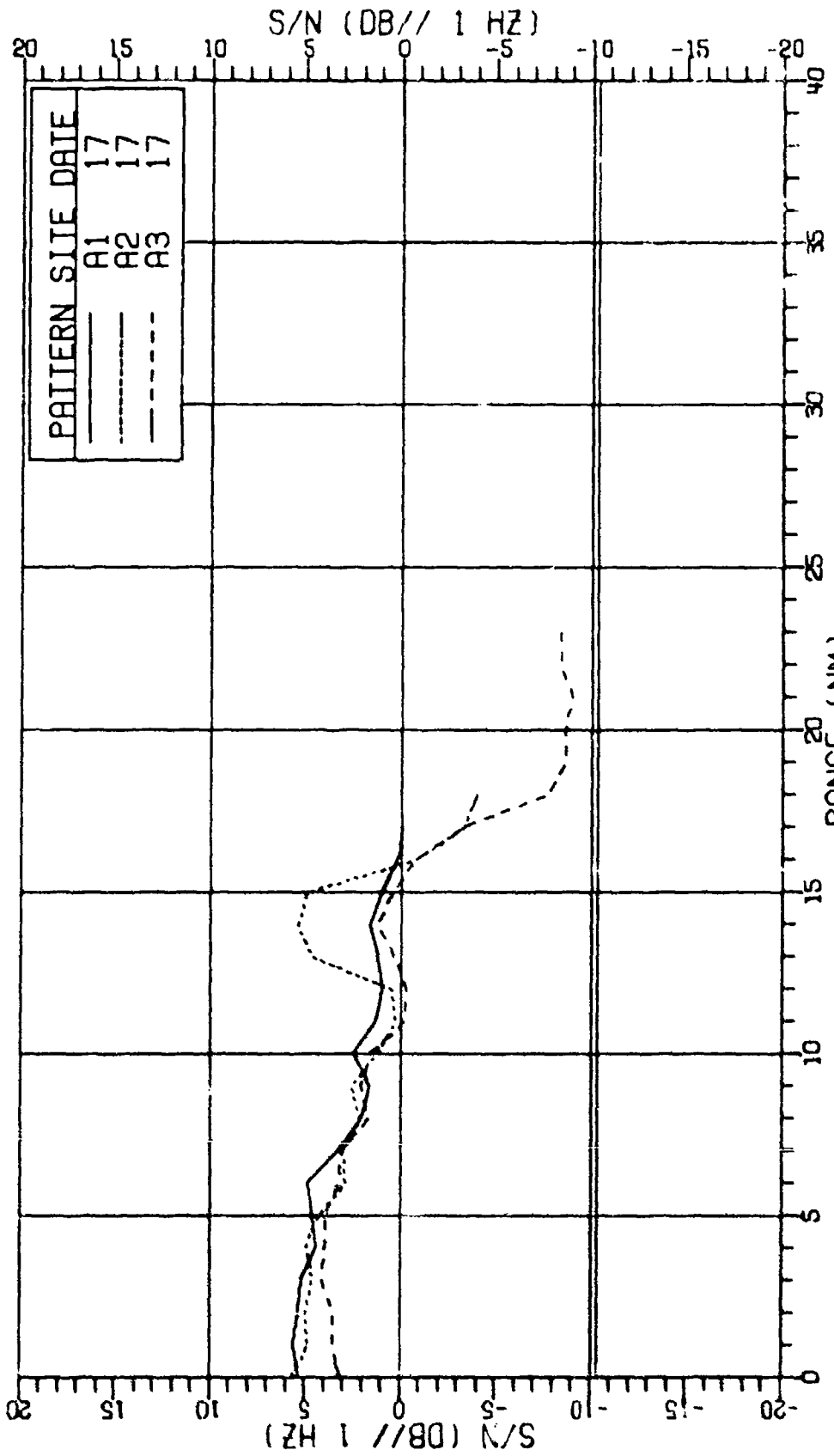

FIGURE II-276
MSS-FVT NEAR BOTTOM [illegible] CARDIOIDS SENSOR
SIGNAL-TO-NOISE RESUL[illegible]R 260HZ AT 147DB (U)

AS-77-3203

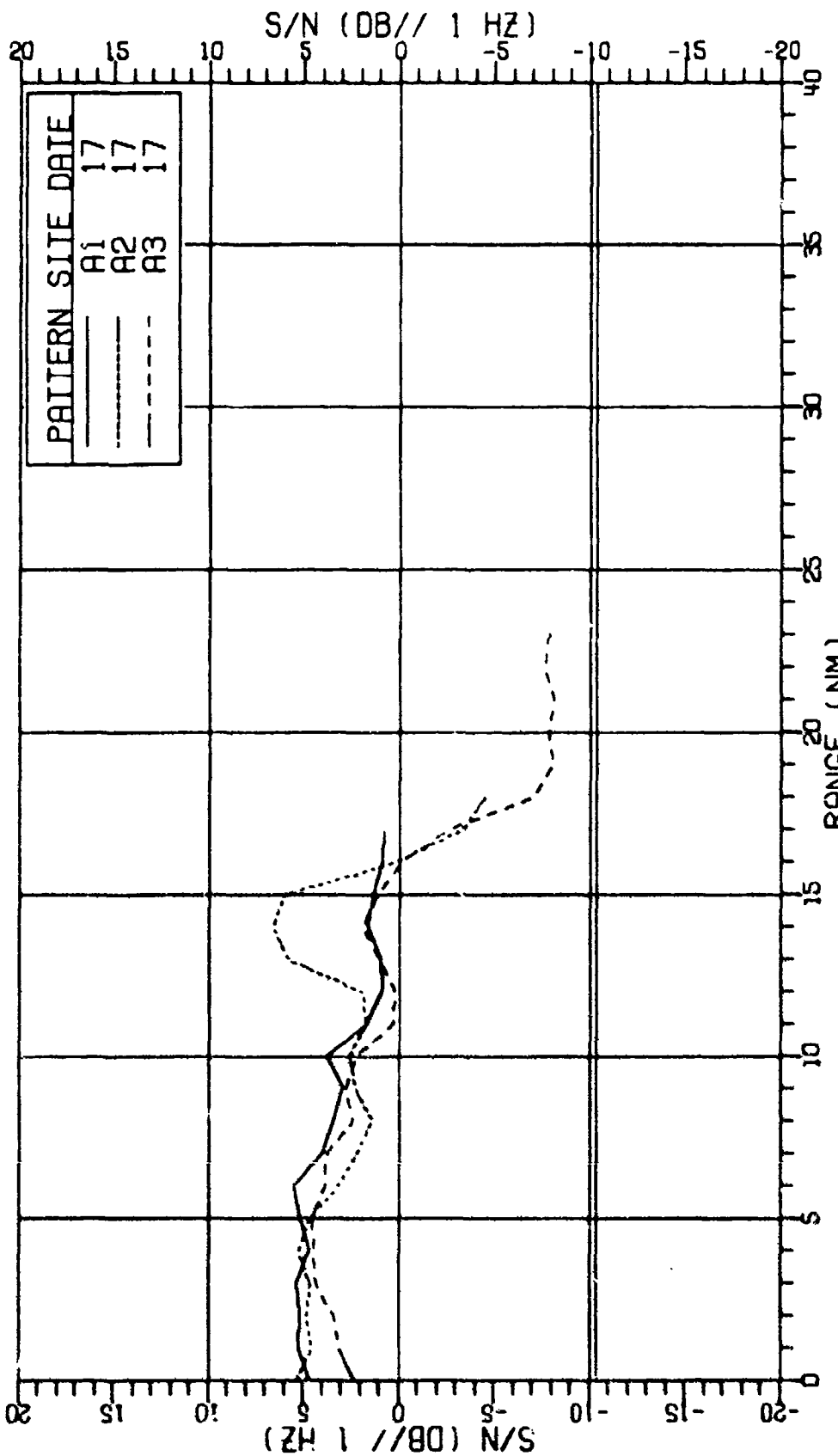

FIGURE II-277
MSS-FVT NEAR BOTTOM MAX GAIN LIMACONS SENSOR
SIGNAL-TO-NOISE RESULTS FOR 260HZ AT 147DB (U)

AS-77-3204

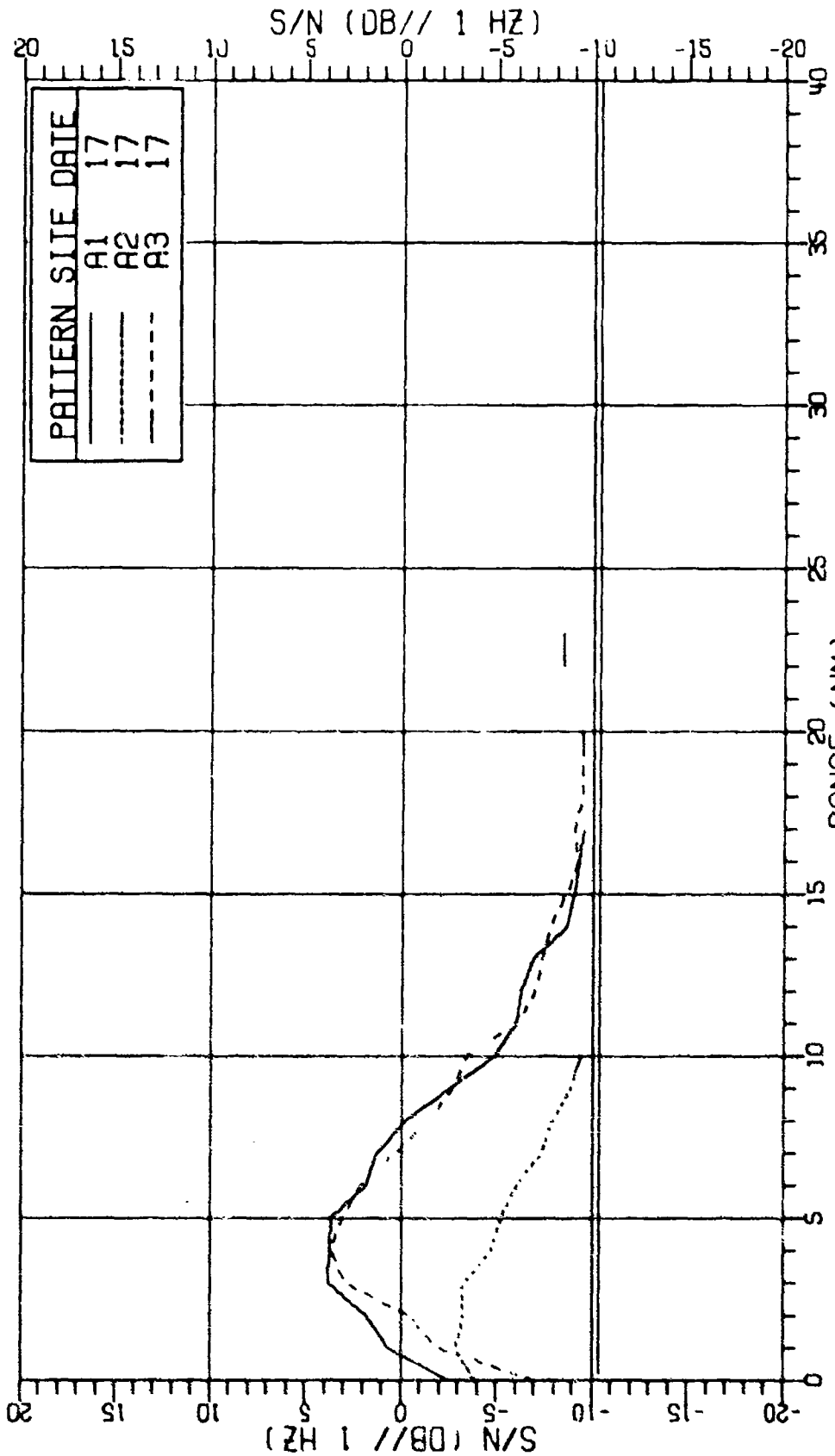

FIGURE II-278
MSS-FVT NEAR BOTTOM VERTICAL DIPOLE SENSOR
SIGNAL-TO-NOISE RESULTS FOR 260HZ AT 147DB (U)

AS-77-

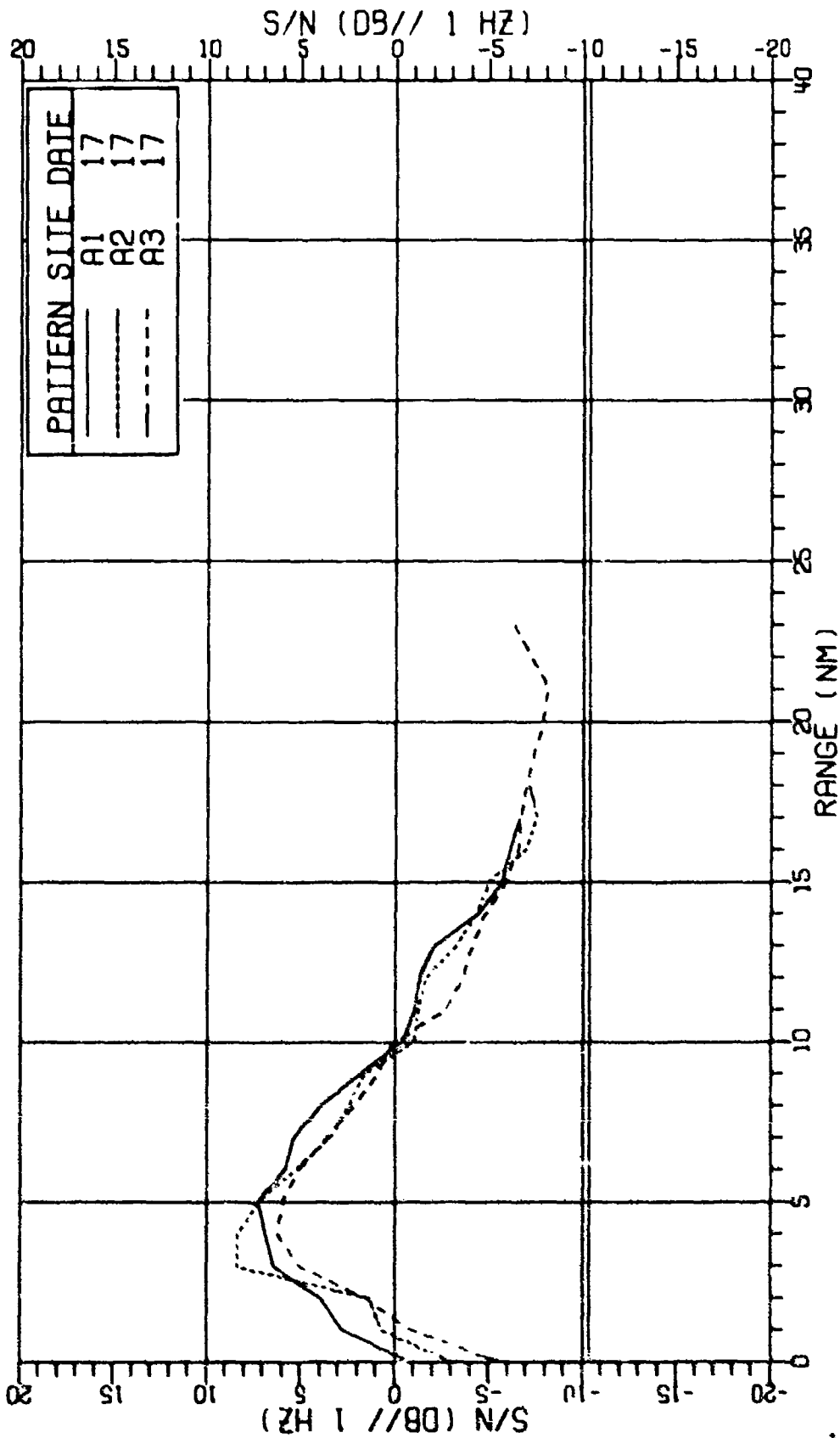

FIGURE II-279
MSS-FVT NEAR BOTTOM DIFFERENCED CARDIOIDS SENSOR
SIGNAL-TO-NOISE RESULTS FOR 260HZ AT 1470B (U)

AS-77-3206

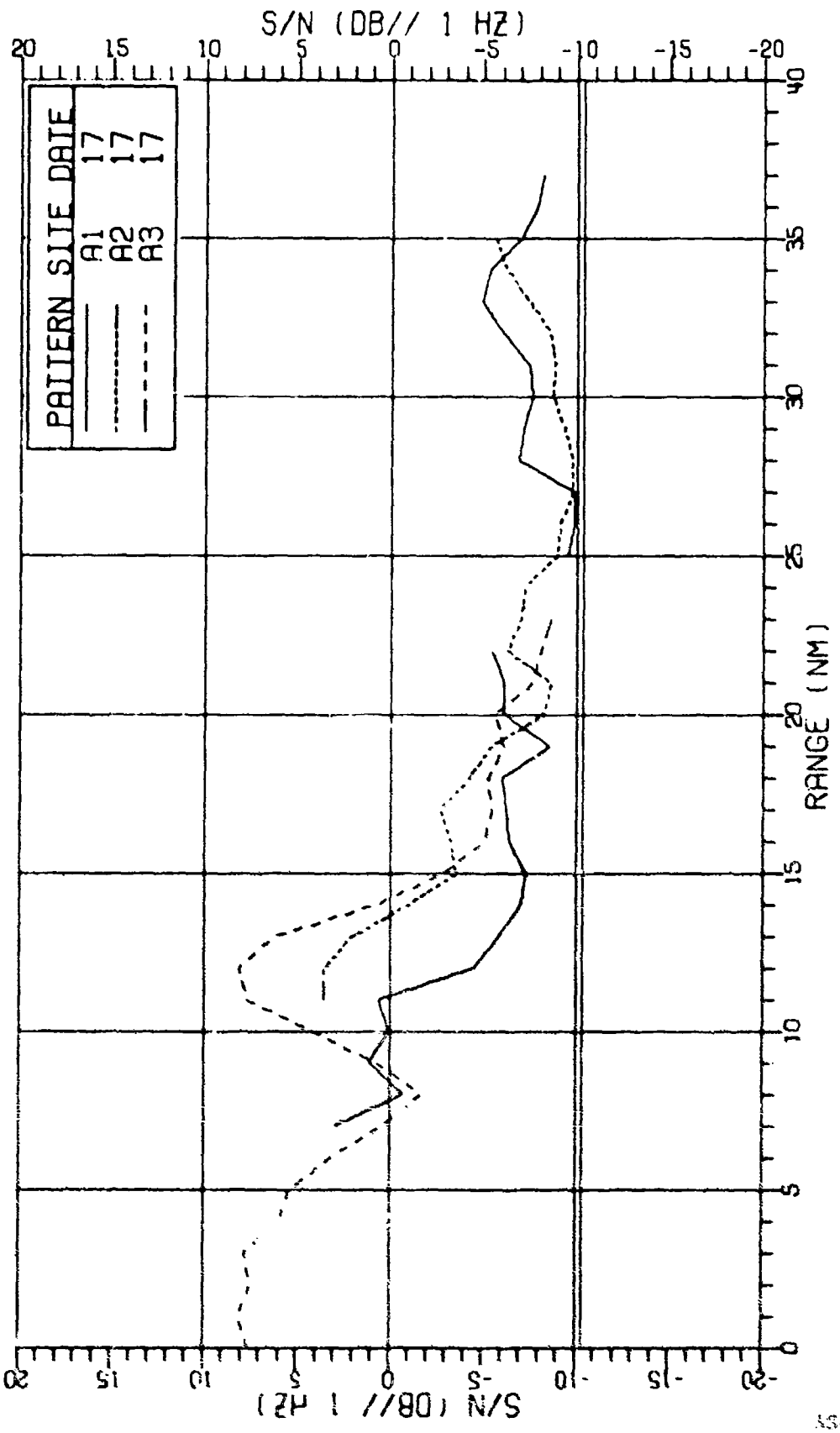

FIGURE II-280
MSS-FVT NEAR BOTTOM OMNIDIRECTIONAL SENSOR
SIGNAL-TO-NOISE RESULTS FOR 70HZ AT 1660B (U)

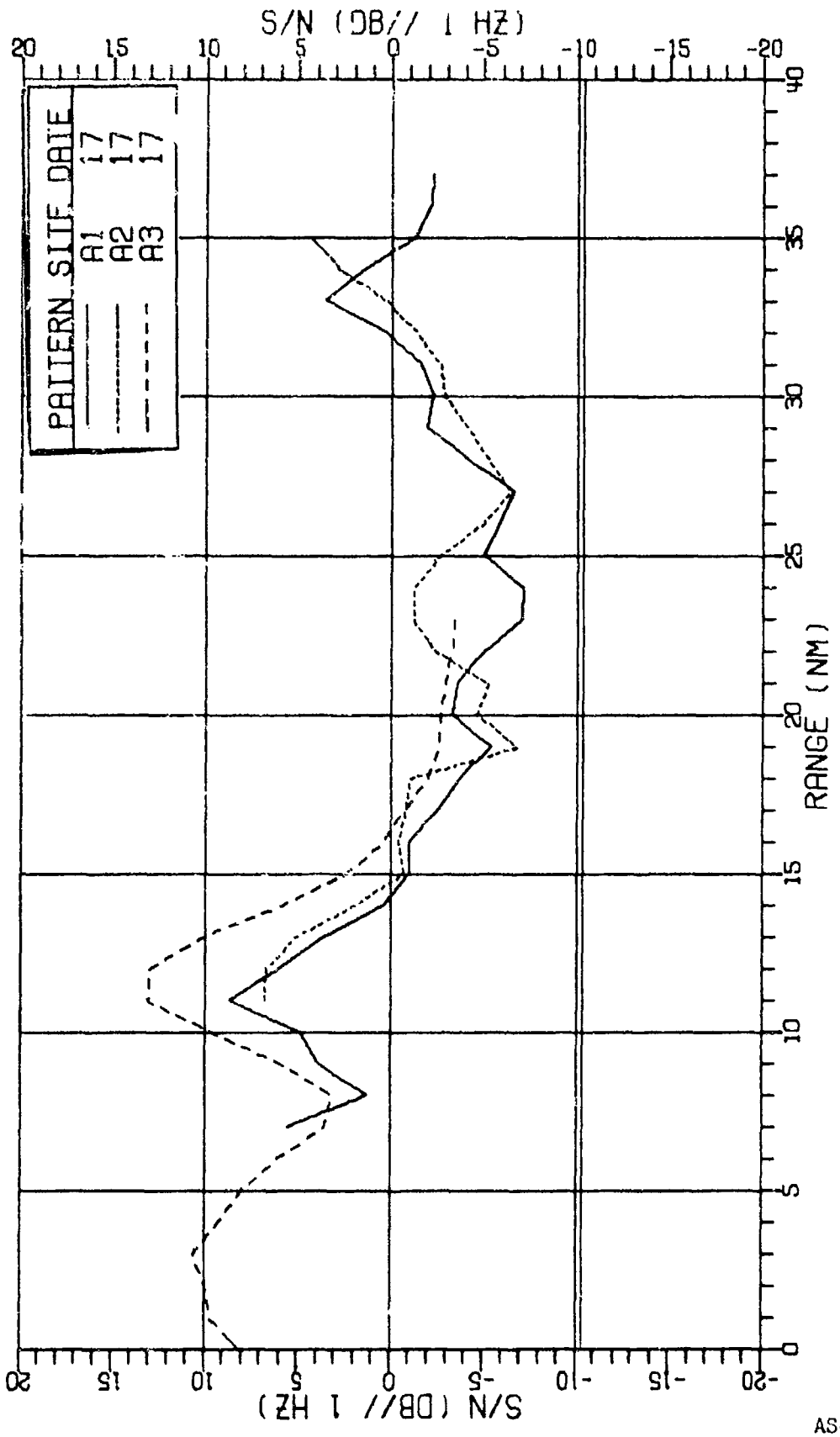

FIGURE II-281
MSS-FVT NEAR BOTTOM SINGLE CARDIOIDS SENSOR
SIGNAL-TO-NOISE RESULTS FOR 70HZ AT 166DB (U)

AS-77-3208

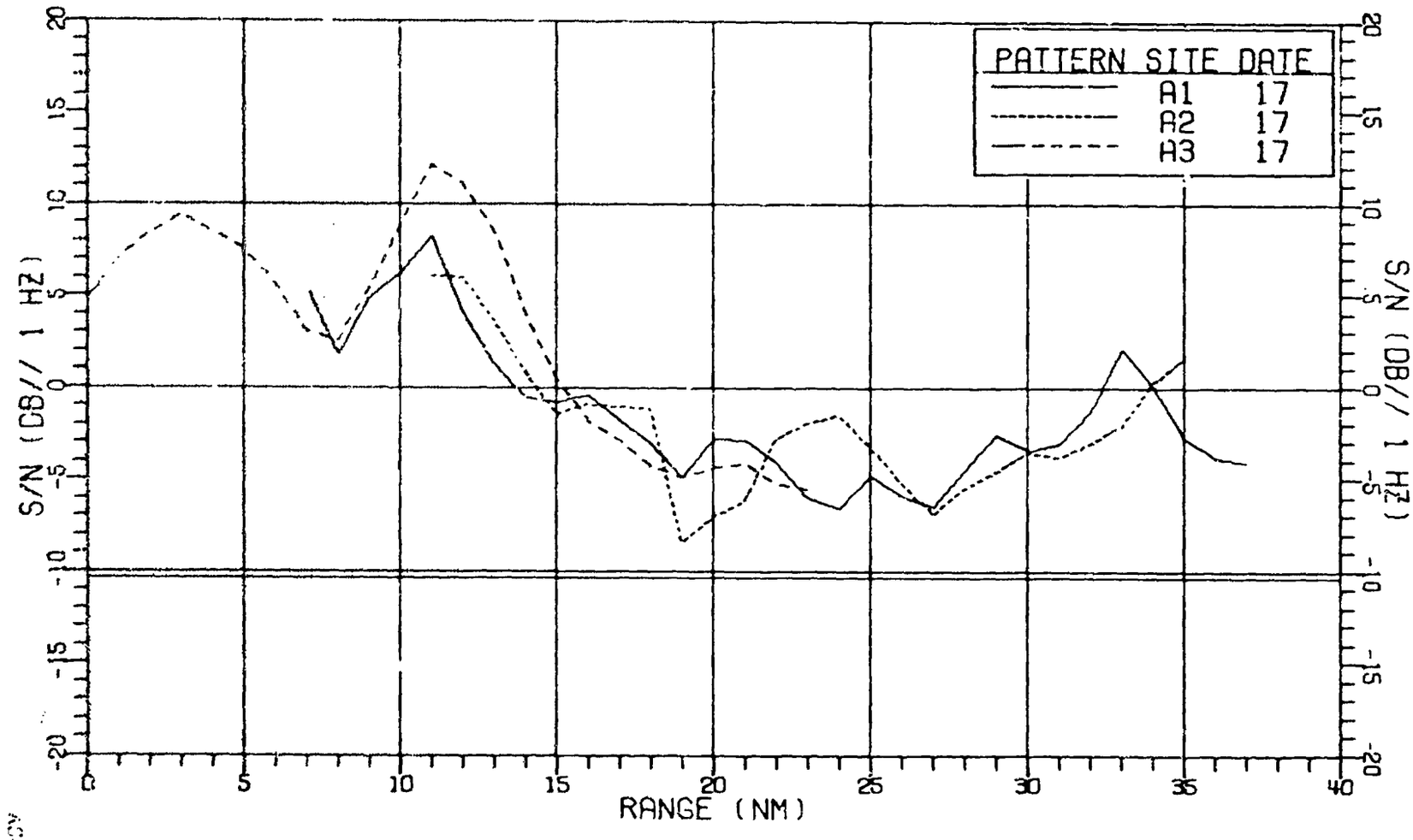

FIGURE II-282
MSS-FVT NEAR BOTTOM MAX GAIN LIMACONS SENSOR
SIGNAL-TO-NOISE RESULTS FOR 70HZ AT 166DB (U)

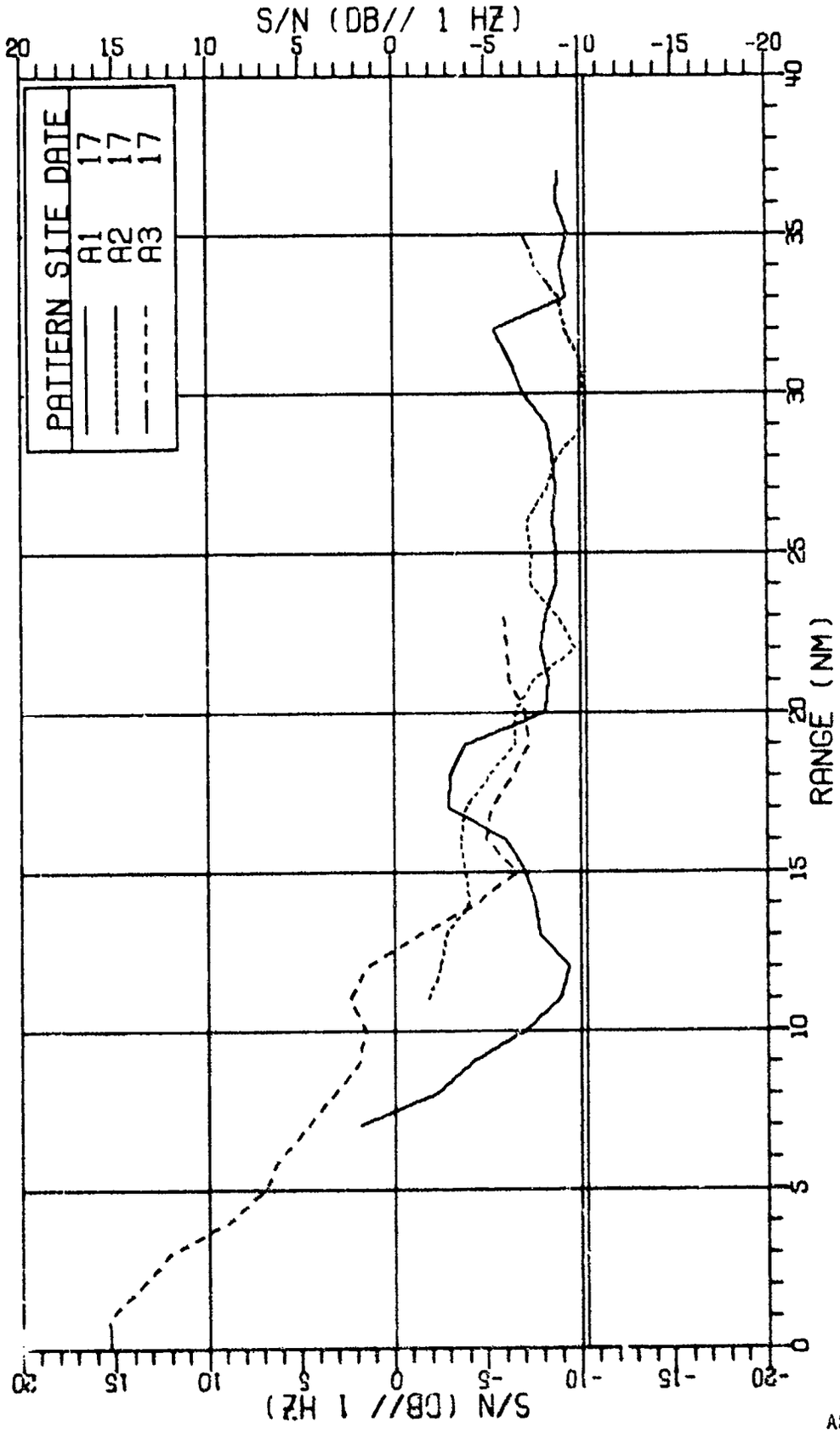

FIGURE II-283
MSS-FVT NEAR BOTTOM VERTICAL DIPOLE SENSOR
SIGNAL-TO-NOISE RESULTS FOR 70HZ AT 1660B (U)

AS-77-3210

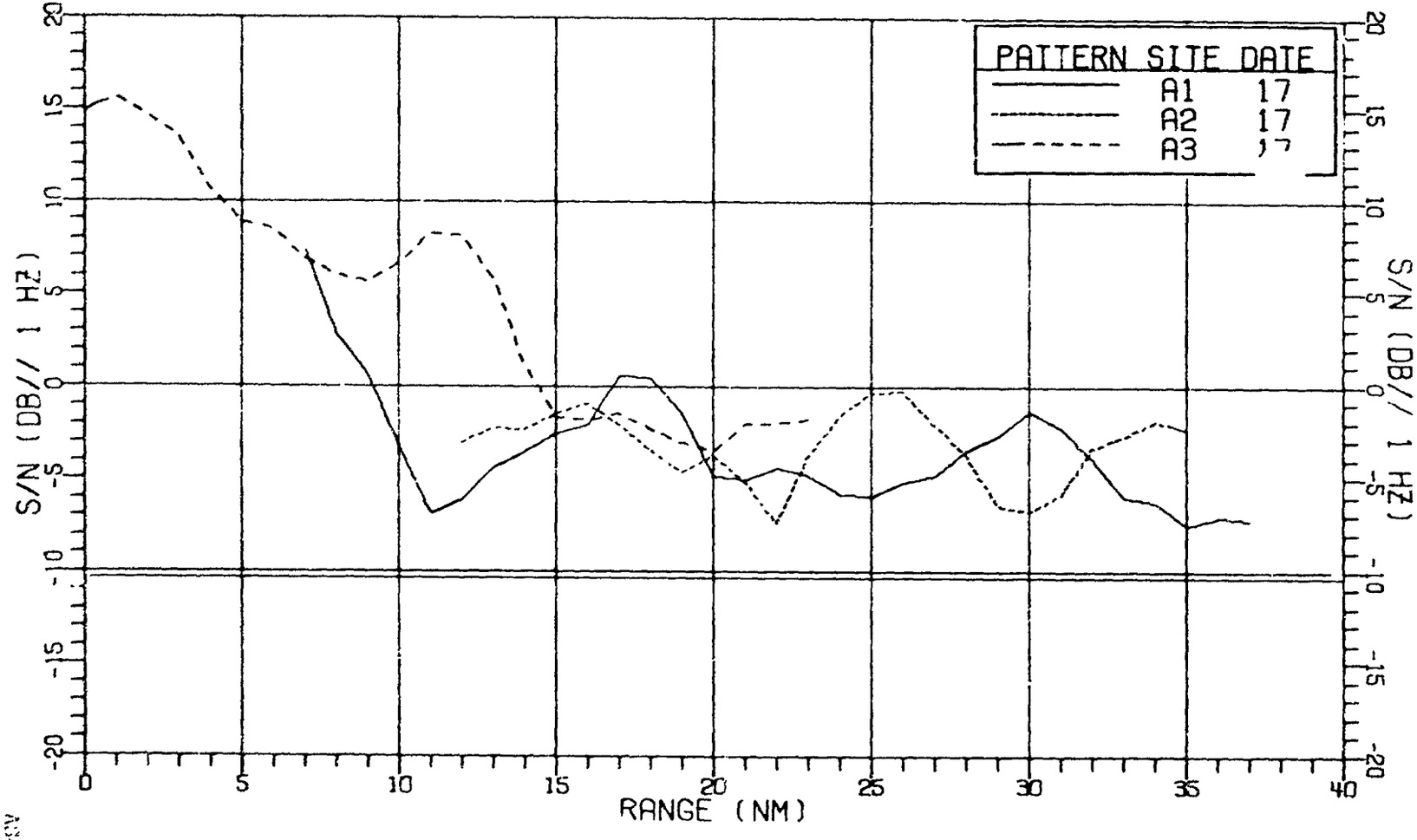

FIGURE II-284
MSS-FVT NEAR BOTTOM DIFFERENCED CARDIOIDS SENSOR
SIGNAL-TO-NOISE RESULTS FOR 70HZ AT 166DB (U)

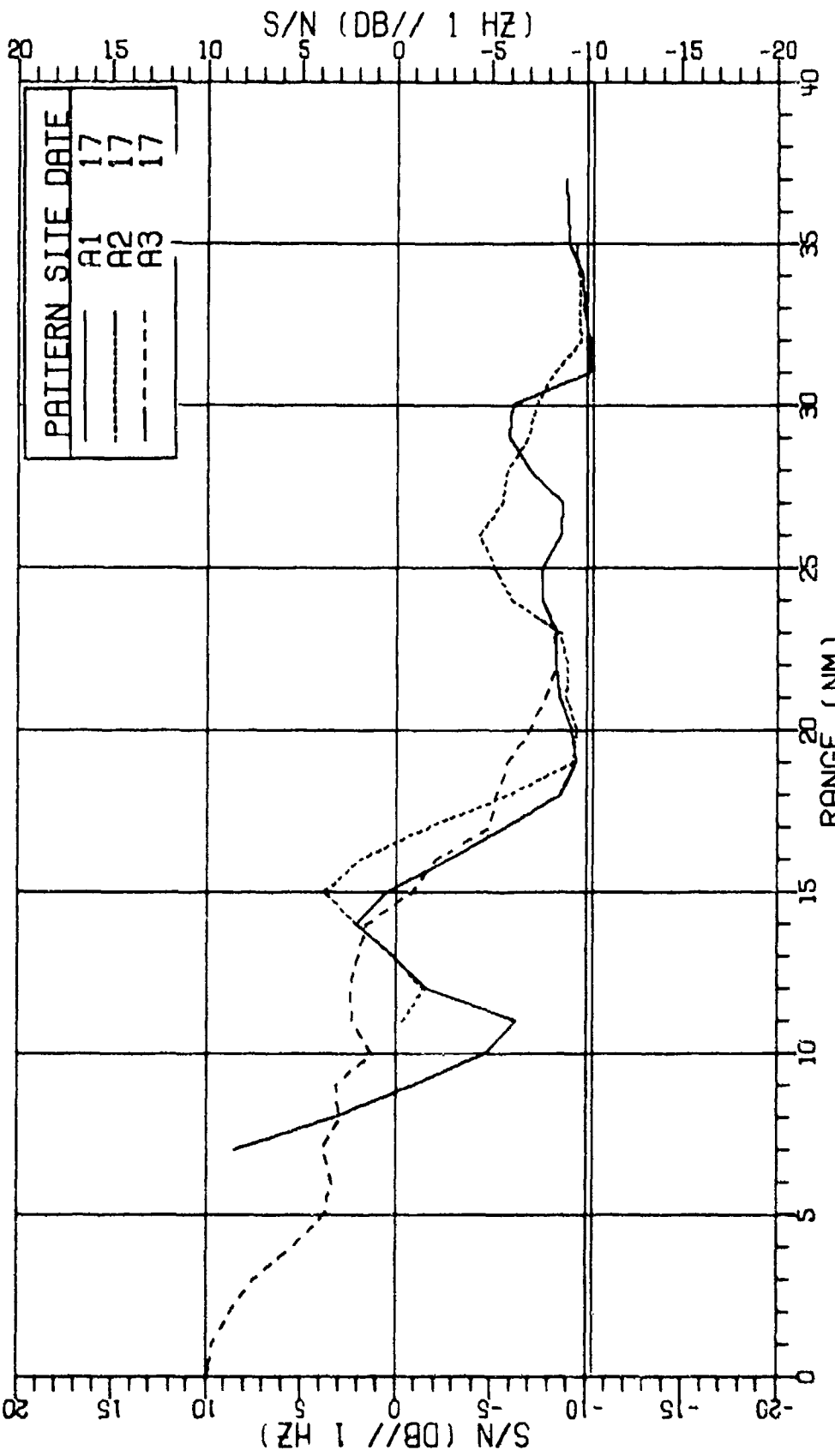

FIGURE II-285
MSS-FVT NEAR BOTTOM OMNIDIRECTIONAL SENSOR
SIGNAL-TO-NOISE RESULTS FOR 170HZ AT 156DB (U)

AS-77-3212

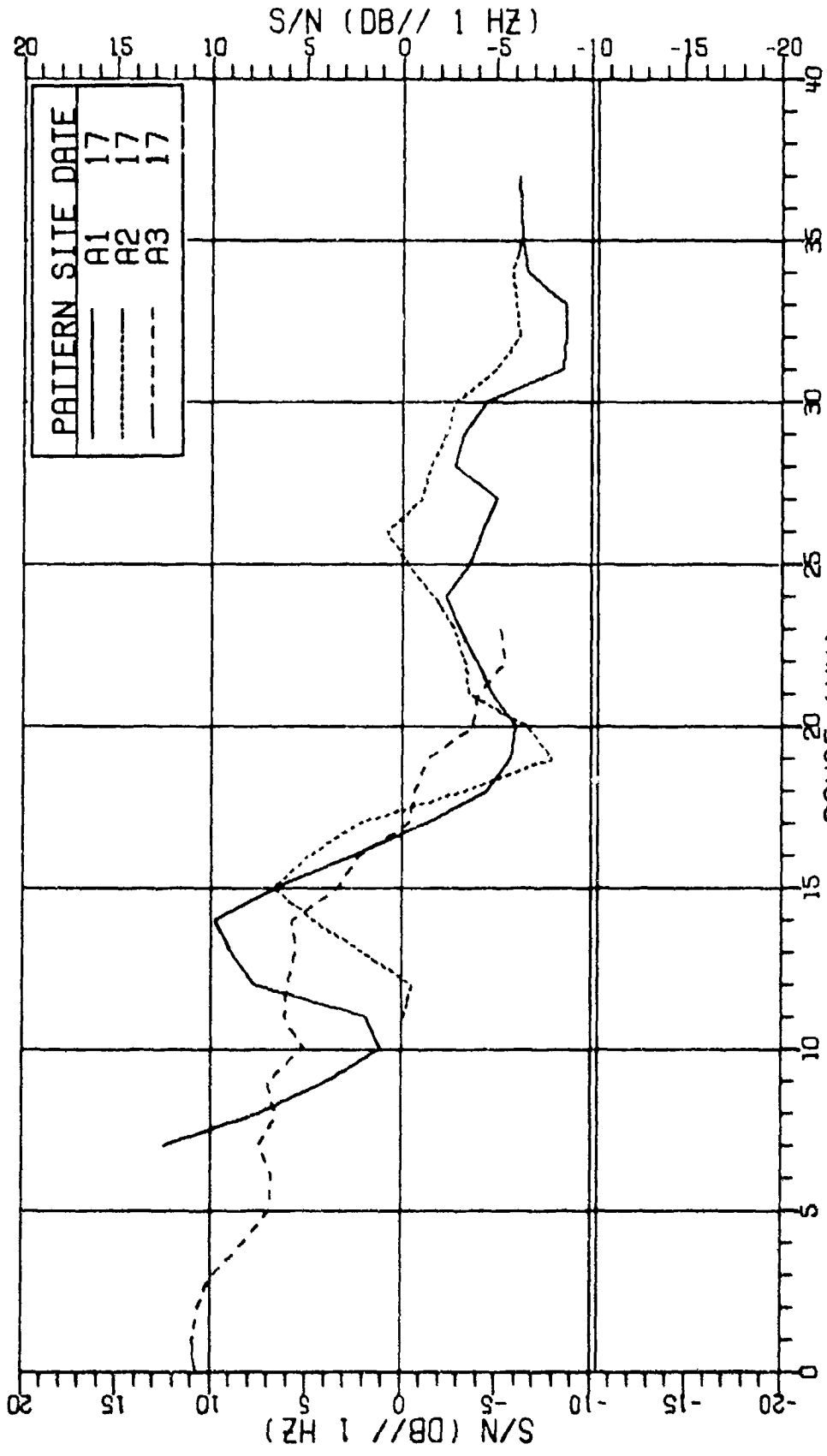

FIGURE II-286
MSS-FVT NEAR BOTTOM SINGLE CARDIOIDS SENSOR
SIGNAL-TO-NOISE RESULTS FOR 170HZ AT 156DB (U)

AS-77-3213

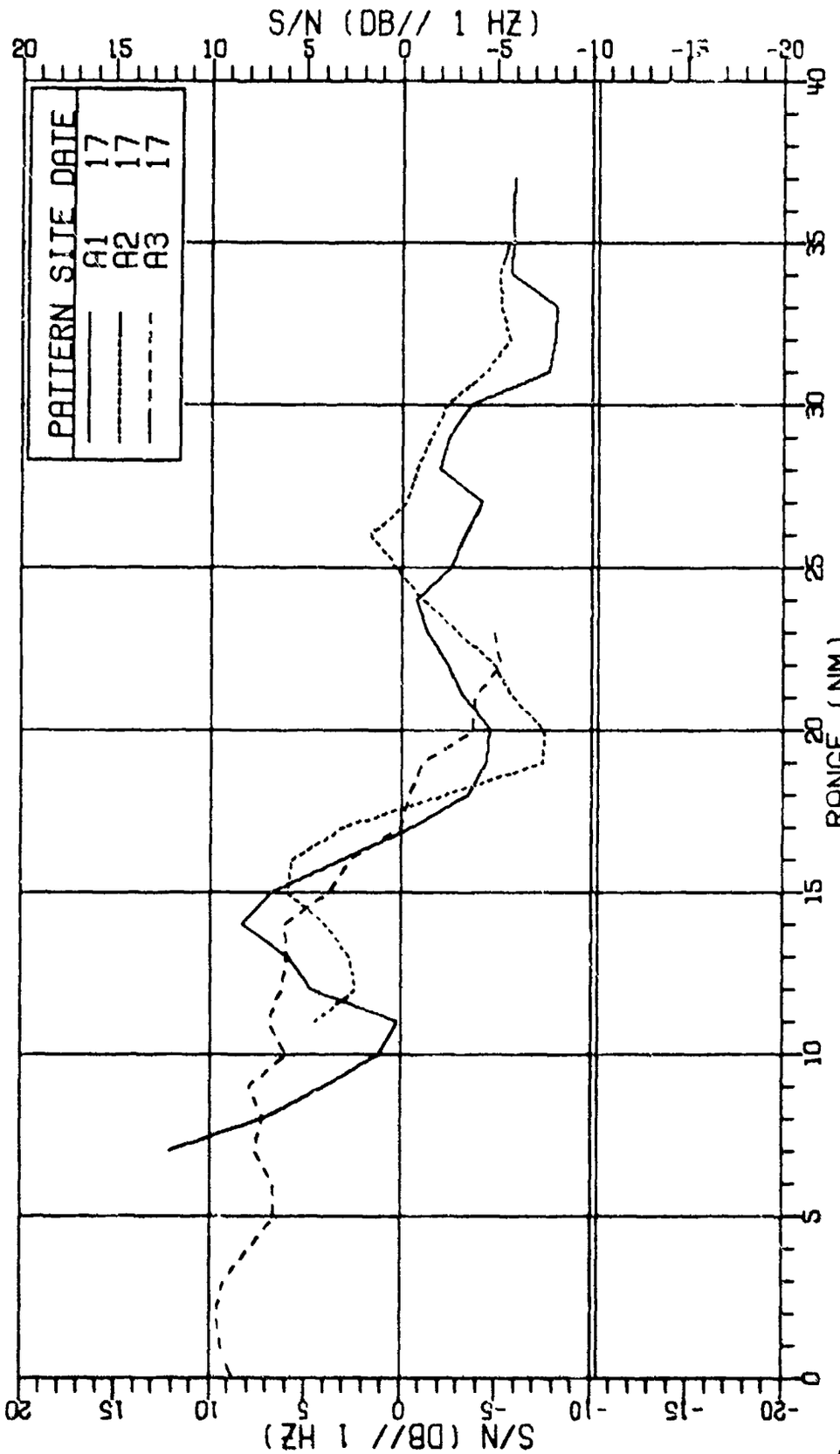

FIGURE II-287
MSS-FVT NEAR BOTTOM MAX GAIN LIMACONS SENSOR
SIGNAL-TO-NOISE RESULTS FOR 170HZ AT 156DB (U)

AS-77-3214

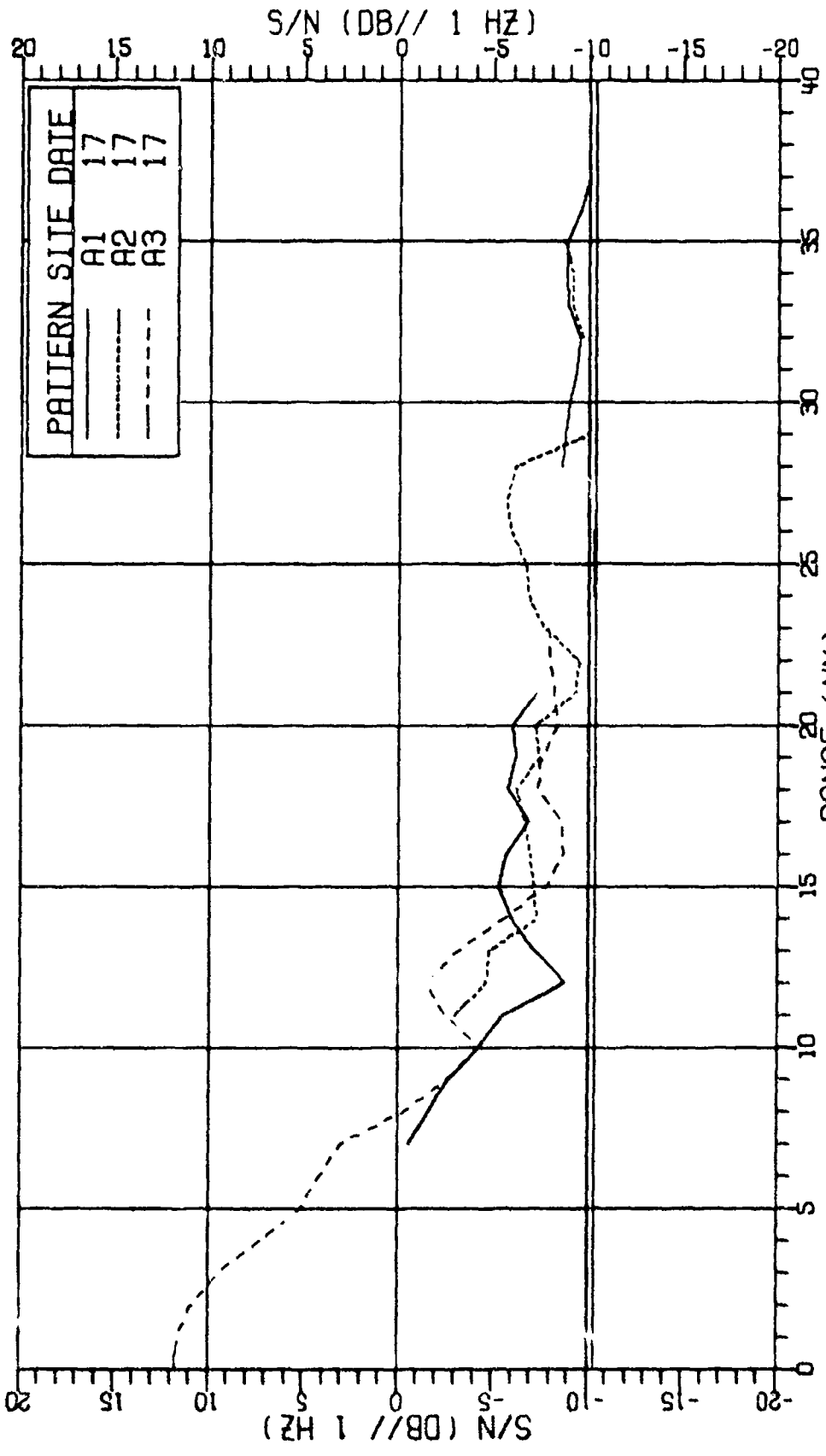

FIGURE II-288
MSS-FVT NEAR BOTTOM VERTICAL DIPOLE SENSOR
SIGNAL-TO-NOISE RESULTS FOR 170HZ AT 156DB (U)

A[illegible]-77-3215

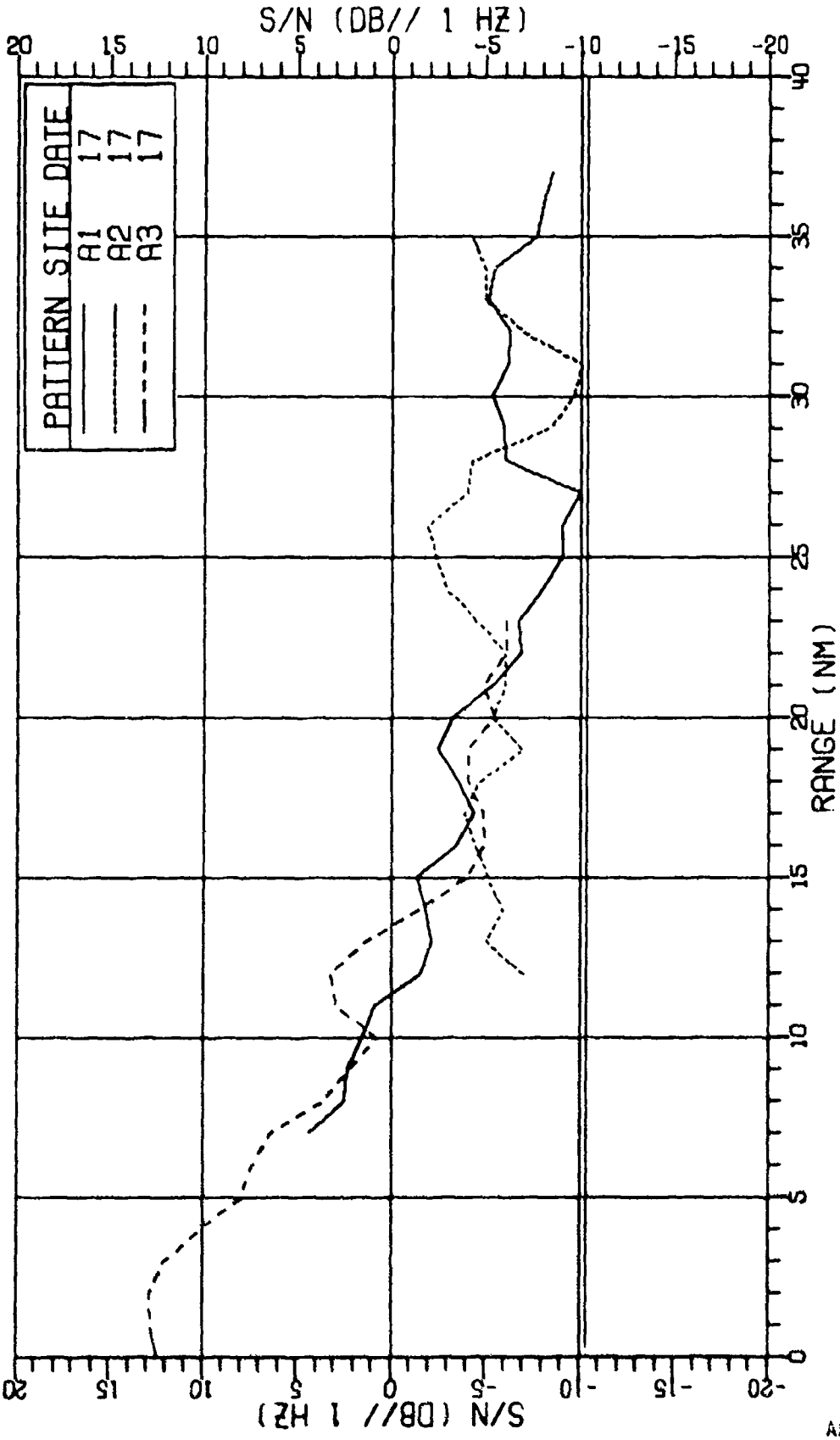

FIGURE II-289
MSS-FVT NEAR BOTTOM DIFFERENCED CARDIOIDS SENSOR
SIGNAL-TO-NOISE RESULTS FOR 170HZ AT 156DB (U)

AS-77-3216

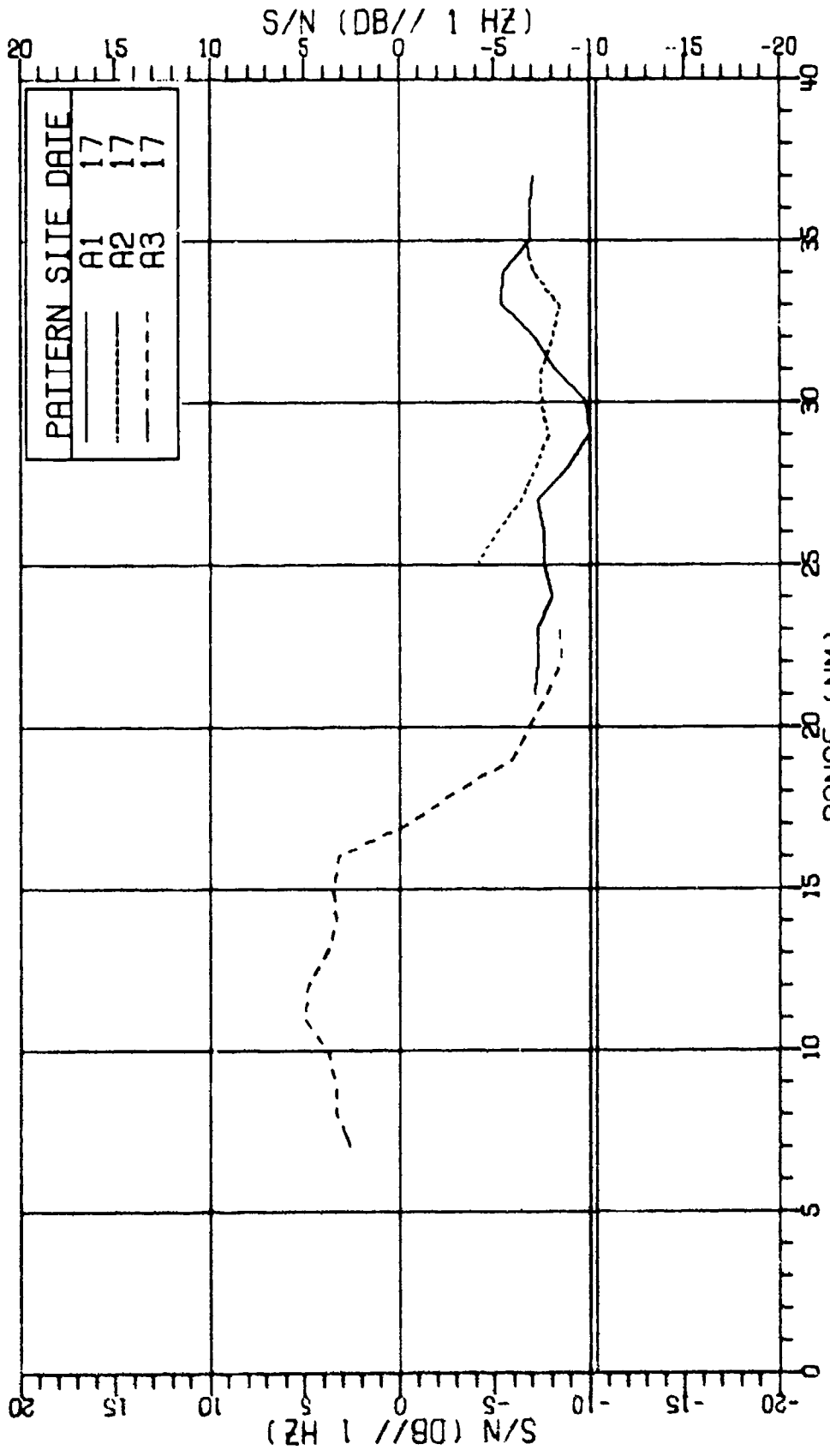

FIGURE II-290
MSS-FVT NEAR BOTTOM OMNIDIRECTIONAL SENSOR
SIGNAL-TO-NOISE RESULTS FOR 335HZ AT 154DB (U)

AS-77-3217

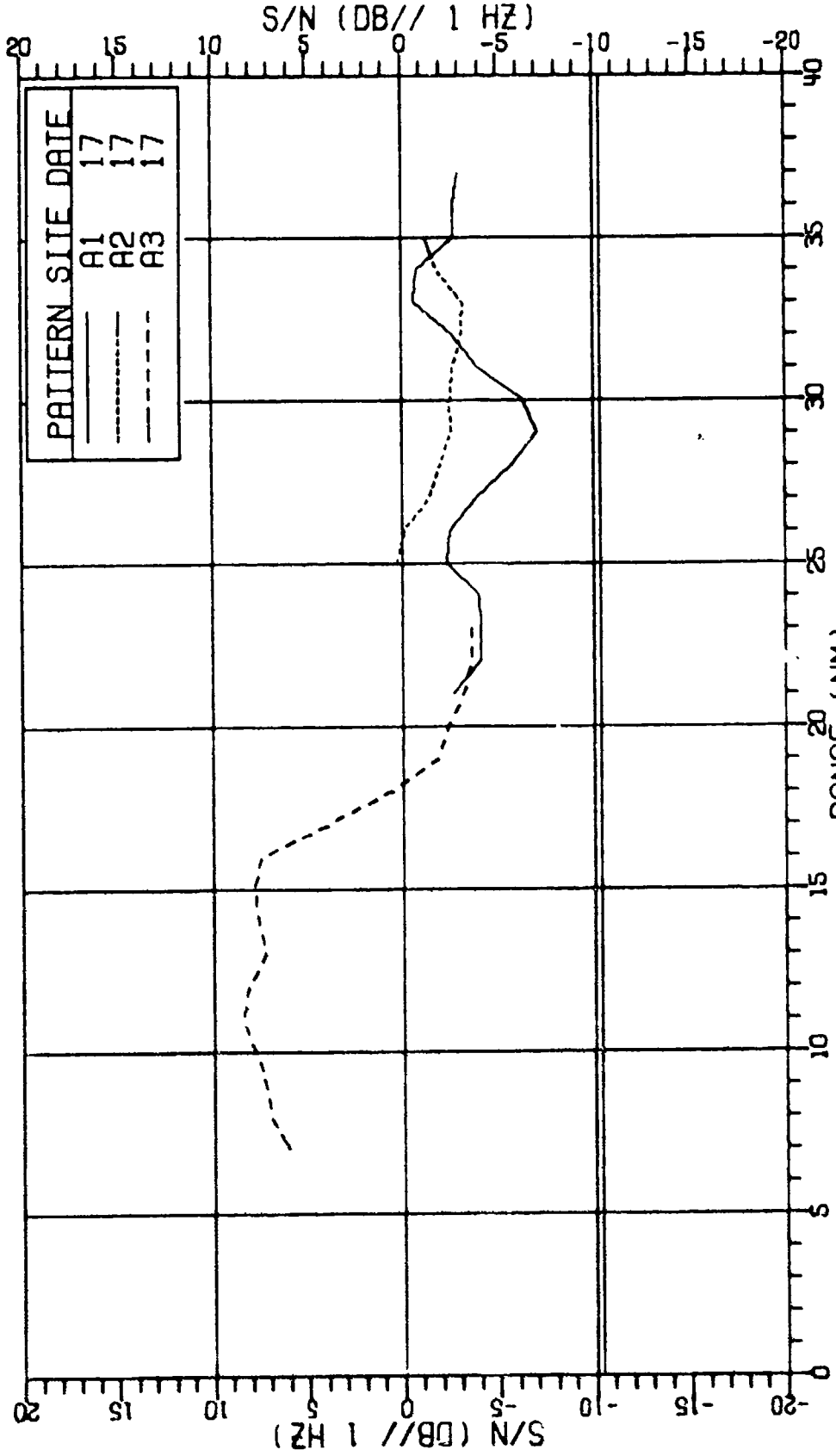

FIGURE II-291
MSS-FVT NEAR BOTTOM SINGLE CARDIOIDS SENSOR
SIGNAL-TO-NOISE RESULTS FOR 335HZ AT 154DB (U)

AS-77-3218

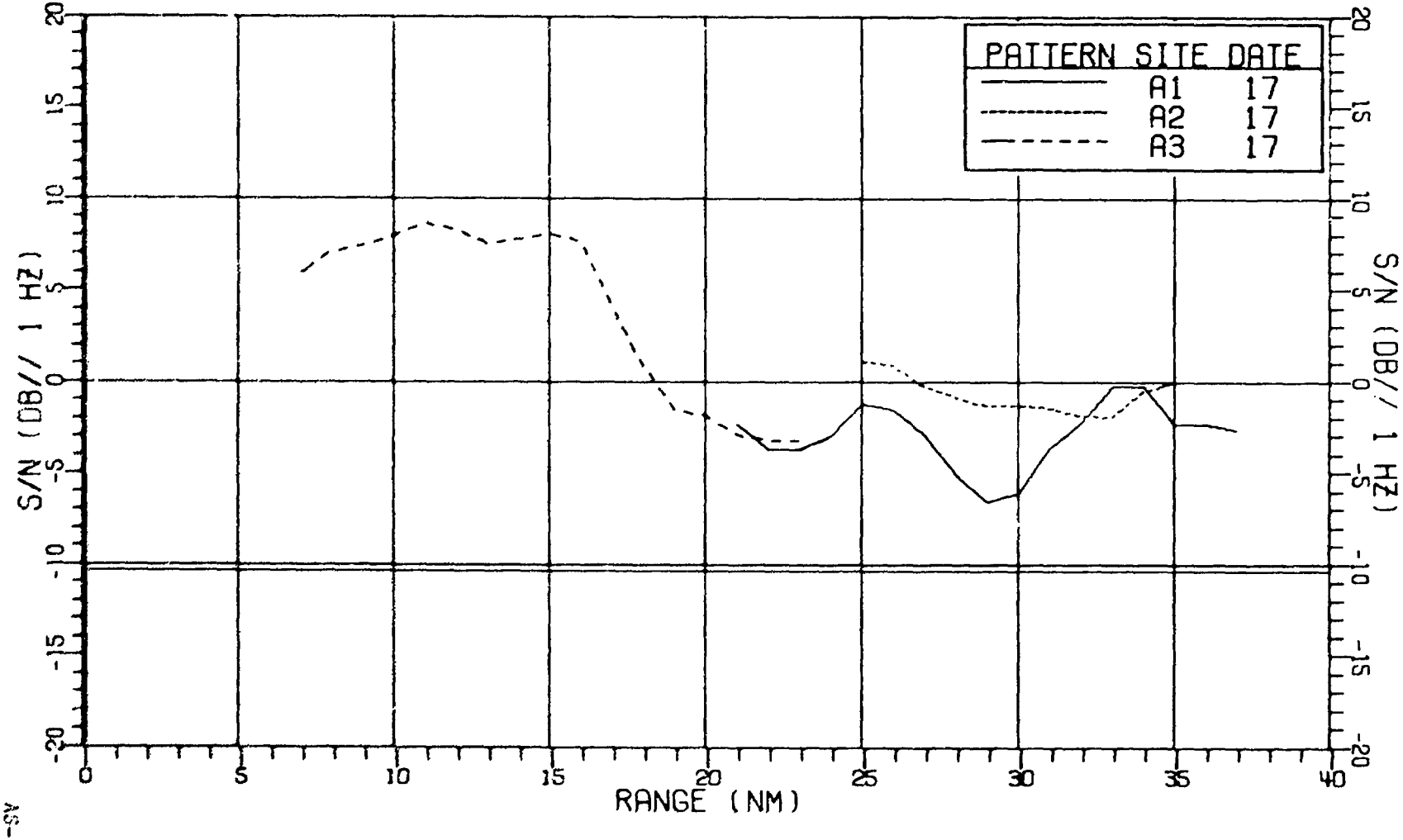

AS-11-3219

FIGURE II-292
MSS-FVT NEAR BOTTOM MAX GAIN LIMACONS SENSOR
SIGNAL-TO-NOISE RESULTS FOR 335HZ AT 154DB (U)

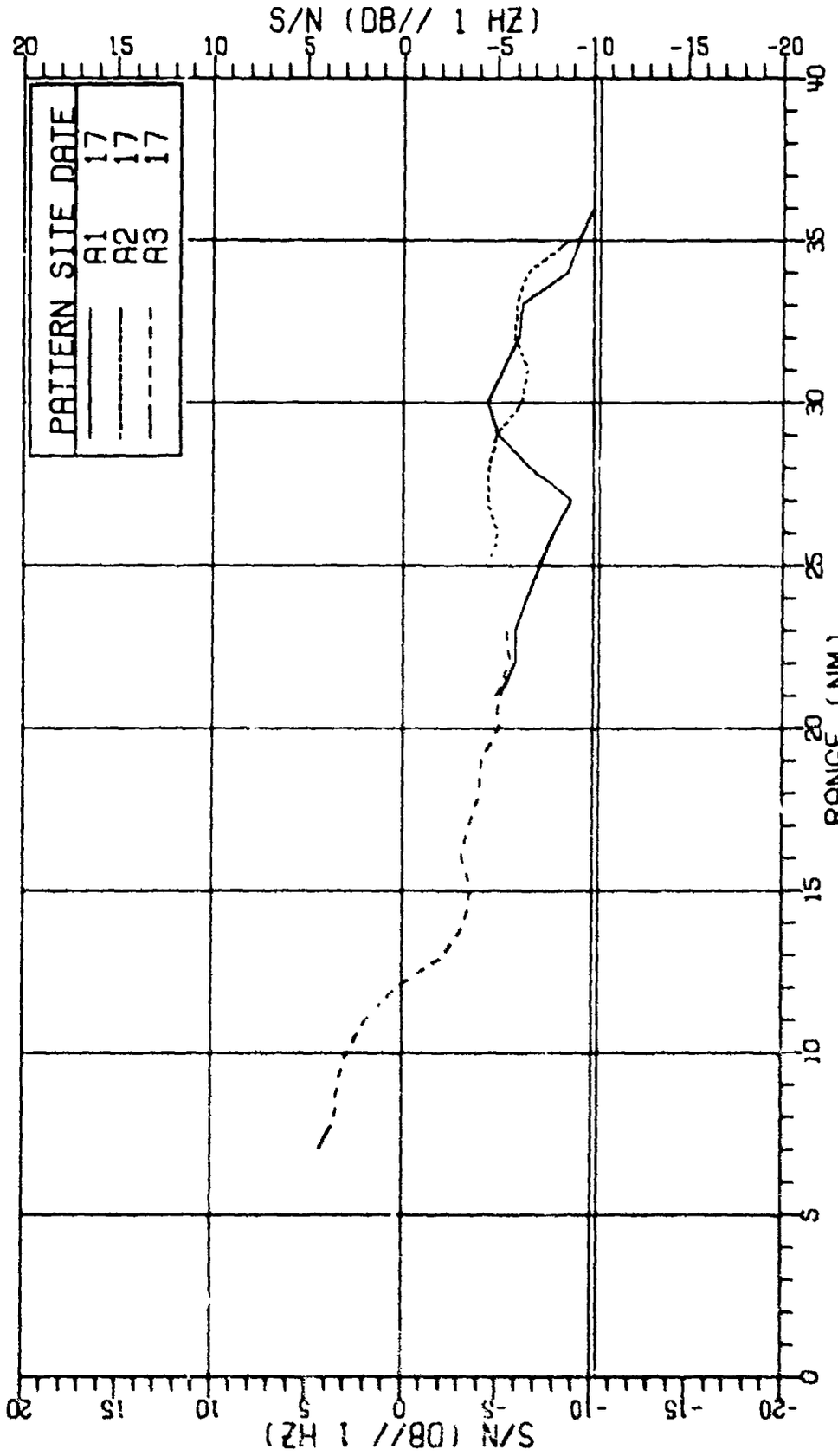

FIGURE II-293
MSS-FVT NEAR BOTTOM VERTICAL DIPOLE SENSOR
SIGNAL-TO-NOISE RESULTS FOR 335HZ AT 154DB (U)

AS-77-3220

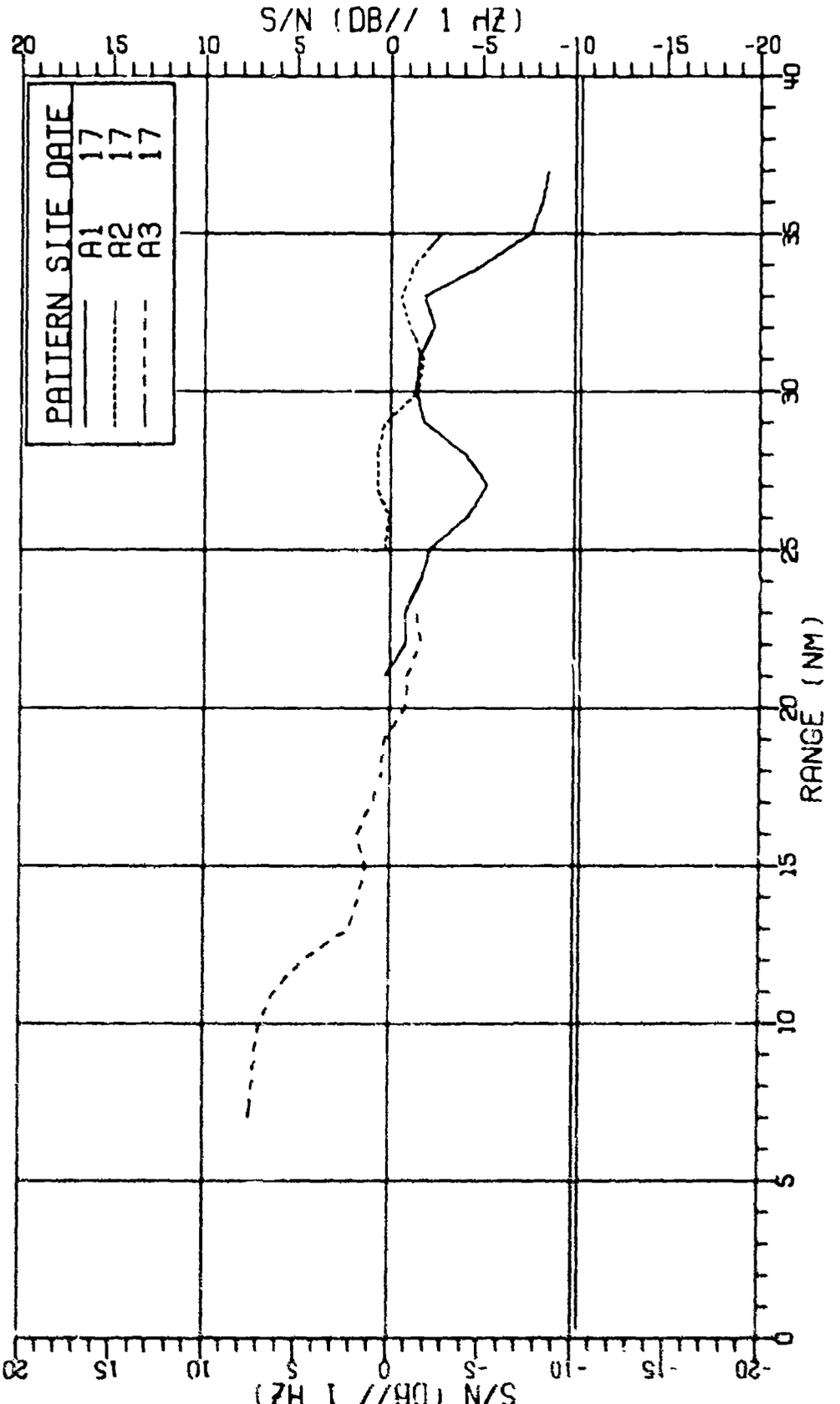

FIGURE II-294
MSS-FVT NEAR BOTTOM DIFFERENCED CARDIOIDS SENSOR
SIGNAL-TO-NOISE RESULTS FOR 335HZ AT 154DB (U)

AR-77-

'The reverse of this page is blank.'

APPENDIX H

AMBIENT SOUND FIELD LEVEL versus FREQUENCY CURVES (U)

(FIGURES H-295 - H-297)

(The reverse of this page is blank.)

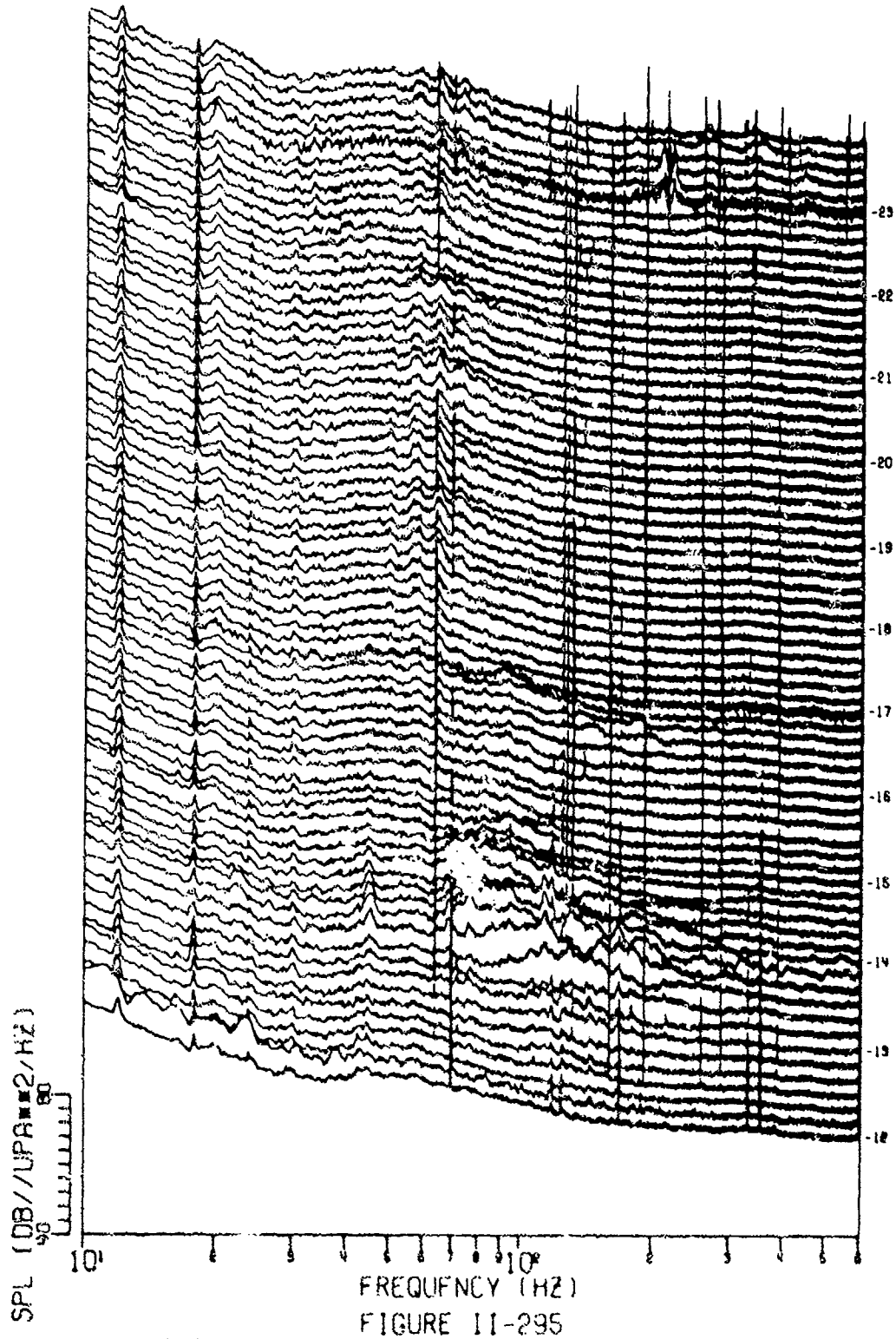

FIGURE II-295
MSS-FVT PHASE II SITE A1 OMNIDIRECTIONAL SENSOR
3D REPRESENTATION THE AMBIENT SOUND FIELD LEVELS
DURING THE 17 NOV FIELD EVENT (U)

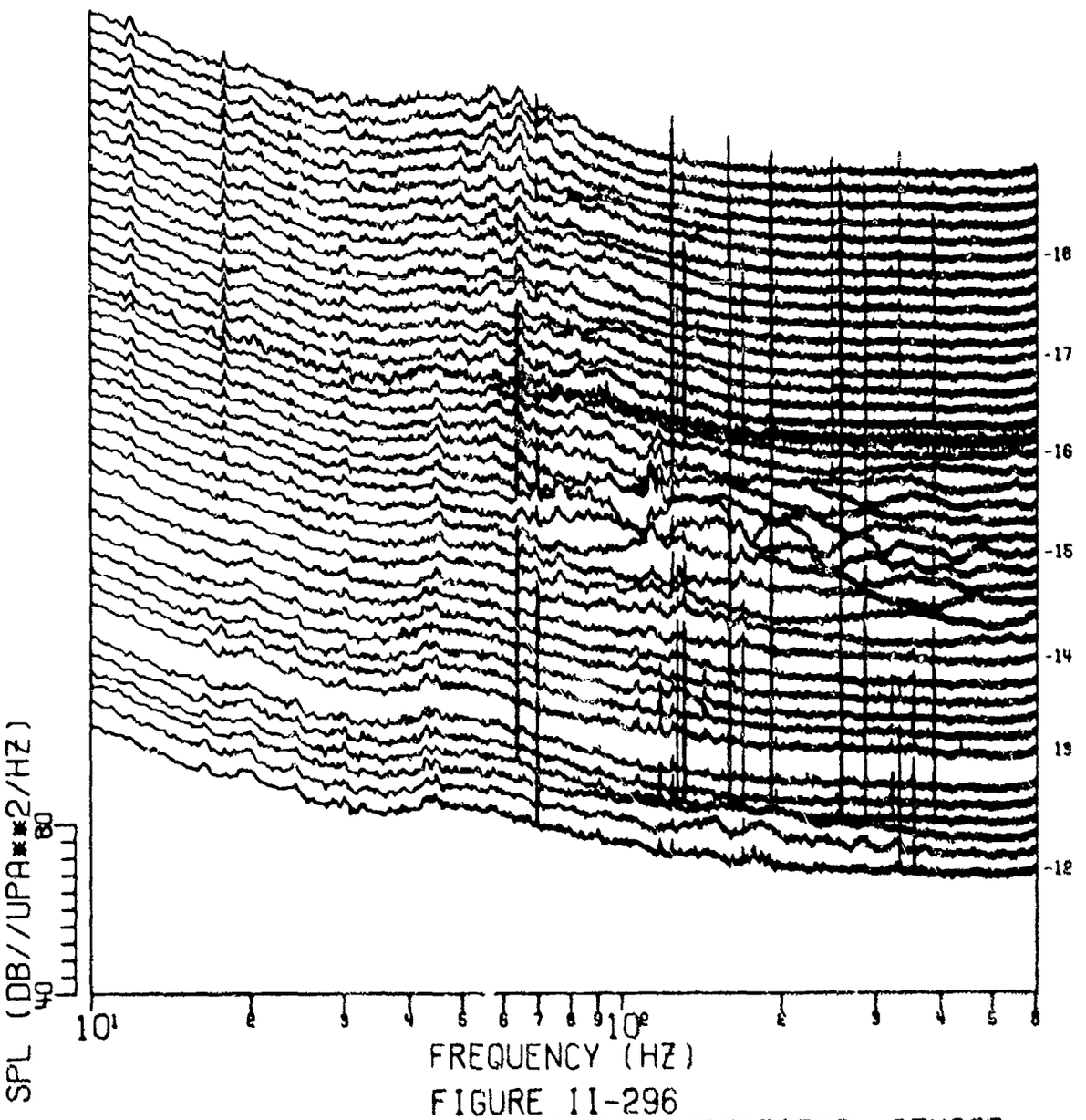

FIGURE II-296
MSS-FVT PHASE II SITE A2 OMNIDIRECTIONAL SENSOR
3D REPRESENTATION THE AMBIENT SOUND FIELD LEVELS
DURING THE 17 NOV FIELD EVENT (U)

AS-77-3310

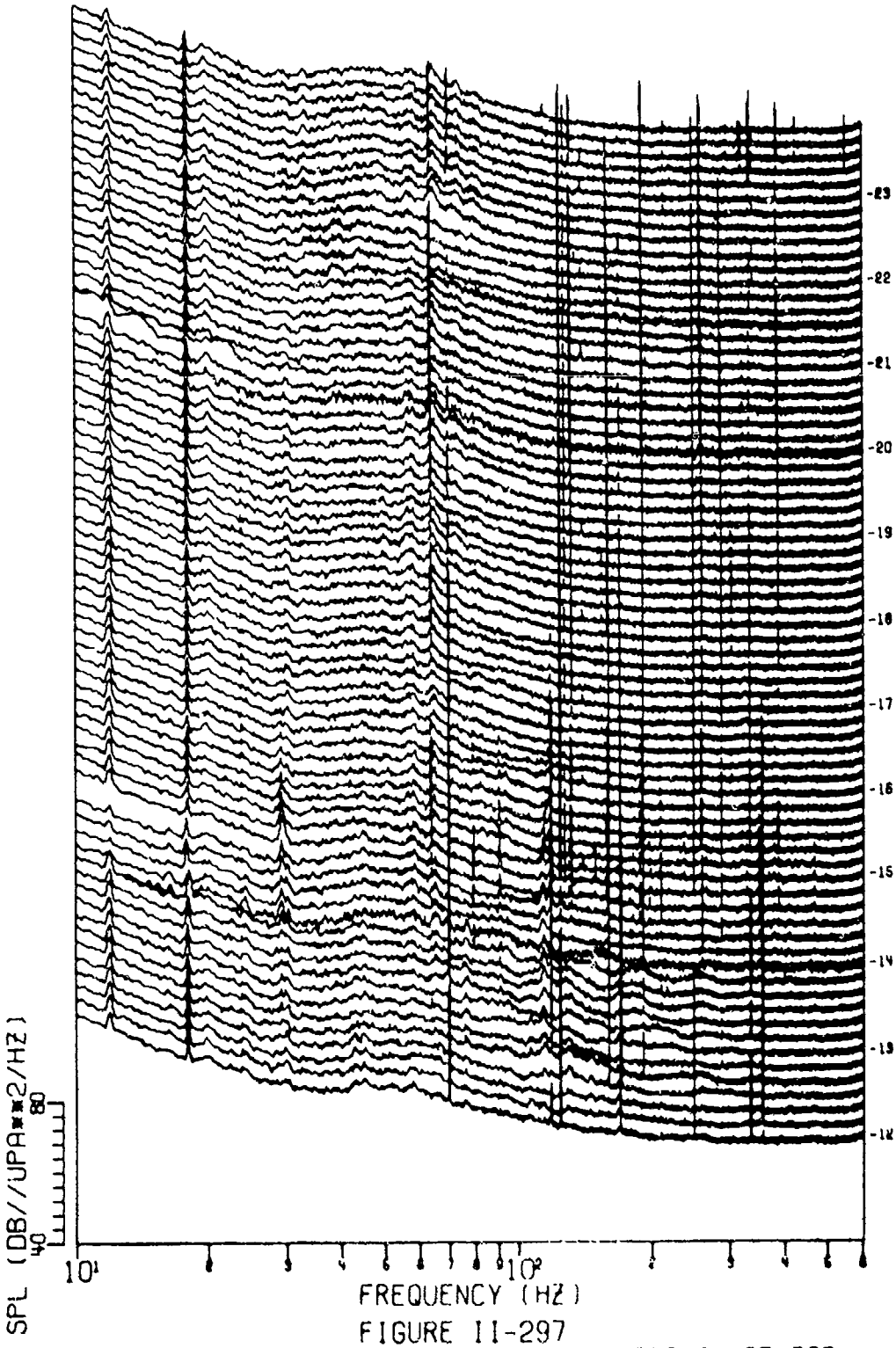

FIGURE II-297
MSS-FVT PHASE II SITE A3 OMNIDIRECTIONAL SENSOR
3D REPRESENTATION THE AMBIENT SOUND FIELD LEVELS
DURING THE 17 NOV FIELD EVENT (U)

AS-77-3311

(The reverse of this page is blank.)

APPENDIX I

NOISE GAIN TIMESERIES CURVES (U)

(FIGURES II-298 - II-327)

(The reverse of this page is blank.)

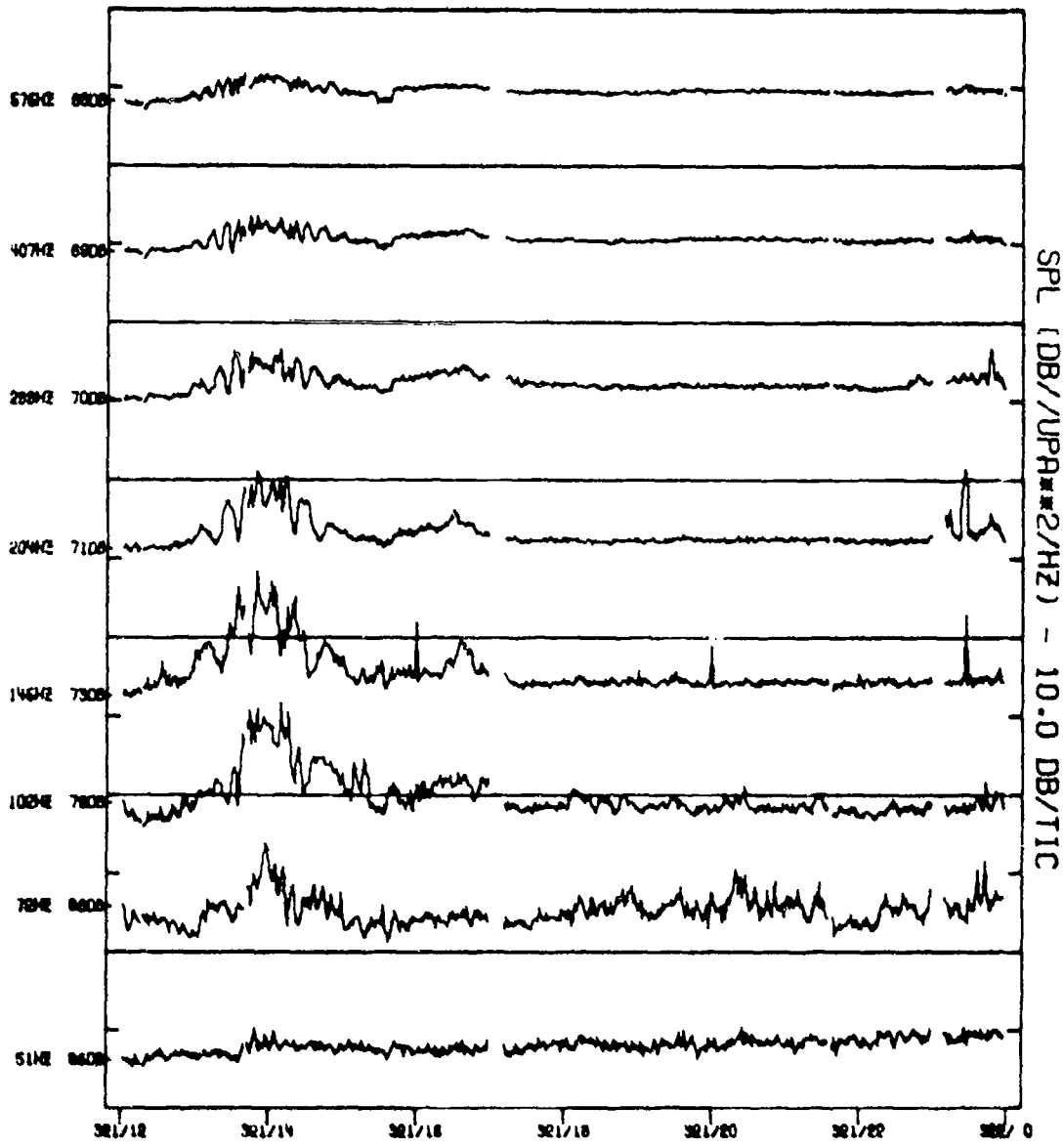

FIGURE II-298
MSS-FVT PHASE II SITE A1 OMNIDIRECTIONAL SENSOR
TIME SERIES OF 1 MIN INTENSITY-AVERAGED SOUND PRESSURE LEVELS
THROUGH 1/10-OCTAVE BANDS DURING THE 17 NOV FIELD EVENT (U)

AS-77-3312

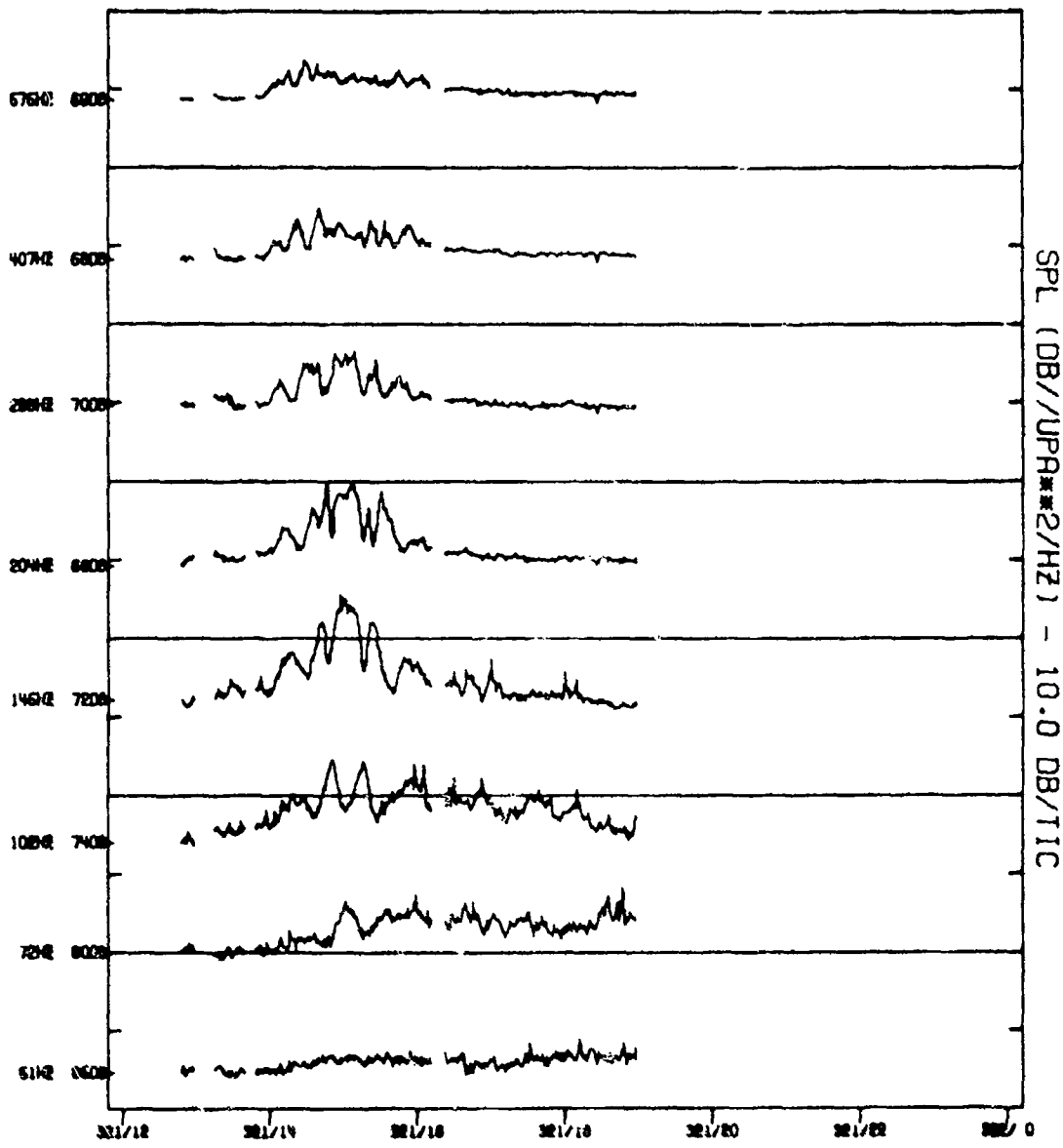

FIGURE II-299
MSS-FVT PHASE II SITE A2 OMNIDIRECTIONAL SENSOR
TIME SERIES OF 1 MIN INTENSITY-AVERAGED SOUND PRESSURE LEVELS
THROUGH 1/10-OCTAVE BANDS DURING THE 17 NOV FIELD EVENT (U)

AS-77-3313

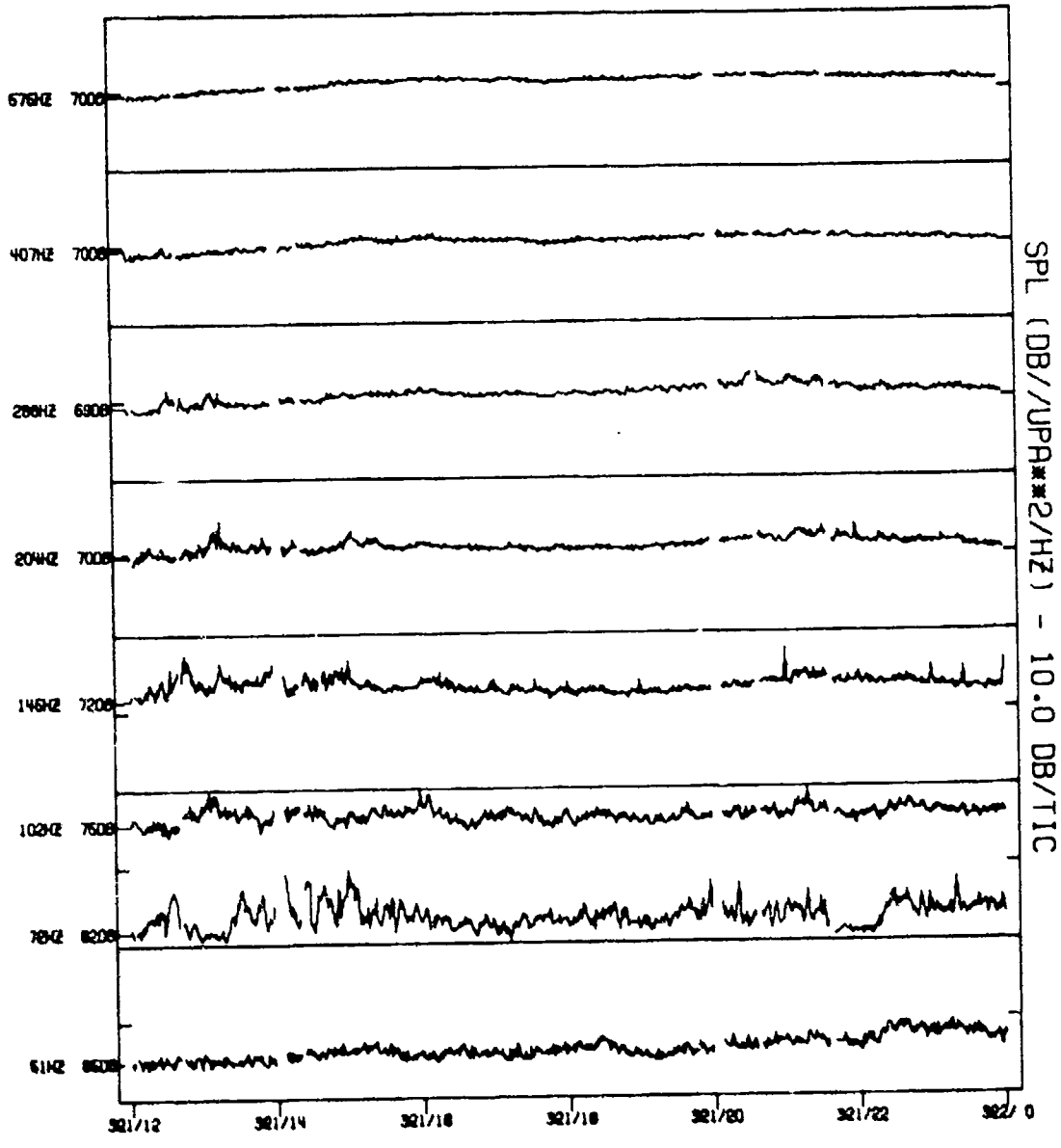

FIGURE II-300
MSS-FVT PHASE II SITE A3 OMNIDIRECTIONAL SENSOR
TIME SERIES OF 1 MIN INTENSITY-AVERAGED SOUND PRESSURE LEVELS
THROUGH 1/10-OCTAVE BANDS DURING THE 17 NOV FIELD EVENT (U)

AS-77-3314

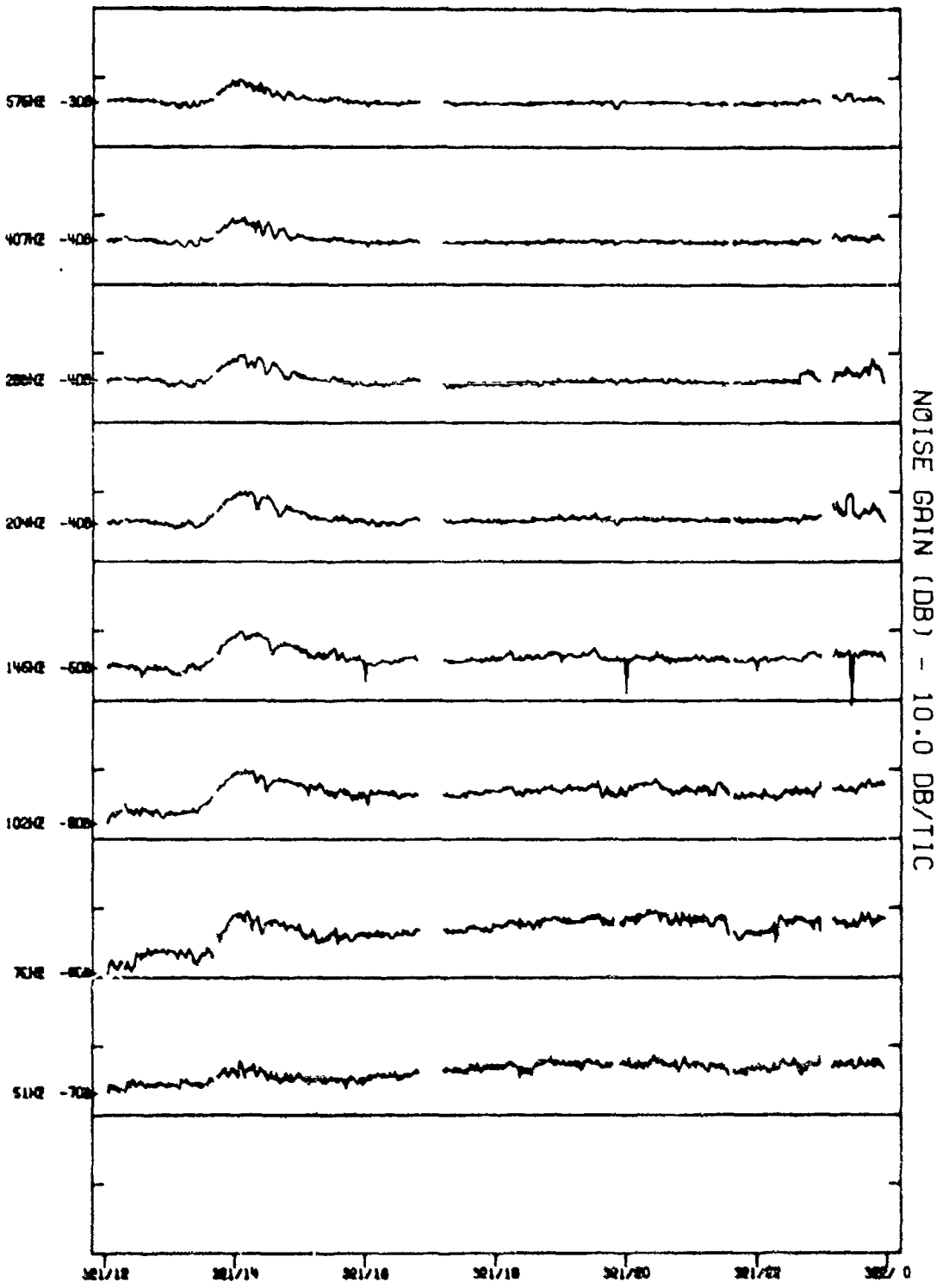

FIGURE II-301
MSS FVT PHASE II SITE A1 NORTH CARDIOID
TIME SERIES OF 1 MIN INTENSITY AVERAGED NOISE GAINS
THROUGH 1/10-OCTAVE BANDS DURING THE 17 NOV FIELD EVENT (U)

AS-77-3315

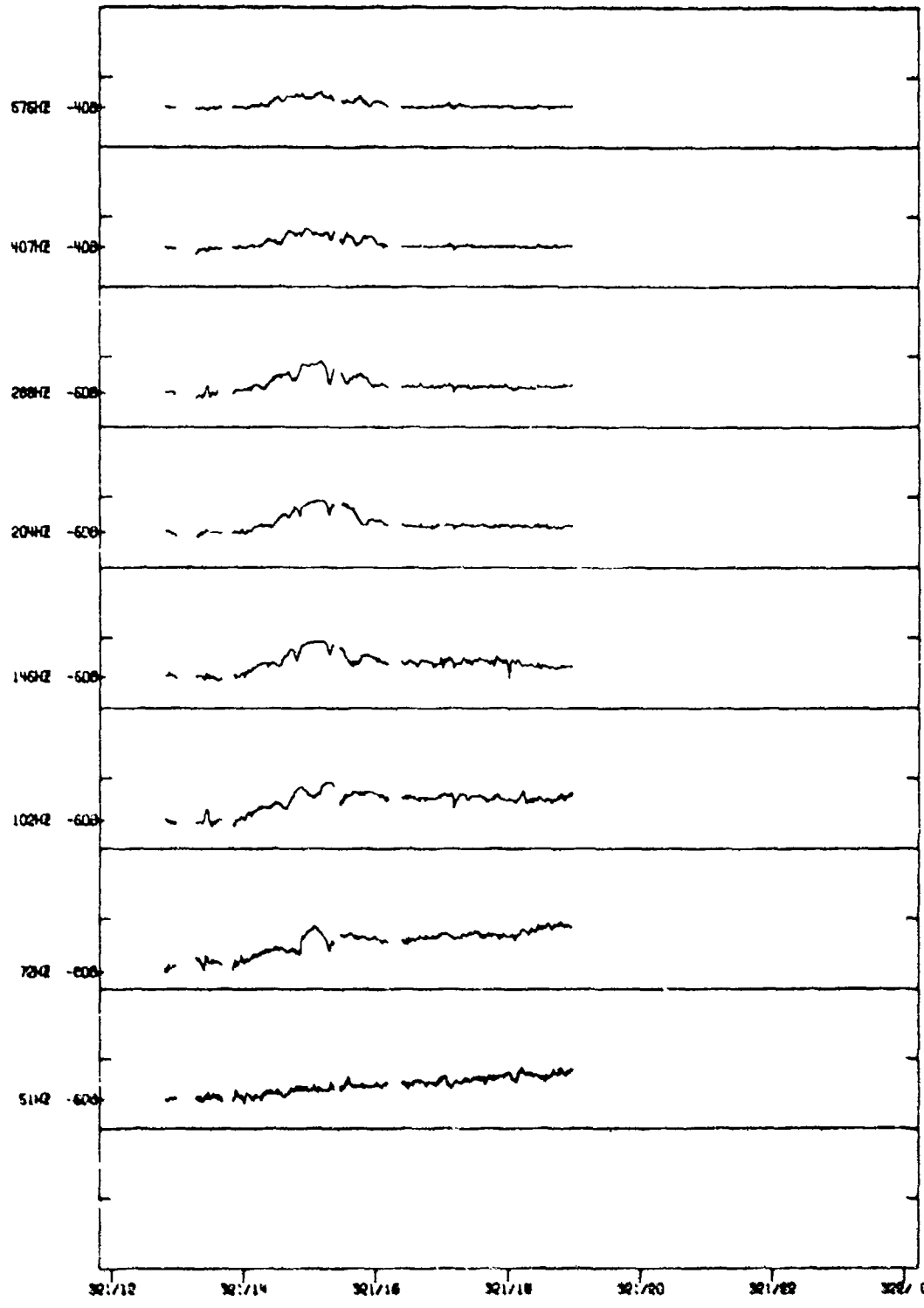

FIGURE II-302
MSS-FVT PHASE II SITE A2 NORTH CARDIOID
TIME SERIES OF 1 MIN INTENSITY-AVERAGED NOISE GAINS
THROUGH 1/10-OCTAVE BANDS DURING THE 17 NOV FIELD EVENT (U)

AS-77-3316

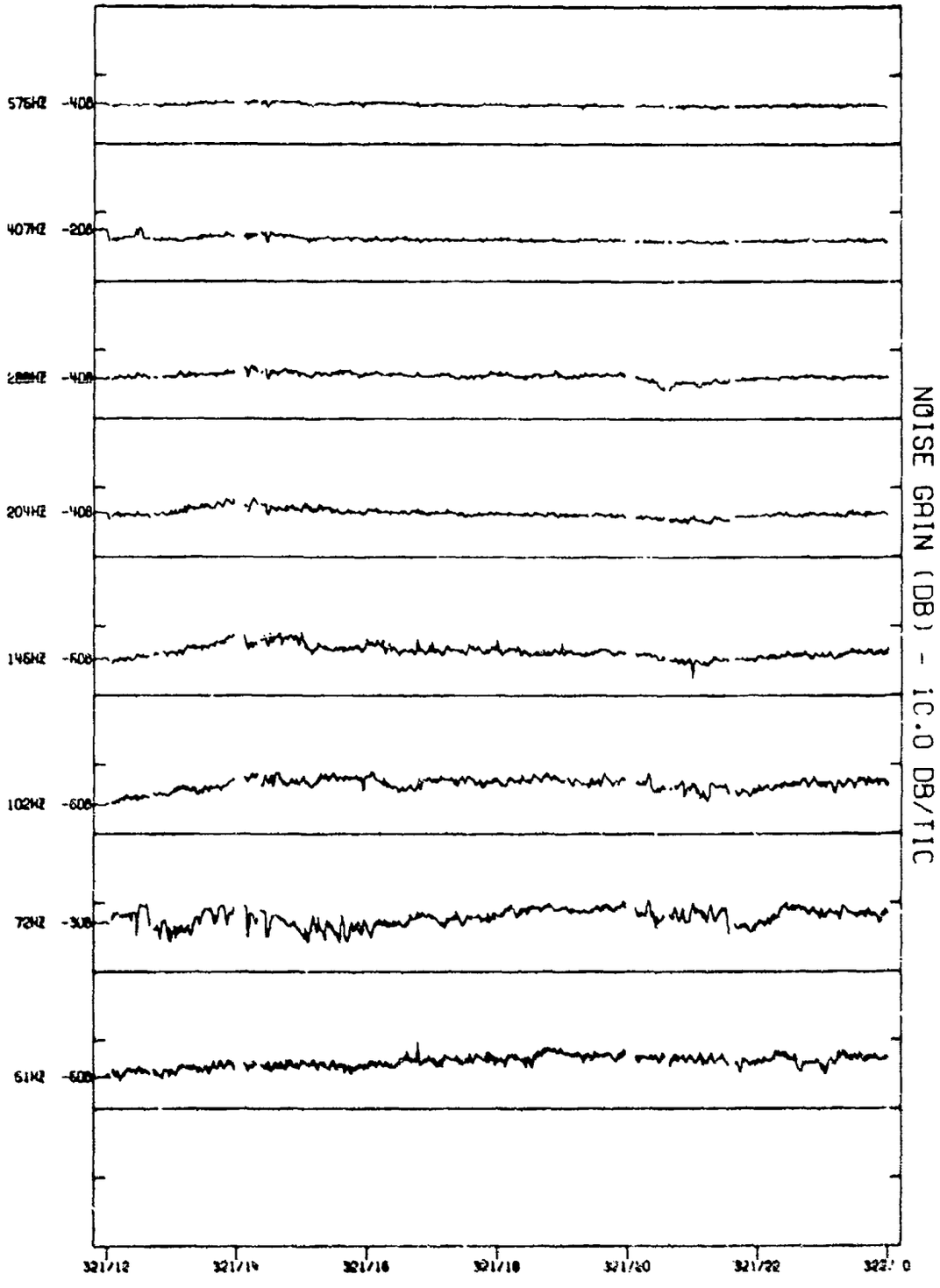

FIGURE II-303
MSS-FVT PHASE II SITE A3 NORTH CARDIOID
TIME SERIES OF 1 MIN INTENSITY-AVERAGED NOISE GAINS
THROUGH 1/10-OCTAVE BANDS DURING THE 17 NOV FIELD EVENT (U)

AS-77-3317

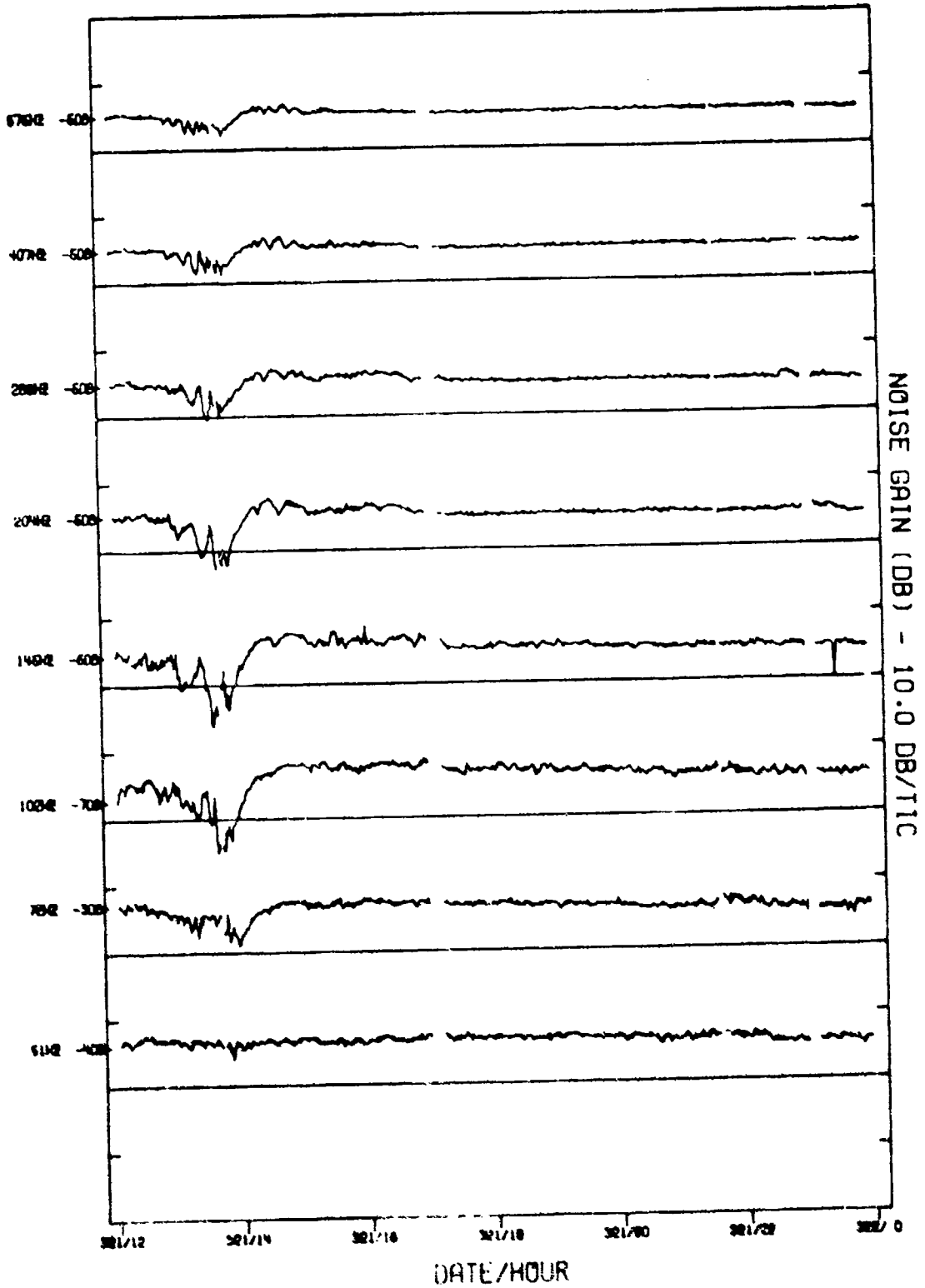

FIGURE II-304
MSS-FVT PHASE II SITE A1 EAST CARDIOID
TIME SERIES OF 1 MIN INTENSITY-AVERAGED NOISE GAINS
THROUGH 1/10-OCTAVE BANDS DURING THE 17 NOV FIELD EVENT (U)

AS-77-3318

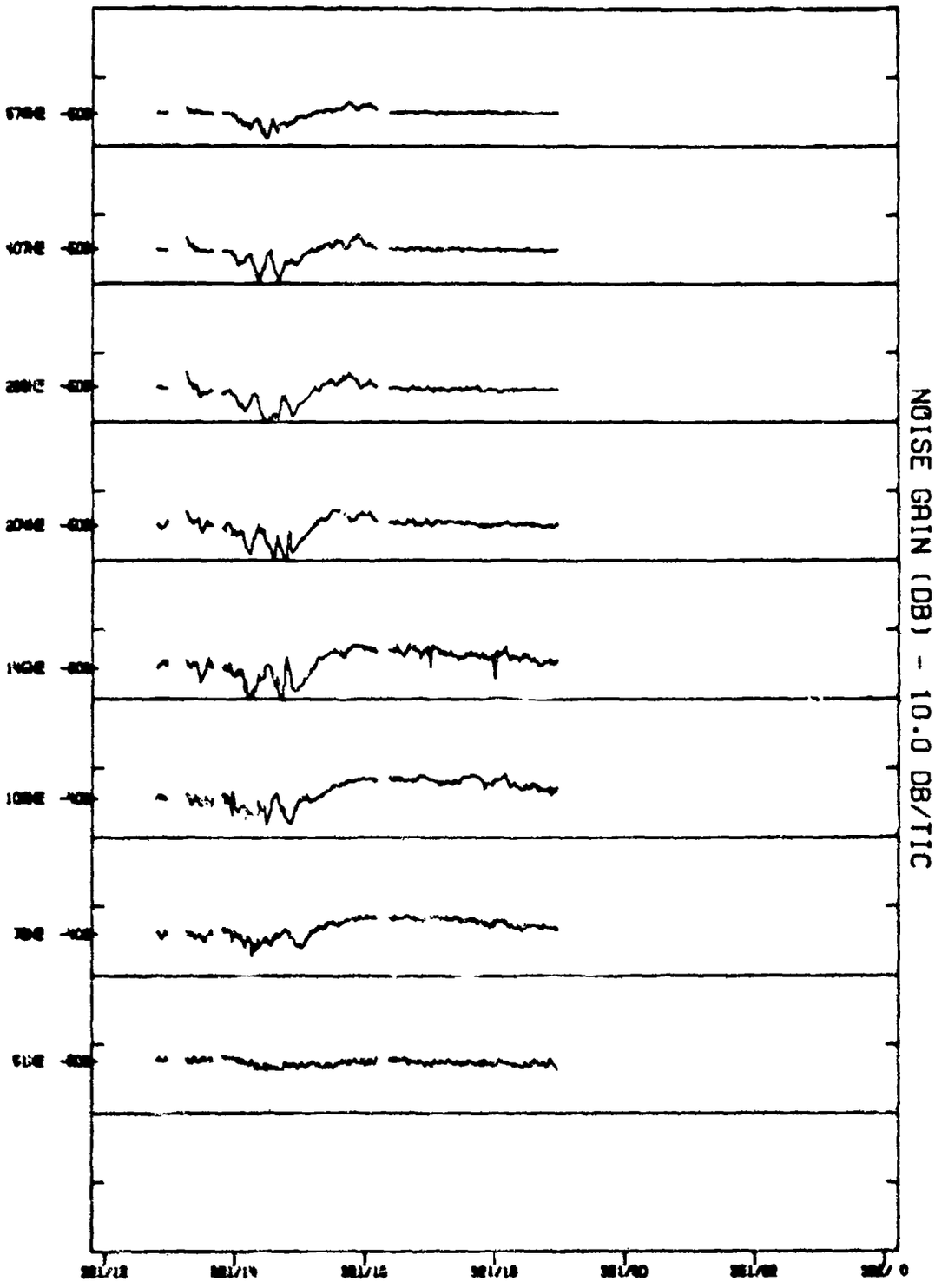

FIGURE II-305
MSS-[illegible]VT PHASE II SITE A2 EAST CARDIOID
TIME SERIES OF 1 MIN INTENSITY-AVERAGED NOISE GAINS
THROUGH 1/10-OCTAVE BANDS DURING THE 17 NOV FIELD EVENT (U)

AS-77-3319

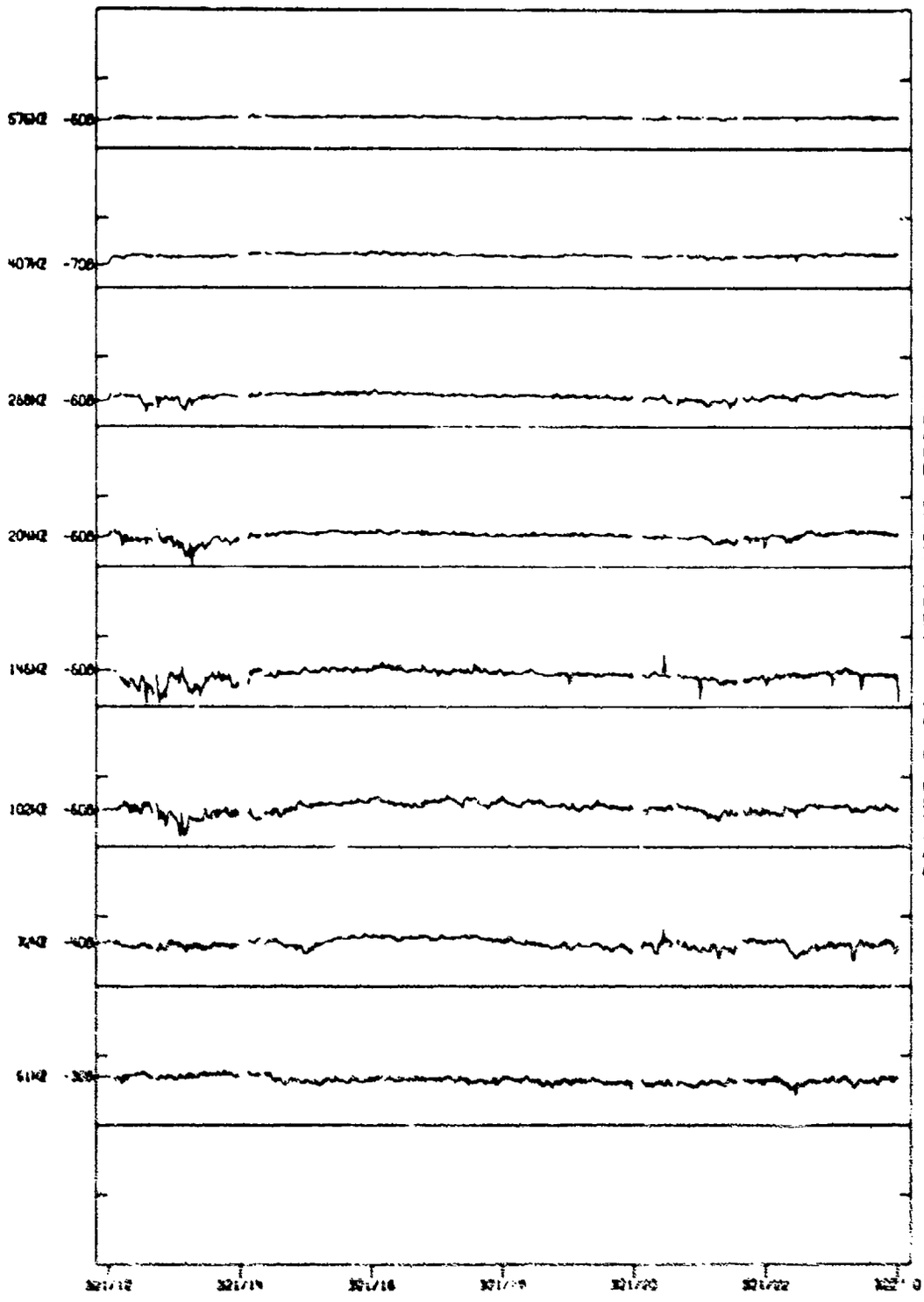

FIGURE II-306
MSS-FVT PHASE II SITE A3 EAST CARDIOID
TIME SERIES OF 1 MIN INTENSITY-AVERAGED NOISE GAINS
THROUGH 1/10-OCTAVE BANDS DURING THE 17 NOV FIELD EVENT (U)

AS-77-3320

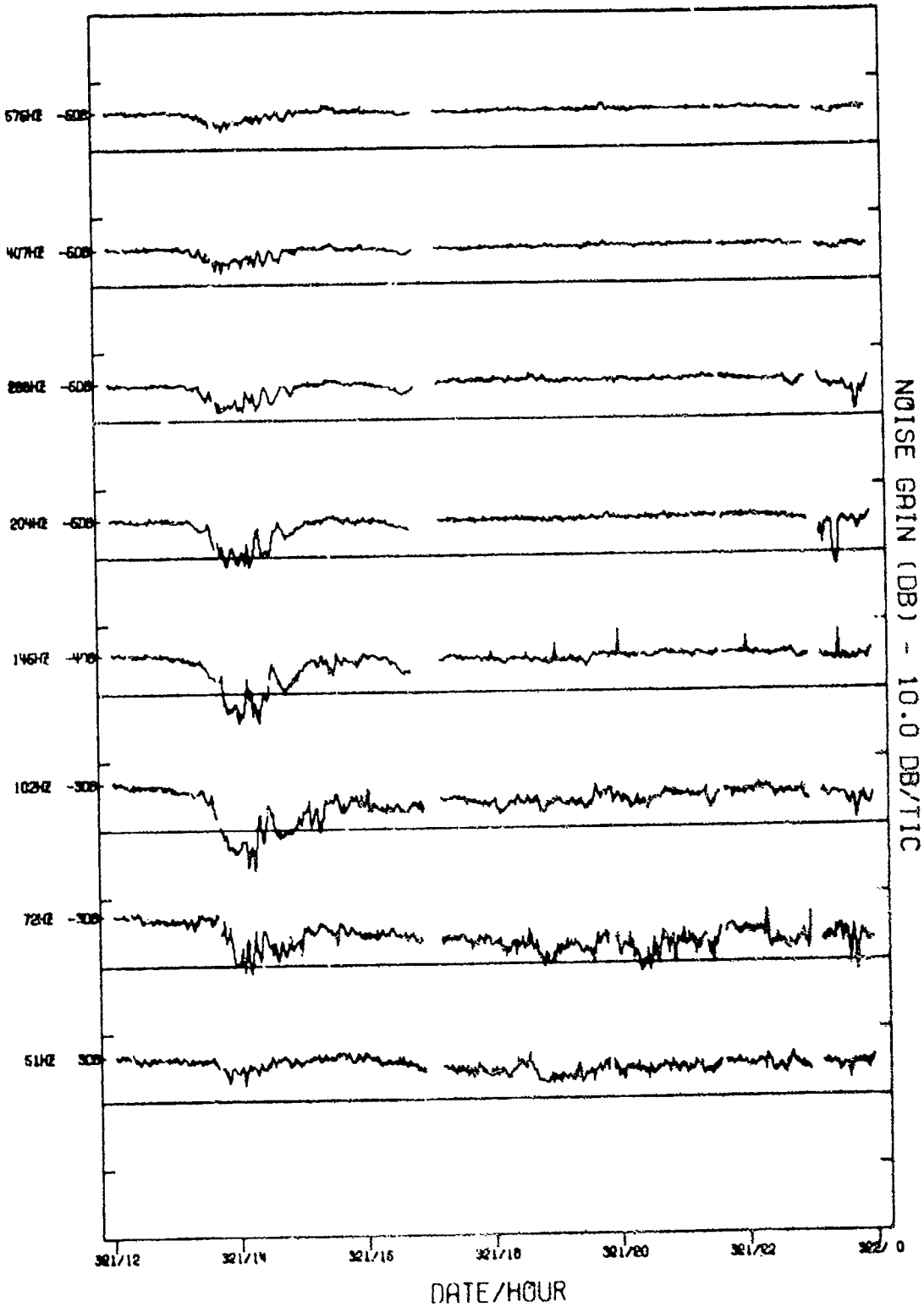

FIGURE II-307
MSS-FVT PHASE II SITE A1 SOUTH CARDIOID
TIME SERIES OF 1 MIN INTENSITY-AVERAGED NOISE GAINS
THROUGH 1/10-OCTAVE BANDS DURING THE 17 NOV FIELD EVENT (U)

AS-77-3321

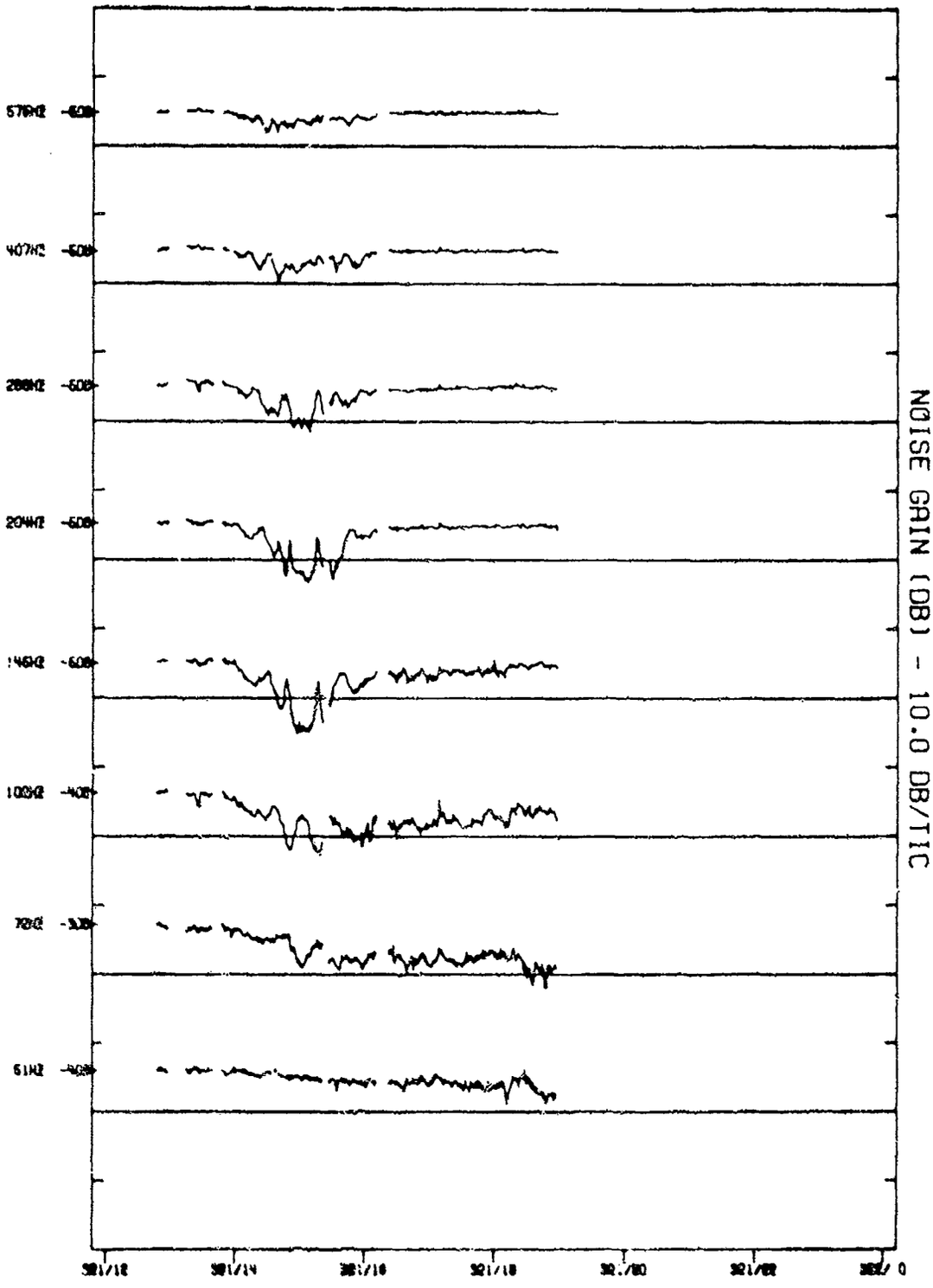

FIGURE II-308
MSS-FVT PHASE II SITE A2 SOUTH CARDIOID
TIME SERIES OF 1 MIN INTENSITY-AVERAGED NOISE GAINS
THROUGH 1/10-OCTAVE BANDS DURING THE 17 NOV FIELD EVENT (U)

AS-77-3322

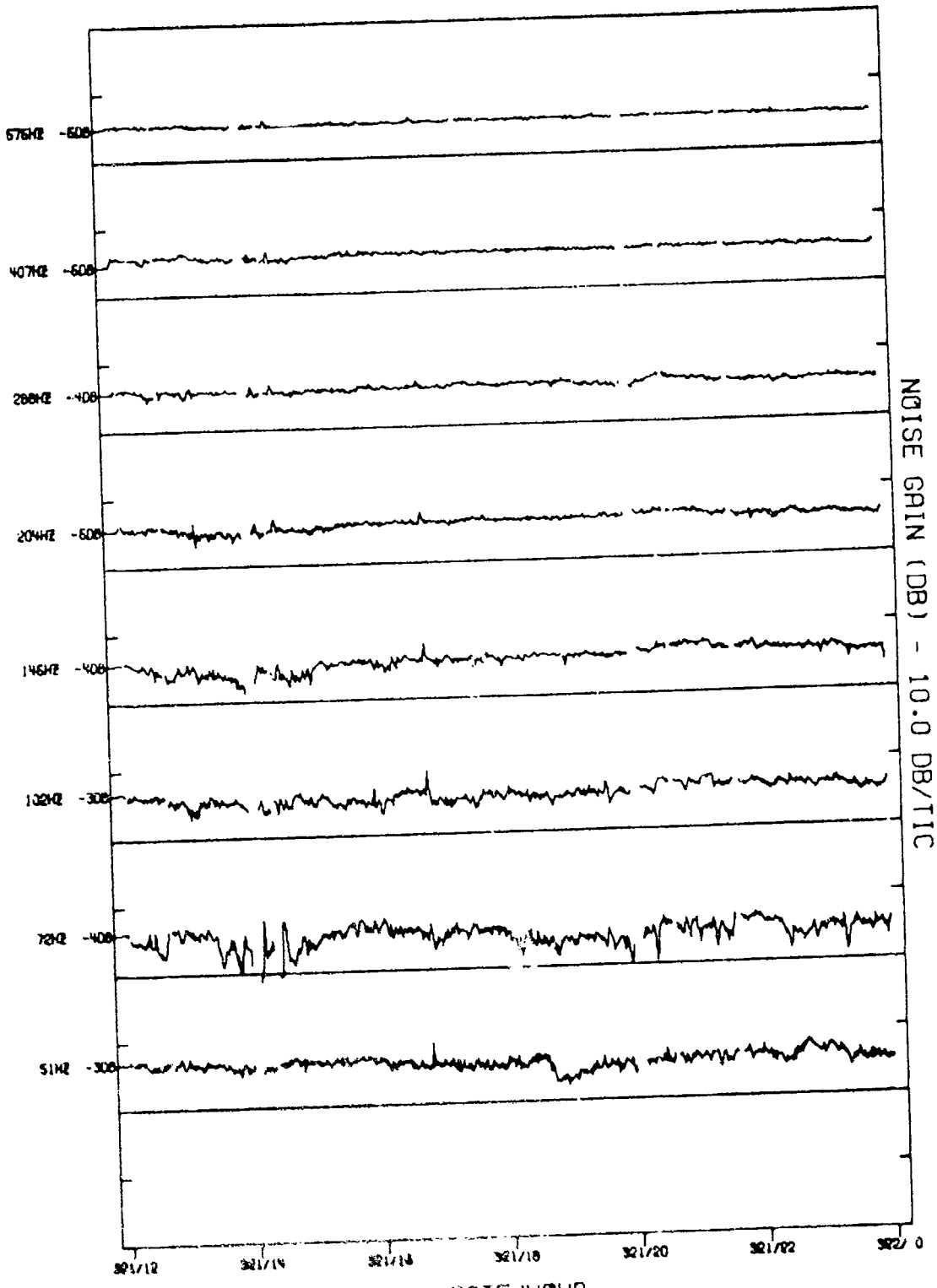

FIGURE II-309
MSS-FVT PHASE II SITE A3 SOUTH CARDIOID
TIME SERIES OF 1 MIN INTENSITY-AVERAGED NOISE GAINS
THROUGH 1/10-OCTAVE BANDS DURING THE 17 NOV FIELD EVENT (U)

AS-77-3323

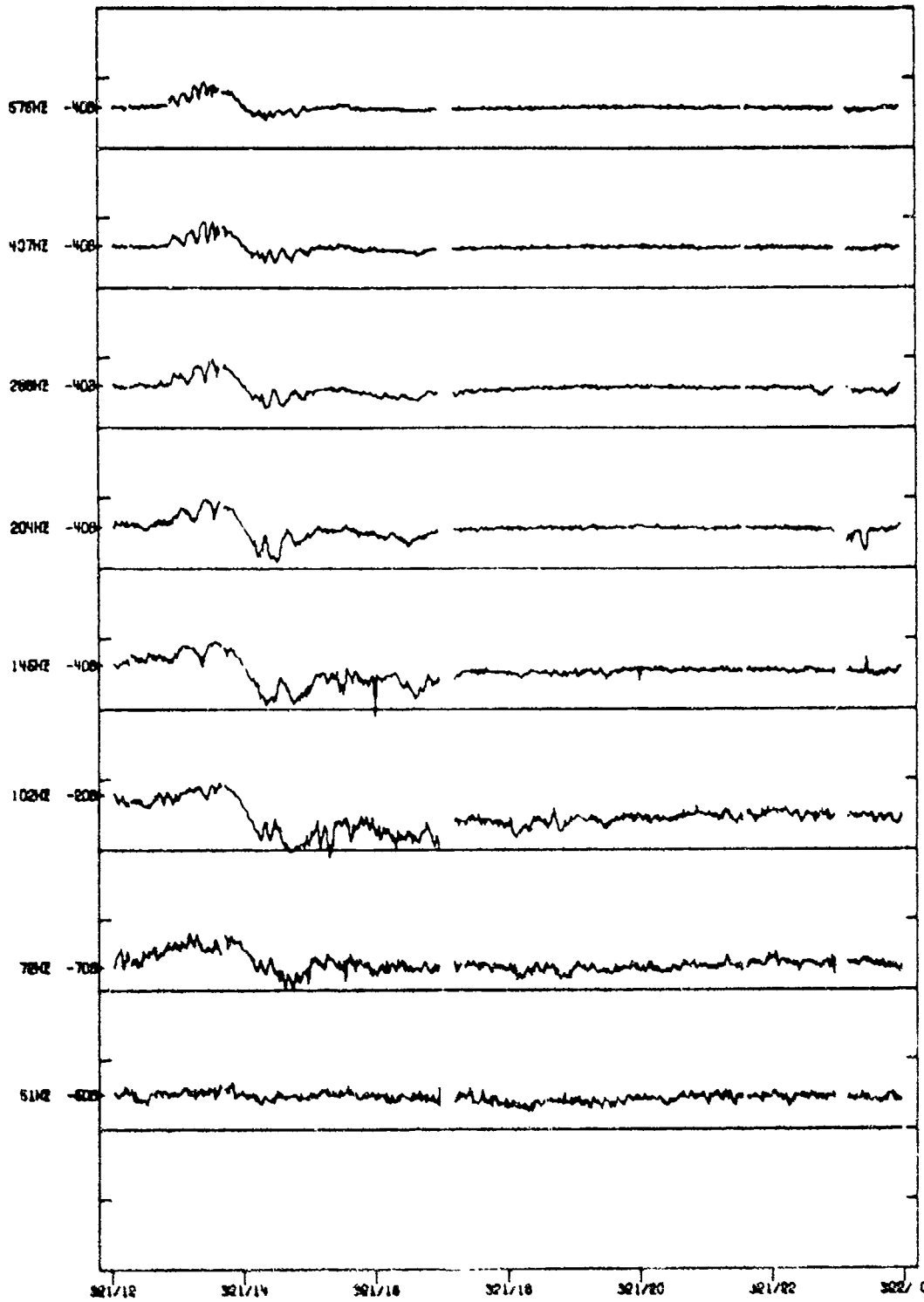

FIGURE II-310
MSS-FVT PHASE II SITE A1 WEST CARDIOID
TIME SERIES OF 1 MIN INTENSITY-AVERAGED NOISE GAINS
THROUGH 1/10-OCTAVE BANDS DURING THE 17 NOV FIELD EVENT (U)

AS-77-3324

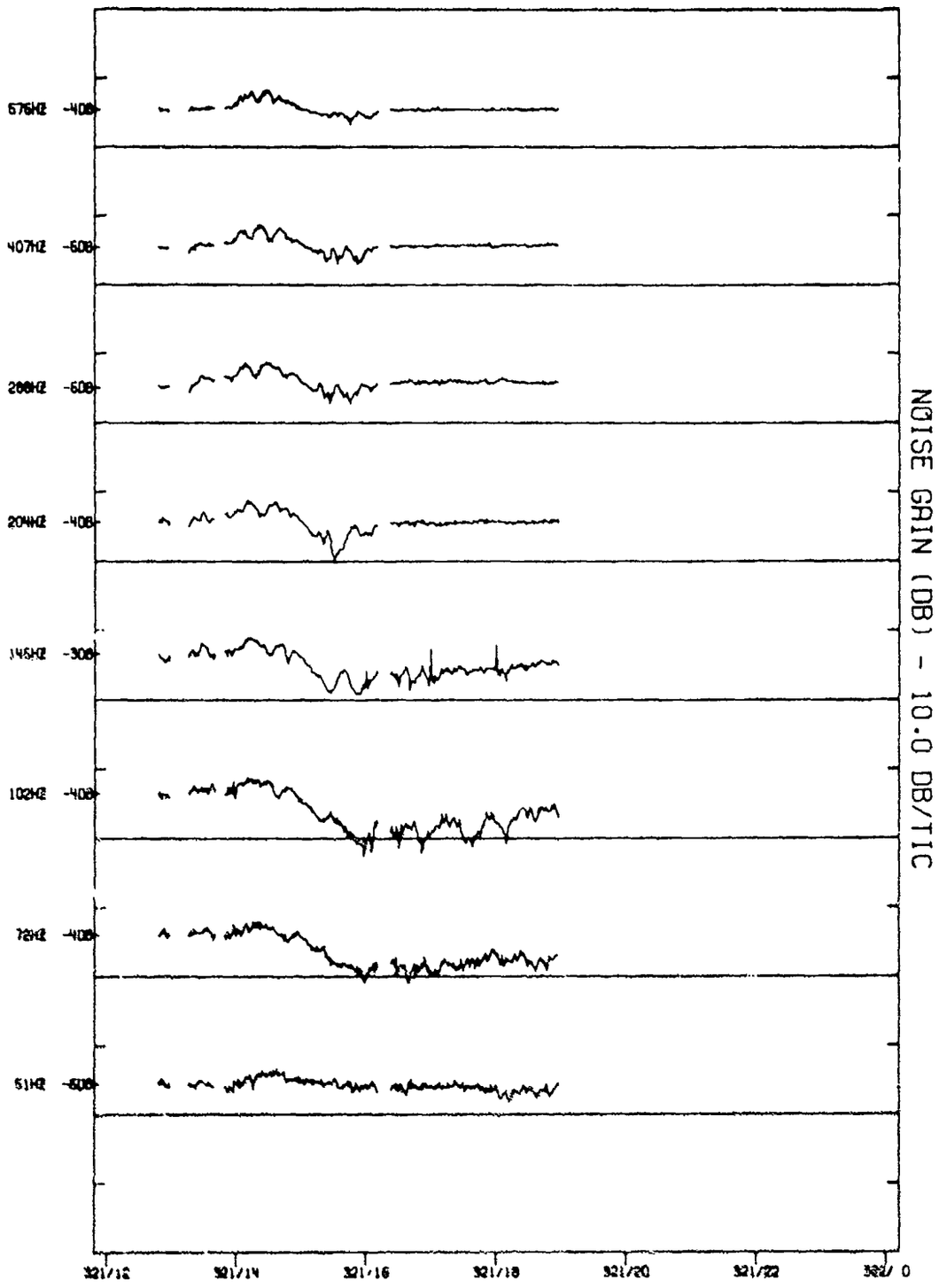

FIGURE II-311
MSS-FVT PHASE II SITE A2 WEST CARDIOID
TIME SERIES OF 1 MIN INTENSITY-AVERAGED NOISE GAINS
THROUGH 1/10-OCTAVE BANDS DURING THE 17 NOV FIELD EVENT (U)

AS-77-3325

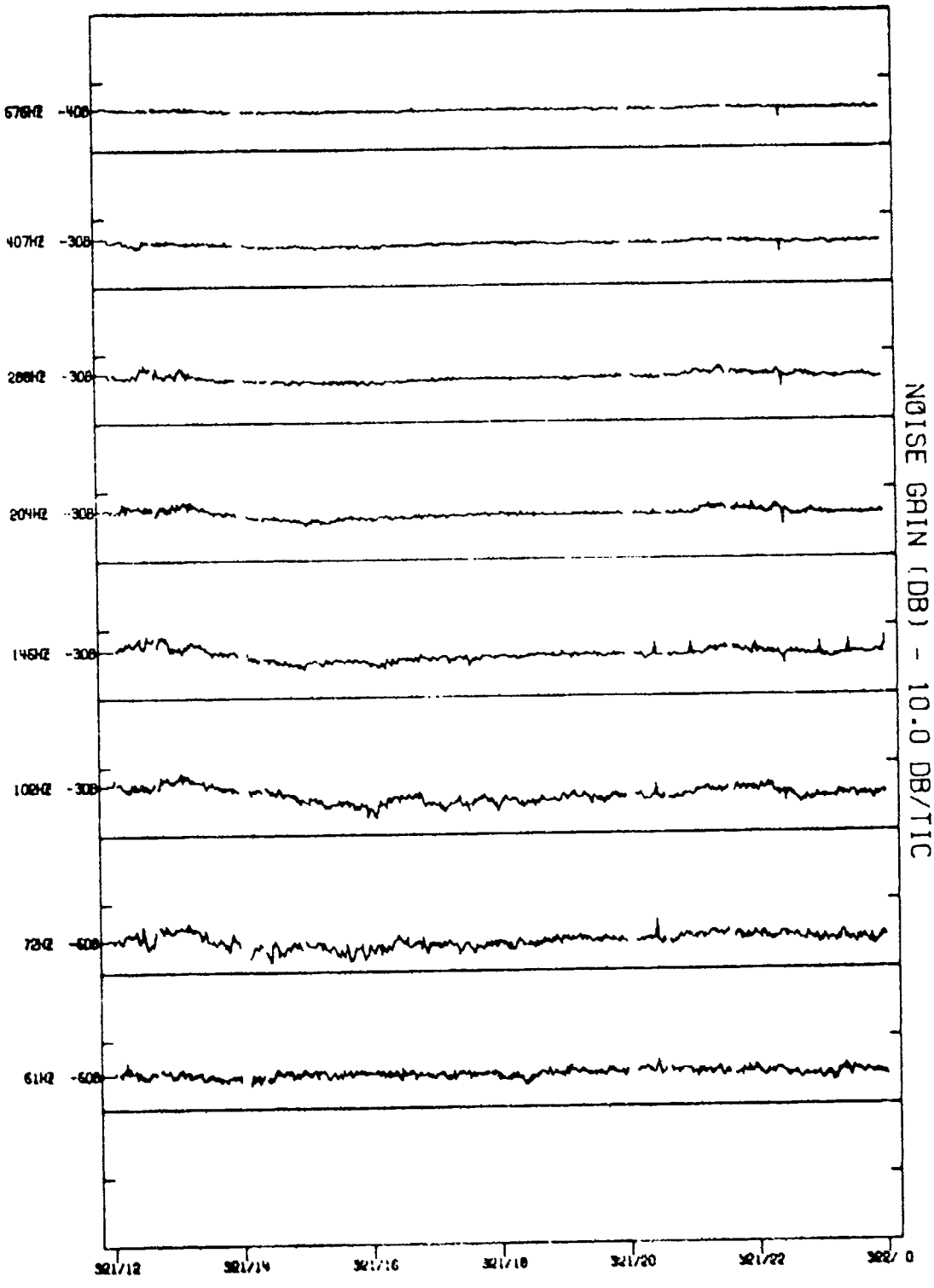

FIGURE II-312
MSS-FVT PHASE II SITE A3 WEST CARDIOID
TIME SERIES OF 1 MIN INTENSITY-AVERAGED NOISE GAINS
THROUGH 1/10-OCTAVE BANDS DURING THE 17 NOV FIELD EVENT (U)

AS-77-3326

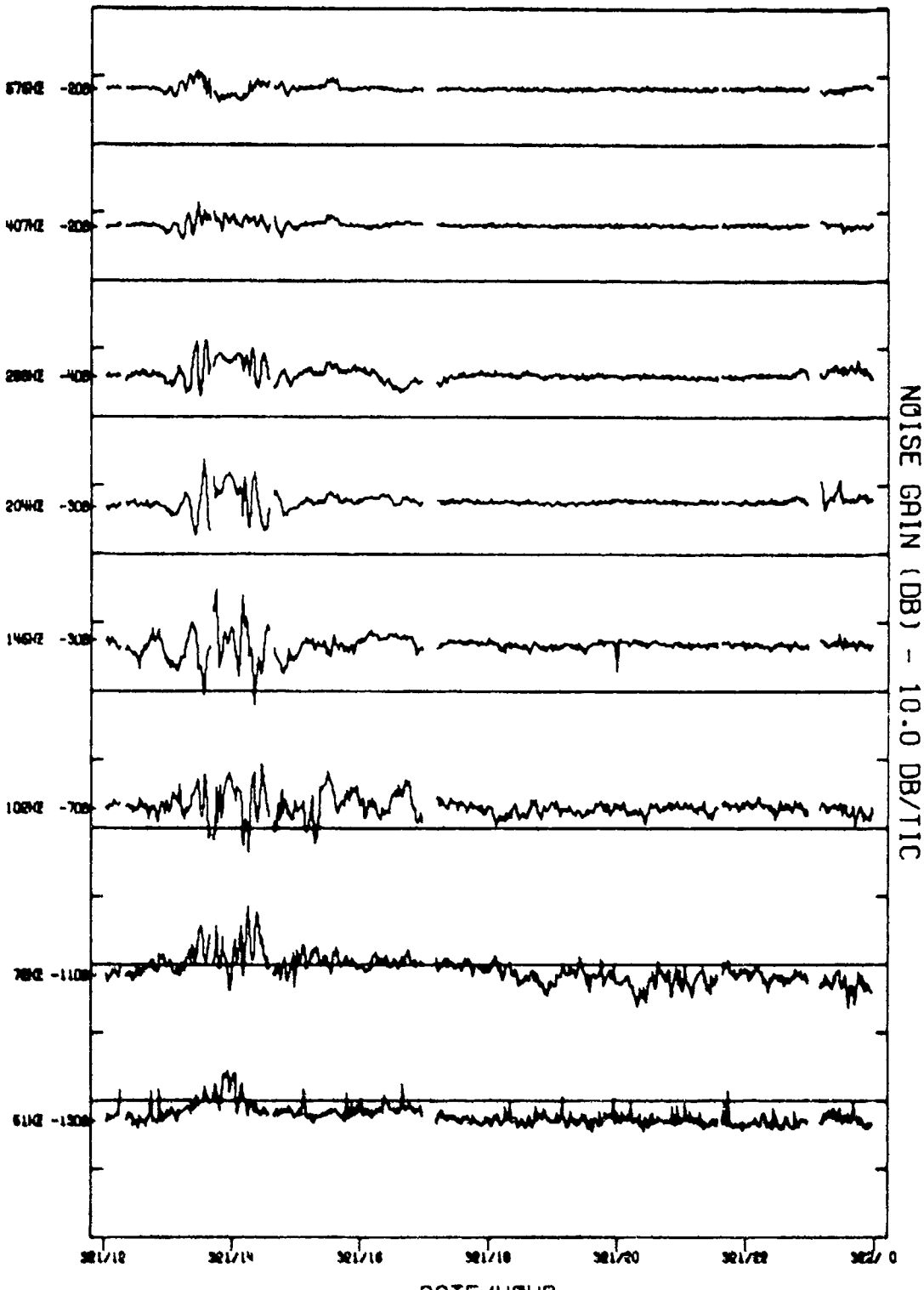

FIGURE II-313
MSS-FVT PHASE II SITE A1 VERTICAL DIPOLE SENSOR
TIME SERIES OF 1 MIN INTENSITY-AVERAGED NOISE GAINS
THROUGH 1/10-OCTAVE BANDS DURING THE 17 NOV FIELD EVENT (U)

AS-77-3327

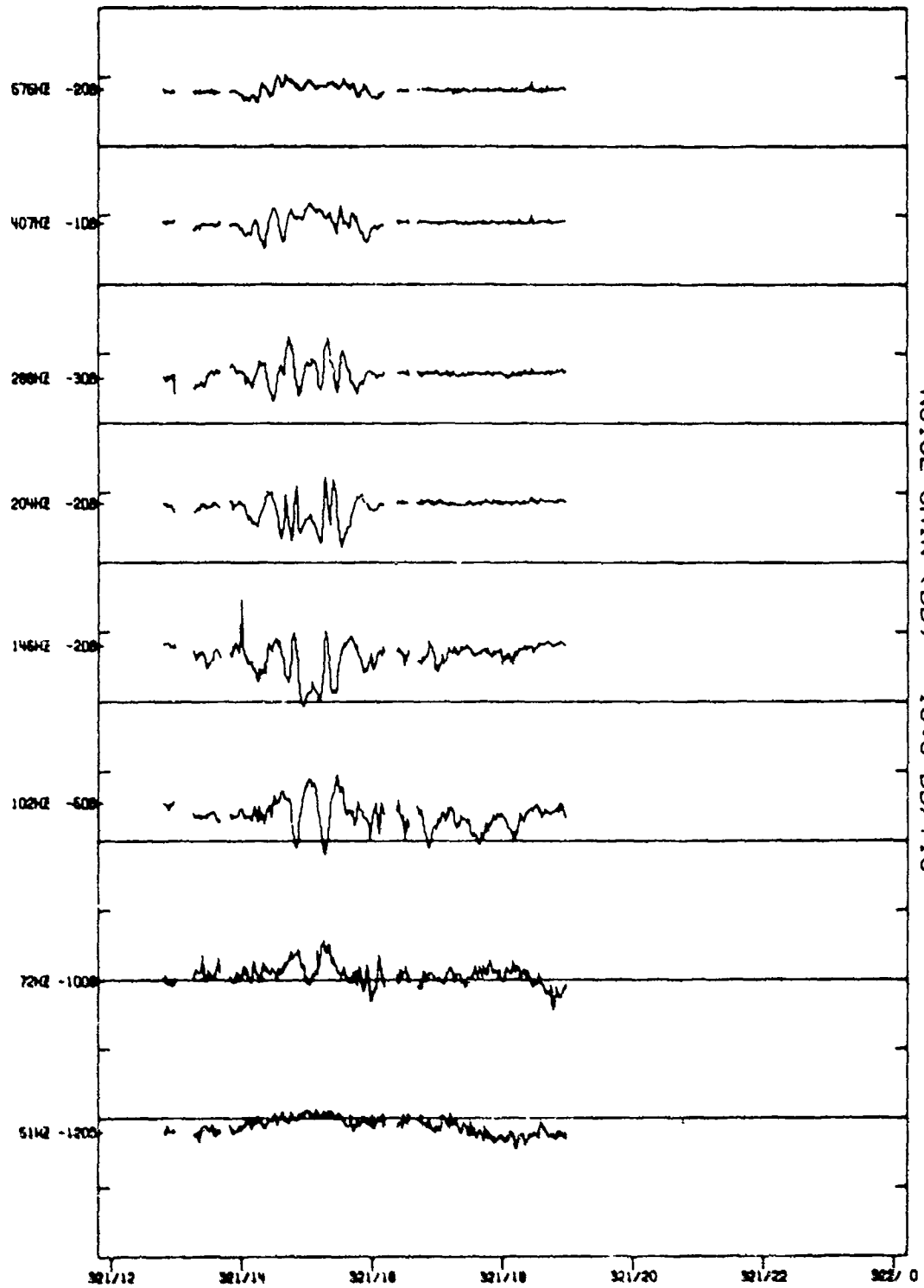

FIGURE II-314
MSS-FVT PHASE II SITE A2 VERTICAL DIPOLE SENSOR
TIME SERIES OF 1 MIN INTENSITY-AVERAGED NOISE GAINS
THROUGH 1/10-OCTAVE BANDS DURING THE 17 NOV FIELD EVENT (U)

AS-77-3328

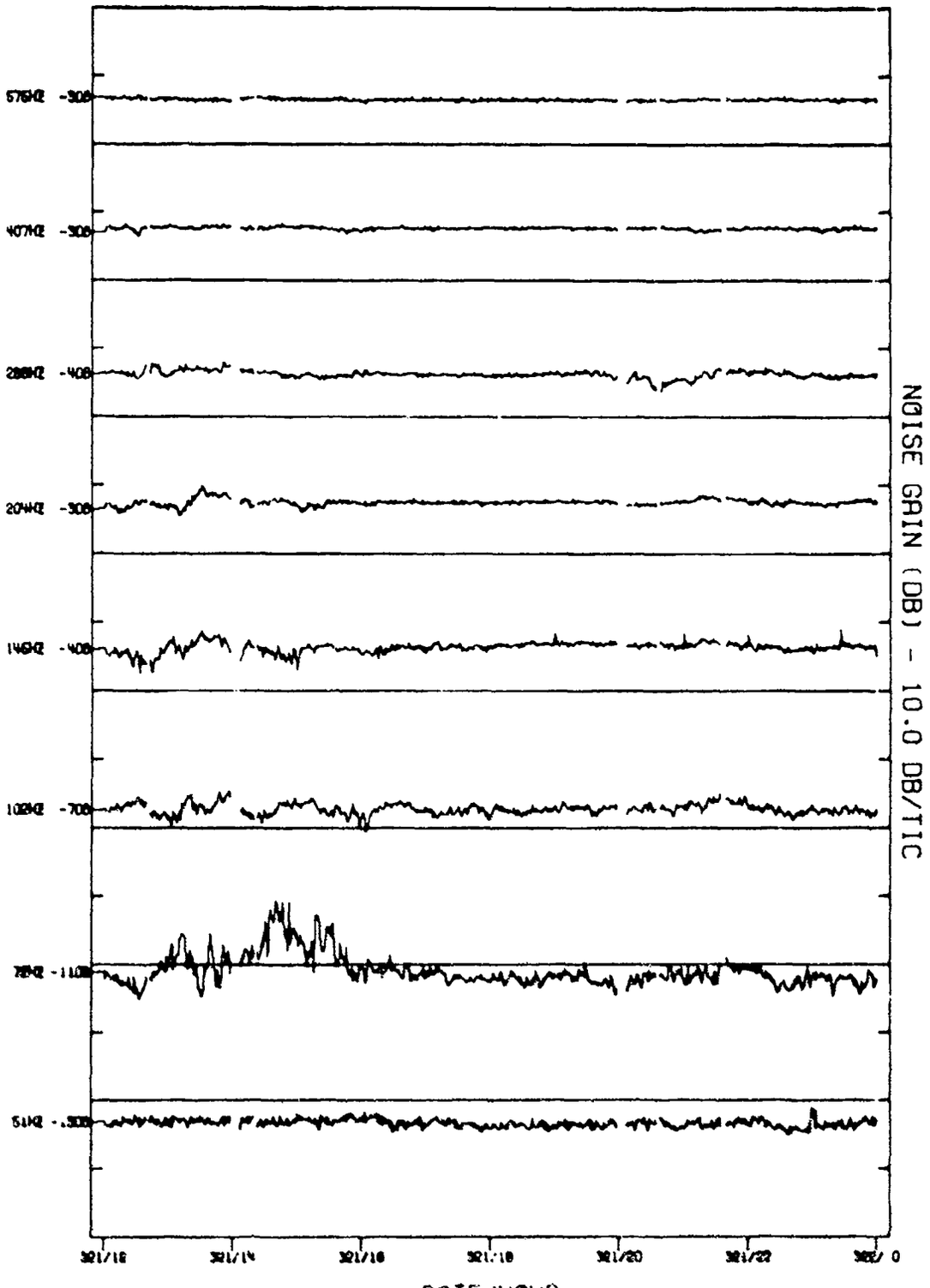

FIGURE II-315
MSS-FVT PHASE II SITE A3 VERTICAL DIPOLE SENSOR
TIME SERIES OF 1 MIN INTENSITY-AVERAGED NOISE GAINS
THROUGH 1/10-OCTAVE BANDS DURING THE 17 NOV FIELD EVENT (U)

AS-77-3329

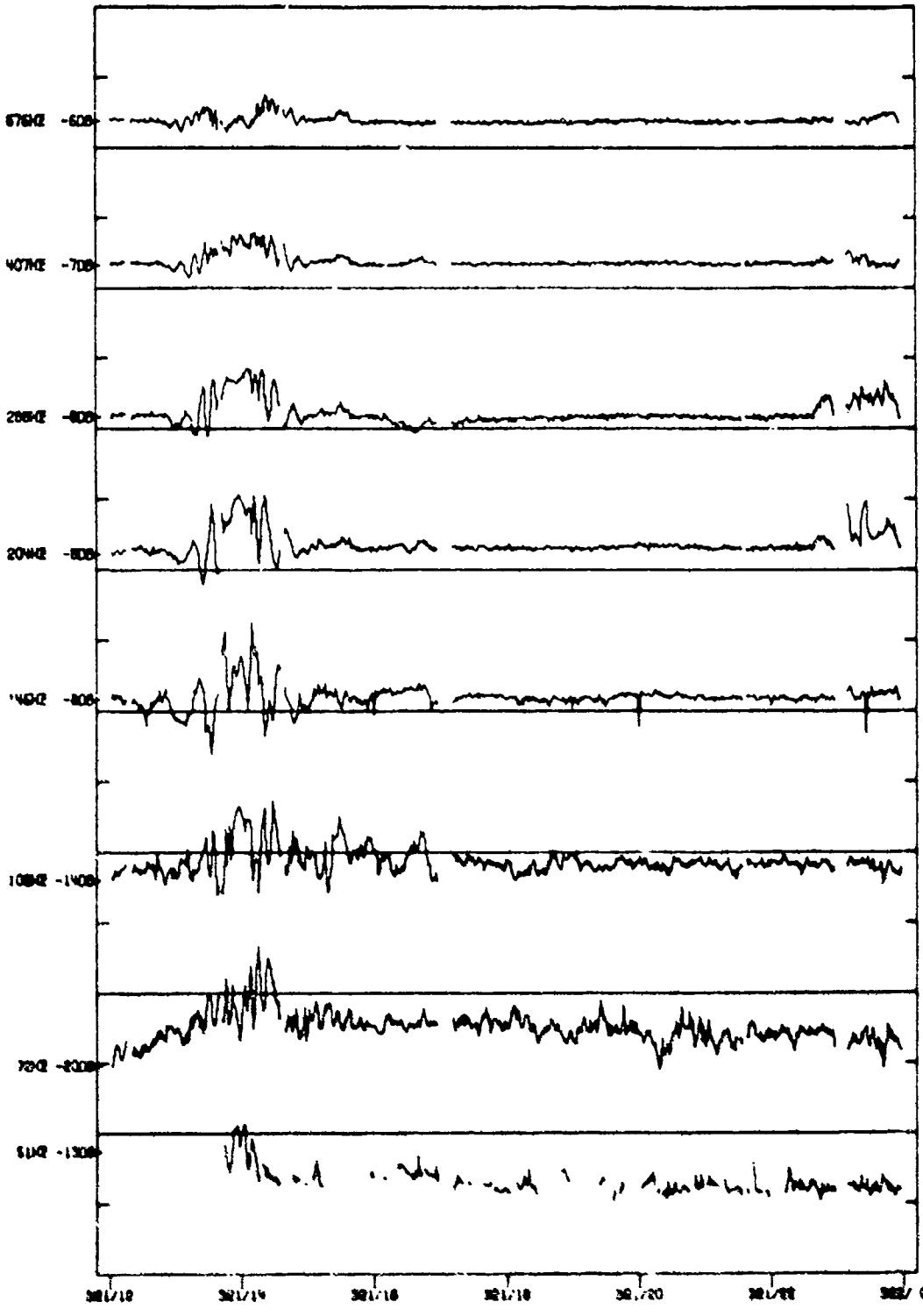

FIGURE II-316
MSS-FVT PHASE II SITE A1 DIFFERENCED NORTH CARDIOID
TIME SERIES OF 1 MIN INTENSITY-AVERAGED NOISE GAINS
THROUGH 1/10-OCTAVE BANDS DURING THE 17 NOV FIELD EVENT (U)

AS-77-3330

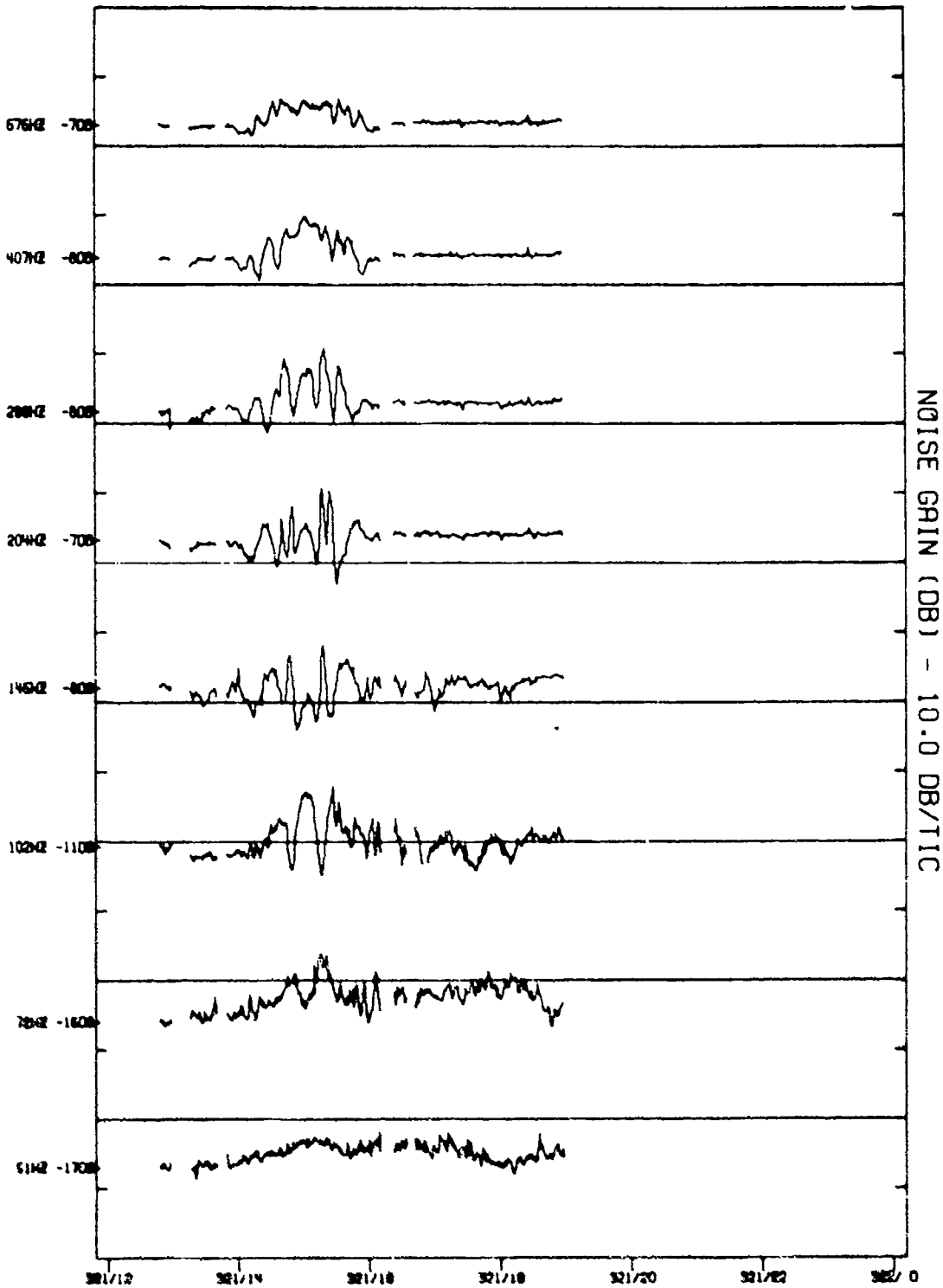

FIGURE II-317
MSS-FVT PHASE II SITE A2 DIFFFRENCED NORTH CARDIOID
TIME SERIES OF 1 MIN INTENSITY-AVERAGED NOISE GAINS
THROUGH 1/10-OCTAVE BANDS DURING THE 17 NOV FIELD EVENT (U)

AS-77-3331

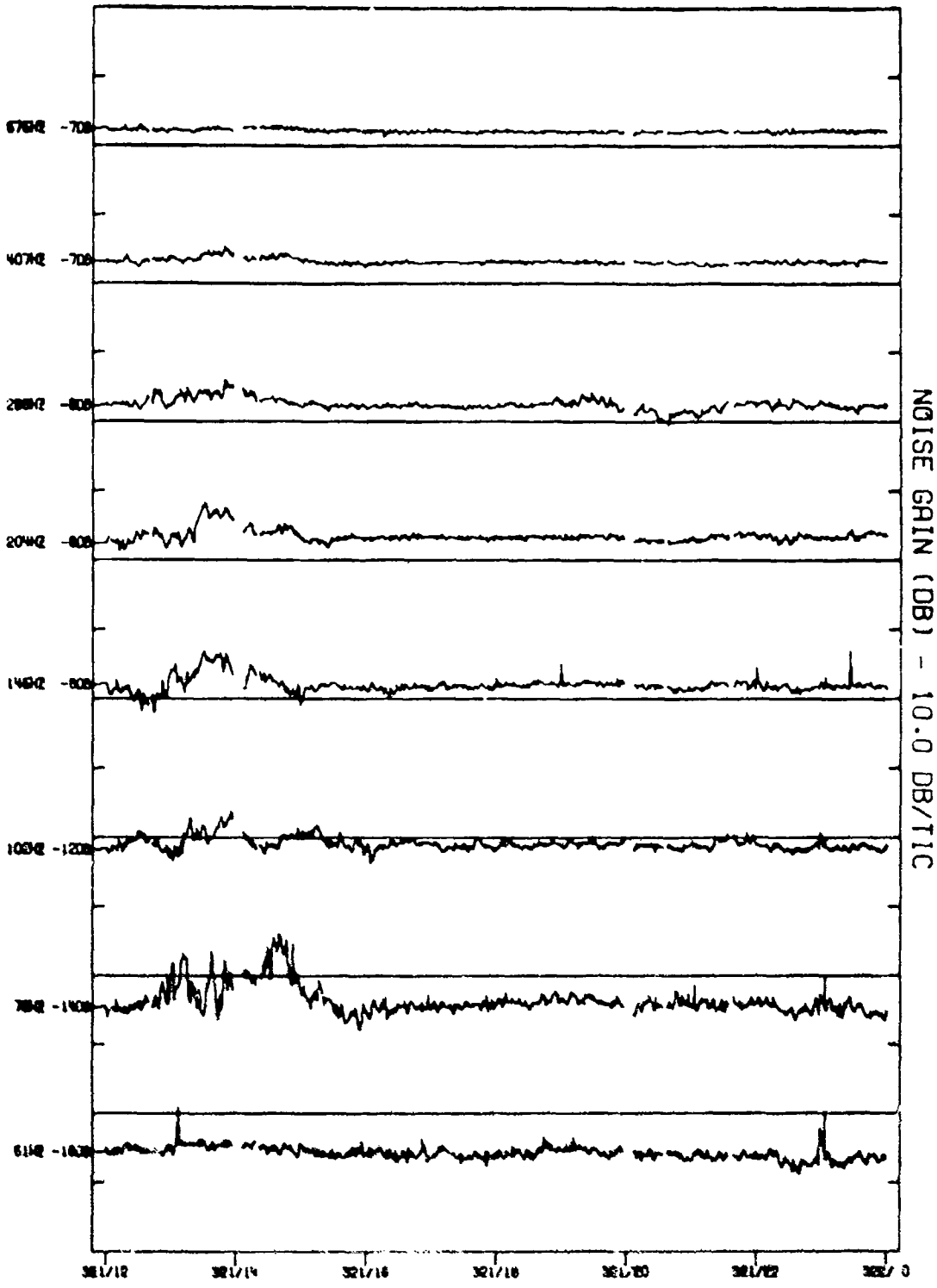

FIGURE II-318
MSS-FVT PHASE II SITE A3 DIFFERENCED NORTH CARDIOID
TIME SERIES OF 1 MIN INTENSITY-AVERAGED NOISE GAINS
THROUGH 1/10-OCTAVE BANDS DURING THE 17 NOV FIELD EVENT (U)

AS-77-3332

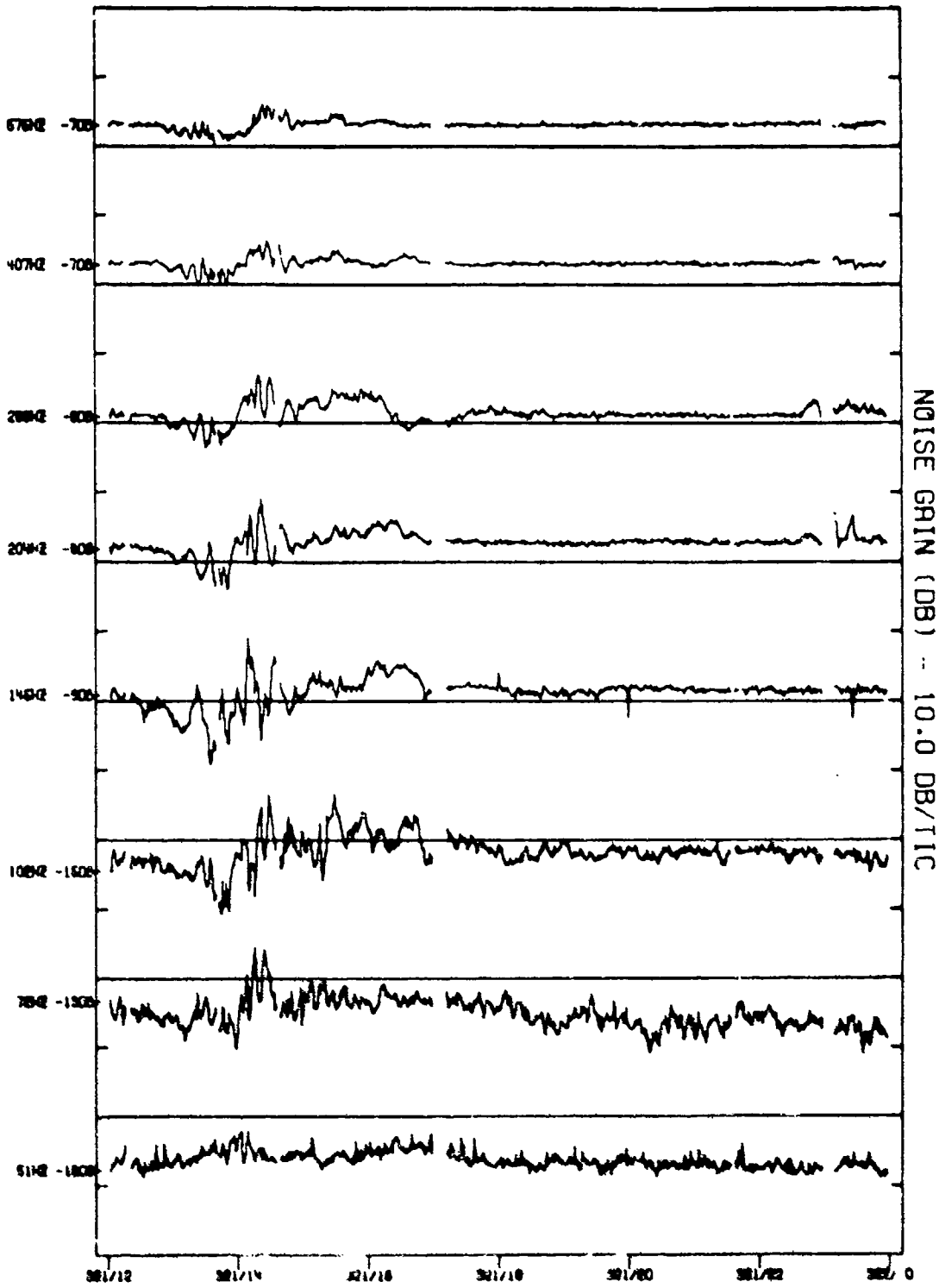

FIGURE II-319
MSS-FVT PHASE II SITE A1 DIFFERENCED EAST CARDIOID
TIME SERIES OF 1 MIN INTENSITY-AVERAGED NOISE GAINS
THROUGH 1/10-OCTAVE BANDS DURING THE 17 NOV FIELD EVENT (U)

AS-77-3333

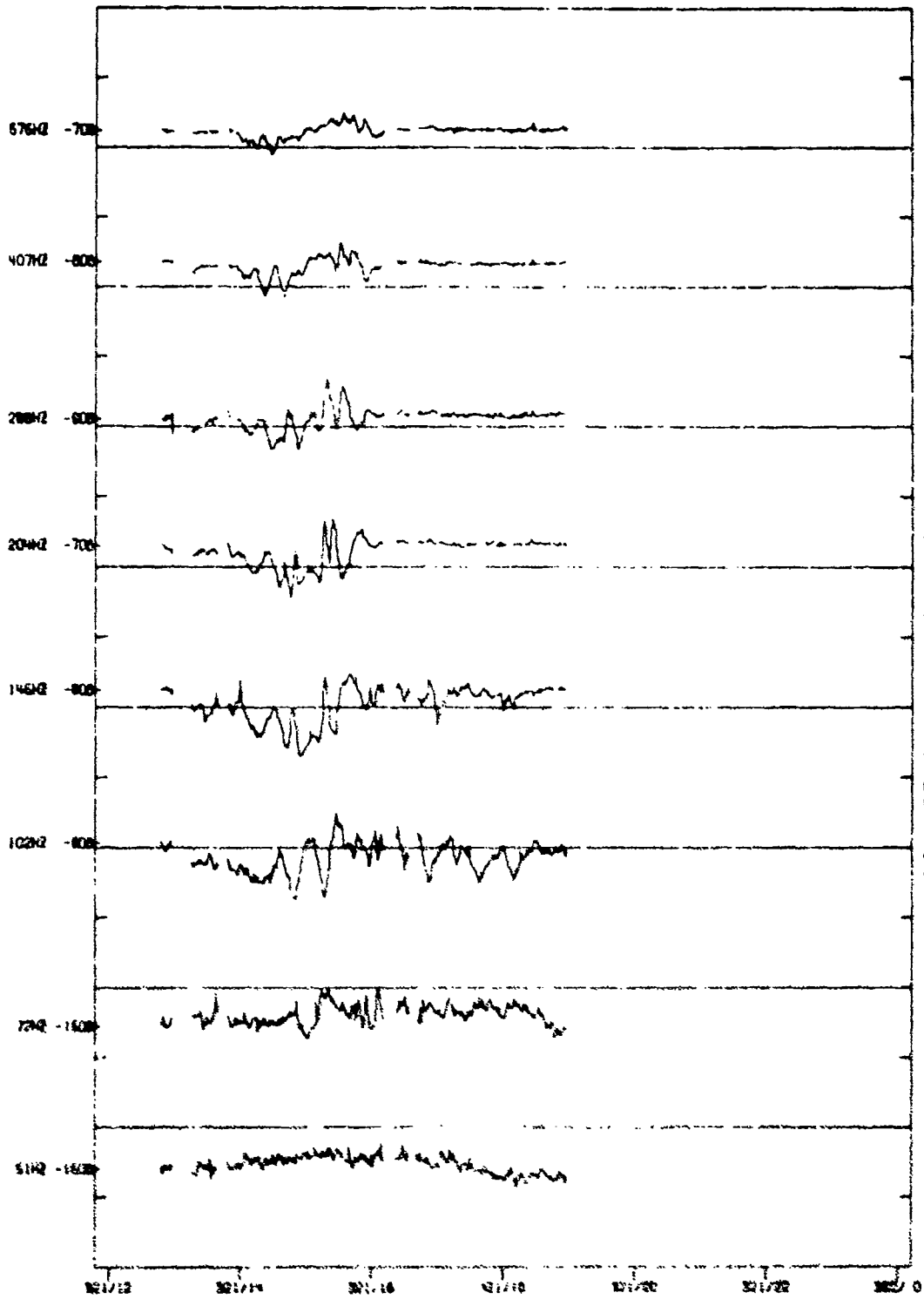

FIGURE II-320
MSS-FVT PHASE II SITE RX DIFFERENCED EAST CARDIOID
TIME SERIES OF 1 MIN INTENSITY-AVERAGED NOISE GAINS
THROUGH 1/10-OCTAVE BANDS DURING THE 17 NOV FIELD EVENT (U)

AS-77-3334

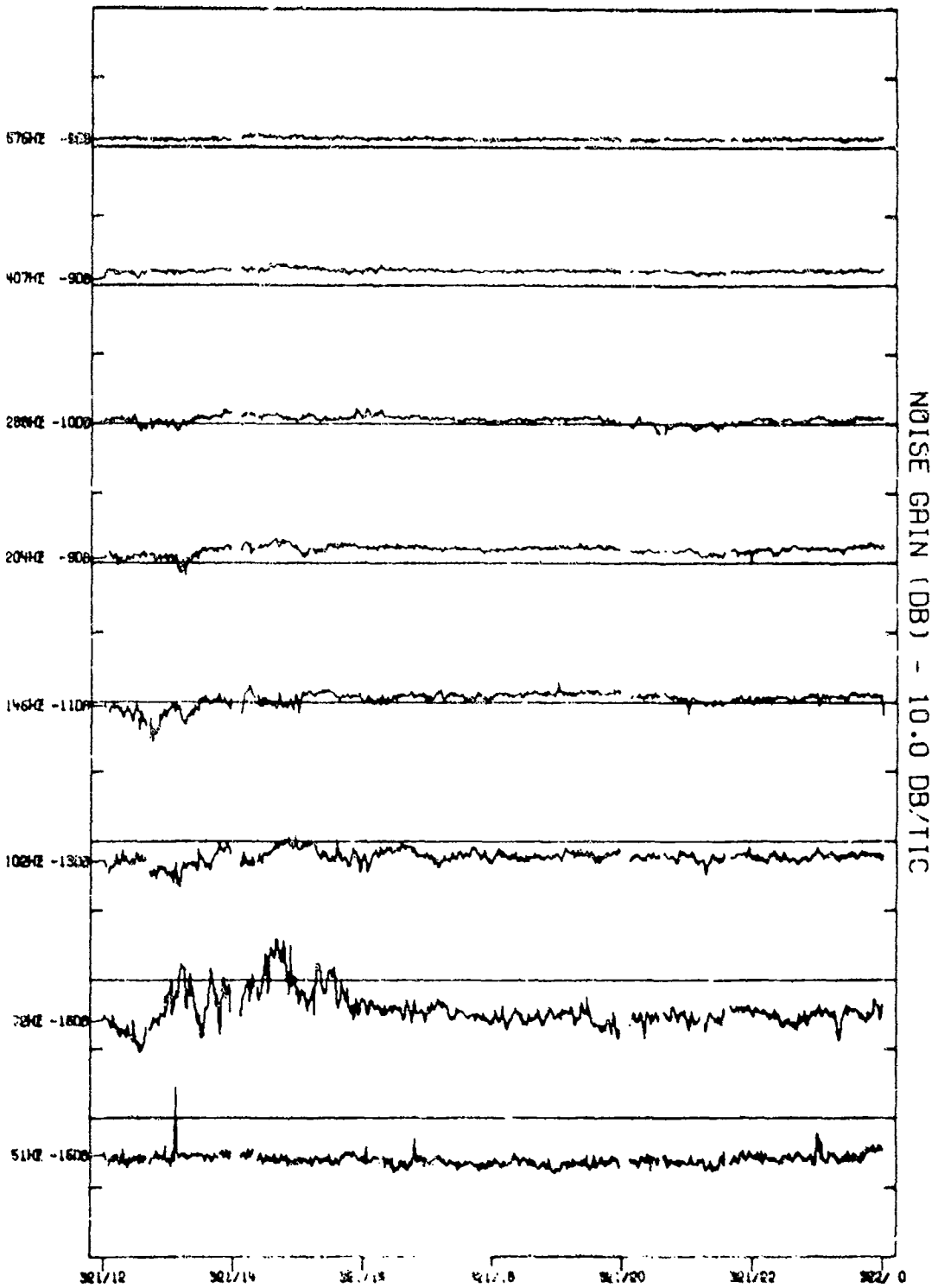

FIGURE II-321
MSS-FVT PHASE II SITE H2 DIFFERENCED EAST CARDIOID
TIME SERIES OF 1 MIN INTENSITY-AVERAGED NOISE GAINS
THROUGH 1/10-OCTAVE BANDS DURING THE 17 NOV FIELD EVENT (U)

AS-77-3335

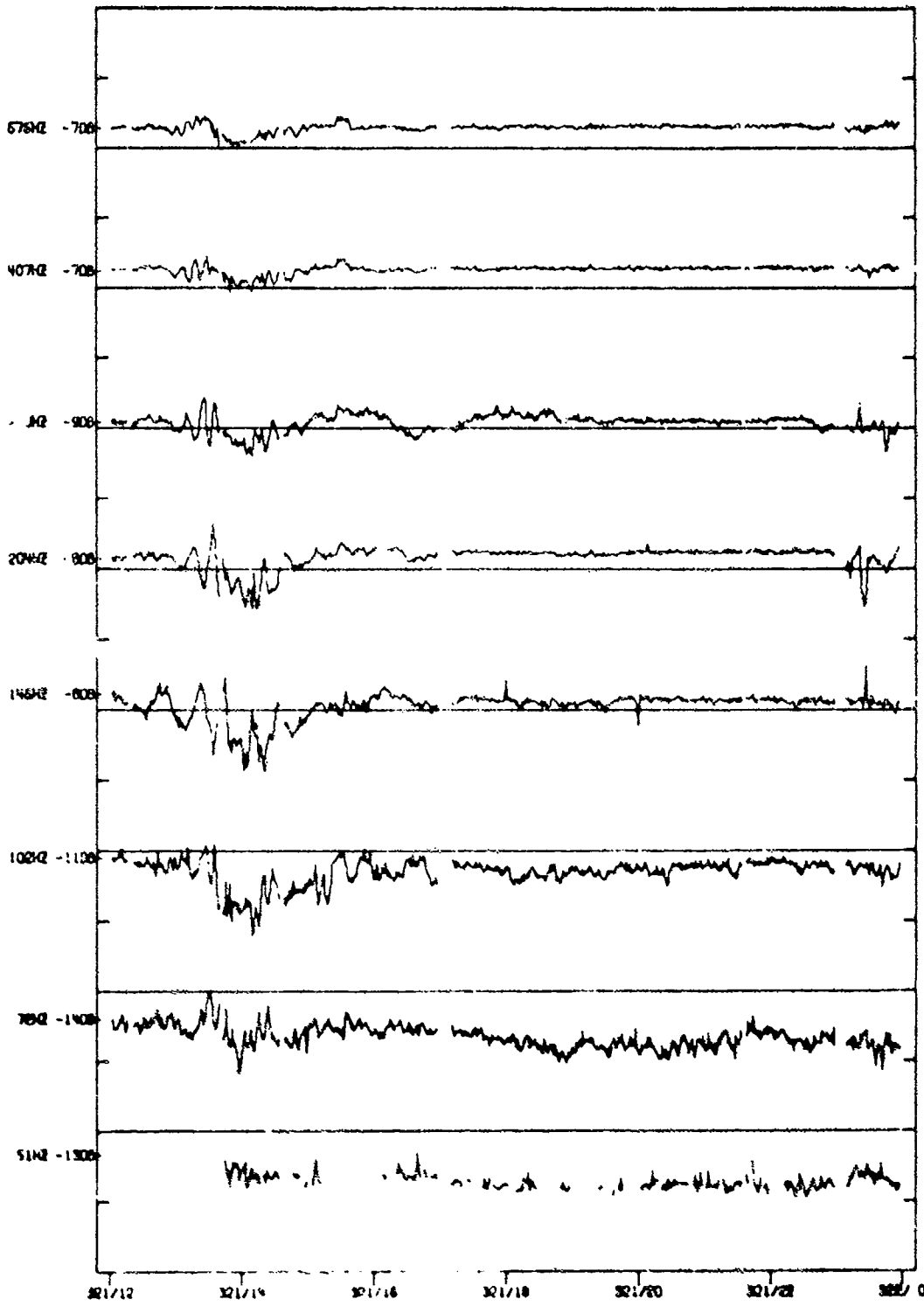

FIGURE II-322
MSS-FVT PHASE II SITE A1 DIFFERENCED SOUTH CARDIOID
TIME SERIES OF 1 MIN INTENSITY-AVERAGED NOISE GAINS
THROUGH 1/10-OCTAVE BANDS DURING THE 17 NOV FIELD EVENT (U)

AS-77-3336

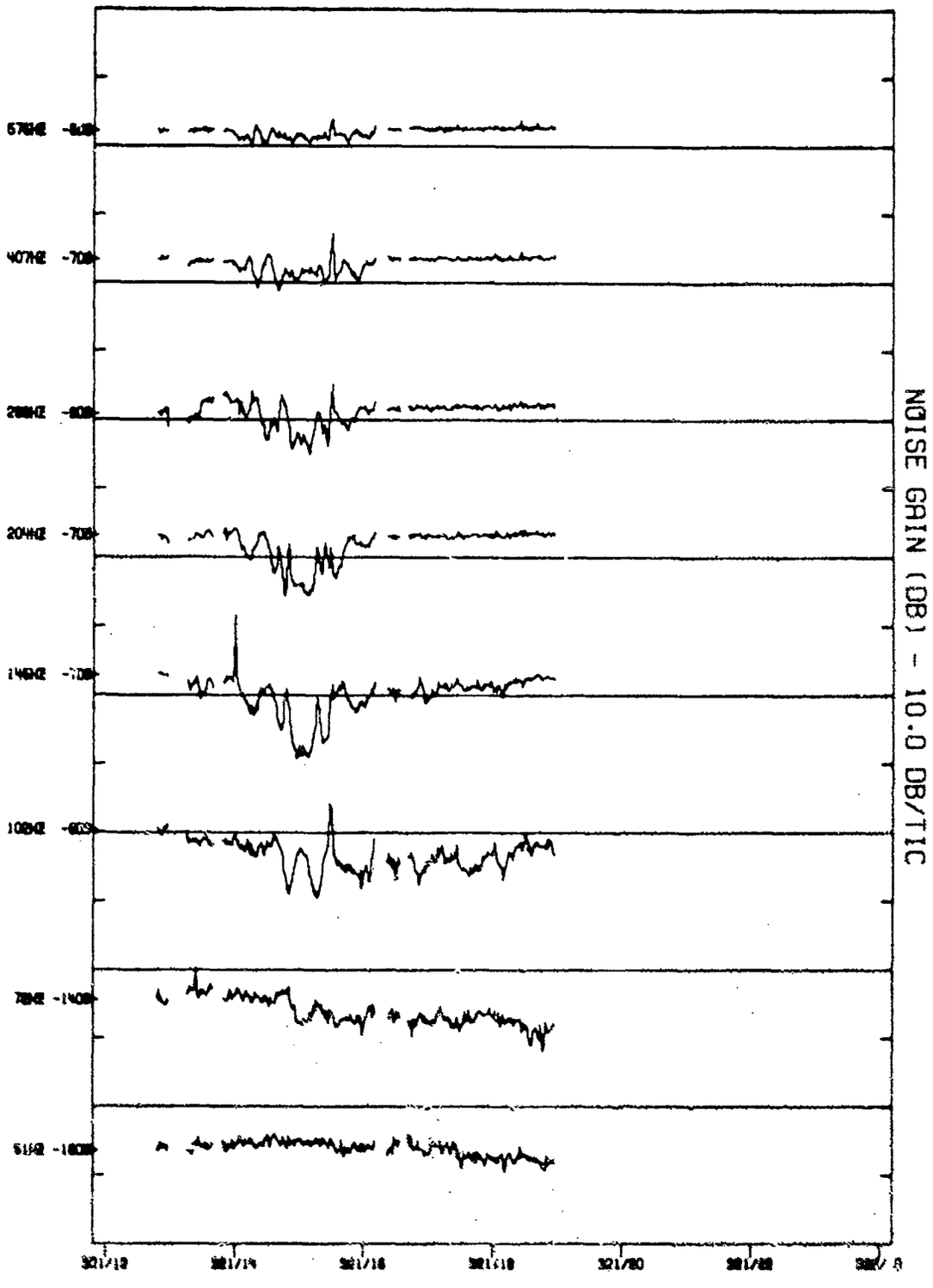

FIGURE II-323
MSS-FVT PHASE II SITE A2 DIFFERENCED SOUTH CARDIOID
TIME SERIES OF 1 MIN INTENSITY-AVERAGED NOISE GAINS
THROUGH 1/10-OCTAVE BANDS DURING THE 17 NOV FIELD EVENT (U)

AS-77-3337

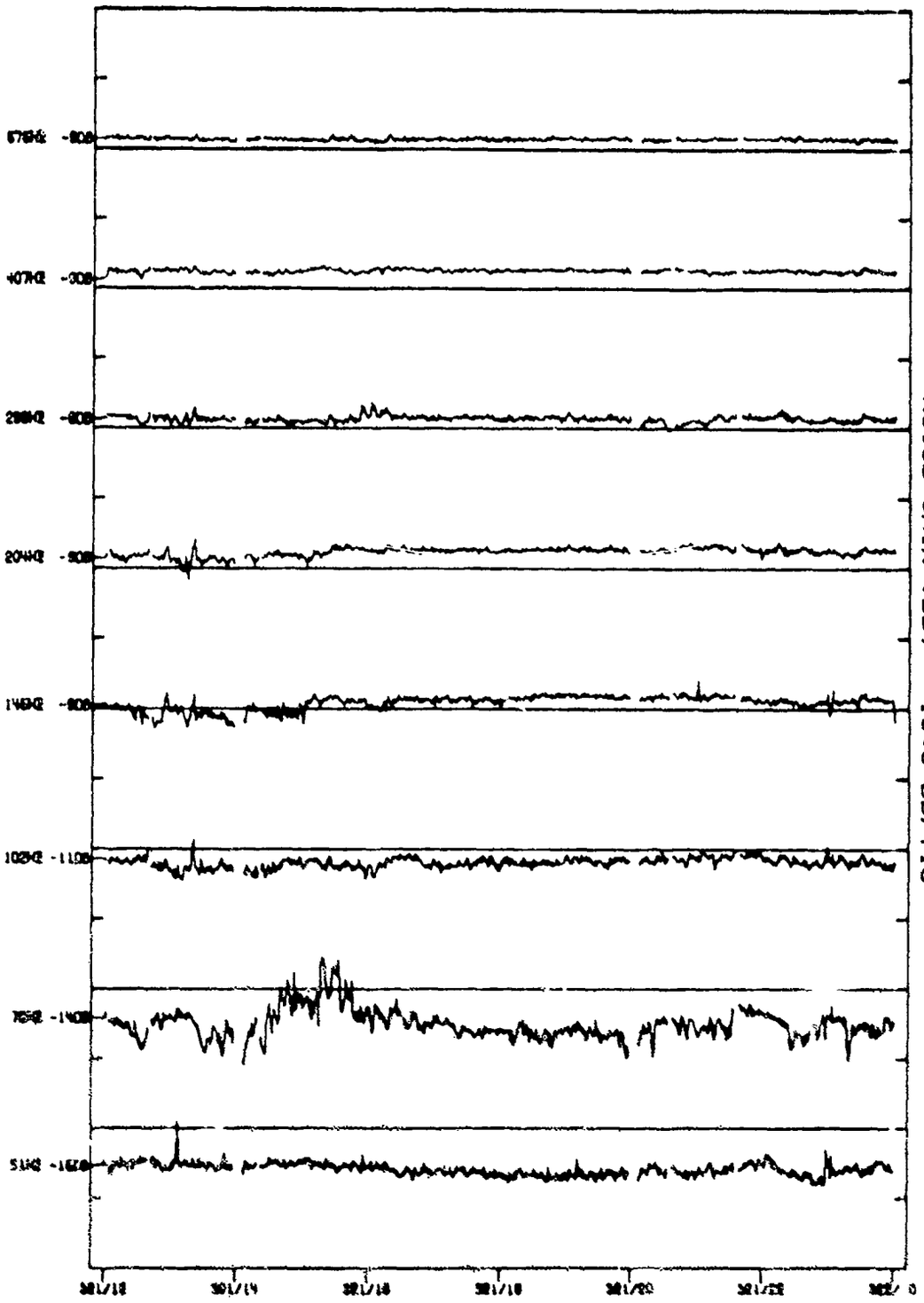

FIGURE II-324
MSS-FVT PHASE II SITE A3 DIFFERENCED SOUTH CARDIOID
TIME SERIES OF 1 MIN INTENSITY-AVERAGED NOISE GAINS
THROUGH 1/10-OCTAVE BANDS DURING THE 17 NOV FIELD EVENT (U)

AS-77-3338

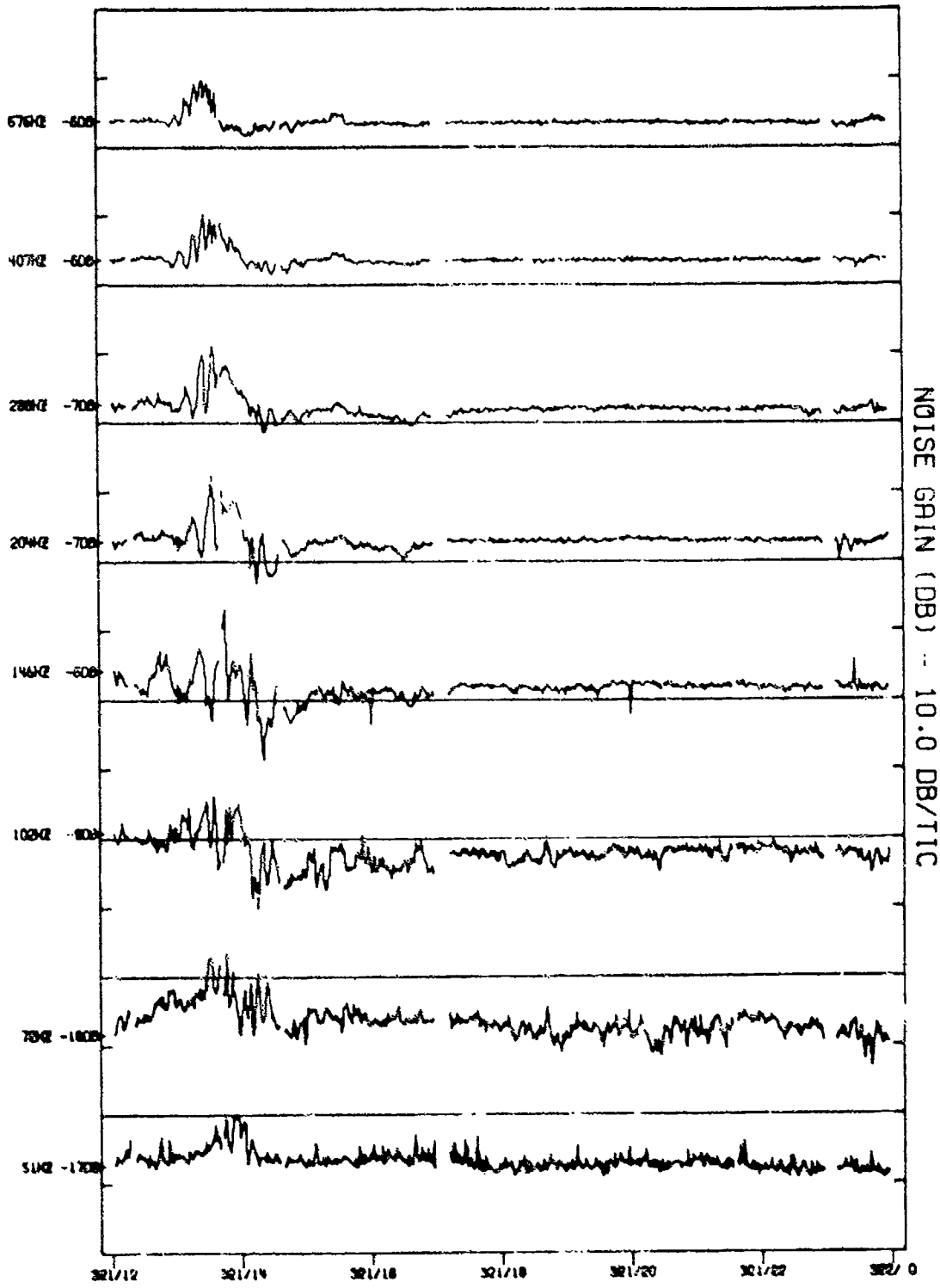

FIGURE II-325
MSS-FVT PHASE II SITE A1 DIFFERENCED WEST CARDIOID
TIME SERIES OF 1 MIN INTENSITY-AVERAGED NOISE GAINS
THROUGH 1/10-OCTAVE BANDS DURING THE 17 NOV FIELD EVENT (U)

AS-77-3339

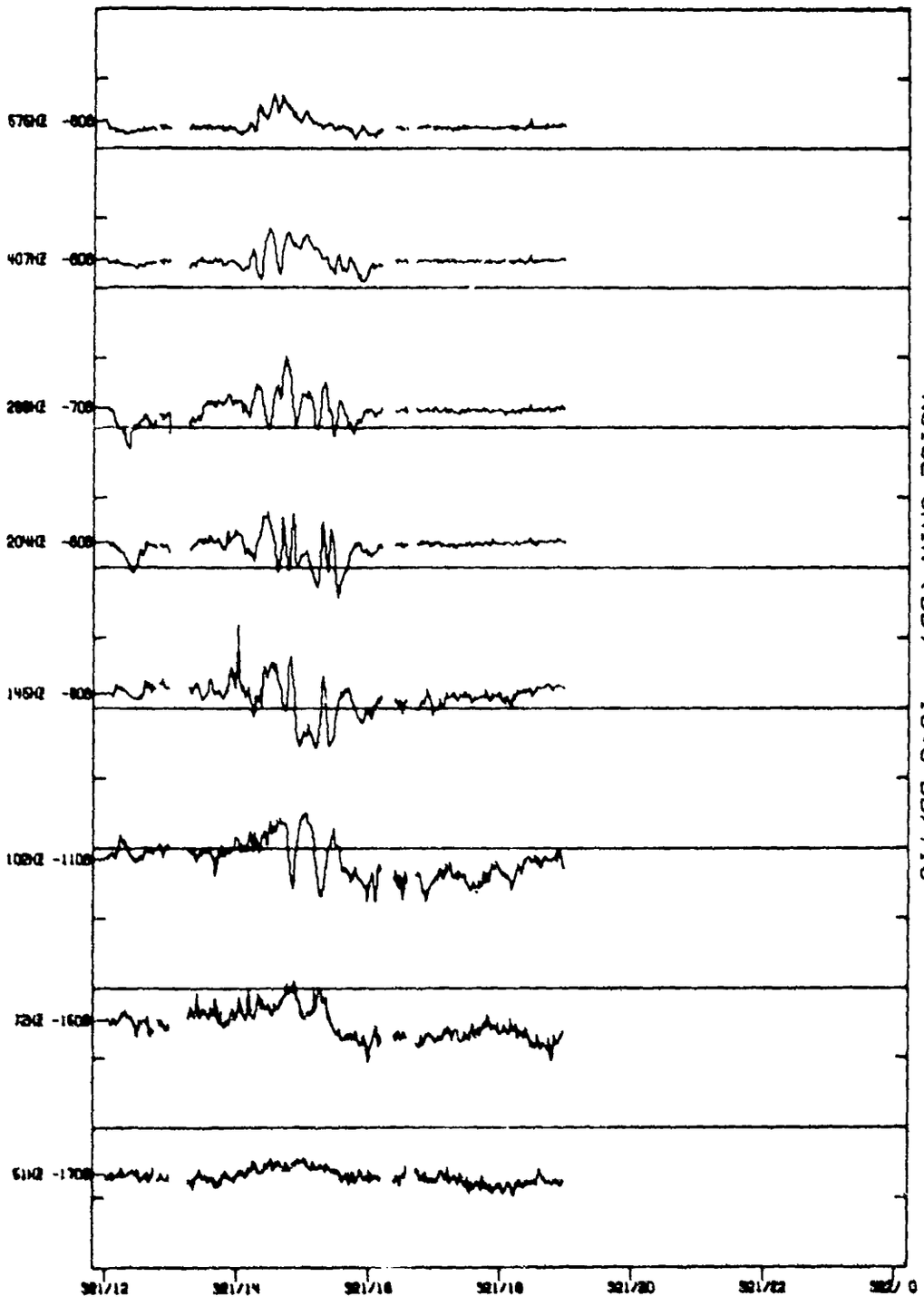

FIGURE II-326
MSS-FVT PHASE II SITE A2 DIFFERENCED WEST CARDIOID
TIME SERIES OF 1 MIN INTENSITY-AVERAGED NOISE GAINS
THROUGH 1/10-OCTAVE BANDS DURING THE 17 NOV FIELD EVENT (U)

AS-77-3340

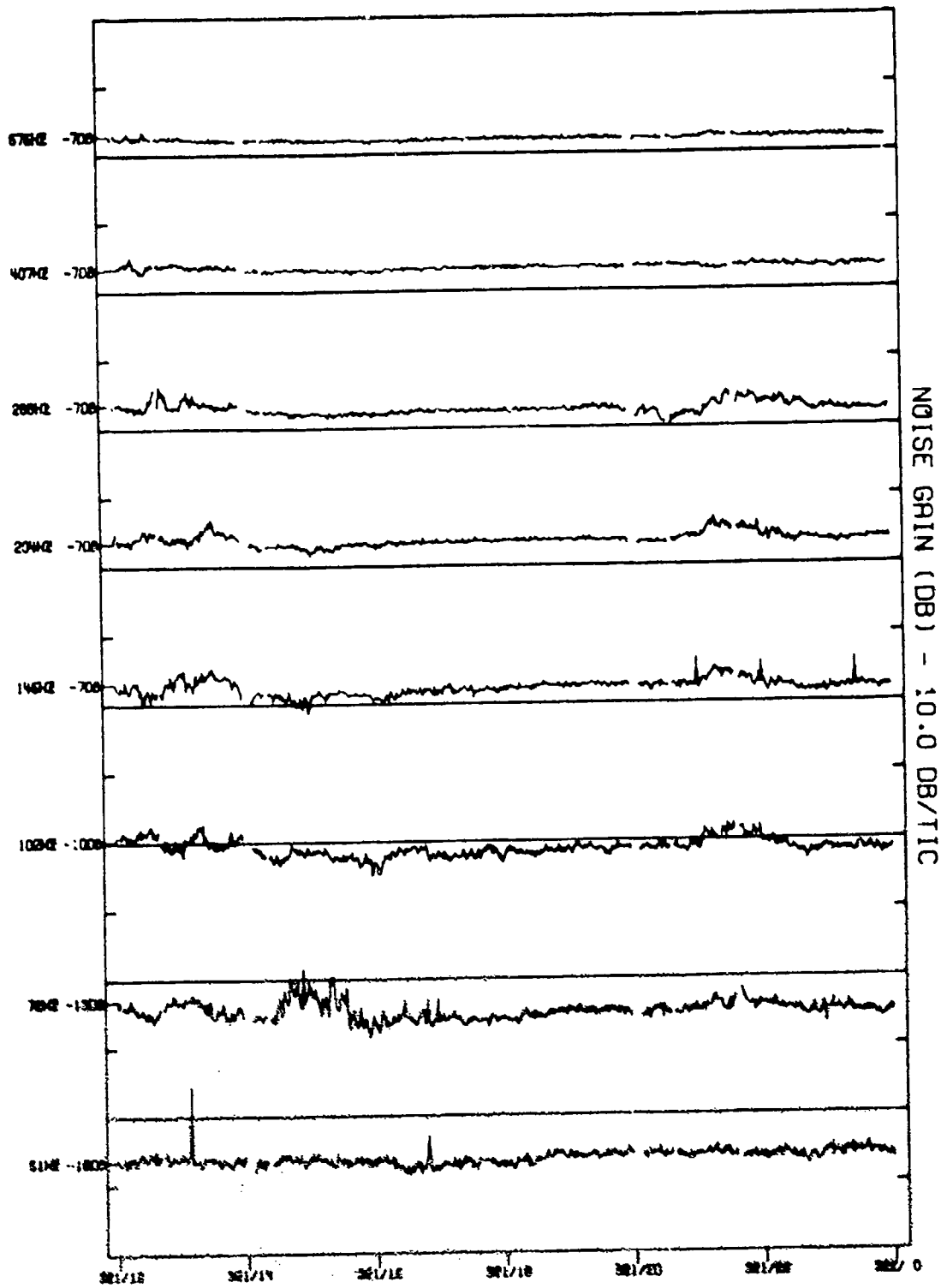

FIGURE II-327
MSS-FVT PHASE II SITE A3 DIFFERENCED WEST CARDIOID
TIME SERIES OF 1 MIN INTENSITY-AVERAGED NOISE GAINS
THROUGH 1/10-OCTAVE BANDS DURING THE 17 NOV FIELD EVENT (U)

AS-77-3341

APPENDIX J

AMBIENT SOUND FIELD PERCENTILE LEVEL versus FREQUENCY CURVES (U)

(FIGURES II-328 - II-357)

(The reverse of this page is blank.)

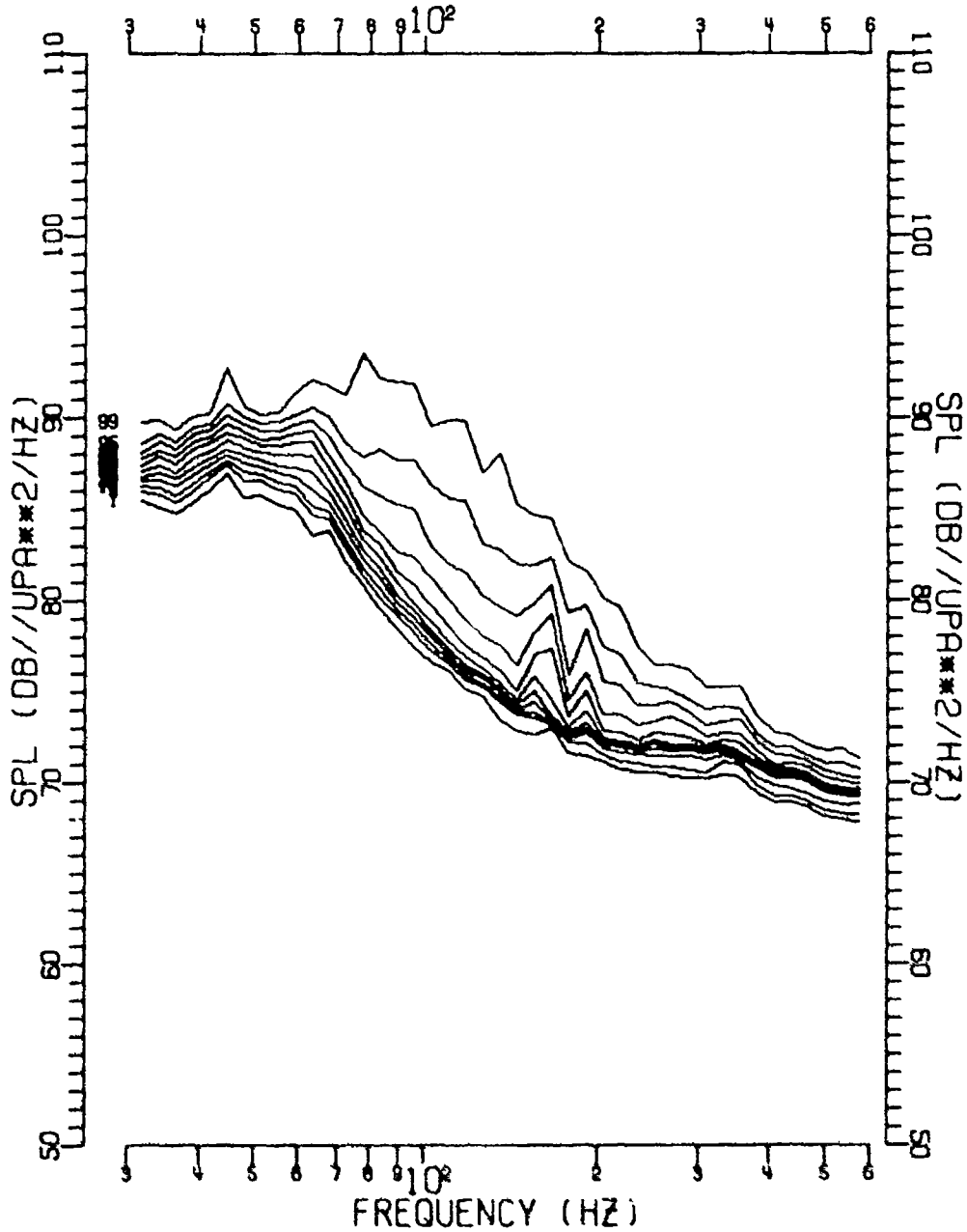

FIGURE II-328
MSS-FVT PHASE II SITE A1 OMNIDIRECTIONAL SENSOR
PERCENTILE LEVELS OF 1 MIN AVERAGED SOUND PRESSURE LEVELS
THROUGH 1/10-OCTAVE BANDS DURING THE 17 NOV FIELD EVENT (U)

AS-77-3342

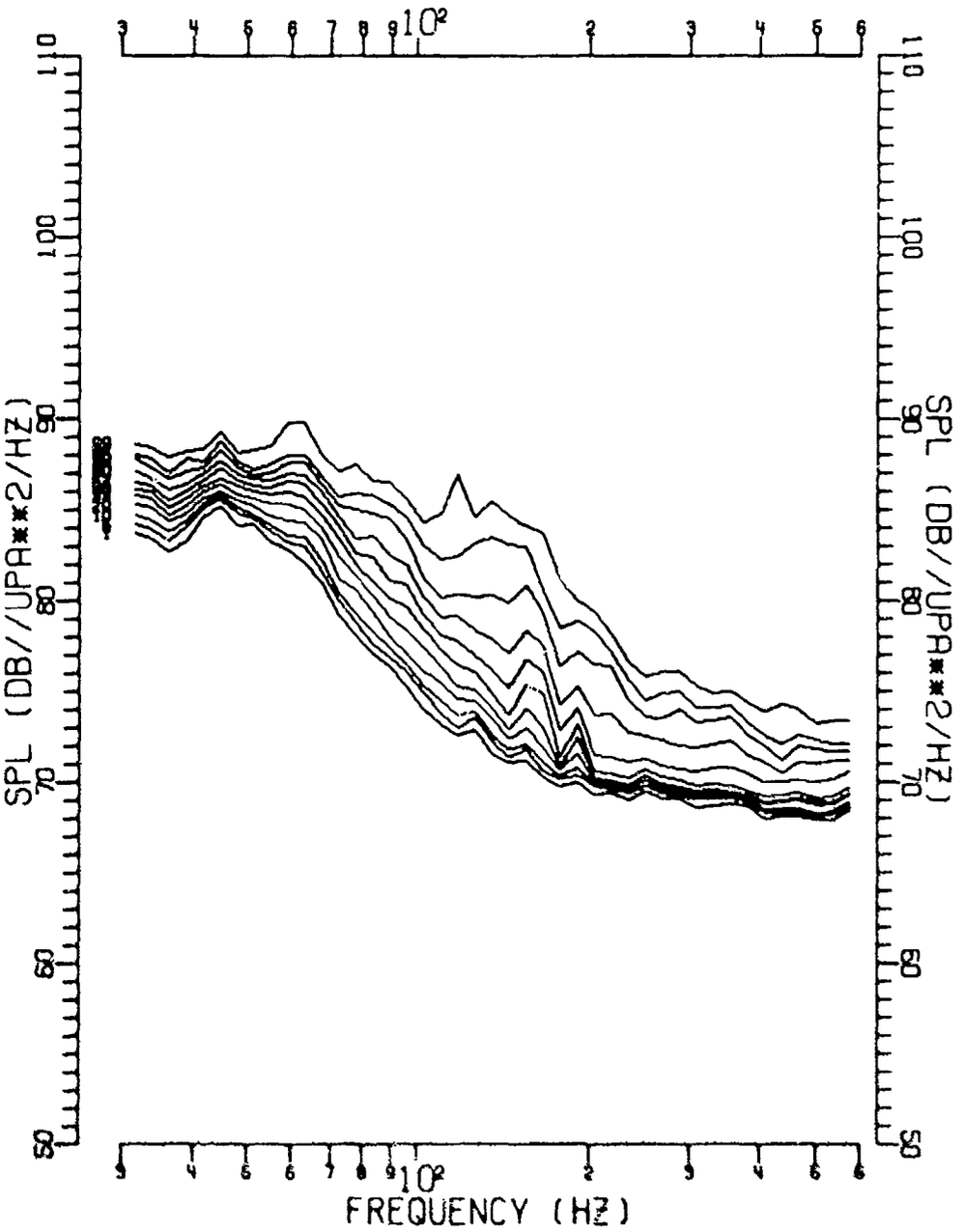

FIGURE II-329
MSS-FVT PHASE II SITE A2 OMNIDIRECTIONAL SENSOR
PERCENTILE LEVELS OF 1 MIN AVERAGED SOUND PRESSURE LEVELS
THROUGH 1/10-OCTAVE BANDS DURING THE 17 NOV FIELD EVENT (U)

AS-77-3343

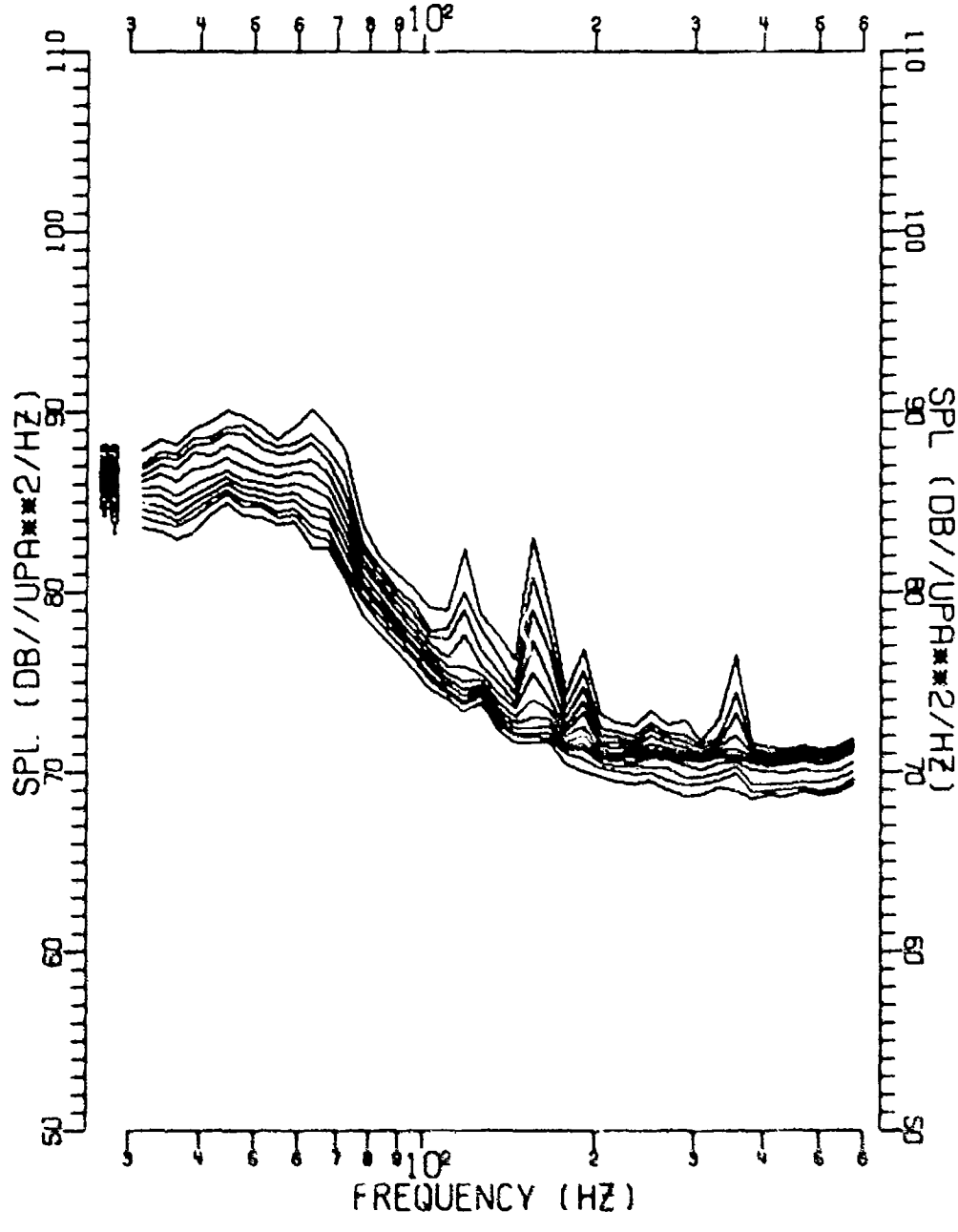

FIGURE II-330
MSS-FVT PHASE II SITE A3 OMNIDIRECTIONAL SENSOR
PERCENTILE LEVELS OF 1 MIN AVERAGED SOUND PRESSURE LEVELS
THROUGH 1/10-OCTAVE BANDS DURING THE 17 NOV FIELD EVENT (U)

AS-77-3344

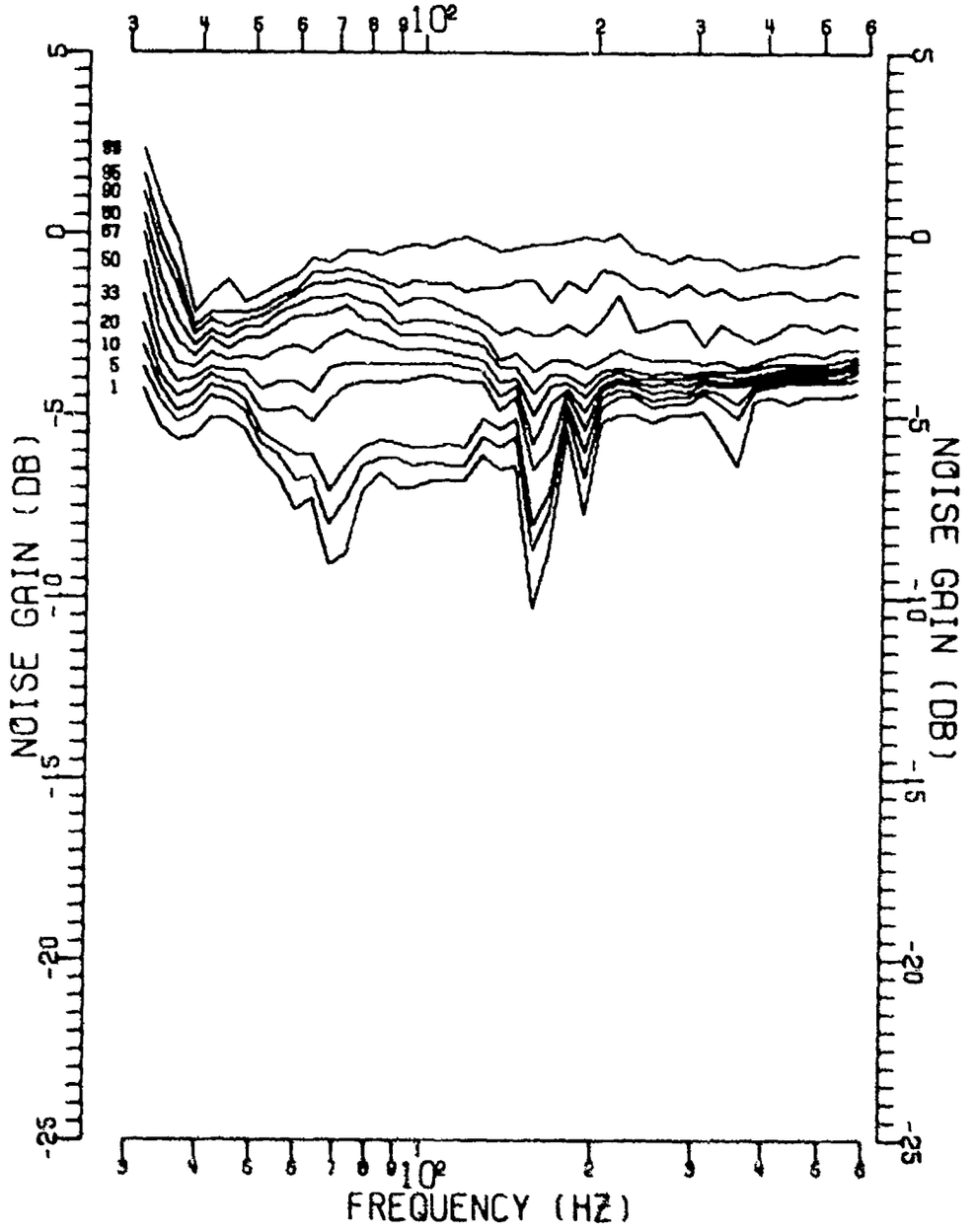

FIGURE II-331
MSS-FVT PHASE II SITE A1 NORTH CARDIOID
PERCENTILE LEVELS OF 1 MIN AVERAGED NOISE GAINS
THROUGH 1/10-OCTAVE BANDS DURING THE 17 NOV FIELD EVENT (U)

AS-77-3345

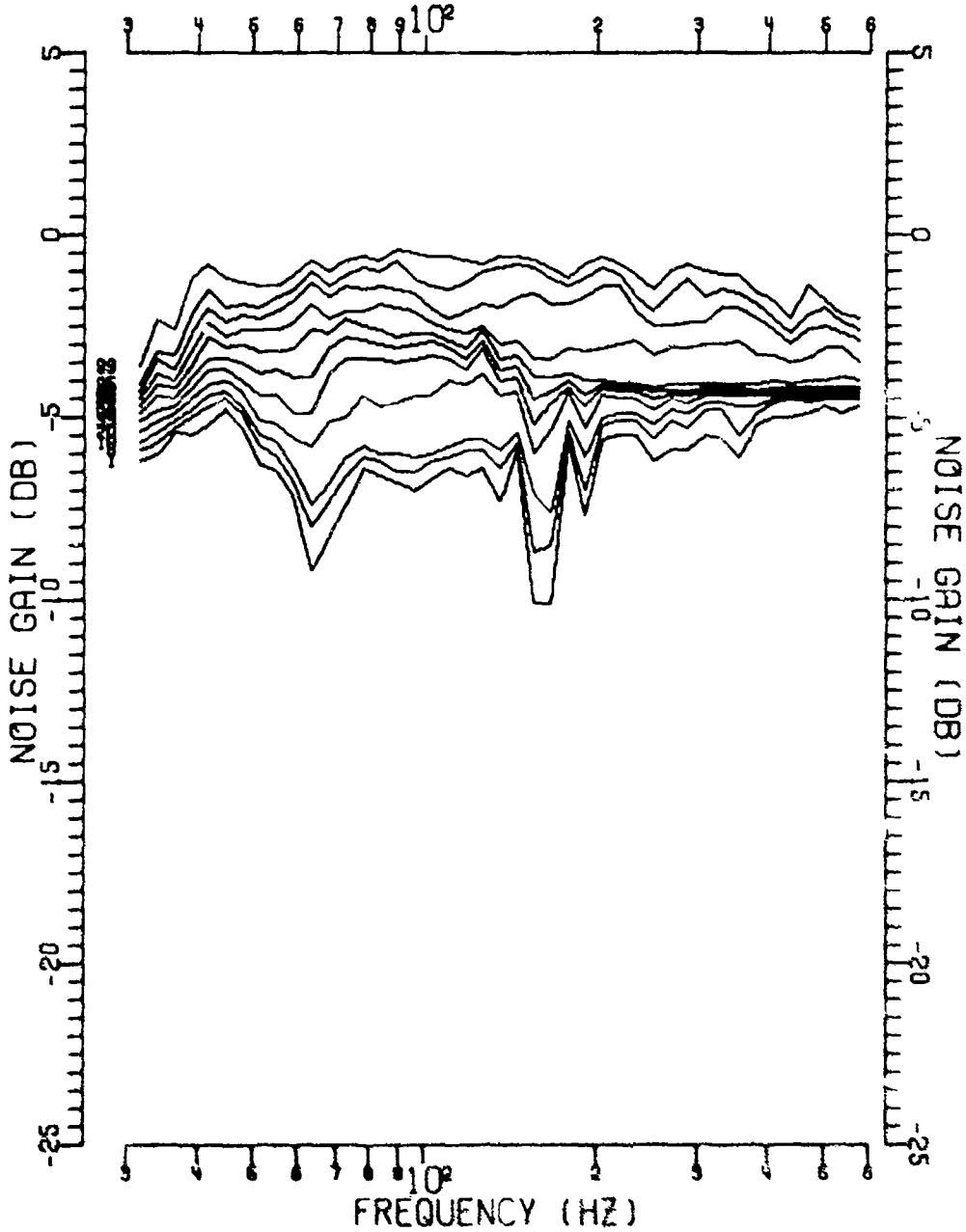

FIGURE II-332
MSS-FVT PHASE II SITE A2 NORTH CARDIOID
PERCENTILE LEVELS OF 1 MIN AVERAGED NOISE GAINS
THROUGH 1/10-OCTAVE BANDS DURING THE 17 NOV FIELD EVENT (U)

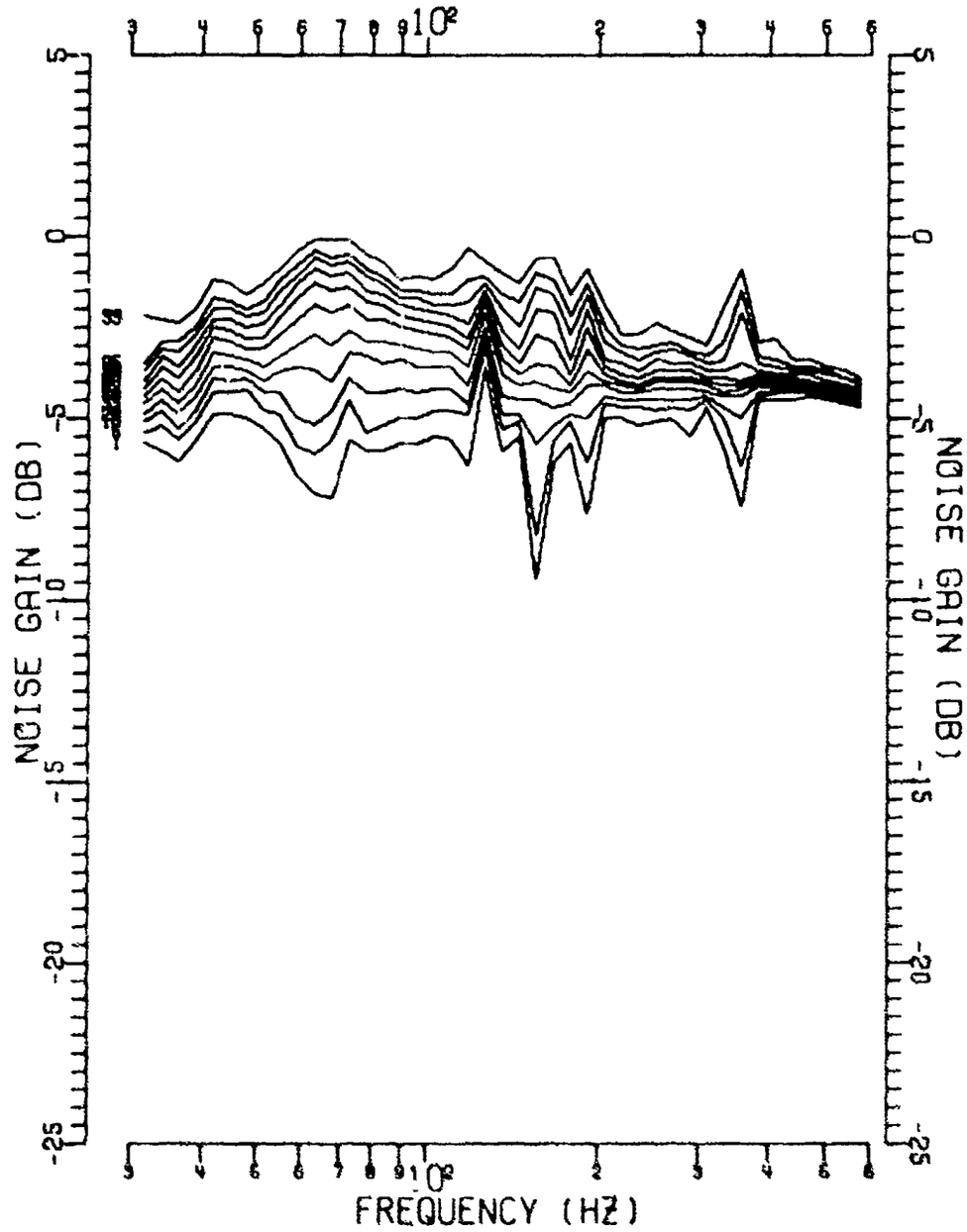

FIGURE II-333
MSS-FVT PHASE II SITE A3 NORTH CARDIOID
PERCENTILE LEVELS OF 1 MIN AVERAGED NOISE GAINS
THROUGH 1/10-OCTAVE BANDS DURING THE 17 NOV FIELD EVENT (U)

AS-77-5347

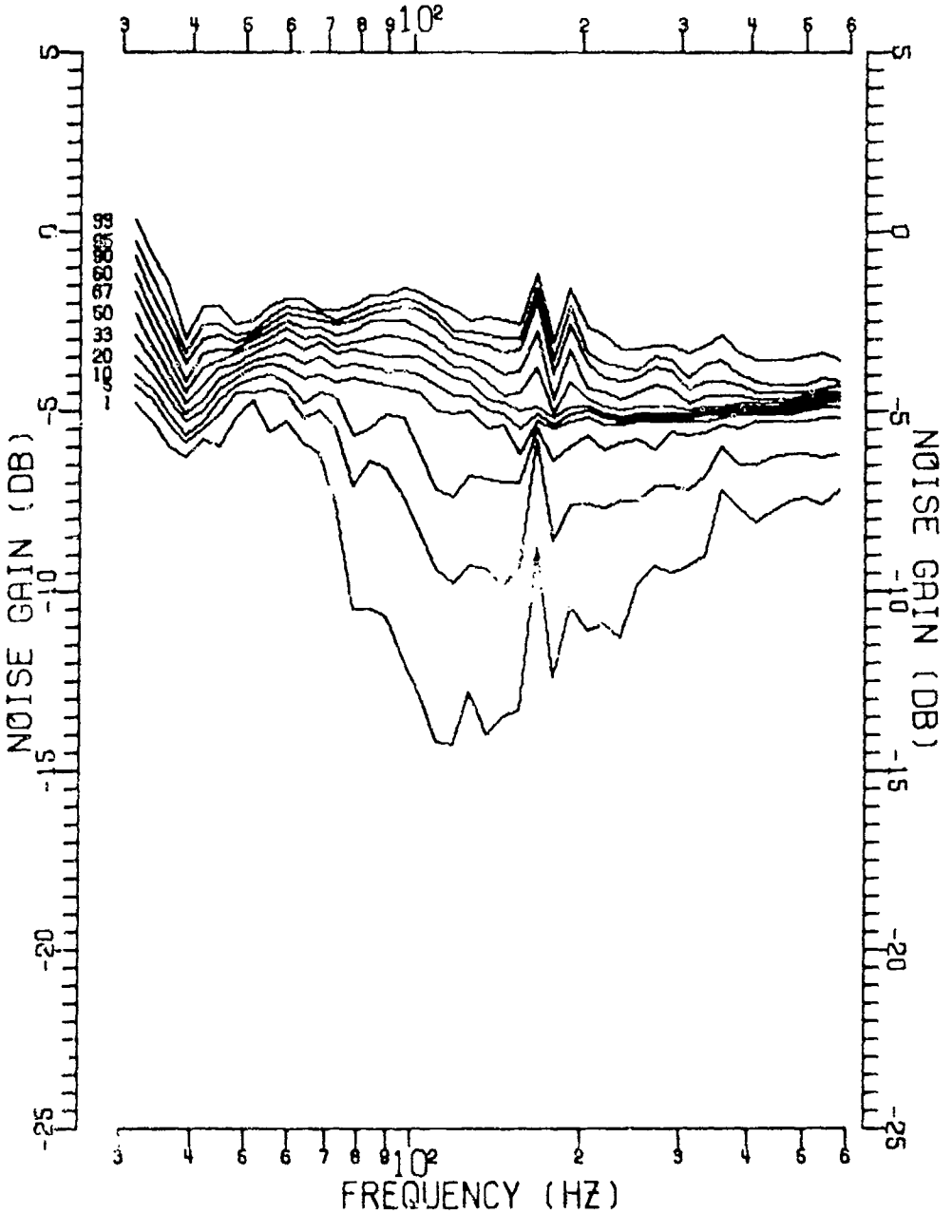

FIGURE II-334
MSS-FVT PHASE II SITE A1 EAST CARDIOID
PERCENTILE LEVELS OF 1 MIN AVERAGED NOISE GAINS
THROUGH 1/10-OCTAVE BANDS DURING THE 17 NOV FIELD EVENT (U)

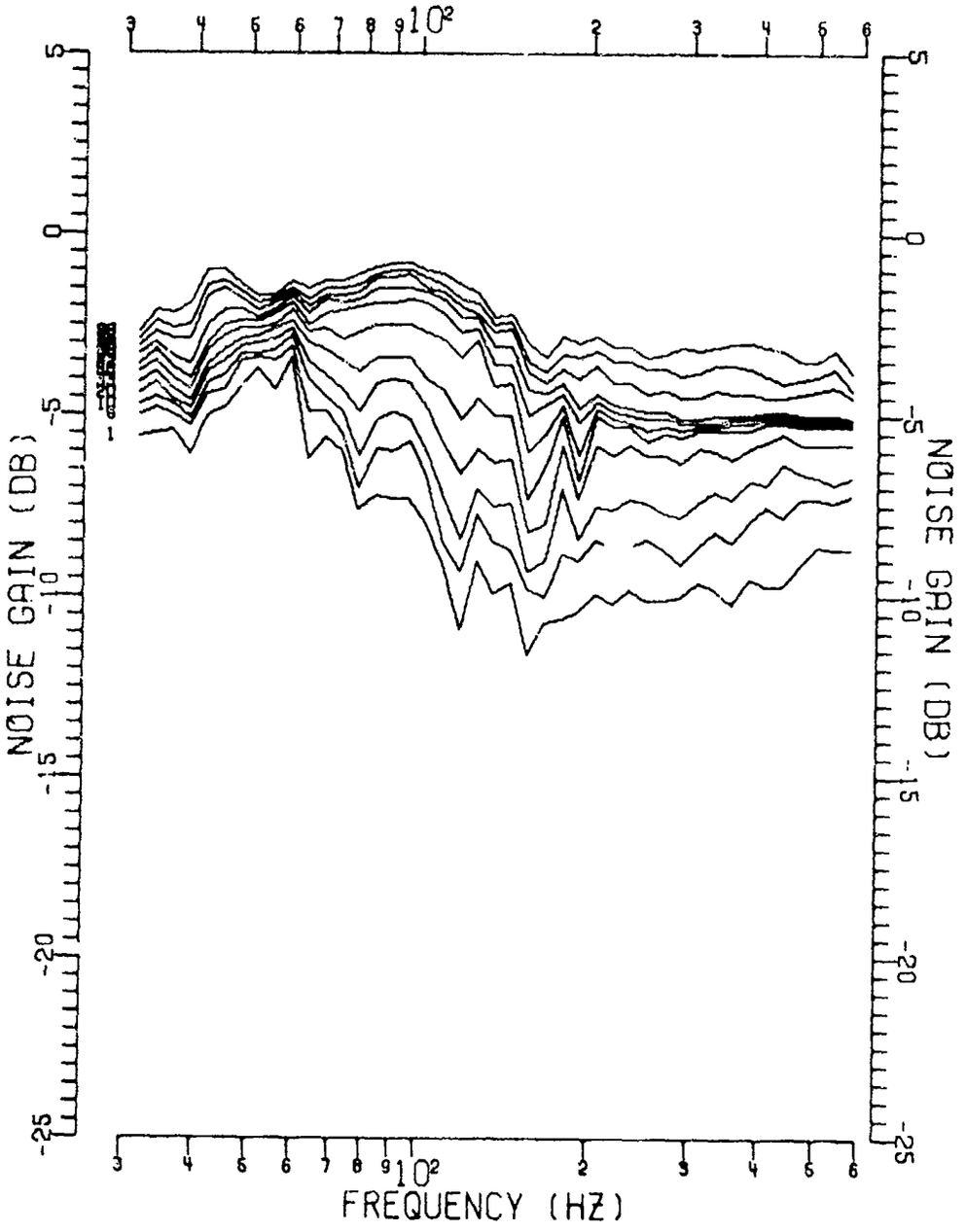

FIGURE II-335
MSS-FVT PHASE II SITE A2 EAST CARDIOID
PERCENTILE LEVELS OF 1 MIN AVERAGED NOISE GAINS
THROUGH 1/10-OCTAVE BANDS DURING THE 17 NOV FIELD EVENT (U)

AS-77-3349

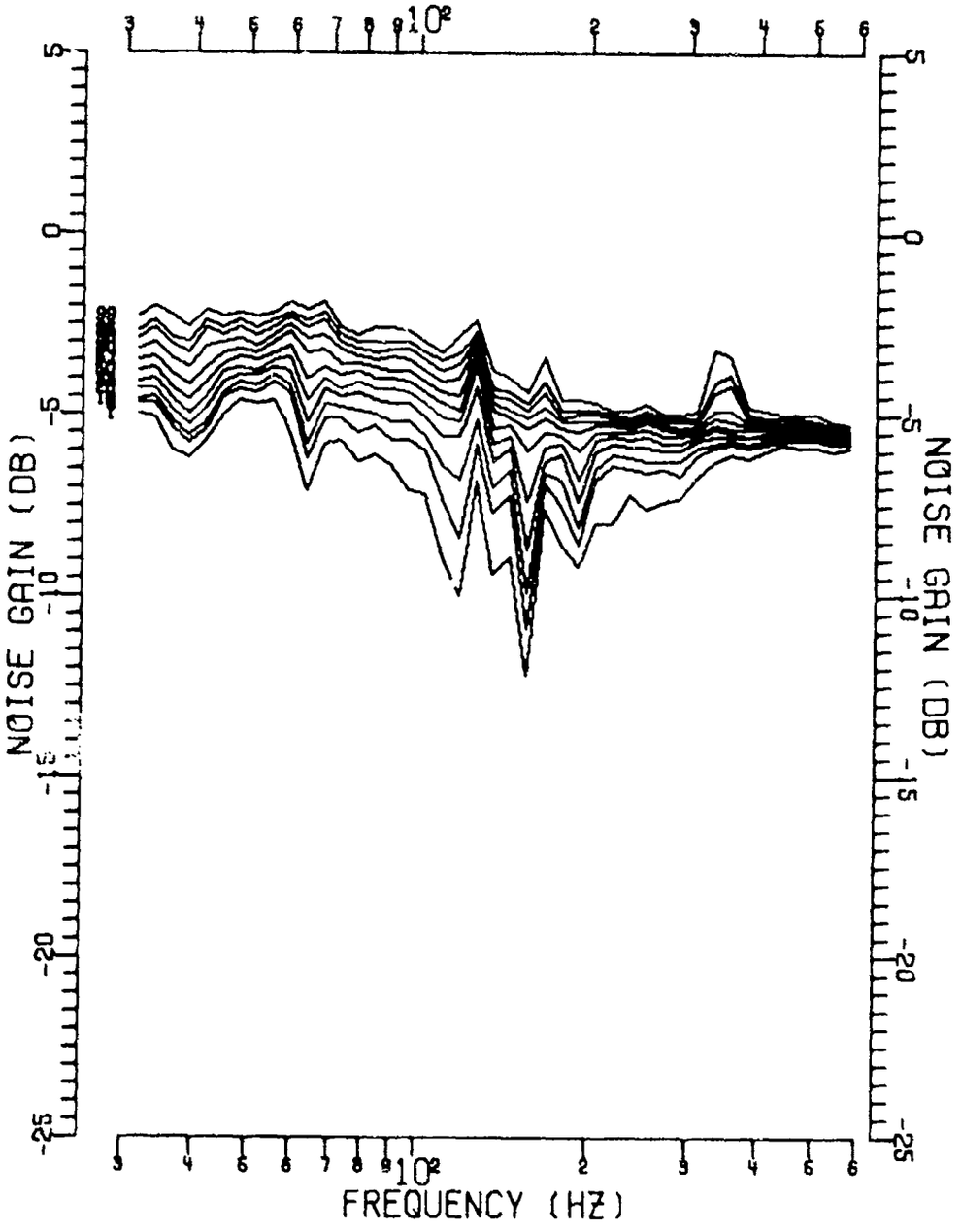

FIGURE II-336
MSS-FVT PHASE II SITE A3 EAST CARDIOID
PERCENTILE LEVELS OF 1 MIN AVERAGED NOISE GAINS
THROUGH 1/10-OCTAVE BANDS DURING THE 17 NOV FIELD EVENT (U)

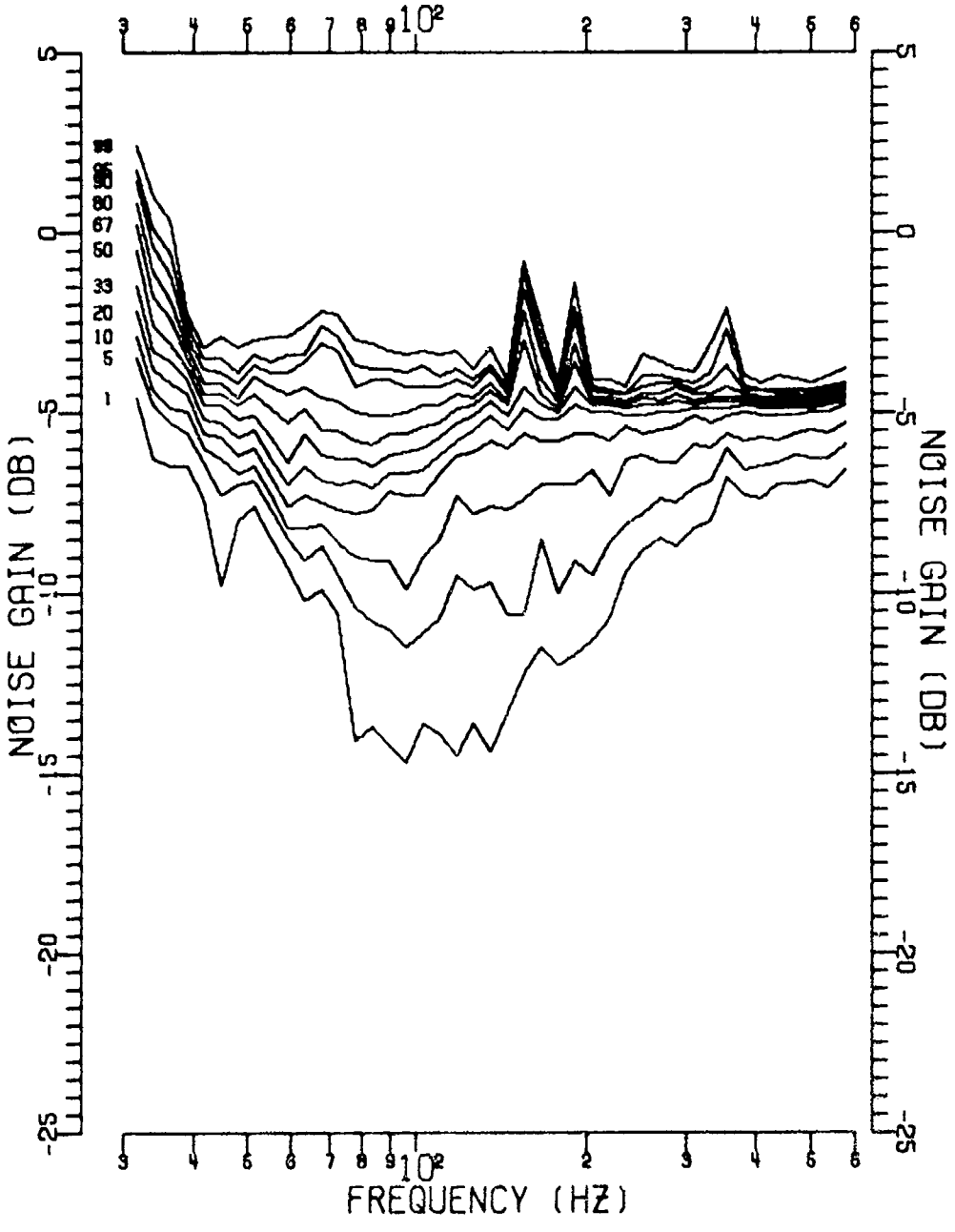

FIGURE II-337
MSS-FVT PHASE II SITE A1 SOUTH CARDIOID
PERCENTILE LEVELS OF 1 MIN AVERAGED NOISE GAINS
THROUGH 1/10-OCTAVE BANDS DURING THE 17 NOV FIELD EVENT (U)

AS-77-3351

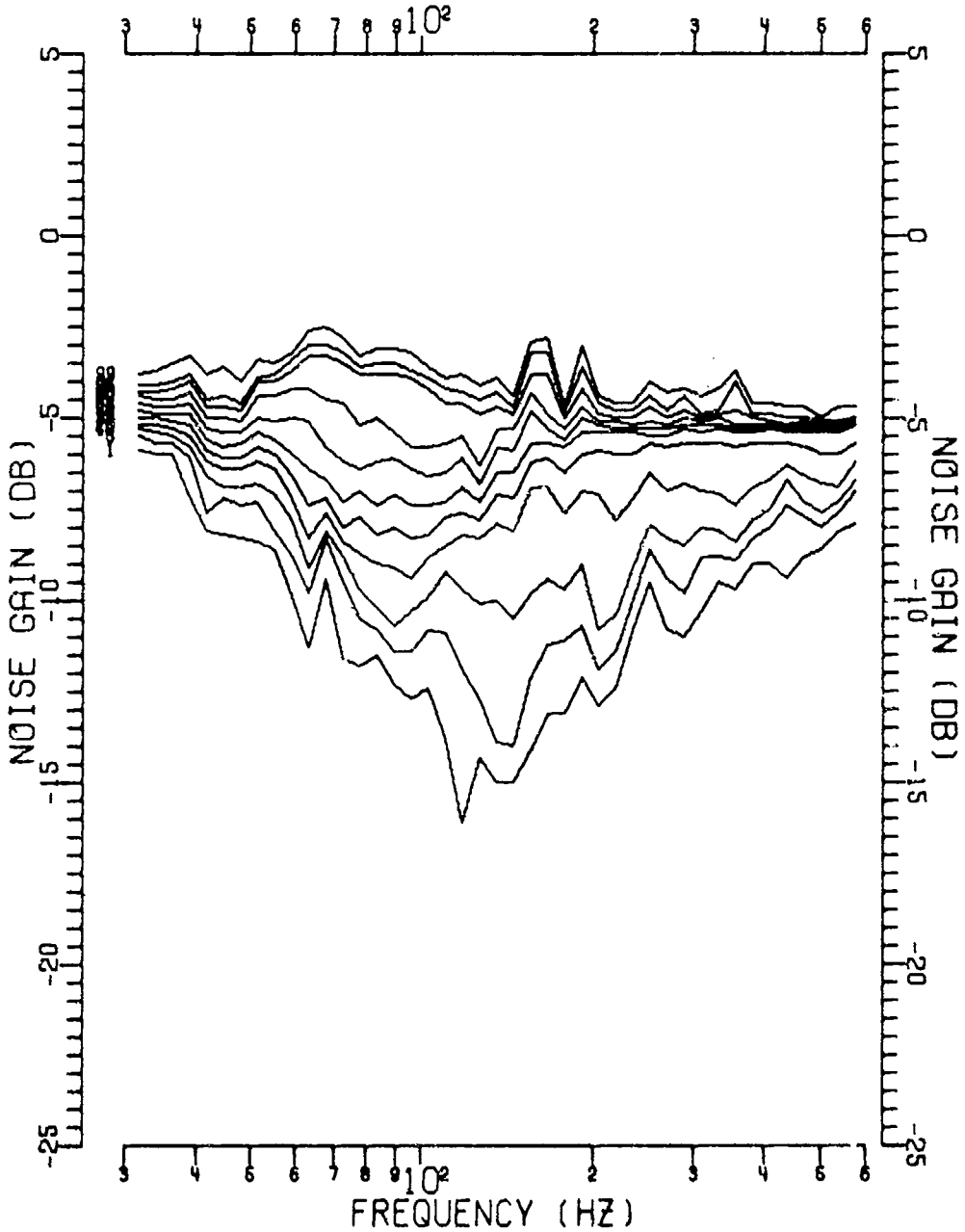

FIGURE II-338
MSS-FVT PHASE II SITE A2 SOUTH CARDIOID
PERCENTILE LEVELS OF 1 MIN AVERAGED NOISE GAINS
THROUGH 1/10-OCTAVE BANDS DURING THE 17 NOV FIELD EVENT (U)

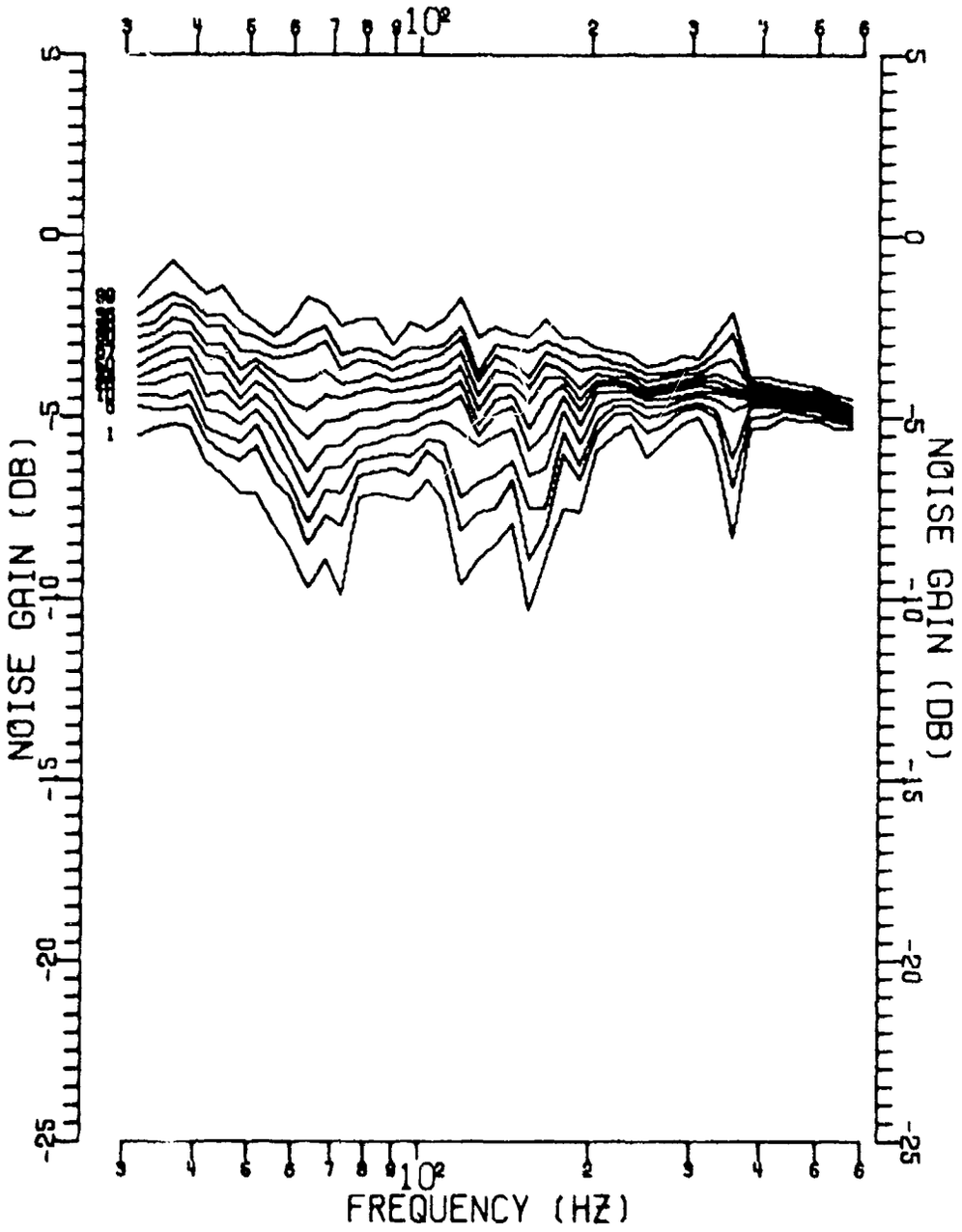

FIGURE II-339
MSS-FVT PHASE II SITE A3 SOUTH CARDIOID
PERCENTILE LEVELS OF 1 MIN AVERAGED NOISE GAINS
THROUGH 1/10-OCTAVE BANDS DURING THE 17 NOV FIELD EVENT (U)

AS-77-3353

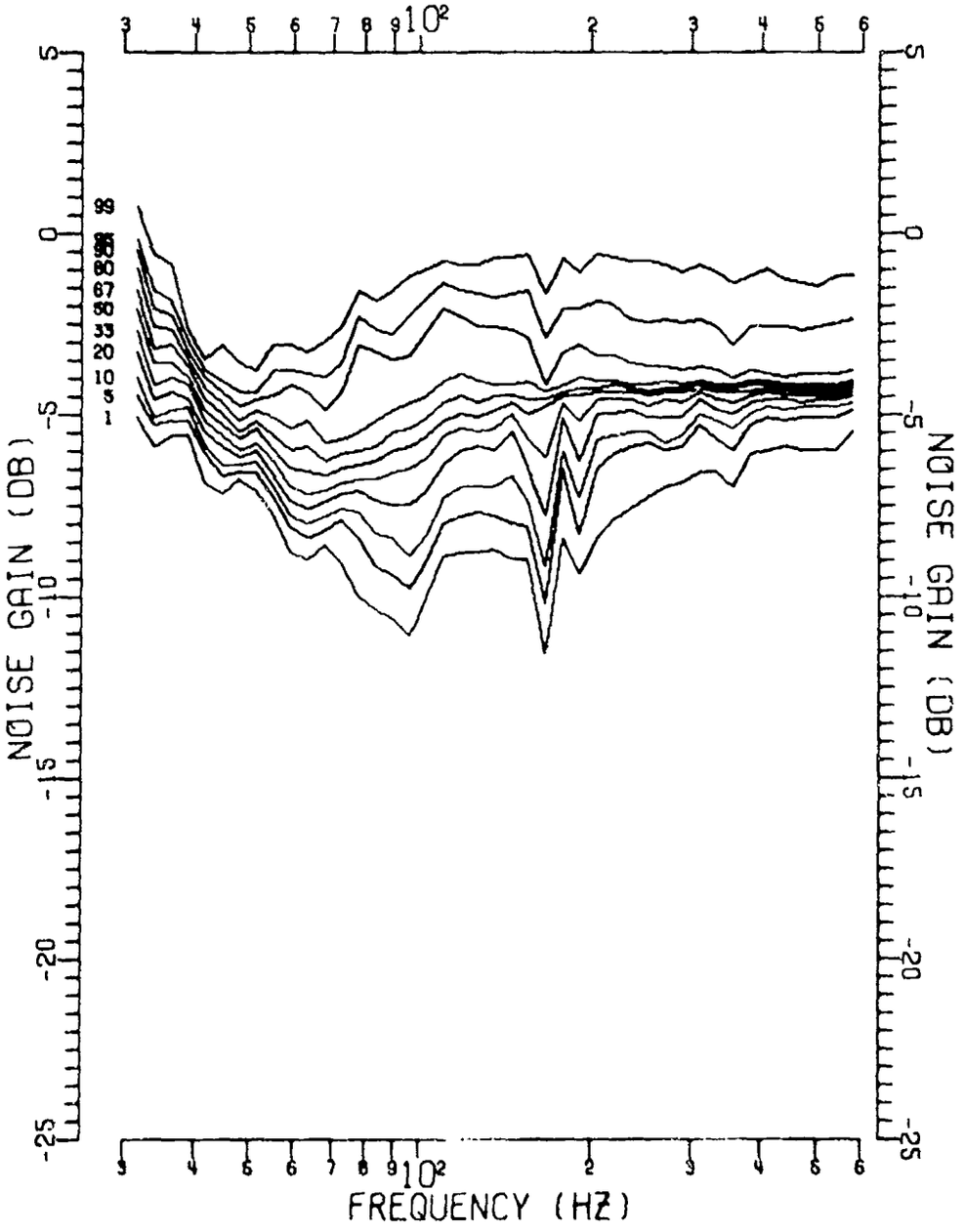

FIGURE II-340
MSS-FVT PHASE II SITE A1 WEST CARDIOID
PERCENTILE LEVELS OF 1 MIN AVERAGED NOISE GAINS
THROUGH 1/10-OCTAVE BANDS DURING THE 17 NOV FIELD EVENT (U)

AS-77-3354

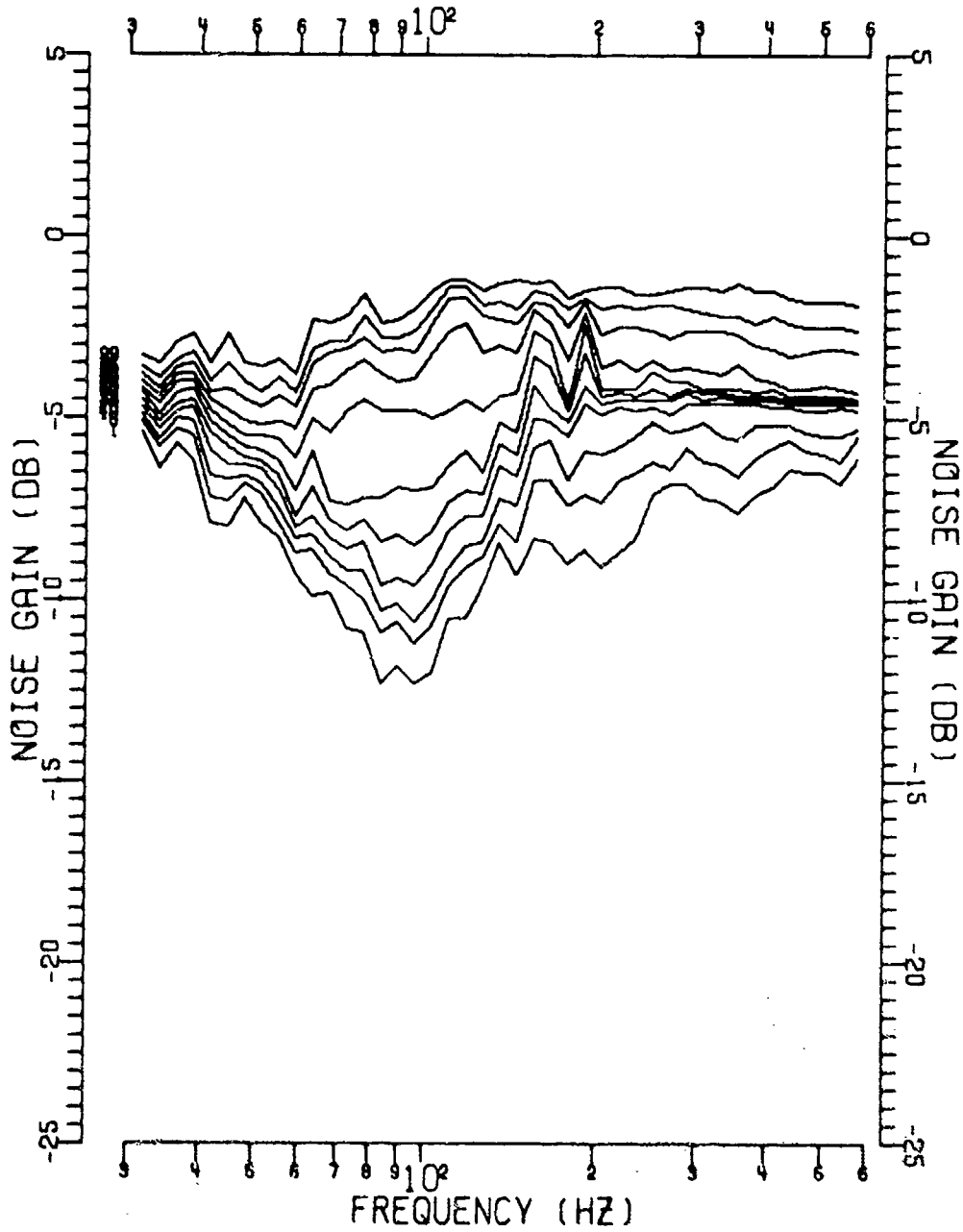

FIGURE II-341
MSS-FVT PHASE II SITE A2 WEST CARDIOID
PERCENTILE LEVELS OF 1 MIN AVERAGED NOISE GAINS
THROUGH 1/10-OCTAVE BANDS DURING THE 17 NOV FIELD EVENT (U)

AS-77-3355

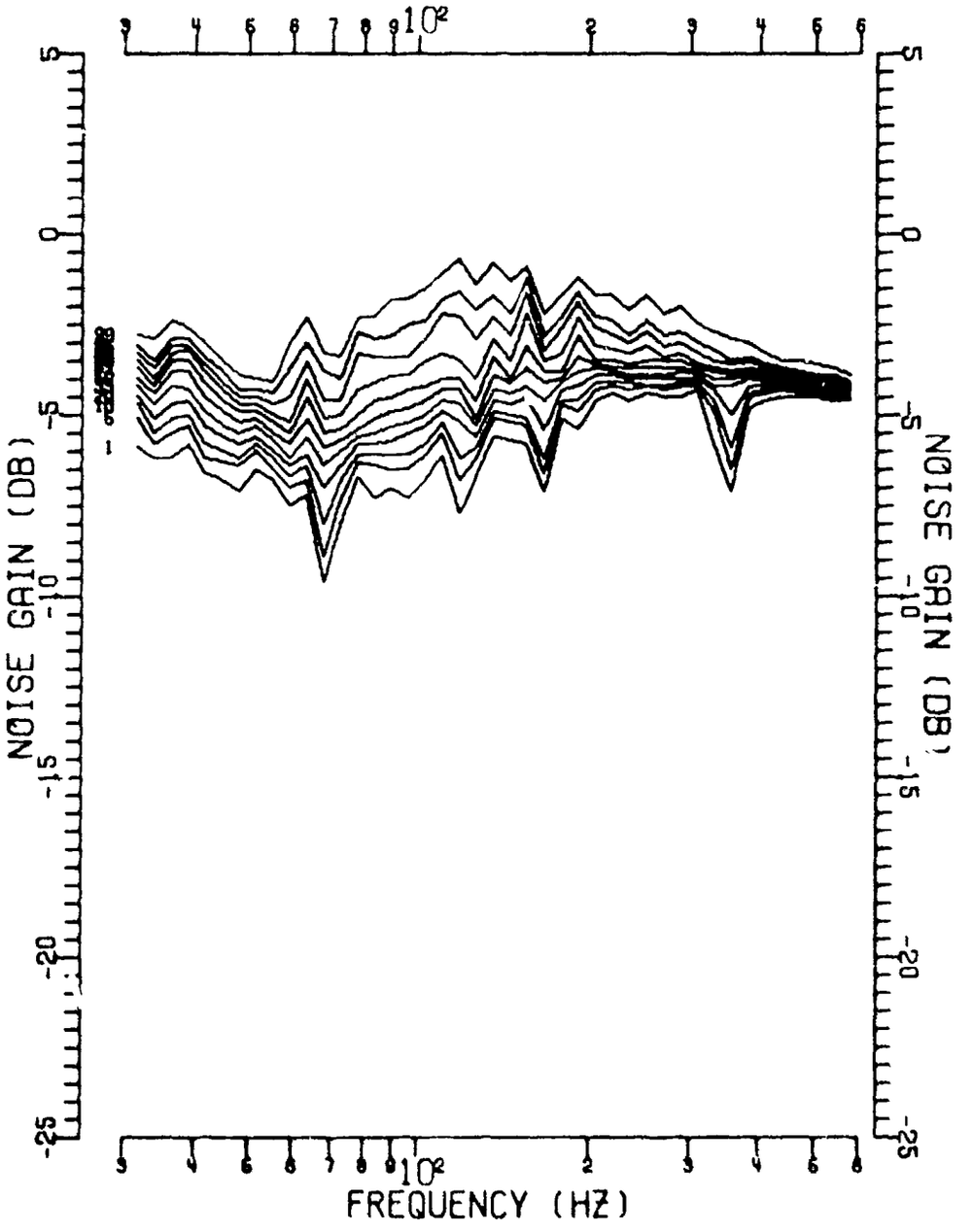

FIGURE II-342
MSS-FVT PHASE II SITE A3 WEST CARDIOID
PERCENTILE LEVELS OF 1 MIN AVERAGED NOISE GAINS
THROUGH 1/10-OCTAVE BANDS DURING THE 17 NOV FIELD EVENT (U)

AS-77-3356

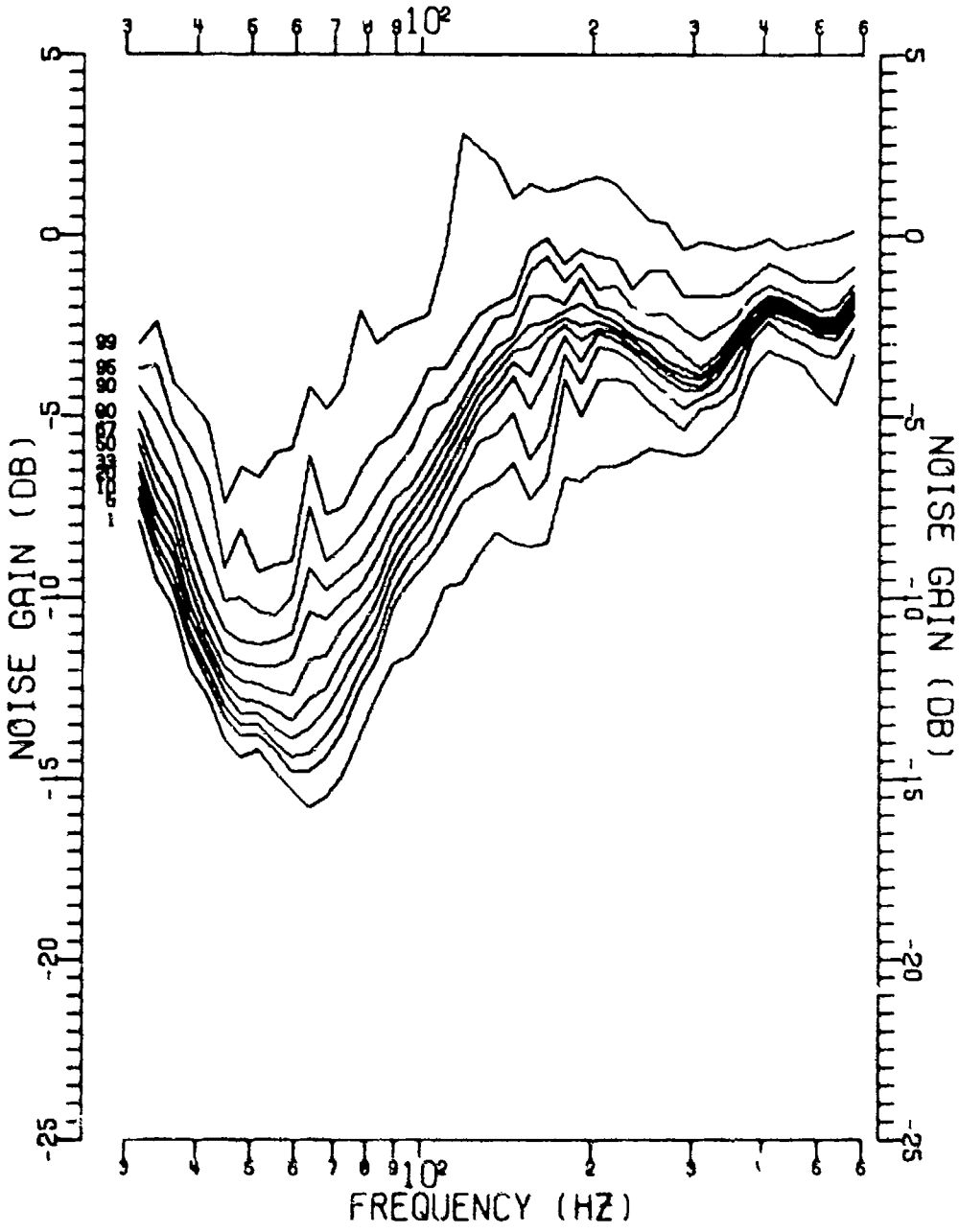

FIGURE II-343
MSS-FVT PHASE II SITE A1 VERTICAL DIPOLE SENSOR
PERCENTILE LEVELS OF 1 MIN AVERAGED NOISE GAINS
THROUGH 1/10-OCTAVE BANDS DURING THE 17 NOV FIELD EVENT (U)

AS-77-3357

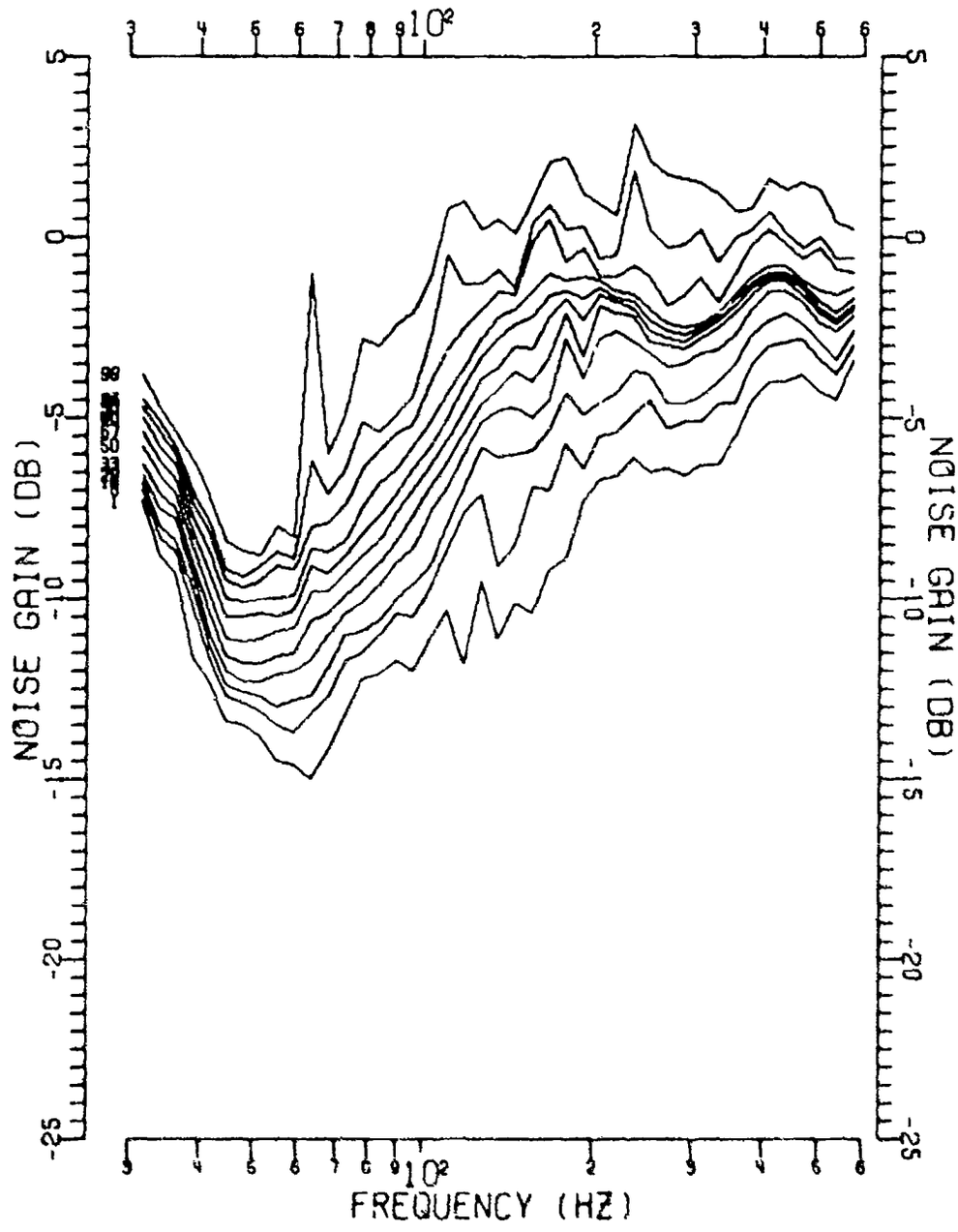

FIGURE II-344
MSS-FVT PHASE II SITE A2 VERTICAL DIPOLE SENSOR
PERCENTILE LEVELS OF 1 MIN AVERAGED NOISE GAINS
THROUGH 1/10-OCTAVE BANDS DURING THE 17 NOV FIELD EVENT (U)

AS-77-3358

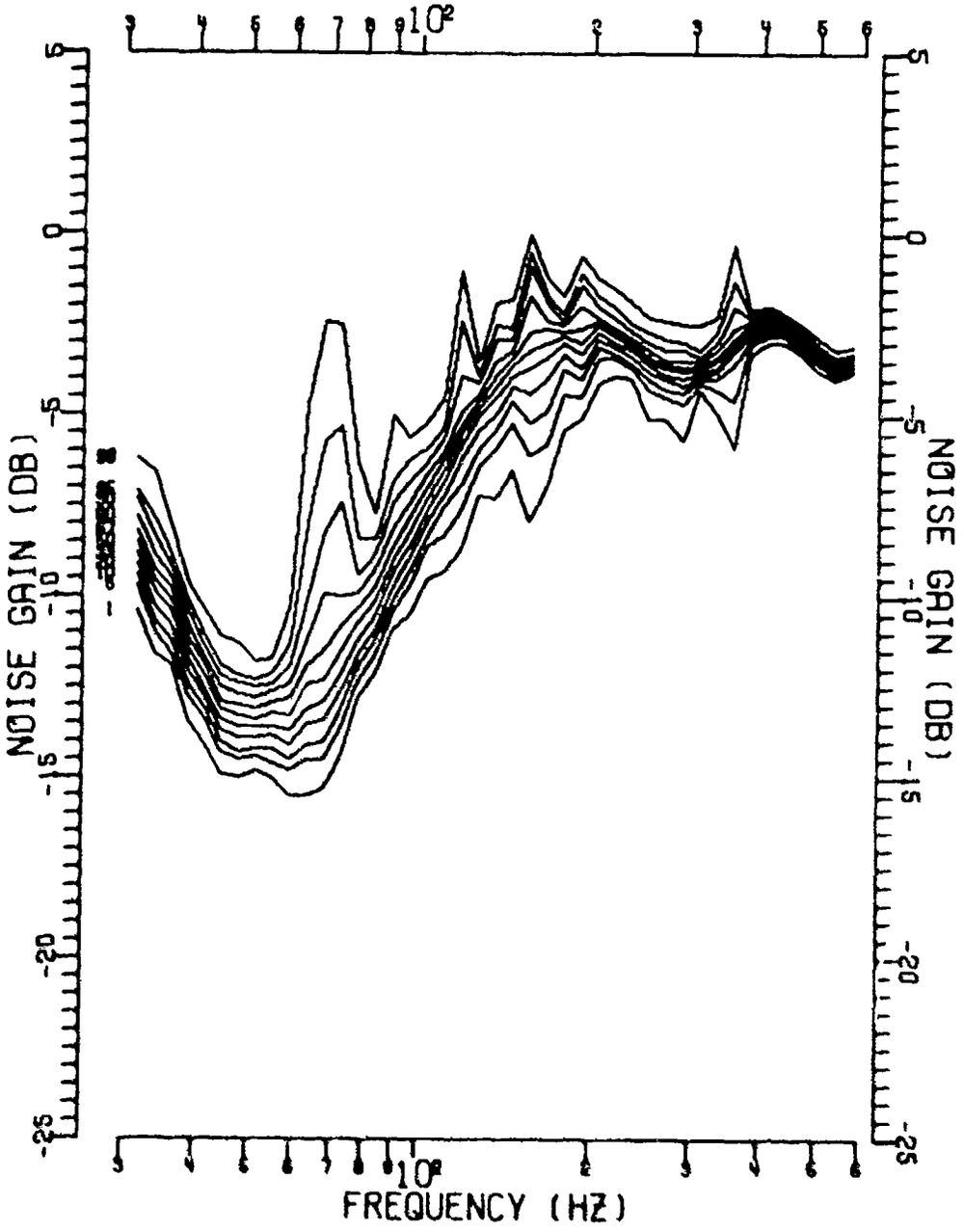

FIGURE II-345
MSS-FVT PHASE II SITE 93 VERTICAL DIPOLE SENSOR
PERCENTILE LEVELS OF 1 MIN AVERAGED NOISE GAINS
THROUGH 1/10-OCTAVE BANDS DURING THE 17 NOV FIELD EVENT (U)

AS-77-3359

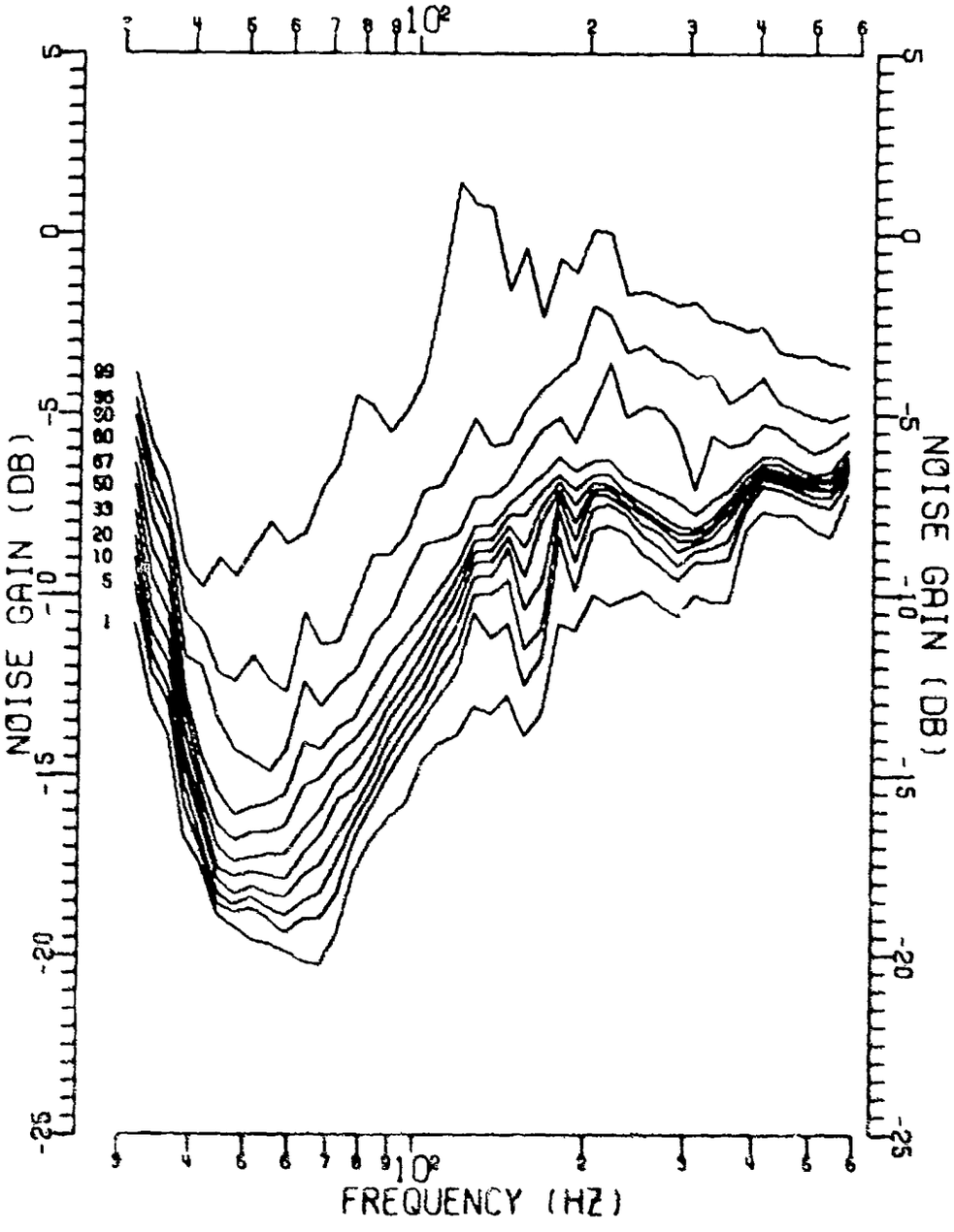

FIGURE II-346
MSS-FVT PHASE II SITE A1 DIFFERENCED NORTH CARDIOID
PERCENTILE LEVELS OF 1 MIN AVERAGED NOISE GAINS
THROUGH 1/10-OCTAVE BANDS DURING THE 17 NOV FIELD EVENT (U)

AS-77-3360

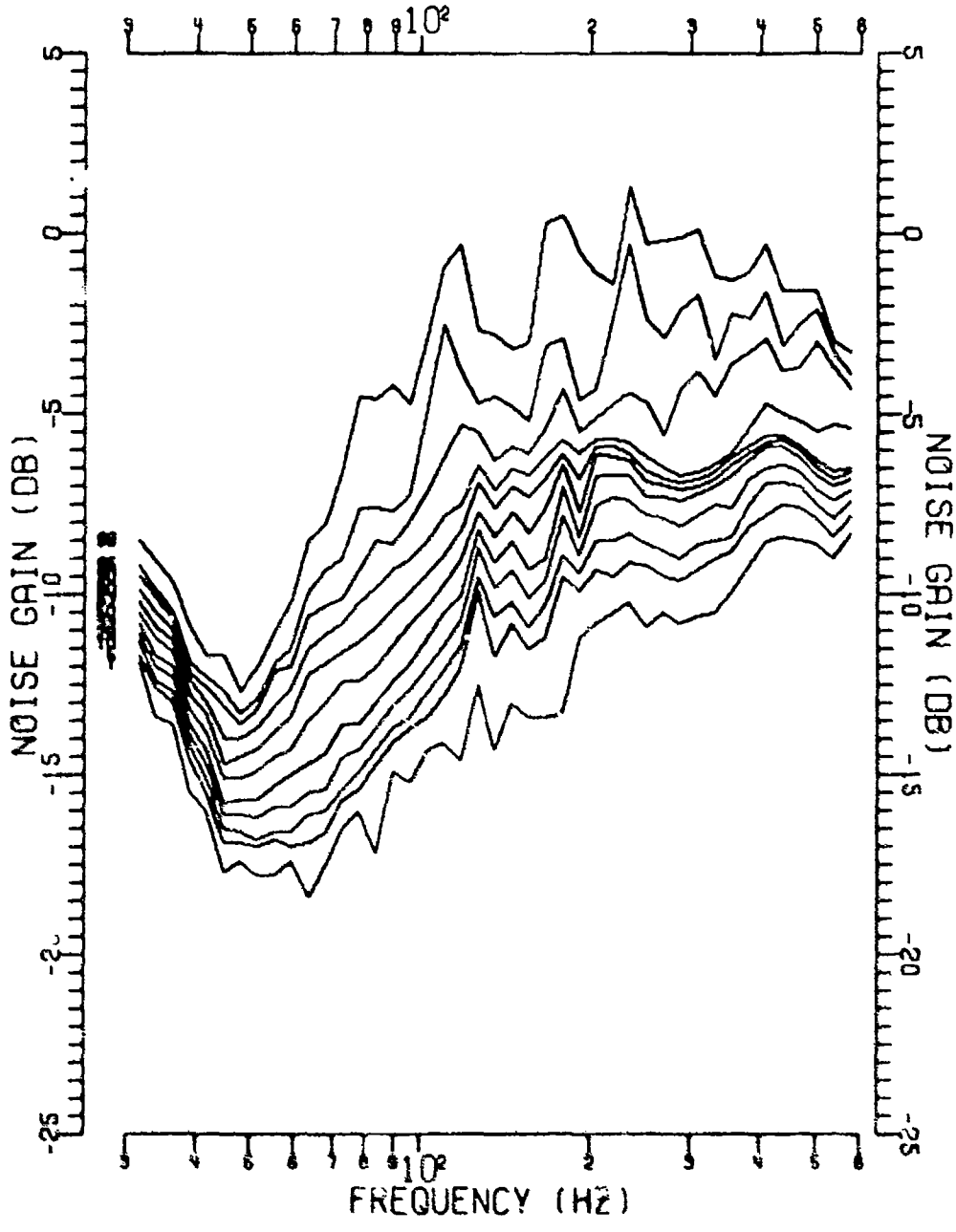

FIGURE II-347
MSS-FVT PHASE II SITE A2 DIFFERENCED NORTH CARDIOID
PERCENTILE LEVELS OF 1 MIN AVERAGED NOISE GAINS
THROUGH 1/10-OCTAVE BANDS DURING THE 17 NOV FIELD EVENT (U)

77-3361

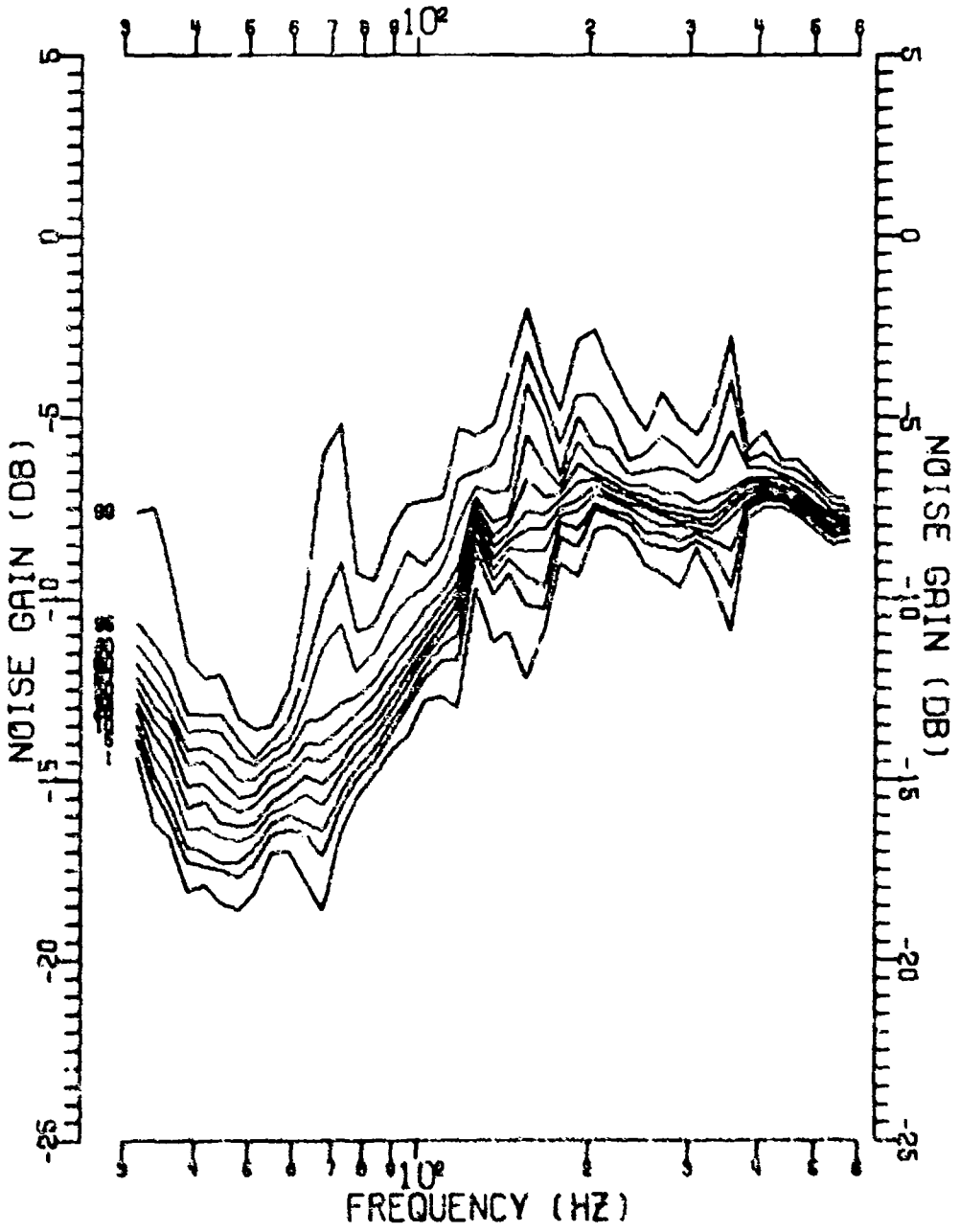

FIGURE II-348
MSS-FVT PHASE II SITE A3 DIFFERENCED NORTH CARDIOID
PERCENTILE LEVELS OF 1 MIN AVERAGED NOISE GAINS
THROUGH 1/10-OCTAVE BANDS DURING THE 17 NOV FIELD EVENT (U)

AS-77-3362

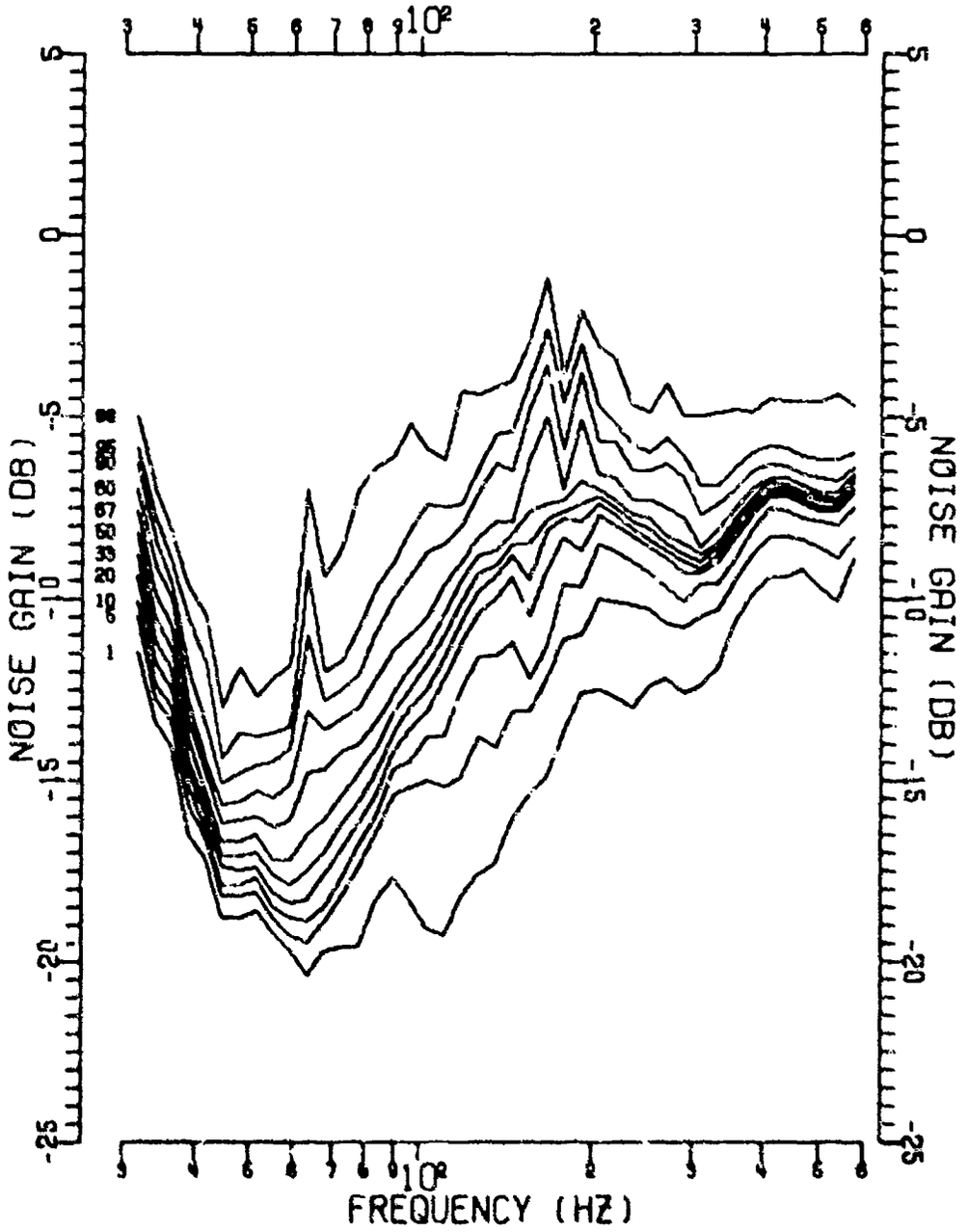

FIGURE II-349
MSS-FVT PHASE II SITE A1 DIFFERENCED EAST CARDIOID
PERCENTILE LEVELS OF 1 MIN AVERAGED NOISE GAINS
THROUGH 1/10-OCTAVE BANDS DURING THE 17 NOV FIELD EVENT (U)

AS-77-3363

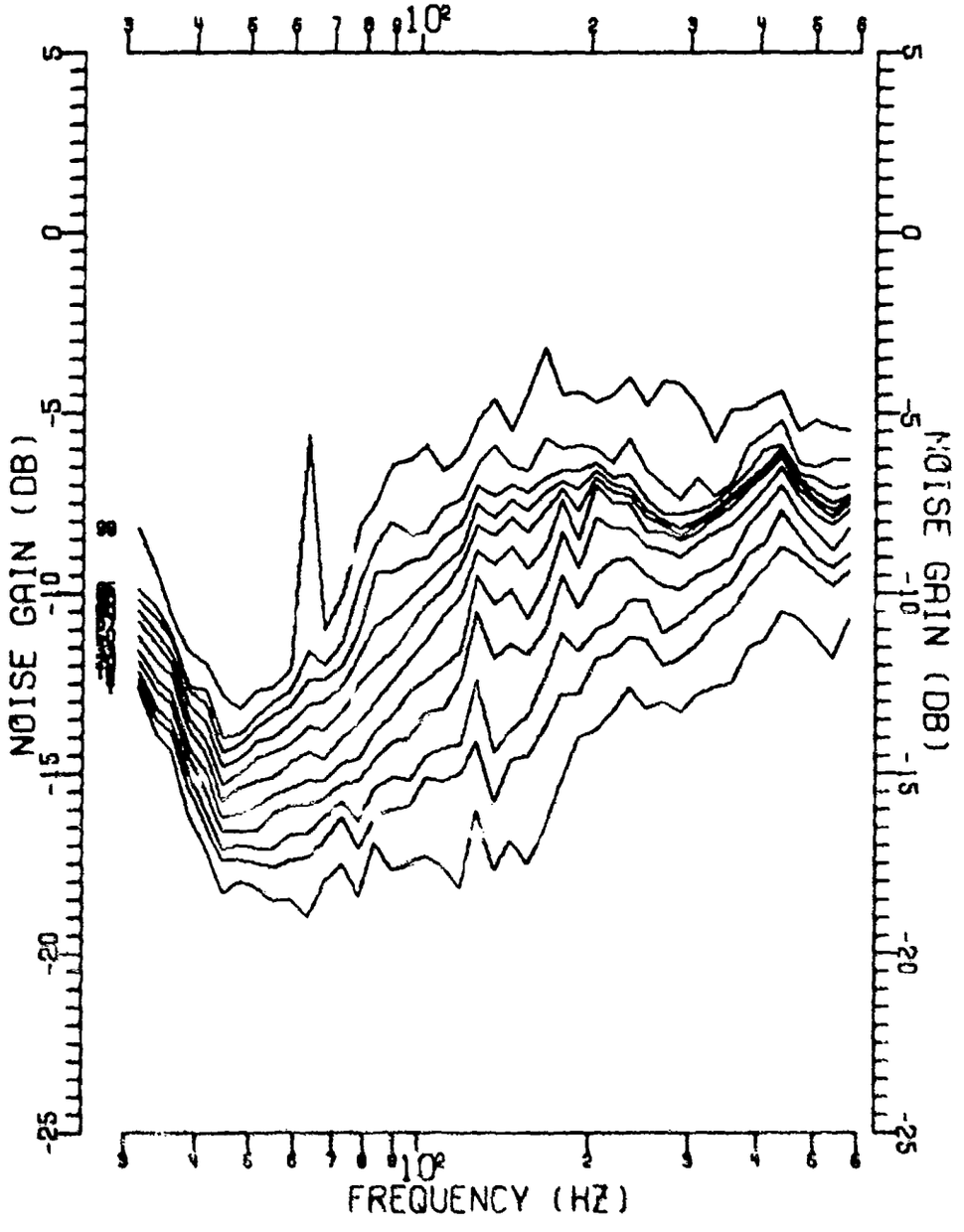

FIGURE II-350
MSS-FVT PHASE II SITE A2 DIFFERENCED EAST CARDIOID
PERCENTILE LEVELS OF 1 MIN AVERAGED NOISE GAINS
THROUGH 1/10-OCTAVE BANDS DURING THE 17 NOV FIELD EVENT (U)

AS-77-3364

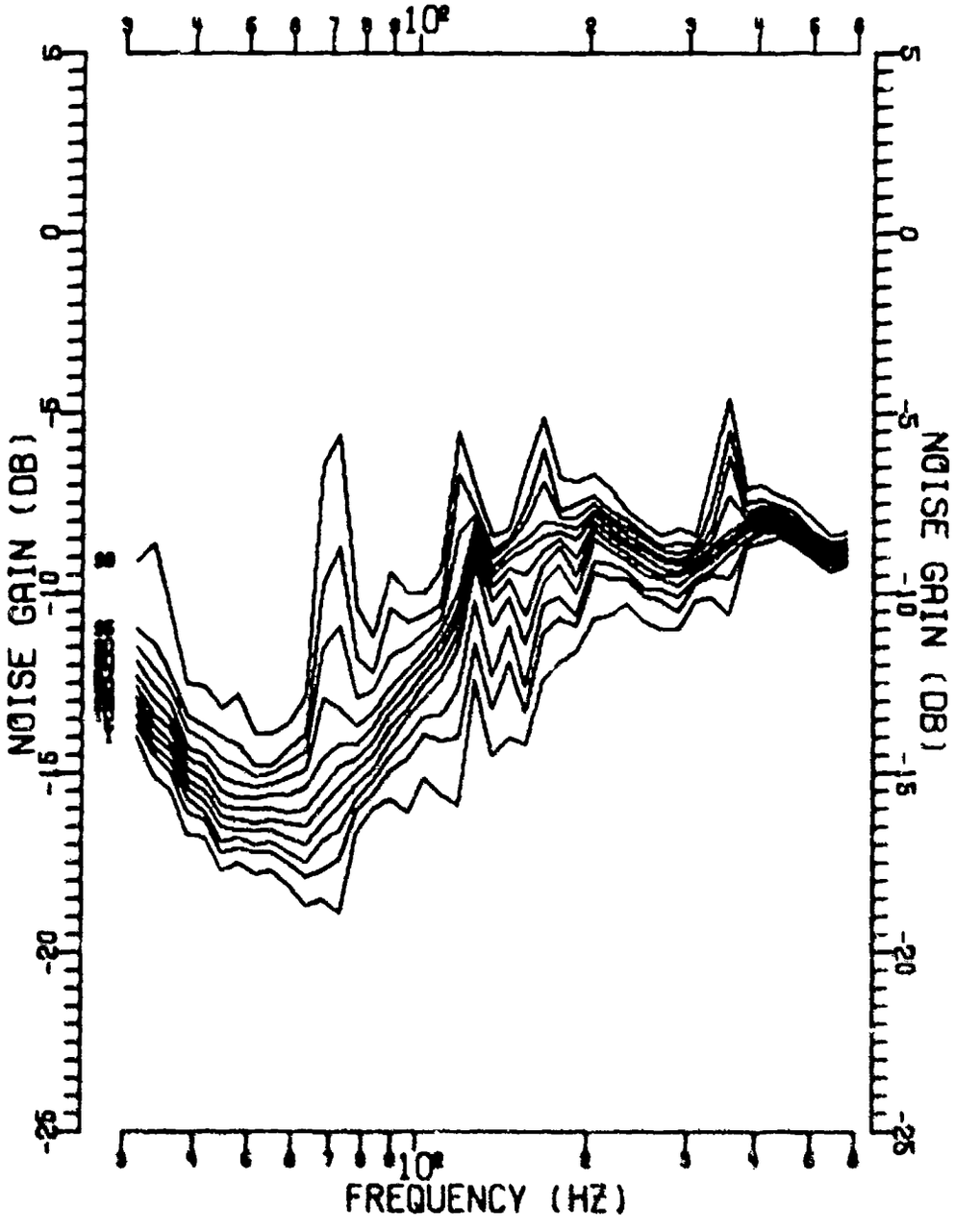

FIGURE II-351
MSS-FVT PHASE II SITE A3 DIFFERENCED EAST CARDIOID
PERCENTILE LEVELS OF 1 MIN AVERAGED NOISE GAINS
THROUGH 1/10-OCTAVE BANDS DURING THE 17 NOV FIELD EVENT (U)

AS-77-3365

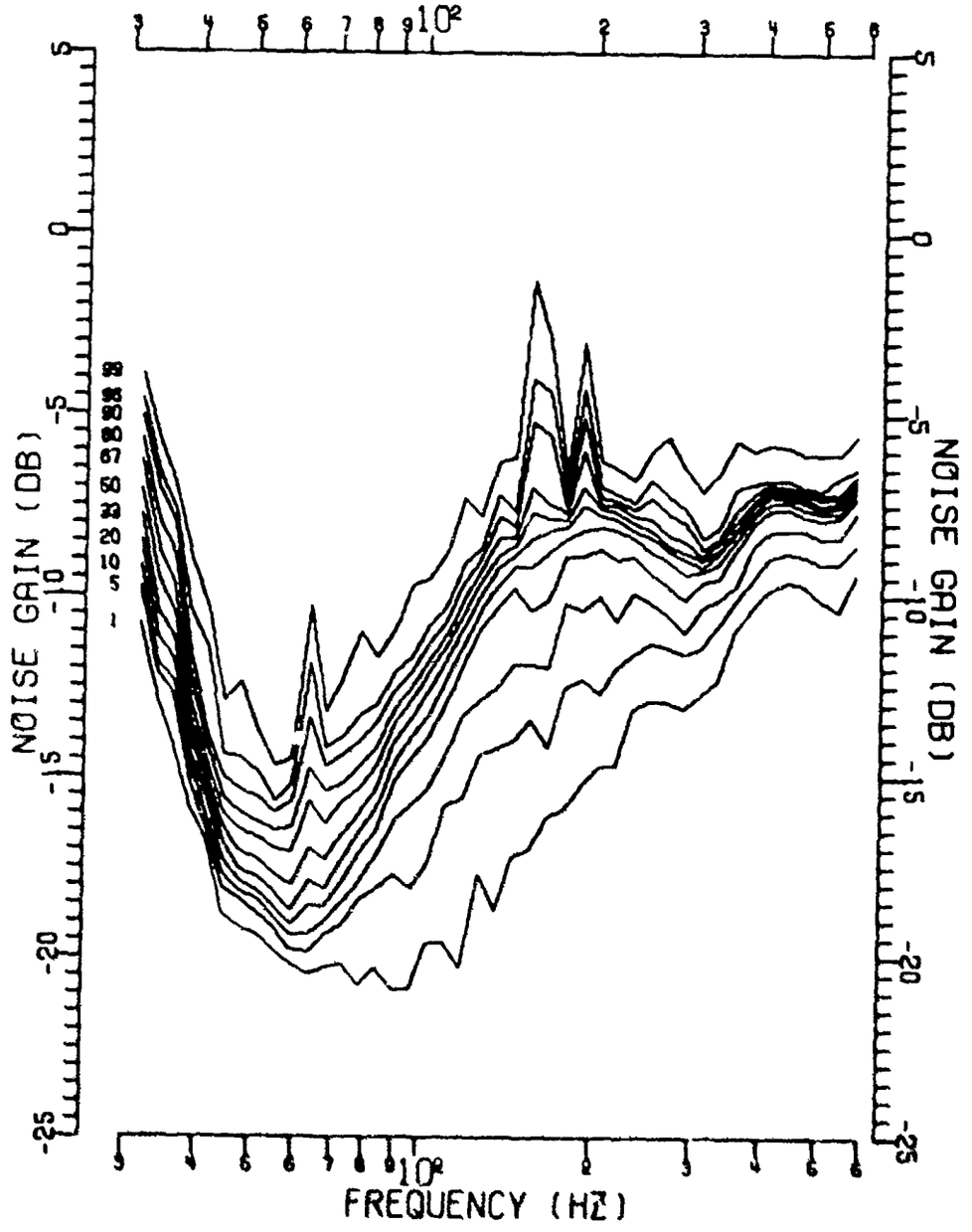

FIGURE II-352
MSS-FVT PHASE II SITE A1 DIFFERENCED SOUTH CARDIOID
PERCENTILE LEVELS OF 1 MIN AVERAGED NOISE GAINS
THROUGH 1/10-OCTAVE BANDS DURING THE 17 NOV FIELD EVENT (U)

AS-77-3366

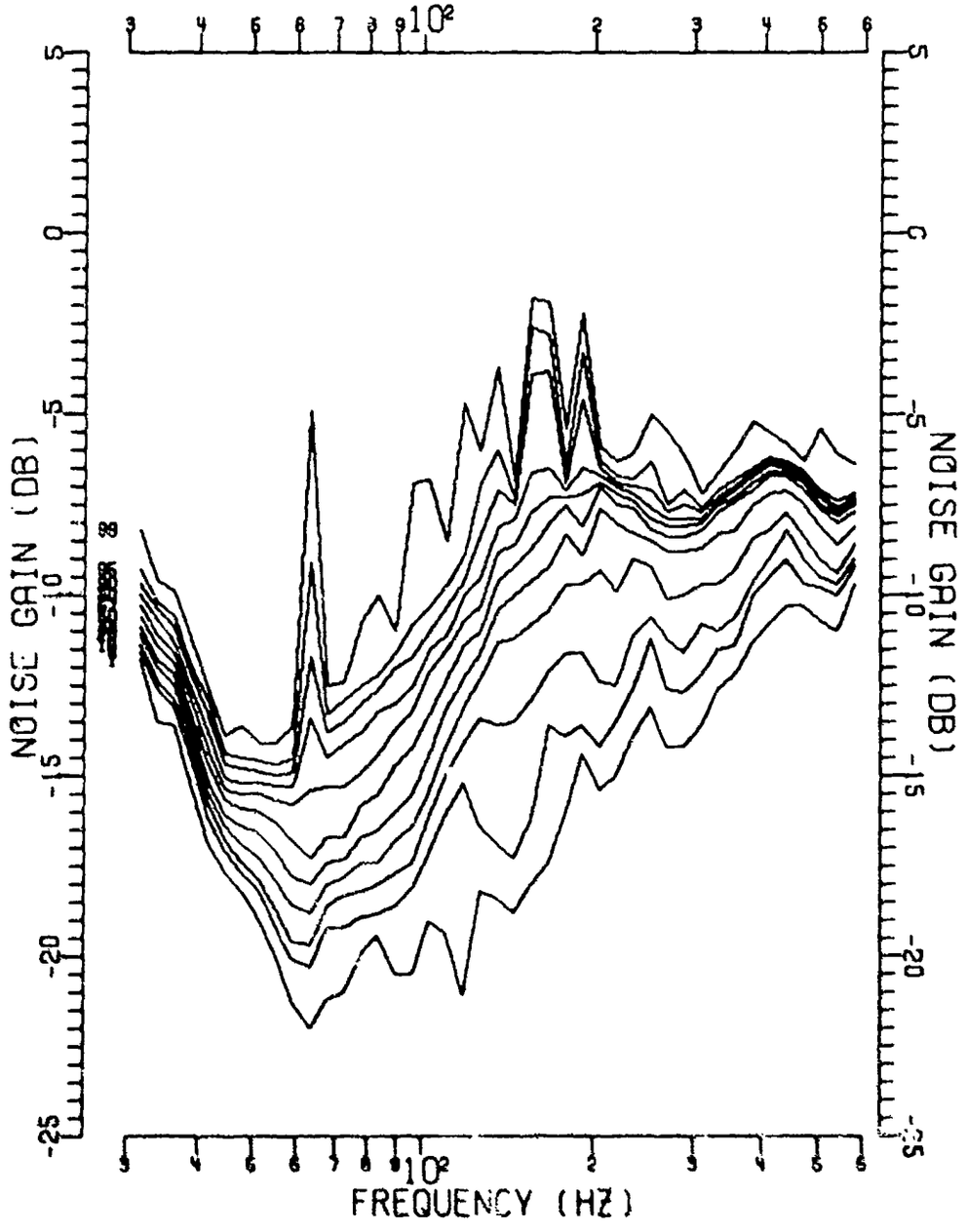

FIGURE II-353
MSS-FVT PHASE II SITE A2 DIFFERENCED SOUTH CARDIOID
PERCENTILE LEVELS OF 1 MIN AVERAGED NOISE GAINS
THROUGH 1/10-OCTAVE BANDS DURING THE 17 NOV FIELD EVENT (U)

AS-77-3367

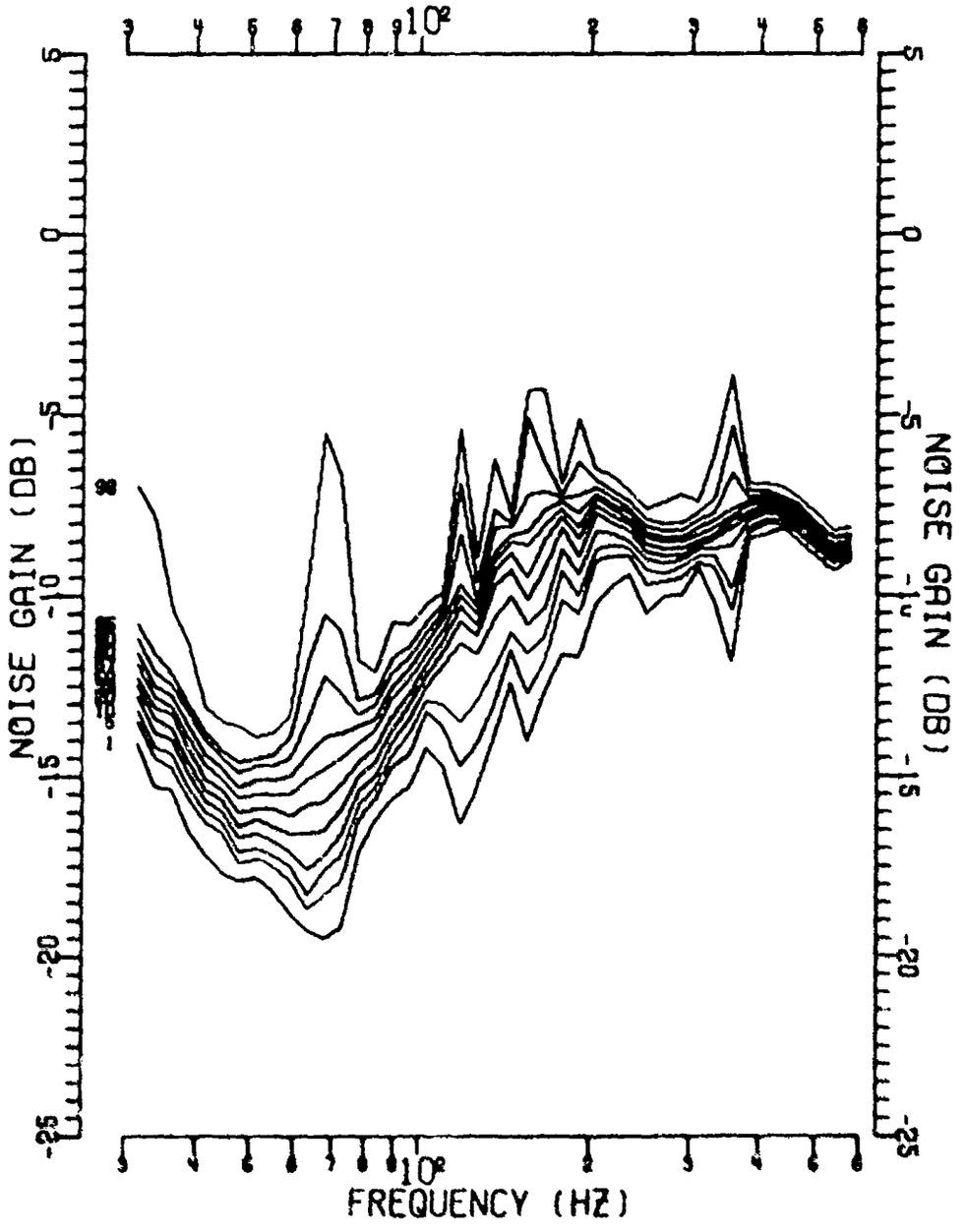

FIGURE II-354
MSS-FVT PHASE II SITE A3 DIFFERENCED SOUTH CARDIOID
PERCENTILE LEVELS OF 1 MIN AVERAGED NOISE GAINS
THROUGH 1/10-OCTAVE BANDS DURING THE 17 NOV FIELD EVENT (U)

AS-77-3368

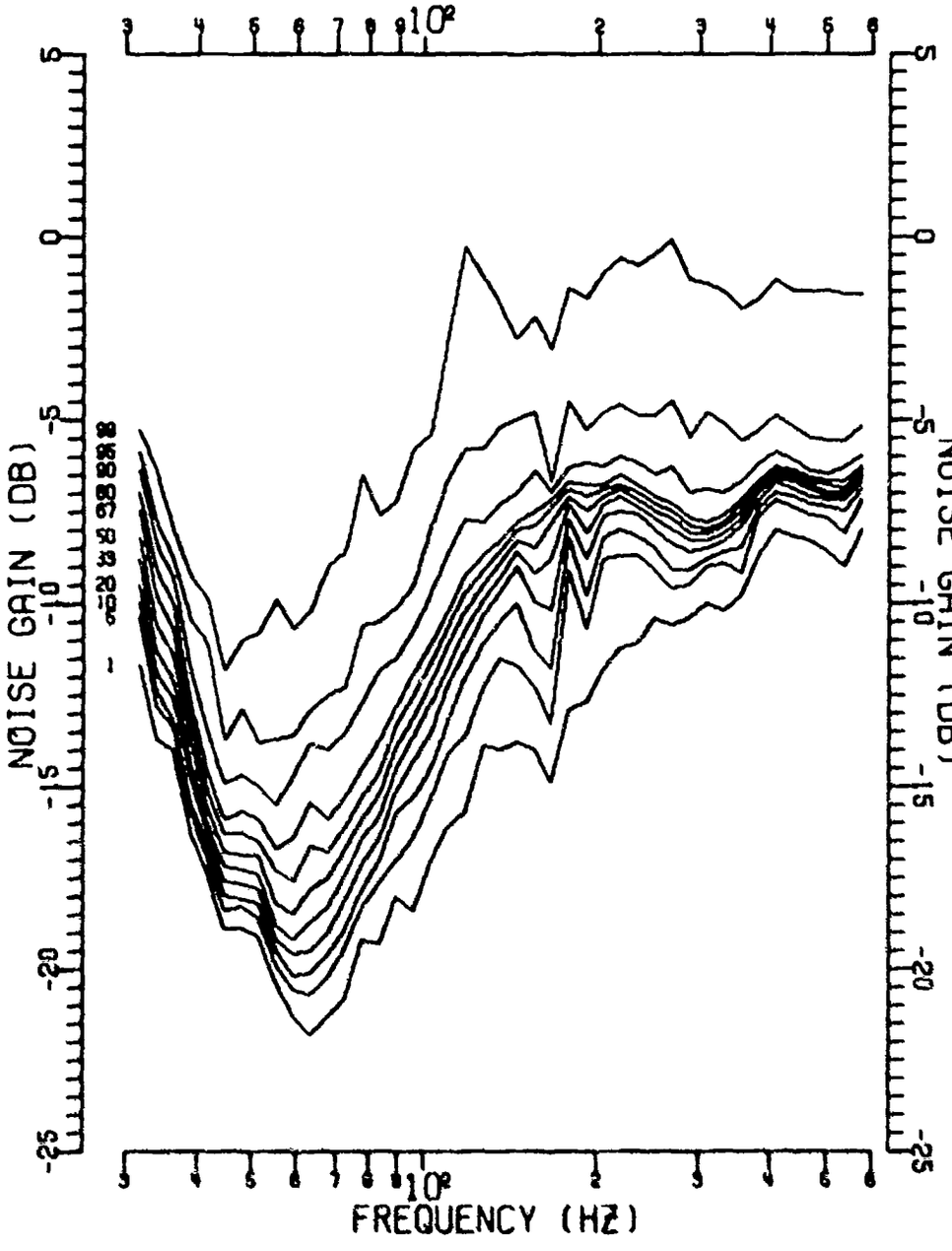

FIGURE II-355
MSS-FVT PHASE II SITE A1 DIFFERENCED WEST CARDIOID
PERCENTILE LEVELS OF 1 MIN AVERAGED NOISE GAINS
THROUGH 1/10-OCTAVE BANDS DURING THE 17 NOV FIELD EVENT (U)

AS-77-3369

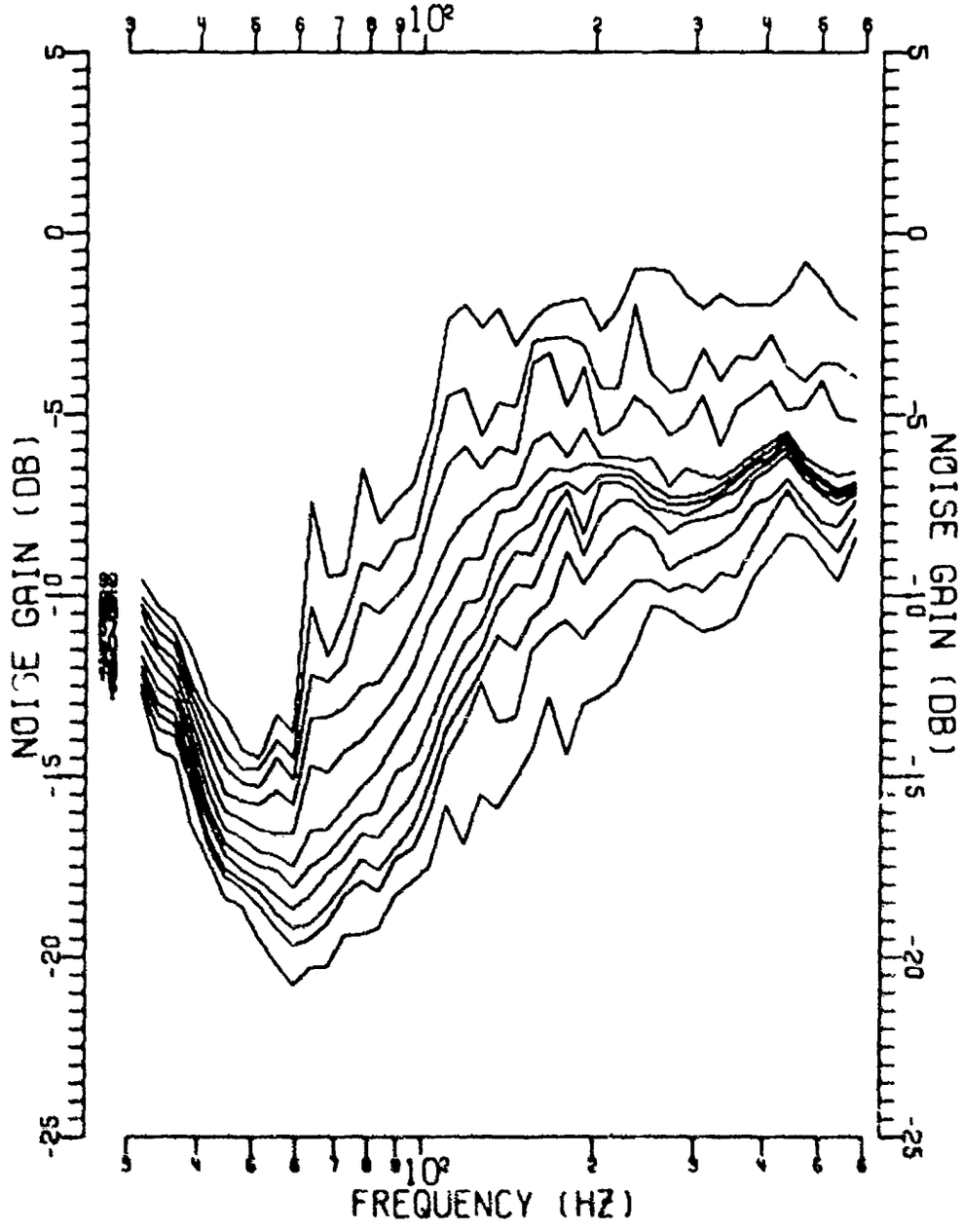

FIGURE II-356
MSS-FVT PHASE II SITE A2 DIFFERENCED WEST CARDIOID
PERCENTILE LEVELS OF 1 MIN AVERAGED NOISE GAINS
THROUGH 1/10-OCTAVE BANDS DURING THE 17 NOV FIELD EVENT (U)

AS-77-3370

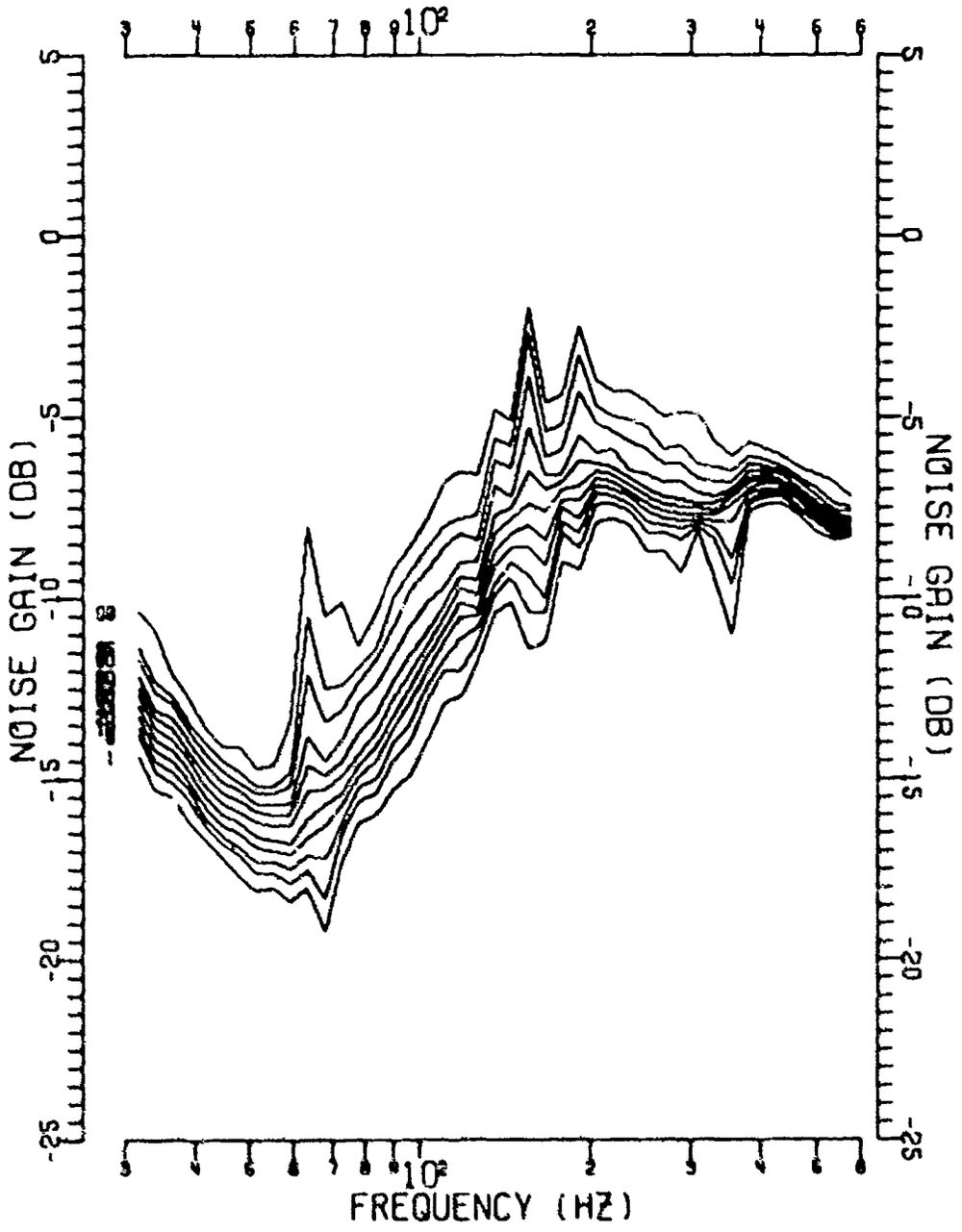

FIGURE II-357
MSS-FVT PHASE II SITE A3 DIFFERENCED WEST CARDIOID
PERCENTILE LEVELS OF 1 MIN AVERAGED NOISE GAINS
THROUGH 1/10-OCTAVE BANDS DURING THE 17 NOV FIELD EVENT (U)

AS-77-3371

APPENDIX K

CLUTTER TIMESERIES CURVES (U)

(FIGURES II-358 - II-372)

(The reverse of this page is blank.)

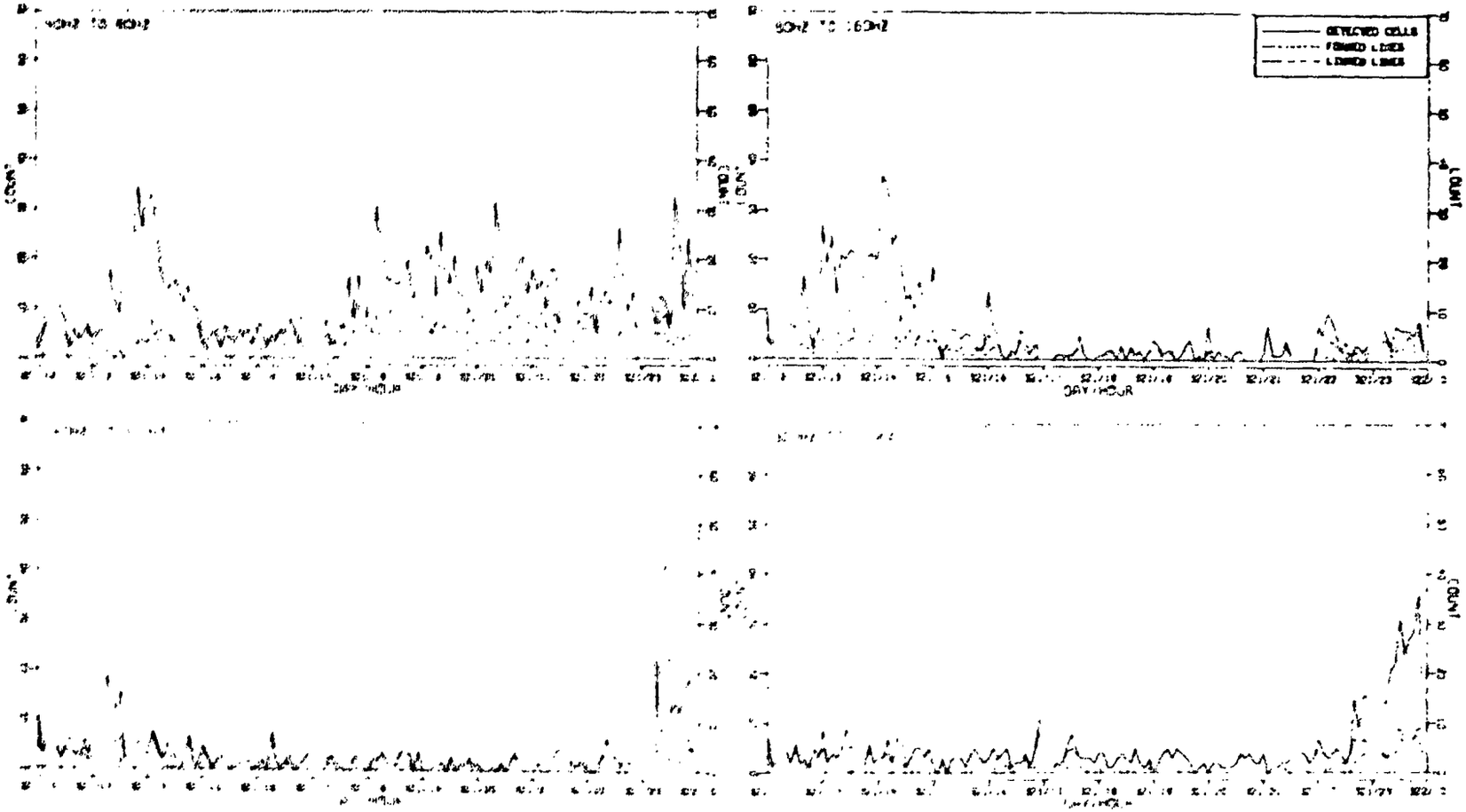

FIGURE II-358
MSS-FVT STANDARD RESOLUTION CLUTTER RESULTS
FOR THE OMNIDIRECTIONAL SENSOR
AT SITE A1 DURING THE 17 NOV FIELD EVENT (U)

AS77-3372

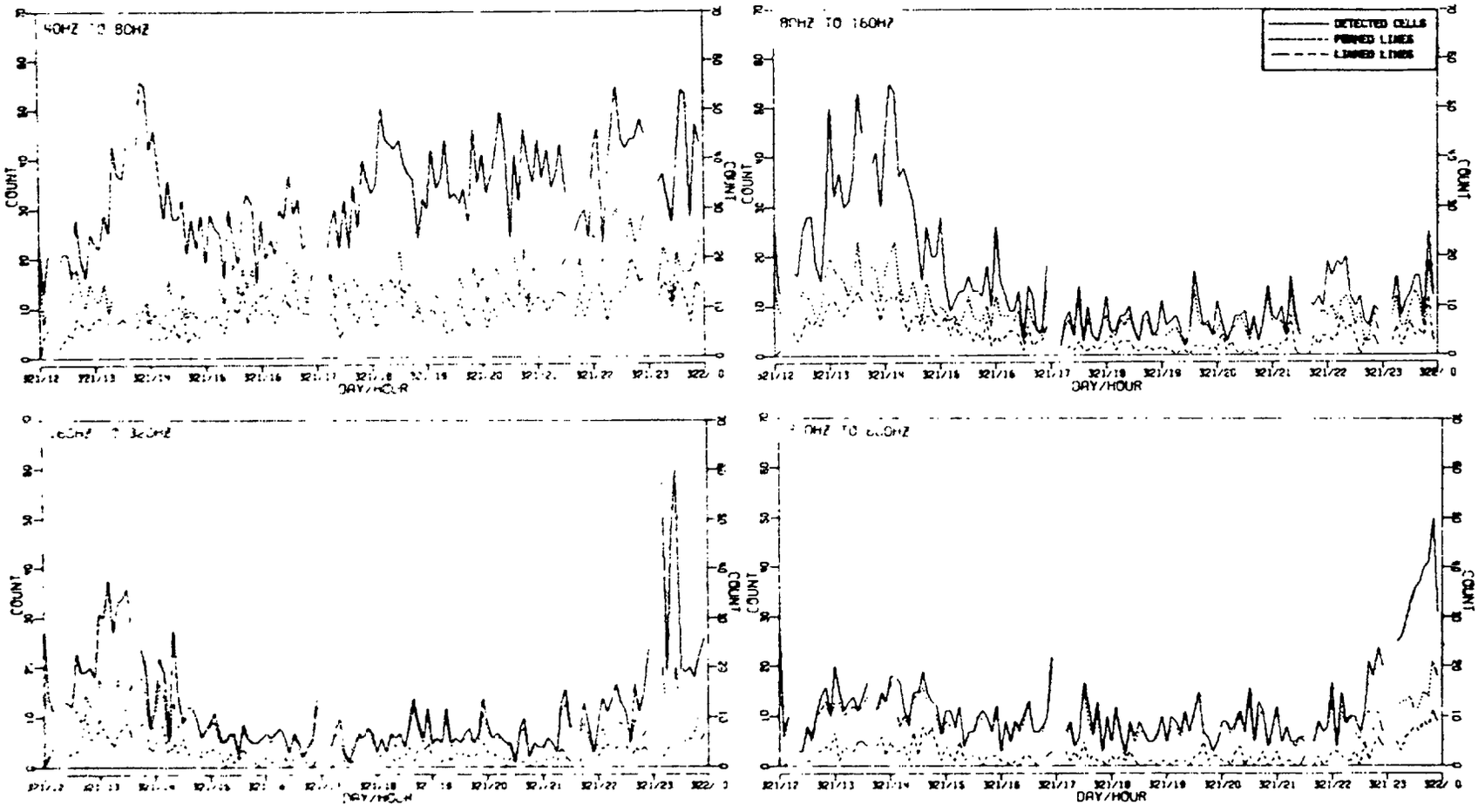

FIGURE II-359
MSS-FVT STANDARD RESOLUTION CLUTTER RESULTS
FOR THE SINGLE CARDIOIDS SENSOR
AT SITE A1 DURING THE 17 NOV FIELD EVENT (U)

AS-77-3373

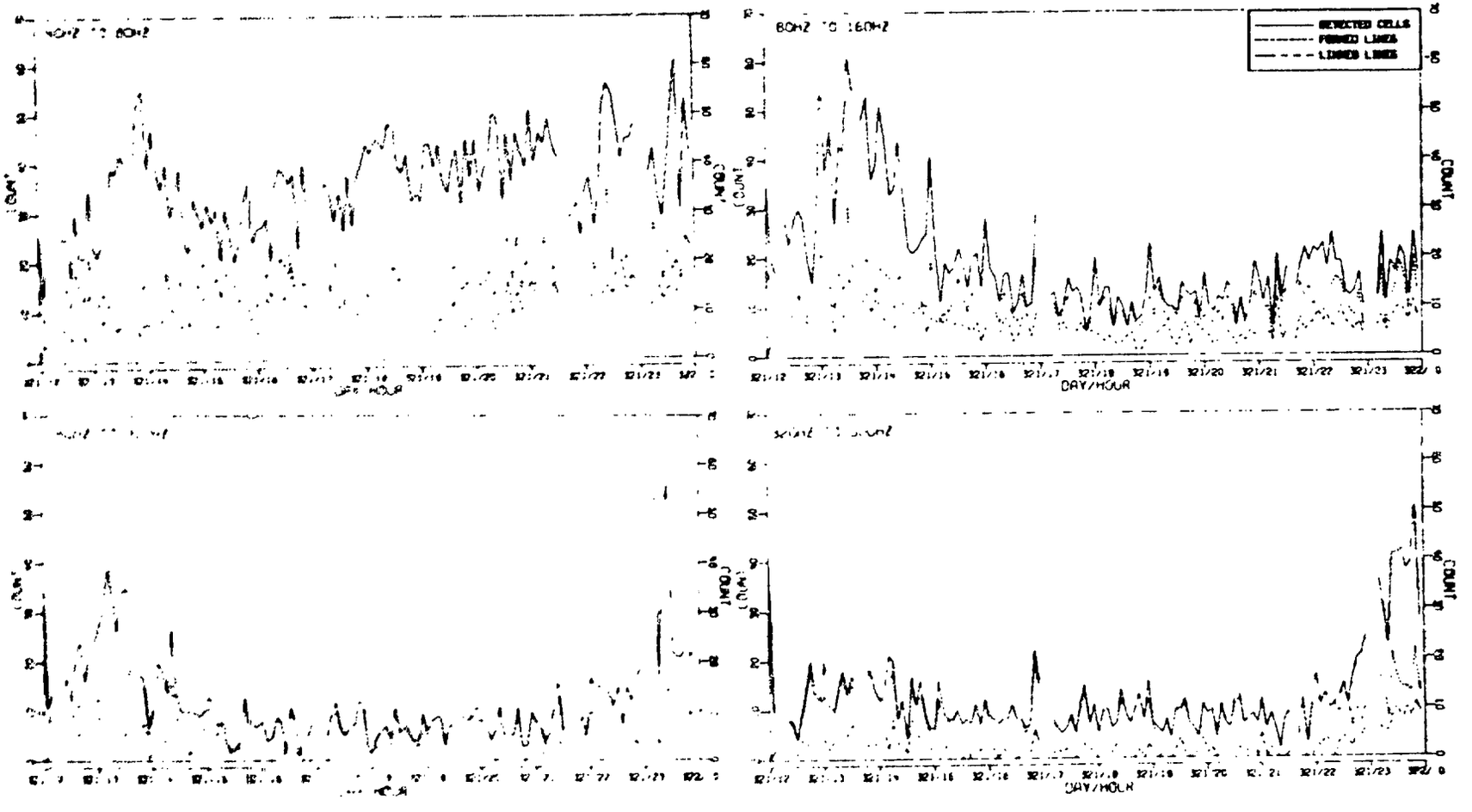

FIGURE II-360
MSS-FVT STANDARD RESOLUTION CLUTTER RESULTS
FOR THE MAX GAIN LIMACONS SENSOR
AT SITE A1 DURING THE 17 NOV FIELD EVENT (U)

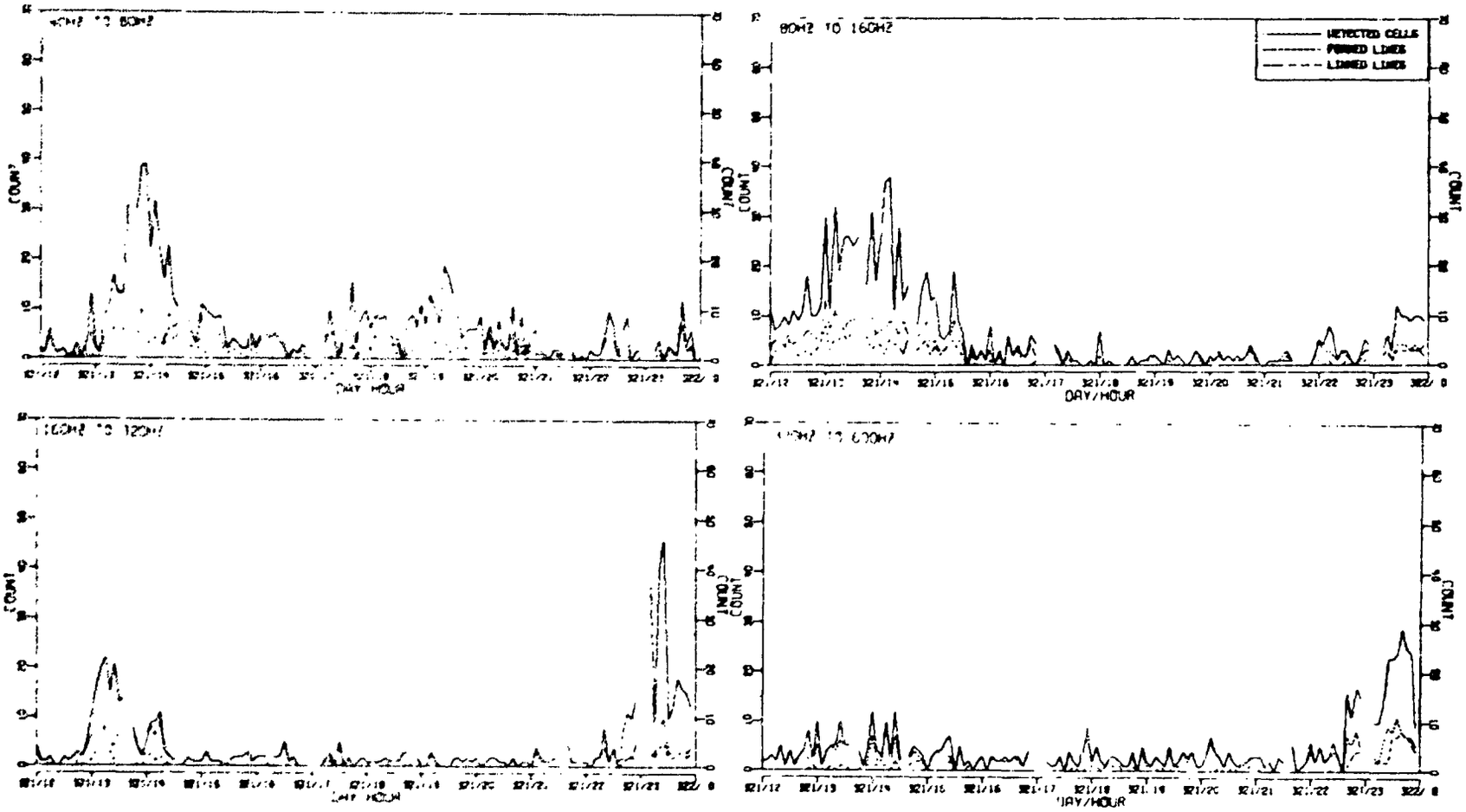

FIGURE II-361
MSS-FVT STANDARD RESOLUTION CLUTTER RESULTS
FOR THE VERTICAL DIPOLE SENSOR
AT SITE A1 DURING THE 17 NOV FIELD EVENT (U)

AS-77-3375

CONFIDENTIAL

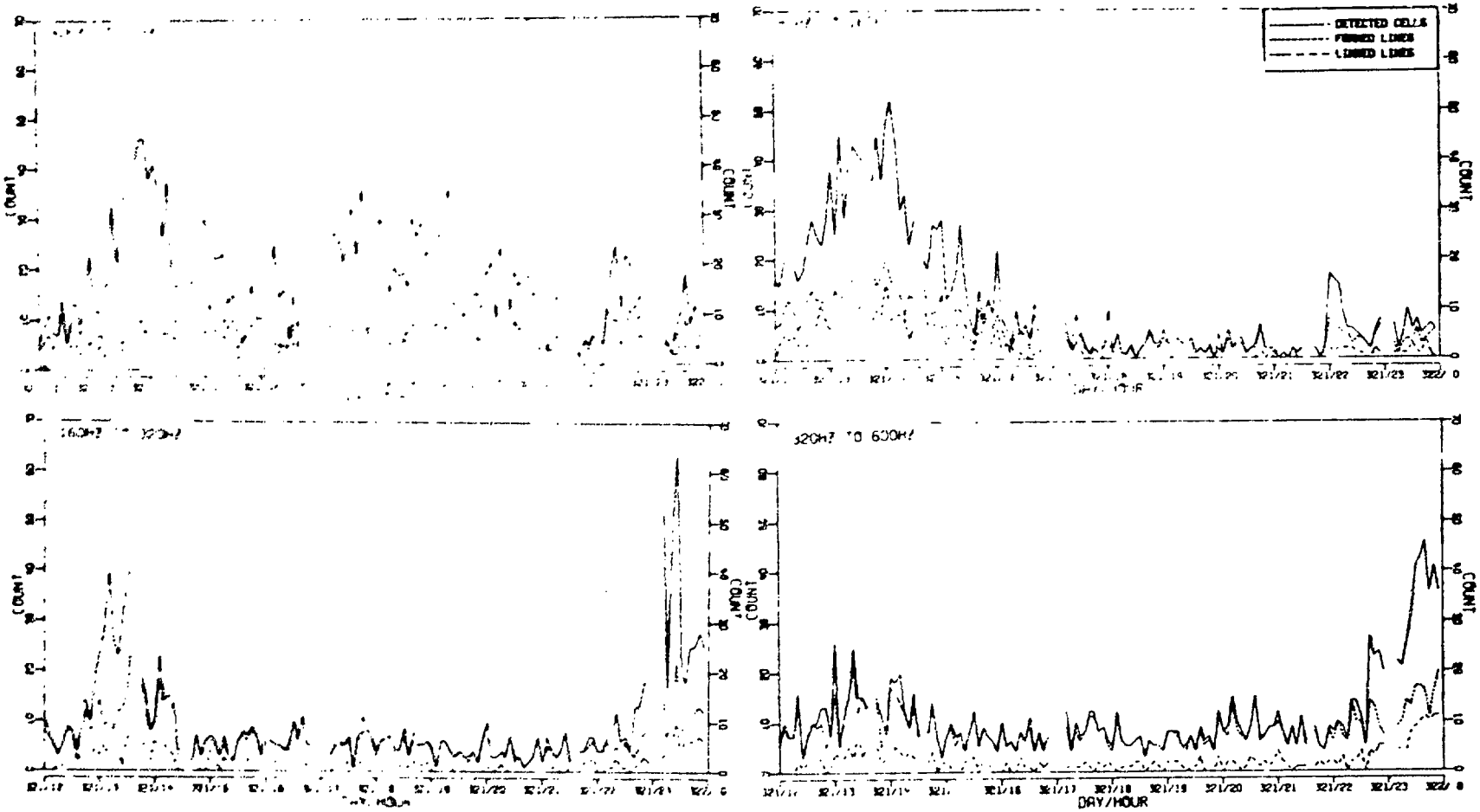

FIGURE II-362
MSS-FVT STANDARD RESOLUTION CLUTTER RESULTS
FOR THE DIFFERENCED CARDIOIDS SENSOR
AT SITE A1 DURING THE 17 NOV FIELD EVENT (U)

AS77-3376

CONFIDENTIAL

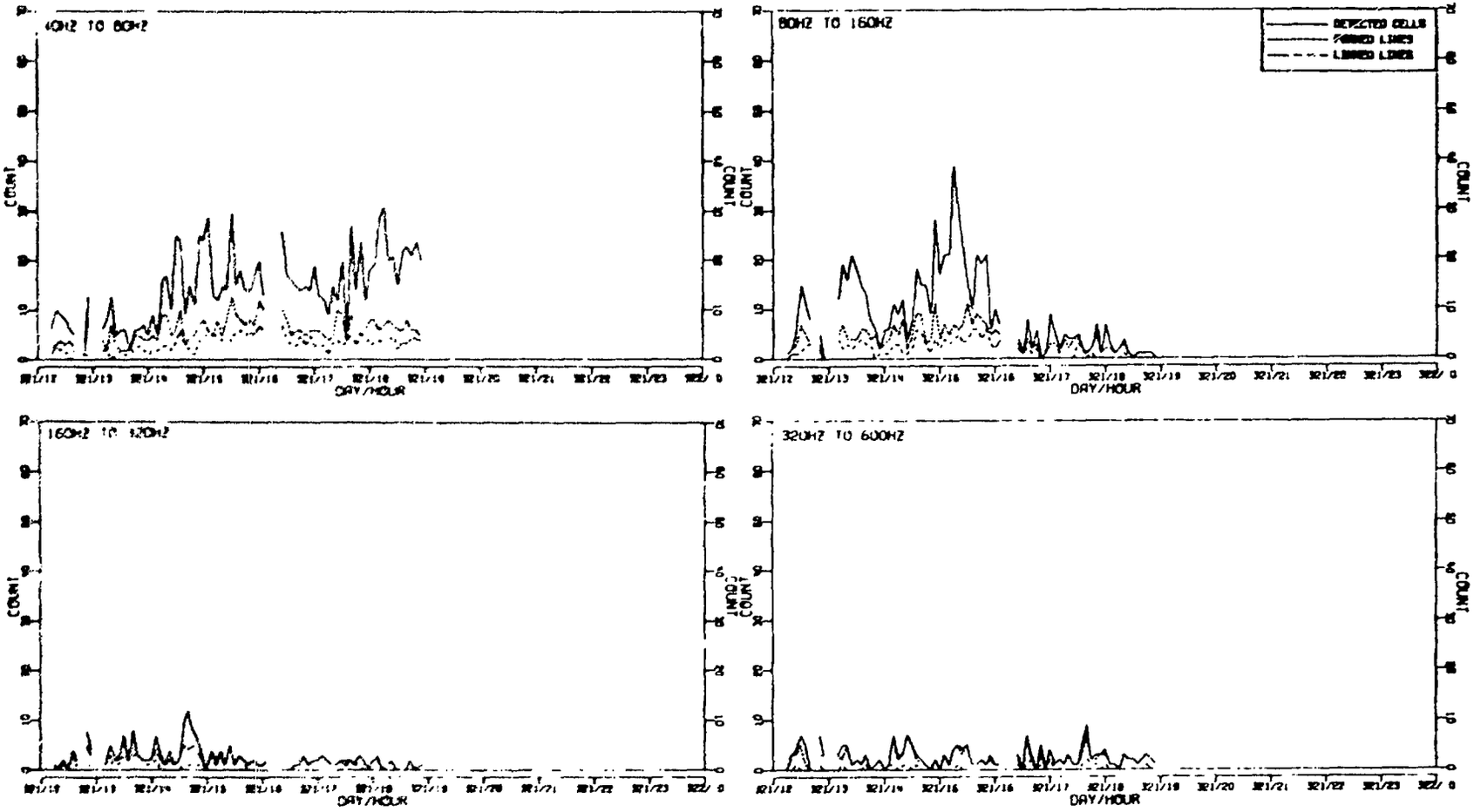

FIGURE II-363
MSS-FVT STANDARD RESOLUTION CLUTTER RESULTS
FOR THE OMNIDIRECTIONAL SENSOR
AT SITE A2 DURING THE 17 NOV FIELD EVENT (U)

AS-77-3377

CONFIDENTIAL

CONFIDENTIAL

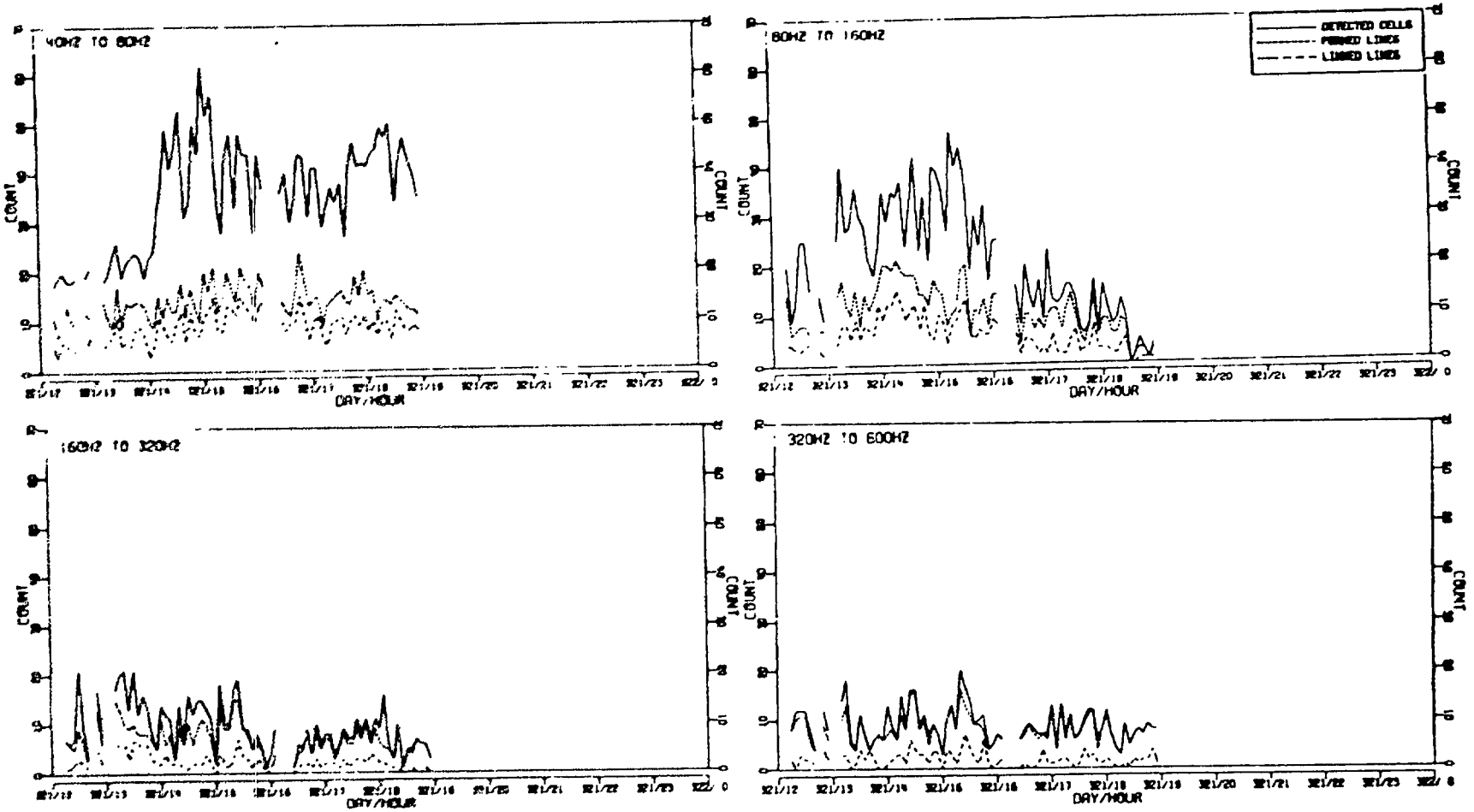

FIGURE II-364
MSS-FVT STANDARD RESOLUTION CLUTTER RESULTS
FOR THE SINGLE CARDIOIDS SENSOR
AT SITE A2 DURING THE 17 NOV FIELD EVENT (U)

AS-77-3378

CONFIDENTIAL

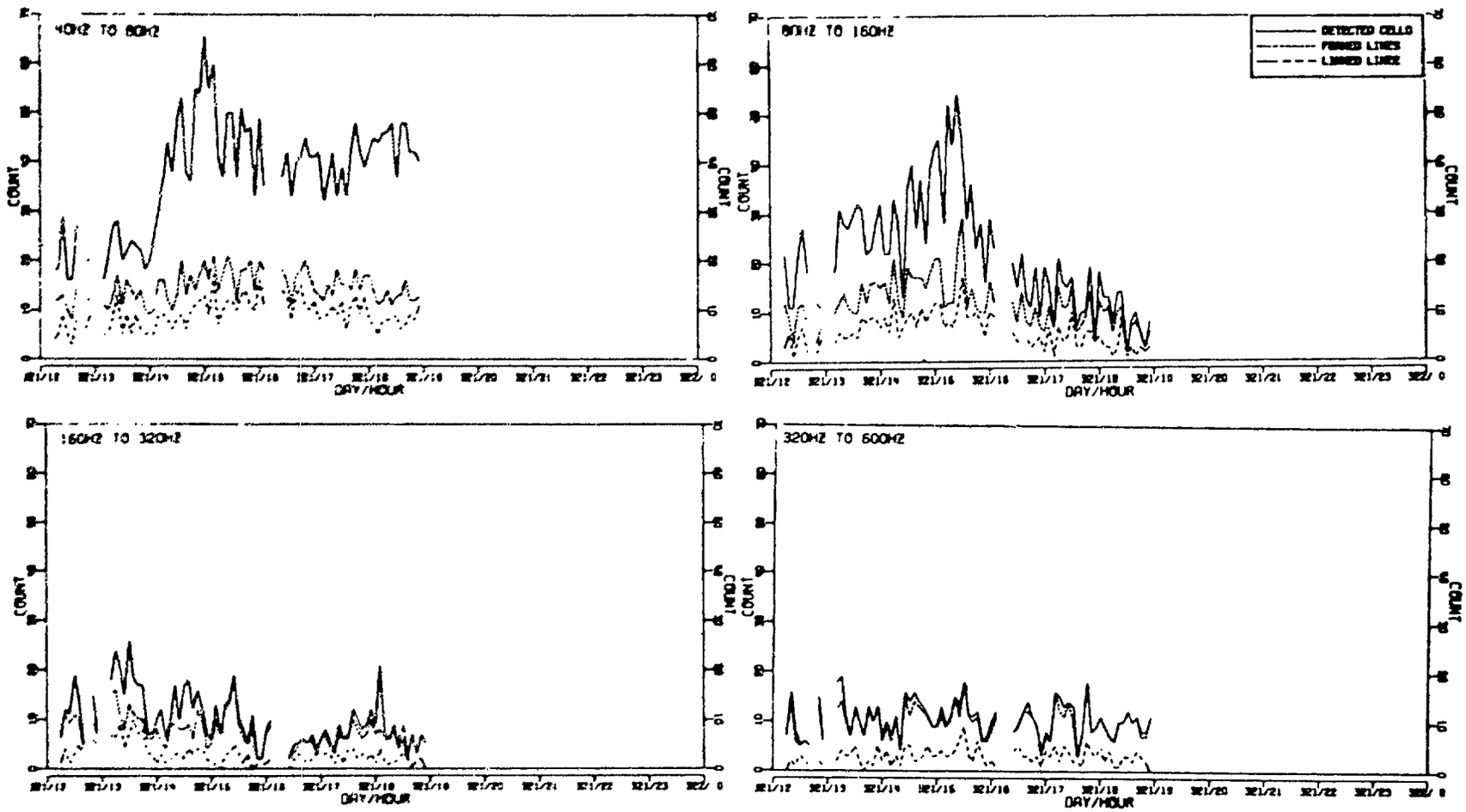

FIGURE II-365
MSS-FVT STANDARD RESOLUTION CLUTTER RESULTS
FOR THE MAX GAIN LIMACONS SENSOR
AT SITE A2 DURING THE 17 NOV FIELD EVENT (U)

AS-77-3379

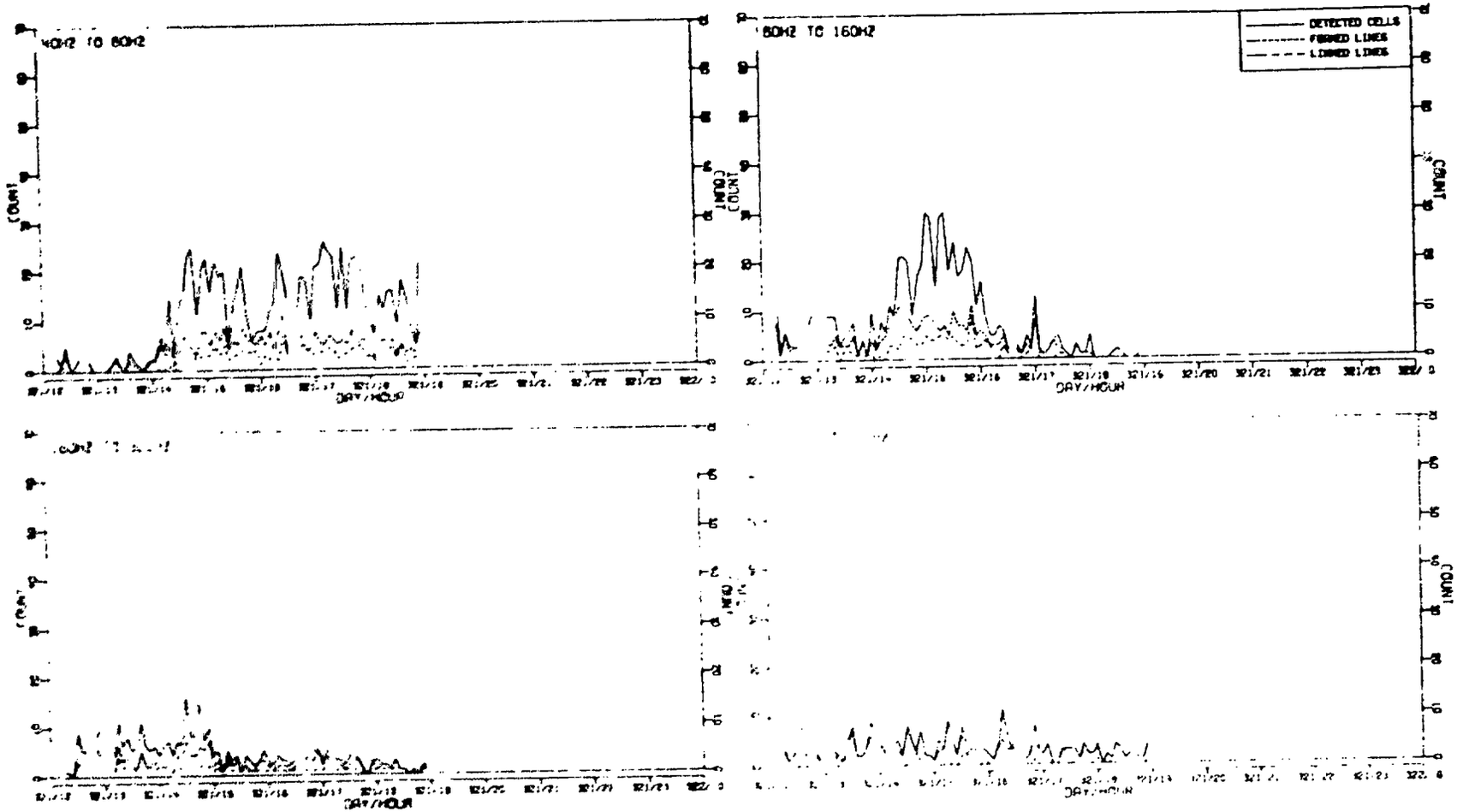

FIGURE II-386
MSS-FVT STANDARD RESOLUTION CLUTTER RESULTS
FOR THE VERTICAL DIPOLE SENSOR
AT SITE A2 DURING THE 17 NOV FIELD EVENT (U)

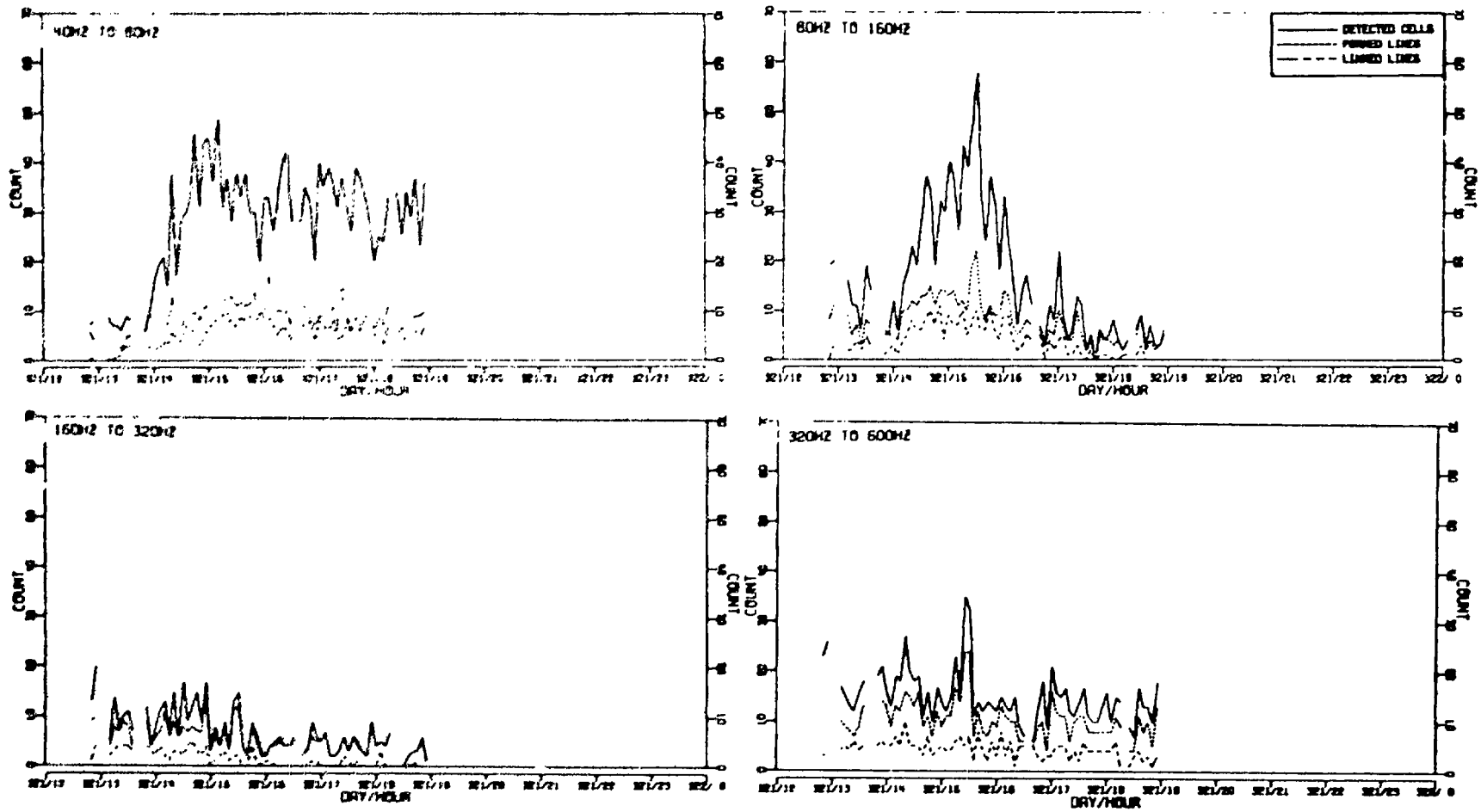

FIGURE II-367
MSS-FVT STANDARD RESOLUTION CLUTTER RESULTS
FOR THE DIFFERENCED CARDIOIDS SENSOR
AT SITE A2 DURING THE 17 NOV FIELD EVENT (U)

AS-77-3381

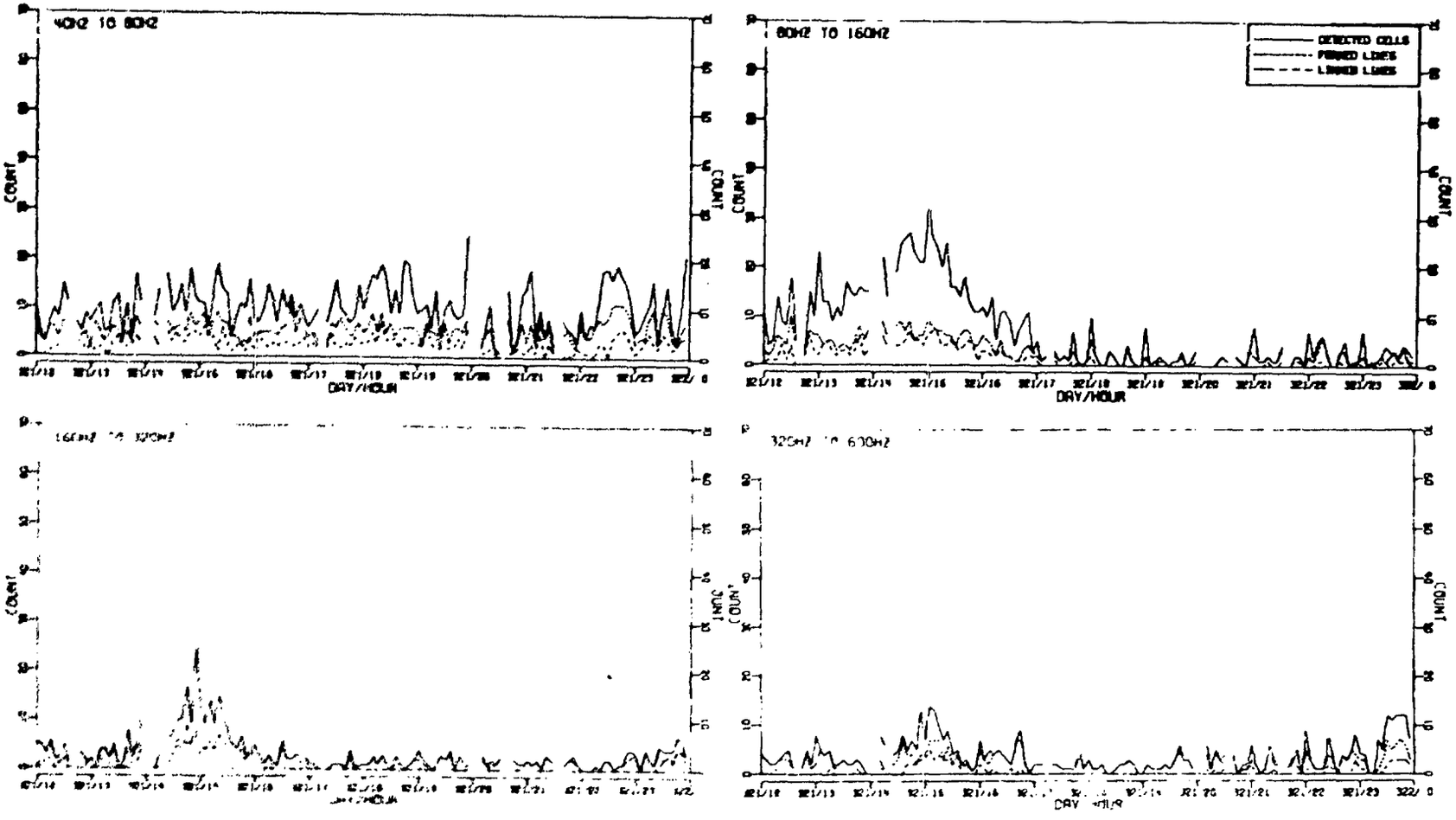

FIGURE II-368
MSS-FVT STANDARD RESOLUTION CLUTTER RESULTS
FOR THE OMNIDIRECTIONAL SENSOR
AT SITE A3 DURING THE 17 NOV FIELD EVENT (U)

AS-77-3182

CONFIDENTIAL

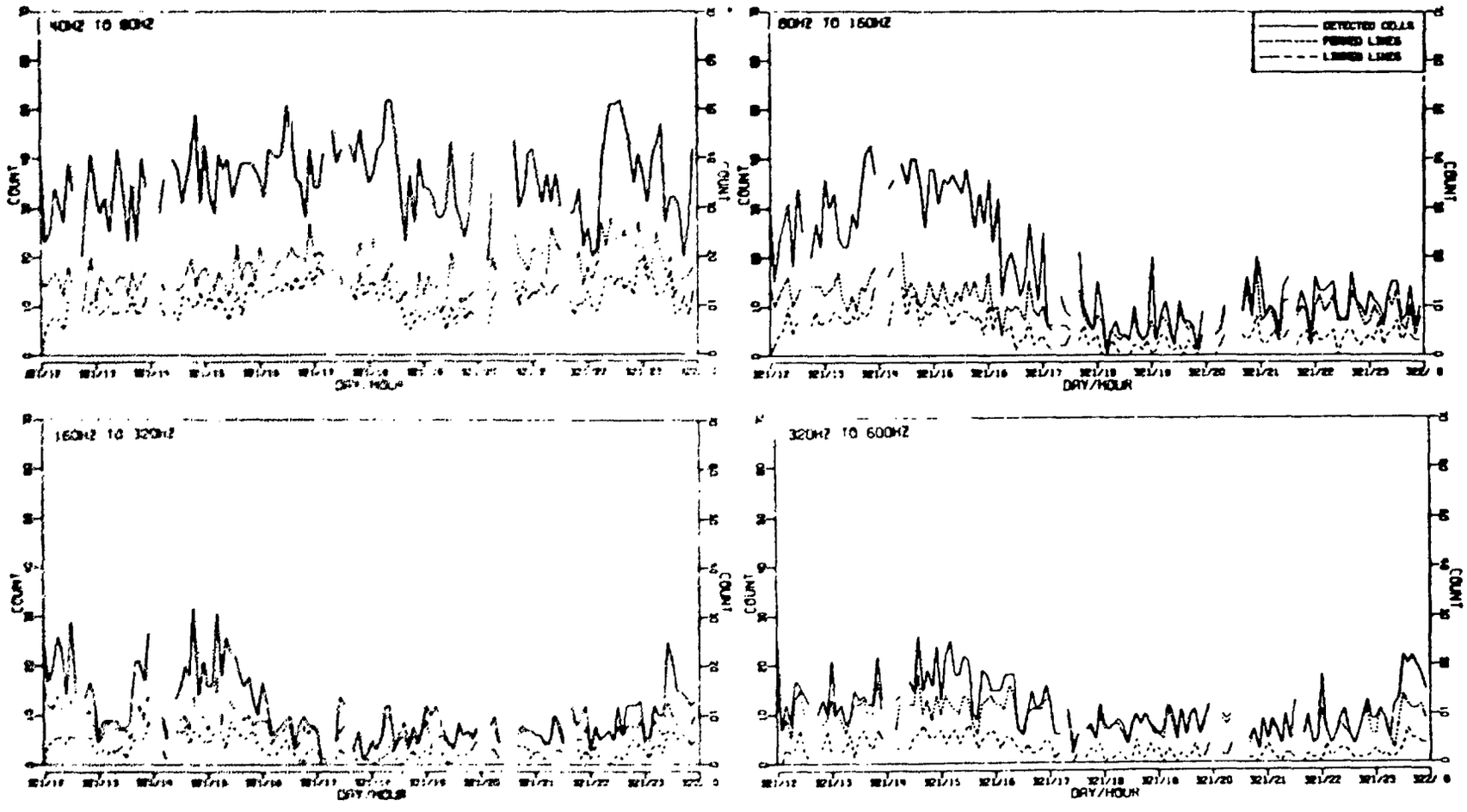

FIGURE II-369
MSS-FVT STANDARD RESOLUTION CLUTTER RESULTS
FOR THE SINGLE CARDIOIDS SENSOR
AT SITE A3 DURING THE 17 NOV FIELD EVENT (U)

AS-77-3383

CONFIDENTIAL

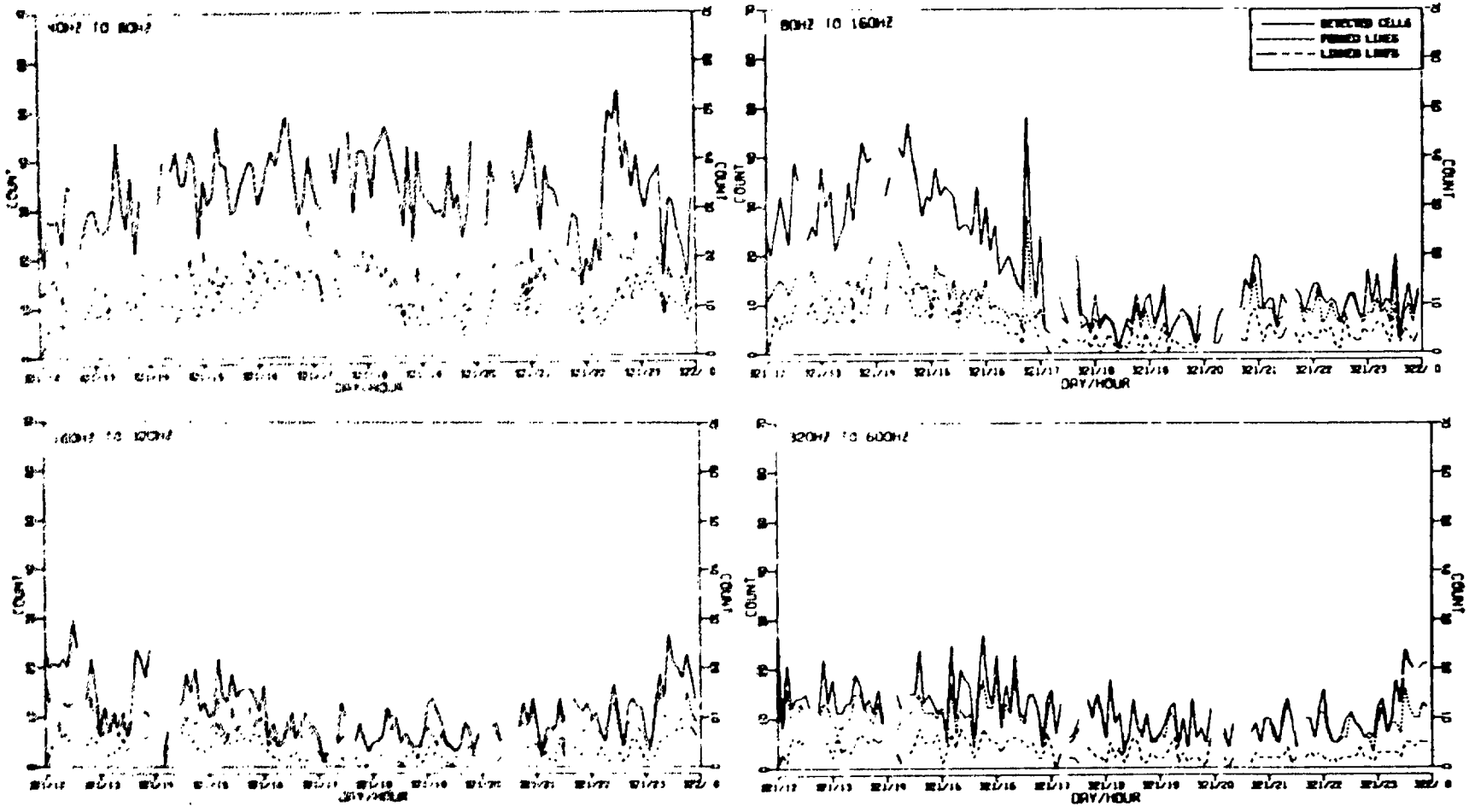

FIGURE II-370
MSS-FVT STANDARD RESOLUTION CLUTTER RESULTS
FOR THE MAX GAIN LIMACONS SENSOR
AT SITE A3 DURING THE 17 NOV FIELD EVENT (U)

CONFIDENTIAL

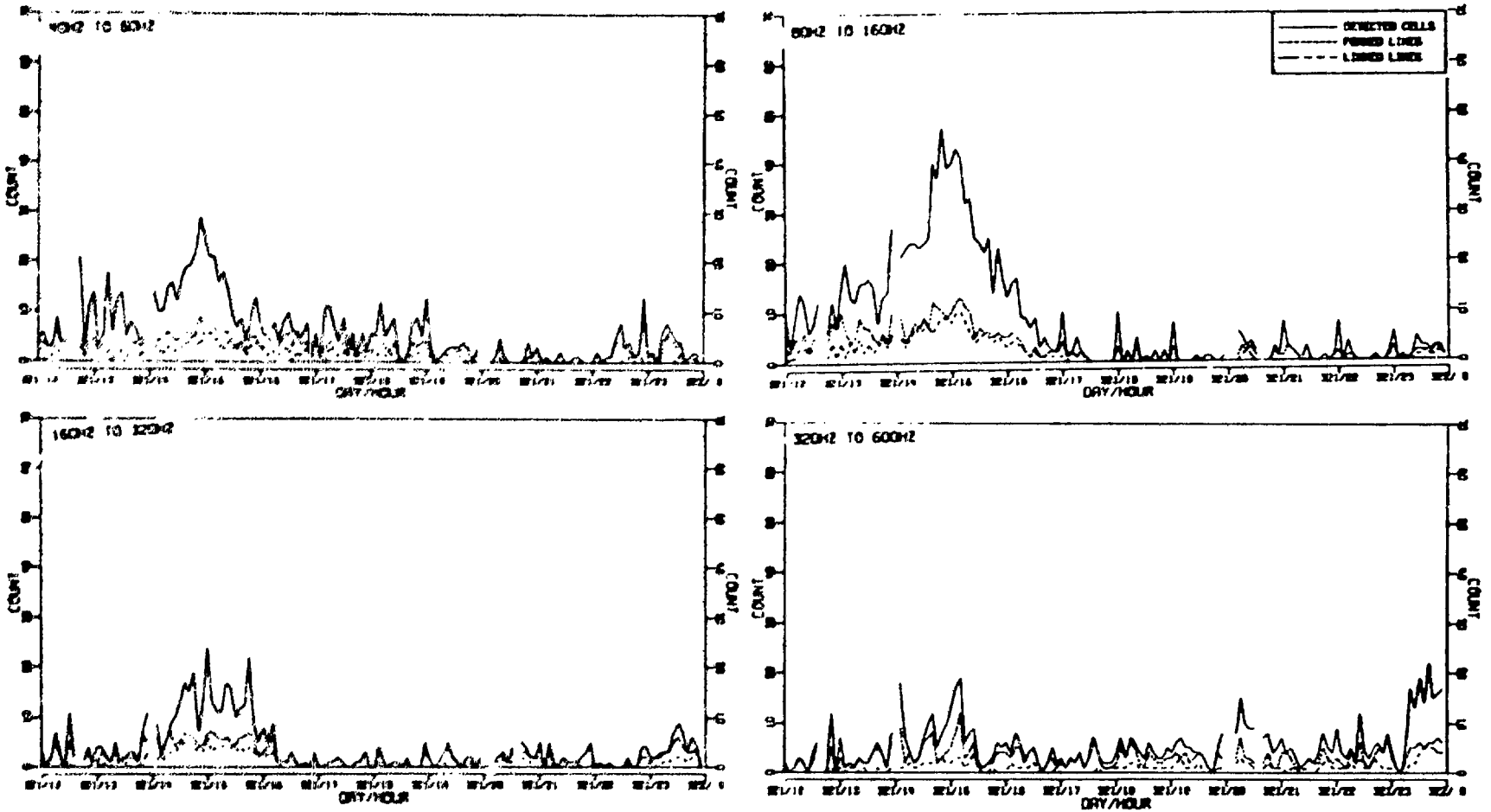

FIGURE II-371
MSS-FVT STANDARD RESOLUTION CLUTTER RESULTS
FOR THE VERTICAL DIPOLE SENSOR
AT SITE A3 DURING THE 17 NOV FIELD EVENT (U)

AS-77-3385

CONFIDENTIAL

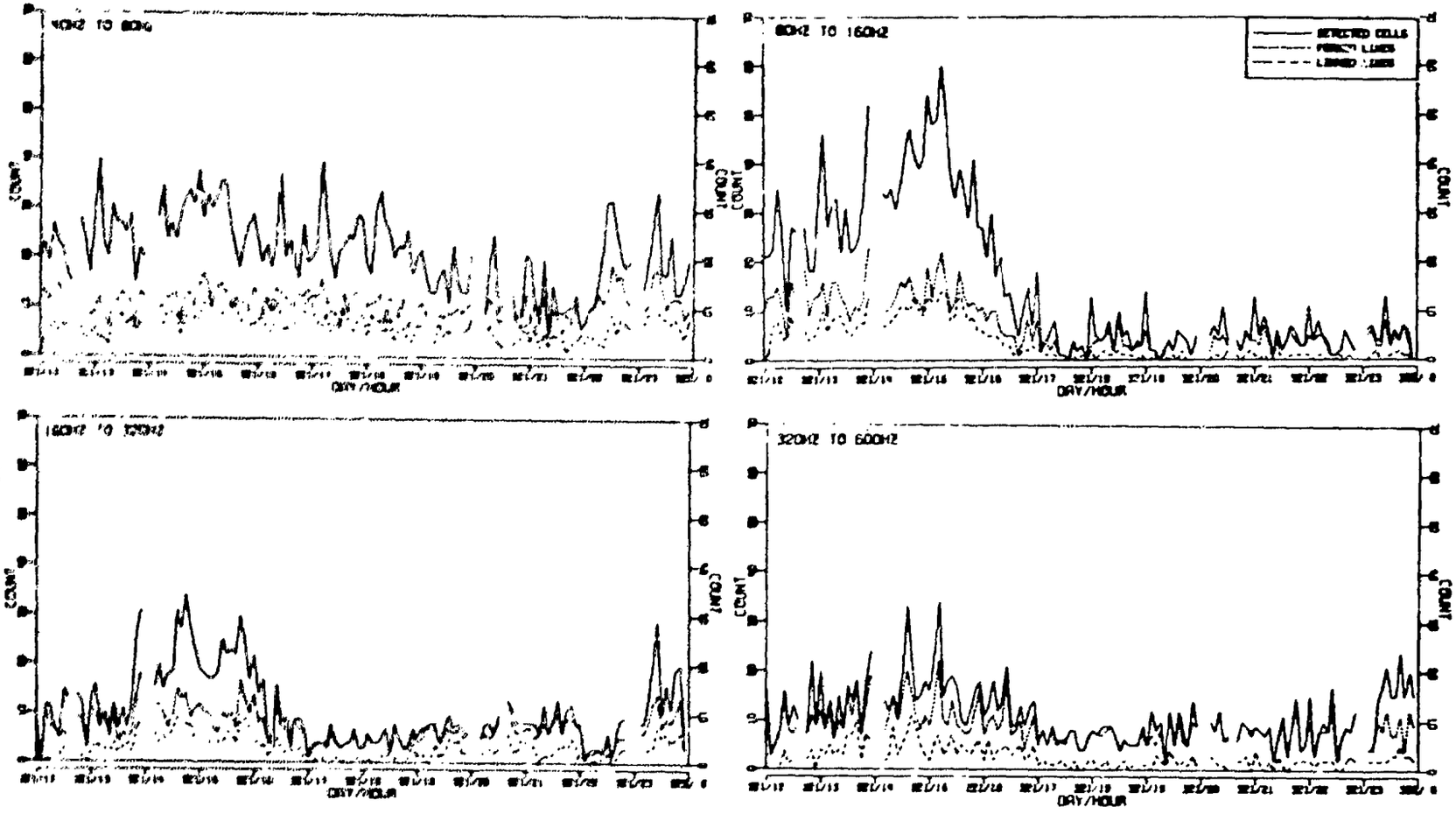

FIGURE II-372
MSS-FVT STANDARD RESOLUTION CLUTTER RESULTS
FOR THE DIFFERENCED CARDIOIDS SENSOR
AT SITE A3 DURING THE 17 NOV FIELD EVENT (U)

AS-77-3386

CONFIDENTIAL

31 December 1978

DISTRIBUTION LIST FOR
ARL-TR-78-2
FINAL REPORT UNDER CONTRACT N00039-77-C-0003, (ITEMS 0003 AND 0004)
SECRET

Copy No.

Commander
Naval Electronic Systems Command
Department of the Navy
Washington, DC 20360
1 Attn: PME 124
2 PME 124-30
3 PME 124-40
4 PME 124-60
5 PME 124TA
6 ELEX 320

7 Office of Assistant Secretary of the Navy
(RE&S) Room 5E813, Pentagon
Washington, DC 20360
Attn: Mr. G. Cann

Chief of Naval Operations
Department of the Navy
Washington, DC 20350
8 Attn: OP-095
9 OP-951F
10 OP-951F1
11 OP-981

Commander
Naval Air Development Center
Department of the Navy
Warminster, PA 18974
12 Attn: Code 3091
13 Code 303

14 Commander
Naval Air Systems Command
Department of the Navy
Washington, DC 20360
Attn: Code PMA-264A

Dist. List for ARL-TR-78-2 under Contract N00039-77-C-0003, Items 0003 and 0004 (Cont'd)

Copy No.

15 Commanding Officer
Naval Intelligence Support Center
4301 Suitland Road
Washington, DC 20390
Attn: Code 222

16 Project Manager
Anti-Submarine Warfare Systems Project Office
Department of the Navy
Washington, DC 20360
Attn: ASW 01T

Commanding Officer
Naval Ocean Research and Development Activity
Department of the Navy
NSTL Station, MS 39529
17 Attn: S. Marshall, Code 340
18 G. Lewis, Code 500

19 - 20 Commanding Officer and Director
Defense Documentation Center
Cameron Station, Building 5
5010 Duke Street
Alexandria, VA 22314

21 TRW, INC.
TRW Defense and Space Systems Group
Washington Operation
7600 Colshire Drive
McLean, VA 22101
Attn: W. Morley

22 Sanders Associates, Inc.
95 Canal Street
Nashua, NH 03606
Attn: L. Gagne

23 Office of Naval Research
Resident Representative
Room 508, Federal Building
Austin, TX 78701

24 Glen E. Ellis, ARL:UT

25 Loyd D. Hampton, ARL:UT

Dist. List for ARL-TR-78-2 under Contract N00039-77-C-0003, Items 0003 and 0004 (Cont'd)

Copy No.

26	Kenneth E. Hawker, ARL:UT
27	Stephen K. Mitchell, ARL:UT
28	Clark S. Penrod, ARL:UT
29	Jack A. Shooter, ARL:UT
30	Library, ARL:UT

DEPARTMENT OF THE NAVY
OFFICE OF NAVAL RESEARCH
875 NORTH RANDOLPH STREET
SUITE 1425
ARLINGTON VA 22203-1995

IN REPLY REFER TO:

5510/1
Ser 321OA/011/06
31 Jan 06

MEMORANDUM FOR DISTRIBUTION LIST

Subj: DECLASSIFICATION OF LONG RANGE ACOUSTIC PROPAGATION PROJECT (LRAPP) DOCUMENTS

Ref: (a) SECNAVINST 5510.36

Encl: (1) List of DECLASSIFIED LRAPP Documents

1. In accordance with reference (a), a declassification review has been conducted on a number of classified LRAPP documents.

2. The LRAPP documents listed in enclosure (1) have been downgraded to UNCLASSIFIED and have been approved for public release. These documents should be remarked as follows:

   Classification changed to UNCLASSIFIED by authority of the Chief of Naval Operations (N772) letter N772A/6U875630, 20 January 2006.

   DISTRIBUTION STATEMENT A: Approved for Public Release; Distribution is unlimited.

3. Questions may be directed to the undersigned on (703) 696-4619, DSN 426-4619.

BRIAN LINK
By direction

Subj: DECLASSIFICATION OF LONG RANGE ACOUSTIC PROPAGATION PROJECT (LRAPP) DOCUMENTS

DISTRIBUTION LIST:

NAVOCEANO (Code N121LC – Jaime Ratliff)
NRL Washington (Code 5596.3 – Mary Templeman)
PEO LMW Det San Diego (PMS 181)
DTIC-OCQ (Larry Downing)
ARL, U of Texas
Blue Sea Corporation (Dr.Roy Gaul)
ONR 32B (CAPT Paul Stewart)
ONR 321OA (Dr. Ellen Livingston)
APL, U of Washington
APL, Johns Hopkins University
ARL, Penn State University
MPL of Scripps Institution of Oceanography
WHOI
NAVSEA
NAVAIR
NUWC
SAIC

Declassified LRAPP Documents

Report Number	Personal Author	Title	Publication Source (Originator)	Pub. Date	Current Availability	Class.
Unavailable	Penrod, C. S., et al.	MOORED SURVEILLANCE SYSTEM FIELD VALIDATION TEST SENSOR PERFORMANCE ANALYSIS. VOLUME I. DATA COLLECTION AND MESUREMENT SYSTEM DESCRIPTION	University of Texas, Applied Research Laboratories	781231	ADC018009	C
Unavailable	Watkins, S. L., et al.	MOORED SURVEILLANCE SYSTEM FIELD VALIDATION TEST SENSOR PERFORMANCE ANALYSIS. VOLUME III. VERNIER RESOLUTION DATA PRODUCTS	University of Texas, Applied Research Laboratories	781231	ADC018373	C
Unavailable	Watkins, S. L., et al.	MOORED SURVEILLANCE SYSTEM FIELD VALIDATION TEST SENSOR PERFORMANCE ANALYSIS. VOLUME II. STANDARD RESOLUTION DATA PRODUCTS	University of Texas, Applied Research Laboratories	781231	ADC018374	C
NORDATN44	Bucca, P. J.	ENVIRONMENTAL VARIABILITY DURING THE CHURCH STROKE II CRUISE FIVE EXERCISE (U)	Naval Ocean R&D Activity	790201	ADC020353; NS; AU; ND	C
NADC7820830	Balonis, R. M.	TEST STEERED VERTICAL LINE ARRAY (TSVLA) MEASUREMENTS FOR BEARING STAKE SURVEYS (U)	Naval Air Systems Command	790301	ADC018003; NS; ND	C
USIControl674779	Williams, W., et al.	REPORT OF THE LRAPP EXERCISE PLANNING WORKSHOP TRACOR INC ROCKVILLE MD 16 - 17 OCTOBER 1978 (U)	Underwater Systems, Inc.	790302	NS; ND	C
NOSCTR357	Hamilton, E. L., et al.	GEOACOUSTIC MODELS OF THE SEAFLOOR: GULF OF OMAN, ARABIAN SEA, AND SOMALI BASIN (U)	Naval Ocean Systems Center	790615	ND	C
Unavailable	Unavailable	RAPIDLY DEPLOYABLE SURVEILLANCE SYST (RDSS) ACOUSTIC VALIDATION TEST (AVT) EXERCISE PLAN (U)	Naval Electronic Systems Command	790625	AU	C
LRAPPRC79027	Brunson, B. A., et al.	GULF OF MEXICO AND CARIBBEAN SEA DATA AND MODEL BASE REPORT (U)	Tracor, Inc.	790701	ADC019153; NS; ND	C
Unavailable	Unavailable	BEARING STAKE BMS DATA QUALITY ASSESSMENT REPORT (U)	University of Texas, Applied Research Laboratories	790705	AU	C
PME12430	Unavailable	RAPIDLY DEPLOYABLE SURVEILLANCE SYSTEM (RDSS) ACOUSTIC VALIDATION TEST (AVT) DATA REDUCTION AND ANALYSIS PLAN (U)	Naval Electronic Systems Command	790815	NS; AU	C
Unavailable	Unavailable	RAPIDLY DEPLOYABLE SURVEILLANCE SYSTEM (RDSS) ACOUSTIC VALIDATION TEST (AVT) EXERCISE PLAN (U)	Naval Electronic Systems Command	790917	AU	C
NOSCTR467	Pedersen, M. A., et al.	PROPAGATION LOSS ASSESSMENT OF THE BEARING STAKE EXERCISE (U)	Naval Ocean Systems Center	790928	ADC020845; NS; AU; ND	C
NOSCTR466	Anderson, A. L., et al.	BEARING STAKE ACOUSTIC ASSESSMENT (U)	Naval Ocean Systems Center	790928	ADC020797; NS; AU; ND	C